Report No. FAA-R-6750.2
AAF-420

LEVEL

IN-SERVICE IMPROVEMENTS TO RELIABILITY AND

MAINTAINABILITY OF THE INSTRUMENT LANDING SYSTEM

Avionics Engineering Center
Department of Electrical Engineering
Ohio University
Athens, Ohio 45701
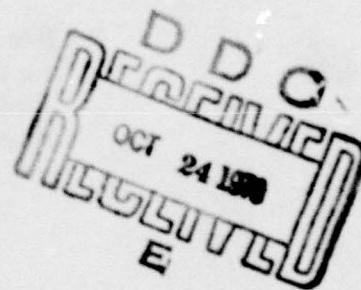
MAY 1979

FINAL REPORT

Document is available to the public through the
National Technical Information Service
Springfield, Virginia 22161

Prepared for

U.S. DEPARTMENT OF TRANSPORTATION
FEDERAL AVIATION ADMINISTRATION
Airway Facilities Sector
Washington, D.C. 20591

79 10 23 017

NOTICE

This document is disseminated under the sponsorship of the Department of Transportation in the interest of information exchange. The United States Government assumes no liability for the contents or use thereof.

TECHNICAL REPORT STANDARD TITLE PAGE

1. Report No. FAA-R-675U.2 AAF-420	2. Government Accession No.	3. Recipient's Catalog No.
4. Title and Subtitle IN-SERVICE IMPROVEMENTS TO RELIABILITY AND MAINTAINABILITY OF THE INSTRUMENT LANDING SYSTEM		5. Report Date May 1979
		6. Performing Organization Code
7. Author(s) Avionics Engineering Center Staff		8. Performing Organization Report No. EER-40-1
9. Performing Organization Name and Address Avionics Engineering Center Department of Electrical Engineering Ohio University Athens, Ohio 45701		10. Work Unit No.
		11. Contract or Grant No. DOT-FA78WA-4062
12. Sponsoring Agency Name and Address U.S. Department of Transportation Federal Aviation Administration Airway Facilities Sector Washington, D.C. 20591		13. Type of Report and Period Covered Final Report October 1977 to May 1979.
		14. Sponsoring Agency Code

15. Supplementary Notes

487

16. Abstract

This report documents results of task efforts undertaken by Ohio University between October 1977 and May 1979. Engineering data resulting from a study of the sideband reference, glide-slope system baseline operating parameters and the effects of specific faults are presented. A series of perturbational studies conducted at commissioned sideband reference facilities and numerous field experiments at Ohio University's Tamiami, Florida site facility are described. Suggested technical improvements and text changes for existing technical manuals have also resulted.

The effects of a wide range of terrain profiles on the performance of sideband reference, null reference, and capture effect systems are compiled in album form. Sideband reference system setup procedures are reviewed, the electrical and physical requirements for the counterpoise are explored, and an introductory look at threshold-plane DDM profiles is presented.

ILS anomaly investigations have resulted in the design, testing, and implementation of a modification to the Type FA-5723 clearance transmitter. Also, predictions of complete glide-slope performance for a proposed site on Runway 22L at Boston Logan are presented.

The maximum allowable VSWR for the 15-element V-Ring and the O-Ring localizers are investigated based on theoretical and experimental work. The findings are that the maximum VSWR is not that of a simple specification but rather that of values that are within the bounds of worst- and best-case conditions depending on the value of the complex reflection coefficient.

Finally, outlines for two one-week seminars and a one-day short course conducted by Ohio University at the FAA Aeronautical Center, Oklahoma City, Oklahoma and Southern Region Headquarters, Atlanta, Georgia, respectively, are given.

17. Key Words Glide Slope, Localizer, Sideband Reference, Seminar, Clearance, Terrain Effects, Boston Logan, Modulation Unbalance, Perturbational Study, V-Ring, O-Ring, Counterpoise	18. Distribution Statement This document is available to the U.S. public through the National Technical Information Service, Springfield, Virginia 22161.

19. Security Classif. (of this report) Unclassified	20. Security Classif. (of this page) Unclassified	21. No. of Pages 465	22. Price

Form DOT F 1700.7 (8-69)

267460

METRIC CONVERSION FACTORS

ii

TABLE OF CONTENTS

TABLE OF CONTENTS (CONTINUED)

iv

TABLE OF CONTENTS (CONTINUED)

TABLE OF CONTENTS (CONTINUED)

LIST OF FIGURES

LIST OF FIGURES (Continued)

LIST OF FIGURES (Continued)

LIST OF FIGURES (Continued)

LIST OF FIGURES (Continued)

LIST OF FIGURES (Continued)

LIST OF TABLES

LIST OF TABLES (Continued)

FOREWORD

For nearly two decades (since 1963) the Avionics Engineering Center at Ohio University (Athens, Ohio) has been engaged in research and engineering directed toward improving and better understanding the Instrument Landing System. The Federal Aviation Administration has supported this effort under a series of contracts with its Systems Research and Development Service and its Airway Facilities Service.

This Final Report describes results obtained during Contract DOT-FA78WA-4062 through its 1977-79 period of performance.

The Avionics Engineering Center is an integral part of the Department of Electrical Engineering at Ohio University. Accordingly, the Center is able to offer opportunities to graduate and undergraduate students and faculty members, for participation in the ongoing FAA-sponsored work. Benefits accrue to the FAA, the Center, and to the individual, through participation in real-world engineering tasks with their requirement for quality work on schedule. The FAA and the aviation industry benefit from the availability of trained and educated engineers with experience in existing and developmental navigation and communication systems.

I. INTRODUCTION AND SUMMARY

This report presents results of FAA-supported work on improvement and documentation of ILS glide slope and localizer systems. Detailed report sections on each of the major work efforts are presented. Due to the diverse nature of project activity, results and conclusions are distributed throughout the report, being placed in those sections to which they apply.

Section II presents results of the sideband reference glide slope studies, first at a near-ideal site and finally at existing installations in the eastern states. Use is made of computer modeling in establishing relationships among baseline parameters and in comparing performance predictions for sideband reference, null reference, and capture effect glide slopes on non-ideal terrain.

Section III discusses ILS anomaly investigations. A description is given of the FA-5723 clearance monitor modification made to remove certain debilitating malfunctions. A computer study of the Runway 22L site at Boston Logan Airport is presented that reveals the capture effect system can be operated satisfactorily provided monitor tolerances are tightened to protect from cumulative tide effects. Allowable VSWR's of V-Ring and O-Ring localizers are identified within a context of best and worst-case bounds. VSWR is shown to be an incomplete specification for precise identification of performance. Description of a complex reflection coefficient is needed.

Section IV outlines the seminars and short course which constituted the educational support function of the project.

Set-up procedures are discussed in the Appendices.

The general conclusion is that the ILS remains a highly flexible and important navigational aid with possibilities for improvement and better and more effective application still waiting to be fully realized.

II.   SIDEBAND REFERENCE GLIDE-SLOPE PERTURBATION AND MONITOR STUDY

Calculated responses of the sideband reference glide-slope system to specific faults and adjustments have been validated experimentally and are herein reported graphically. Both far-field behavior and near-field vertical profiles of the glide-slope structure are presented for some fault conditions. The question of integral versus near-field monitoring is investigated.

Calculated performances for null reference, sideband reference, and capture effect glide-slope systems for different terrain profiles are compared and studies of selected operational glide slopes are included.

A. A Documentation of the Sideband Reference Glide-Slope System Response to Specific Faults.

1. Summary and Conclusions. A study has been made of the response of the sideband reference (SBR), image, glide-slope system to specific faults. Various faults were introduced into the transmitting equipment and RF distribution network. These faults are intended to be representative of those which might be expected to occur in practice due to either a component failure or improper adjustment of the station equipment. As each fault was introduced into the system, glide path (operating) parameters for the nearly ideal site at Tamiami Airport were measured using an instrumented aircraft and the results compared to those predicted by the flat earth option of OUGS, a computer model for image glide slope systems developed at Ohio University.

The validation tests involved both integral and near-field monitor pickups. The validation process yielded data that showed the measured values were typically to 2% of the predicted values. The integral monitoring provided good data, but the well-used components in the associated transmission lines network introduced some problems with stability.

The conclusions reached as a result of this investigation are:

(1) In the SBR system the path angle is controlled in part and is critically dependent on the sideband power division between the upper and lower antennas. This power must be carefully controlled and monitored. The existence of vagaries in power splitting devices and the resetting of controls offers potential for path angle maintenance problems.

(2) Present instructions for setting the near-field monitor antennas are in one case misleading, and in the other result in an overly sensitive sample. In general, the current monitor set-up as specified for the SBR system must be considered a fault detector and not an analog representation of the far-field conditions.

-2-

(3) A major advantage to use of the SBR system is that the lower antenna heights used not only permit locating the array closer to runway areas but also require only a modest ground plane in the reflecting area.

(4) For antenna phasing using airborne or ground-based methods, a quadrature section of line (90 electrical degrees) should be inserted in the sideband feedline going to the APCU or the upper antenna and the sideband line to the lower antenna dummied. It should be noted that for the flat plane case simply inserting the quadrature section in the sideband line going to the APCU is sufficient without changes in the lower antenna.

(5) The present monitoring set-up is overly sensitive to ground-plane conditions in the near-field reflecting zone. The use of a ground screen (counterpoise) ignores the basic principle of representativeness since the screen does not significantly influence the far field.

(6) Integral monitors gave indications in most cases of being an analog of the far field.

(7) Ground phasing with the use of probes is possible if phase distribution among the dipoles or "effective phase center" of each antenna or relative phase of the monitor port output with respect to radiated signal is known.

2. Introduction and Purpose. The purpose of this report section is to document the performance of the sideband reference glide-slope system. Such documentation can be useful not only for troubleshooting and other maintenance tasks, but can also provide insight into expected monitor performance as well as set-up procedures.

a. SBR Theory of Operation. The sideband reference glide slope, as presently employed, requires two antennas arranged vertically one above the other with the upper antenna offset toward the runway to minimize proximity effects in the near-threshold zone along the centerline. These antennas may be at various height ratios ranging from 2.5 to 1, to 4 to 1. For convenience it is simpler to discuss a specific installation since the principle, once understood, is easily generalized to any other ratio. The specific system designed for use in the Tamiami (TMB) tests has antennas at height ratio of 3 to 1 and a glide-slope angle of 3°. To achieve this, the upper antenna was placed at a height of one-half wavelength divided by the sine of 4°, thus producing a null at 4°. The lower antenna was placed at a height of one-half wavelength divided by the sine of 12° and produced a null at 12°. These heights are based on calculations made using the far-field approximation. Figure 1 illustrates these field strength variations with altitude expressed as path angle. A simple trigonometric calculation shows that if the maxima of the two patterns are equal, the signals will also be equal at 3° and 9°. The lower antenna radiates modulated carrier (modulation index 0.4, 150 and 90 Hz sidebands both in phase with the carrier) plus sideband-only (suppressed carrier) signals which subtract from the 150 and add to the 90 Hz carrier sidebands. The upper antenna
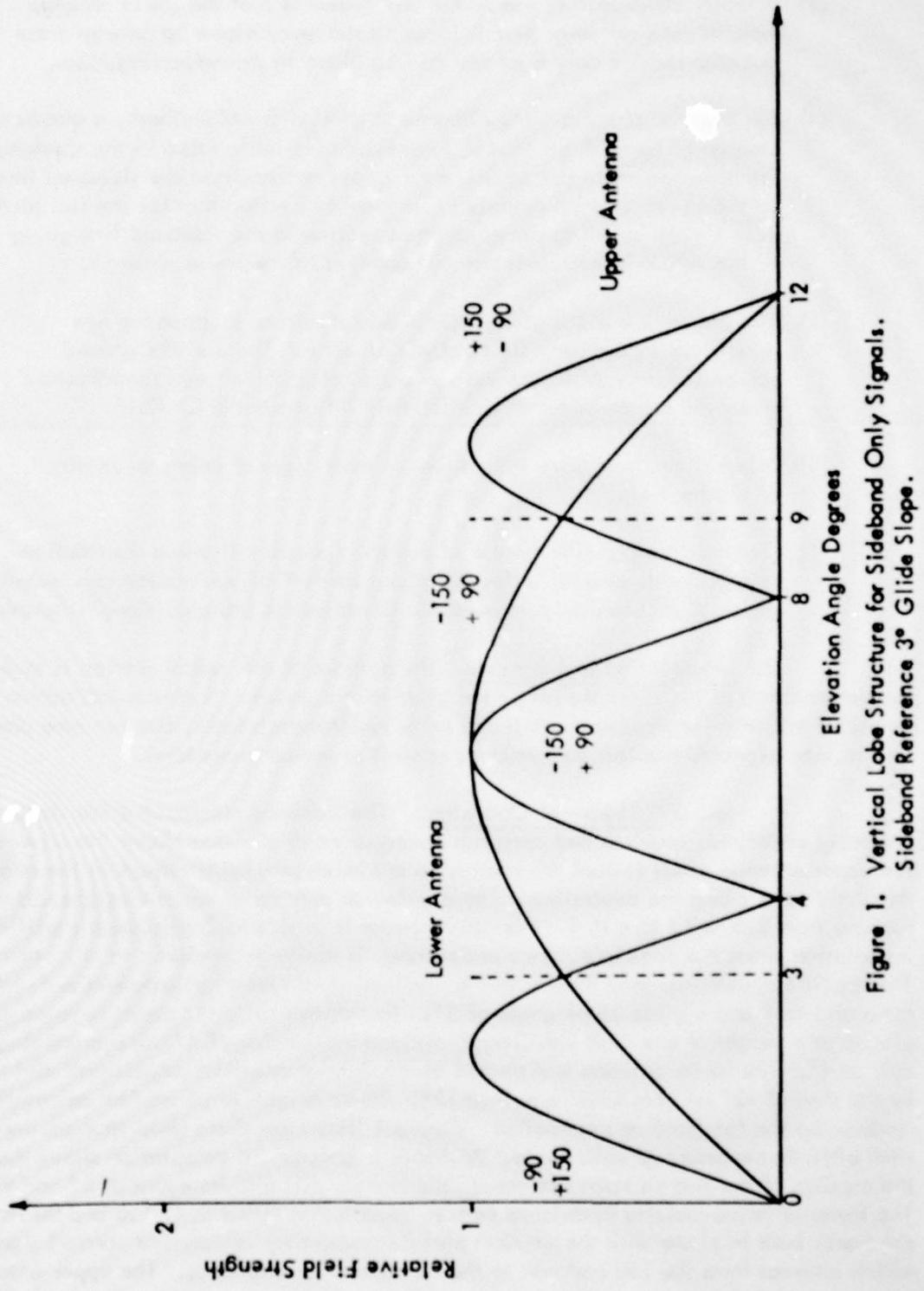
Figure 1. Vertical Lobe Structure for Sideband Only Signals. Sideband Reference 3° Glide Slope.

radiates sideband only (suppressed carrier) signals with the 150 Hz sidebands and the 90 Hz sidebands reversed with respect to those in the lower antenna. Where these sideband only signals have equal magnitude (at 3° and 9° as shown in Figure 1) the result is cancellation of the depth of modulation increments and 0 DDM (difference in depth of modulation).

Since the TMB location is extremely flat, the ray-optic method may be used for calculation of the spatial patterns of CDI (course deviation indicator) current. Calculating the path length for antenna to observer and image to observer (using the method of images) one obtains the formulation:

$$CDI = K \{ \frac{\sin 180(\gamma_4 - \gamma_1)}{\sin 180(\gamma_3 - \gamma_2)} \cos 180(\gamma_4 + \gamma_1 - \gamma_3 - \gamma_2) - 1 \} \quad \text{indicator current}$$

where

$$\gamma_1 = ((x-e)^2 + y^2 + (z-H)^2)^{\frac{1}{2}}$$

$$\gamma_2 = (x^2 + y^2 + (z-h)^2)^{\frac{1}{2}}$$

$$\gamma_3 = (x^2 + y^2 + (z+h)^2)^{\frac{1}{2}}$$

$$\gamma_4 = ((x-e)^2 + y^2 + (z+H)^2)^{\frac{1}{2}}$$

h is the height of the lower antenna

H is the height of the upper antenna

e is the offset of the upper antenna.

The antenna tower is at the origin of the coordinate system (Cartesian), y is measured parallel to the runway centerline, x is perpendicular to the runway centerline, and z is the vertical distance above ground. Distances are measured in wavelengths.

It is interesting to note that the sideband reference system consists of the superposition of a null-reference-like pattern (4° slope) and a constant CDI pattern. This concept is useful in visualizing some of the peculiarities of the near-field region.

3. Data Collection. The SBR data collection was accomplished at Ohio University's experimental ILS test site at the New Tamiami Airport. A Mark 1C glide-slope transmitter was used as a signal source. Two APC type FA-8976 glide-slope antennas were installed at a height of 7.09' (2.161m) and 21.27' (6.483m) above ground for the SBR configuration.

The APCU implemented for these tests facilitates accurate fault introduction and when used in conjunction with selected transmitter controls is capable of effecting a wide range of perturbations. Figure 2 shows a simplified schematic of the SBR test APCU.

The path angle was found to be 3.02° with a width of 0.68°. The system was then perturbed as noted in Table 1. Airborne measurements of the path angle and width were obtained using the Ohio University Minilab Mark III, an airborne instrumentation package flown in a Beechcraft Model V35A.

Table 1 also contains the predicted responses of the system as determined by the computer model OUGS. Very good correlation is evident with percent difference typically amounting to 1%.

    4. Discussion of Data. In preparation for the setup and test to be made on the sideband reference glide slope at Tamiami, the glide slope was modeled with the OUGS computer model and a series of perturbations applied to the model. Figures 3 through 6 are plots of path angle and path edge loci vs. perturbation derived from these runs in which the observation point was brought in at constant altitude along the extended centerline (pattern B) and also moved vertically up at the 360°, 300°, and 180° proximity points. All perturbations to be used in anticipated fault tests were thus treated. Use of these data permitted efficient planning of fault study flight checks by making possible the selection of faults which would bring the monitors to alarm limits.

By simulating vertical runs at various points in the near field, data was obtained from which Figures 7, 8, and 9 were constructed. Figure 7 was calculated for the sideband reference glide slope with normal antenna currents and a perfectly reflecting ground plane (reflection coefficient 1.000 at 180°). Figures 8 and 9 show the effect of an imperfectly reflecting ground. Figure 8 was plotted for a complex dielectric constant of (ϵ_r = 20. -j 0.60) while Figure 9 represents the effects of using a dielectric constant of (ϵ_r = 2.25 -j 0.255).

A major reason for the profile study is to furnish information concerning the correlation existing between points accessible to ground based measurements and the far field. Such information is vital to the framing of a set-up procedure which can guarantee minimum flight check expense requirements. Appendix A contains some of these set-up procedures and includes preliminary experimental data taken in the vertical plane containing the runway threshold.

An interesting use of the profile of Figure 7 was made during the set-up at Tamiami. When an attempt was made to carry out the instructions in Handbook 6750.6B, paragraph 26b3, a frustrating impasse arose in that the required 0 DDM could not be found. The profile showed why this was the case, and thus avoided lost time and effort while also pointing to a correction which should be made in future editions of the instructions.

Another application of theoretical modeling to the set-up at TMB involved airborne phasing of the upper antenna as described in Handbook 6750.6B, section 24f1, which calls for the addition of a 90° line section to the sideband line. The ambiguity

-6-
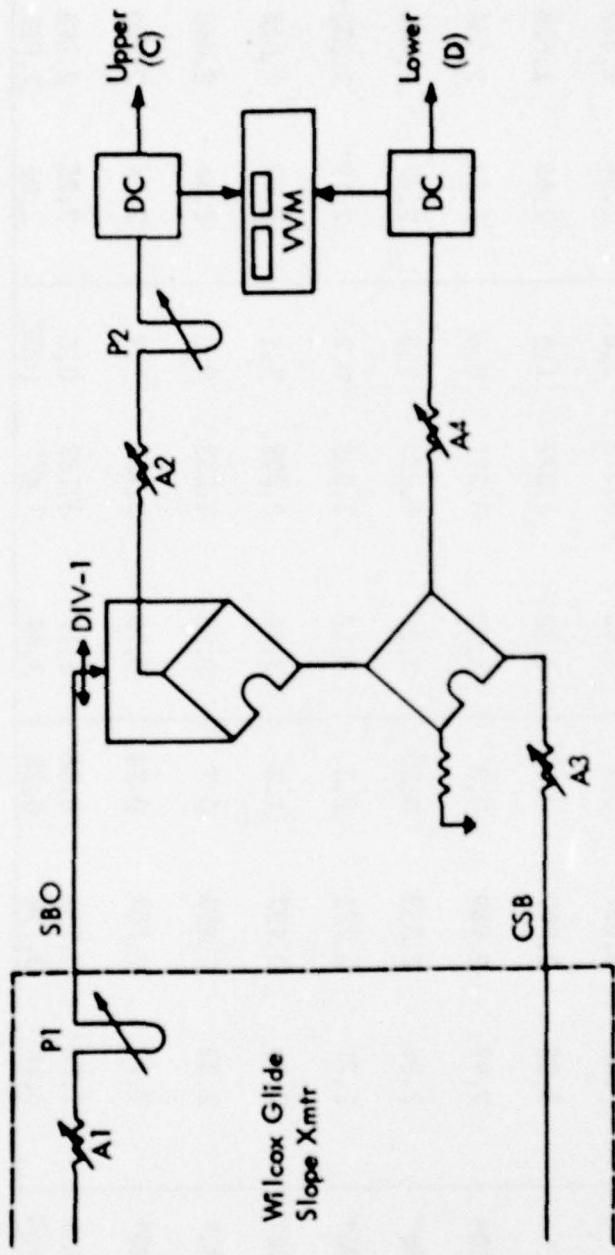
Figure 2. Simplified Block Diagram of SBR APCU/Test Setup.

RUN	0 CDI (°)			UPPER 75 uAmp.(°)			LOWER 75 uAmp.(°)		
	MEAS.	CALC.	% Off	MEAS.	CALC.	% Off	MEAS.	CALC.	% Off
NORMAL	3.02	3.000	0.67	3.37	3.350	0.6	2.69	2.650	1.5
CSB +30°	3.01	3.001	0.3	3.52	3.406	3.3	2.57	2.597	1.0
CSB -30°	2.96	2.998	1.3	3.30	3.404	3.0	2.62	2.594	1.0
CSB +20°	3.02	3.001	0.6	3.46	3.373	2.6	2.64	2.629	0.4
CSB -20°	3.00	2.999	0.03	3.32	3.372	1.5	2.66	2.626	1.3
Upper -20°	2.93	2.939	0.3	3.33	3.311	0.6	2.54	2.566	1.0
Upper -30°	2.86	2.853	0.25	3.21	3.253	1.3	2.47	2.444	1.1
Upper -36°	2.71	2.775	2.3	3.18	3.205	0.8	2.19*	2.333*	6.1*
Upper +20°	2.90	2.937	1.3	3.24	3.309	2.1	2.52	2.563	1.7
Upper +30°	2.83	2.850	0.7	3.28	3.253	0.8	2.36	2.440	3.3
Upper +40°	2.71	2.703	0.26	3.10	3.159	1.9	2.24	2.230	0.44
Upper -2dB	2.74	2.750	0.36	3.17	3.189	0.6	2.25	2.298	3.1
Lower -2dB	3.16	3.198	0.25	3.49	3.479	0.32	2.86	2.921	2.1

*A defective phase adjustor prevented the attainment of the full 40° phase delay. This situation was later corrected when repair was possible without loss of flight time.

Table 1. Comparison of Flight Measurements with Calculated Theoretical Values.

Curve 1 – Pattern B

Curve 2 – 360° Point

Curve 3 – 300° Point
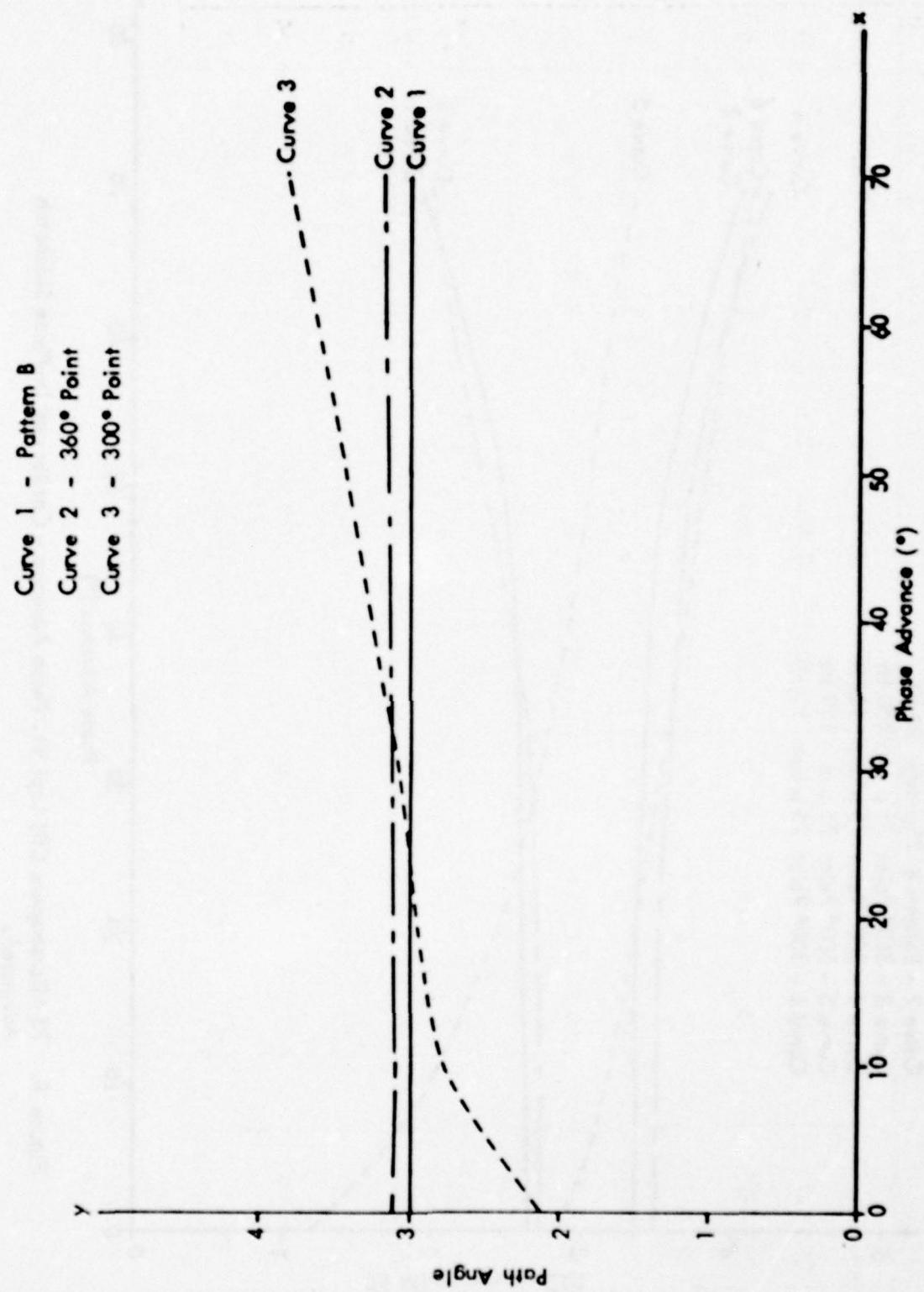
Figure 3. Path Angle Vs. Phase Advance – Carrier and In-Phase Sidebands Advanced.

Curve 1 – Pattern B 75 μ amp 150 Hz
Curve 2 – Pattern B 75 μ amp 90 Hz
Curve 3 – 360° Point 75 μ amp 150 Hz
Curve 4 – 360° Point 75 μ amp 90 Hz
Curve 5 – 300° Point 75 μ amp 150 Hz
Curve 6 – 300° Point 75 μ amp 90 Hz

Phase Advance (°)
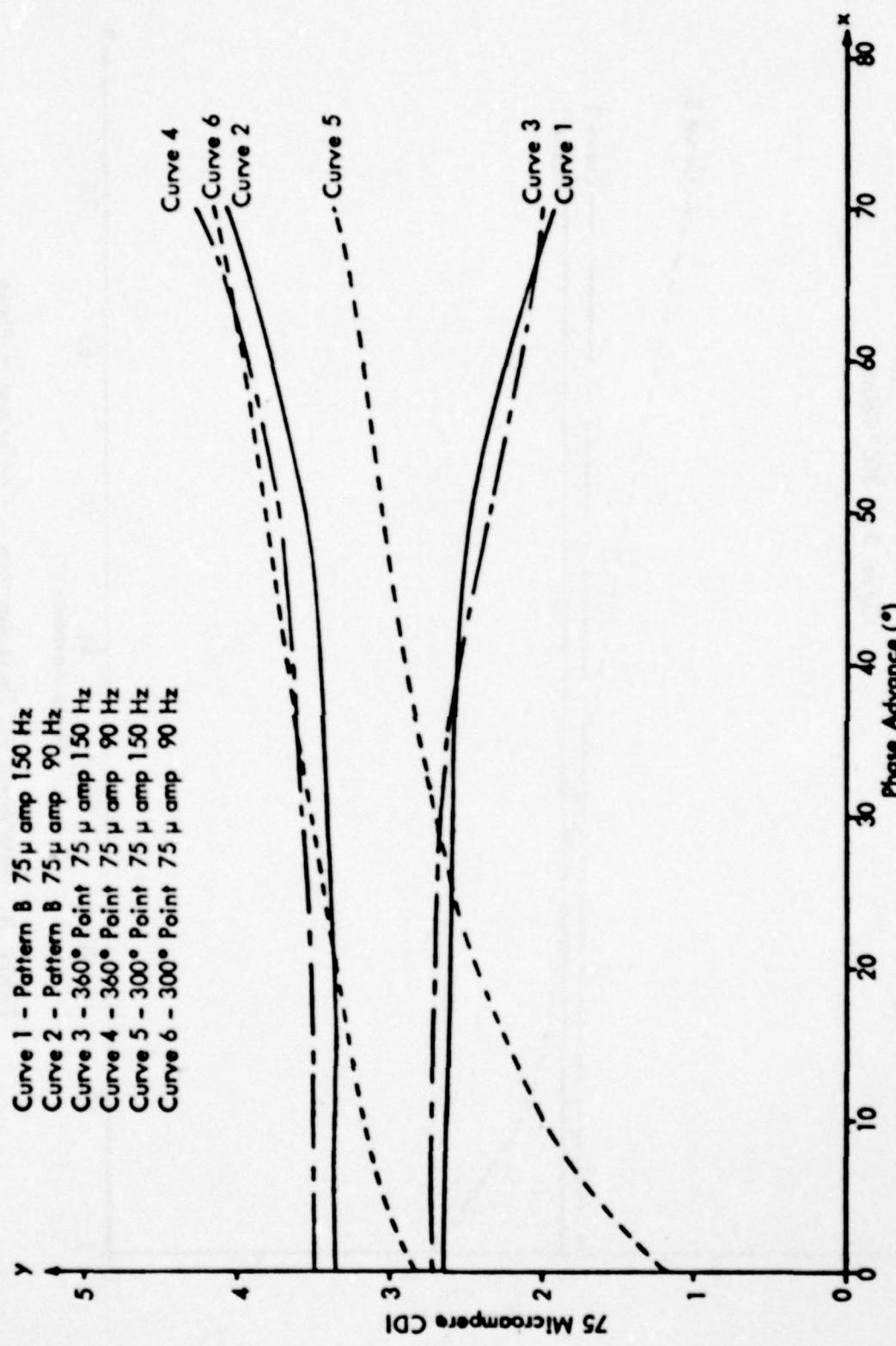
75 Microampere CDI

Figure 4.   75 Microampere CDI Loci Vs. Phase Advance – Carrier and In-Phase Sidebands Advanced.

Curve 1 - Pattern B

Curve 2 - 360° Point

Curve 3 - 300° Point
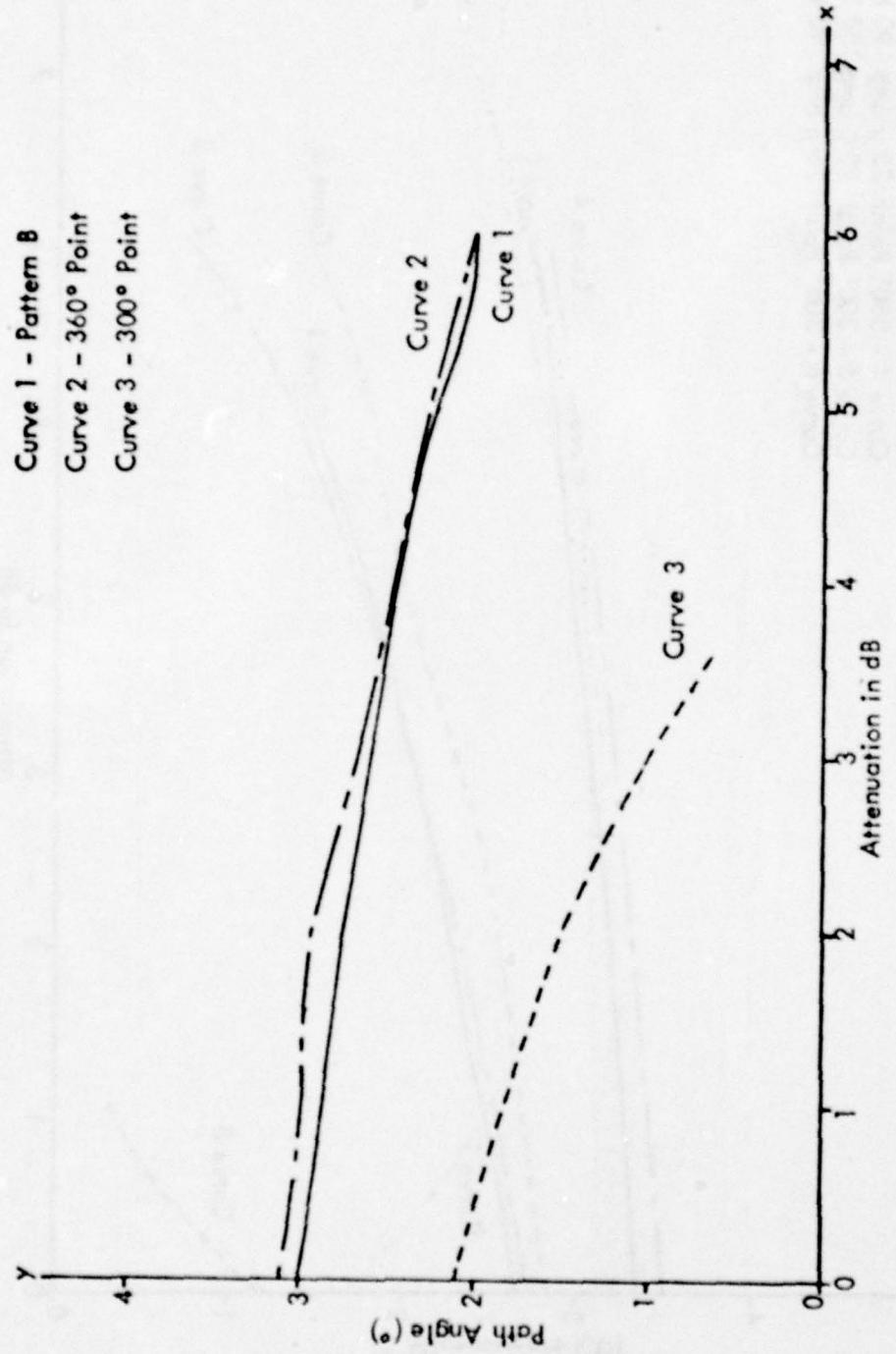
Figure 5. Path Angle Vs. Attenuation–Upper Antenna Power Attenuated.

-11-

Curve 1 – Pattern B 75 μ amp 150 Hz
Curve 2 – Pattern B 75 μ amp 90 Hz
Curve 3 – 360° Point 75 μ amp 150 Hz
Curve 4 – 360° Point 75 μ amp 90 Hz
Curve 5 – 300° Point 75 μ amp 150 Hz
Curve 6 – 300° Point 75 μ amp 90 Hz
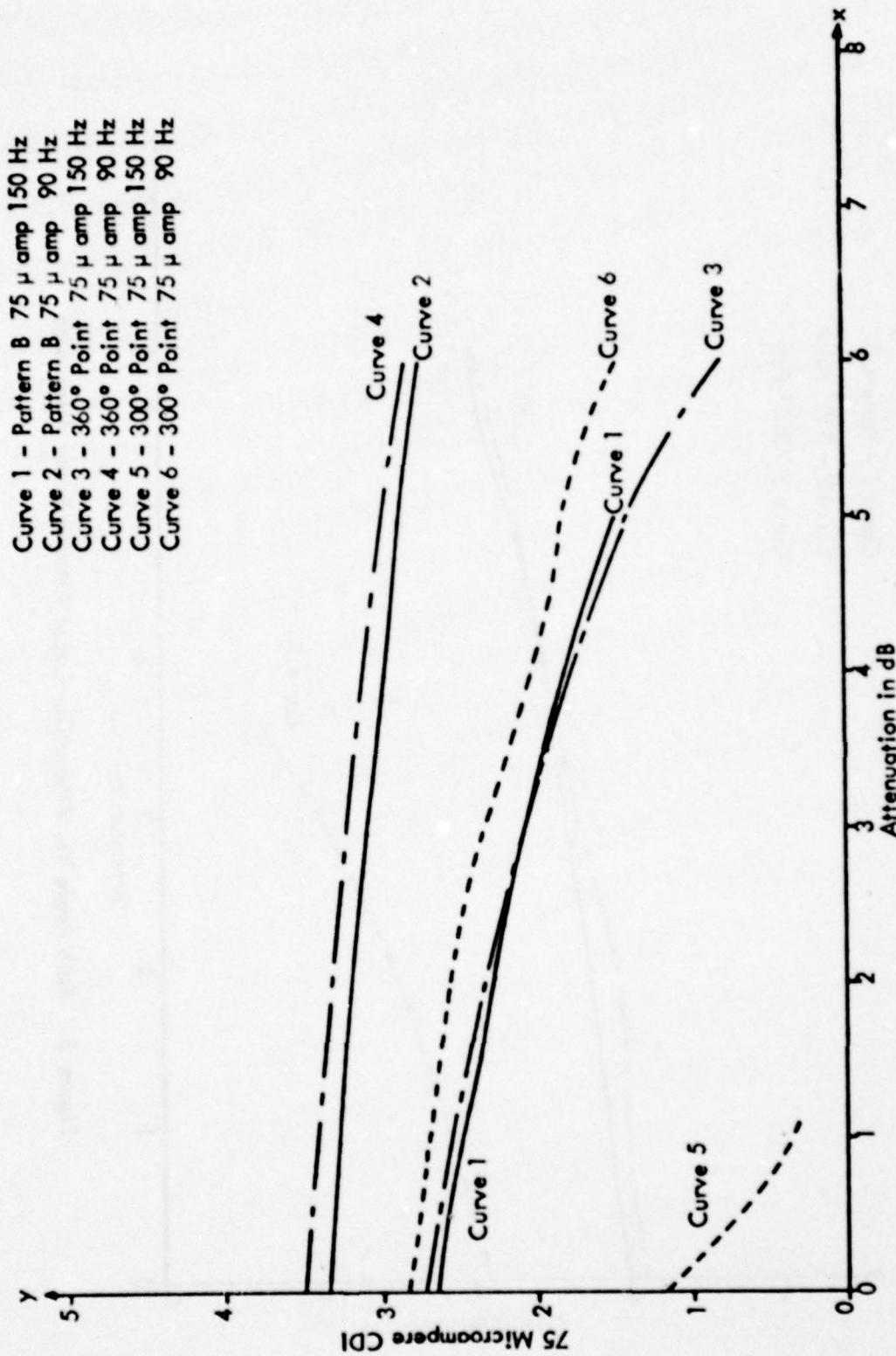
Figure 6.   75 Microampere CDI Loci Vs. Attenuation – Upper Antenna Power Attenuated.
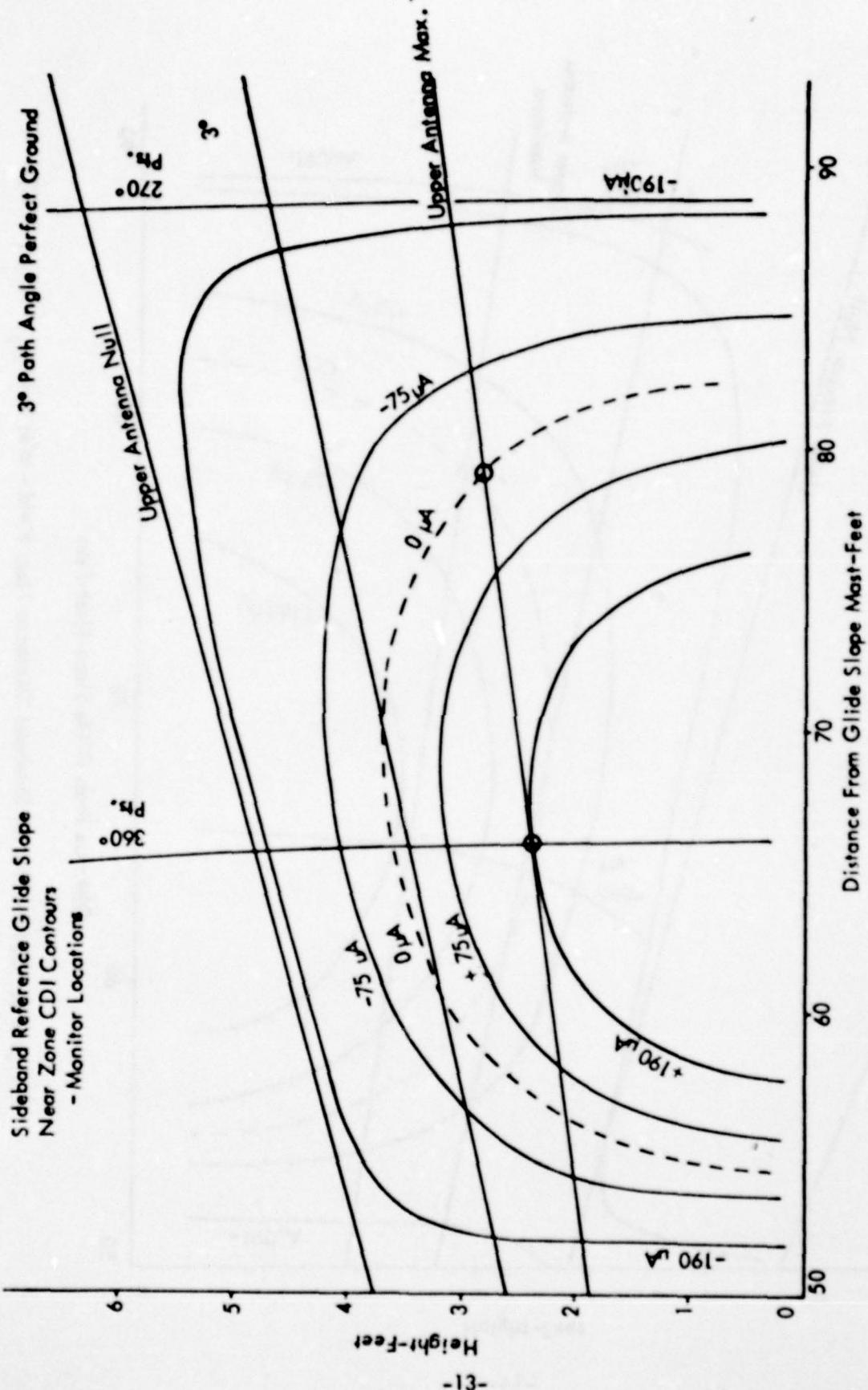
Figure 7. CDI Profiles for Sideband Reference Near Field – Perfect Ground.
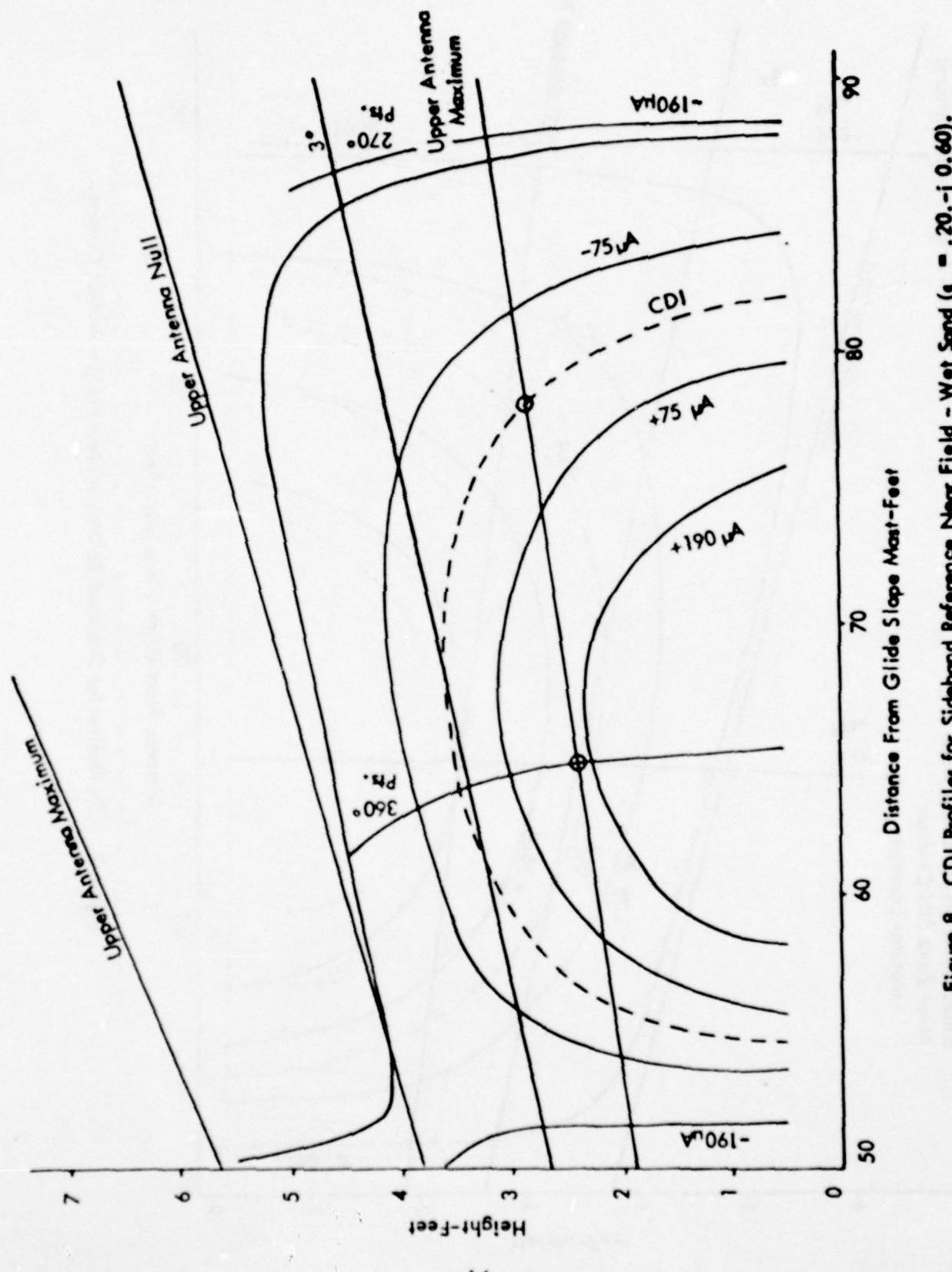
Figure 8. CDI Profiles for Sideband Reference Near Field – Wet Sand (ϵ_r = .20.–j 0.60).

-14-
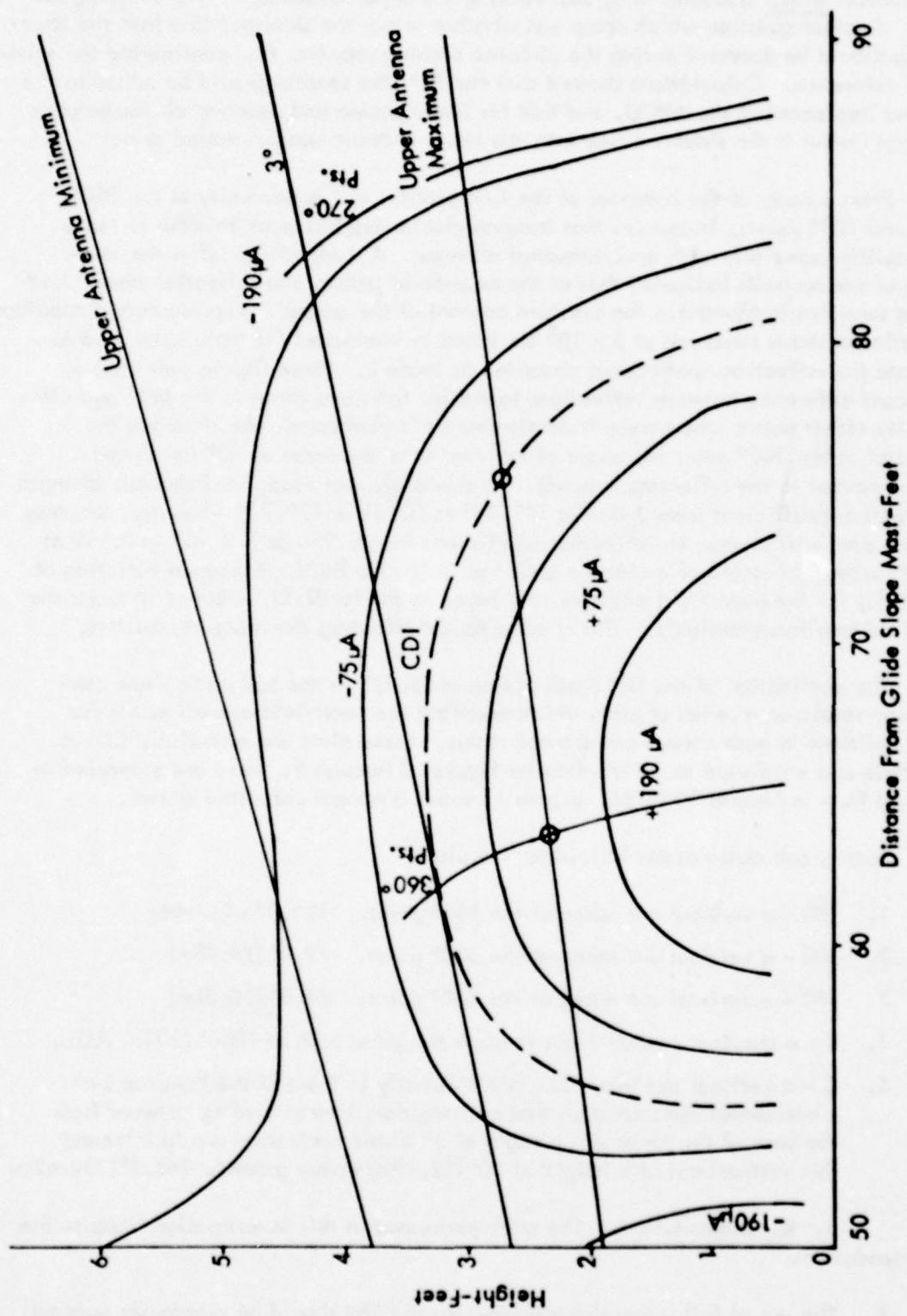
Figure 9. CDI Profiles for Sideband Reference Near Field - Dry Sand (e_r = 2.55 -j.0255).

here involves which sideband line, that feeding the upper antenna, or that entering the APCU. Another question which arose was whether or not the sideband line into the lower antenna should be dummied during the airborne phasing process, thus configuring the system as null reference. Calculations showed that the 90° line section should be added to the sideband line entering the APCU, and that for ideal ground and receiver characteristics it did not matter if the sideband line into the lower antenna were dummied or not.

From a study of the behavior of the CDI profiles in the proximity of the 360°, 300°, and 180° points, it appears that integral monitoring has much to offer in terms of reliability especially with environmental changes. A study of the reflection pro-perties of various soils indicated that at the near-field points, the reflection coefficient is quite sensitive to changes in the moisture content of the ground. Representative complex dielectric constants measured at 3×10^8 Hz listed in vonHippel [1] have been used to calculate the reflection coefficients compiled in Table 2. These figures point out a significant difference between reflections to the far field and those to the 360° and other proximity effect points where near-field monitoring is performed. At 3° above the horizontal at the 360° point the angle of incident is of the order of 70° (measured from the normal to the reflecting ground). At this angle wet sand, for instance, changes its reflection coefficient from 0.855 at 179.86° to 0.581 at 179.75° when dry, whereas the same sand will change its reflection coefficient from 0.976 at 179.98° to 0.919 at 179.97° where the angle of incidence is 87° as in the far field. The great variation of reflectivity for the near-field monitors, not found in the far field, is bound to make the near-field monitors unreliable. This is not a factor affecting the integral monitors.

The application of the flat earth option of OUGS to the SBR glide slope con-figuration results in a series of plots which describes the near field as well as the far field conditions in both normal and faulted status. These plots are essentially CDI vs. path angle and were used to derive data for Figures 4 through 9. They are presented in graphical form in Figures 10 to 54. Figure 10 shows a normal unfaulted system.

Each graph contains the following five plots:

1. 180 - a vertical cut taken at the 180° point. 134.0' (40.84m)

2. 300 - a vertical cut taken at the 300° point. 79.0' (24.08m)

3. 360 - a vertical cut taken at the 360° point. 65.8' (20.06m)

4. B - a standard pattern B cut through the glide path at 1000' (300m) AGL.

5. C - a vertical cut taken at a point directly in front of the tower and at a horizontal distance such that an imaginary line extending outward from the base of the tower at an angle of 3° above horizontal would intersect this vertical cut at a height of 40' (12.19m) above ground. 763.2' (232.62m)

5. Recommendations. The work performed in this investigation leads to the recommendations:

1. The use of full integral monitoring for the SBR should be vigorously pursued.

θ	SAND				LOAM				CLAY			
	Dry		Wet		Dry		Wet		Dry		Wet	
	ρ	Φ	ρ	Φ	ρ	Φ	ρ	Φ	ρ	Φ	ρ	Φ
45	0.339	179.54	0.724	179.71	0.330	179.69	0.726	178.48	0.320	178.98	0.746	175.73
50	0.371	179.57	0.745	179.74	0.362	179.71	0.748	178.62	0.351	179.05	0.766	176.11
60	0.457	179.65	0.795	179.79	0.448	179.76	0.797	178.92	0.437	179.23	0.8l2	176.97
70	0.581	179.75	0.855	179.86	0.573	179.83	0.856	179.26	0.563	179.45	0.867	179.45
80	0.757	179.87	0.923	179.93	0.752	179.91	0.924	179.62	0.745	179.71	0.930	178.94
82	0.800	179.90	0.938	179.94	0.795	179.93	0.939	179.70	0.790	179.77	0.944	179.15
84	0.846	179.92	0.953	179.96	0.842	179.95	0.954	179.77	0.837	179.82	0.957	179.36
86	0.894	179.95	0.969	179.97	0.891	179.96	0.969	179.85	0.888	179.88	0.971	179.57
88	0.945	179.97	0.984	179.99	0.944	179.98	0.984	179.92	0.942	179.94	0.986	179.79
90	1.000	180.00	1.000	180.00	1.000	180.00	1.000	180.00	1.000	180.00	1.000	180.00

Dry Sand $2.55-j0.0255$
Wet Sand $20. \quad -j0.6$
Dry Loam $2.47-j0.0161$
Wet Loam $20. \quad -j3.2$
Dry Clay $2.38-j0.0476$
Wet Clay $20. \quad -j10.4$

Table 2. Complex Reflection Coefficient (Polar) for Various Angles of Incidence (Measured from the Normal to the Reflecting Plane) for Typical Soils.
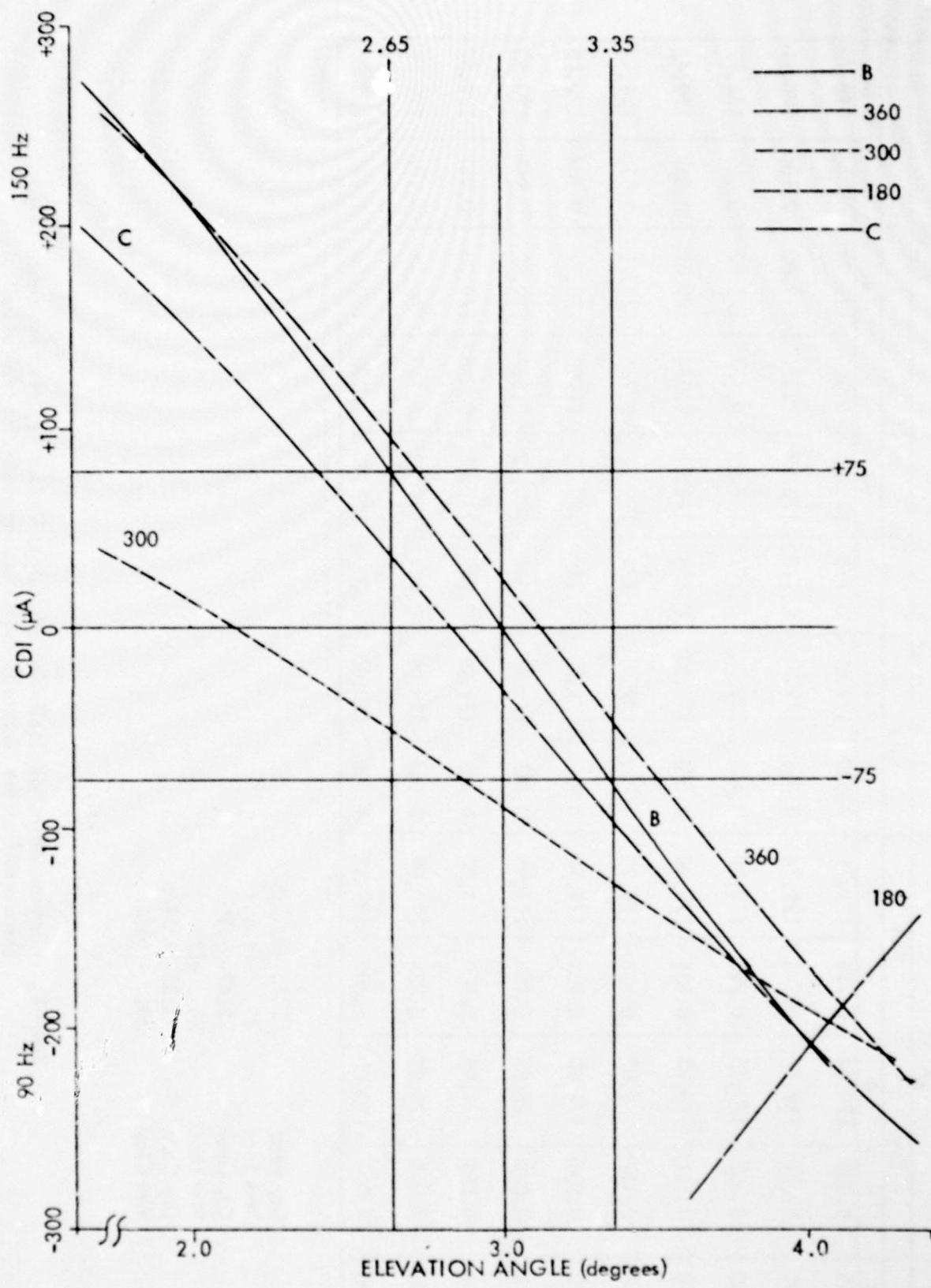
Figure 10.   CDI vs. Angle – Normal Sideband Reference.

-18-
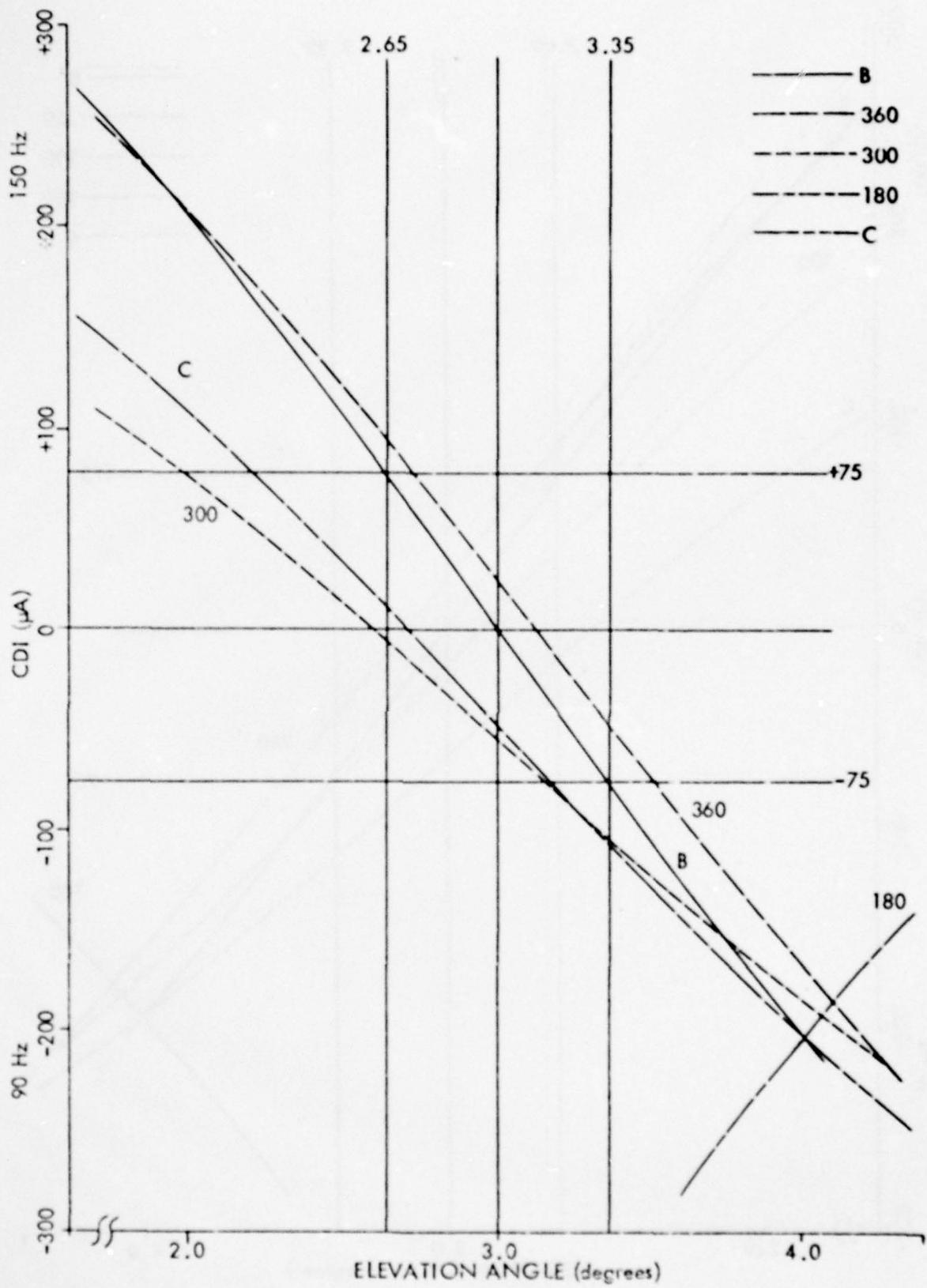
Figure 11. CDI vs. Angle - CSB Advanced 10°.

-19-
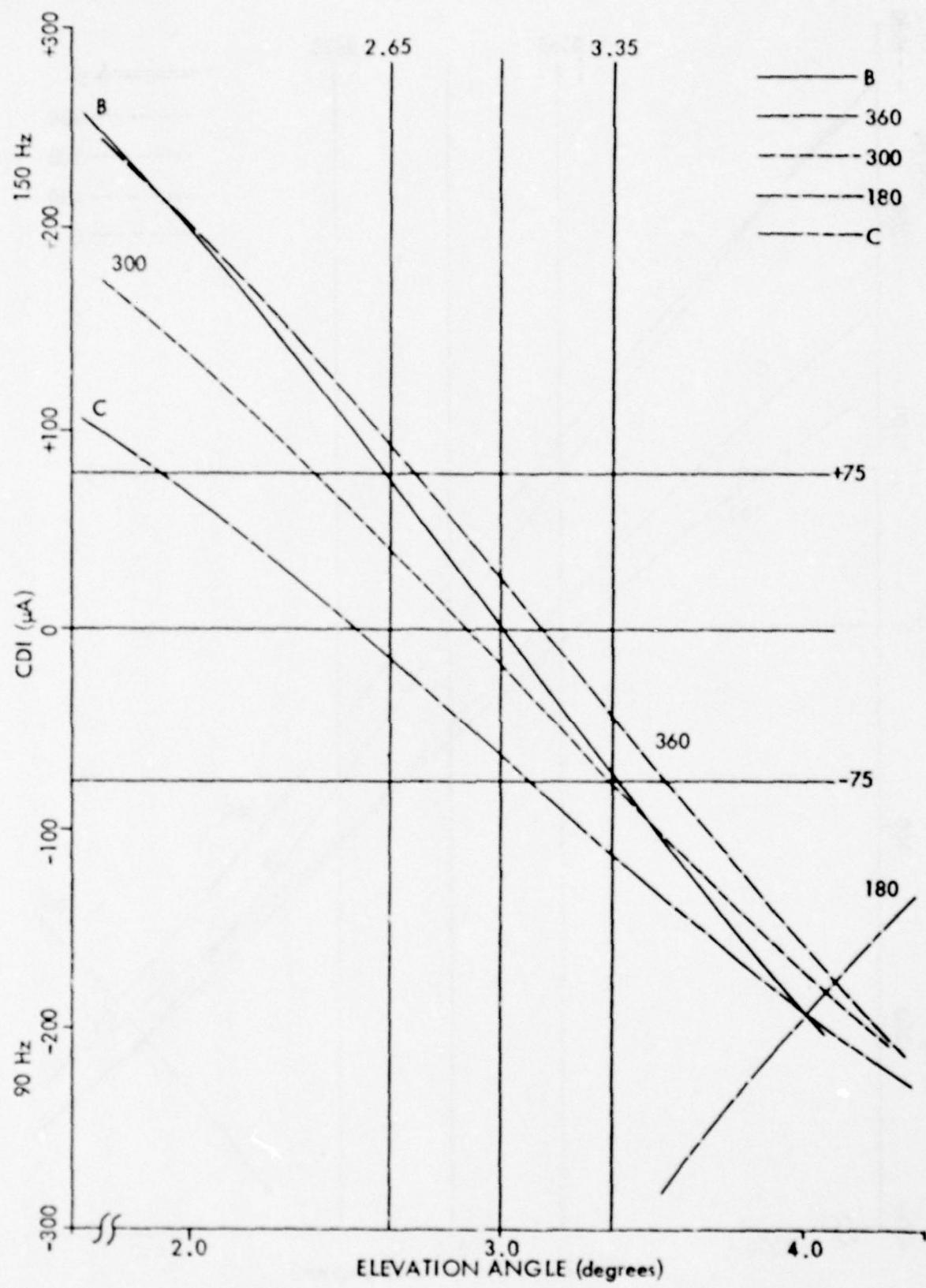
Figure 12. CDI vs. Angle - CSB Advanced 20°.

-20-
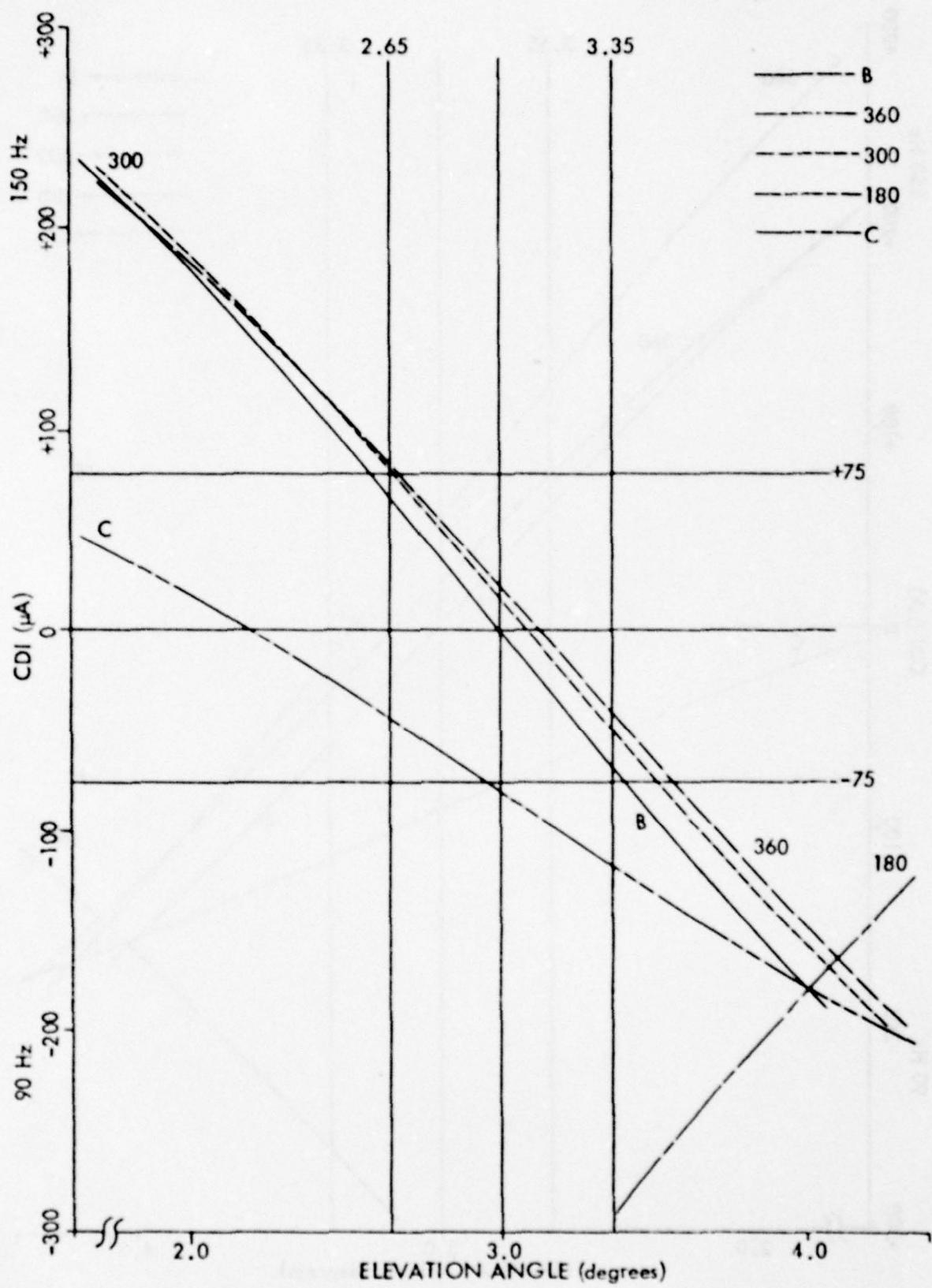
Figure 13. CDI vs. Angle - CSB Advanced 30°.
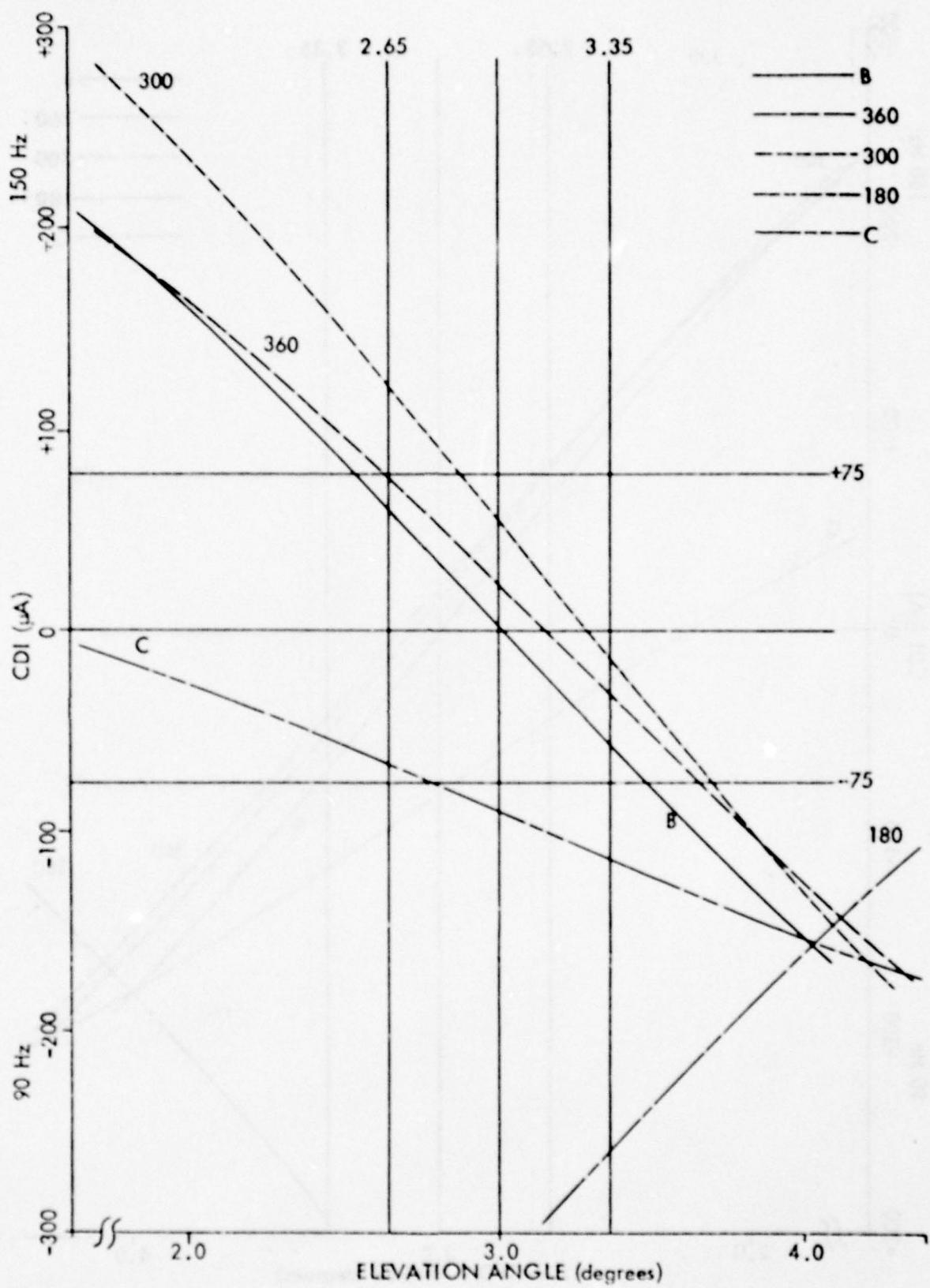
Figure 14.   CDI vs. Angle – CSB Advanced 40°.

-22-
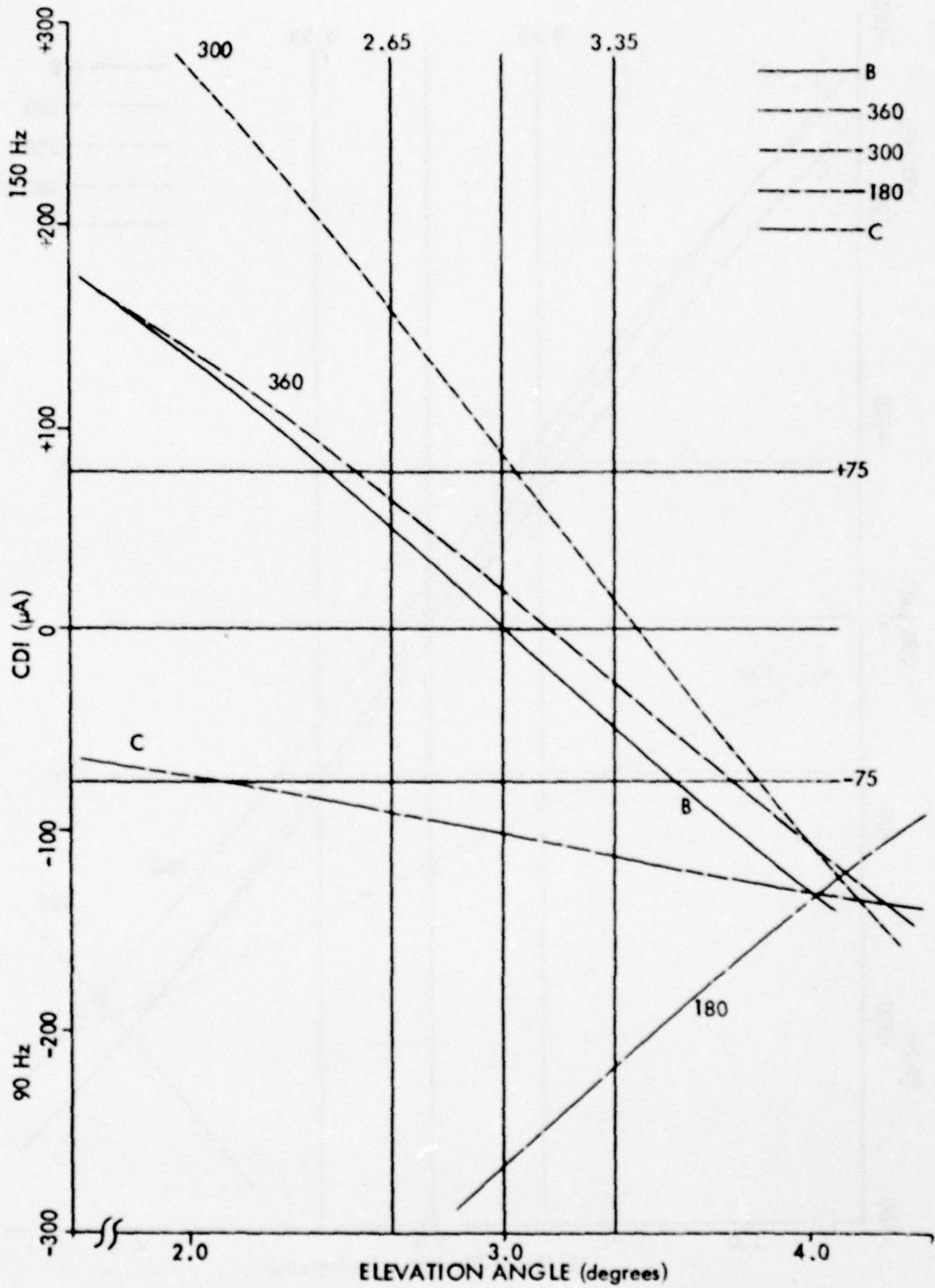
Figure 15. CDI vs. Angle – CSB Advanced 50°.
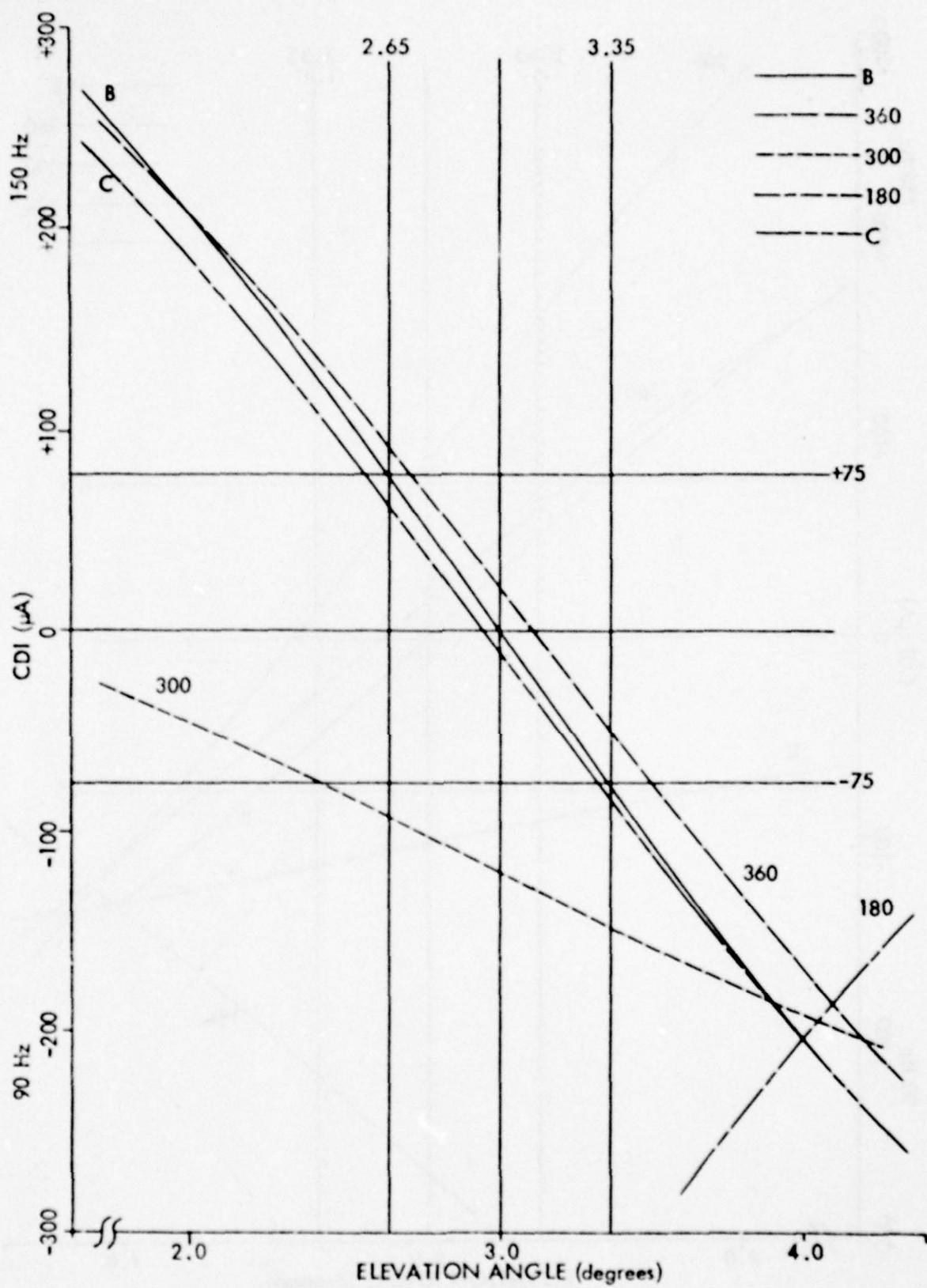
Figure 16. CDI vs. Angle – CSB Retarded 10°.
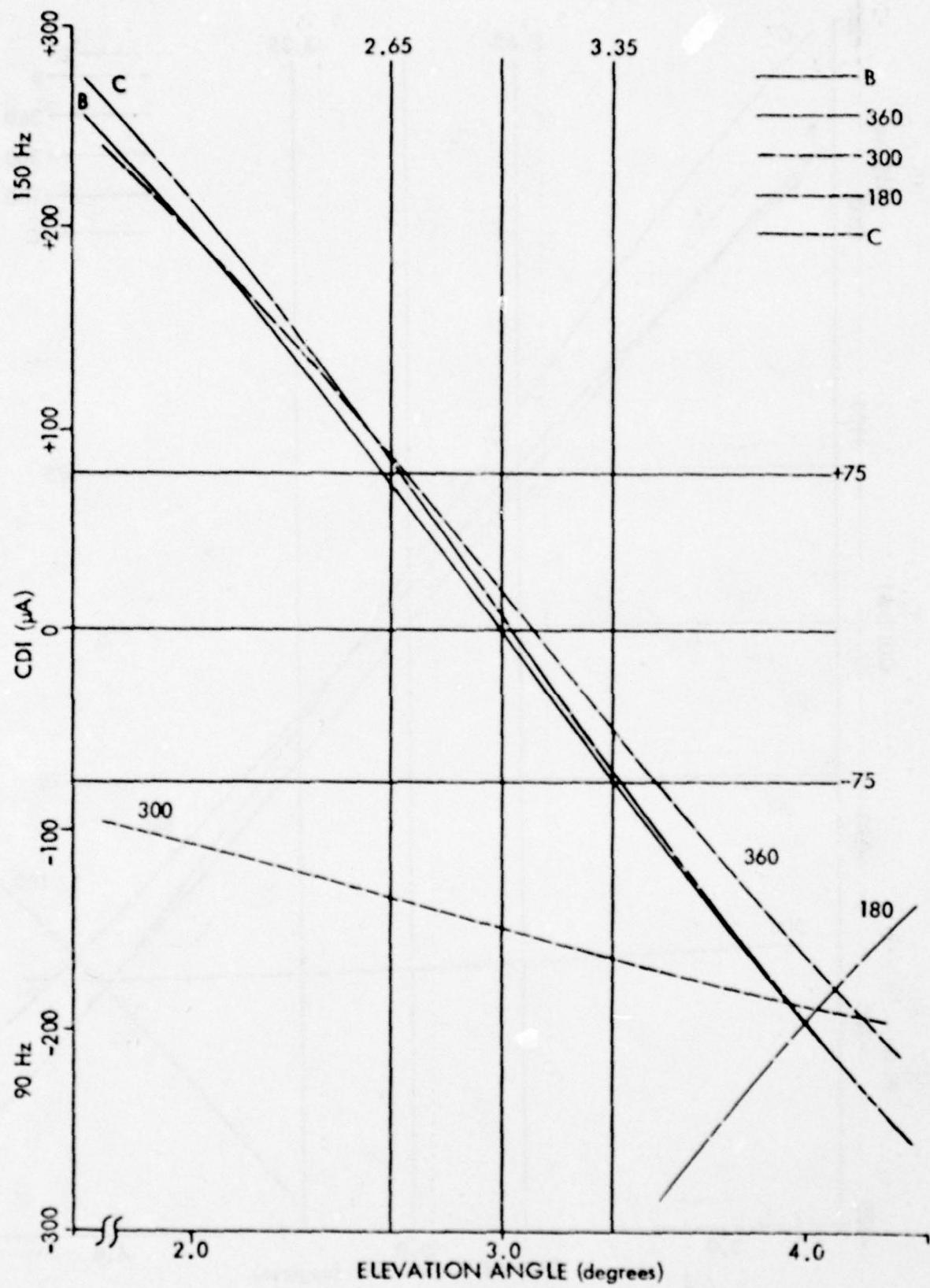
Figure 17. CDI vs. Angle – CSB Retarded 20°.
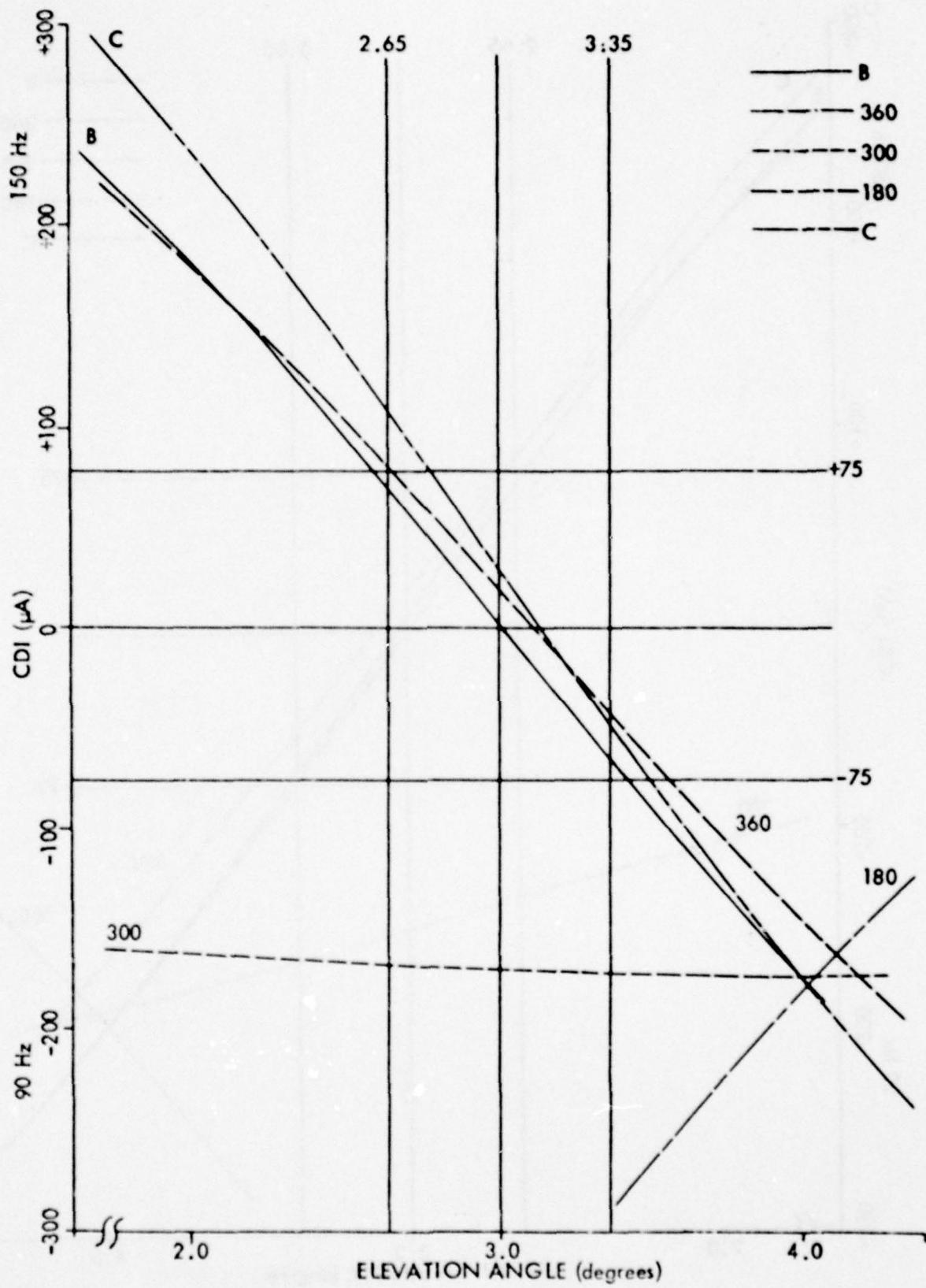
Figure 18. CDI vs. Angle – CSB Retarded 30°.
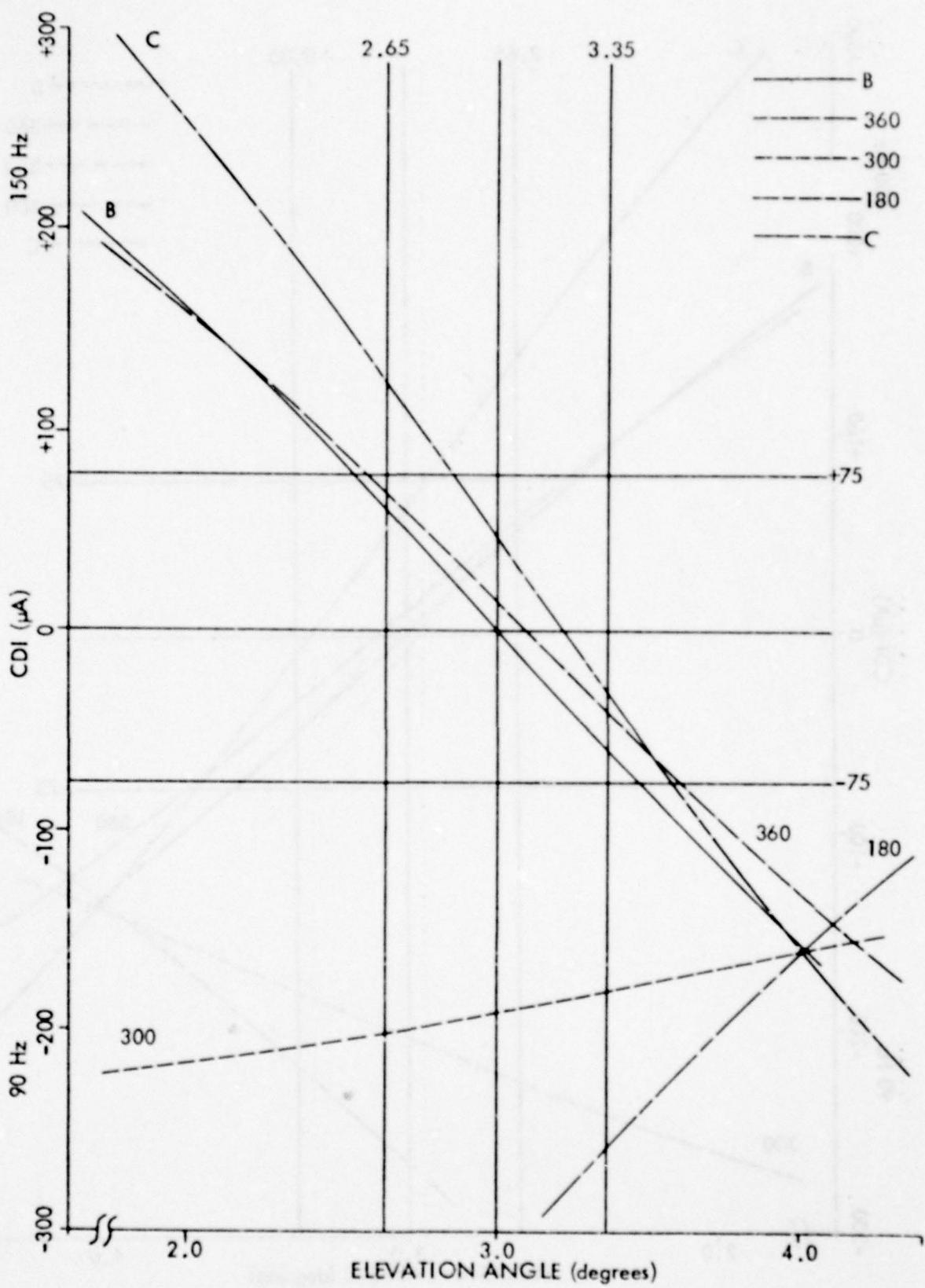
Figure 19.   CDI vs. Angle — CSB Retarded 40°.
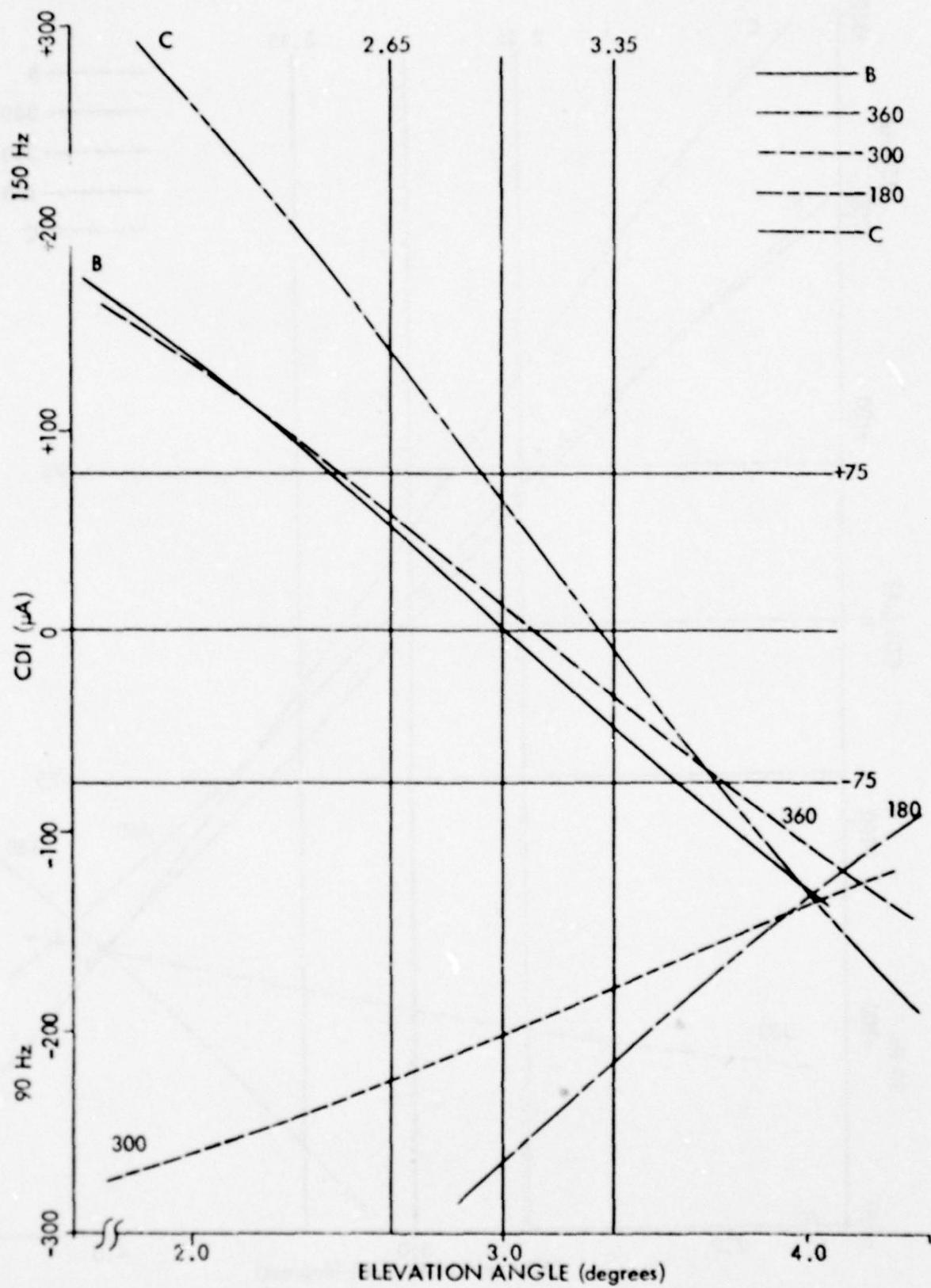
Figure 20. CDI vs. Angle – CSB Retarded 50°.
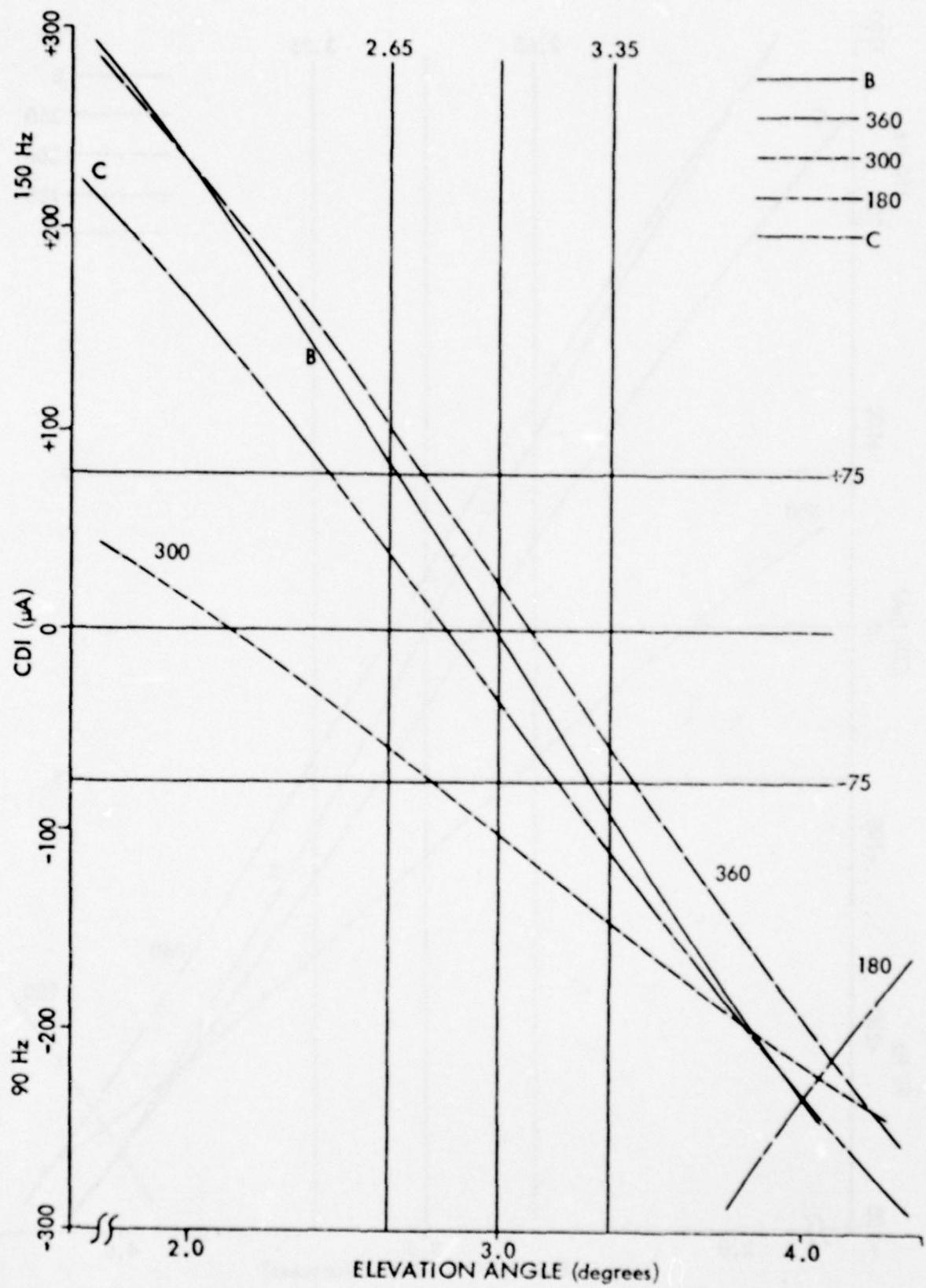
Figure 21. CDI vs. Angle – CSB Attenuated 1 dB.

-29-
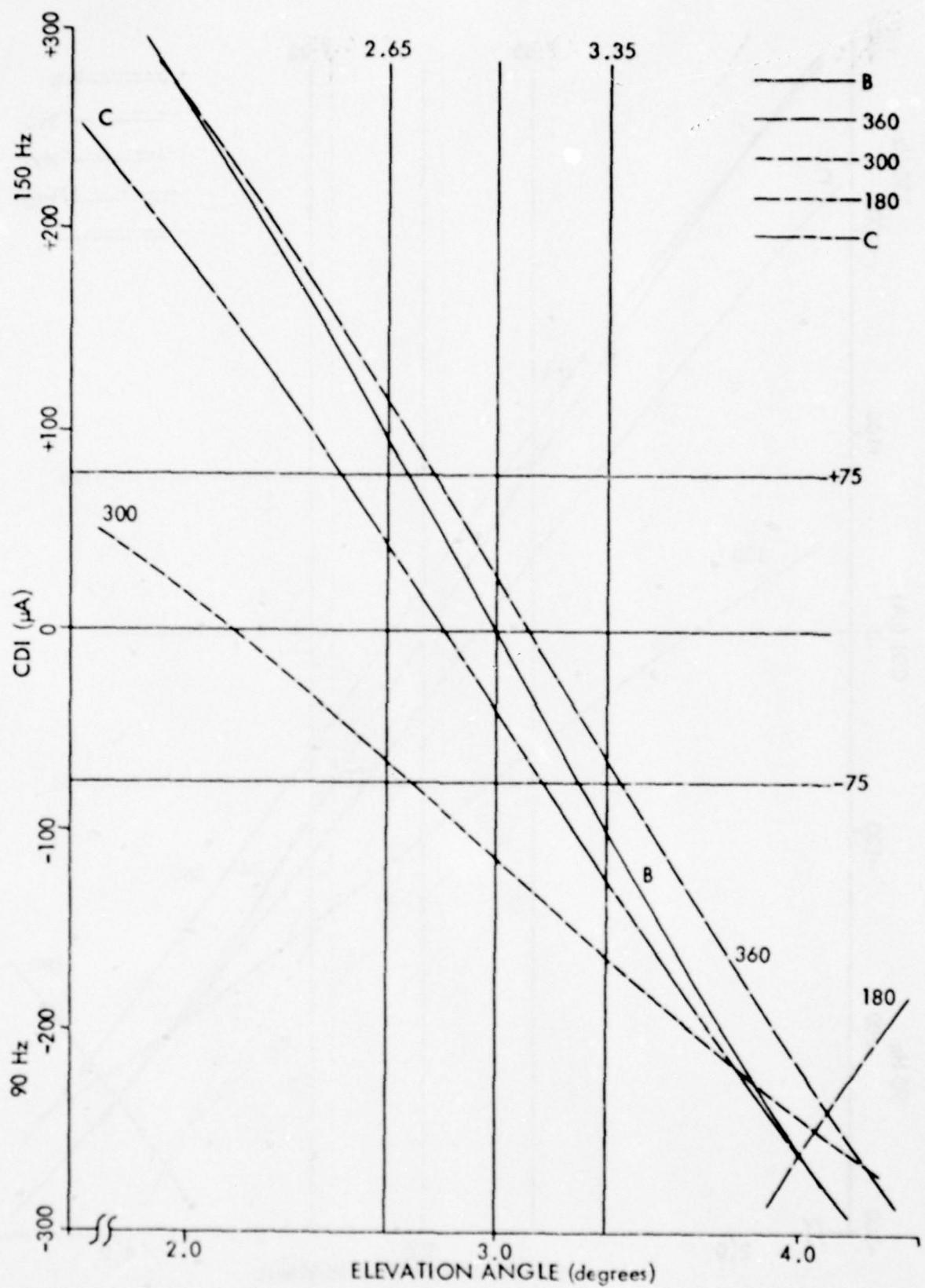
Figure 22.   CDI vs. Angle – CSB Attenuated 2 dB.
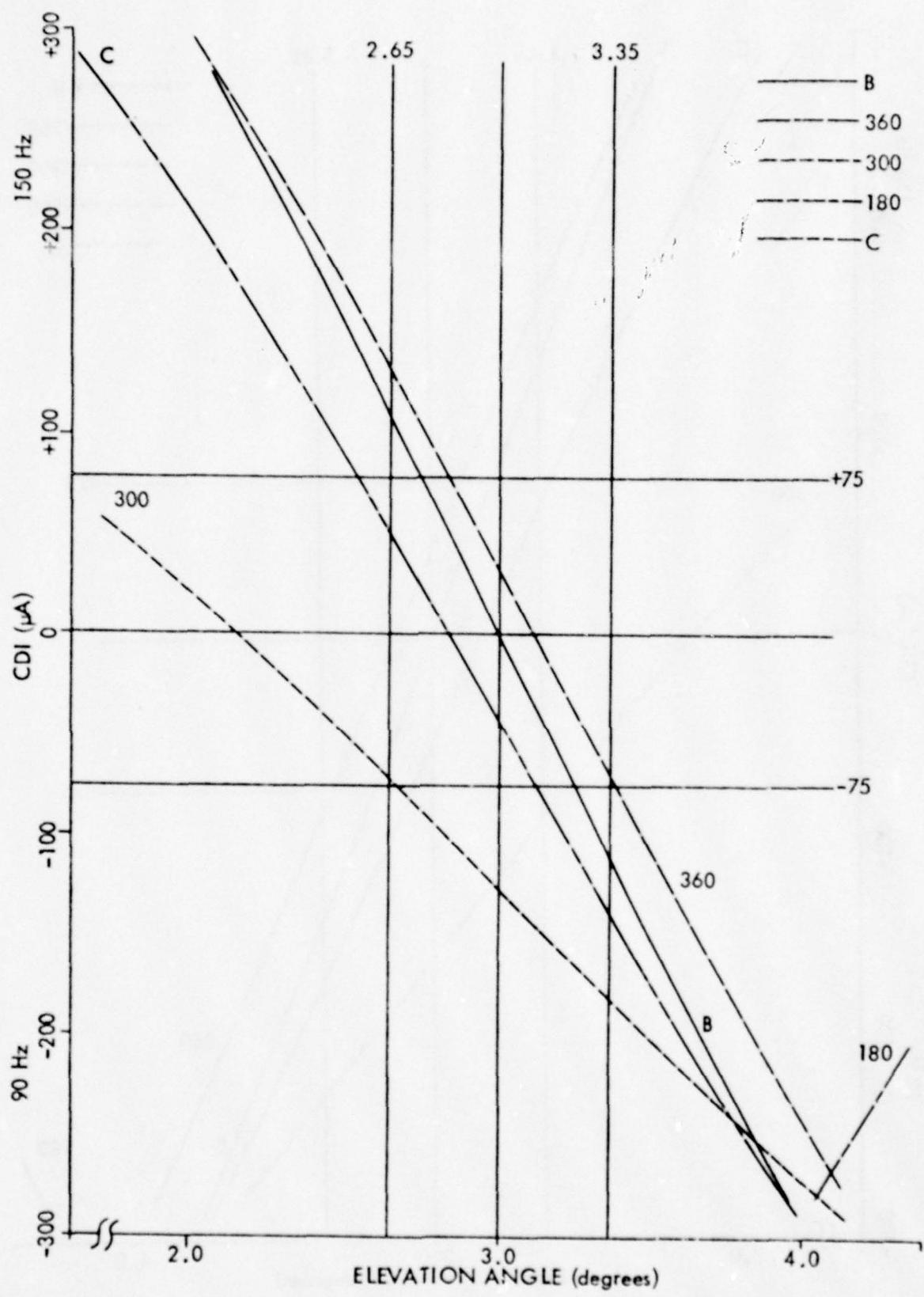
Figure 23. CDI vs. Angle – CSB Attenuated 3 dB.
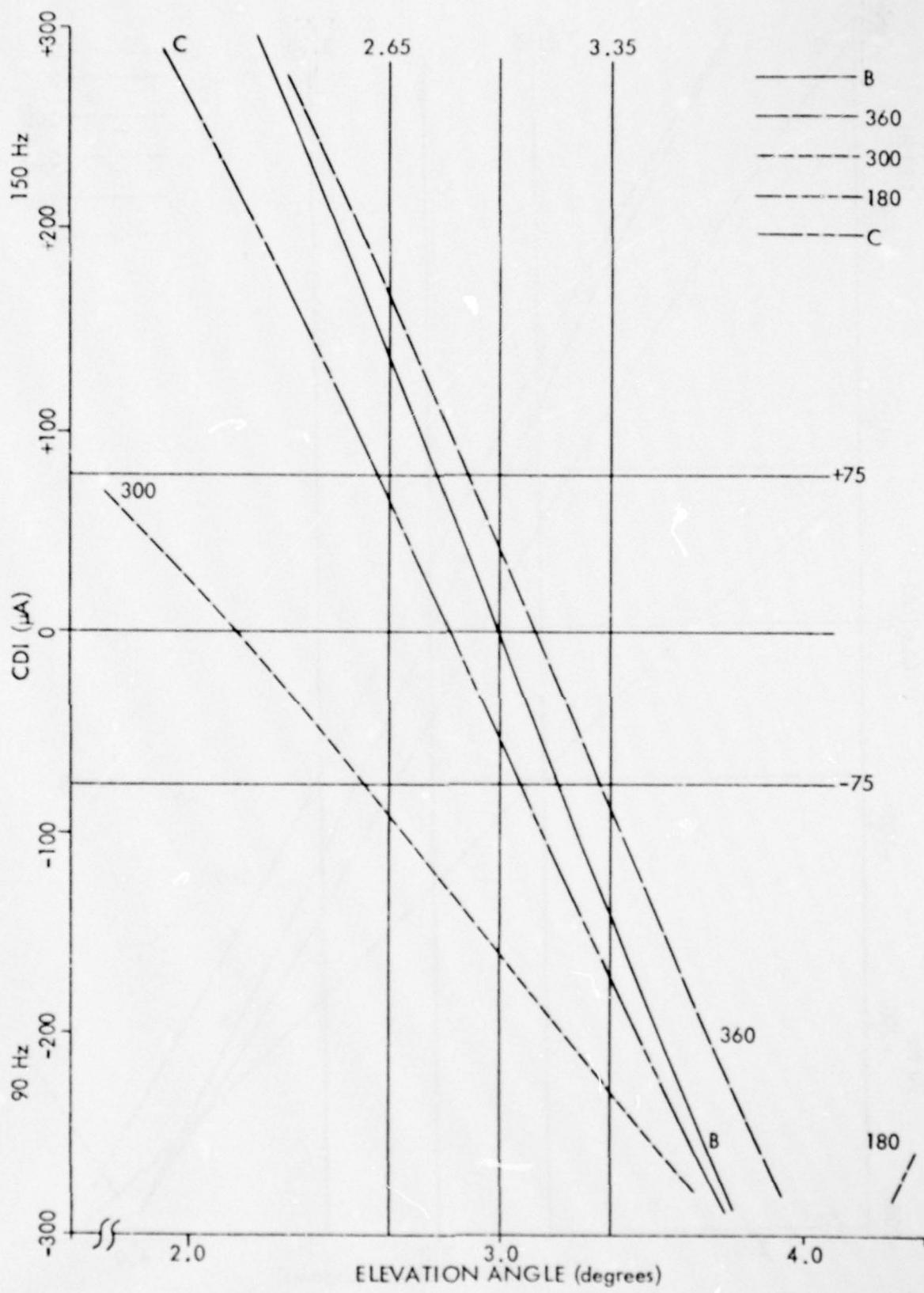
Figure 24. CDI vs. Angle – CSB Attenuated 5 dB.
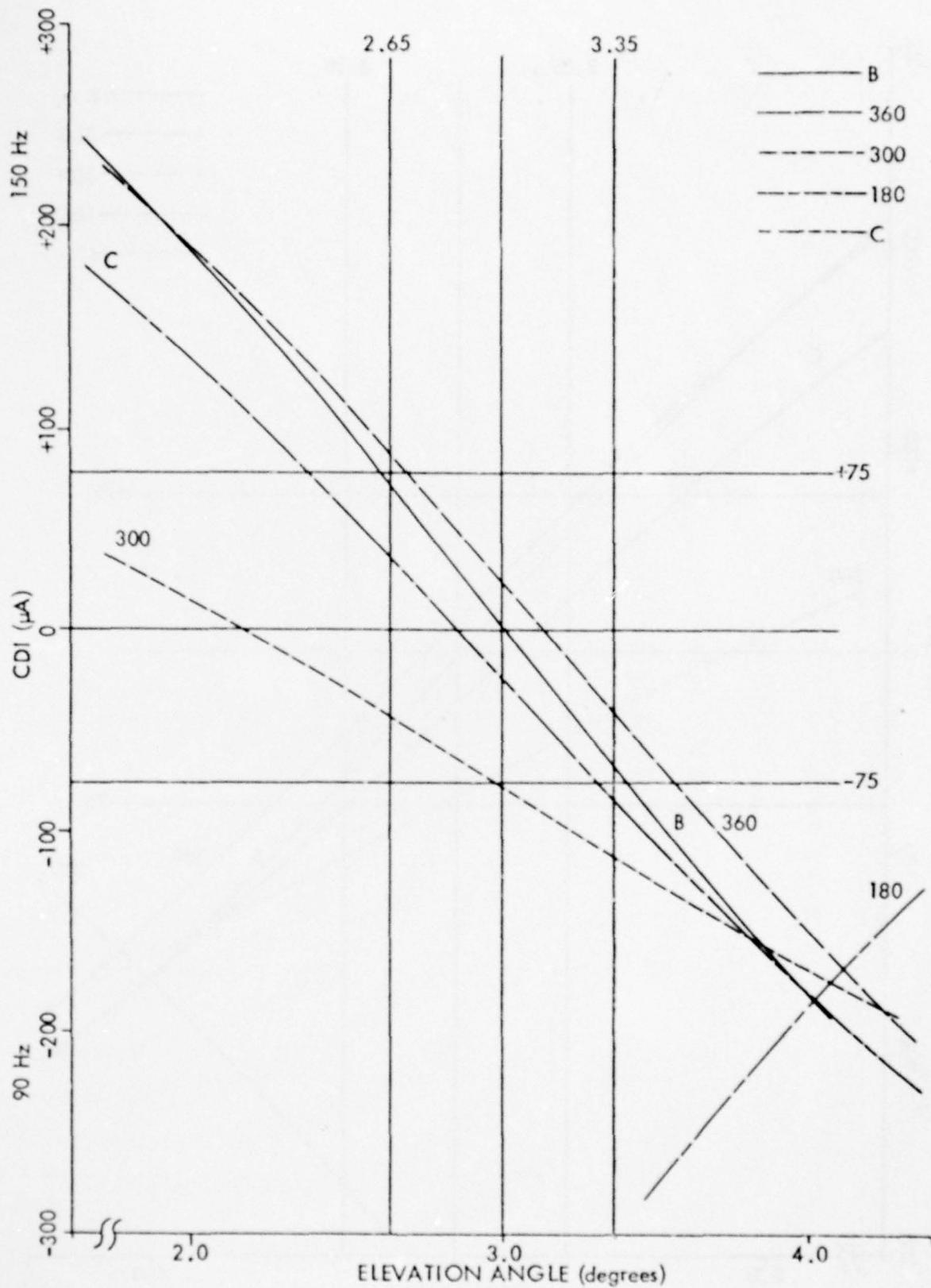
Figure 25. CDI vs. Angle – SBO Attenuated 1 dB.
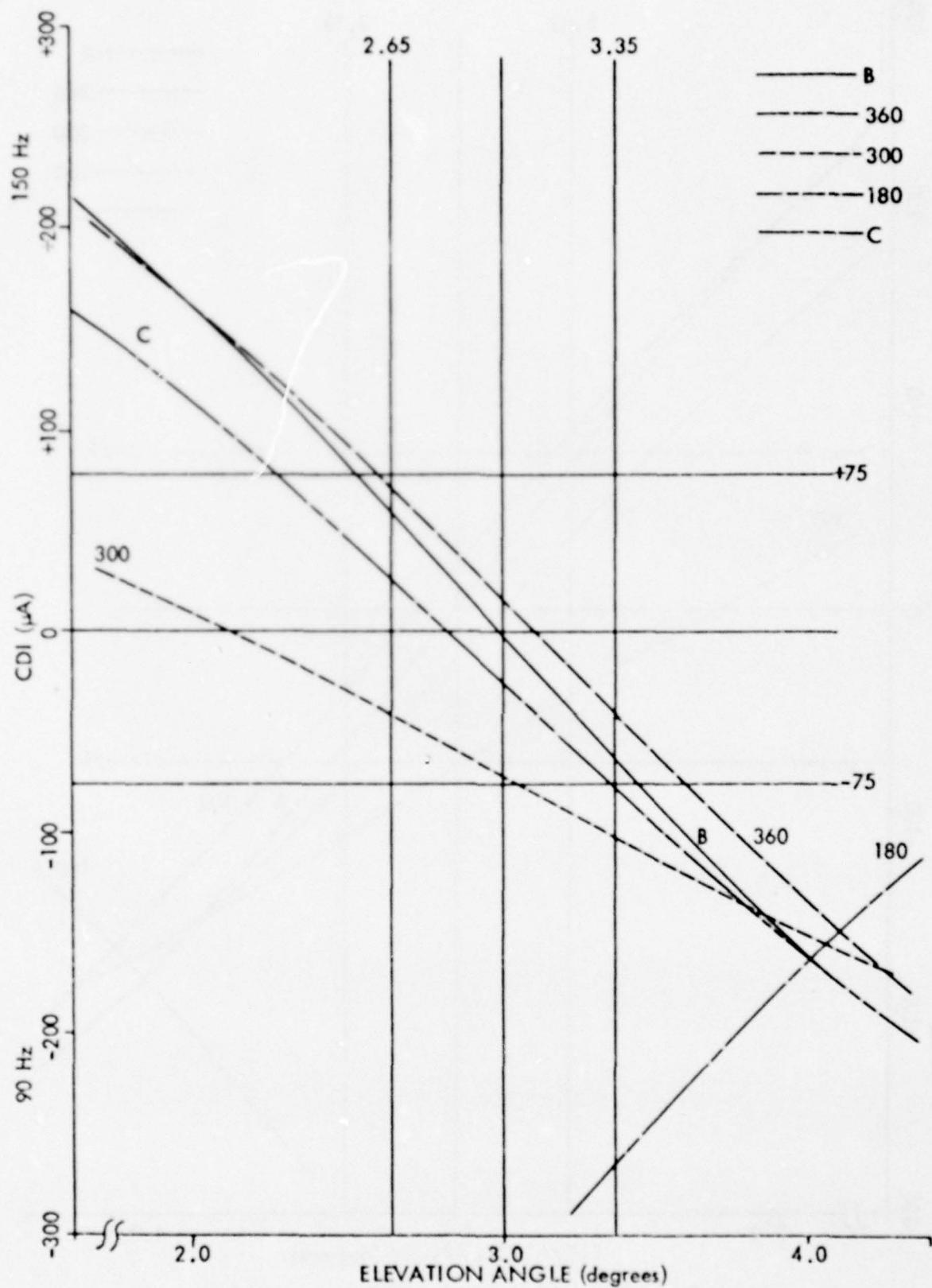
Figure 26. CDI vs. Angle – SBO Attenuated 2 dB.

-34-
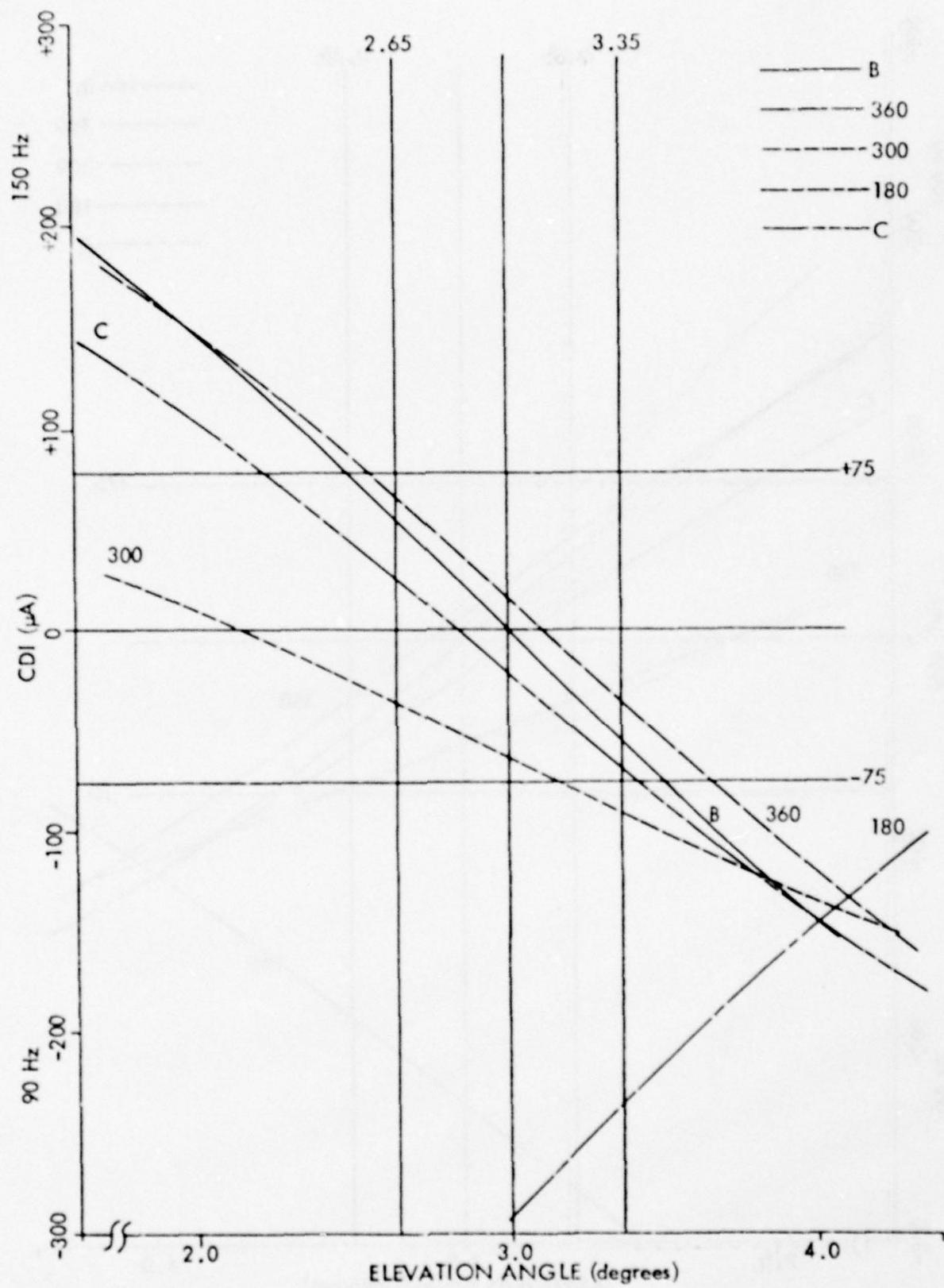
Figure 27. CDI vs. Angle – SBO Attenuated 3 dB.
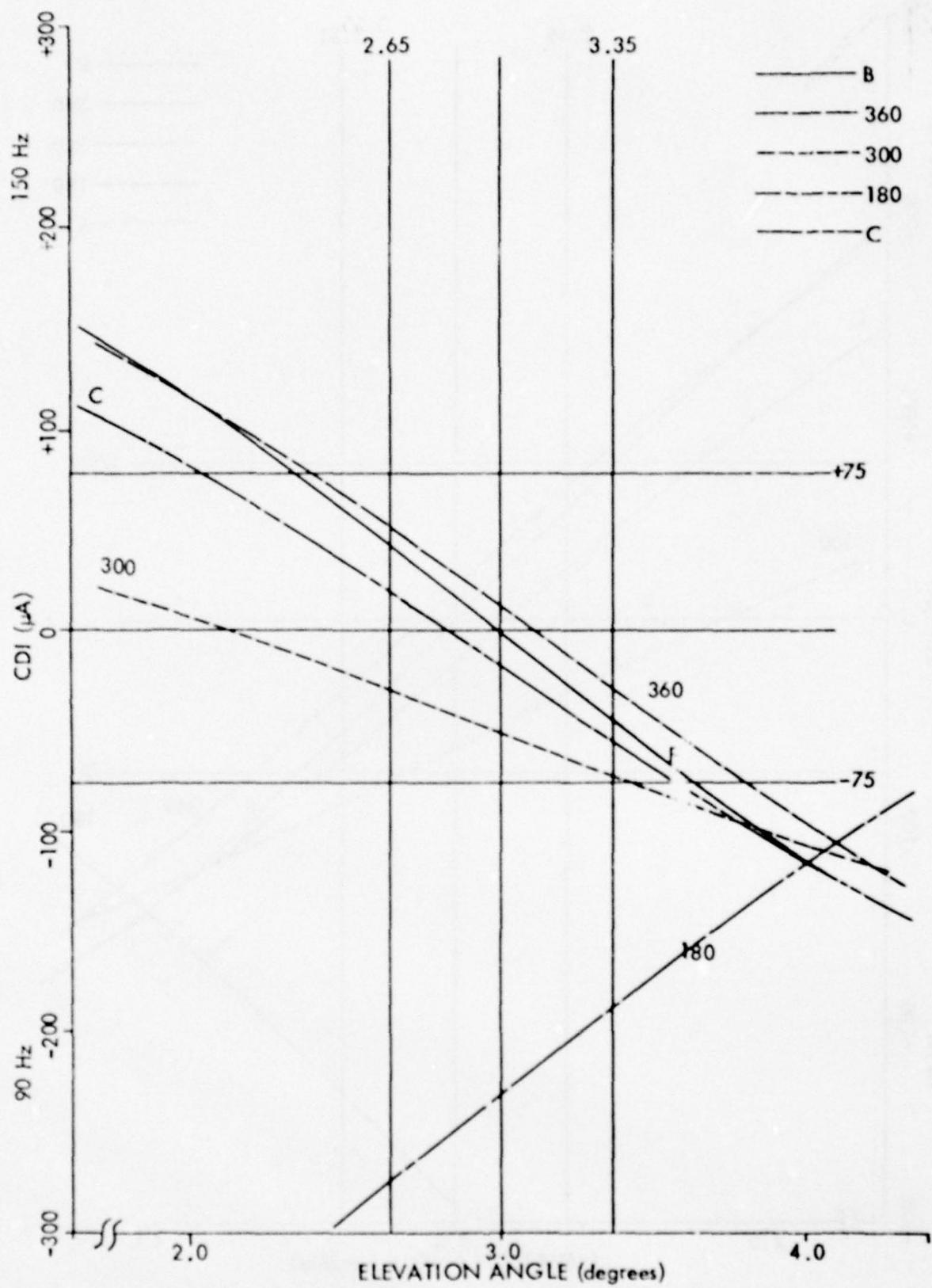
Figure 28. CDI vs. Angle – SBO Attenuated 5 dB.
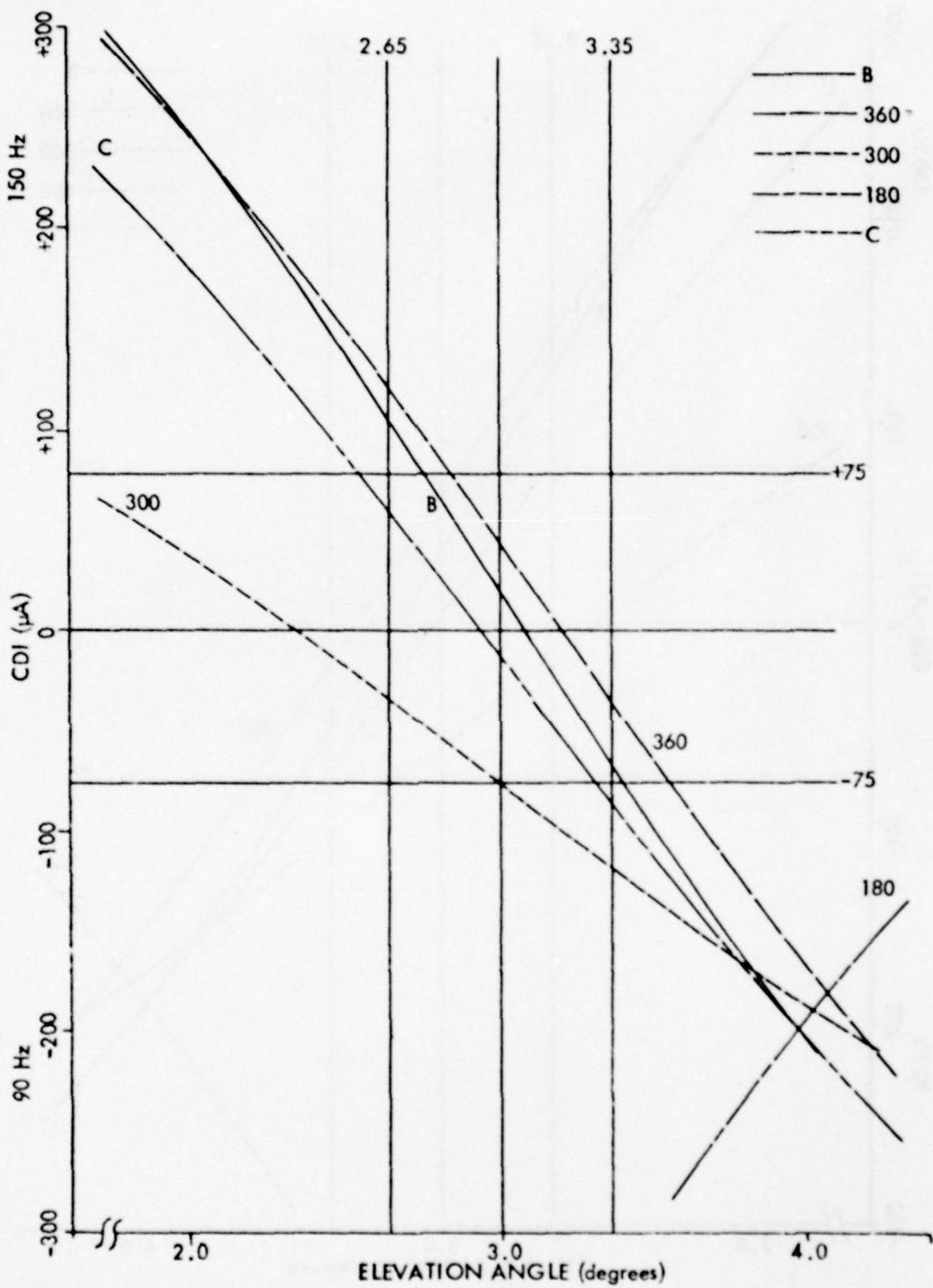
Figure 29. CDI vs. Angle – SBO Power Division: Lower Antenna –0.5 dB, Upper Antenna +0.448 dB.
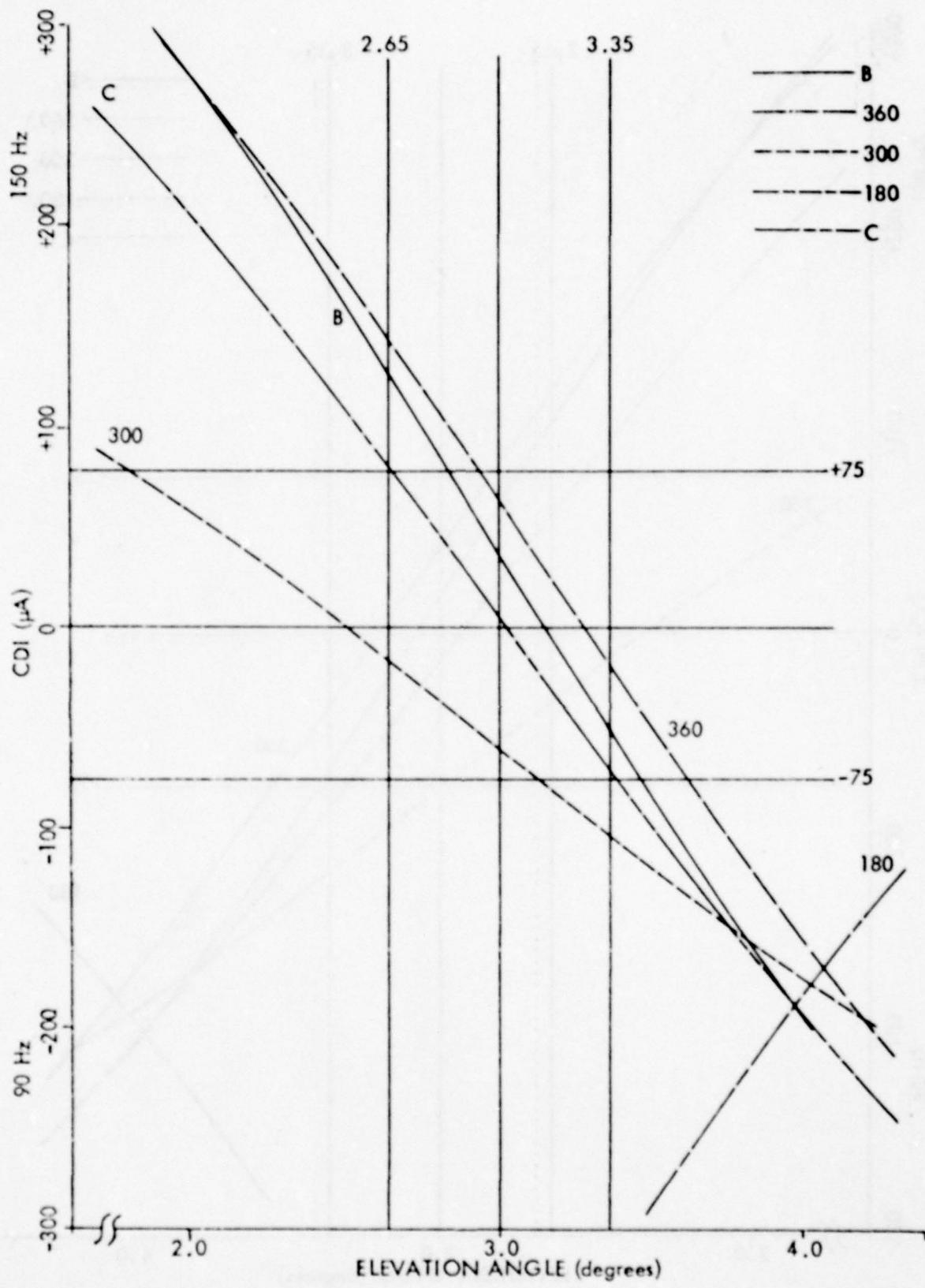
Figure 30.   CDI vs. Angle – SBO Power Division: Lower Antenna –1.0 dB,
Upper Antenna +0.812 dB.

-38-
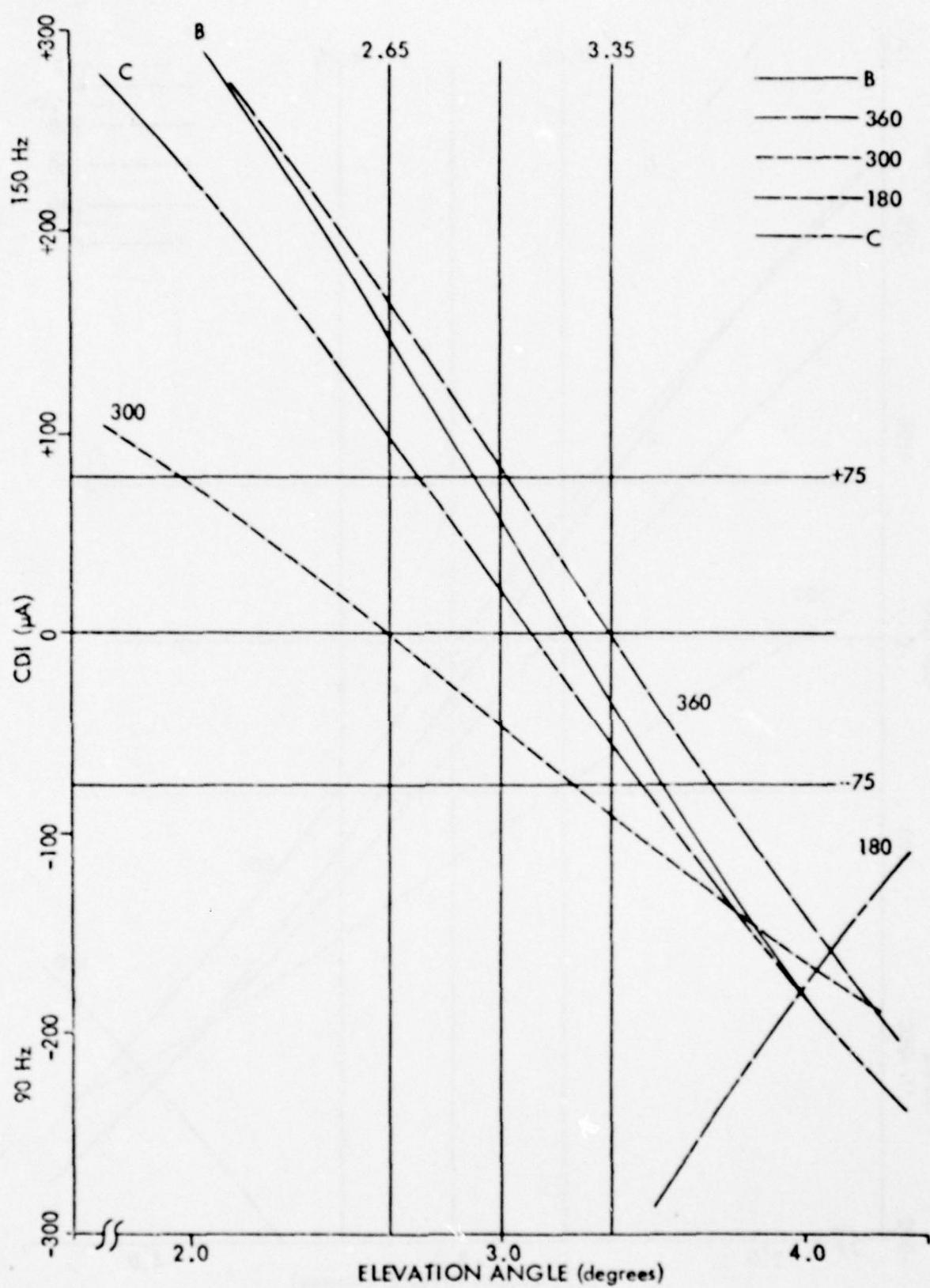
Figure 31.   CDI vs. Angle – SBO Power Division: Lower Antenna –1.5 dB, Upper Antenna +1.113 dB.
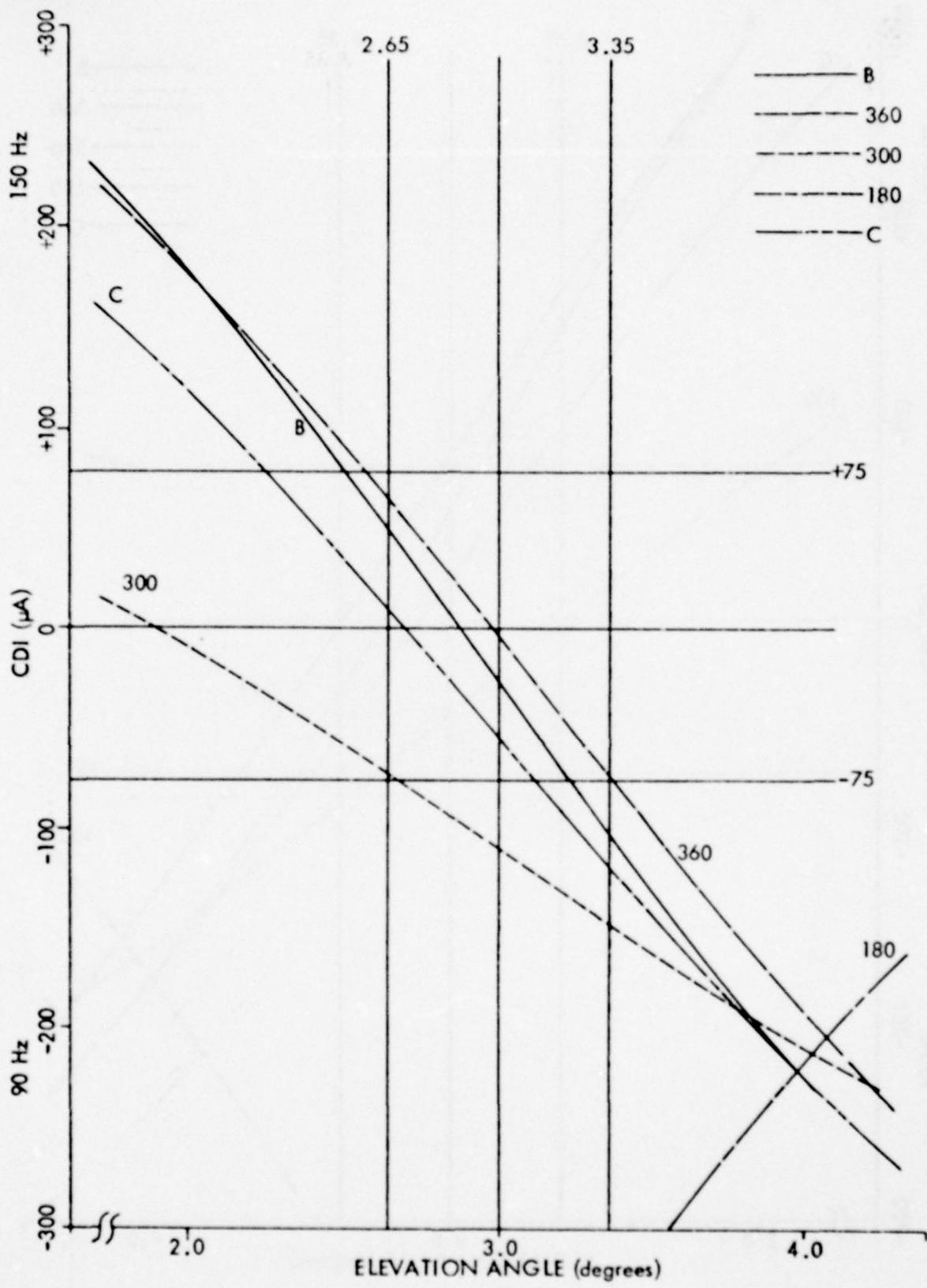
Figure 32. CDI vs. Angle – SBO Power Division: Upper Antenna –0.5 dB, Lower Antenna +0.448 dB.

-40-
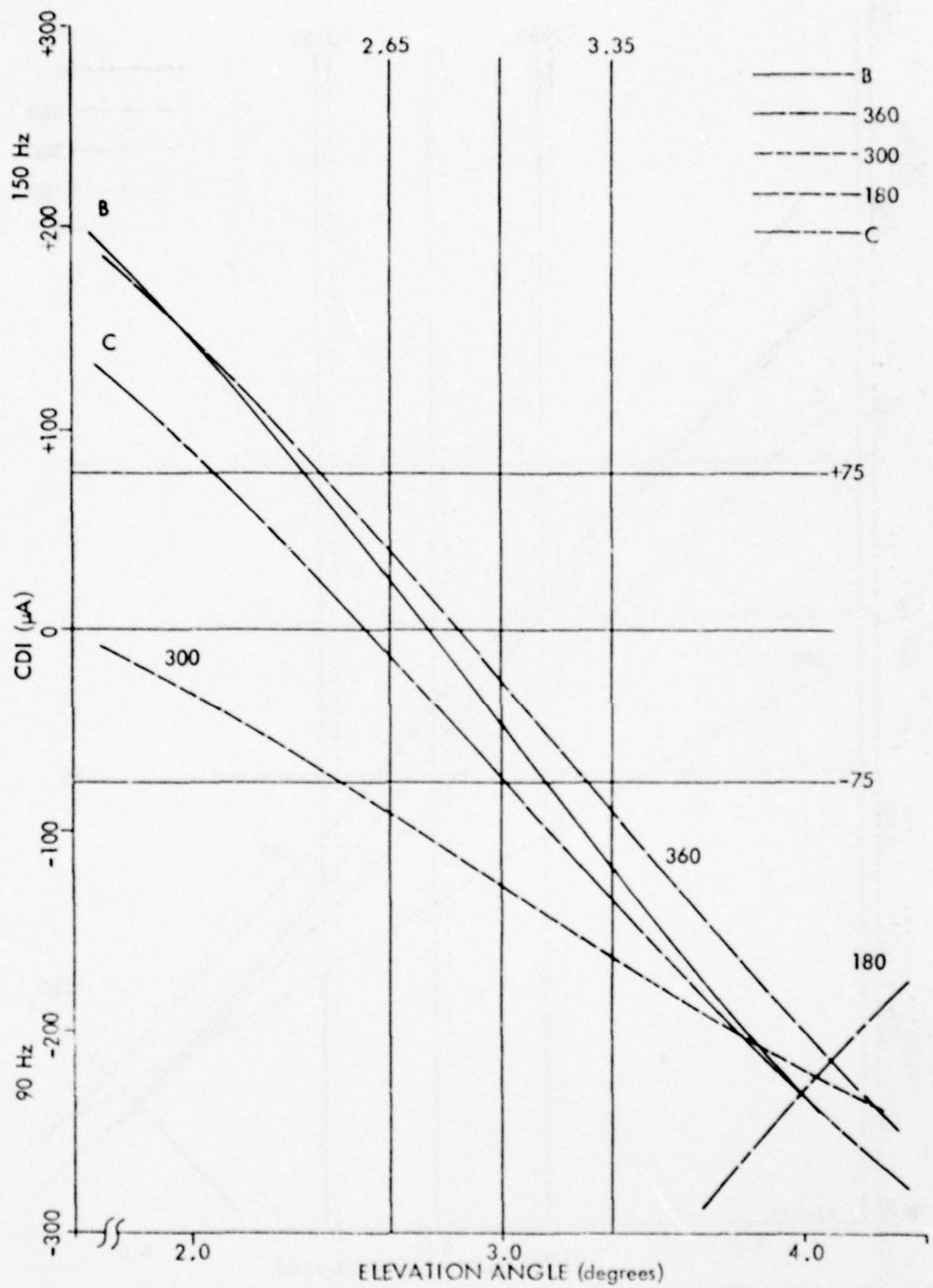
Figure 33. CDI vs. Angle – SBO Power Division: Upper Antenna –1.0 dB, Lower Antenna +0.812 dB.

-41-
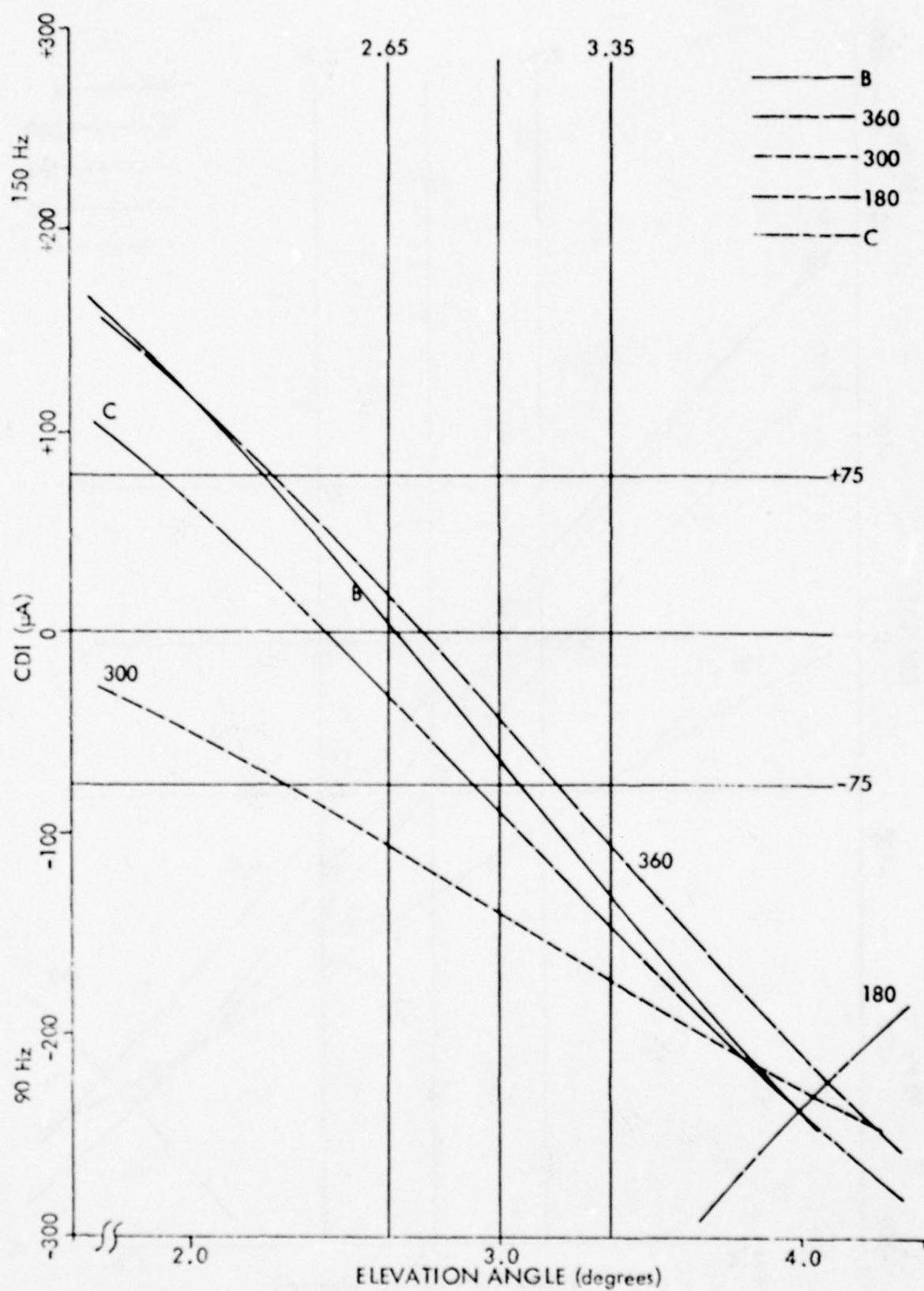
Figure 34. CDI vs. Angle – SBO Power Division: Upper Antenna –1.5 dB, Lower Antenna +1.113 dB.
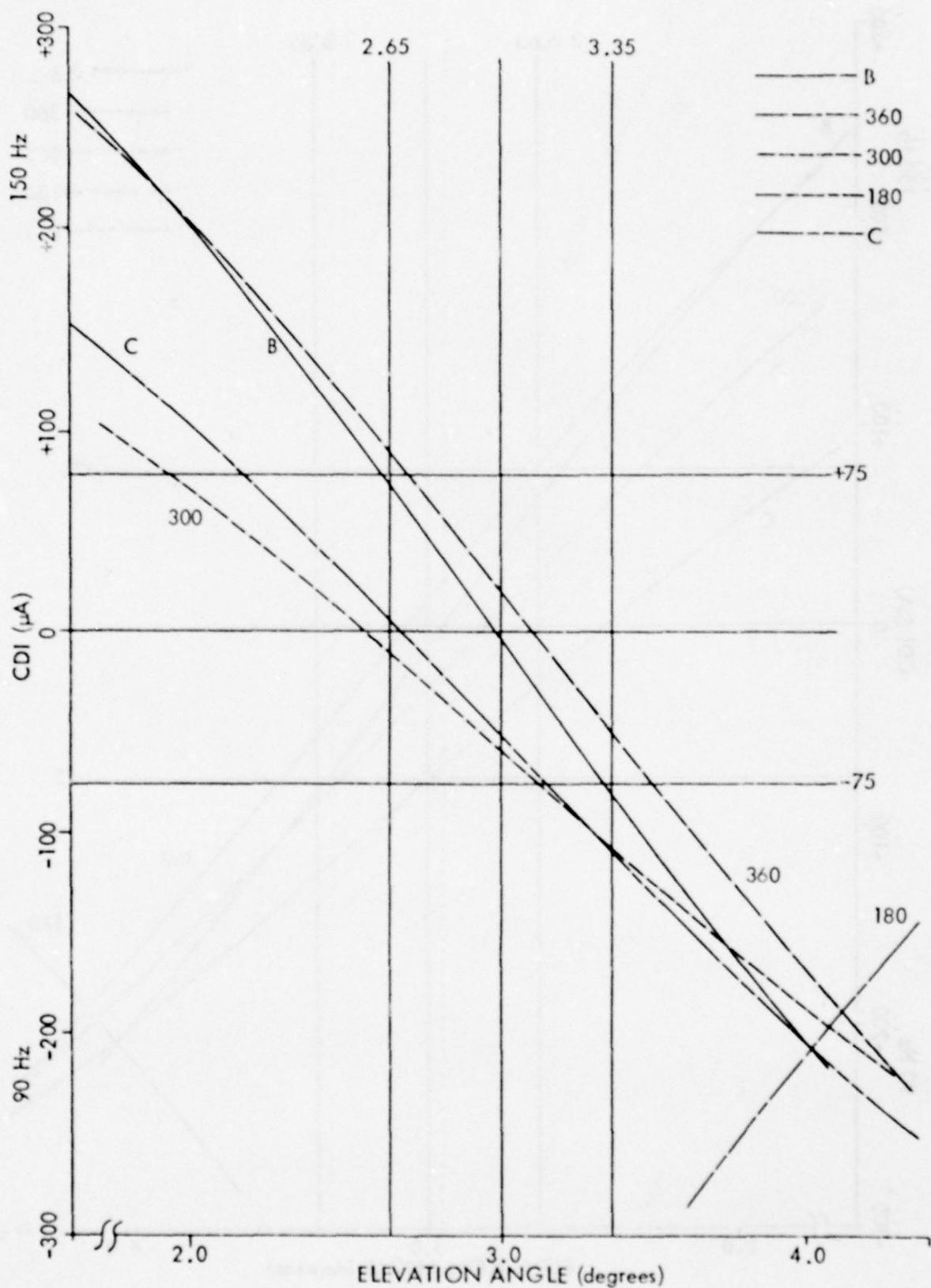
Figure 35. CDI vs. Angle — Lower Antenna Advanced 10°.

-43-
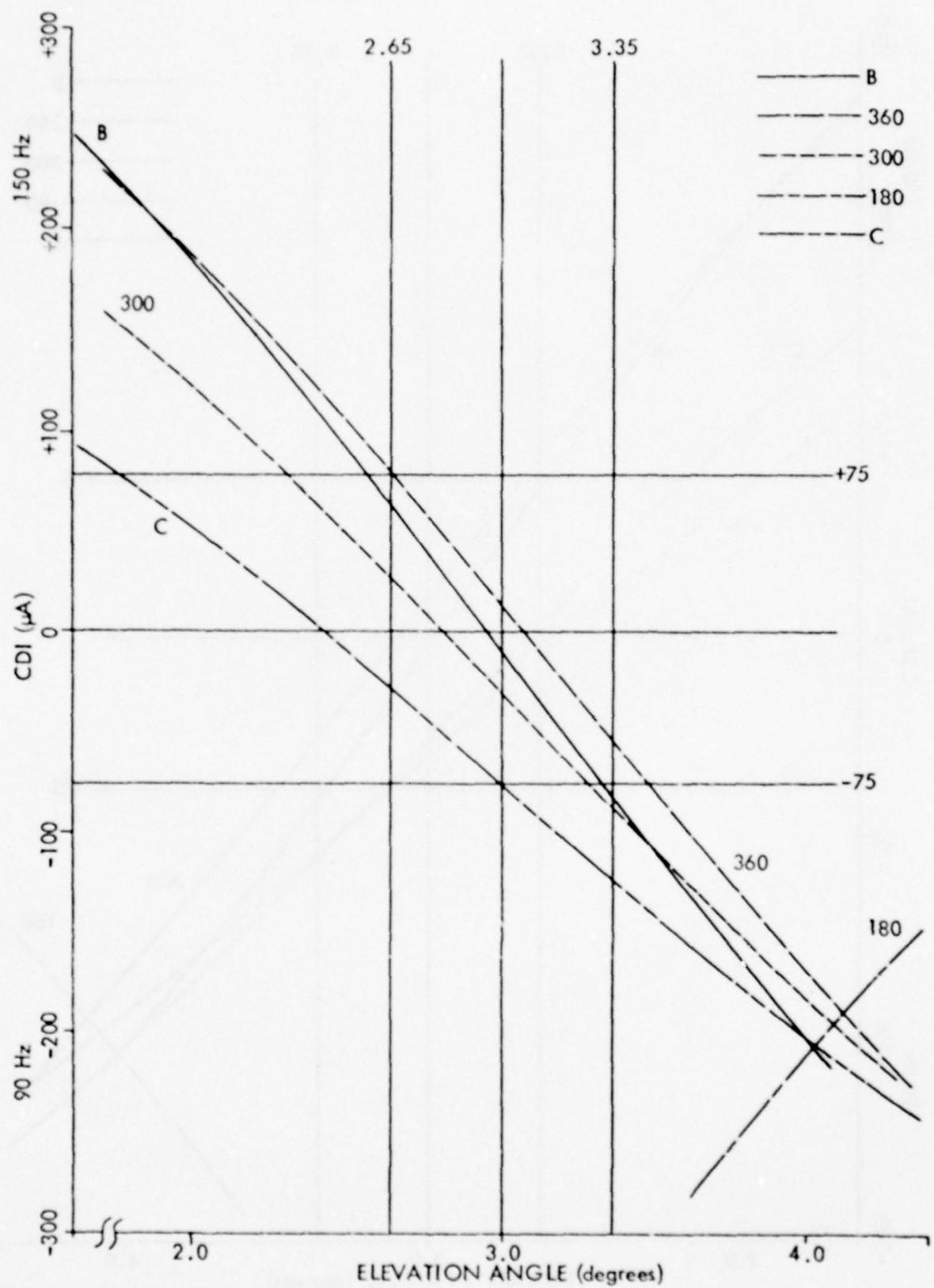
Figure 36. CDI vs. Angle — Lower Antenna Advanced 20°.

-44-
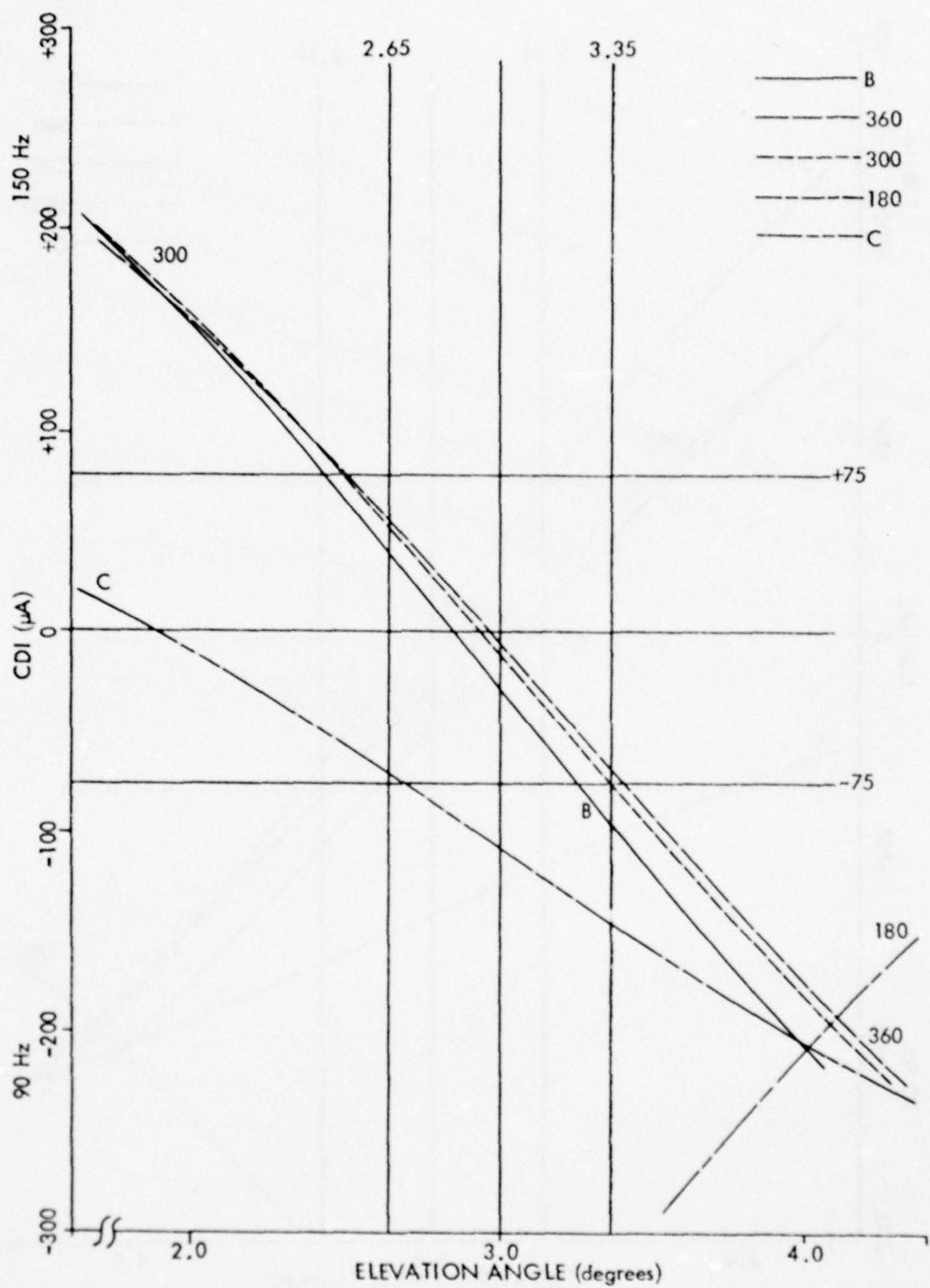
Figure 37.   CDI vs. Angle – Lower Antenna Advanced 30°.
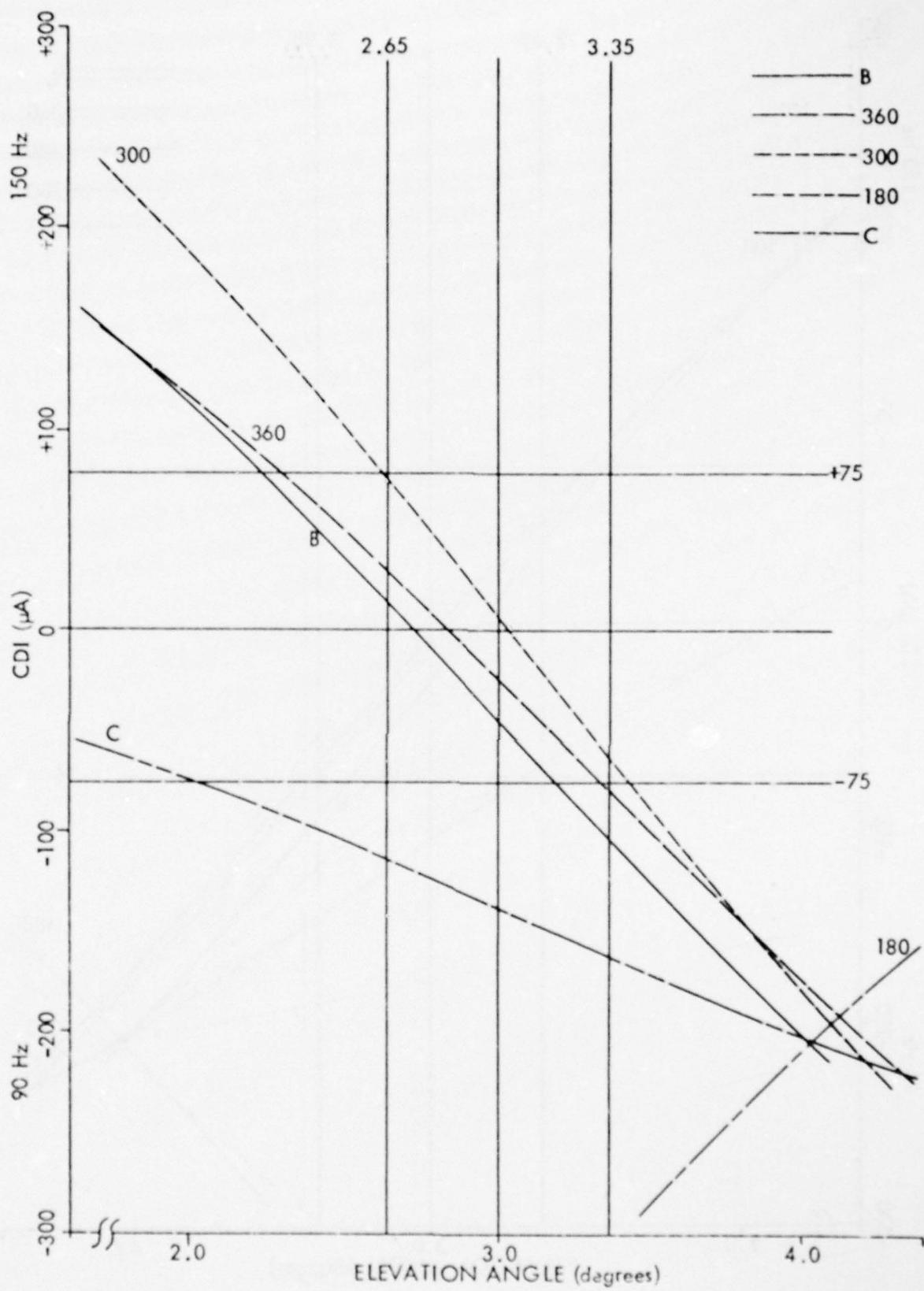
Figure 38. CDI vs. Angle - Lower Antenna Advanced 40°.
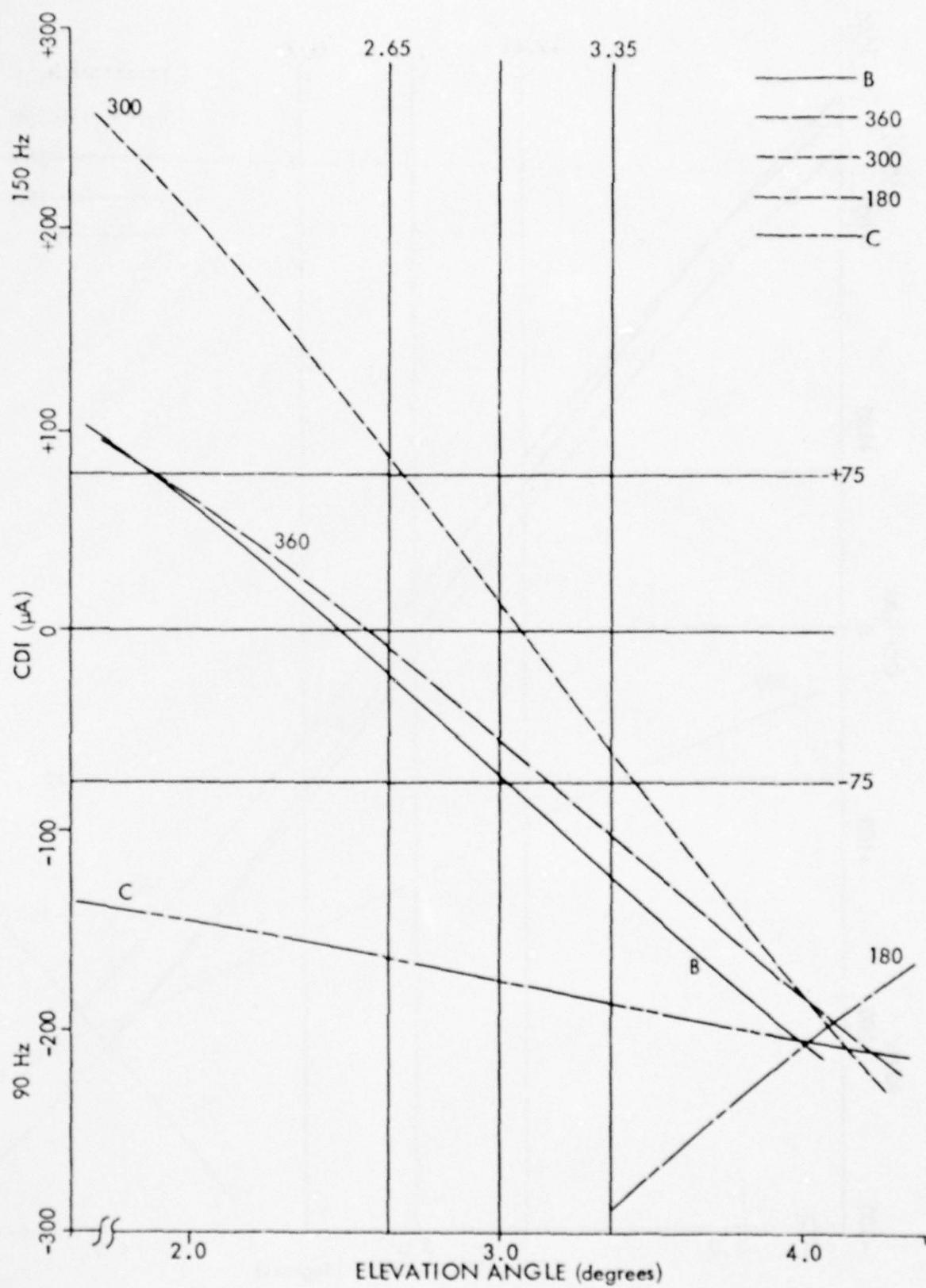
Figure 39. CDI vs. Angle – Lower Antenna Advanced 50°.

-47-
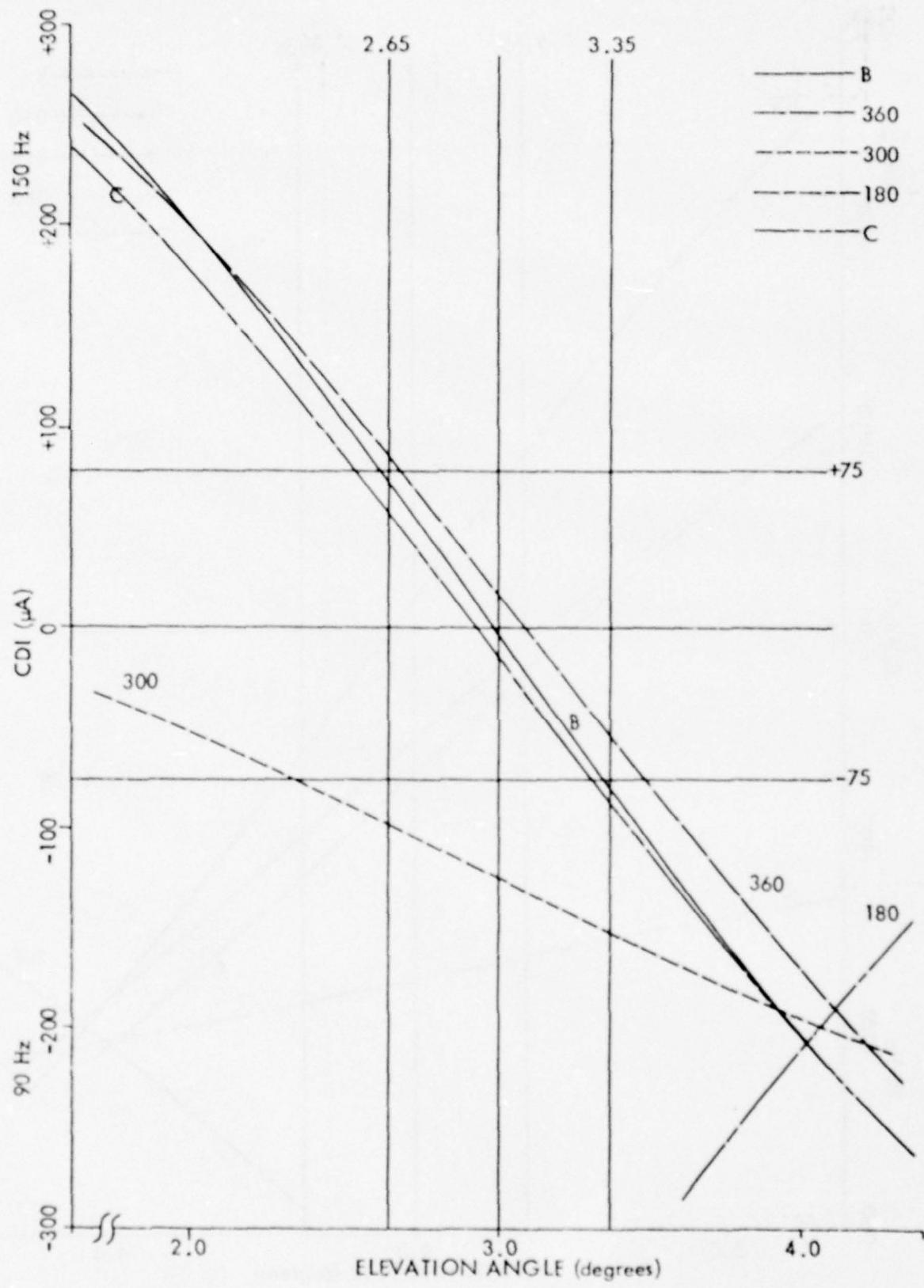
Figure 40. CDI vs. Angle – Upper Antenna Advanced 10°.

-48-
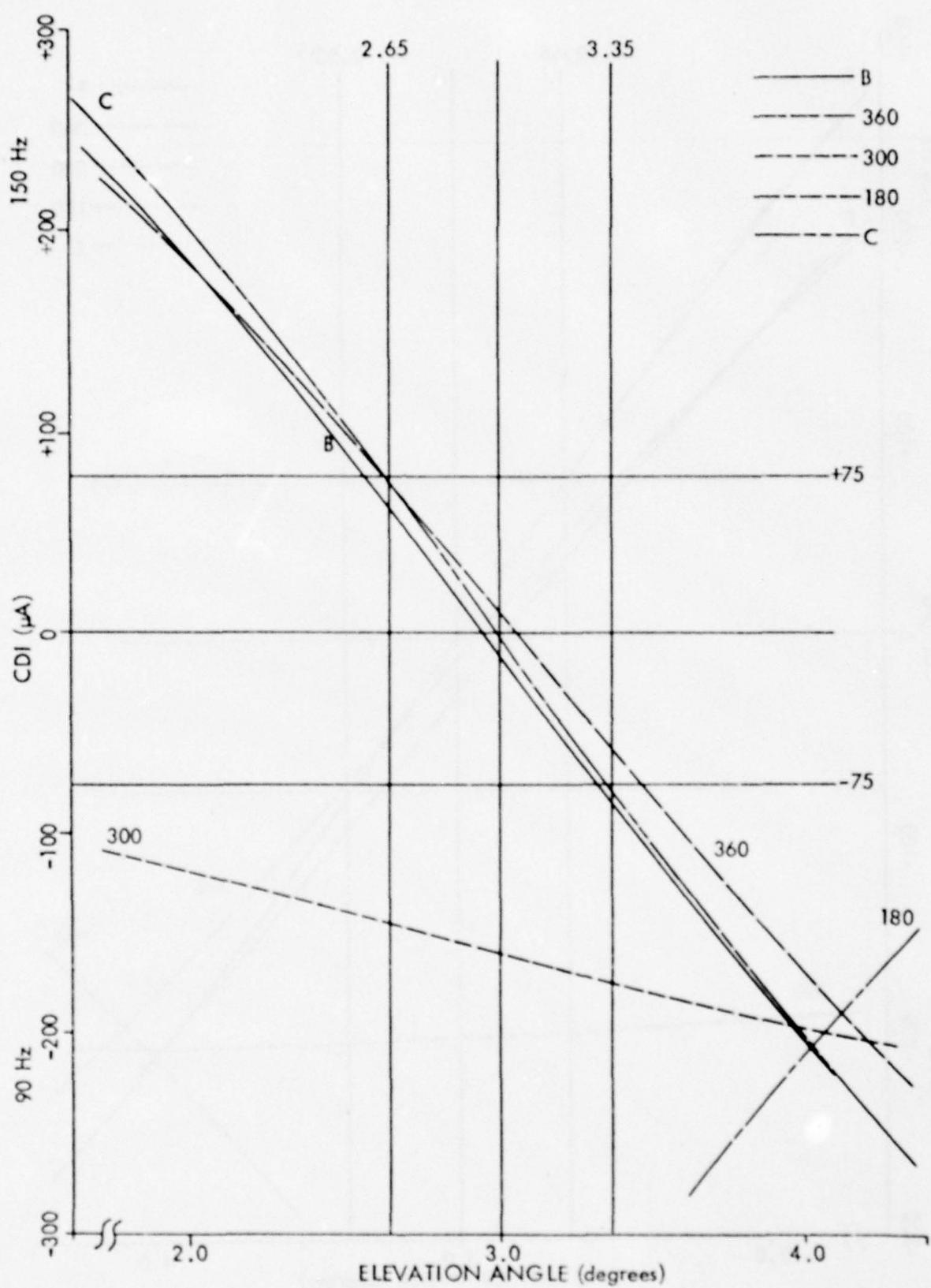
Figure 41. CDI vs. Angle – Upper Antenna Advanced 20°.

-49-
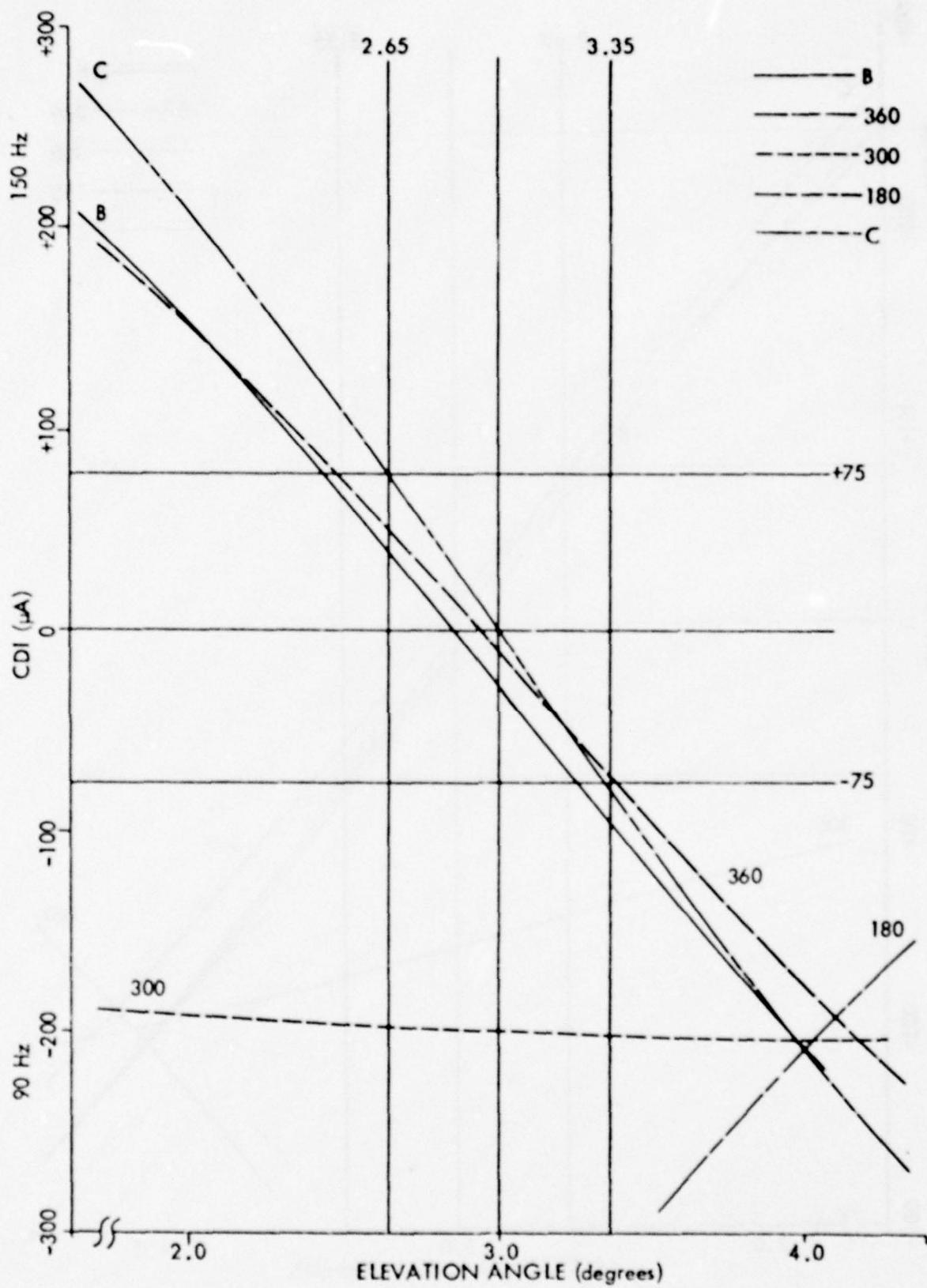
Figure 42. CDI vs. Angle – Upper Antenna Advanced 30°.
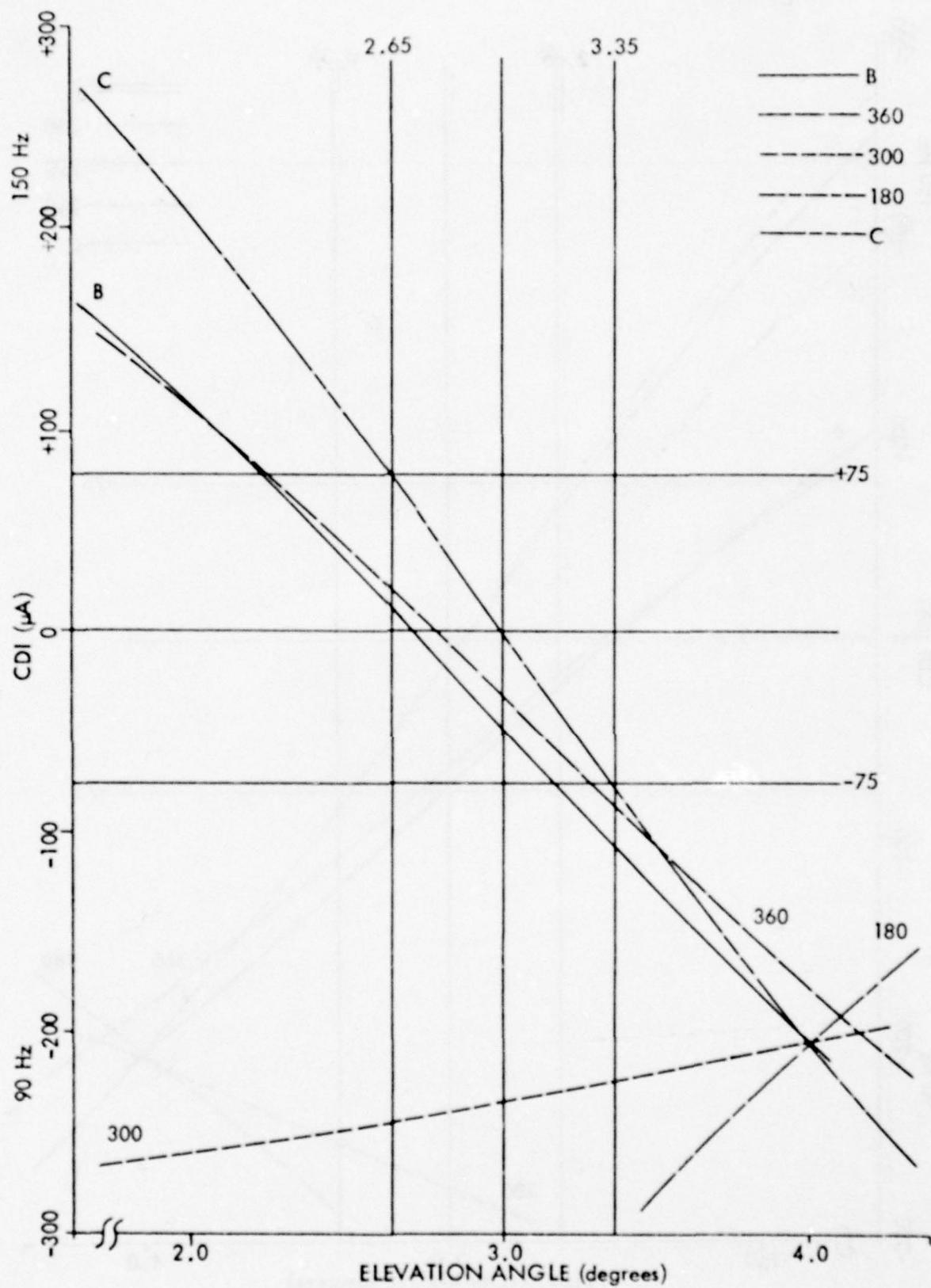
Figure 43. CDI vs. Angle – Upper Antenna Advanced 40°.
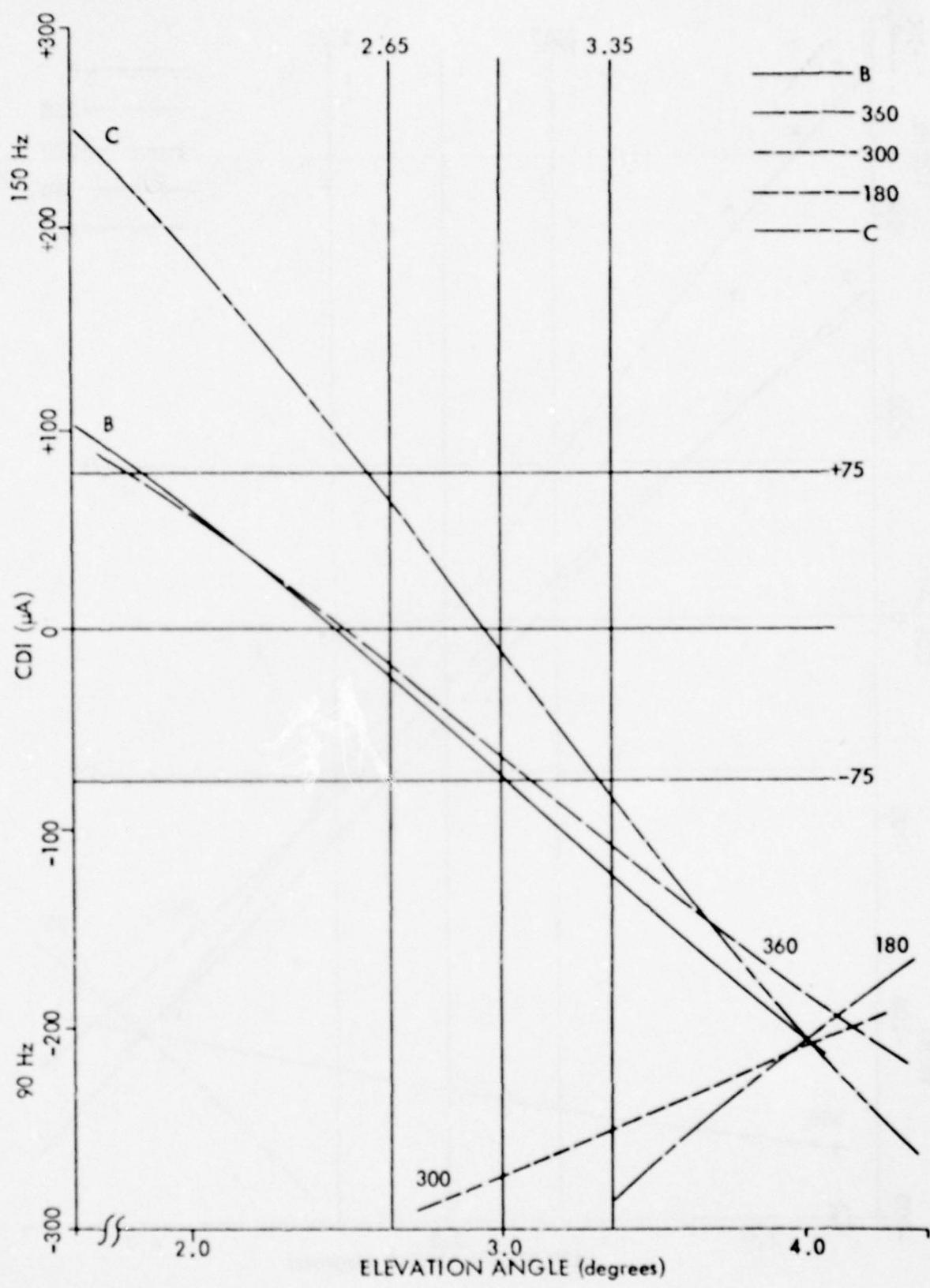
Figure 44. CDI vs. Angle - Upper Antenna Advanced 50°.

-52-
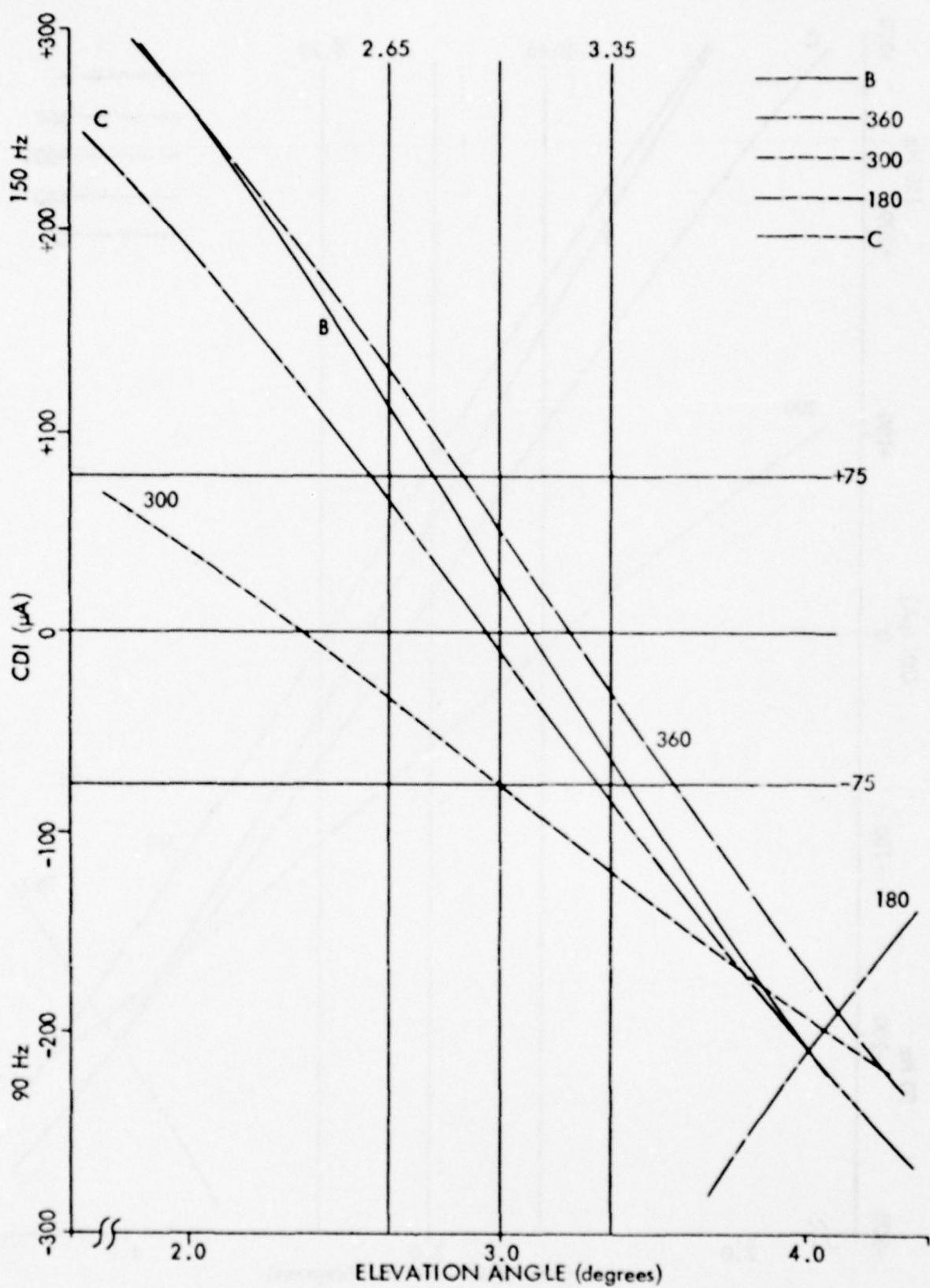
Figure 45. CDI vs. Angle – Lower Antenna Attenuated 1 dB.

-53-
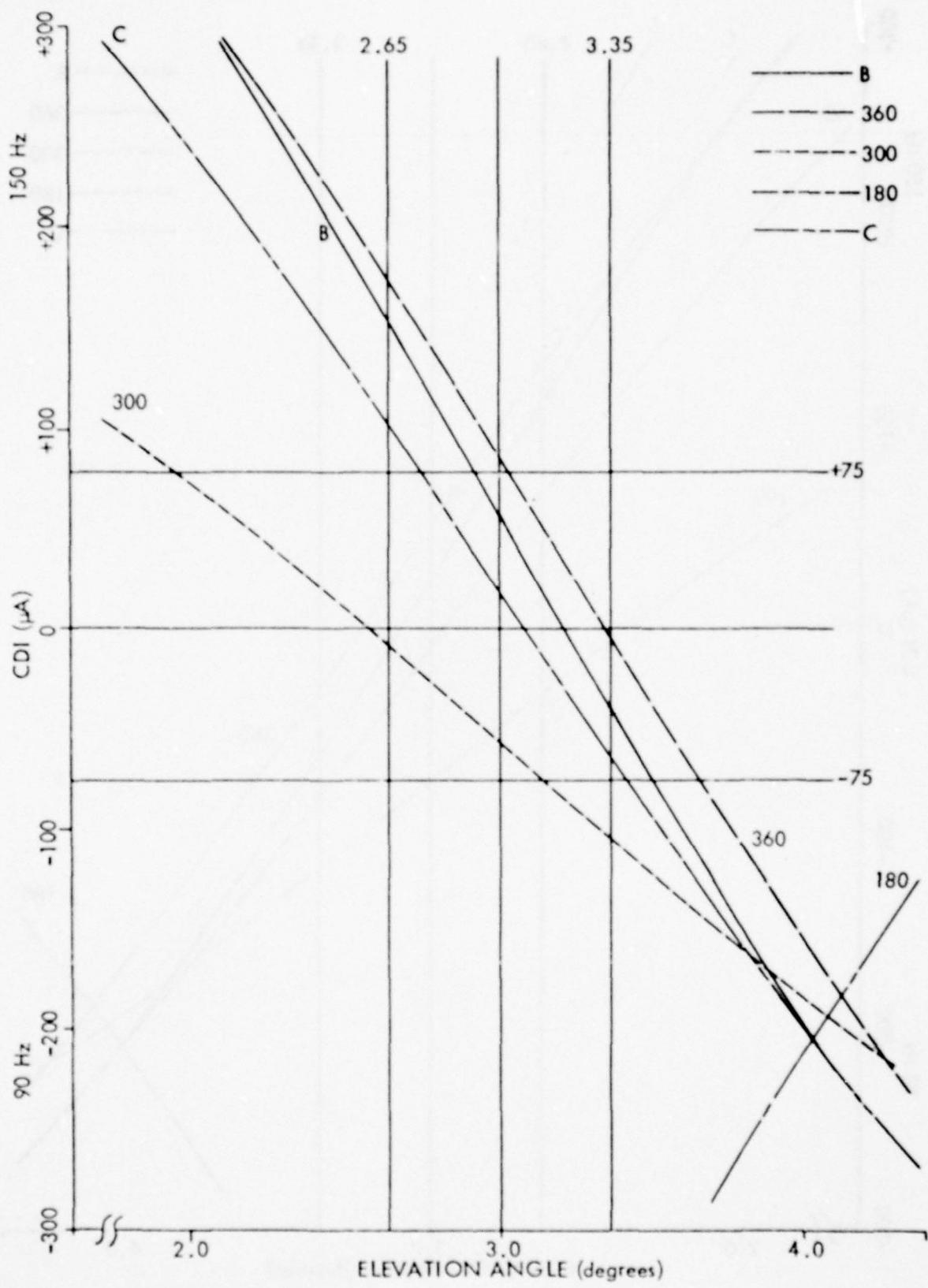
Figure 46. CDI vs. Angle – Lower Antenna Attenuated 2 dB.

-54-
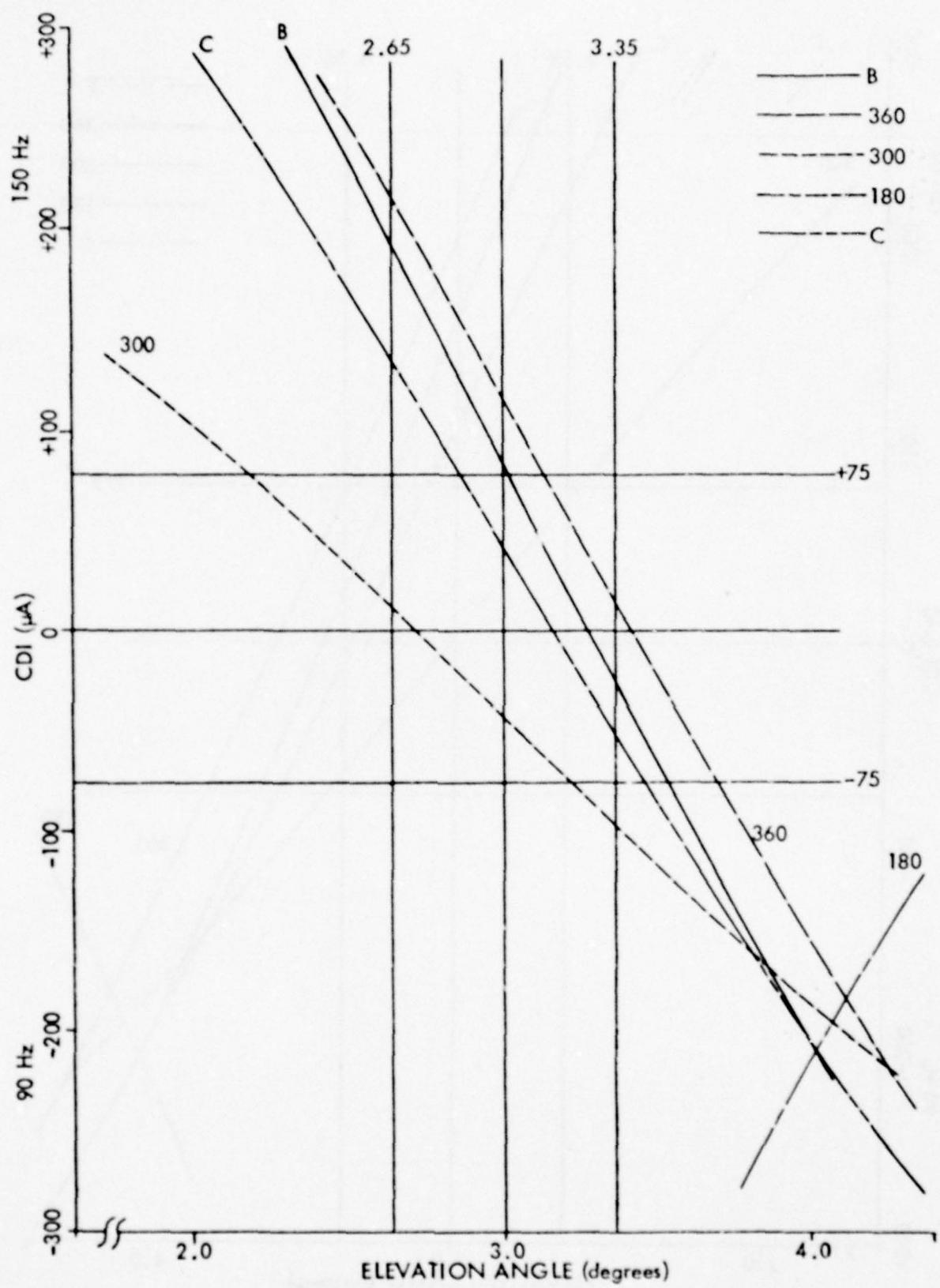
Figure 47. CDI vs. Angle – Lower Antenna Attenuated 3 dB.
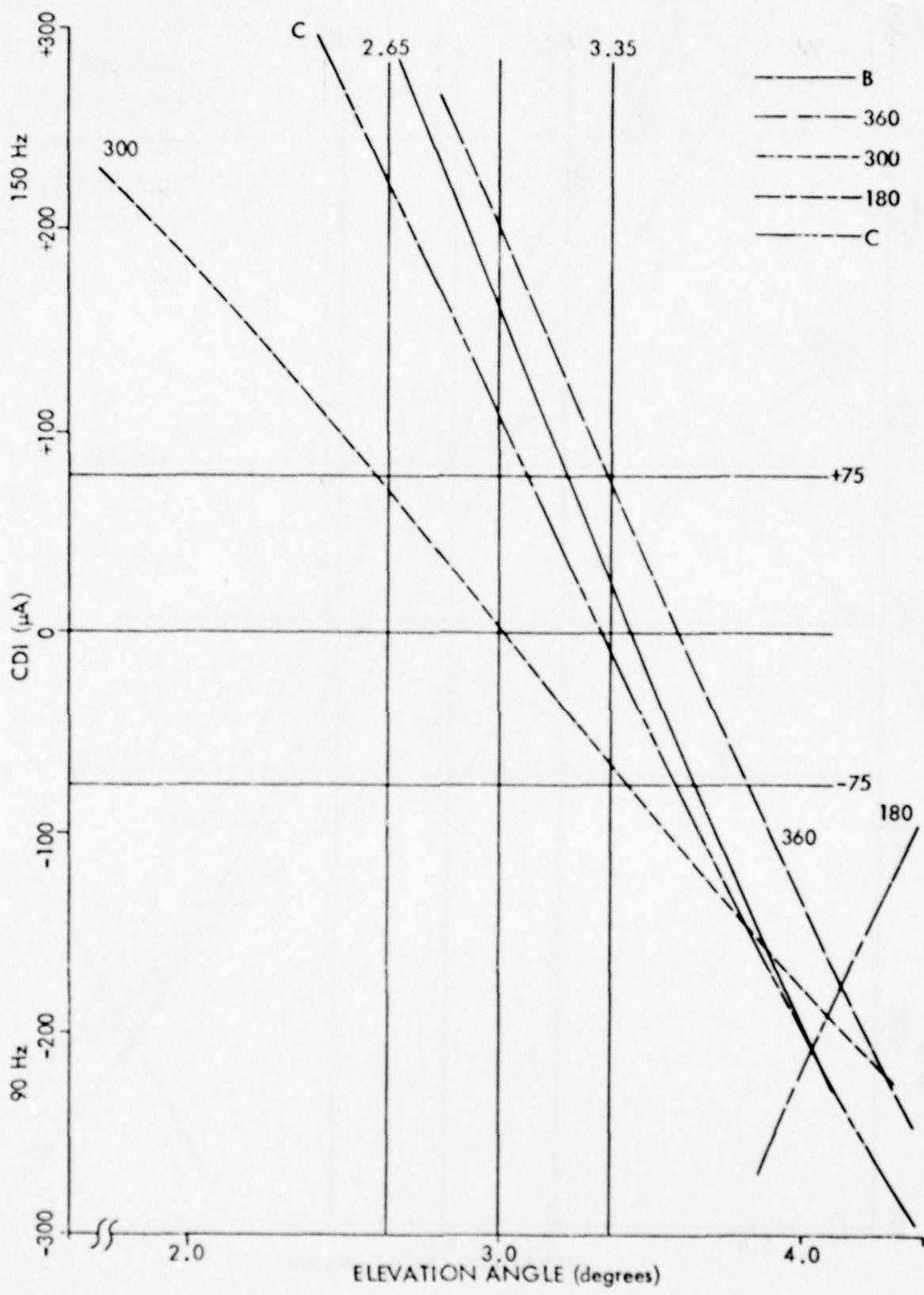
Figure 48. CDI vs. Angle – Lower Antenna Attenuated 5 dB.

-56-
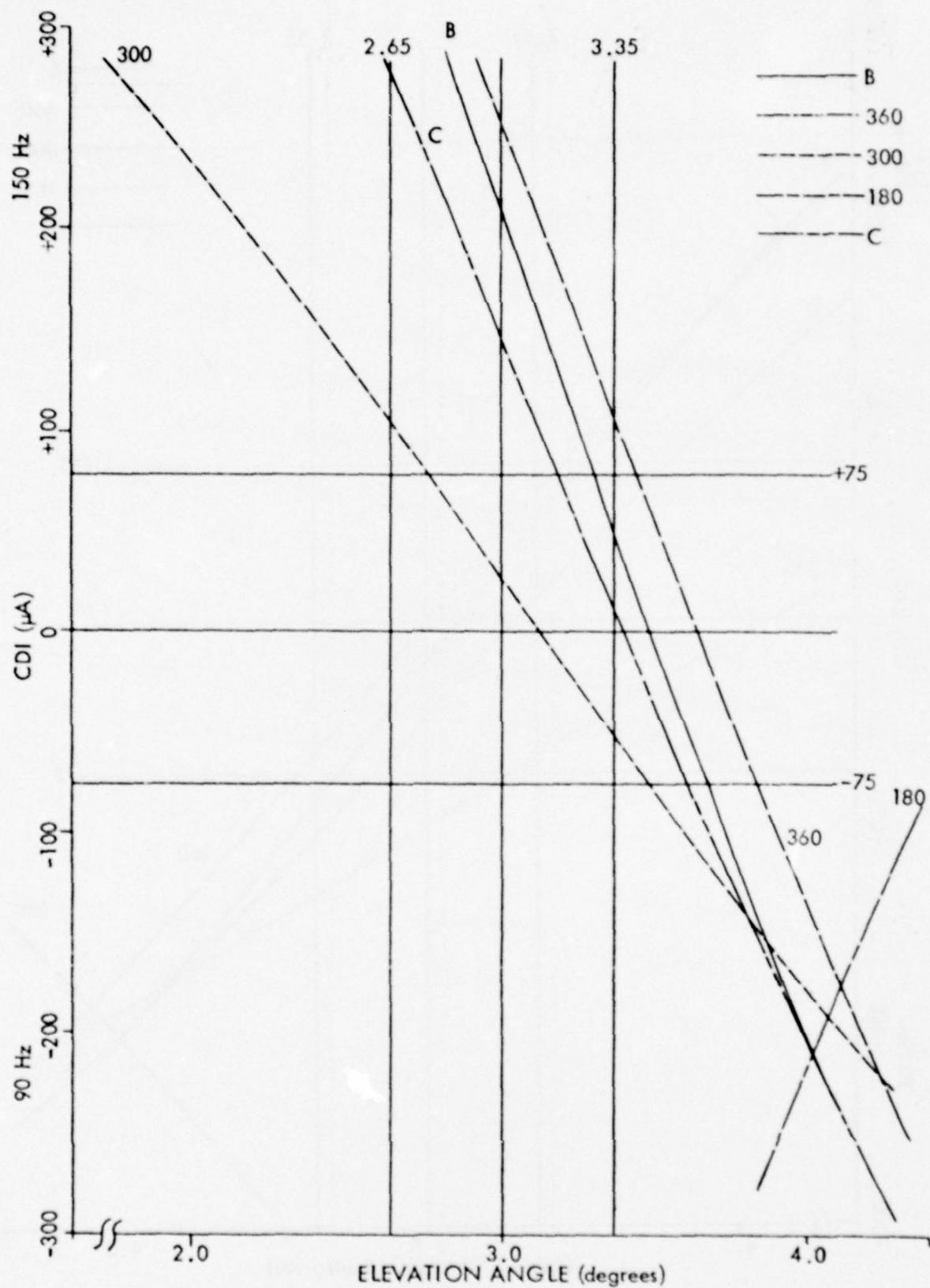
Figure 49. CDI vs. Angle - Lower Antenna Attenuated 6 dB.

-57-
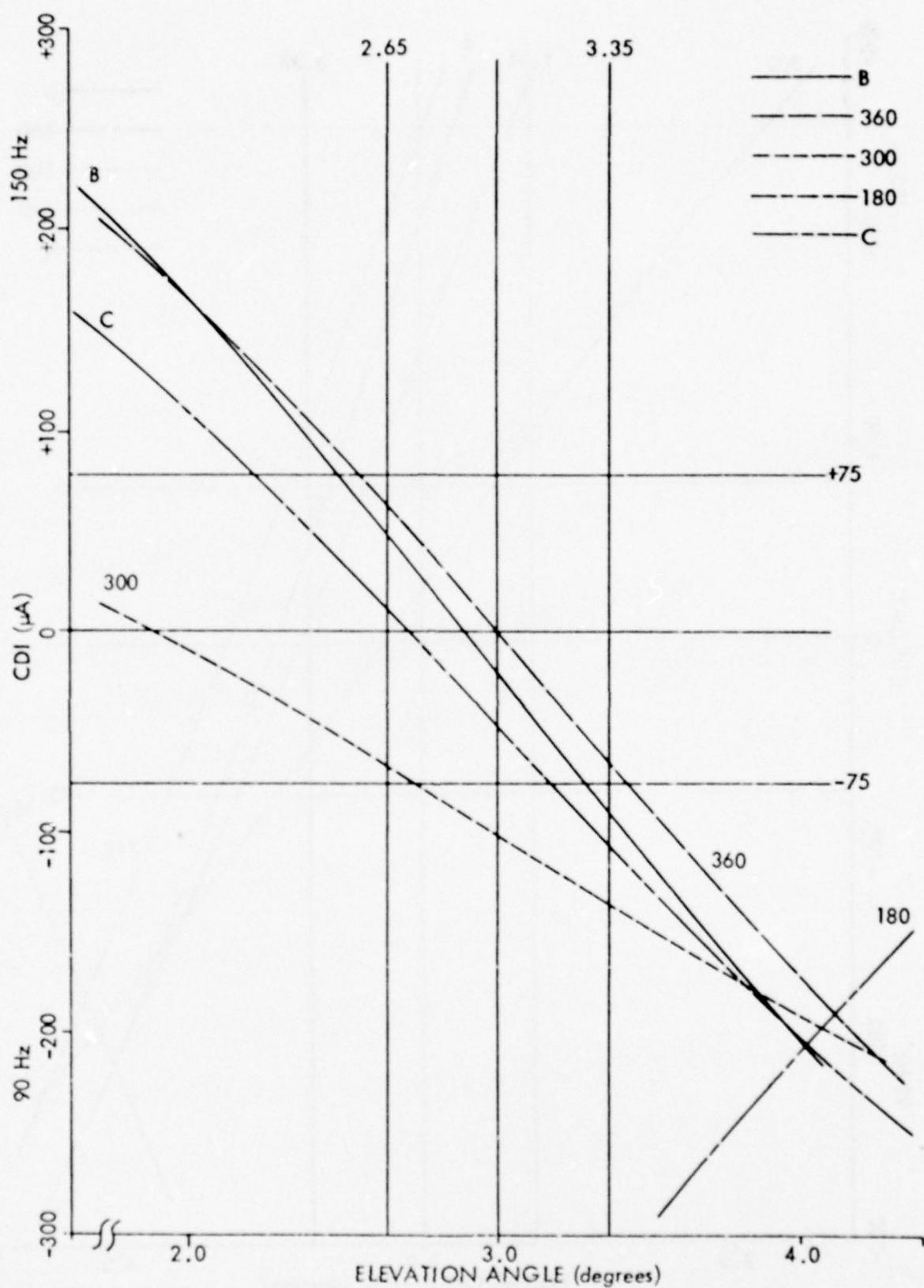
Figure 50. CDI vs. Angle – Upper Antenna Attenuated 1 dB.
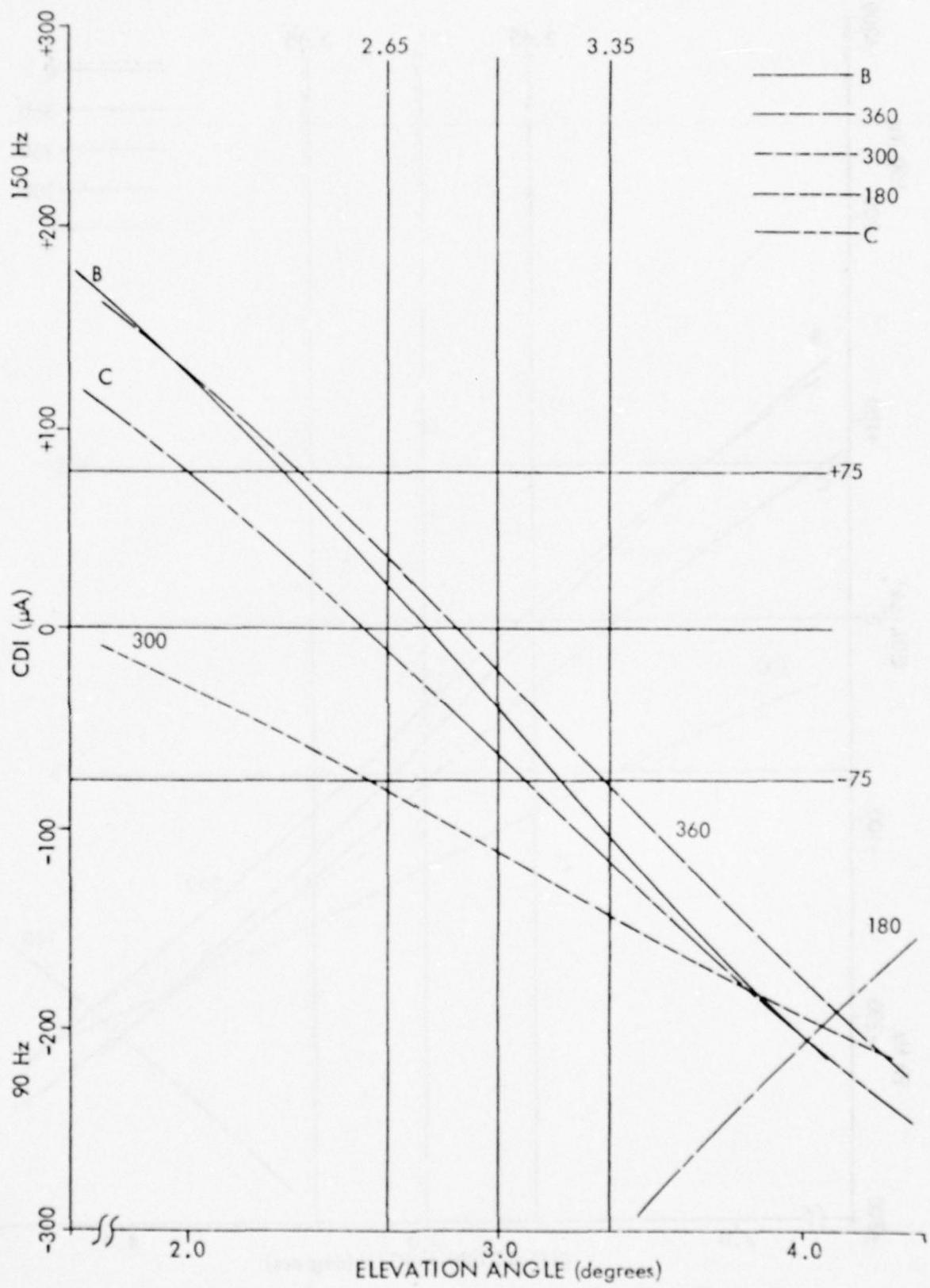
Figure 51. CDI vs. Angle – Upper Antenna Attenuated 2 dB.
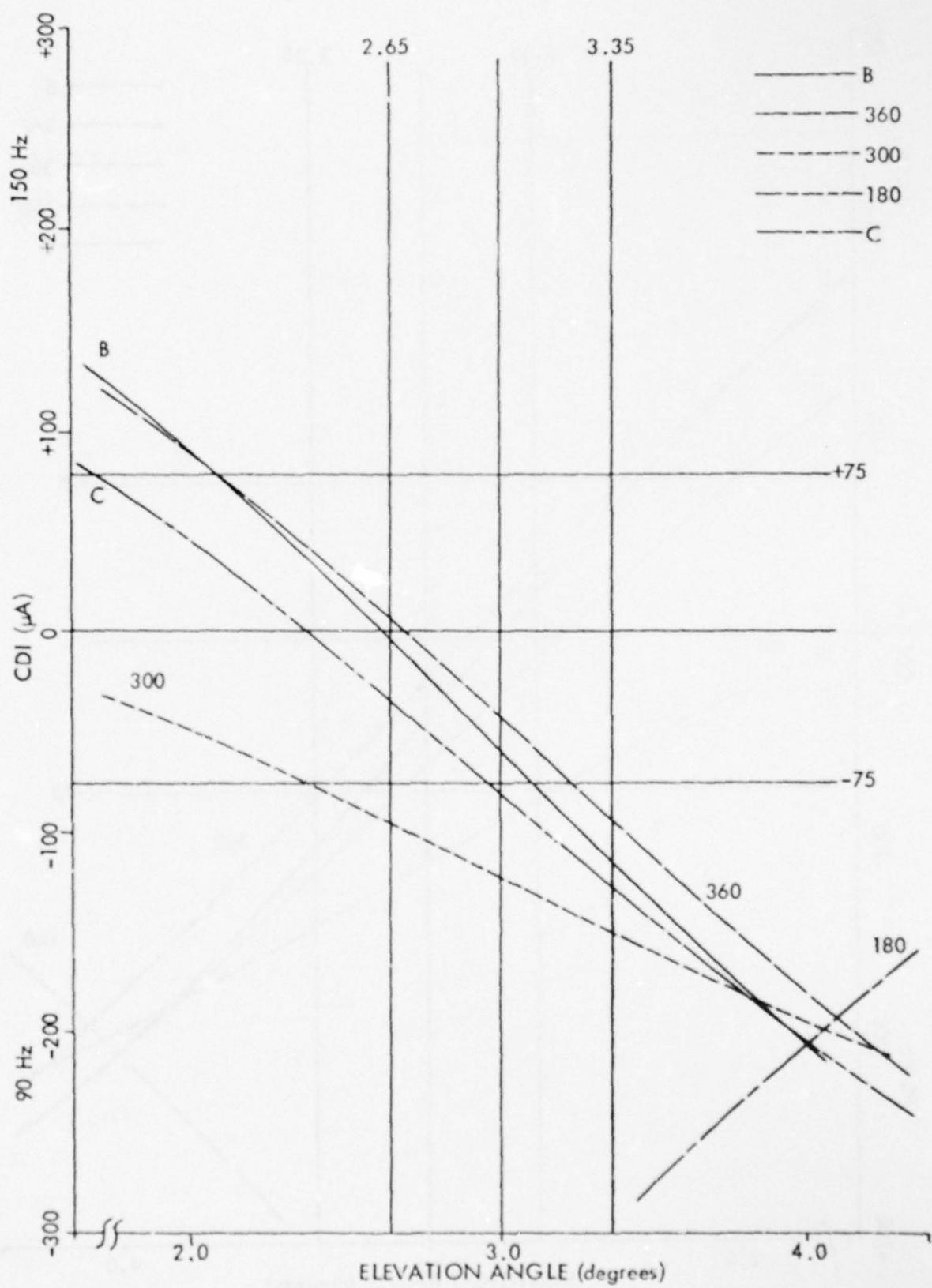
Figure 52. CDI vs. Angle – Upper Antenna Attenuated 3 dB.

-60-
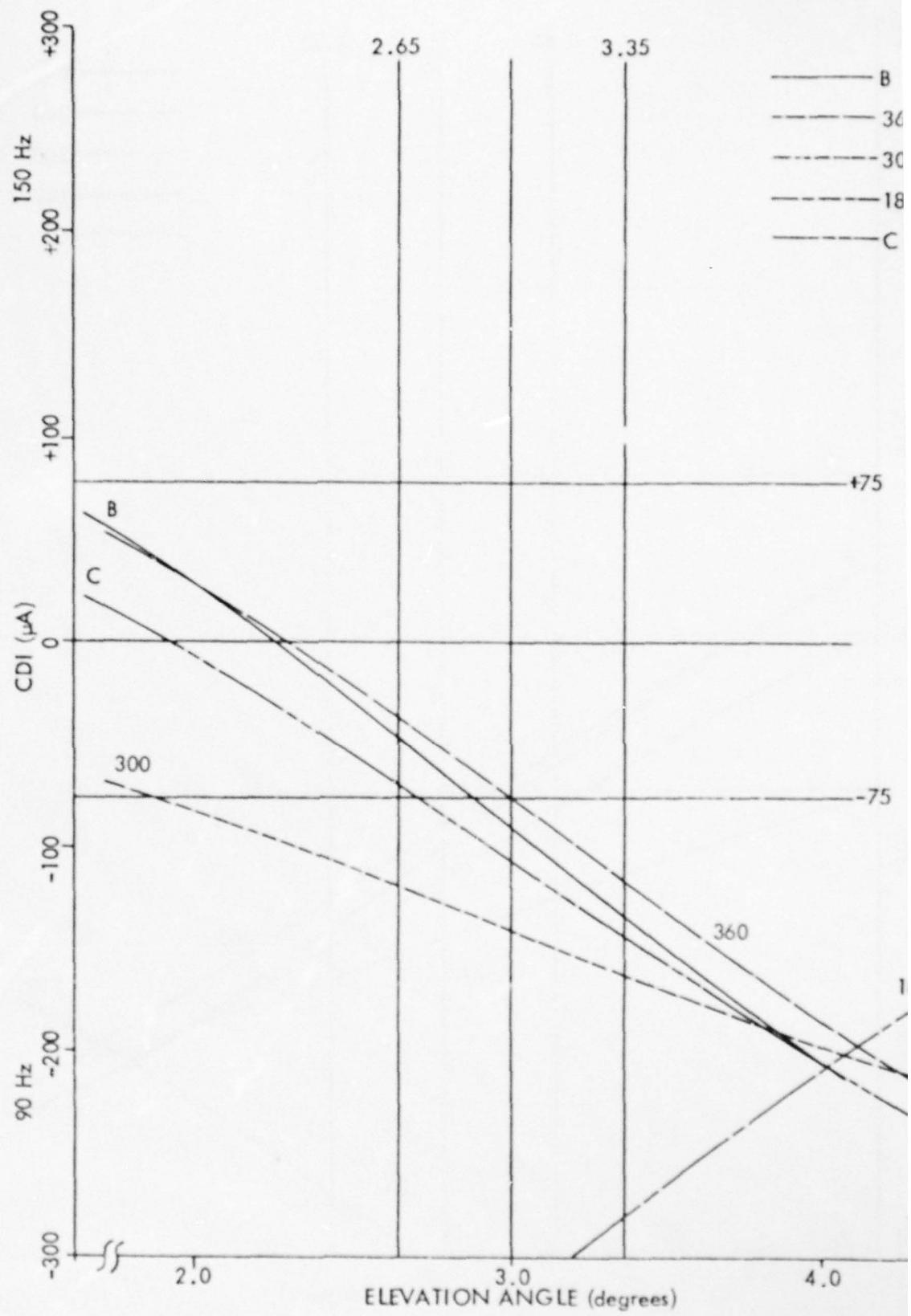
Figure 53. CDI vs. Angle – Upper Antenna Attenuated 5 dB.
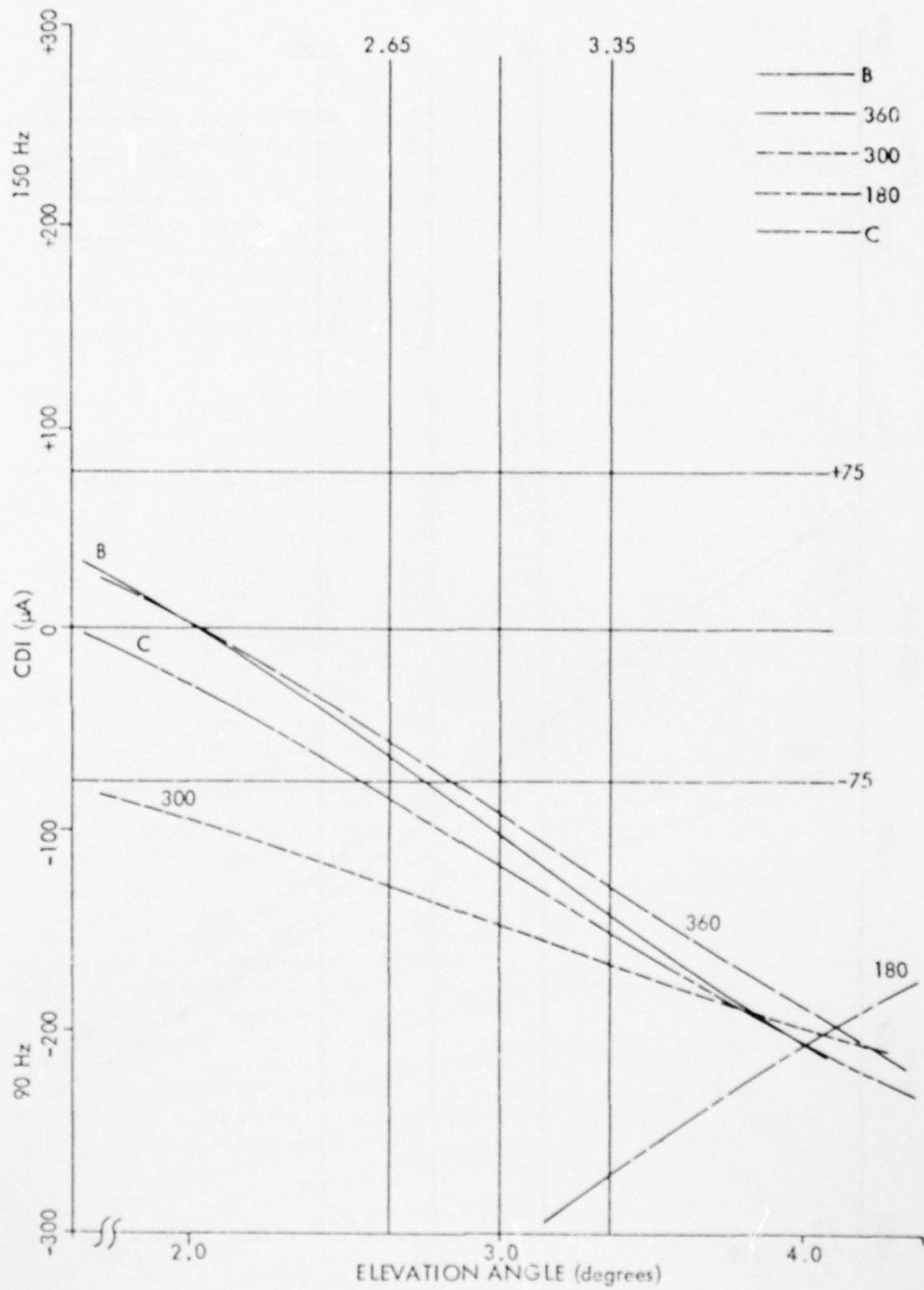
Figure 54. CDI vs. Angle – Upper Antenna Attenuated 6 dB.

2. A set-up method should be developed for the SBR glide-slope system that can be used at any site, starting with the results so far obtained and based on models generated by OUGS for non-ideal sites.

3. Limited perturbation studies should be conducted at commissioned SBR sites to yield data valuable to ILS engineers. Subsequent recommendations for SBR monitoring, integral or otherwise, would benefit from data so obtained. This type of data would supplement that already obtained by the OUGS model, this study, and by work at Ohio University's Albany, Ohio experimental test site.

B. Additional Documentation for Sideband Reference Glide-Slope Performance with Near Field and Integral Analog Monitoring.

1. Summary and Conclusions. As disclosed in the preceding section, the current near-field monitoring for the sideband reference glide-slope system is not only non-analog in nature but overly sensitive to near-field environmental factors. Results of testing documented here suggest that the implementation of integral, analog monitoring for the sideband reference system would provide an improvement to identify system faults accurately and eliminate spurious response to environmental factors, thus reducing system outages.

2. Introduction. Preliminary work was accomplished on implementing analog monitoring using integral pick-ups. The investigation centered on system response to foreign objects on the antennas, changes in the transmission line lengths, and changes in modulation balance, sideband power, and sideband-to-carrier phasing.

During the work described in part A of this section (II-A) on the sideband reference in Tamiami, some peculiar near-field monitor response conditions became evident; hence, motivation was provided for implementation of the integral monitoring.

3. Discussion of Data. In preparation for the integral monitoring testing, a conventional sideband reference (SBR) system was established at the test site. Antenna heights for the 3:1 ratio were established at 7.09' (2.16m) and 21.27' (6.483m). An antenna offset of 6.0 inches (15.2cm) was used. Figure 55 is a view of the site after configuration as a sideband reference system. The system was then phased and found to have a path angle of 3.04° and a path width of 0.68°. At this time an effort was made to find a ground phasing point near the fenceline, approximately 2000' (610m) on the centerline extended. This point was located and found to be displaced from the centerline approximately 35' (11m). This point was permanently marked for future use.
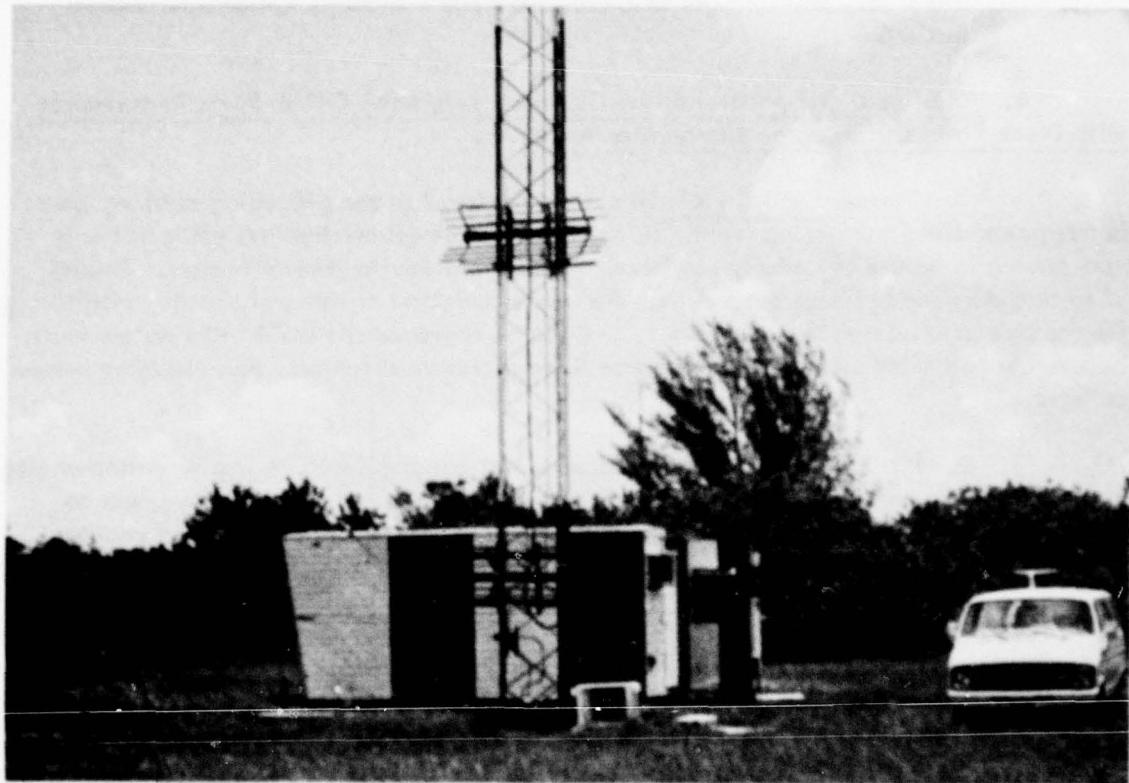
Figure 55.   The SBR System Used for the Analog, Integral
Monitor Testing at the Tamiami Test Site.

With the system now operating normally, the RF recombining for the integral, analog monitors was implemented as shown in Figure 56. The alignment procedure used for the RF recombining unit is as follows:

1. Determine that the glide-slope system is operating normally with the proper path angle and width.

2. Insert the CSB into the SBO input to the APCU and dummy load both the SBO line from the modulator and the CSB input to the APCU.

3. Using CH B of a vector voltmeter to monitor the "path" output of the recombining network, adjust AT-P and PH-P alternately to obtain a minimum RF signal level on CH B. It will be necessary to sample some CSB signal with CH A from some point in the transmitting system.

4. Now sample the "width" output with CH B and alternately adjust AT-W and PH-W for a minimum signal level on CH B.

5. Repeat steps 3 and 4 until both the "path" and the "width" outputs from the network are at a minimum.

6. Return the CSB and SBO inputs to the APCU to normal.

7. With the detectors and monitors connected to the "path" and "width" outputs of the RF recombining network and the system operating normally, both monitors should now read 0 DDM. If not, return to step 1.

8. Now set the DDM offset in the "width" monitor to 087.5/150 (X2)DDM and adjust AT-W (increase) attenuation until the "width" monitor indicator meter reads zero. The "width" monitor now appears to be at the lower path edge and the "path" monitor on the path.

After the analog recombining network and the monitors were properly aligned, Honeywell Electronix 19 strip chart recorders were used to record the monitor variations over a three-day period. During this time no changes or adjustments were made to the transmitting equipment. Diurnal changes for this monitoring scheme were found to be approximately -30%/+15% of width alarm and -25%/+10% of path alarm.

A series of tests was then conducted to determine the response of both the far field and the analog monitor to perturbations in the system. These tests included not only changes in the operating parameters of the transmitting equipment, but also abnormal antenna conditions such as those which might be expected to result from the presence of birds or debris. The far-field data was obtained using the Minilab airborne instrumentation package in a Beechcraft Model 35. [2]
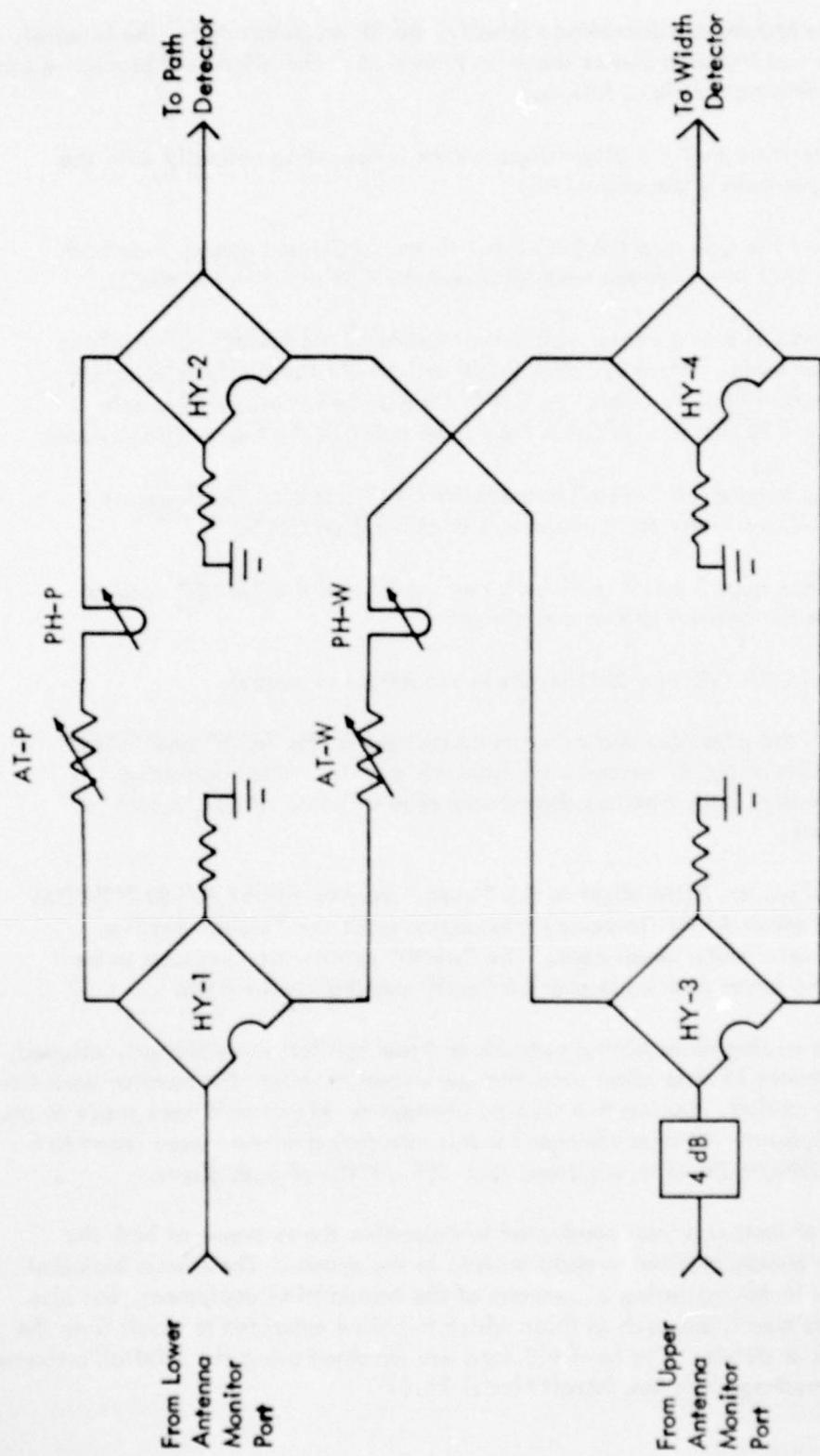
Figure 56. Schematic of the RF Recombining Network Implemented for the Tamiami Integral, Analog Monitor Tests in June, 1978.

-66-

4. Results. The ground phasing point located at the fenceline and displaced approximately 35' (11m) from the centerline extended was used as a reference for several attempts to ground phase the system. Results of ground phasing were very consistent with airborne phasing being a +4°. Phasing by observing a minimum 150 Hz condition in the lower antenna was a -6° from that called for by ground phasing. As would be expected, the minimum 150 Hz indication in the lower antenna was accompanied by a minimum path width indication on the analog width monitor.

The integral, analog monitor implemented with standard MK 1C monitor components as shown in Figure 56, experienced diurnal changes not exceeding 30% of alarm. Results of strip chart recordings of the path and width monitors over a three-day period are shown in Figure 57. No adjustments were made to the transmitting equipment during this time. Time limitations precluded a complete investigation to establish the cause of these variations, but subsequent testing showed the phasors to be unstable.

Alignment of the RF recombining network was complicated due to interaction between the path and width channels. An iterative approach was required.

Table 3 is a summary of the results of the series of perturbational tests conducted to verify satisfactory operation of the analog monitor. Calculated far field, measured far field, and analog monitor values are given for all perturbations.

Satisfactory analog monitor operation in the presence of antenna faults resulting from birds or debris on the antennas is examined. Figure 58 shows a water-soaked rag placed atop the center element of the lower antenna. Figure 59 is a view of a 12" x 24" (30.5cm x 61.0cm) screen mesh [3/4" (1.9cm) square mesh] draped in front of the same center element of the lower antenna. The placement of a wire loop 7" (17.8cm) above the center element is shown in Figure 60. Referring to Table 3, we see that in all cases the analog monitor was conservative, indicating a far-field change greater than was measured.

5. Recommendations. The use of integral, analog monitoring for the sideband reference glide-slope system has been demonstrated. Further testing of the analog monitoring scheme should be done to establish long-term stability performance. Interaction between the path and width channel during alignment of the monitor recombining network should be examined further through an expanded series of tests.

C. Calculated Performance Comparisons for Sideband Reference, Null Reference, and Capture Effect Glide Slope Systems for 19 Different Terrain Profiles.

1. Introduction. This section consists of an album of calculated performances for 19 different non-ideal terrain profiles. The standard reference used to predict the applicability of the various image glide-slope systems (null reference, sideband reference, capture effect) in the presence of uneven terrain is the FAA publication "Siting Criteria for Instrument Landing Systems". [3] Figure 3-12 of this publication is reproduced as Figure 61 and shows 5 classes of terrain profile types with the predicted applicability of the three image glide-slope systems for each profile.
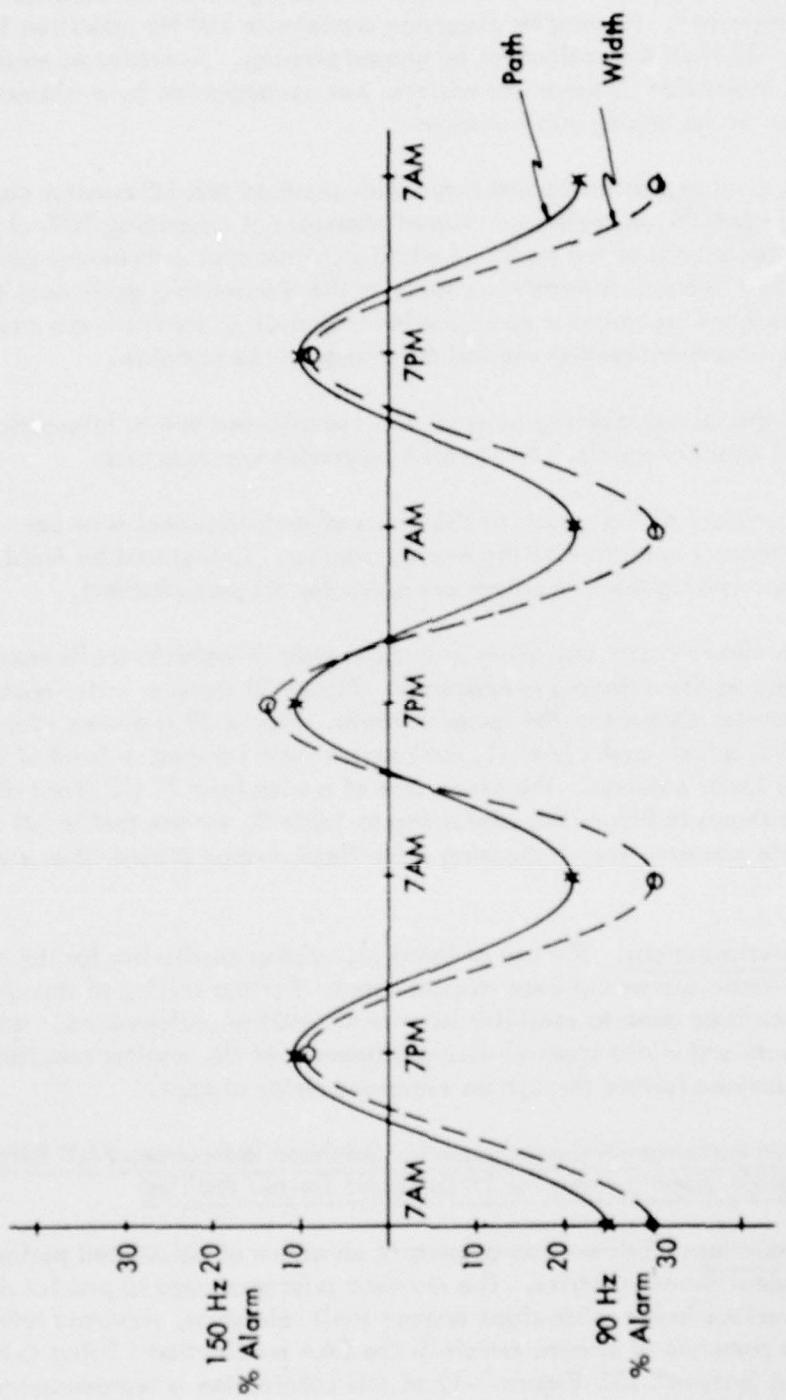
Figure 57. Diurnal Variations in the Integral, Analog Monitor
Output during the Tamiami Tests.

Legend: H = High, L = Low, B = Broad, S = Sharp

Condition	Calculated Far-Field ∠ (°)	% ∠ Alarm	Width (°)	% Width Alarm	Measured For-Field ∠ (°)	% ∠ Alarm	Width (°)	% Width Alarm	Analog Monitor % ∠ Alarm	% Width Alarm
Normal	3.00	0	0.70	0	3.02	0	0.73	0	0	0
Broad Alarm	3.00	0	0.90	100B	3.02	0	0.90	100B	0	100 B
Sharp Alarm	3.00	0	0.50	100S	3.03	5 H	0.49	100S	0	100 S
High Angle	3.20	100 H	0.70	0	3.20	100 H	0.67	26S	100 H	30 S
Low Angle	2.80	100 L	0.70	0	2.83	85 L	0.80	41B	100 L	45 B
SBO Advanced 30°	3.00	0	0.82	60B	3.04	10 H	0.82	53B	0	115 B
SBO Delay 30°	3.00	0	0.82	60B	3.00	10 L	0.82	53B	0	100 B
SBO Advanced 34°	2.99	5L	0.88	88B	3.02	0	0.80	41B	0	100 B
SBO Delay 37°	3.01	5H	0.89	96B	2.90	55L	0.91	106B	0	100 B
Upper Antenna Advanced 15°	2.98	10L	0.72	10B	3.01	5L	0.68	22S	50 L	50 L
Upper Antenna Delay 15°	2.98	10L	0.72	10B	2.95	31L	0.73	0	60 L	20 L
Mod Bal .02 → 90 Hz	2.90	50L	0.70	0	2.86	73L	0.64	36S	105 L	150 S
Mod Bal .02 → 150 Hz	3.10	50H	0.70	0	3.20	190H	0.76	22B	100 H	100 B
Wet Rag Center Dipole (Fig. 4)	-	-	-	-	3.04	11H	0.70	13S	0	0
Screen Center Dipole (Fig. 5)	-	-	-	-	3.00	9L	0.66	30S	20 L	100 S
Wire Loop 7" (17.8cm) Above Center Dipole (Fig. 6)	-	-	-	-	2.95	32L	0.70	13S	100 L	60 S

Table 3. Summary of the Results of the Perturbational Tests on the Sideband Reference Glide-Slope System Using Integral, Analog Monitoring.
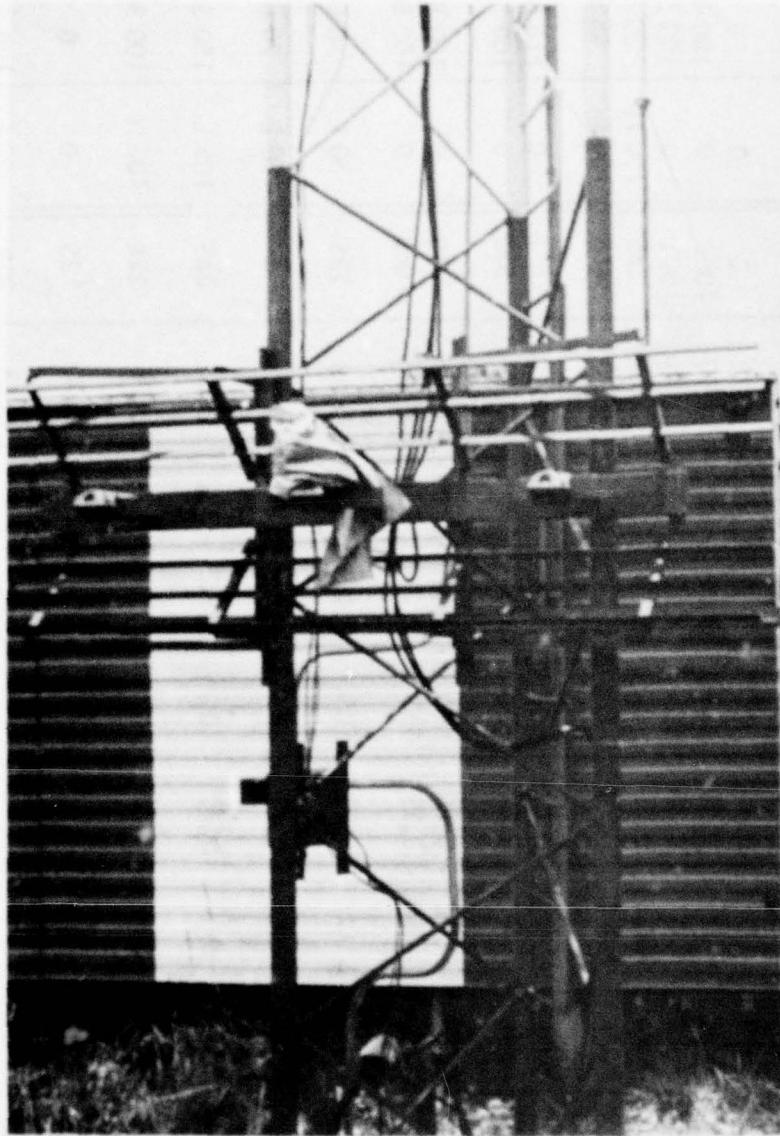
Figure 58.   View of the Water-Soaked Rag Placed on the Center
Element of the Lower Antenna of the Sideband Reference
Array with Integral, Analog Monitoring.
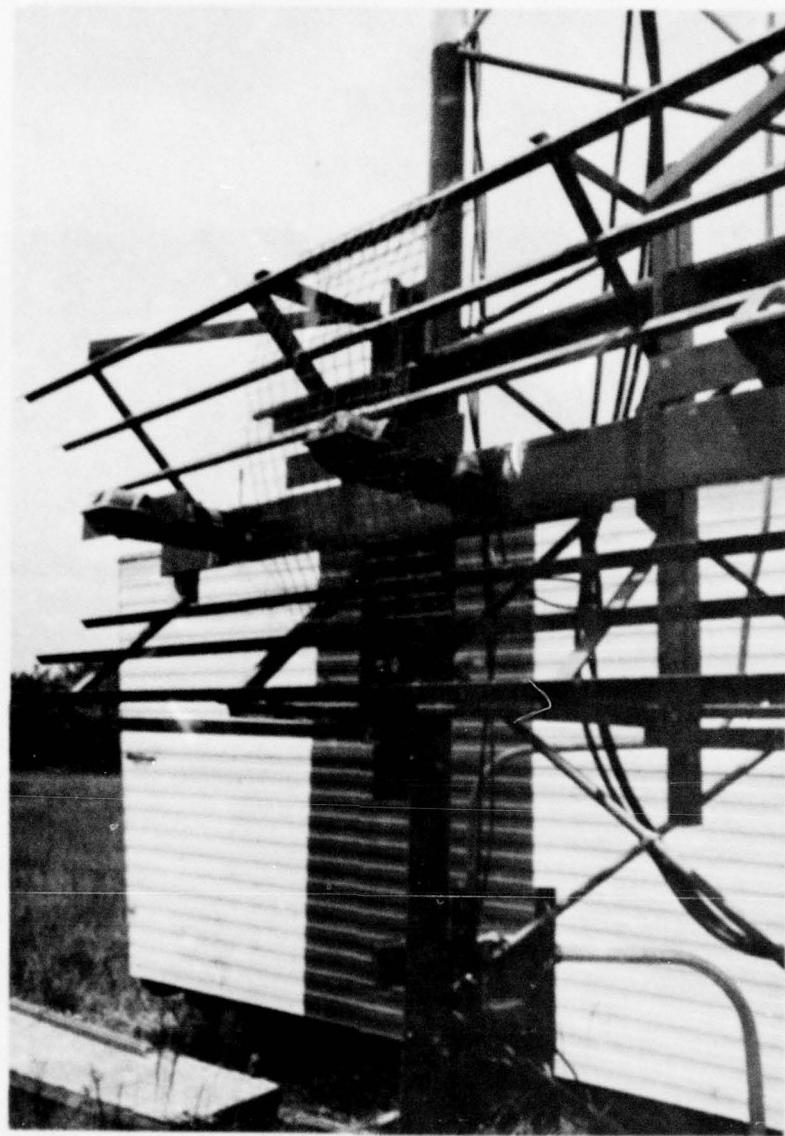
Figure 59.   View of the Simulated Antenna Fault Using a
12" × 24" (3/4" mesh) [30.5cm × 61.0cm(1.9cm
mesh)] Screen Over the Center Element of the
Lower Antenna.

-71-
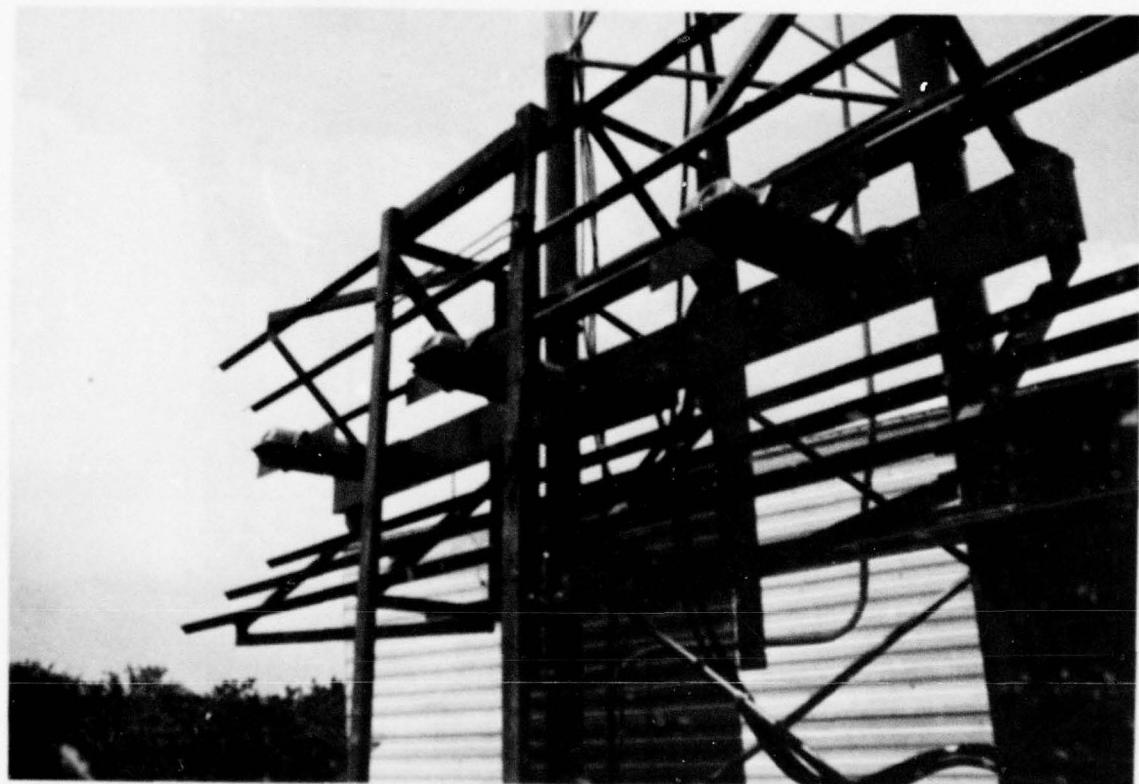
Figure 60. A View of the Wire Loop Placed 7" (17.8cm) Above the Center Dipole Element of the Lower Antenna.
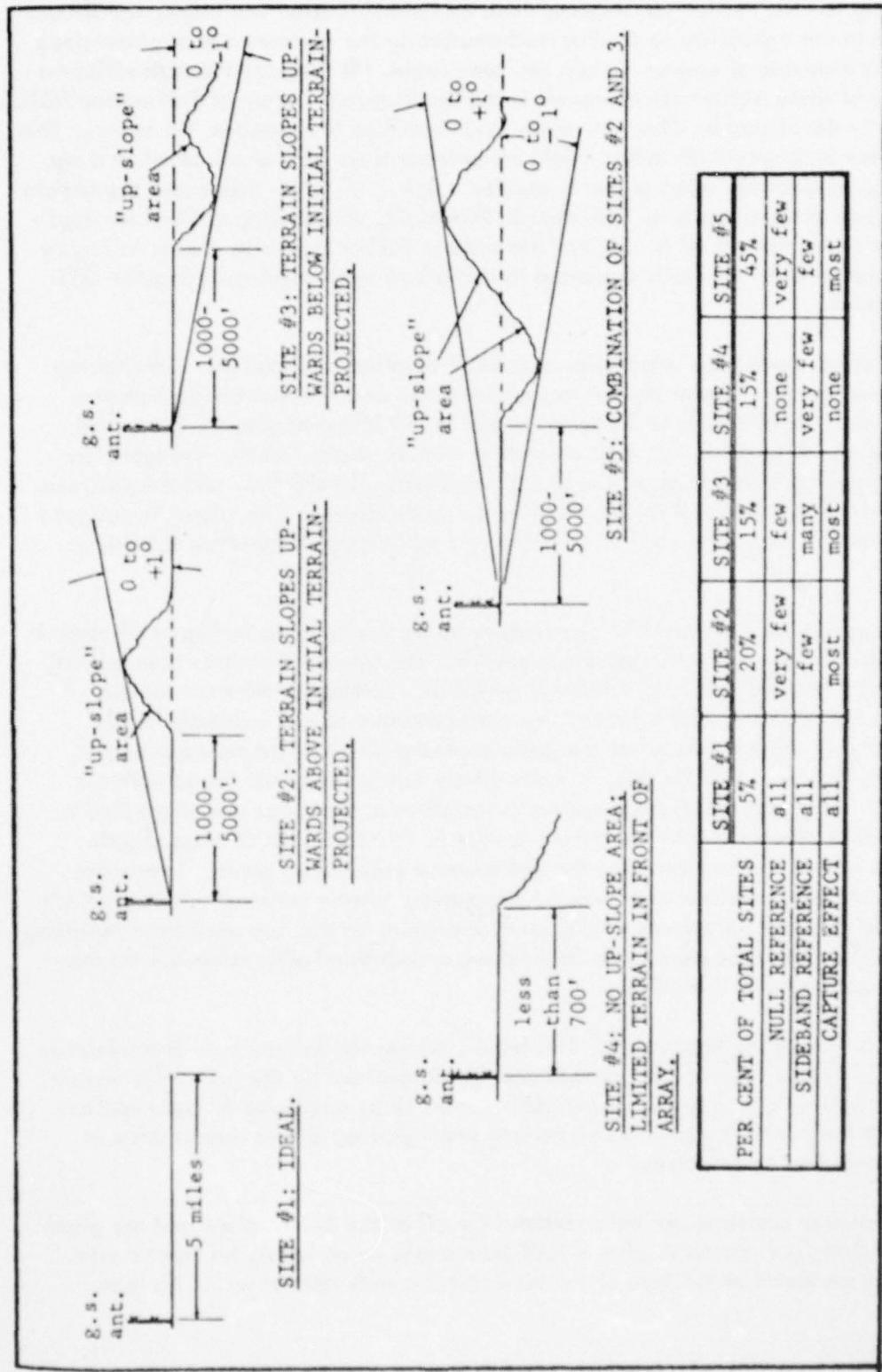
Figure 61. Expected Applicability of Various Types of Glide Slope Systems to Different Siting Conditions. (Taken from Reference [3].)

During the time which has elapsed since this classification was made, significant improvement in the capability to predict mathematically the performance of glide-slope systems in the presence of uneven terrain has been made. [4] Perhaps the most efficient and accurate of these mathematical models is the Geometrical Theory of Diffraction (GTD) model recently developed at Ohio University and described in reference [4] above. This model has been compared with actual flight measurements on several occasions and has been found to be accurate when properly applied.[5,6,7]* With this model the terrain is described two-dimensionally as indicated in Figure 62, thus making it ideal for application to the two-dimensional terrain profiles used to define the 5 site classes in Figure 61. All of the calculated results presented in this album were obtained using the GTD reflection model.

This album contains a substantial amount of detailed information. Considering the performance curves, dephasing curves, and antenna and composite lobe patterns, each profile considered results in 32 curves drawn on 10 different graphs, for a total of 608 curves on 190 graphs. In addition, tables of path angle, width, and symmetry are given for each profile for all of the phase conditions investigated, and the optimum phasing and sideband power (A ratio) are given for each system. This album is designed to be an engineer's tool to be applied to siting and optimizing image-type ILS glide-slope systems.

The predictions in this album correlate quite well with those in Figure 61 regarding applicability of the different systems to specific site types. It must be pointed out, however, that site types 2,3, and 5 include an infinite number of different terrain profiles, and the results obtained for the few representative ones considered in this album probably do not include all of the various effects which might be encountered in actual installations. Despite this, it seems likely that an engineer faced with the task of choosing the best glide-slope system to install at a particular site might find it useful and informative to locate the terrain profile in this album which most closely resembles the actual site and consider the performance predictions given. Even after the system is chosen, problems with phasing the system, setting antenna heights, adjusting the sideband power for correct width, and for capture effect, successfully completing the phase verification procedure, may be avoided or mitigated after reference to the calculations contained in this album.

2. Modeling Parameters. The terrain is assumed to vary two-dimensionally as indicated in Figure 62, with the ground contour determined by the particular terrain profile. The ground is assumed to be perfectly conducting, a reasonably good approximation for the horizontally polarized waves and small grazing angles encountered in glide-slope modeling calculations.

The antenna positions are held constant for all of the calculations and are given in Table 4a. They are chosen to give a 3.0° path angle on an ideal, horizontal site. All angles are measured at the base of the mast and are with respect to the horizon.

---

* Also see Section IIA of this report.

1·0   2·8   2·5

2·15   2·2

3·5   2·0

1·1   1·8

1·25   1·4   1·6

NATIONAL BUREAU OF STANDARDS
MICROCOPY RESOLUTION TEST CHART
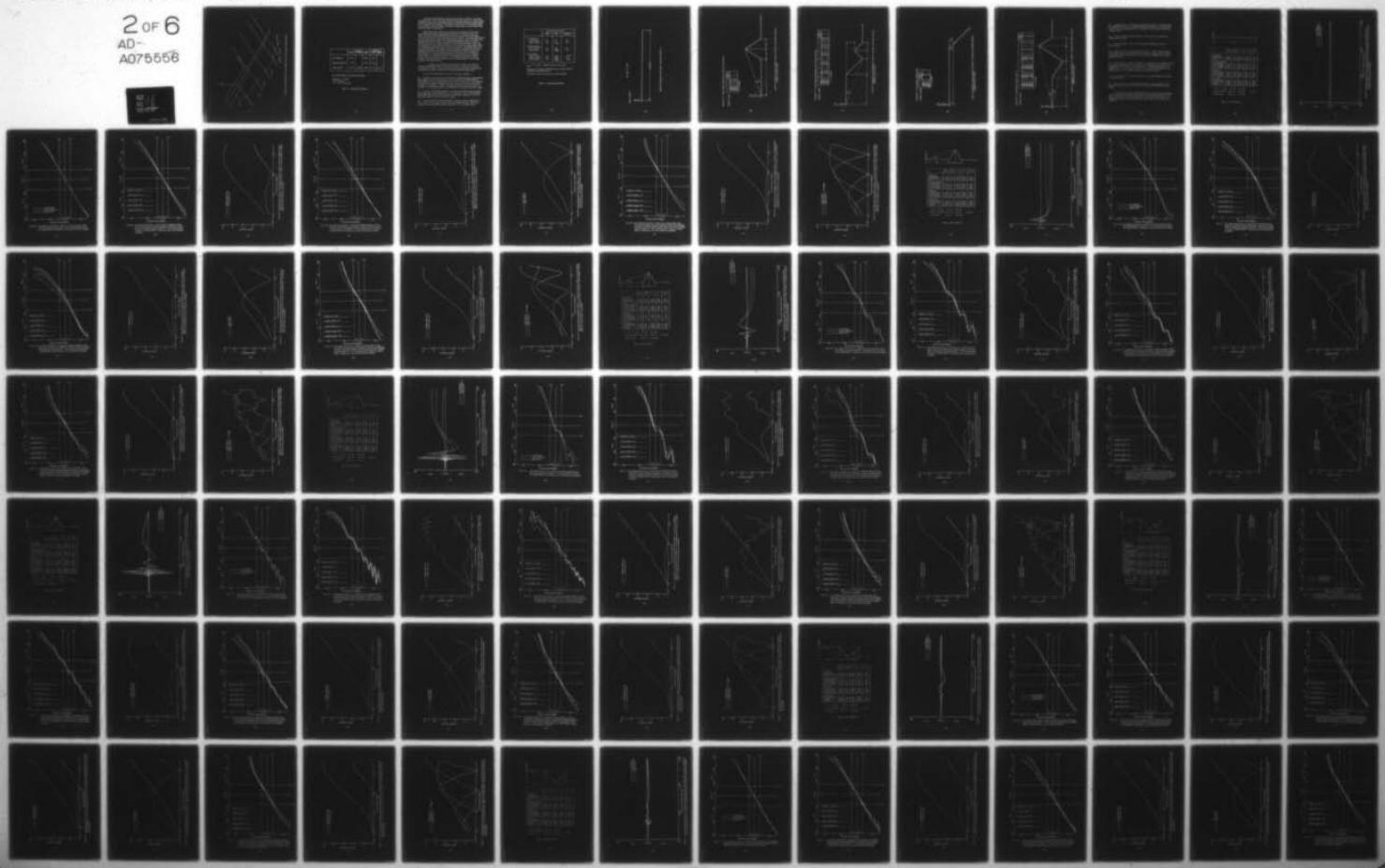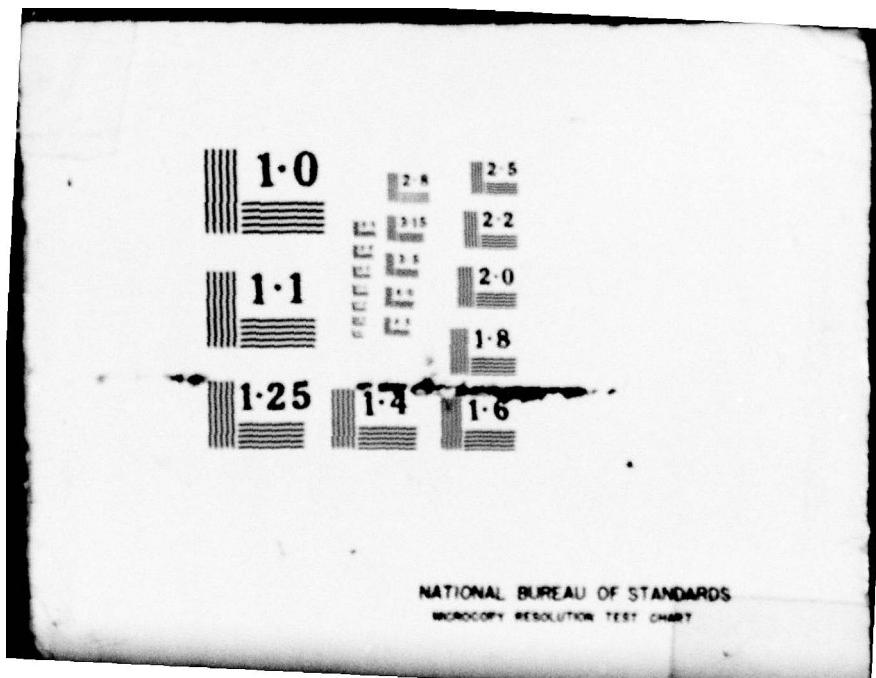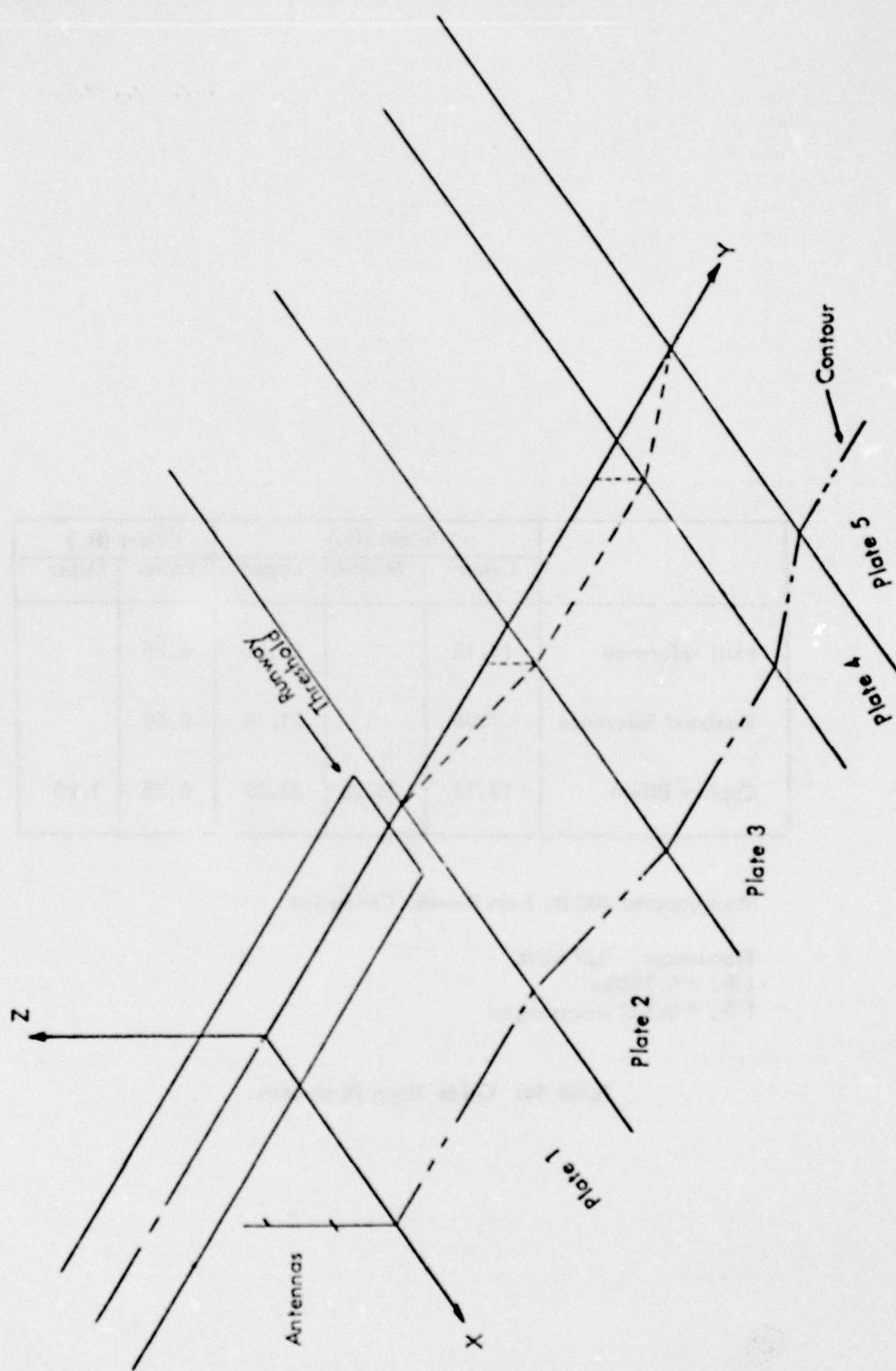
Figure 62. Three-Dimensional Terrain Model from Two-Dimensional Terrain Contour.

	Height (ft.)			Offset (ft.)	
	Lower	Middle	Upper	Lower	Upper
Null Reference	14.13		28.26	0.75	
Sideband Reference	7.06		21.18	0.50	
Capture Effect	14.13	28.26	42.39	0.75	1.25

Mast Located 400 ft. from Runway Centerline

Frequency: 332 MHz
1 ft. = 0.3048m
1 ft. = 0.337 wavelengths

Table 4a. Glide Slope Parameters.

The signal powers delivered to each antenna are given in Table 4b. The powers are normalized to 1 watt carrier power delivered to the lower antenna, but may be linearly scaled to any power level. The sideband power is adjusted for each terrain profile to give a 0.70° path width when possible. The resulting A ratio is given in the parameter tables for each profile, and can be readily converted to sideband power into each antenna using the formula given in Table 4b. [B]

Before determination of the A ratio the antennas are phased so that the total signal from each antenna, including ground reflections, is in phase at a point 1.0° above horizontal and 1000' (300m) directly above the runway centerline (extended). This would correspond to using airborne phasing at an actual site. All phasing perturbations are given relative to this initial antenna phasing determination, which is included in the parameter table for each profile. It is evident that phasing the antennas using this criterion often results in a system that does not have symmetrical changes in path width when dephasing plus and minus symmetrically or, in the case of the capture effect system, will not seemingly satisfy the phasing verification procedure. Consideration of the very rough radiation patterns which result from the uneven terrain reflections indicates that the effects of dephasing will not be the same for uneven terrain as for perfectly flat, horizontal ground. Thus phasing the system for minimum path width, or symmetrical width changes, or to satisfy the phase verification procedure will result in different relative phases when the terrain is uneven. The phasing technique chosen (airborne phasing) is commonly applied in the field due to its relative simplicity, and is simple to apply on the computer as well.

3. Results. The 19 different terrain profiles included in this album are described in Figures 63 through 67. Each profile is given a number, and the results are organized by number. To use the album, find the profile of interest, and look back in the results section for the table and curves pertaining to that profile number.

For each profile the following curves are calculated and plotted:

(a)   Flyability (low approach) for Null Reference, Sideband Reference, Capture Effect. The simulated aircraft is flown above the runway centerline from 30,000' (9000m) to 1000' (300m) from the point opposite the antenna mast at a constant 3.0° angle (measured with respect to horizontal at the base of the mast). The plot is of Course Deviation Indication in microamperes vs. distance. The sideband power (A ratio) and phasing is as indicated in the corresponding table. The effects of CDI meter damping are not included.

(b)   Level Run for NR, SBR, CE Systems. The systems are phased as described above and the A ratio is set (when possible) for a 0.70° path width. The simulated aircraft is flown 1000' (300m) above the runway centerline (extended) at angles from 1.0 to 4.5° above the horizontal. The plot is of CDI vs. angle.

(c)   Level Run for NR with System Dephasing. The lower antenna is dephased +15, -15, +30, and -30° and a level run as in (b) is simulated for each case. The normal phasing case is also repeated from (b) for comparison. CDI vs. angle is plotted.

	Signal Powers (in watts)		
	CSB	SBO	Clearance
Null Reference			
Lower Antenna	1.0	0.0	0.0
Upper Antenna	0.0	P_{SBO}	0.0
Sideband Reference			
Lower Antenna	1.0	P_{SBO}	0.0
Upper Antenna	0.0	P_{SBO}	0.0
Capture Effect			
Lower Antenna	1.0	$\frac{1}{2}P_{SBO}$	.0375
Middle Antenna	0.25	P_{SBO}	0.0
Upper Antenna	0.0	$\frac{1}{2}P_{SBO}$	.0375

$$P_{SBO} = A^2 \cdot (0.4)^2 \cdot (.80235)^2 \text{ where A is the A ratio}$$

Measured with average-responding meter (i.e., Bird or Vector Voltmeter) at the antenna input.

Modulation Indices: 0.4 for Carrier, 0.9 for Clearance

Table 4b. Glide Slope Parameters.

Terrain Profile η_1

Site Type η_1: Ideal

5 Miles (8km)
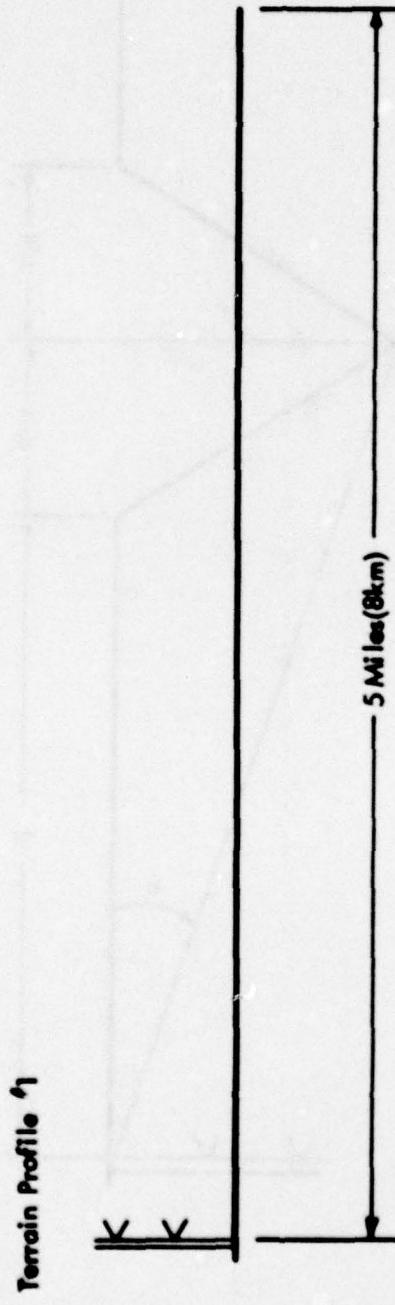
Figure 63. Dimensions of Site Type η_1 and Terrain Profile η_1.

Site Type #2: Terrain Slopes Upwards Above Initial Terrain Projected

Profiles Included:

d	a	Terrain Profile #
1000 ft.	0.5°	2
3000 ft.	0.5°	3
3000 ft.	1.0°	4
5000 ft.	1.0°	5

1 ft. = 0.3048m
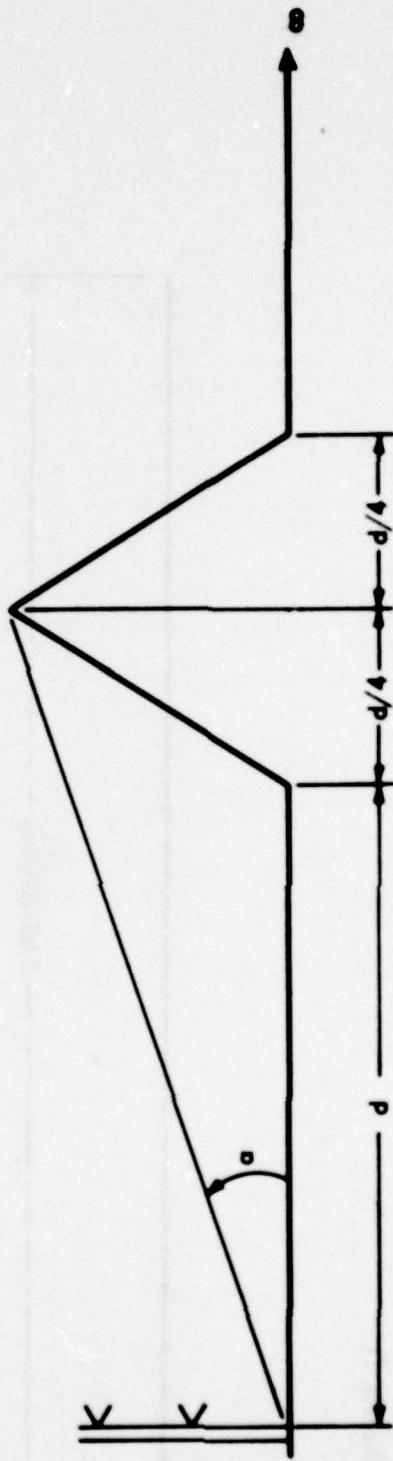
Figure 64. Dimensions of Terrain Profiles 2 through 5 Included in this Album which are Classified as Type #2 Sites.

Site Type #3: Terrain Slopes Upwards Below Initial Terrain Projected.

Profiles Included:

d	e	f	g	h	β	Terrain Profile #
1000 ft.	2,750 ft.	750 ft.	750 ft.	8.2 ft.	0.5°	6
3000 ft.	750 ft.	750 ft.	750 ft.	8.2 ft.	0.5°	7
3000 ft.	750 ft.	750 ft.	750 ft.	16.3 ft.	1.0°	8
5000 ft.	1,250 ft.	1,250 ft.	1,250 ft.	27.2 ft.	1.0°	9

1 ft. = 0.3048m
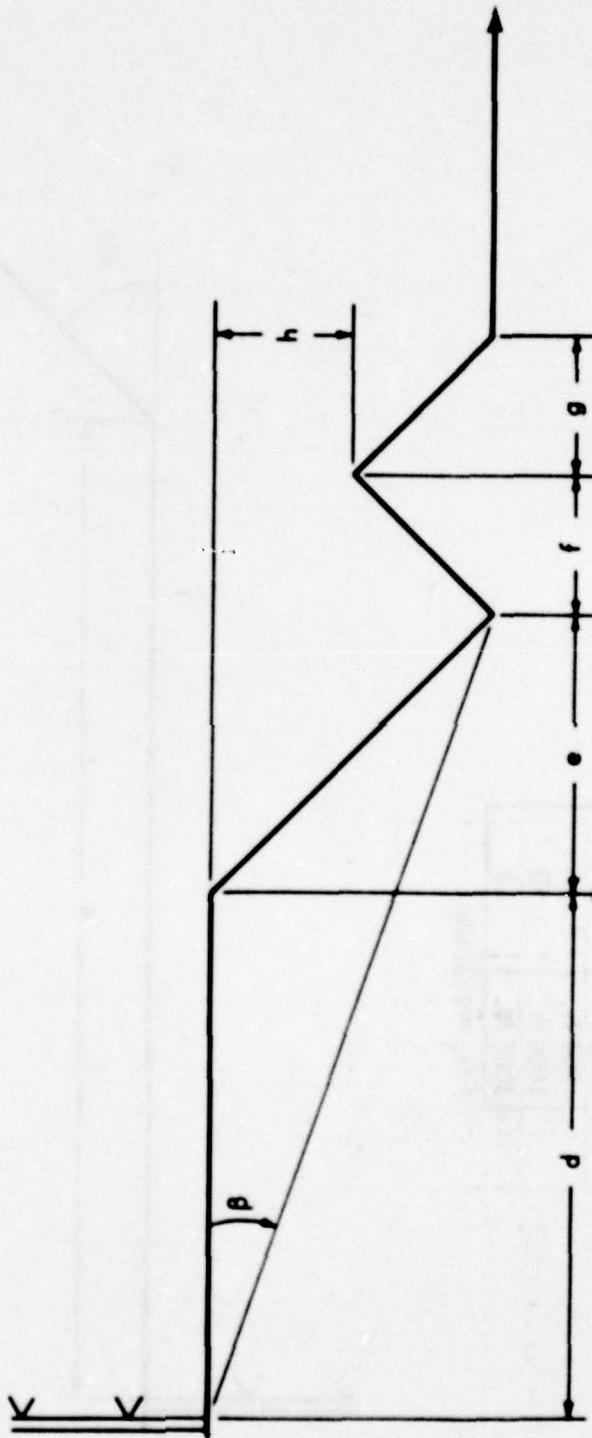
Figure 65. Dimensions of Terrain Profiles 6 through 9 Included in this Album which are Classified as Type #3 Sites.

Site Type #4: No Up-Slope; Limited Terrain

Profiles Included:

d	Terrain Profile #
500 ft.	10
700 ft.	11
1000 ft.	12
3000 ft.	13

1 ft. = 0.3048m
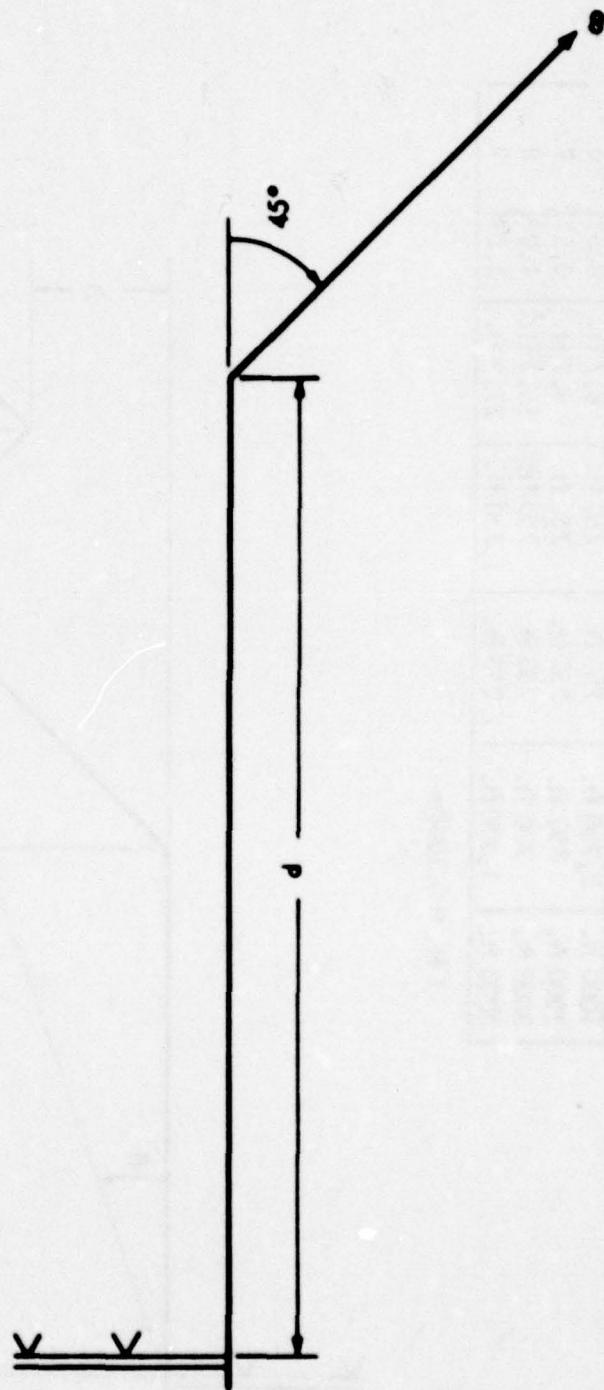
Figure 66. Dimensions of Terrain Profiles 10 through 13 Included in this Album which are Classified as Type #4 Sites.

Site Type #5: Combination of Types #2 and #3

Profiles Included:

d	e	f	g	a	β	Terrain Profile #
1000 ft.	7000 ft.	2000 ft.	2000 ft.	.5°	.5°	14
3000 ft.	5000 ft.	2000 ft.	2000 ft.	.5°	.5°	15
5000 ft.	3000 ft.	2000 ft.	2000 ft.	.5°	.5°	16
1000 ft.	250 ft.	1000 ft.	250 ft.	.5°	.5°	17
3000 ft.	750 ft.	3000 ft.	750 ft.	.5°	.5°	18
5000 ft.	3000 ft.	2000 ft.	2000 ft.	1.0°	1.0°	19

1 ft. = 0.3048m
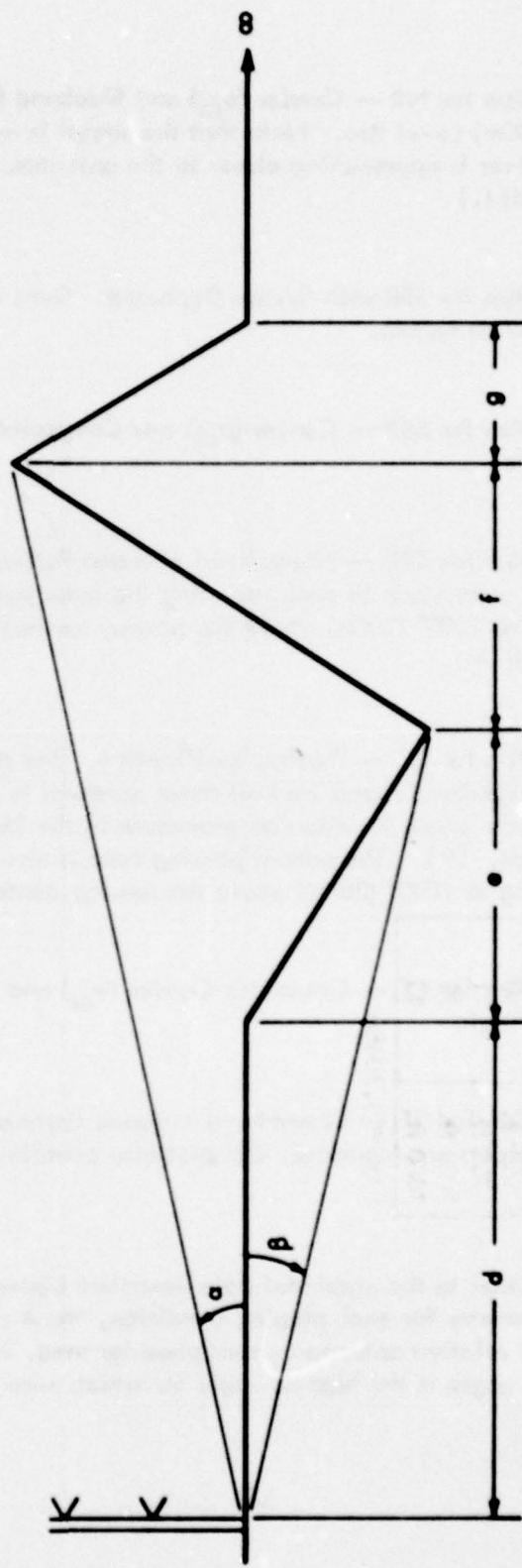
Figure 67. Dimensions of Terrain Profiles 14 through 19 Included in this Album which are Classified as Type #5 Sites.

-83-

(d)   Level Run for NR -- Carrier (e_{cs}) and Sideband (e_{ss}) Signals vs. Elevation Angle for a 1000' (300m) Level Run. Note that the signal levels increase with elevation angle since the receiver is approaching closer to the antennas. (The NR antenna patterns are included in plot j.)

(e)   Level Run for SBR with System Dephased. Same as (c) previous page but for sideband reference system.

(f)   Level Run for SBR -- Carrier (e_{cs}) and Composite Sideband (e_{ss}) Signals vs. Elevation Angle.

(g)   Level Run for SBR -- Normalized Antenna Patterns. Signals radiated by upper and lower SBR antennas with each radiating the same power as measured by a simulated aircraft flying at 1000' (300m) above the runway centerline (extended) with all ground reflections included.

(h)   Level Run for CE -- Phasing Verification. The middle antenna is dephased +15 and -15°, and the sideband signal into all three antennas is dephasing +30 and -30°. This corresponds to the phase verification procedure in the United States Standard Flight Inspection Manual. [9]   The normal phasing case is also repeated for comparison. The aircraft is flying at 1000' (300m) above the runway centerline extended.

(i)   Level Run for CE -- Composite Carrier (e_{cs}) and Composite Sideband (e_{ss}) Signals vs. Elevation Angle.

(j)   Level Run for CE -- Normalized Antenna Patterns. Same as (g) above. Since the antenna heights are identical, this plot also contains the Null Reference antenna patterns.

In addition to the graphical data described above, a table containing path angle, width, and symmetry for each phasing condition, the A ratio required to obtain a 0.70° width, and the relative antenna current phasings used, is given for each profile. The tabulated path angle is the highest angle for which zero CDI occurs on the level run simulation.

5 Miles
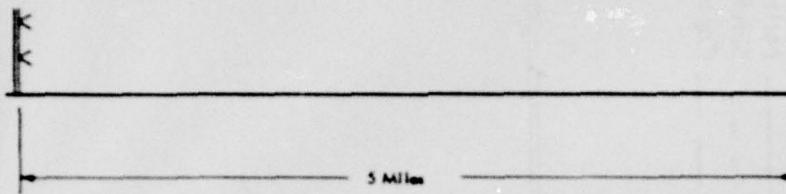
	Path Angle	Width Angle	+75 µA	-75 µA	Symmetry
Normal Phasing					
Null Reference	3.00	.70	2.65	3.35	.50
Sideband Reference	3.00	.70	2.65	3.35	.50
CEGS	3.00	.70	2.65	3.35	.50
Null Reference Dephased					
+15° Lower Antenna	3.00	.73	2.64	3.37	.50
-15° Lower Antenna	3.00	.73	2.64	3.37	.50
+30° Lower Antenna	3.00	.81	2.60	3.41	.50
-30° Lower Antenna	3.00	.81	2.60	3.41	.50
SBR Dephased					
+15° Lower Antenna	2.97	.73	2.61	3.33	.50
-15° Lower Antenna	2.97	.73	2.61	3.33	.50
+30° Lower Antenna	2.86	.82	2.45	3.26	.50
-30° Lower Antenna	2.86	.82	2.45	3.26	.50
CEGS Dephased					
+15° Middle Antenna	3.00	.73	2.63	3.36	.48
-15° Middle Antenna	3.00	.73	2.63	3.36	.48
+30° SBO	3.00	.81	2.60	3.41	.50
-30° SBO	3.00	.81	2.60	3.41	.50

"A" Ratio: NR .300 SBR .300 CEGS .300

Relative Phase NR/CEGS Upper 0° Middle 0° Lower 0°

Relative Phase SBR Upper 0° Lower 0°

Table 5. Terrain Profile #1.
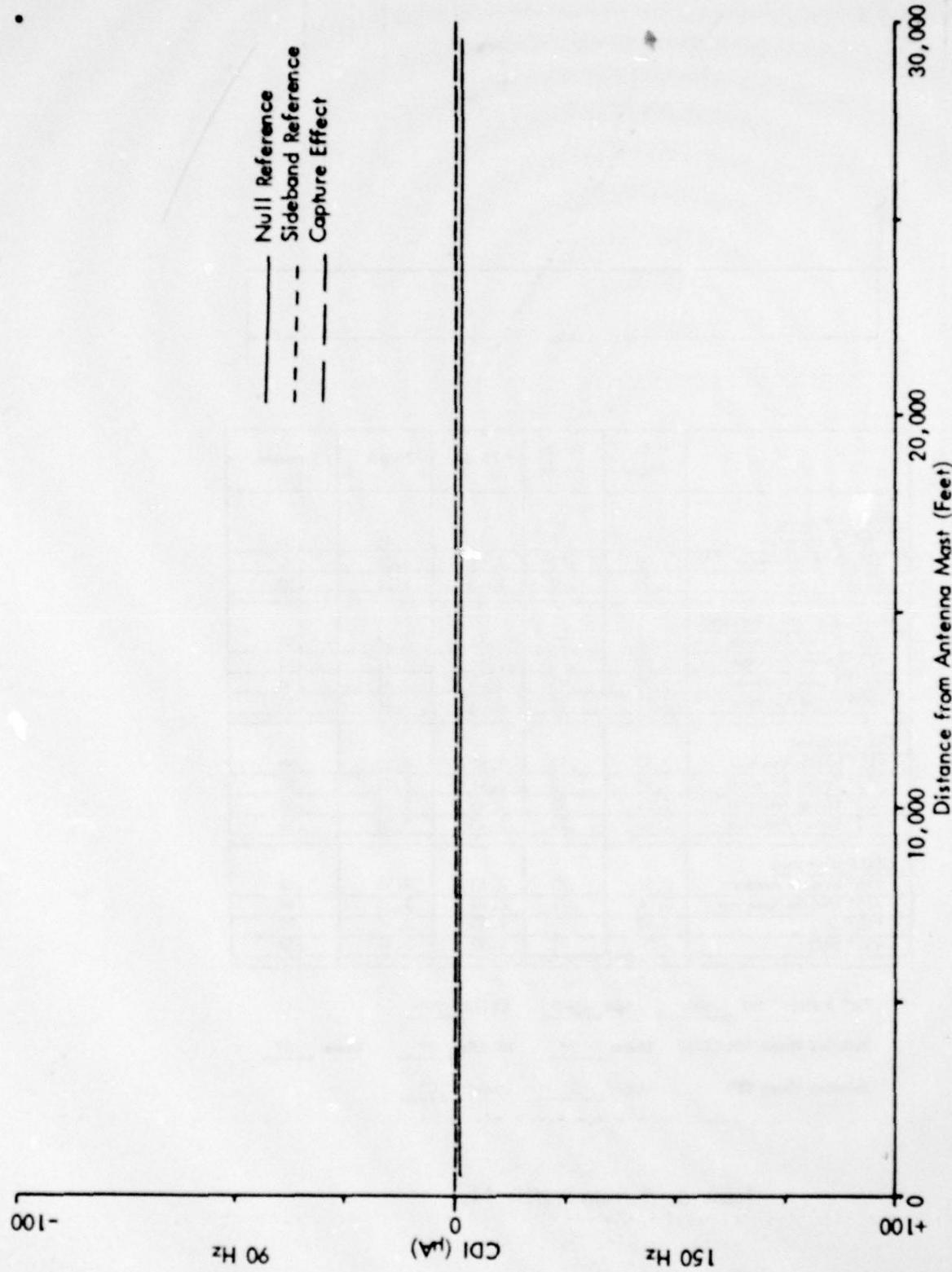
Figure 68a. Calculated Curves of CDI vs. Distance for the Three Image Type Glide-Slope Systems for Terrain Profile #1. The simulated aircraft is flying a constant 3.0 degree low approach over the runway centerline (extended).
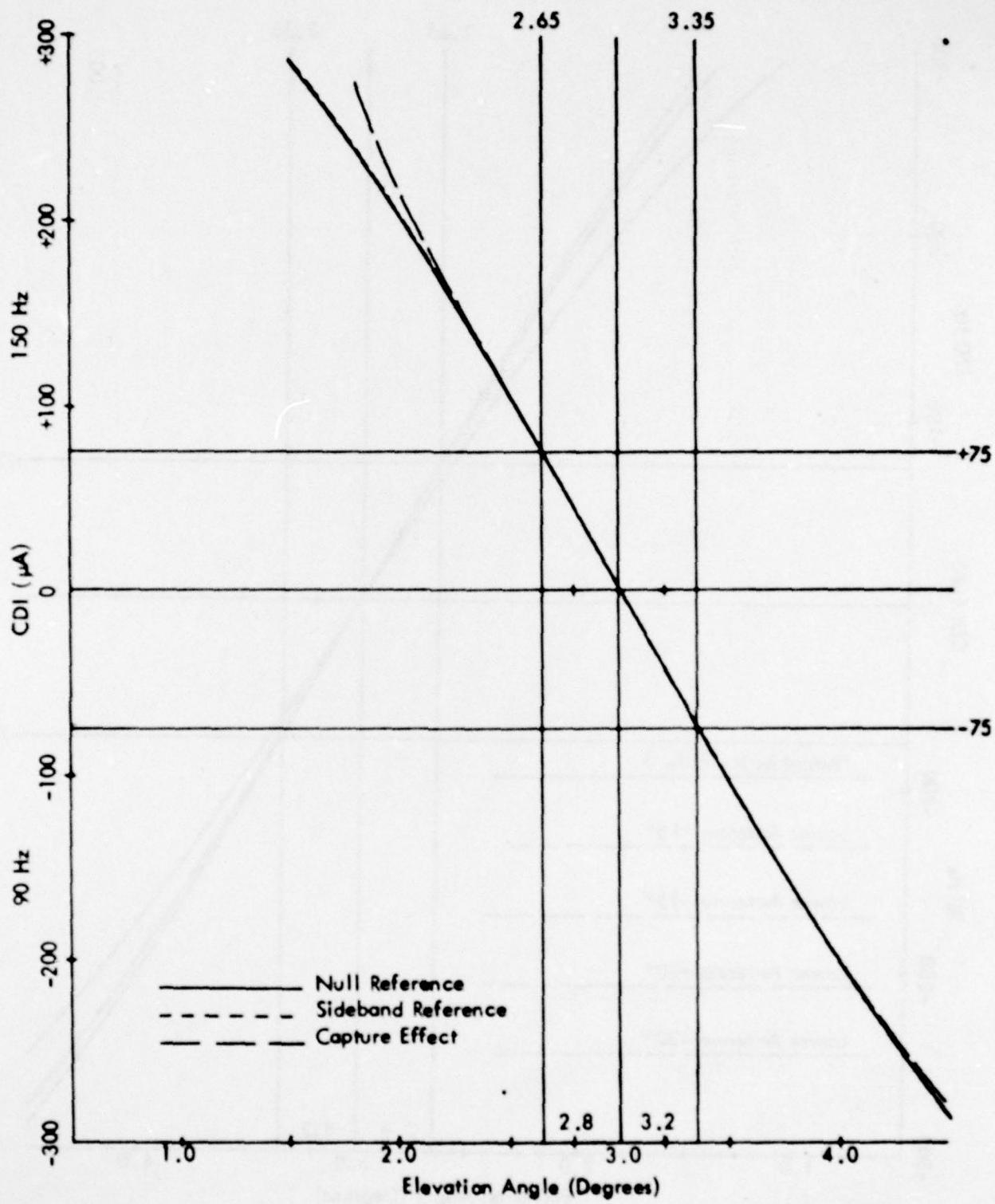
Figure 68b. Calculated Curves of CDI vs. Angle for the Three Image Type Glide-Slope Systems for Terrain Profile #1. The simulated aircraft is flying at a constant 1000 ft. altitude above the runway centerline (extended).
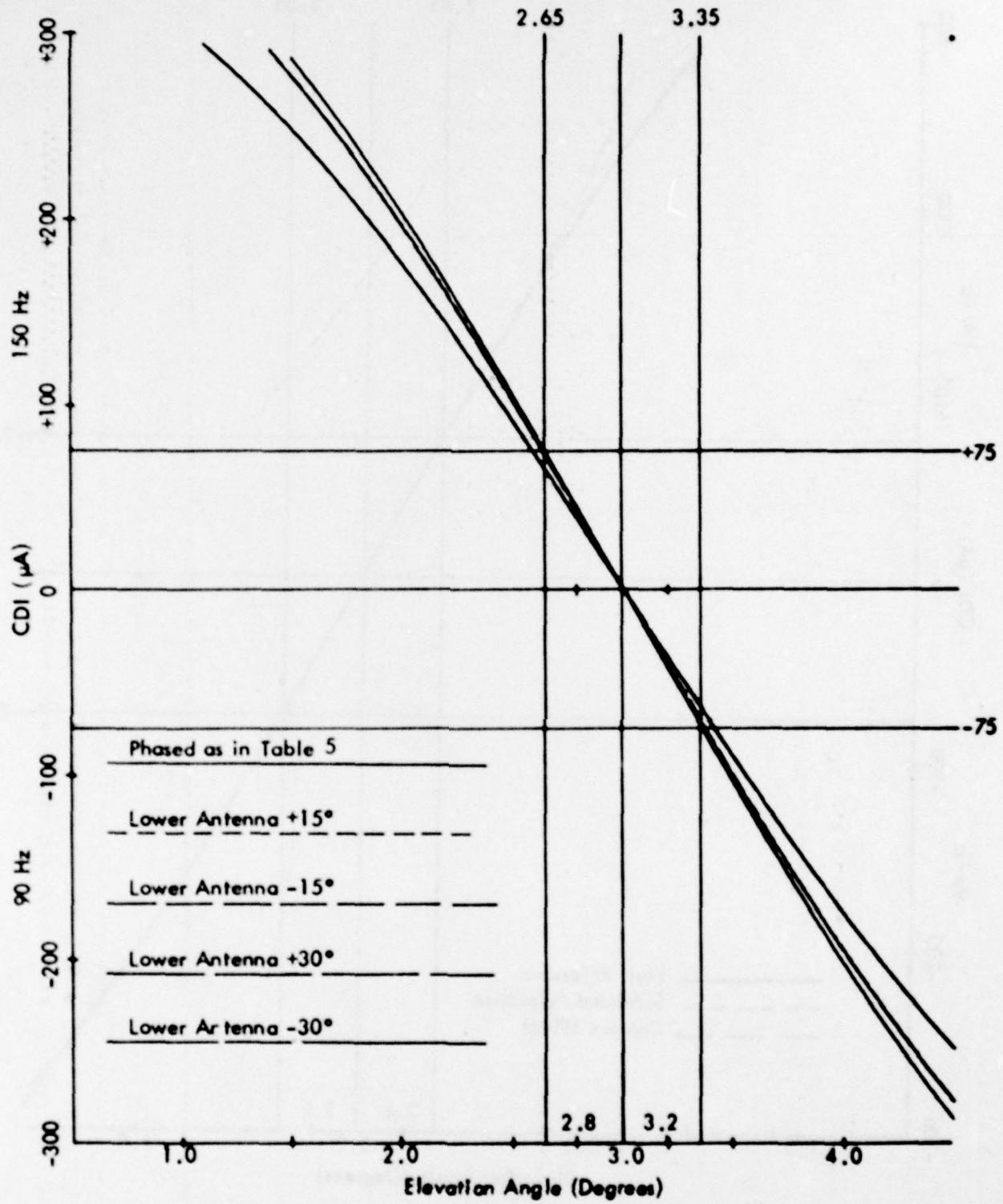
Figure 68c. Calculated Curves of CDI vs. Angle for the Null Reference Glide-Slope with the Normal Phasing (as indicated in Table 5) and Various Amounts of Dephasing for Terrain Profile #1. The simulated aircraft is flying at a constant 1000 ft. altitude above the runway centerline (extended).

-88-
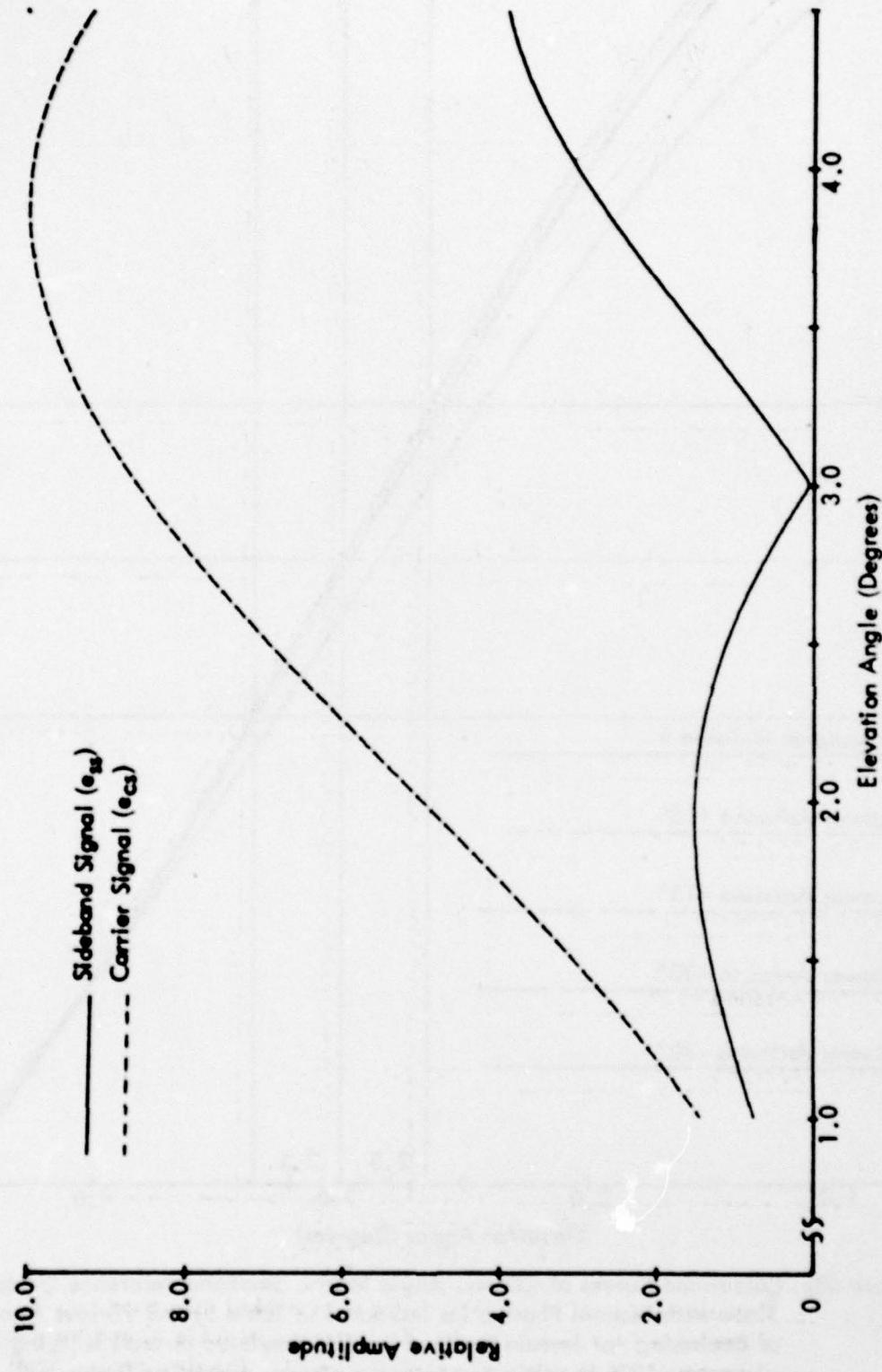
Figure 68d. Calculated Curves of Carrier and Sideband Signals vs. Angle for the Null Reference Glide Slope for Terrain Profile #1. The simulated aircraft is flying at a constant 1000 ft. altitude above the runway centerline (extended).
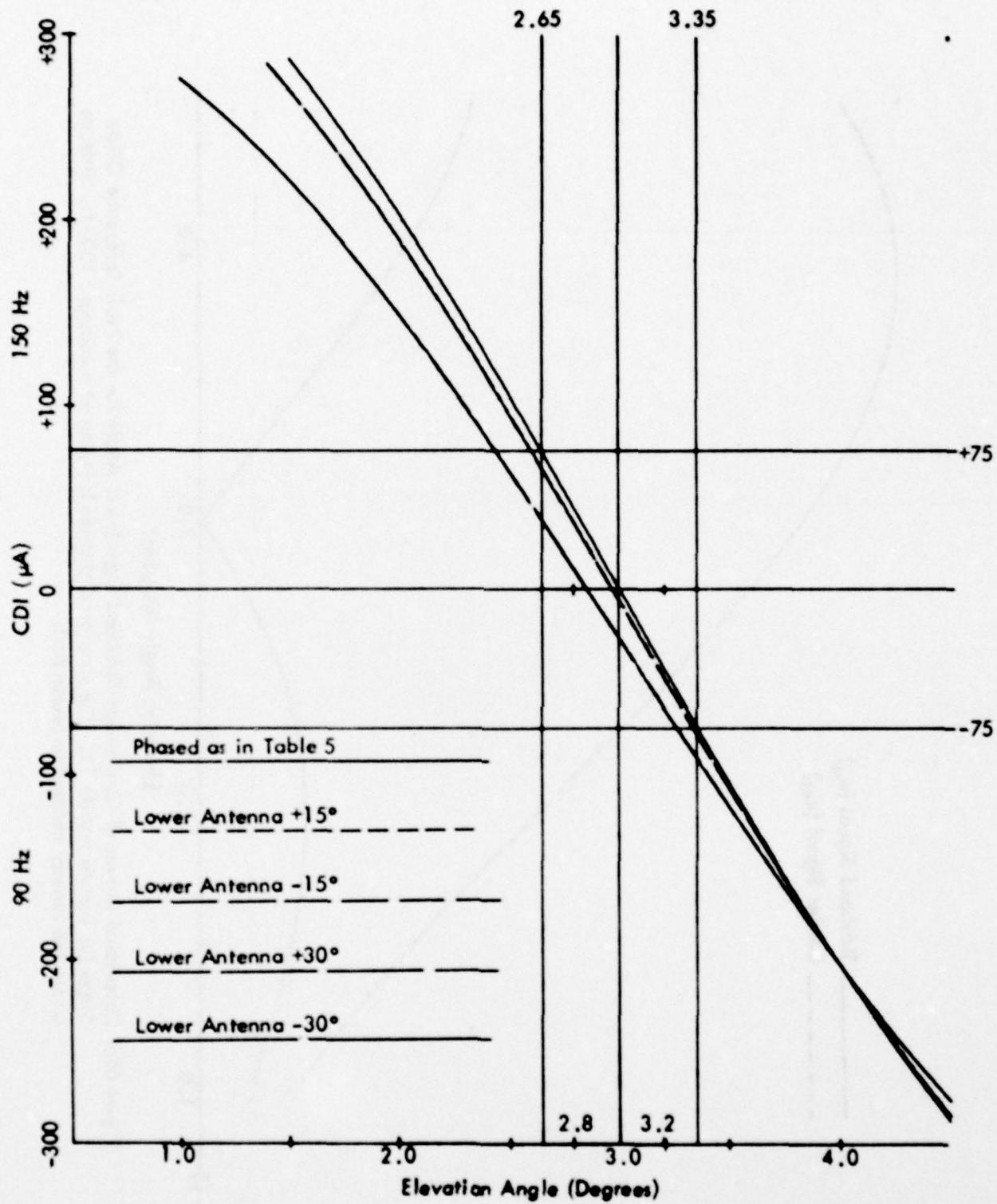
Figure 68e. Calculated Curves of CDI vs. Angle for the Sideband Reference Glide Slope with Normal Phasing (as Indicated in Table 5) and Various Amounts of Dephasing for Terrain Profile #1. The simulated aircraft is flying at a constant 1000 ft. altitude above the runway centerline (extended).

-90-
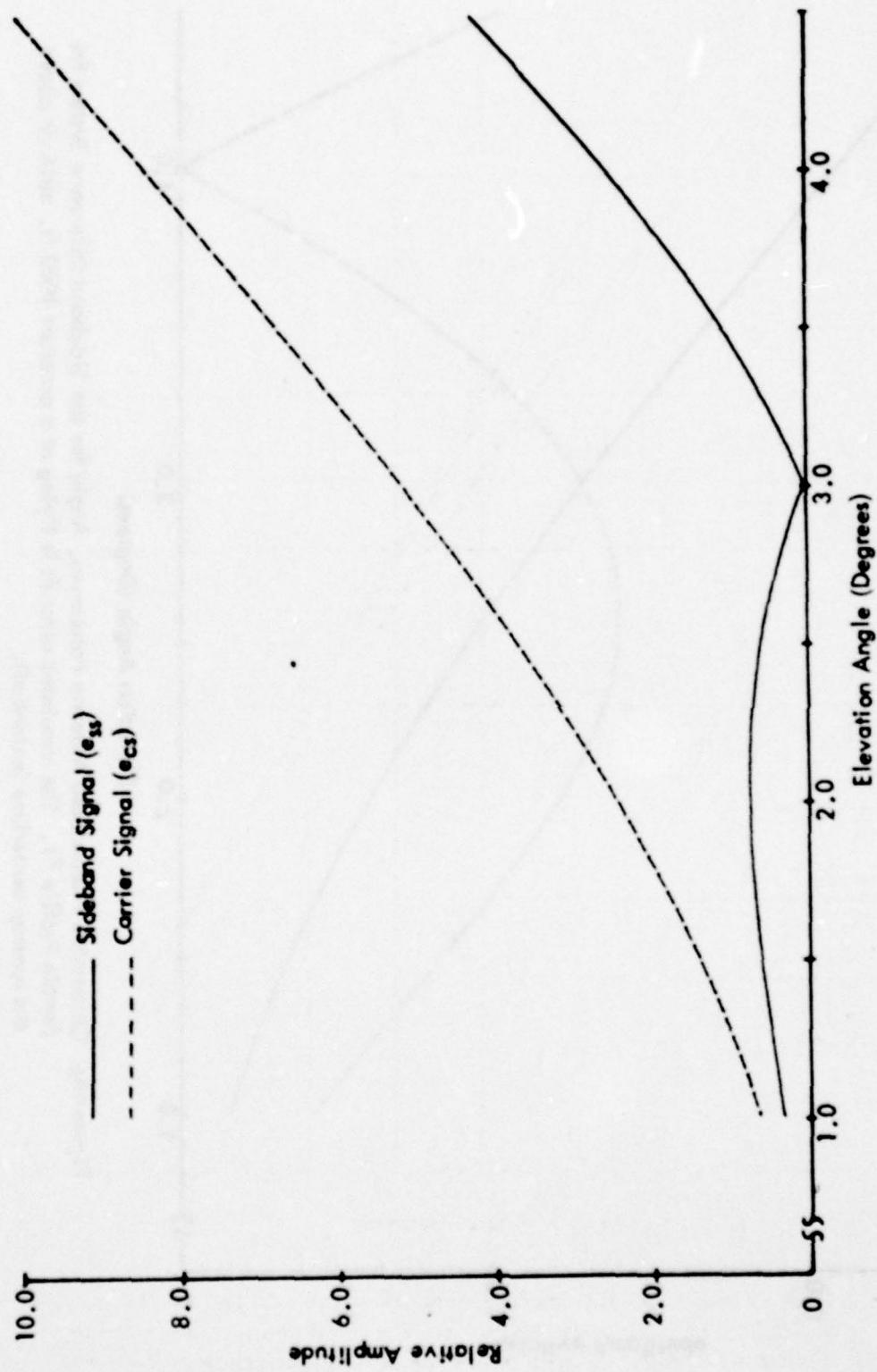
Figure 68f. Calculated Curves of Carrier and Composite Sideband Signals vs. Angle for the Sideband Reference Glide Slope for Terrain Profile #1. The simulated aircraft is flying at a constant 1000 ft. altitude above the runway centerline (extended).
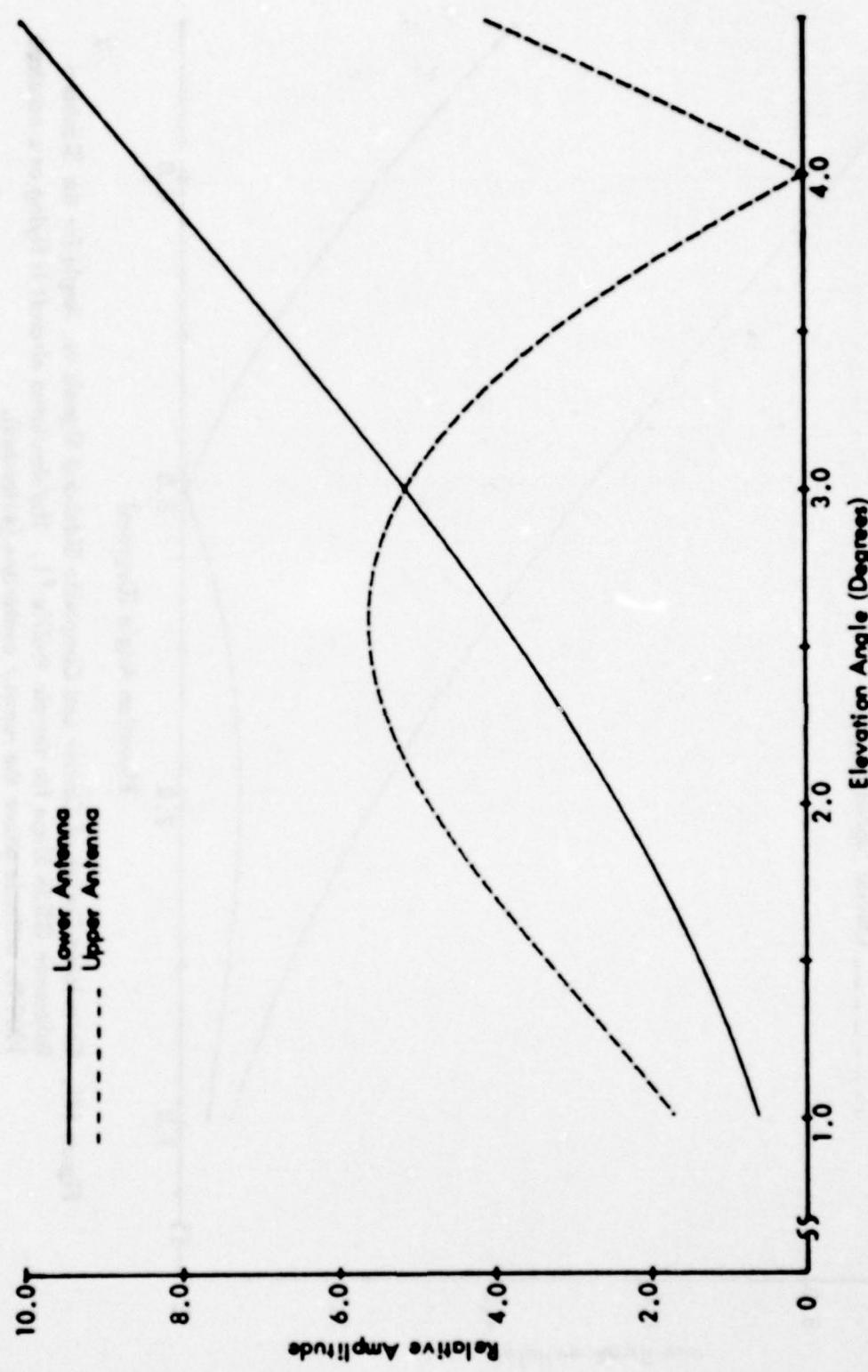
Figure 68g. Calculated Normalized Antenna Patterns vs. Angle for the Sideband Reference System for Terrain Profile #1. The simulated aircraft is flying at a constant 1000 ft. altitude above the runway centerline (extended).

Elevation Angle (Degrees)

Relative Amplitude

—————— Lower Antenna

- - - - - - - Upper Antenna
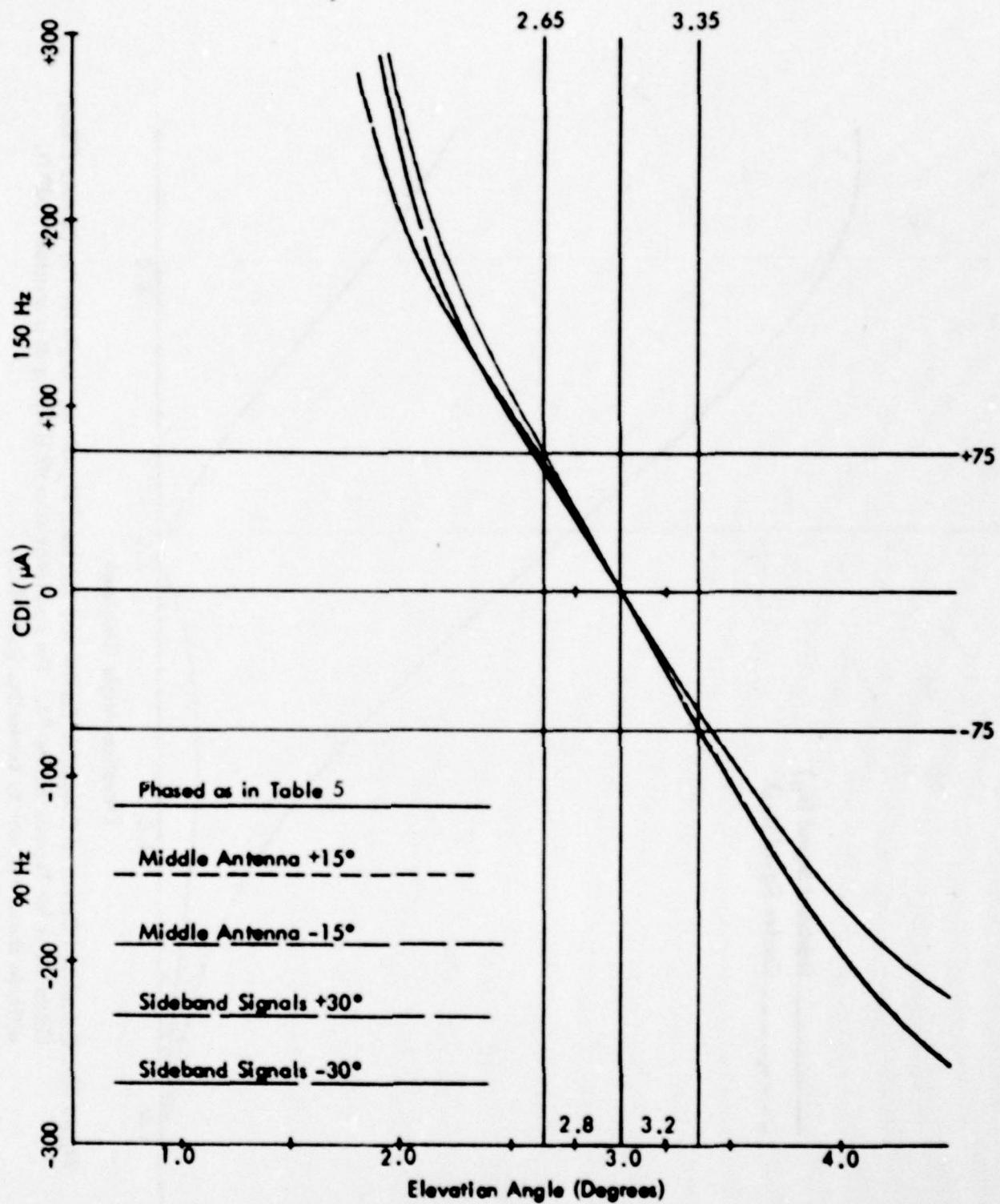
Figure 68h. Calculated Curves of CDI vs. Angle for the Capture Effect Glide
Slope with the Normal Phasing (as Indicated in Table 5) and Dephased
According to the Flight Inspection Manual Phase Verification Procedure
for Terrain Profile #1. The simulated aircraft is flying at a constant
1000 ft. altitude above the runway centerline (extended).

-93-
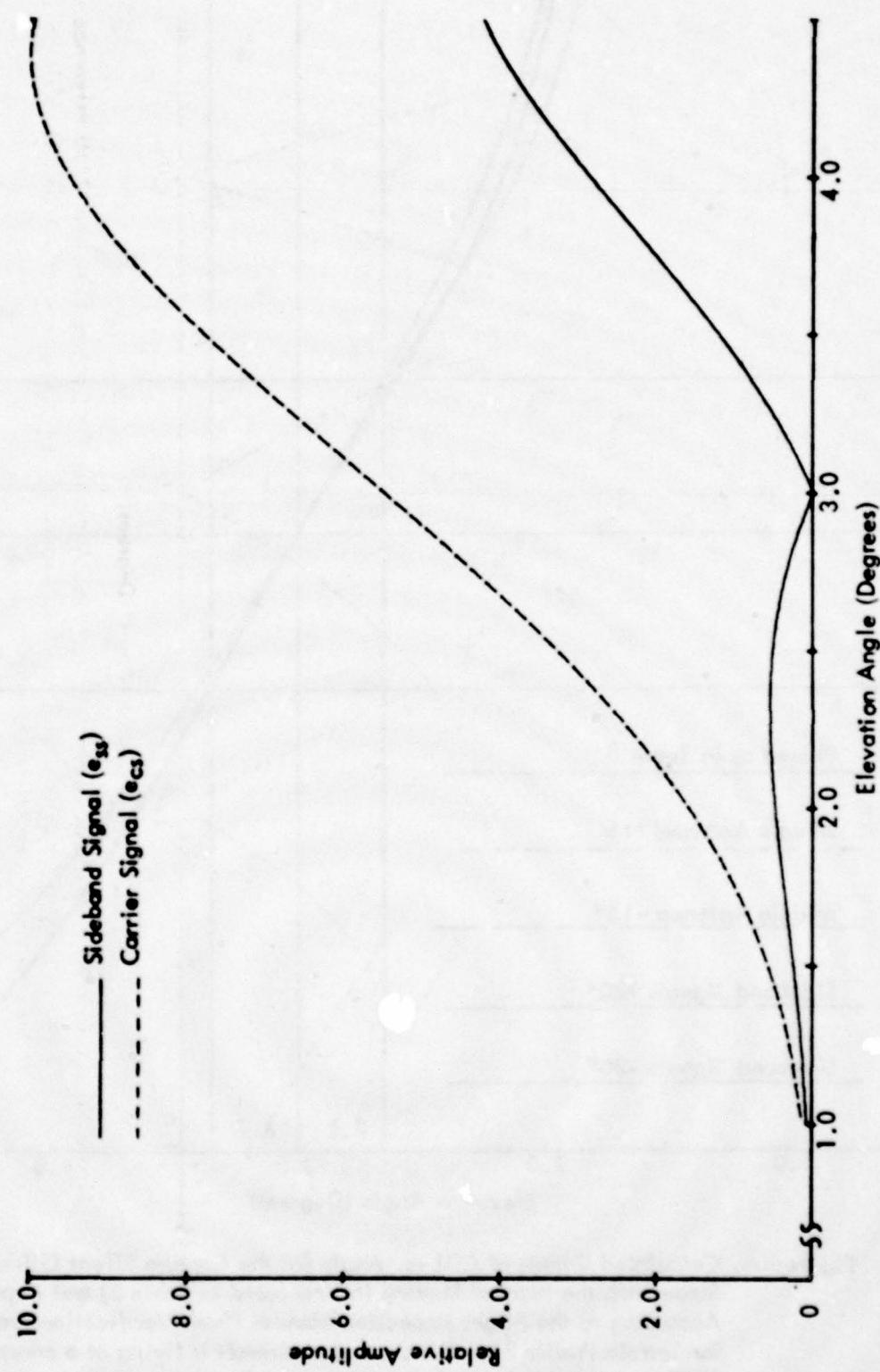
Figure 68i. Calculated Curves of Composite Carrier and Sideband Signals vs. Angle for the Capture Effect Glide Slope for Terrain Profile #1. The simulated aircraft is flying at a constant 1000 ft. altitude above the runway centerline (extended).

Figure 68j. Calculated Normalized Antenna Patterns vs. Angle for the Capture Effect and Null Reference Systems for Terrain Profile #1. The simulated aircraft is flying at a constant 1000 ft. altitude above the runway centerline (extended).

Relative Amplitude

Elevation Angle (Degrees)

Lower Antenna
Middle Antenna (NR Upper)
Upper Antenna
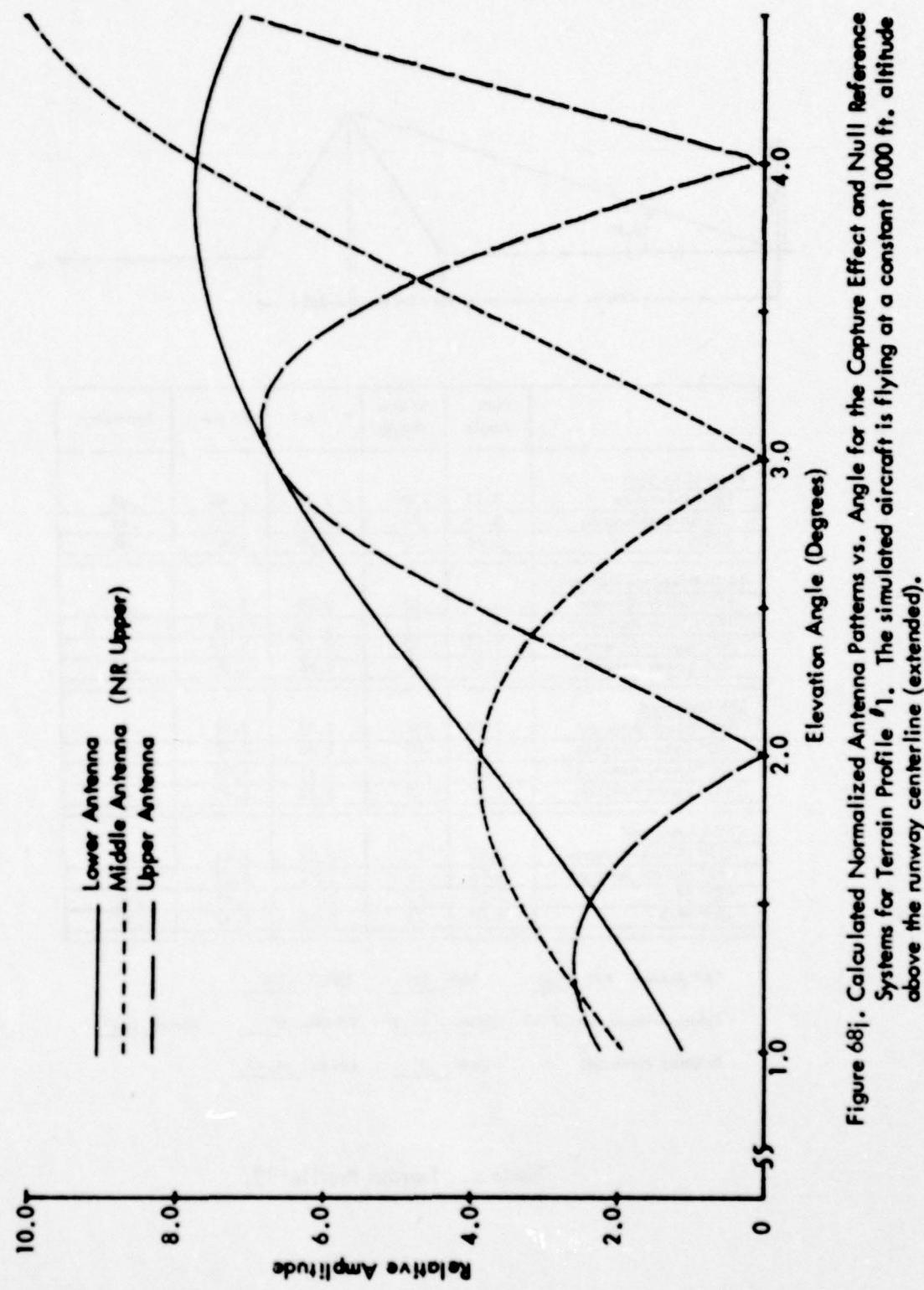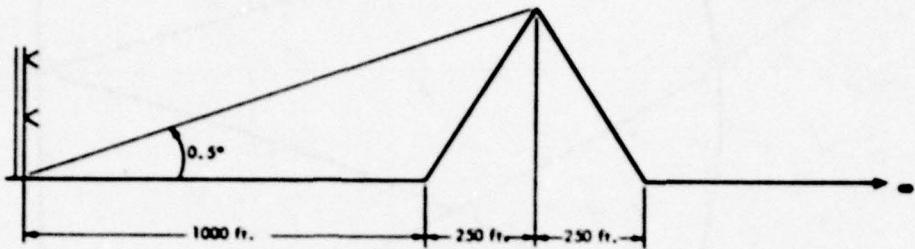
	Path Angle	Width Angle	+ 75 µA	- 75 µA	Symmetry
Normal Phasing					
Null Reference	3.17	.70	2.78	3.48	.44
Sideband Reference	3.14	.70	2.75	3.45	.45
CEGS	3.08	.70	2.70	3.40	.46
Null Reference Dephased					
+15° Lower Antenna	3.15	.67	2.78	3.45	.45
-15° Lower Antenna	3.19	.77	2.75	3.52	.43
+30° Lower Antenna	3.13	.70	2.75	3.45	.45
-30° Lower Antenna	3.22	.93	2.66	3.59	.40
SBR Dephased					
+15° Lower Antenna	3.10	.68	2.73	3.42	.46
-15° Lower Antenna	3.10	.80	2.66	3.46	.44
+30° Lower Antenna	3.01	.74	2.61	3.34	.45
-30° Lower Antenna	2.97	1.08	2.34	3.42	.42
CEGS Dephased					
+15° Middle Antenna	3.09	.87	2.57	3.44	.40
-15° Middle Antenna	3.06	.68	2.71	3.39	.48
+30° SBO	3.08	.85	2.64	3.49	.48
-30° SBO	3.07	.75	2.68	3.43	.47

"A" Ratio: NR .266 SBR .282 CEGS .340

Relative Phase NR/CEGS Upper -8.3° Middle 0° Lower 2.5°

Relative Phase SBR Upper 0° Lower -1.4°

Table 6. Terrain Profile #2.
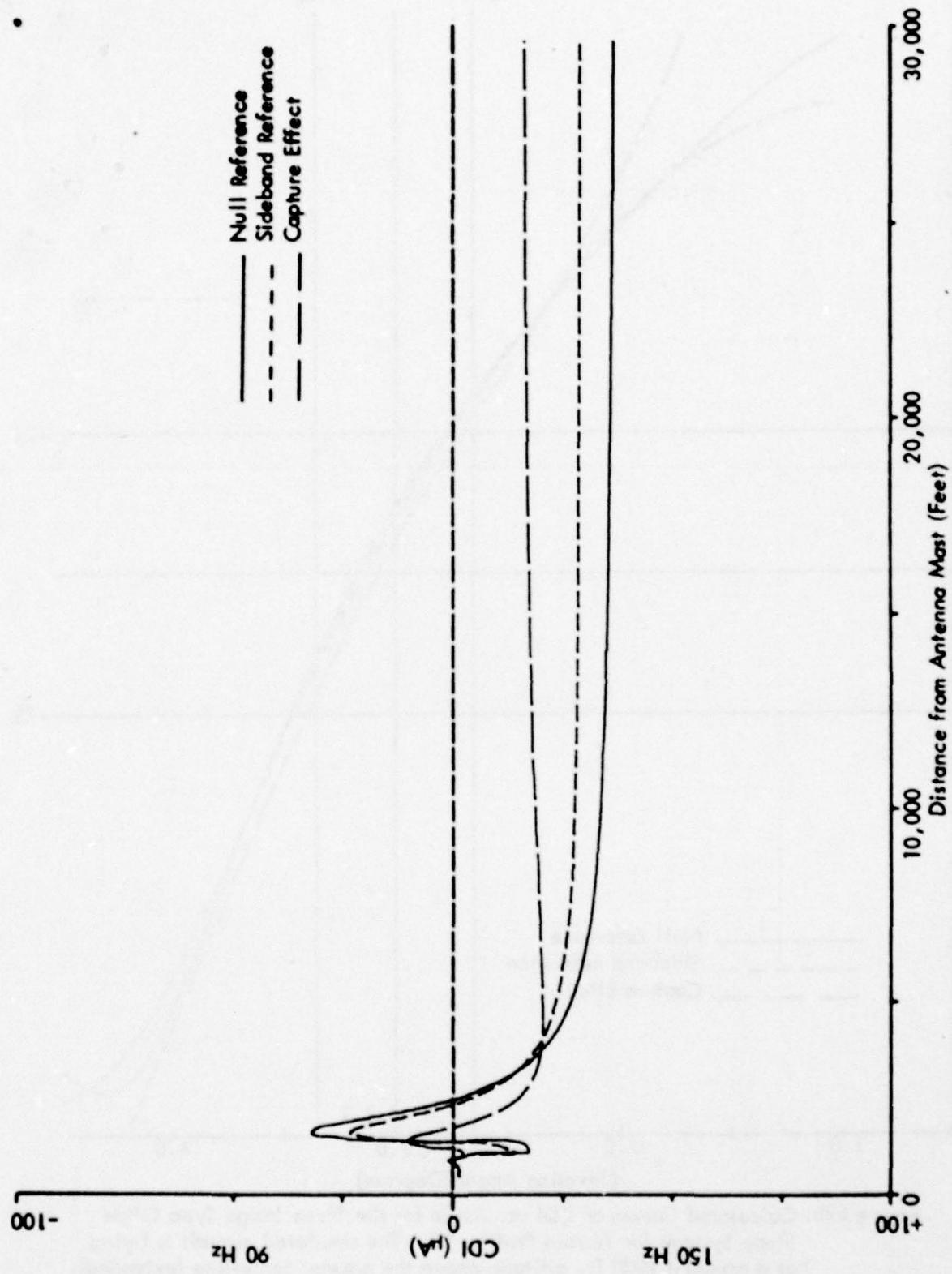
Figure 69a. Calculated Curves of CDI vs. Distance for the Three Image Type Glide Slope Systems for Terrain Profile #2. The simulated aircraft is flying a constant 3.0 degree low approach over the runway centerline (extended).

-97-
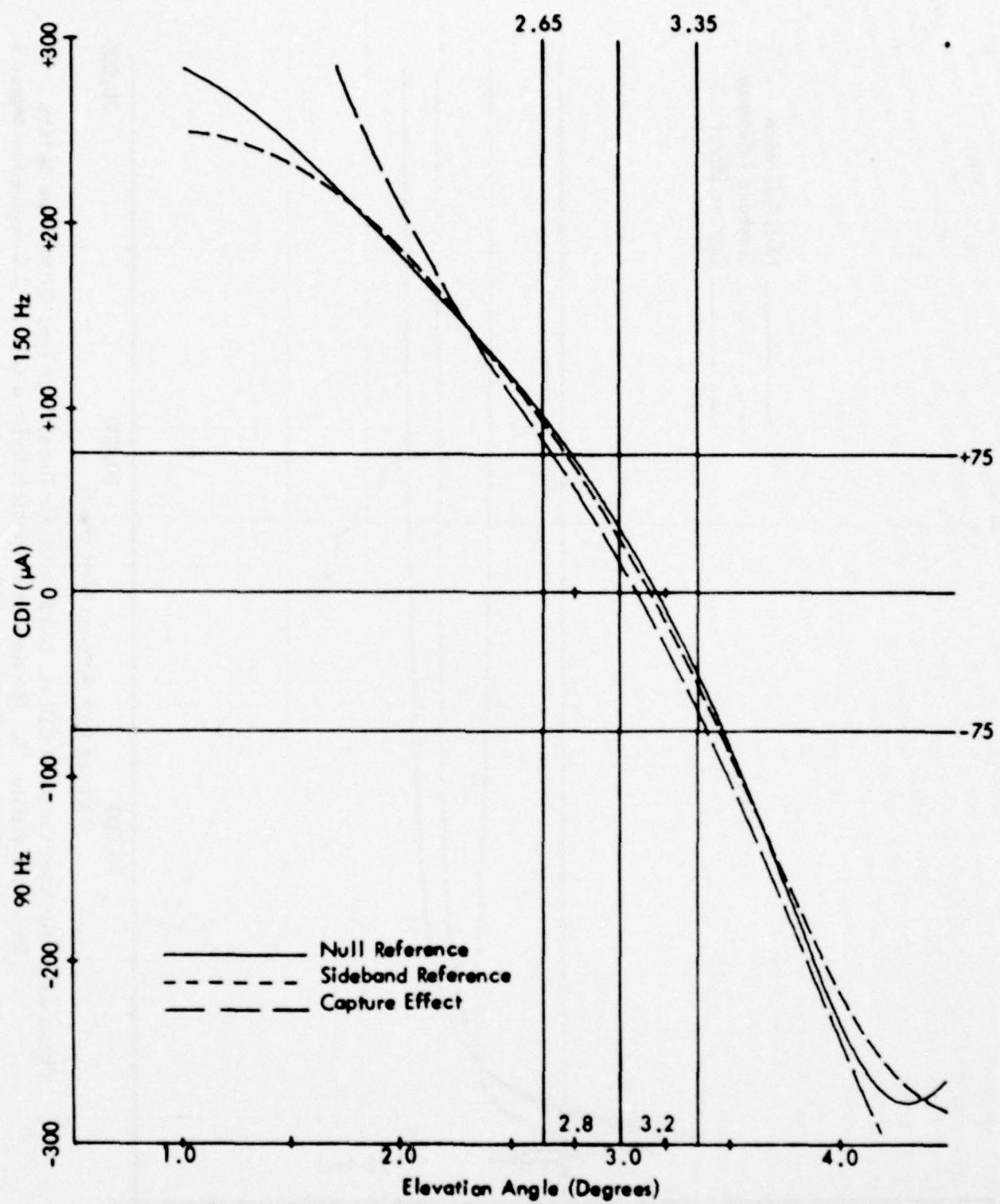
Figure 69b. Calculated Curves of CDI vs. Angle for the Three Image Type Glide Slope Systems for Terrain Profile #2. The simulated aircraft is flying at a constant 1000 ft. altitude above the runway centerline (extended).
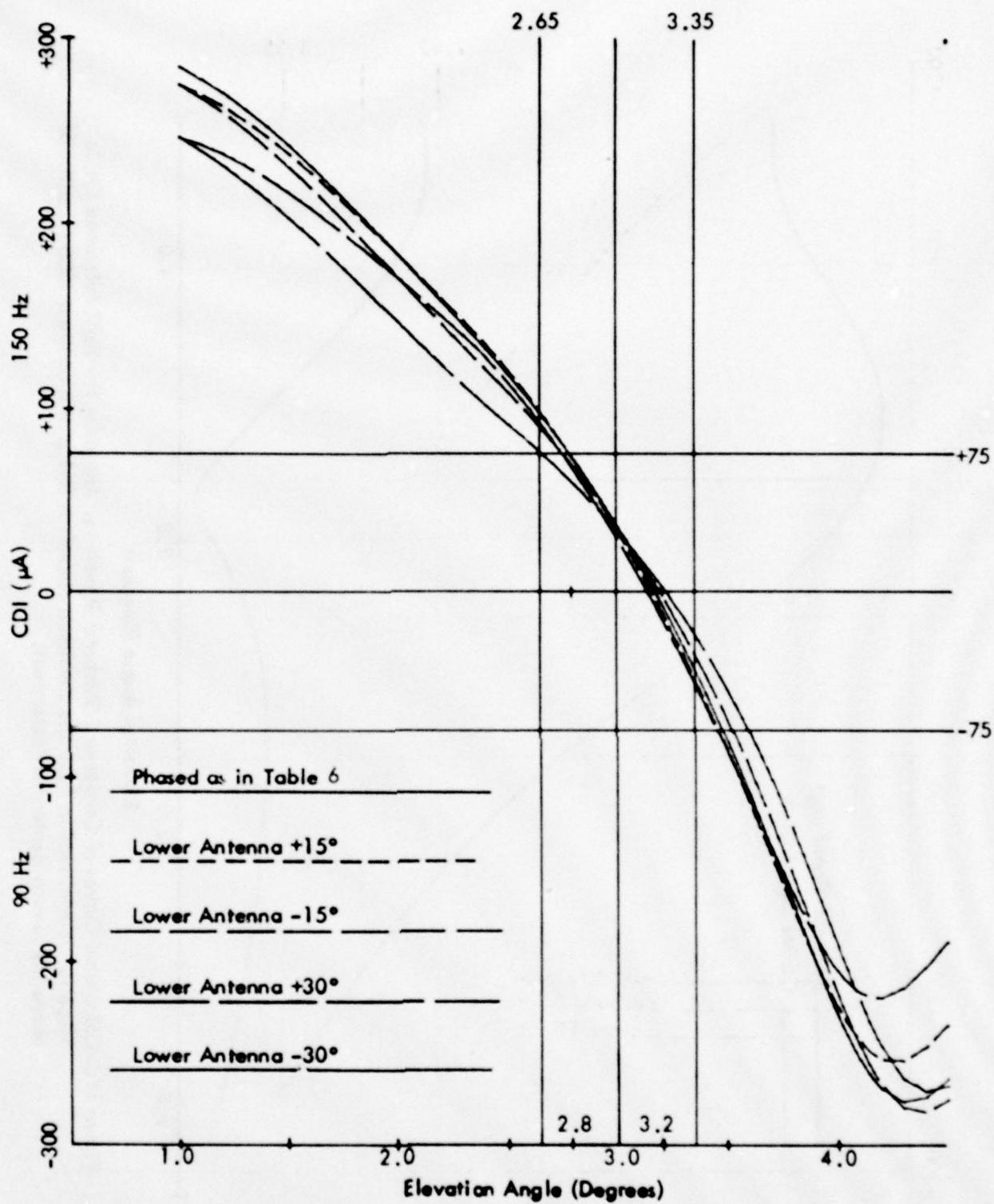
Figure 69c. Calculated Curves of CDI vs. Angle for the Null Reference Glide Slope with the Normal Phasing (as Indicated in Table 6) and Various Amounts of Dephasing for Terrain Profile #2. The simulated aircraft is flying at a constant 1000 ft. altitude above the runway centerline (extended).

-99-
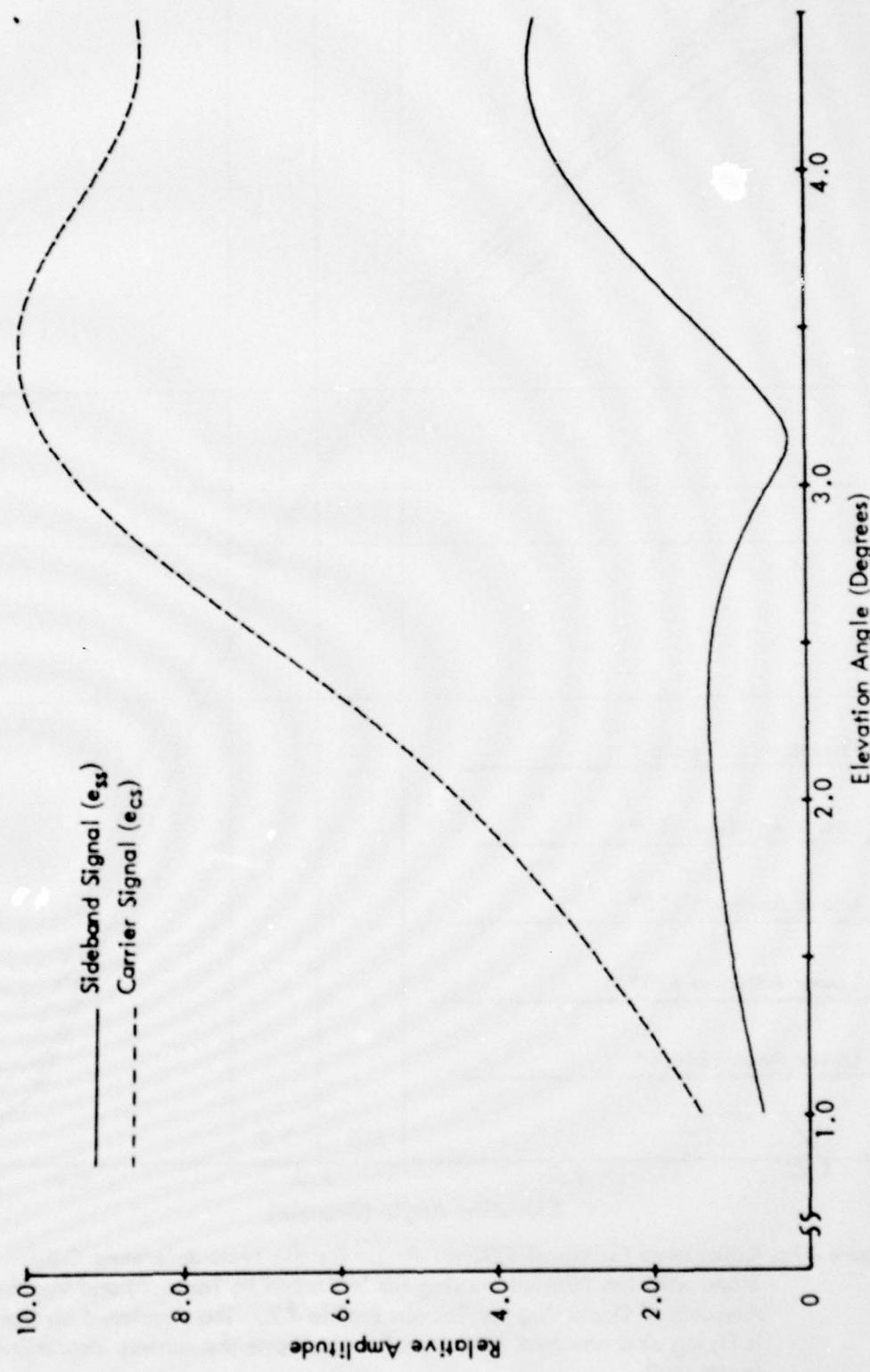
Figure 69d. Calculated Curves of Carrier and Sideband Signals vs. Angle for the Null Reference Glide Slope for Terrain Profile #2. The simulated aircraft is flying at a constant 1000 ft. altitude above the runway centerline (extended).
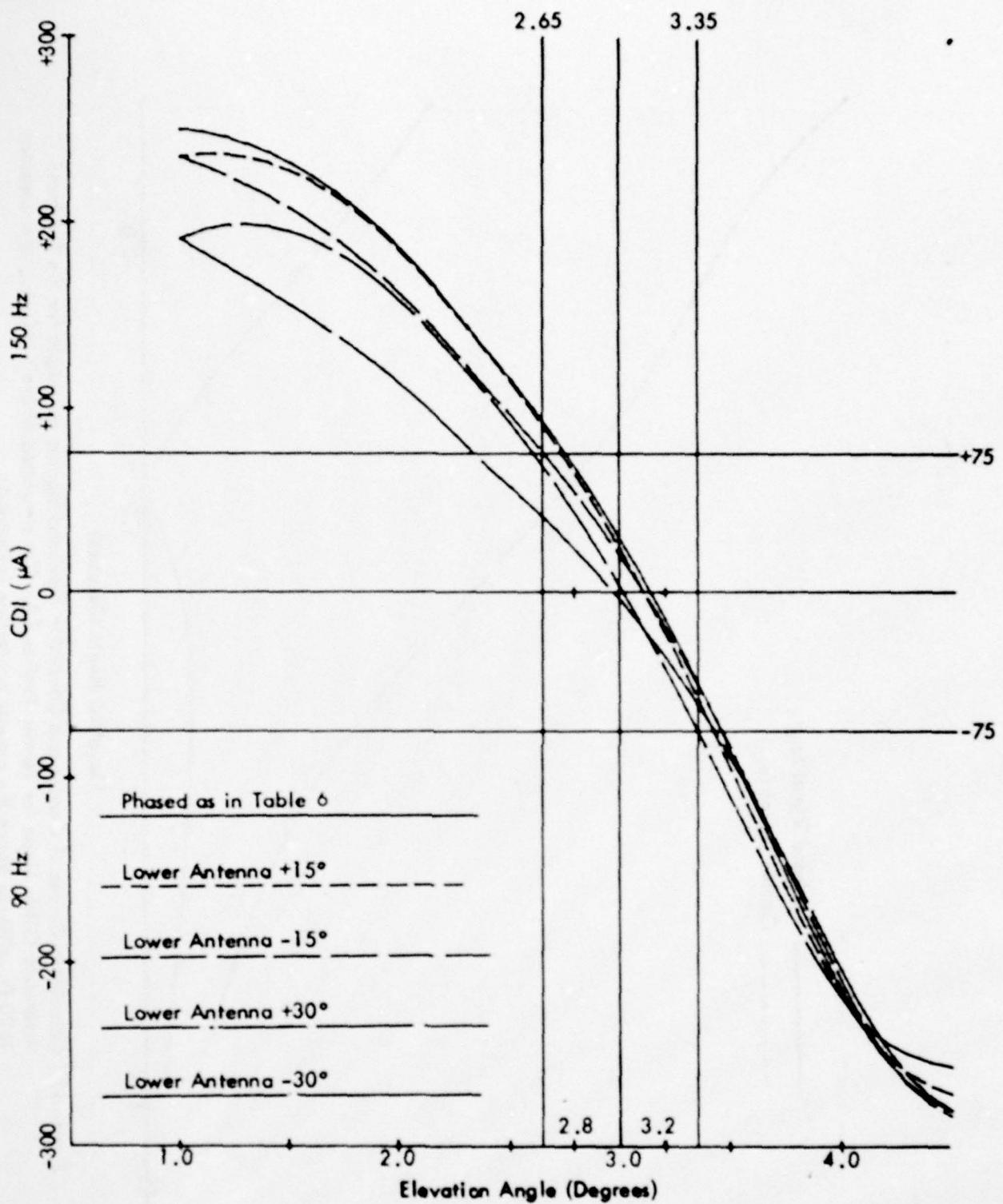
Figure 69e. Calculated Curves of CDI vs. Angle for the Sideband Reference Glide Slope with Normal Phasing (as Indicated in Table 6) and Various Amounts of Dephasing for Terrain Profile #2. The simulated aircraft is flying at a constant 1000 ft. altitude above the runway centerline (extended).
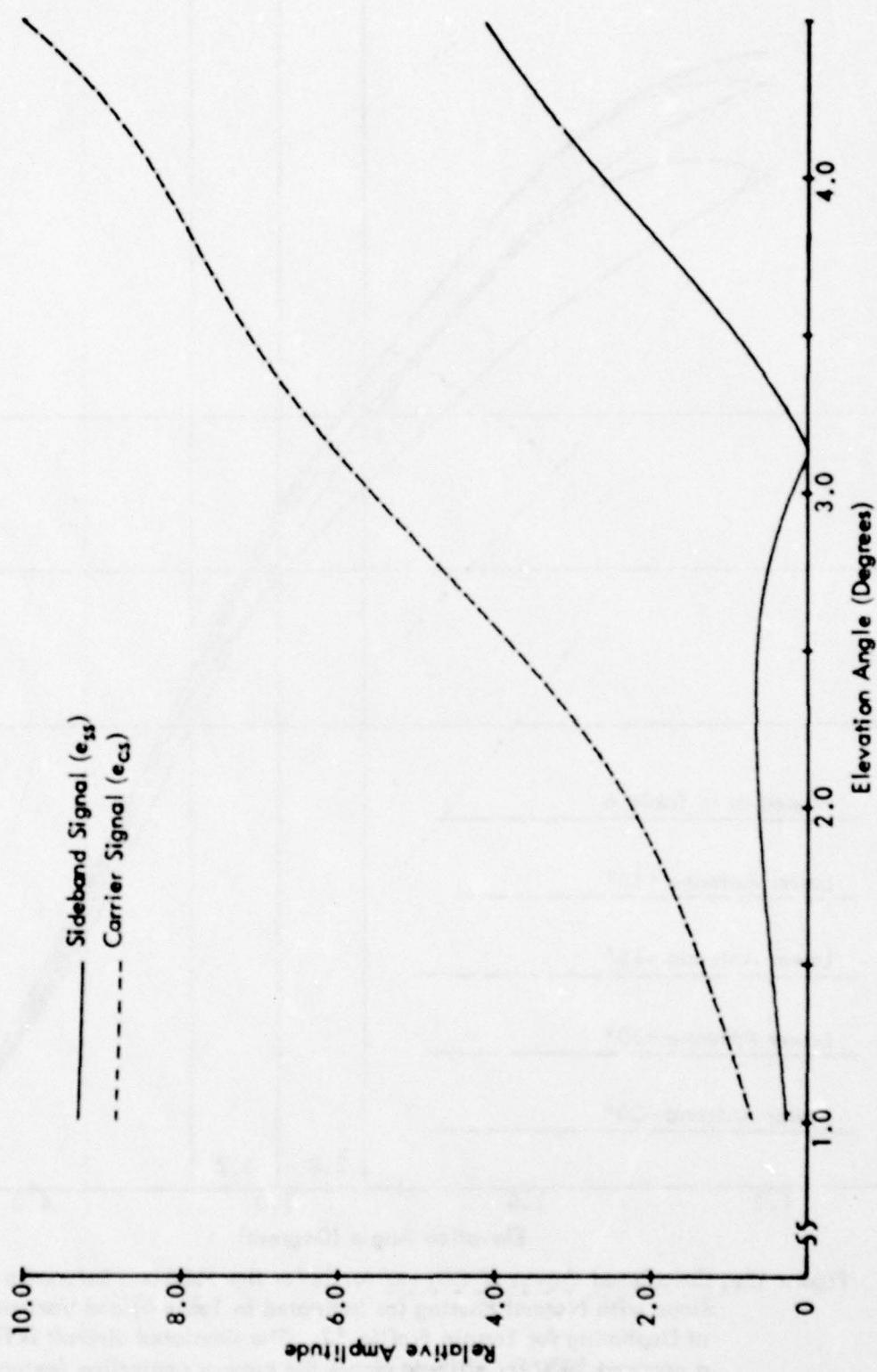
Figure 69f. Calculated Curves of Carrier and Composite Sideband Signals vs. Angle for the Sideband Reference Glide Slope for Terrain Profile #2. The simulated aircraft is flying at a constant 1000 ft. altitude above the runway centerline (extended).
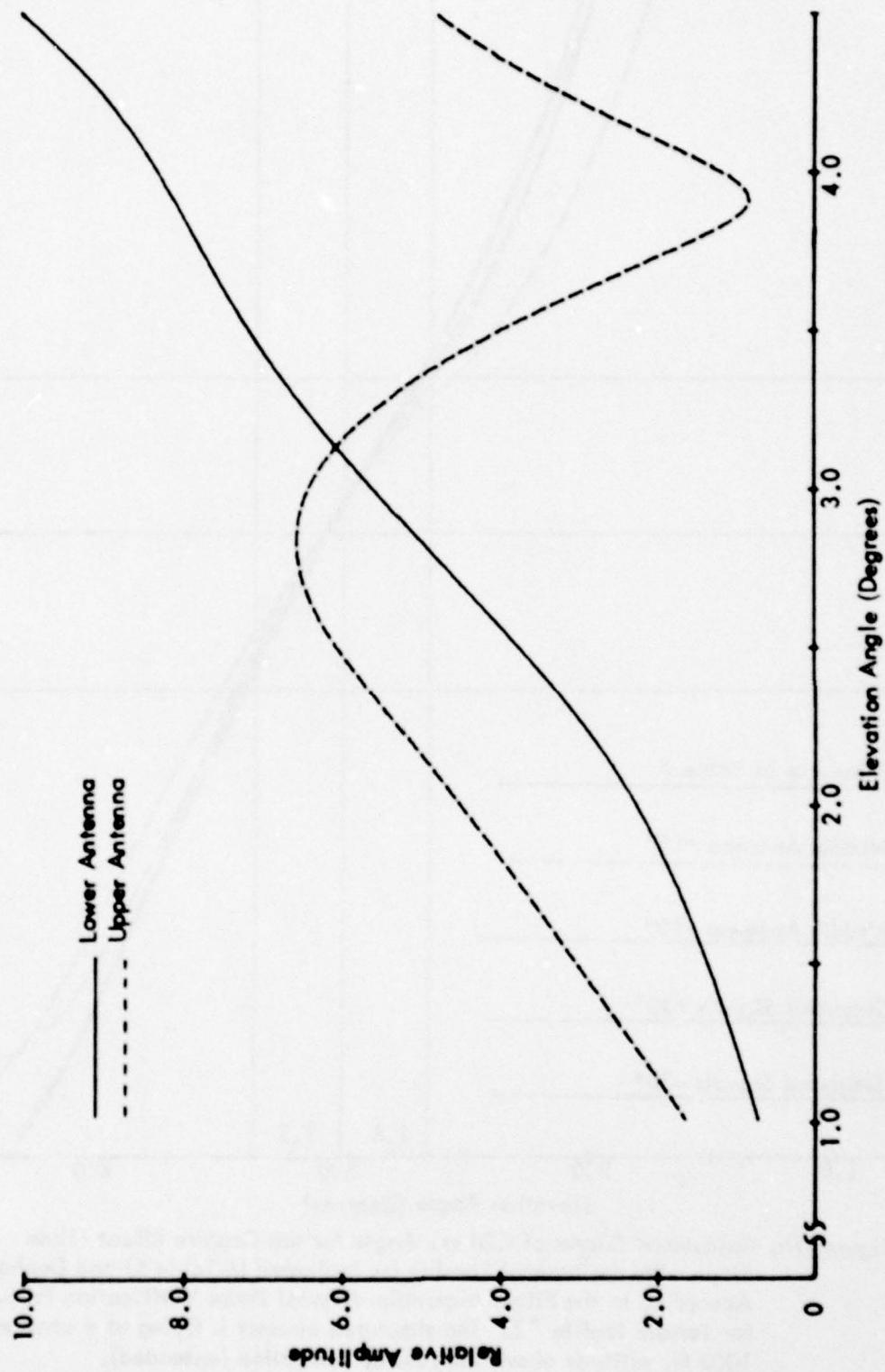
Figure 69g. Calculated Normalized Antenna Patterns vs. Angle for the Sideband Reference System for Terrain Profile #2. The simulated aircraft is flying at a constant 1000 ft. altitude above the runway centerline (extended).
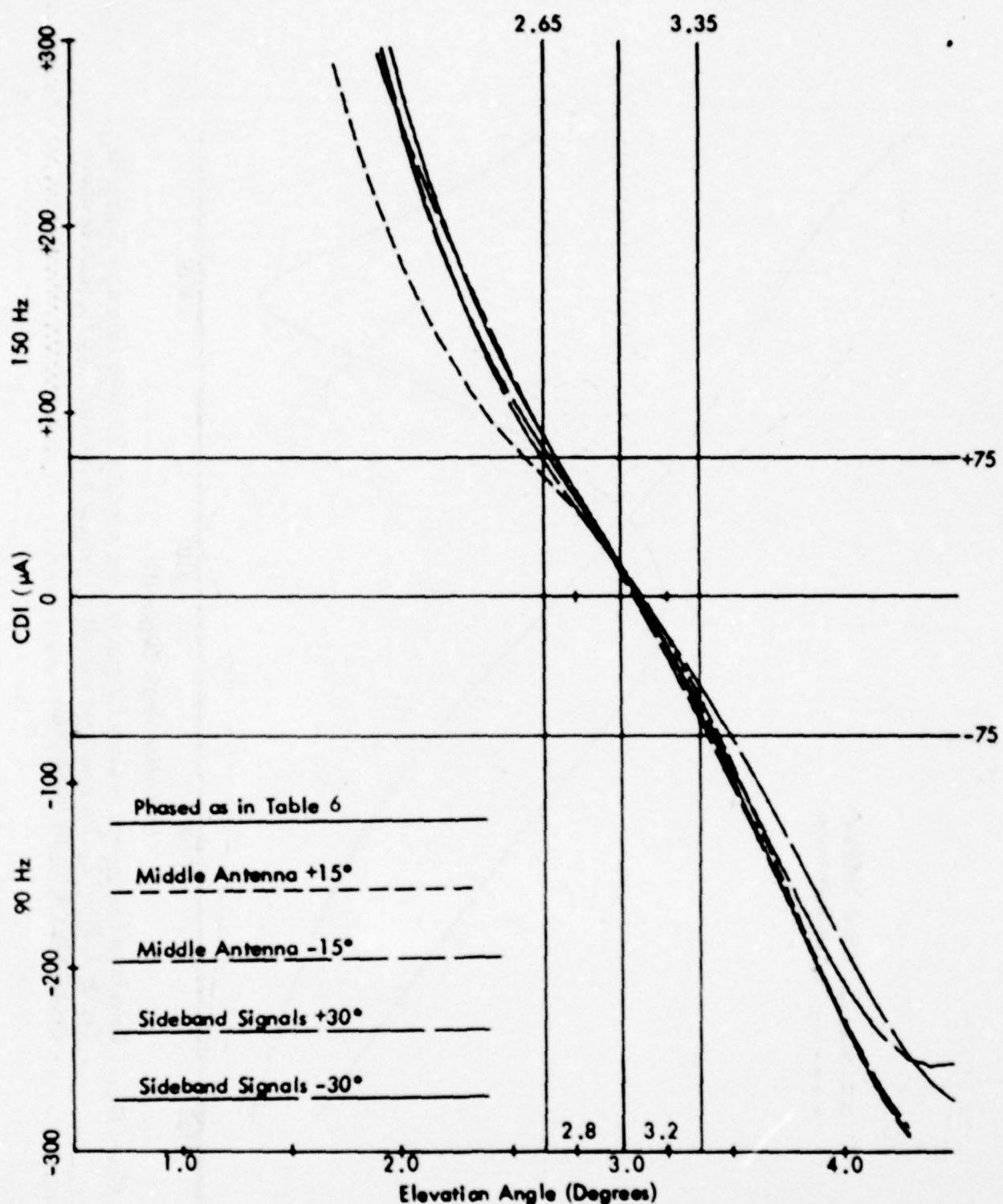
Figure 69h. Calculated Curves of CDI vs. Angle for the Capture Effect Glide
Slope with the Normal Phasing (as Indicated in Table 6) and Dephased
According to the Flight Inspection Manual Phase Verification Procedure
for Terrain Profile #2. The simulated aircraft is flying at a constant
1000 ft. altitude above the runway centerline (extended).
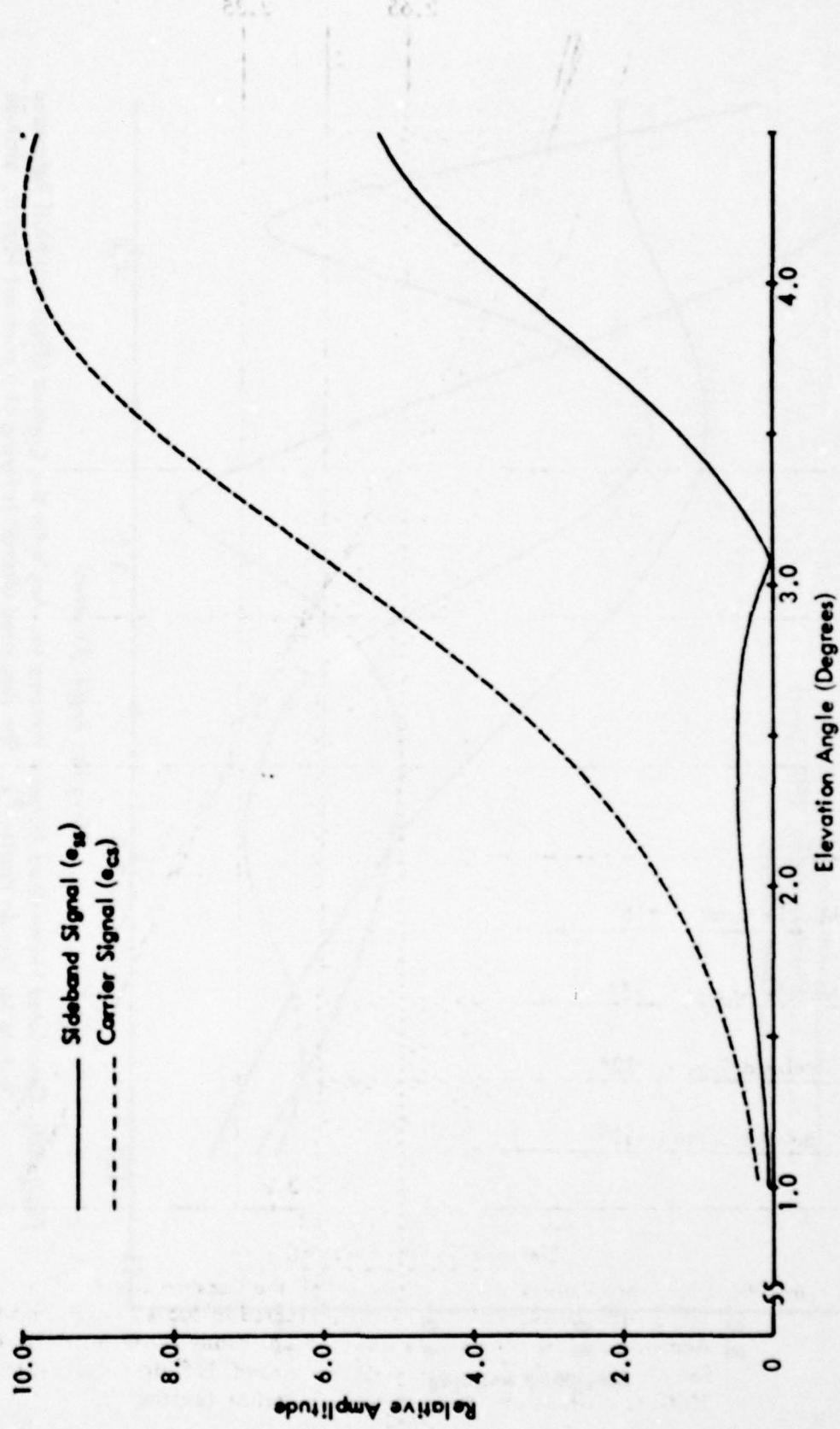
Figure 69i. Calculated Curves of Composite Carrier and Sideband Signals vs. Angle for the Capture Effect Glide Slope for Terrain Profile #2. The simulated aircraft is flying at a constant 1000 ft. altitude above the runway centerline (extended).

Figure 69j. Calculated Normalized Antenna Patterns vs. Angle for the Capture Effect and Null Reference Systems for Terrain Profile #2. The simulated aircraft is flying at a constant 1000 ft. altitude above the runway centerline (extended).

0.5°

3000 ft. — 750 ft. — 750 ft.
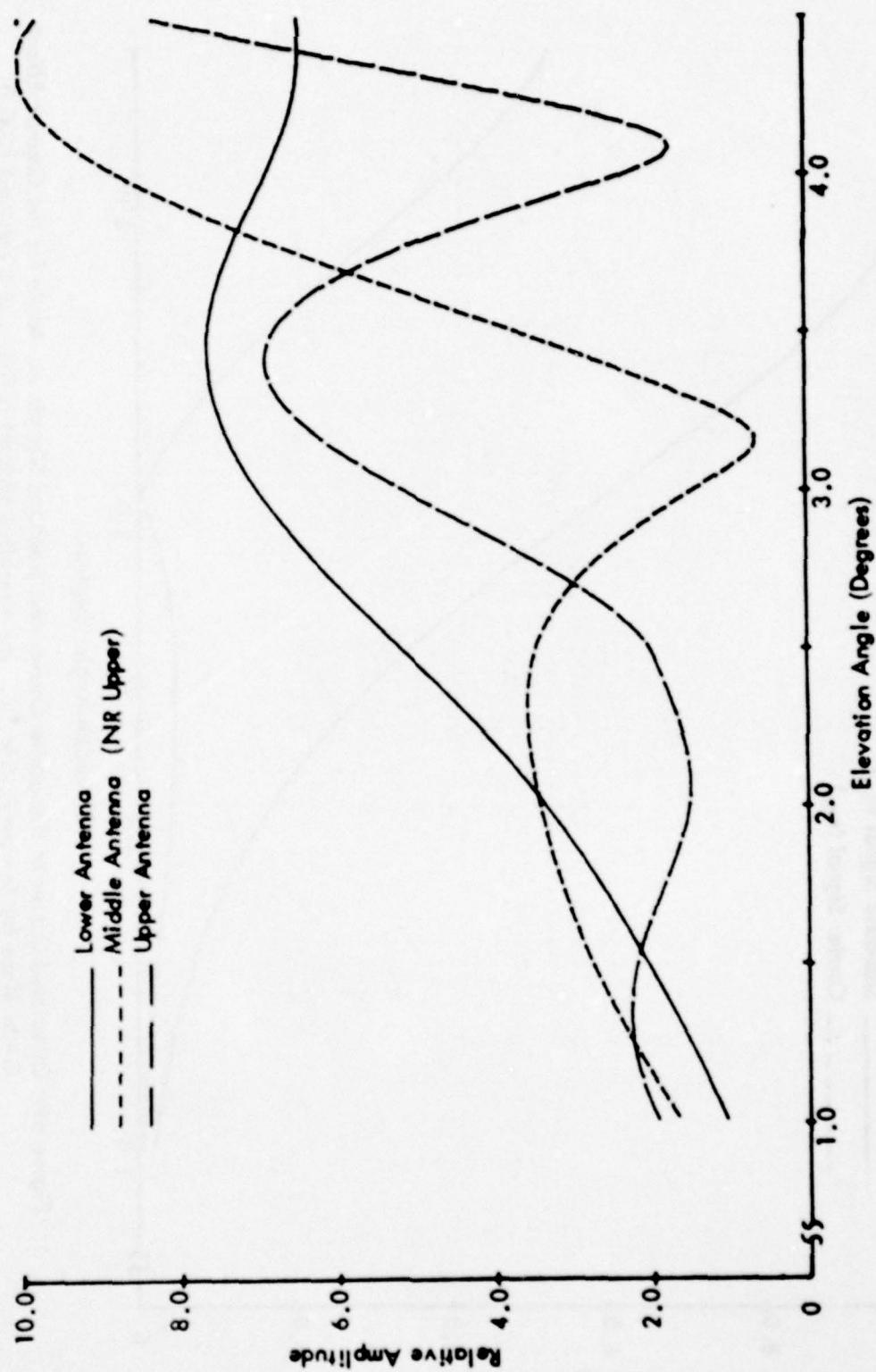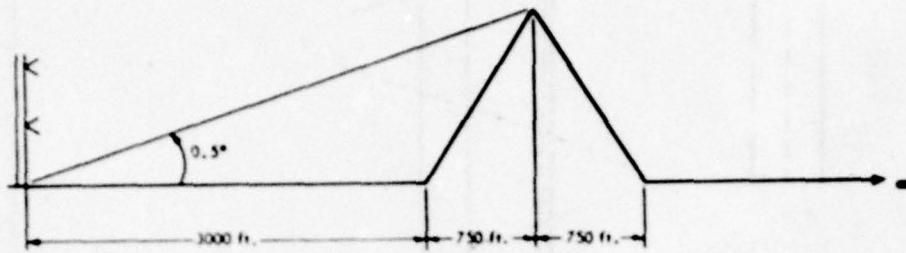
	Path Angle	Width Angle	+75 µA	-75 µA	Symmetry
Normal Phasing					
Null Reference	3.07	.70	2.56	3.25	.27
Sideband Reference	3.05	.70	2.57	3.27	.32
CEGS	3.02	.70	2.63	3.34	.45
Null Reference Dephased					
+15° Lower Antenna	3.06	.71	2.55	3.25	.28
-15° Lower Antenna	3.08	.73	2.54	3.27	.25
+30° Lower Antenna	3.04	1.15	2.46	3.61	.50
-30° Lower Antenna	3.10	.79	2.50	3.29	.23
SBR Dephased					
+15° Lower Antenna	3.00	.79	2.44	3.23	.30
-15° Lower Antenna	3.06	.72	2.56	3.28	.30
+30° Lower Antenna	2.85	.925	2.21	3.14	.32
-30° Lower Antenna					
CEGS Dephased					
+15° Middle Antenna	3.04	.74	2.60	3.33	.40
-15° Middle Antenna	3.00	.73	2.63	3.36	.49
+30° SBO	3.06	.76	2.65	3.41	.46
-30° SBO	2.98	.87	2.49	3.36	.44

"A" Ratio: NR .295   SBR .294   CEGS .305

Relative Phase NR/CEGS   Upper -4.3°   Middle 0°   Lower 4.39°

Relative Phase SBR   Upper 0°   Lower 8.06°

Table 7. Terrain Profile #3.
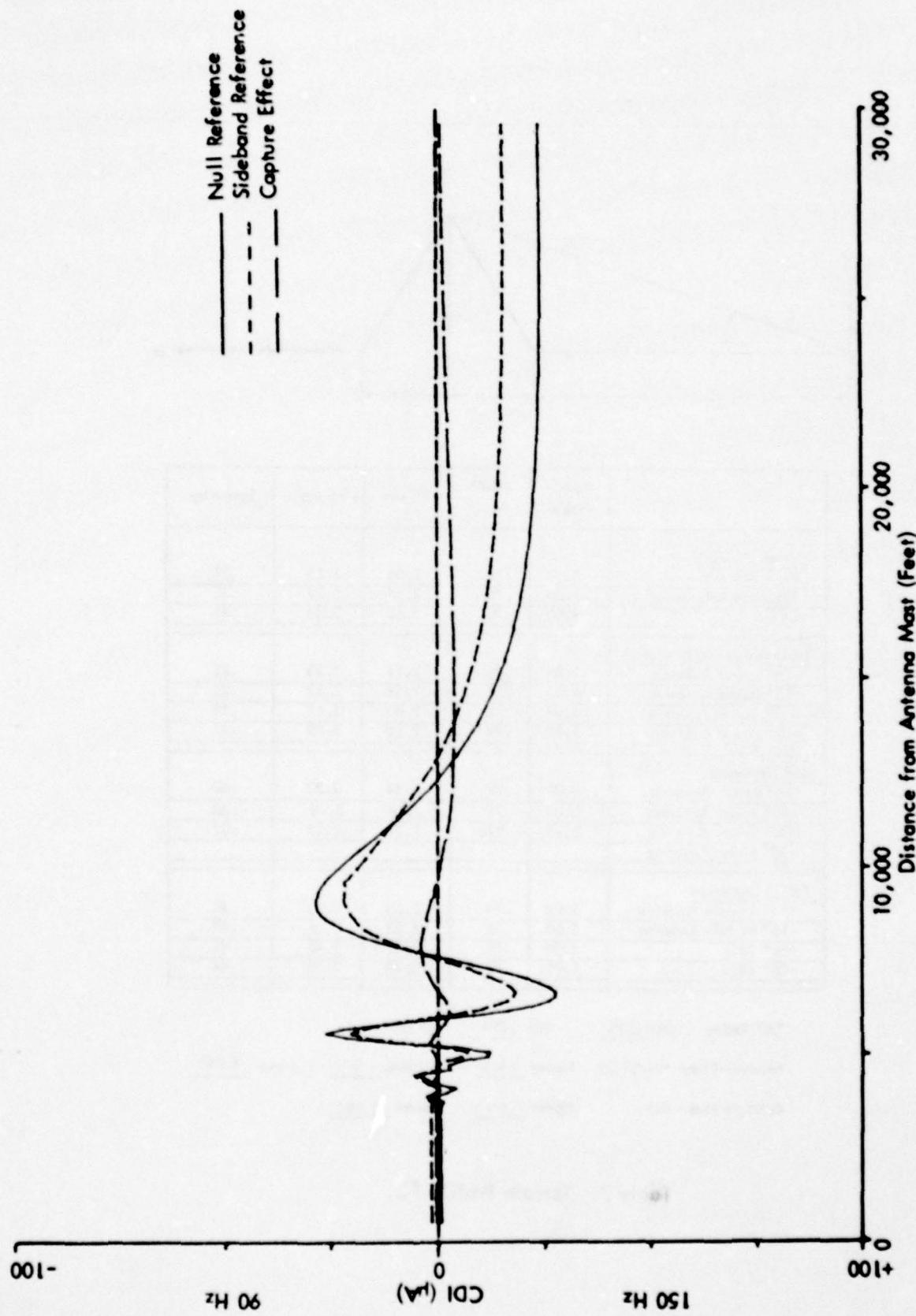
Figure 70b. Calculated Curves of CDI vs. Distance for the Three Image Type Glide-Slope Systems for Terrain Profile #3. The simulated aircraft is flying a constant 3.0 degree low approach over the runway centerline (extended).

-108-
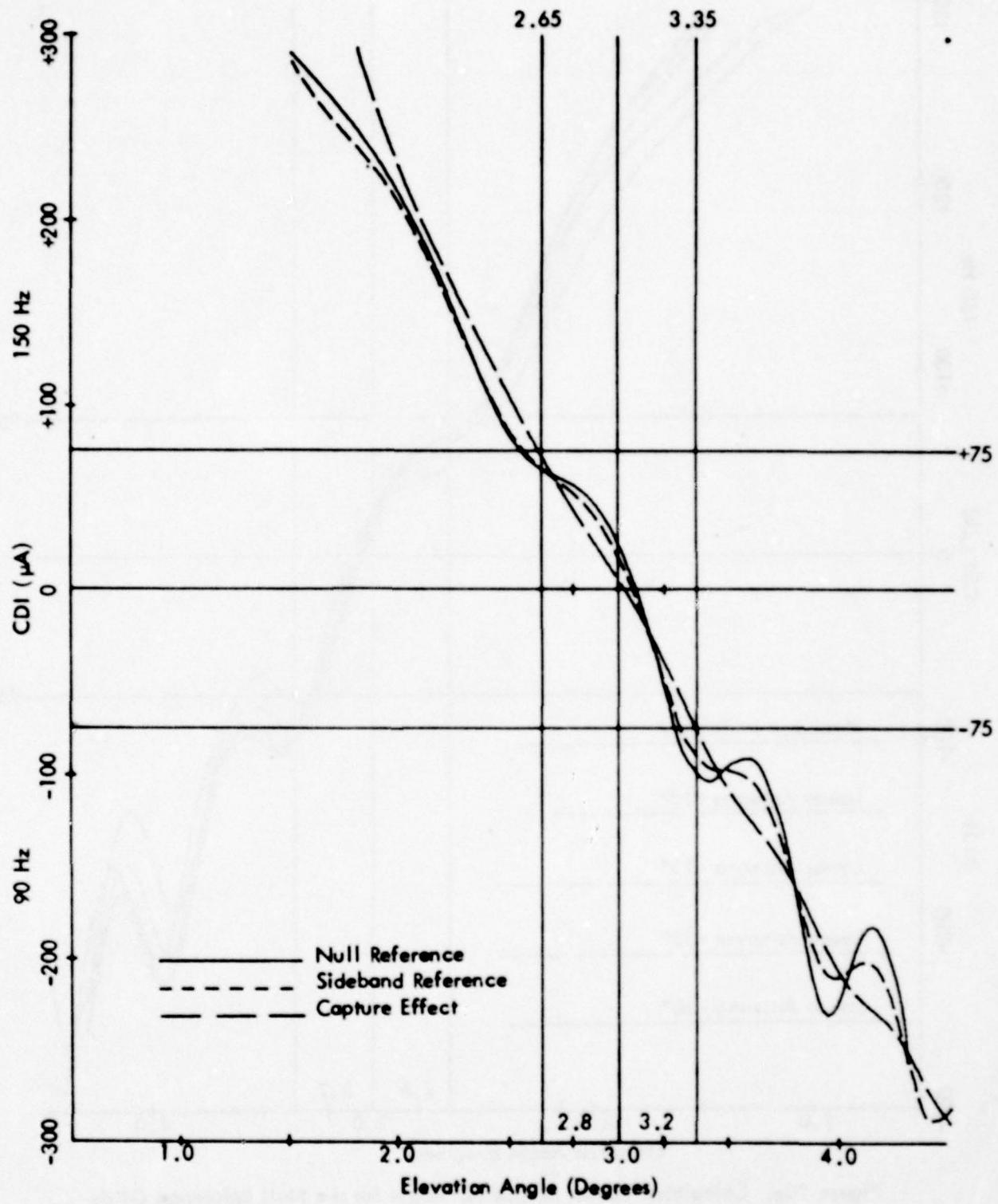
Figure 70b. Calculated Curves of CDI vs. Angle for the Three Image Type Glide-Slope Systems for Terrain Profile #3. The simulated aircraft is flying at a constant 1000 ft. altitude above the runway centerline (extended).
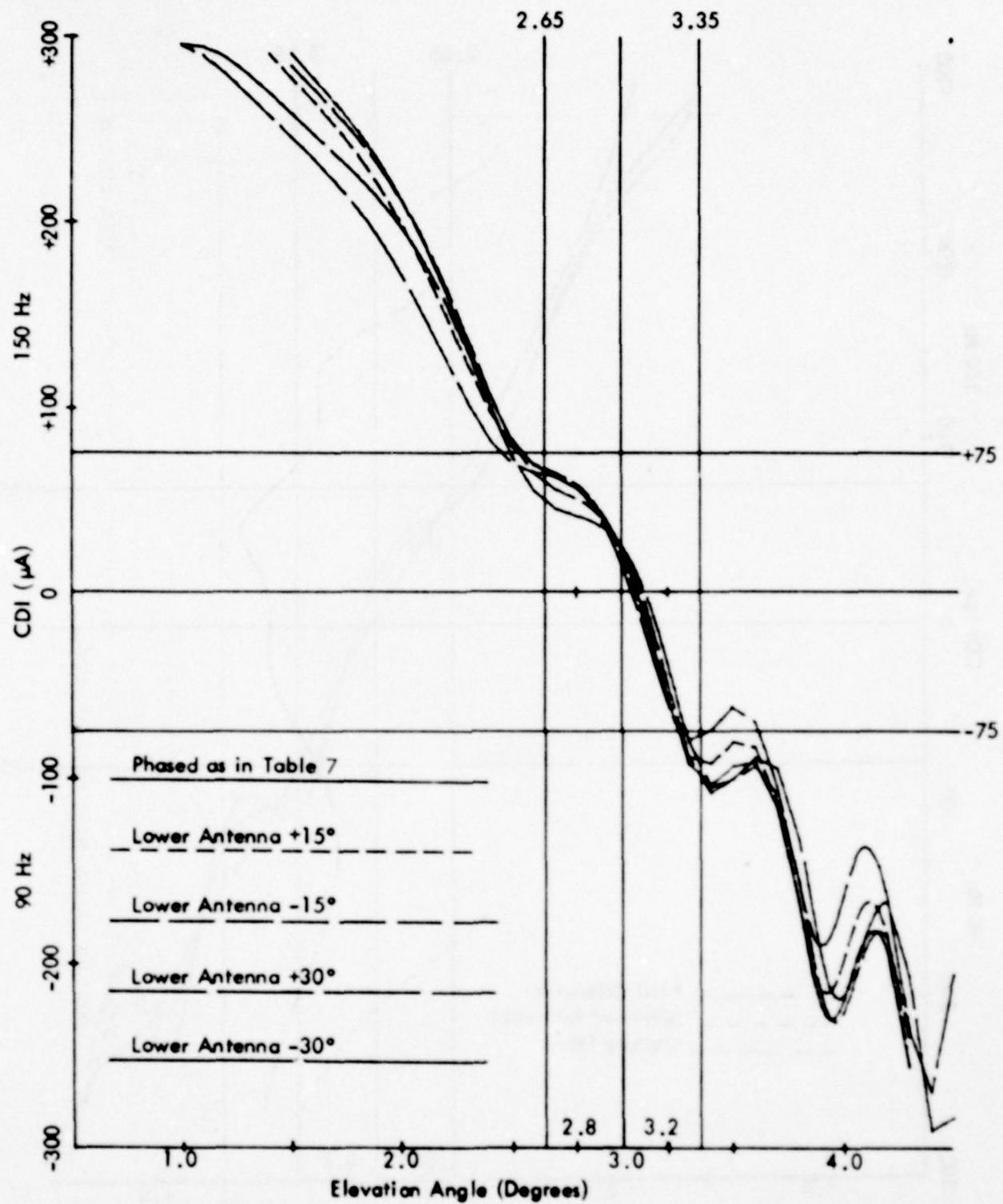
Figure 70c. Calculated Curves of CDI vs. Angle for the Null Reference Glide Slope with the Normal Phasing (as Indicated in Table 7) and Various Amounts of Dephasing for Terrain Profile #3. The simulated aircraft is flying at a constant 1000 ft. altitude above the runway centerline (extended).
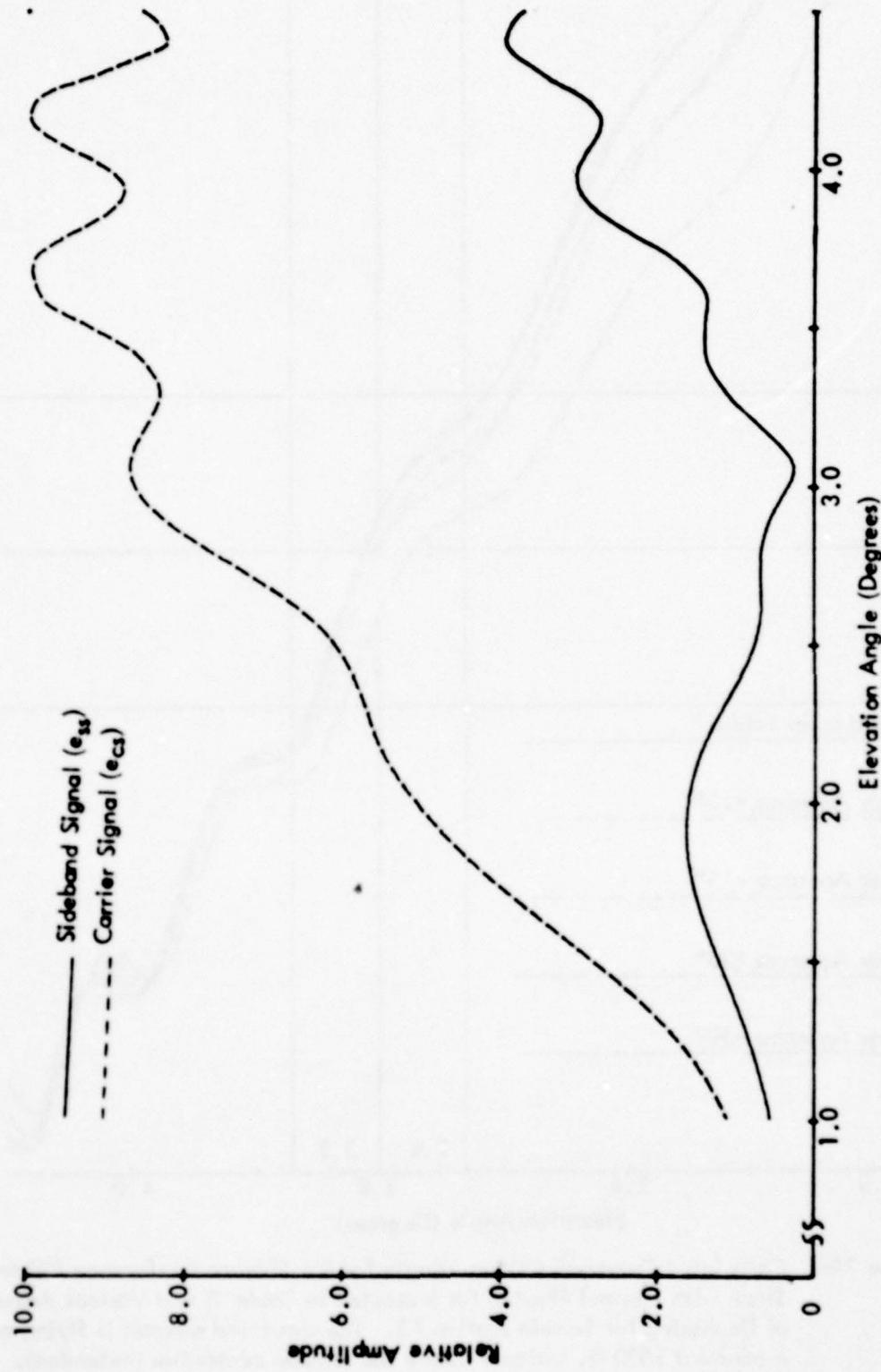
Figure 70d. Calculated Curves of Carrier and Sideband Signals vs. Angle for the Null Reference Glide Slope for Terrain Profile #3. The simulated aircraft is flying at a constant 1000 ft. altitude above the runway centerline (extended).

-111-
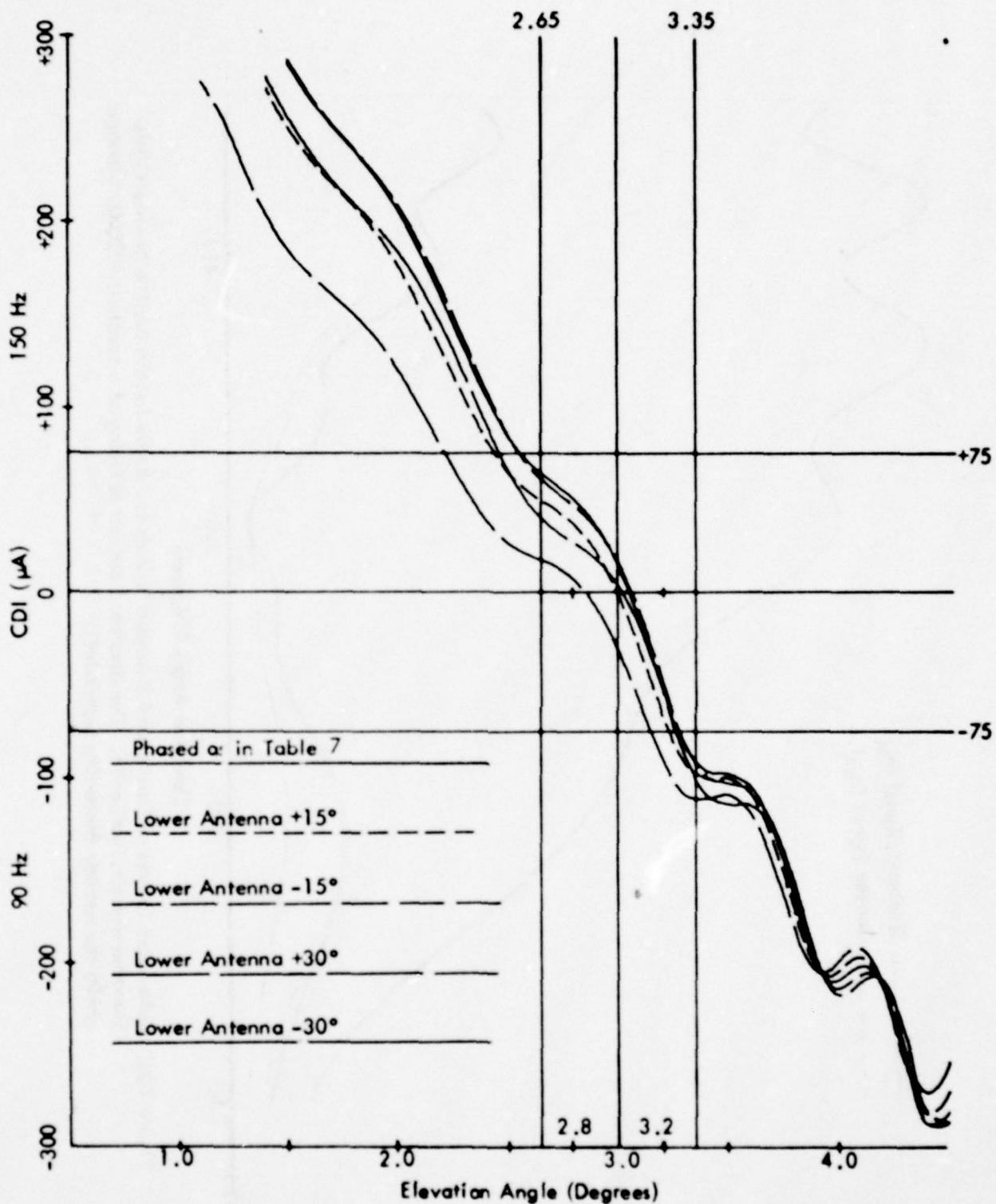
Figure 70e. Calculated Curves of CDI vs. Angle for the Sideband Reference Glide Slope with Normal Phasing (as Indicated in Table 7) and Various Amounts of Dephasing for Terrain Profile #3. The simulated aircraft is flying at a constant 1000 ft. altitude above the runway centerline (extended).
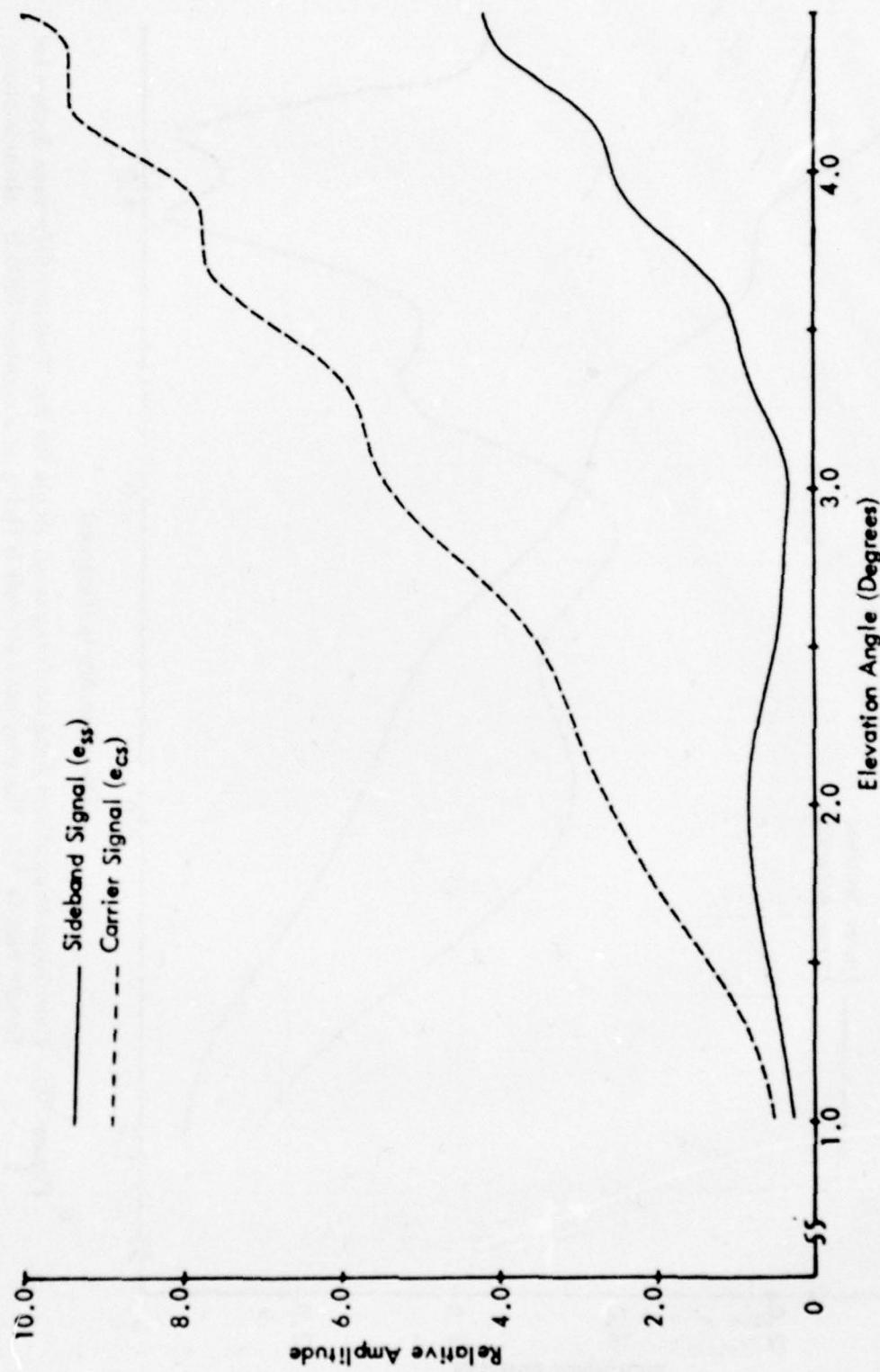
Figure 70f. Calculated Curves of Carrier and Composite Sideband Signals vs. Angle for the Sideband Reference Glide Slope for Terrain Profile #3. The simulated aircraft is flying at a constant 1000 ft. altitude above the runway centerline (extended).

-113-
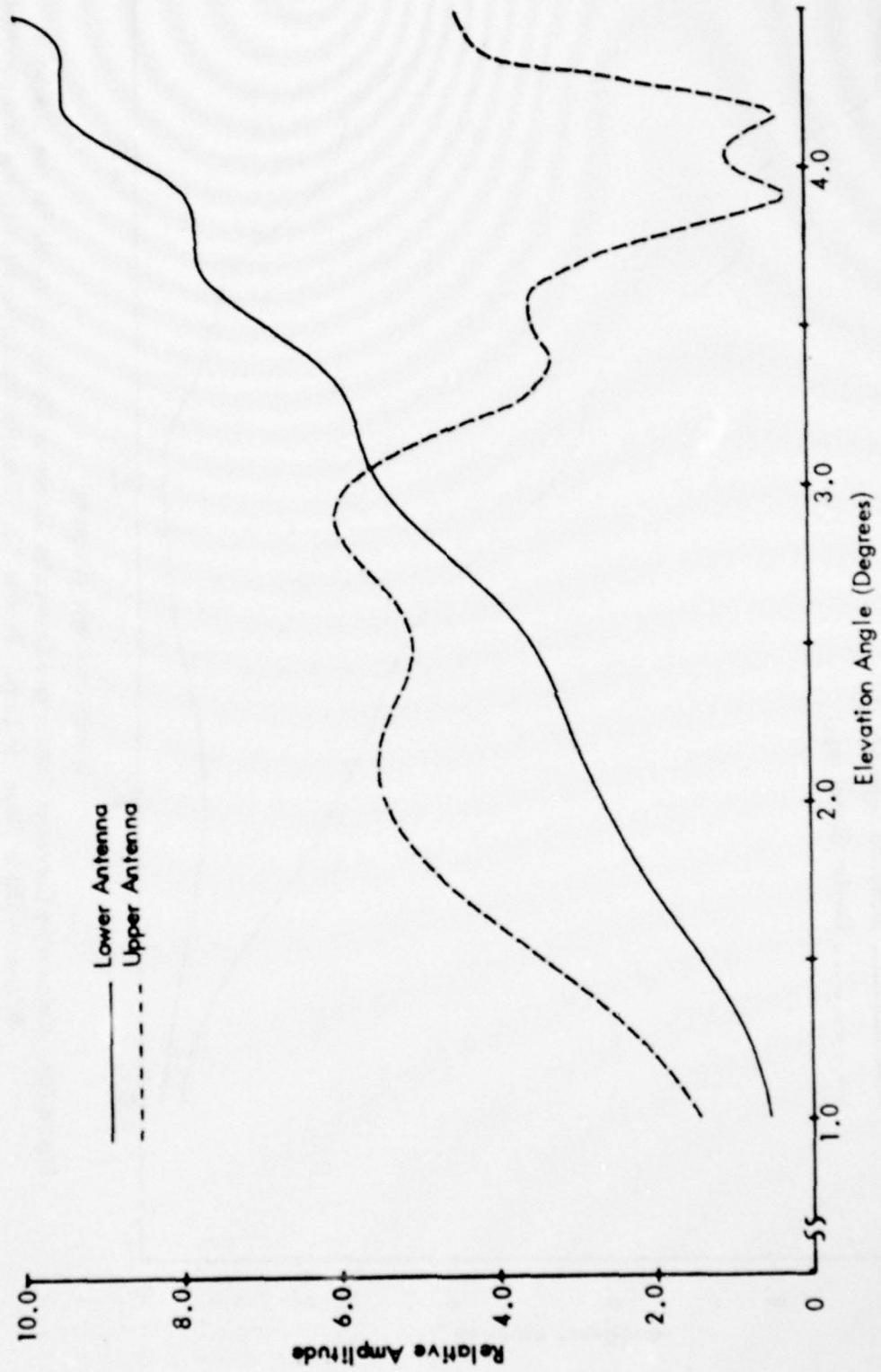
Figure 70g. Calculated Normalized Antenna Patterns vs. Angle for the Sideband Reference System for Terrain Profile #3. The simulated aircraft is flying at a constant 1000 ft. altitude above the runway centerline (extended).
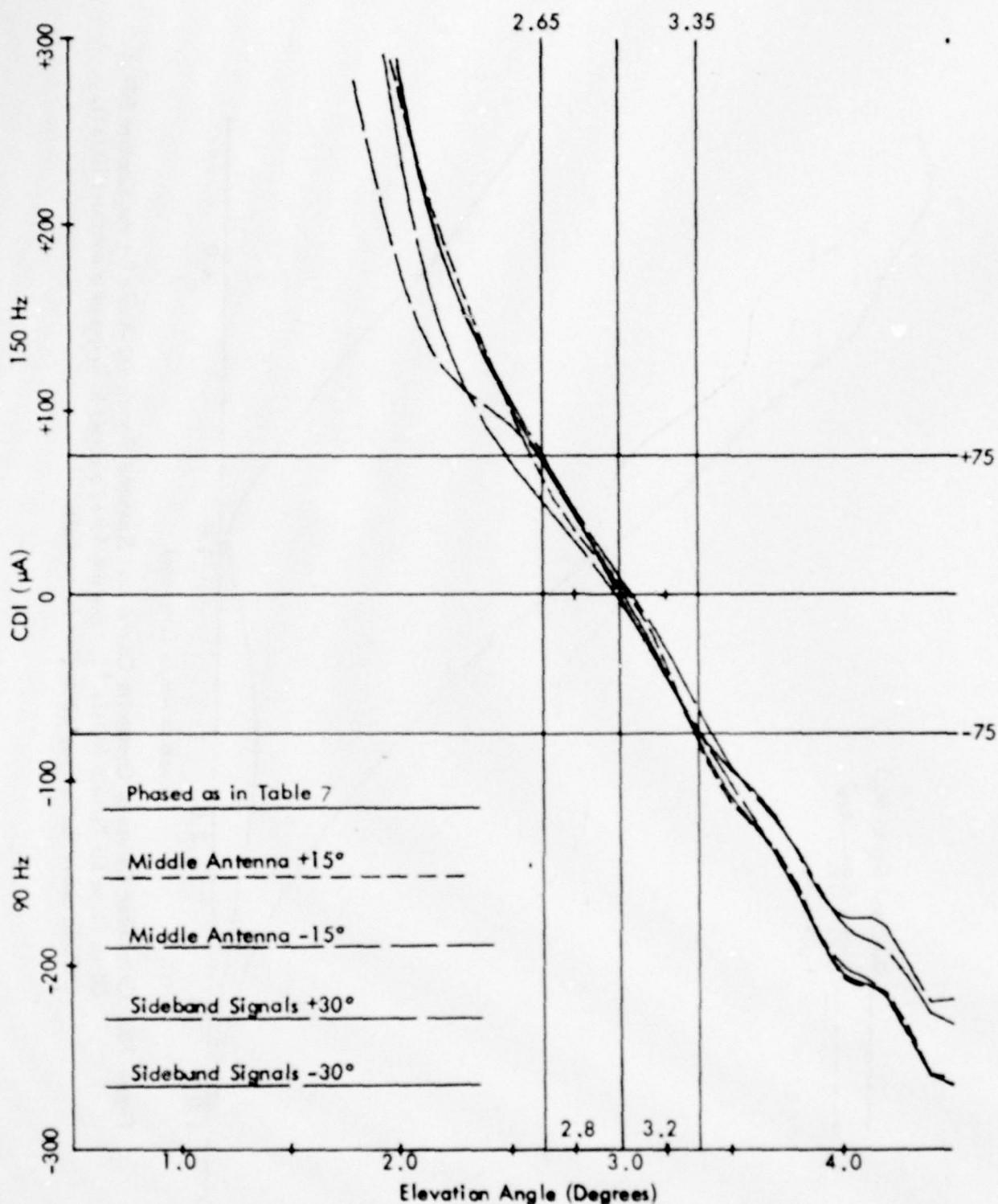
Figure 70h. Calculated Curves of CDI vs. Angle for the Capture Effect Glide Slope with the Normal Phasing (as Indicated in Table 7) and Dephased According to the Flight Inspection Manual Phase Verification Procedure for Terrain Profile #3. The simulated aircraft is flying at a constant 1000 ft. altitude above the runway centerline (extended).

-115-

Figure 70i. Calculated Curves of Composite Carrier and Sideband Signals vs. Angle for the Capture Effect Glide Slope for Terrain Profile #3. The simulated aircraft is flying at a constant 1000 ft. altitude above the runway centerline (extended).
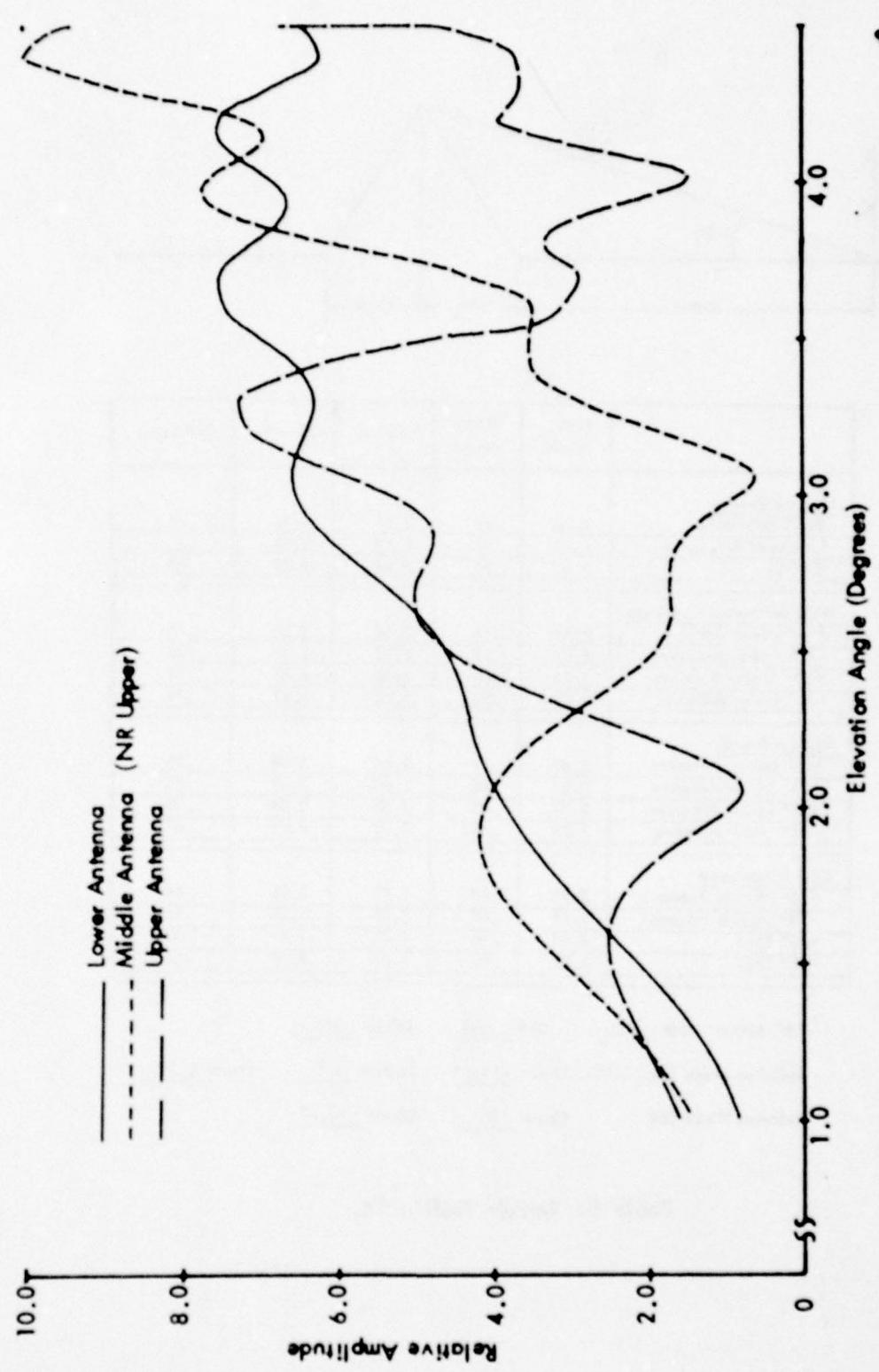
Figure 70i. Calculated Normalized Antenna Patterns vs. Angle for the Capture Effect and Null Reference Systems for Terrain Profile #3. The simulated aircraft is flying at a constant 1000 ft. altitude above the runway centerline (extended).
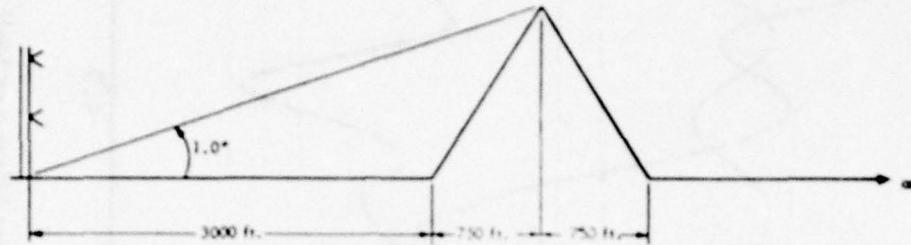
	Path Angle	Width Angle	+75 μA	-75 μA	Symmetry
Normal Phasing					
Null Reference	2.86	.70	2.71	3.41	.78
Sideband Reference	2.89	.70	2.69	3.39	.71
CEGS	2.96	.70	2.68	3.37	.60
Null Reference Dephased					
+15° Lower Antenna	2.85	.73	2.68	3.40	.76
-15° Lower Antenna	2.87	.71	2.72	3.42	.78
+30° Lower Antenna	2.83	.78	2.63	3.41	.74
-30° Lower Antenna	2.88	.75	2.72	3.47	.79
SBR Dephased					
+15° Lower Antenna	2.89	.71	2.67	3.38	.70
-15° Lower Antenna	2.85	.68	2.65	3.32	.70
+30° Lower Antenna	2.82	.75	2.59	3.34	.70
-30° Lower Antenna	2.76	.46	2.52	2.98	.47
CEGS Dephased					
+15° Middle Antenna	2.95	.67	2.71	3.38	.64
-15° Middle Antenna	2.98	.78	2.59	3.38	.51
+30° SBO	3.02	.76	2.71	3.47	.60
-30° SBO	2.89	.84	2.57	3.40	.62

"A" Ratio: NR .398   SBR .366   CEGS .305

Relative Phase NR/CEGS   Upper -11.9°   Middle 0°   Lower 0.7°

Relative Phase SBR   Upper 0°   Lower -7.2°

Table 8. Terrain Profile #4.
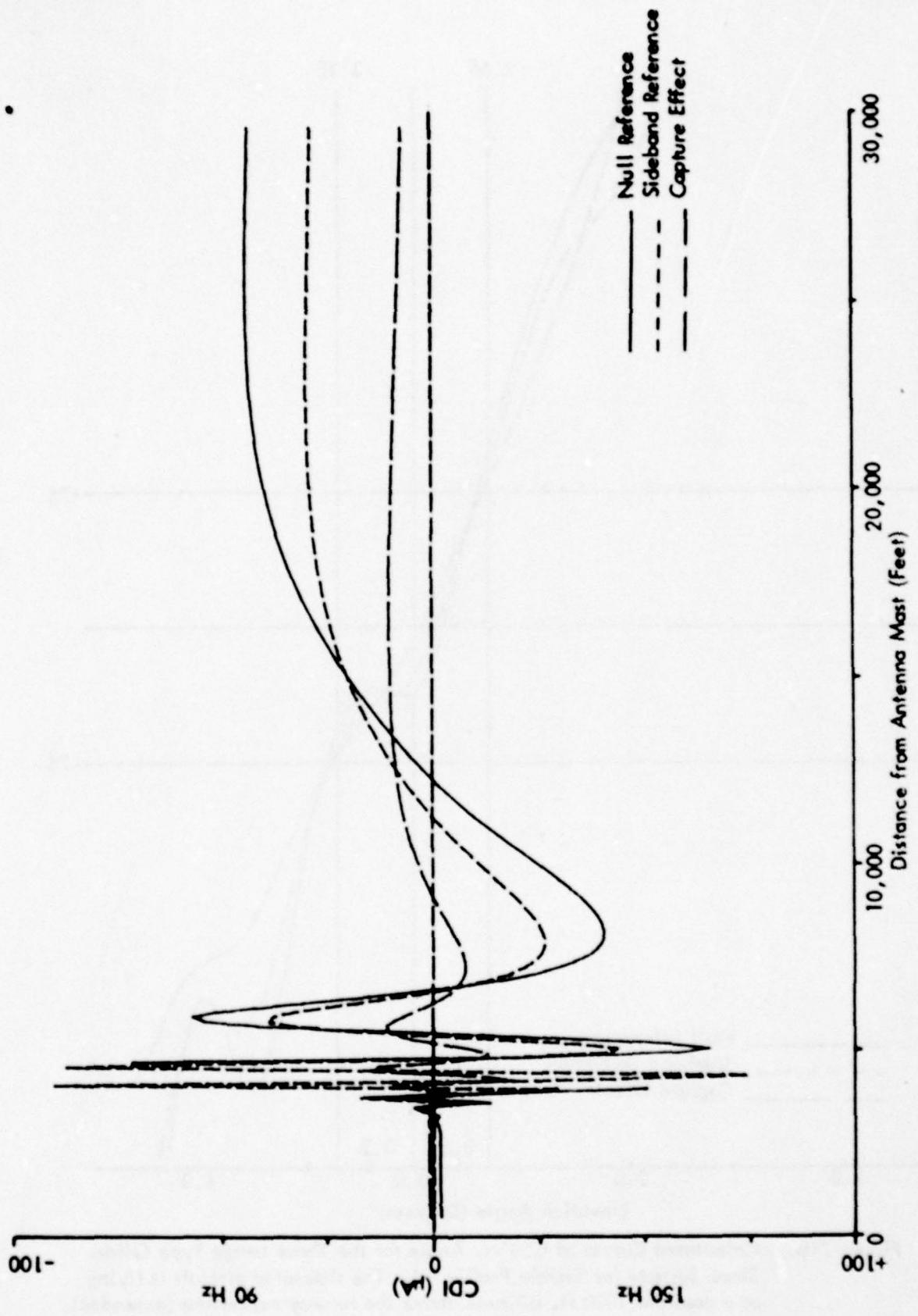
Figure 71a. Calculated Curves of CDI vs. Distance for the Three Image Type Glide-Slope Systems for Terrain Profile #4. The simulated aircraft is flying a constant 3.0 degree low approach over the runway centerline (extended).
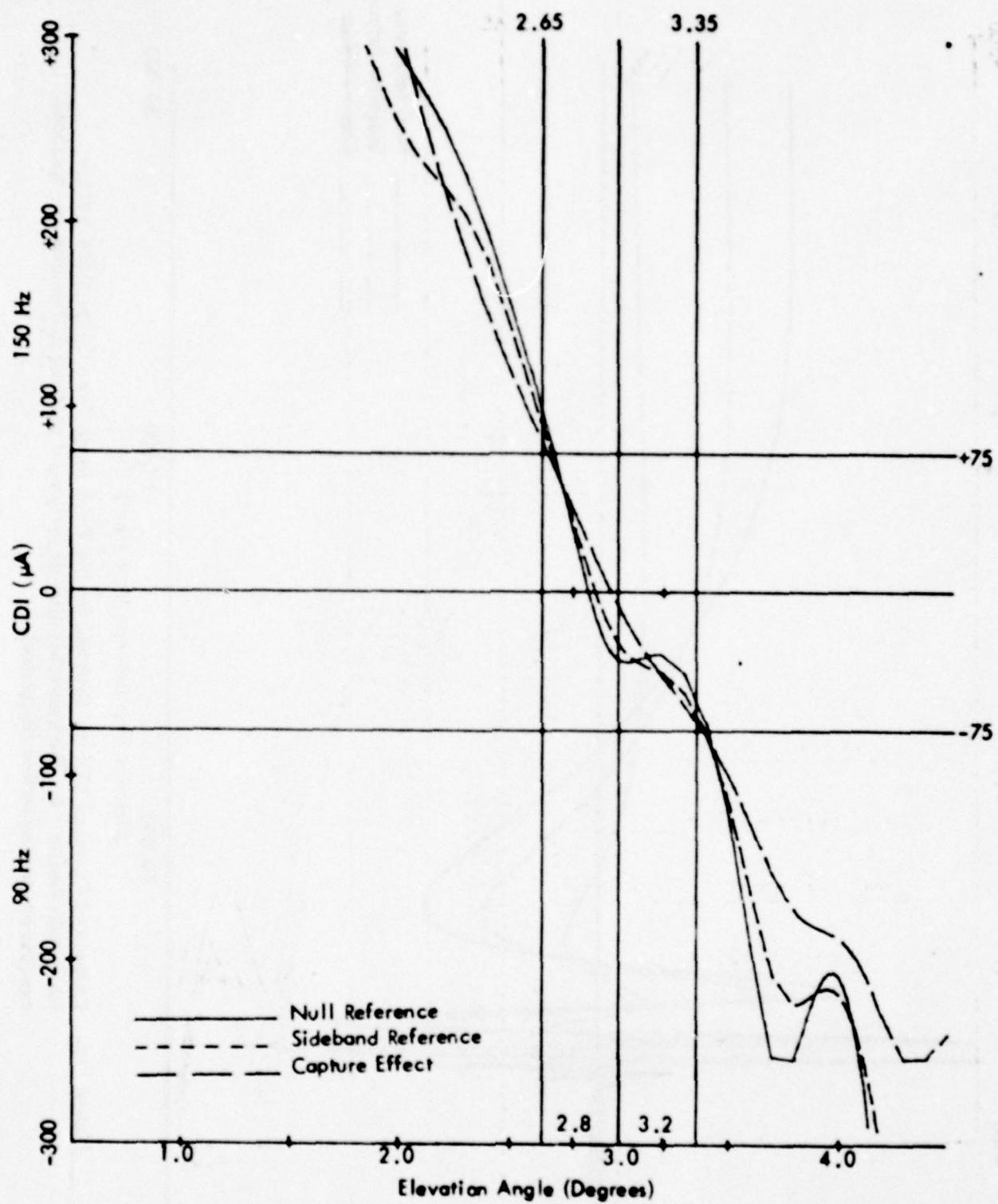
Figure 71b. Calculated Curves of CDI vs. Angle for the Three Image Type Glide-Slope Systems for Terrain Profile #4. The simulated aircraft is flying at a constant 1000 ft. altitude above the runway centerline (extended).

-120-
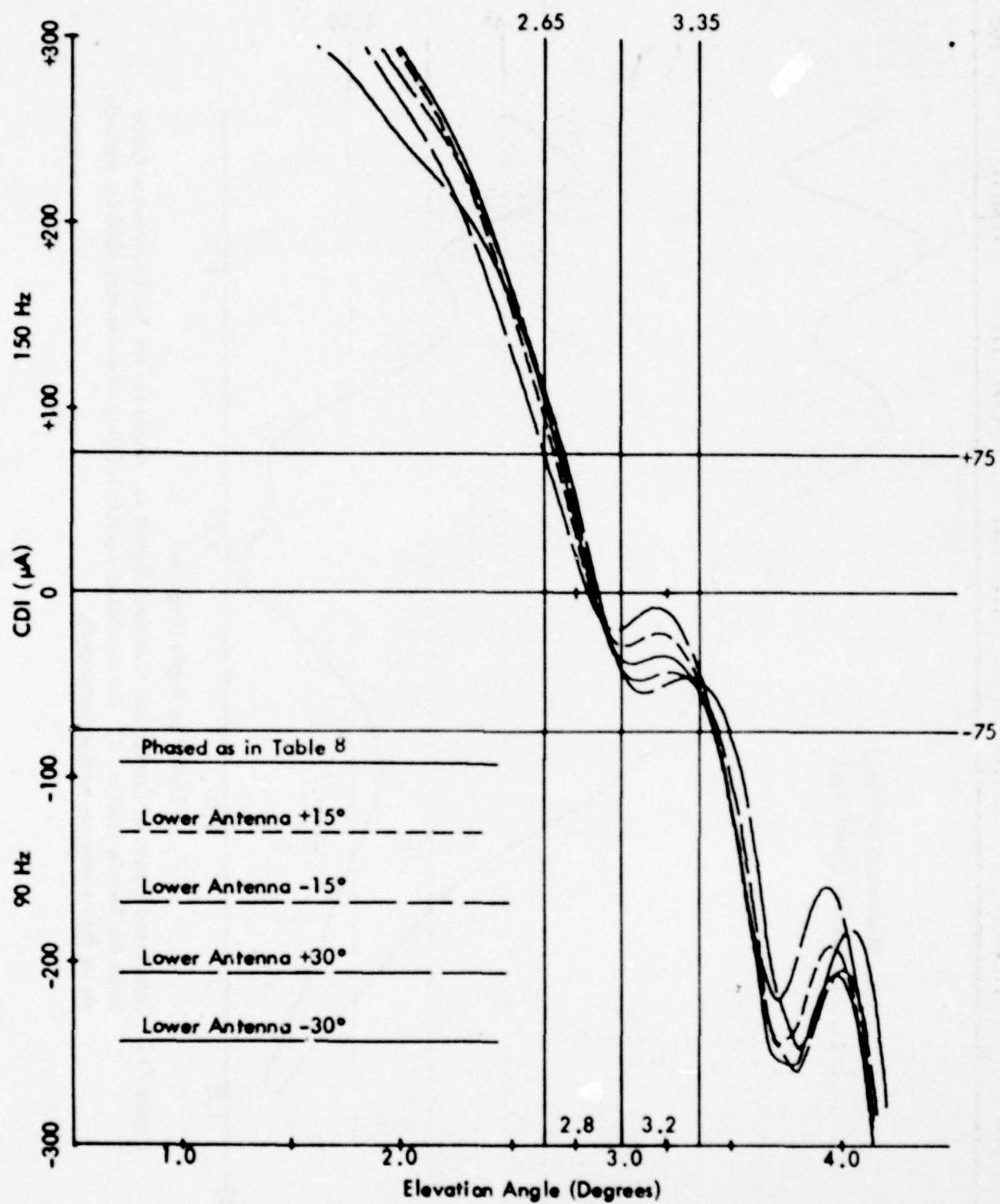
Figure 71c. Calculated Curves of CDI vs. Angle for the Null Reference Glide
Slope with the Normal Phasing (as Indicated in Table 8) and Various
Amounts of Dephasing for Terrain Profile #4. The simulated aircraft
is flying at a constant 1000 ft. altitude above the runway centerline
(extended).

-121-
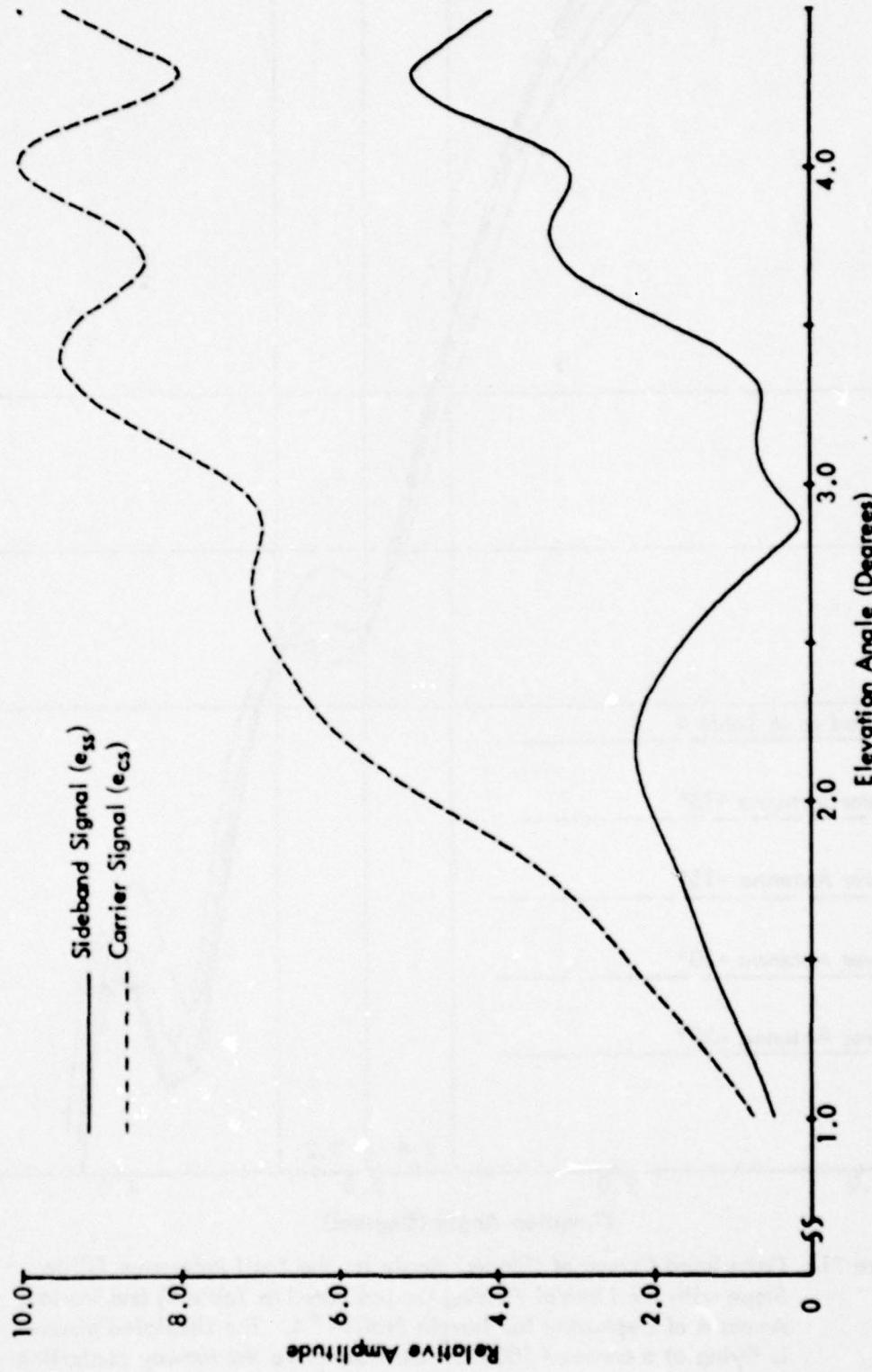
Figure 71d. Calculated Curves of Carrier and Sideband Signals vs. Angle for the Null Reference Glide Slope for Terrain Profile #4. The simulated aircraft is flying at a constant 1000 ft. altitude above the runway centerline (extended).
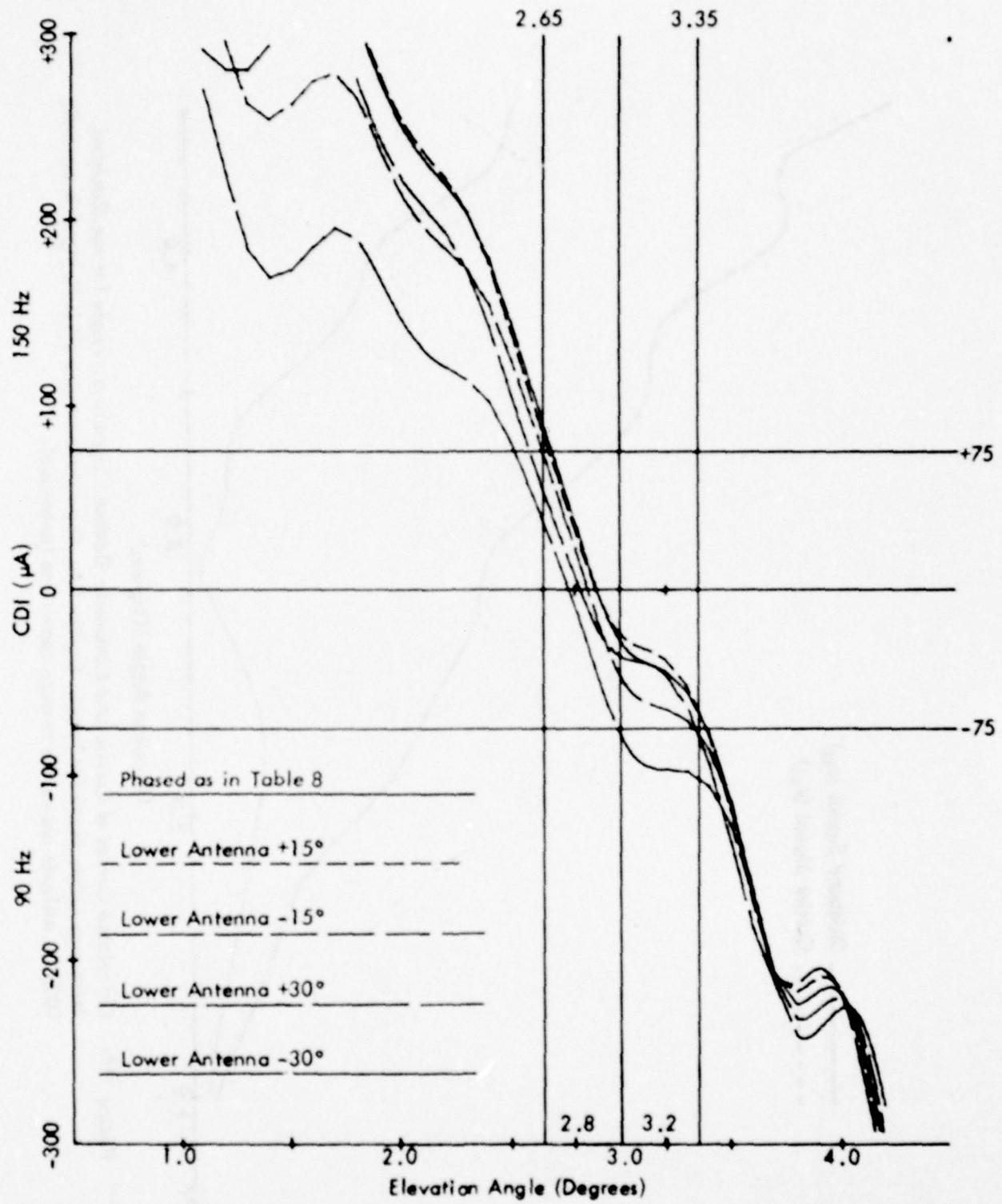
Figure 71e. Calculated Curves of CDI vs. Angle for the Sideband Reference Glide Slope with Normal Phasing (as Indicated in Table 8) and Various Amounts of Dephasing for Terrain Profile #4. The simulated aircraft is flying at a constant 1000 ft. altitude above the runway centerline (extended).
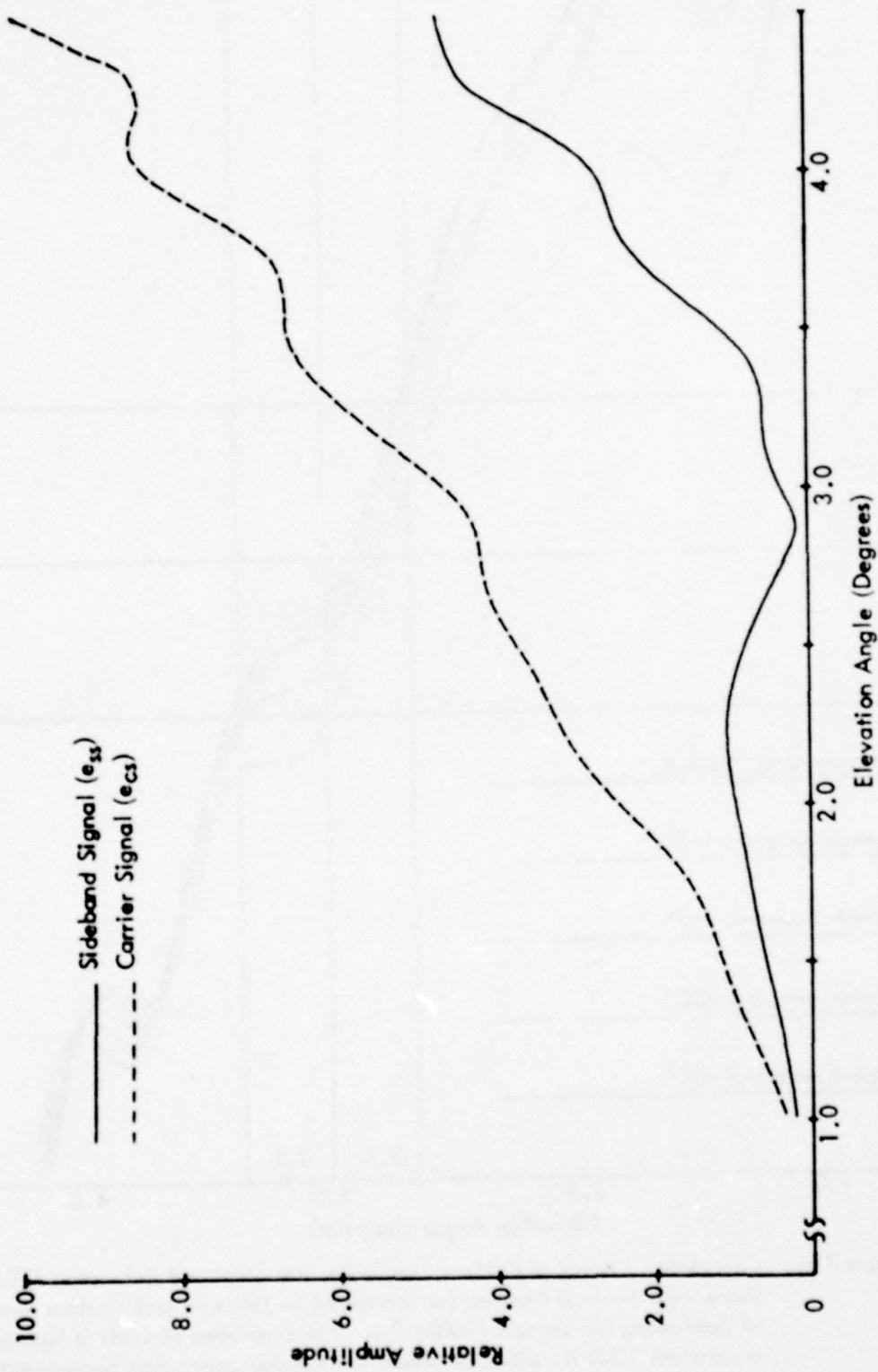
Figure 71f. Calculated Curves of Carrier and Composite Sideband Signals vs. Angle for the Sideband Reference Glide Slope for Terrain Profile #4. The simulated aircraft is flying at a constant 1000 ft. altitude above the runway centerline (extended).

-124-
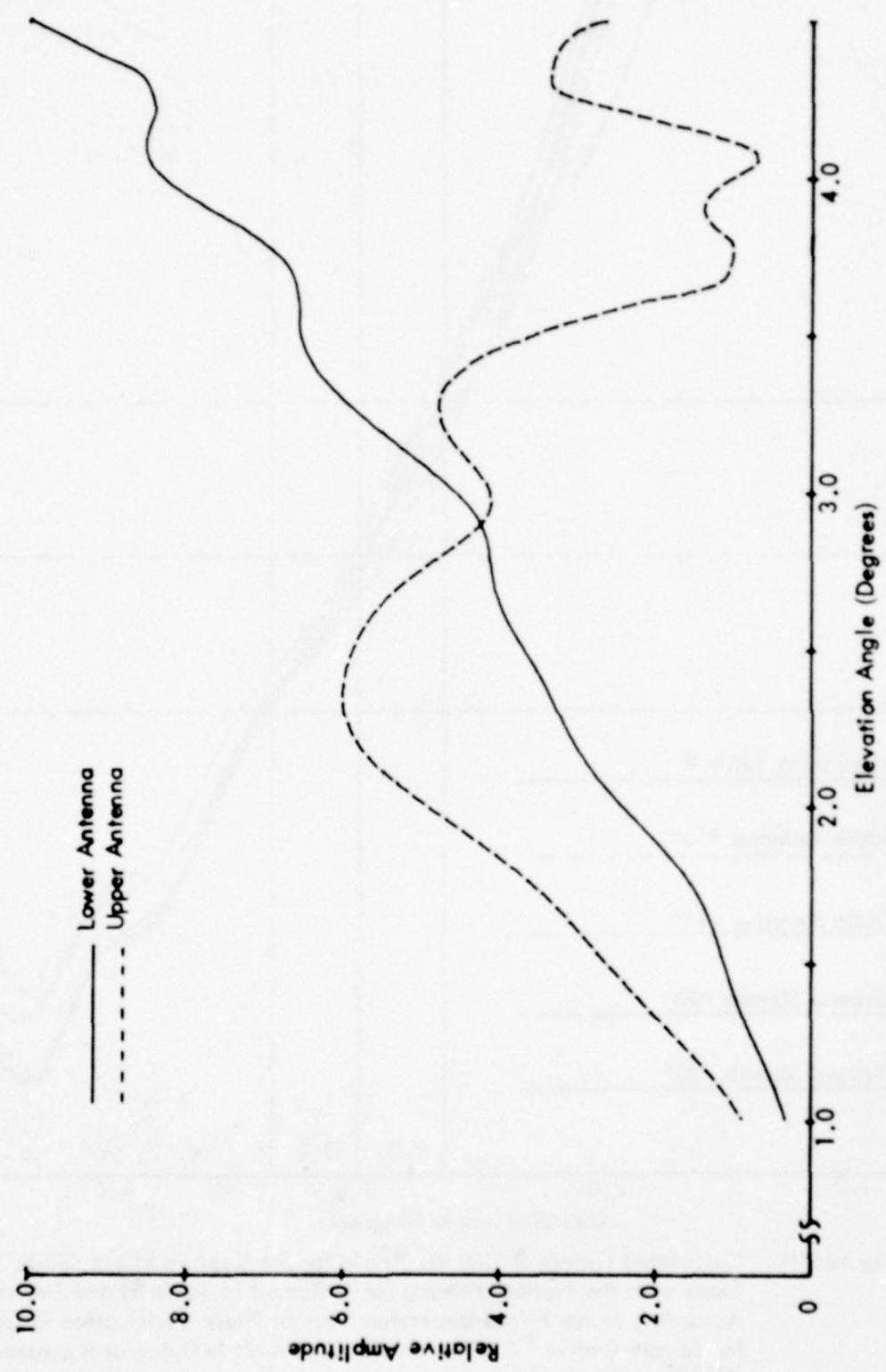
Figure 71g. Calculated Normalized Antenna Patterns vs. Angle for the Sideband Reference System for Terrain Profile #4. The simulated aircraft is flying at a constant 1000 ft. altitude above the runway centerline (extended).
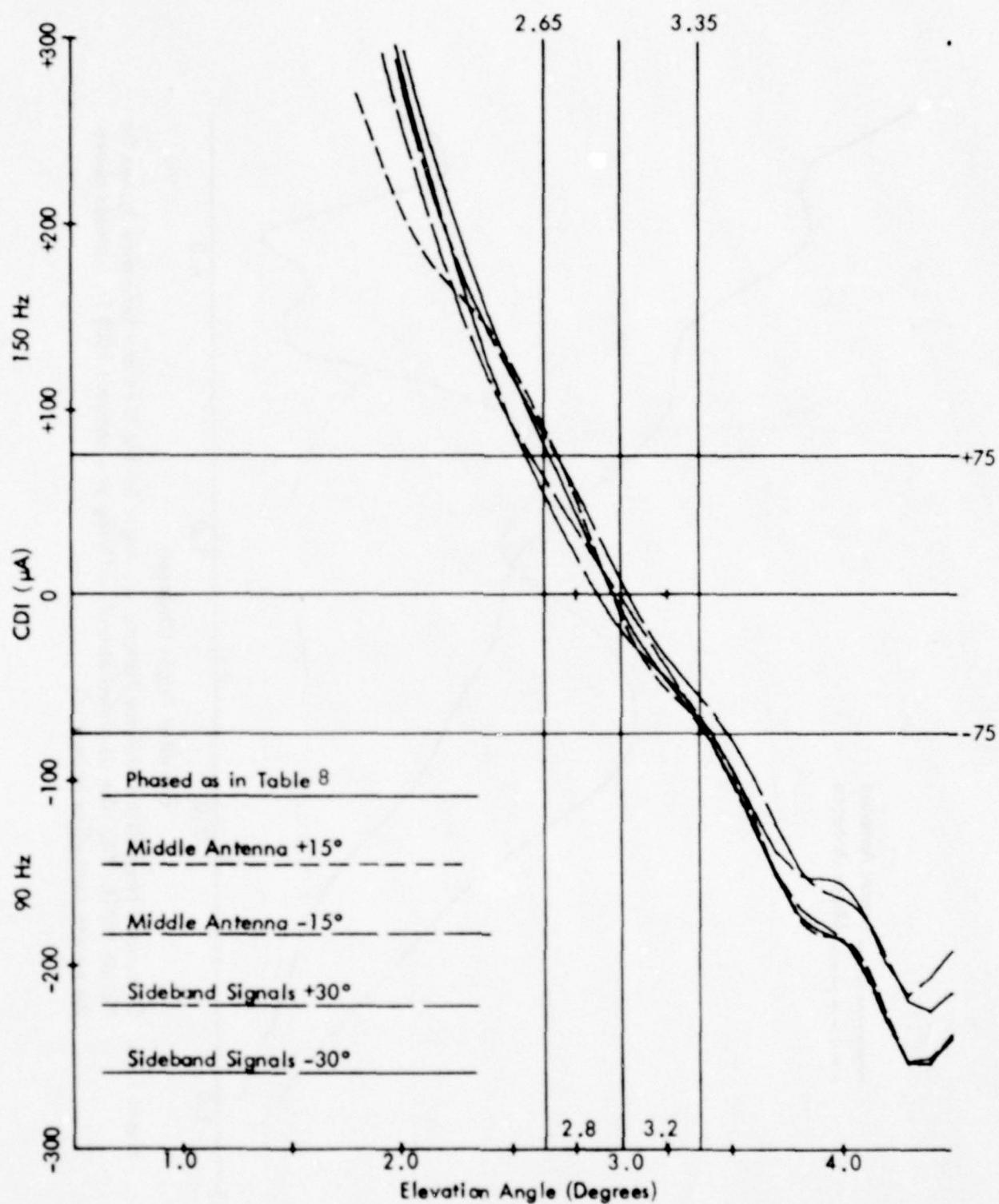
Figure 71h. Calculated Curves of CDI vs. Angle for the Capture Effect Glide Slope with the Normal Phasing (as Indicated in Table 8) and Dephased According to the Flight Inspection Manual Phase Verification Procedure for Terrain Profile #4. The simulated aircraft is flying at a constant 1000 ft. altitude above the runway centerline (extended).
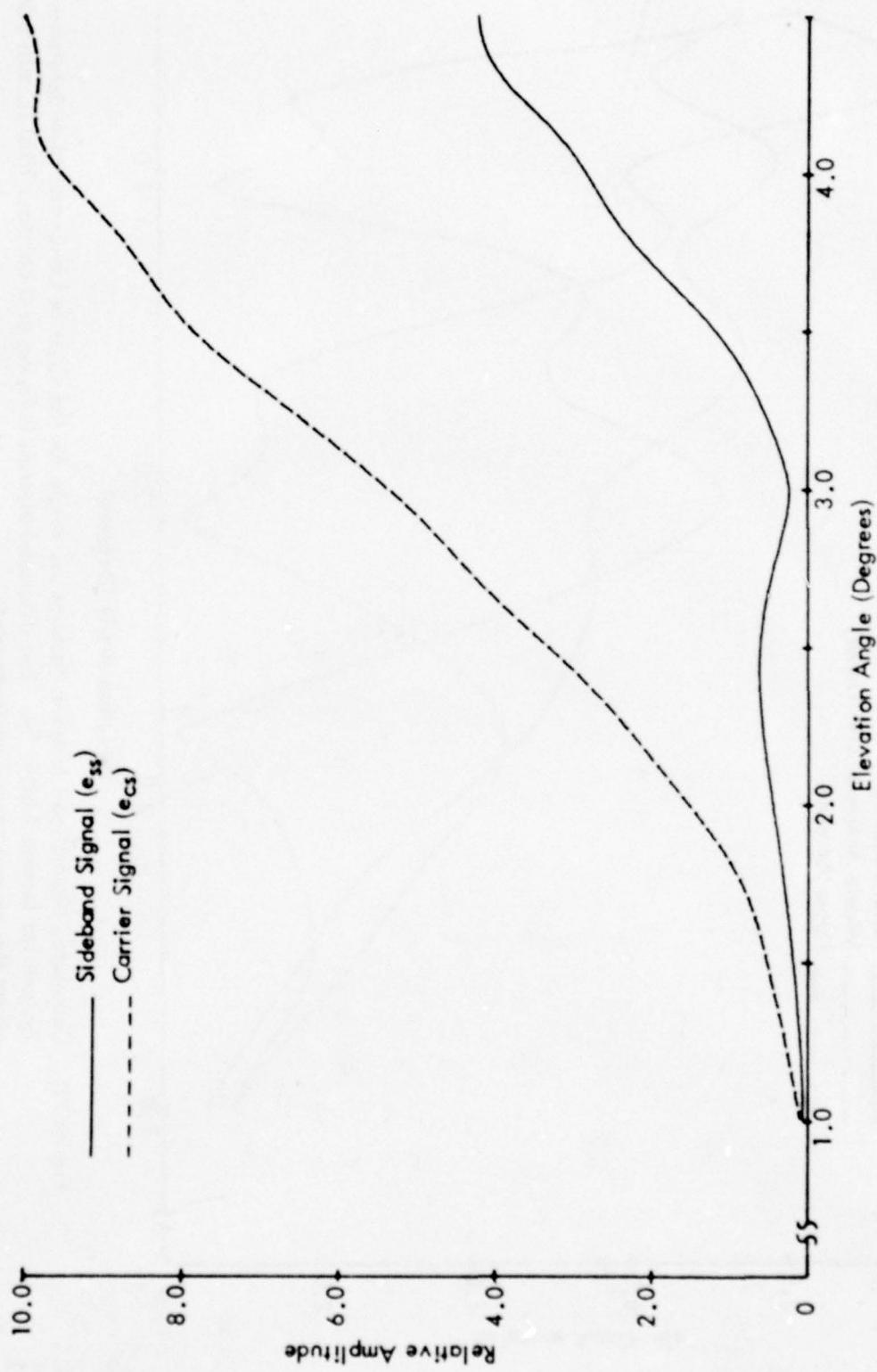
Figure 71i. Calculated Curves of Composite Carrier and Sideband Signals vs. Angle for the Capture Effect Glide Slope for Terrain Profile #4. The simulated aircraft is flying at a constant 1000 ft. altitude above the runway centerline (extended).

Figure 71j. Calculated Normalized Antenna Patterns vs. Angle for the Capture Effect and Null Reference Systems for Terrain Profile #4. The simulated aircraft is flying at a constant 1000 ft. altitude above the runway centerline (extended).

-128-
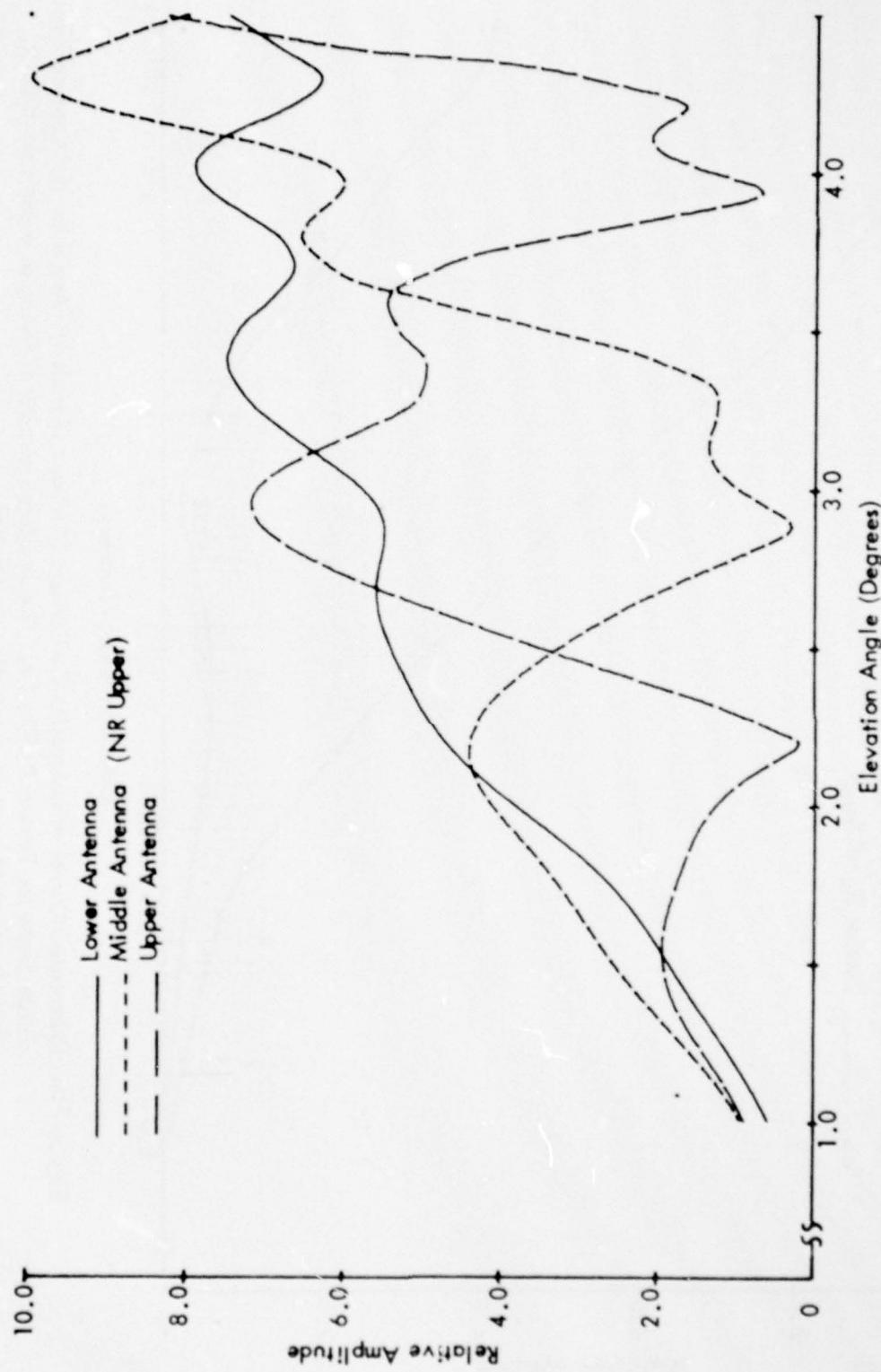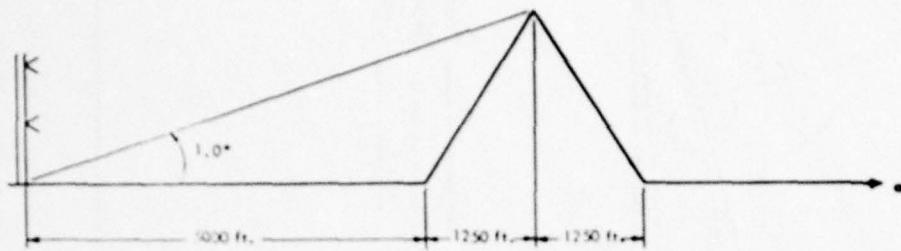
	Path Angle	Width Angle	+ 75 µA	- 75 µA	Symmetry
Normal Phasing					
Null Reference	2.92	.61	2.72	3.33	.66
Sideband Reference	2.93	.70	2.64	3.34	.59
CEGS	2.97	.70	2.64	3.34	.52
Null Reference Dephased					
+15° Lower Antenna	2.91	.82	2.70	3.52	.75
-15° Lower Antenna	2.93	.62	2.71	3.34	.65
+30° Lower Antenna	3.14	.91	2.64	3.55	.44
-30° Lower Antenna	2.94	.86	2.49	3.35	.48
SBR Dephased					
+15° Lower Antenna	2.87	.92	2.38	3.30	.46
-15° Lower Antenna	2.94	.73	2.62	3.35	.57
+30° Lower Antenna	2.77	1.07	2.17	3.24	.44
-30° Lower Antenna	2.91	.92	2.42	3.34	.46
CEGS Dephased					
+15° Middle Antenna	2.97	.74	2.61	3.34	.48
-15° Middle Antenna	2.97	.72	2.62	3.34	.50
+30° SBO	3.04	.71	2.71	3.42	.52
-30° SBO	2.89	.94	2.40	3.34	.48

"A" Ratio: NR .280* SBR .266 CEGS .306

Relative Phase NR/CEGS Upper -9.8° Middle 0° Lower +6.1°

Relative Phase SBR Upper 0° Lower +8.9°

*Could not be adjusted to 0.70° path width.

Table 9. Terrain Profile #5.
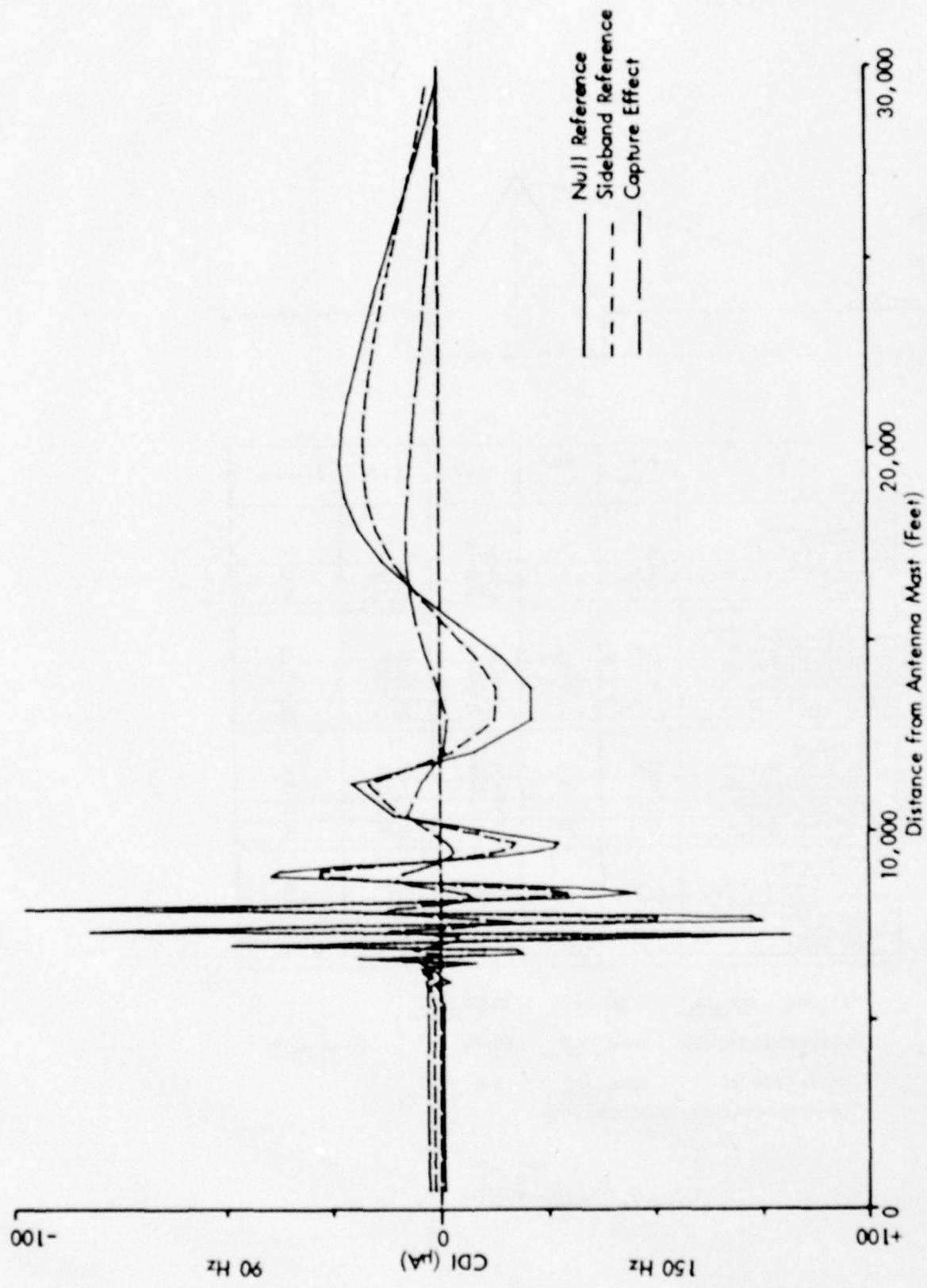
Figure 72a. Calculated Curves of CDI vs. Distance for the Three Image Type Glide-Slope Systems for Terrain Profile #5. The simulated aircraft is flying a constant 3.0 degree low approach over the runway centerline (extended).

-130-
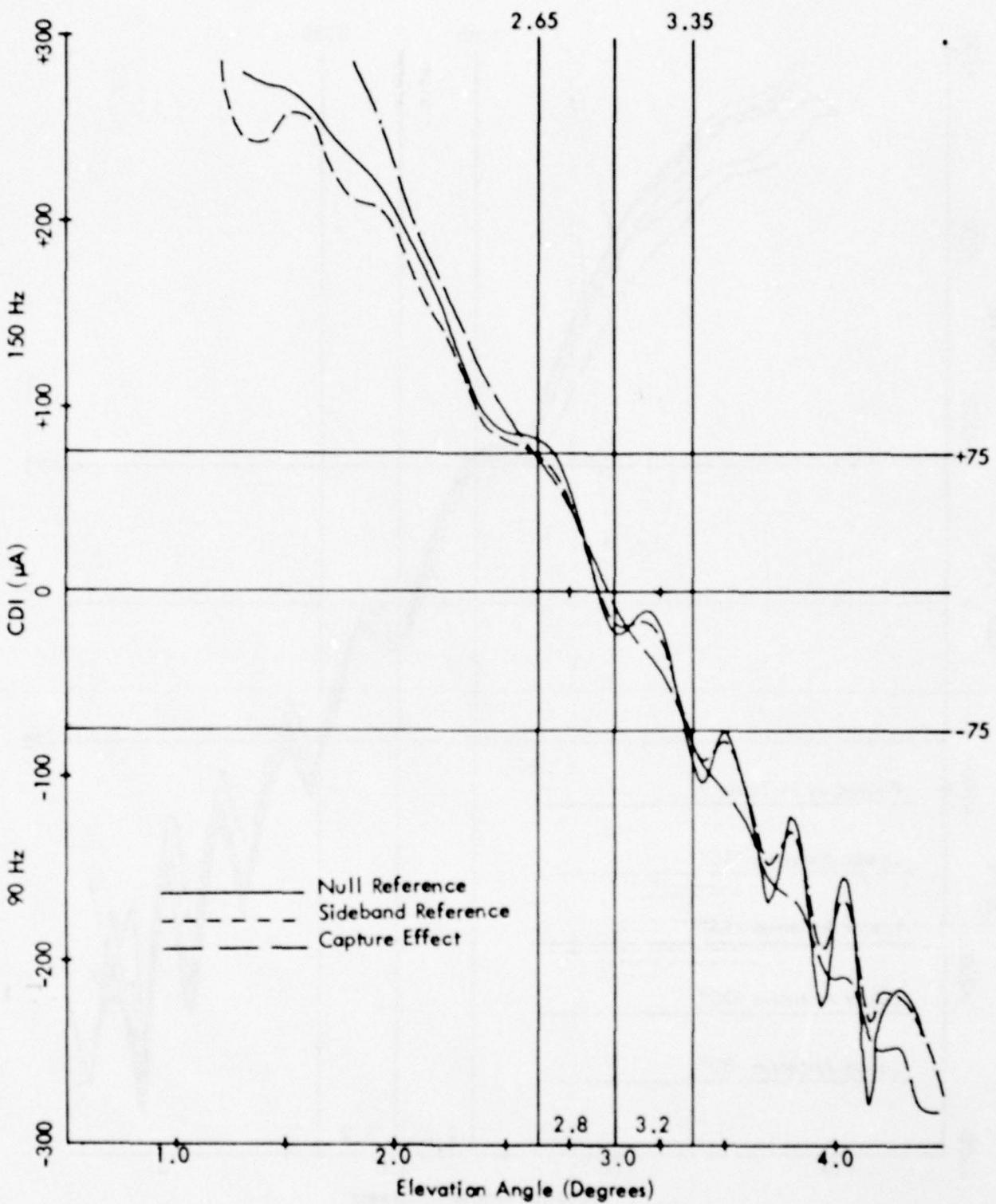
Figure 72b.   Calculated Curves of CDI vs. Angle for the Three Image Type Glide-Slope Systems for Terrain Profile #5. The simulated aircraft is flying at a constant 1000 ft. altitude above the runway centerline (extended).
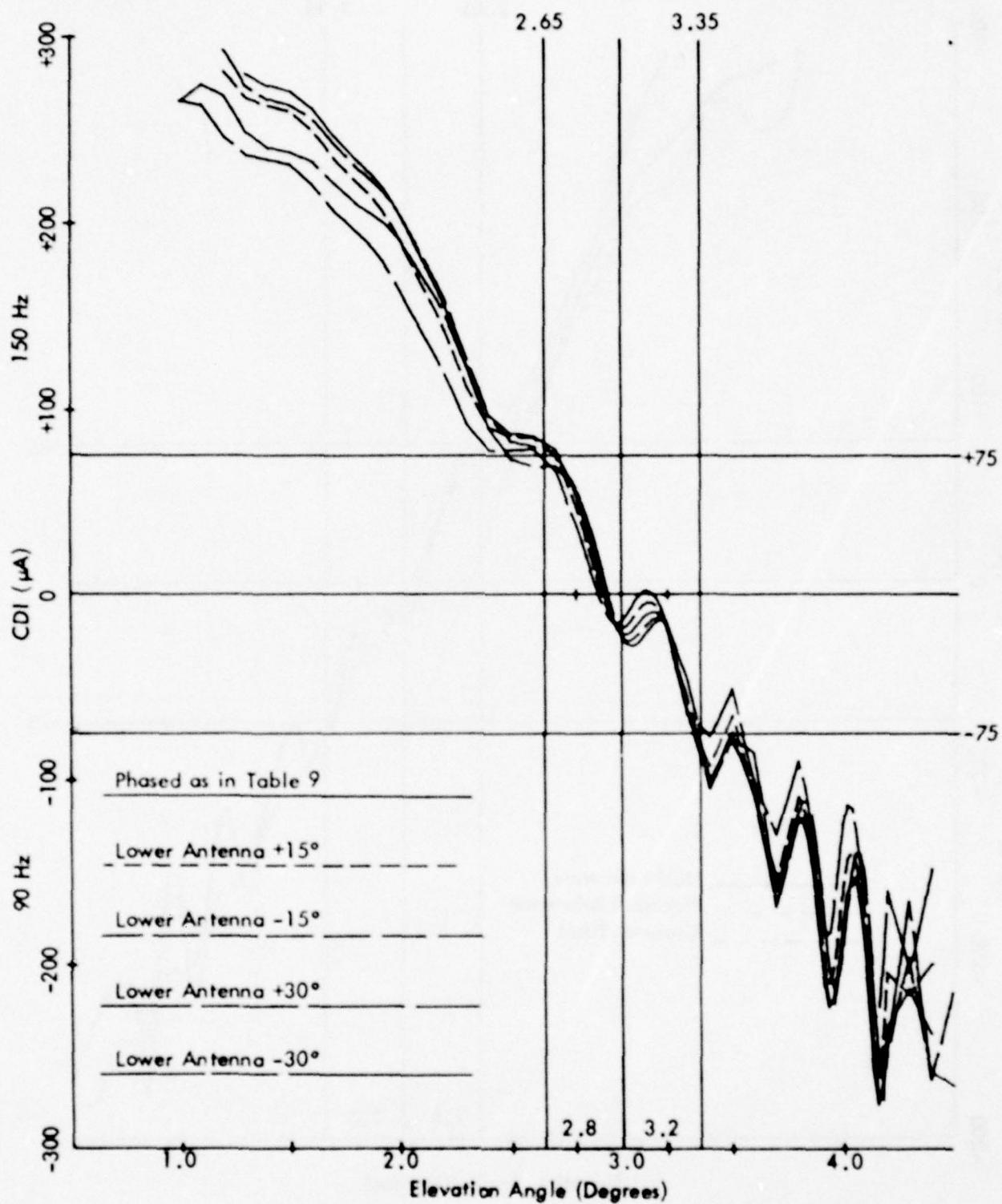
Figure 72c. Calculated Curves of CDI vs. Angle for the Null Reference Glide Slope with the Normal Phasing (as Indicated in Table 9) and Various Amounts of Dephasing for Terrain Profile #5. The simulated aircraft is flying at a constant 1000 ft. altitude above the runway centerline (extended).

-132-
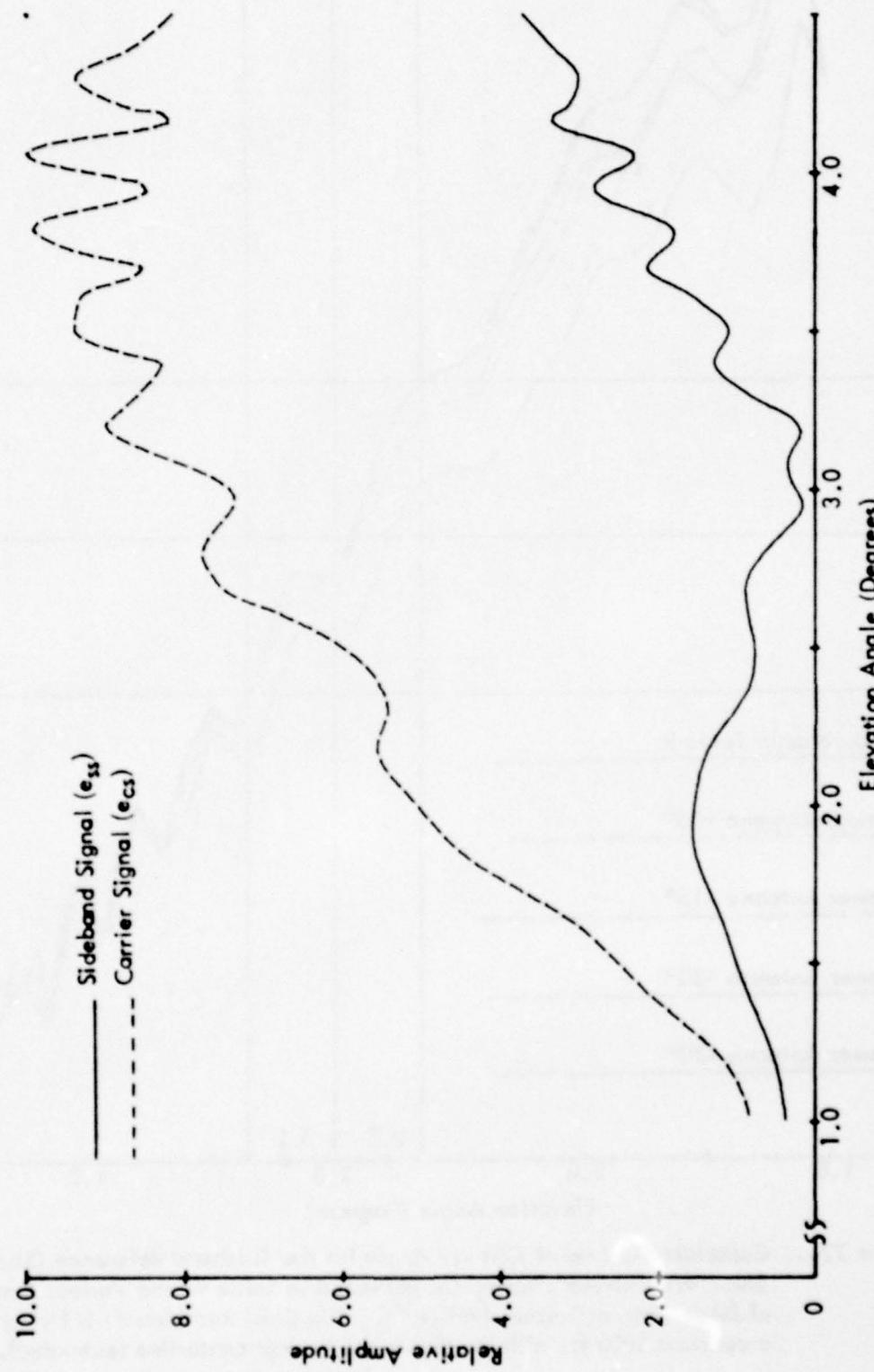
Figure 72d. Calculated Curves of Carrier and Sideband Signals vs. Angle for the Null Reference Glide Slope for Terrain Profile #5. The simulated aircraft is flying at a constant 1000 ft. altitude above the runway centerline (extended).
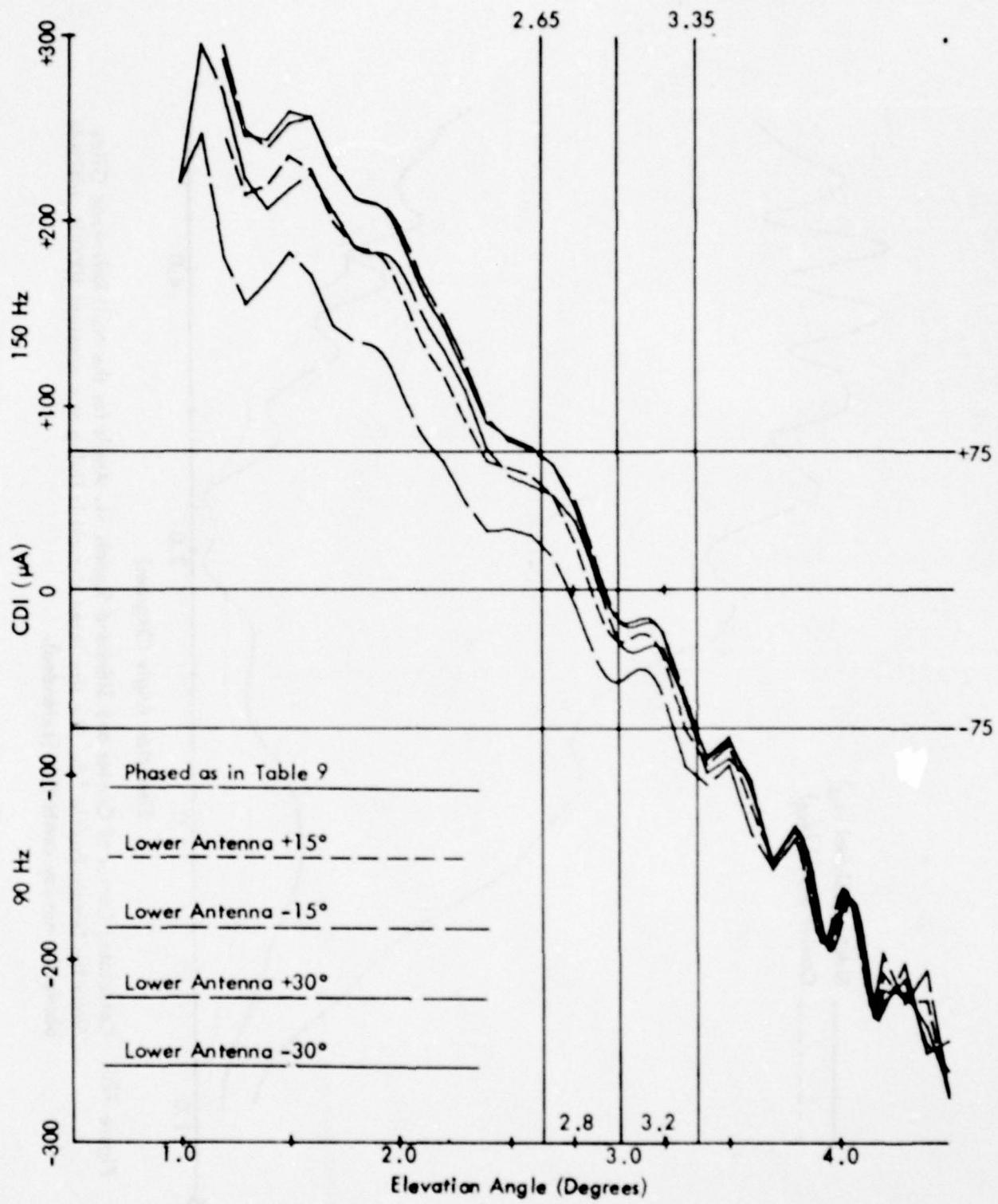
Figure 72e. Calculated Curves of CDI vs. Angle for the Sideband Reference Glide Slope with Normal Phasing (as Indicated in Table 9) and Various Amounts of Dephasing for Terrain Profile #5. The simulated aircraft is flying at a constant 1000 ft. altitude above the runway centerline (extended).
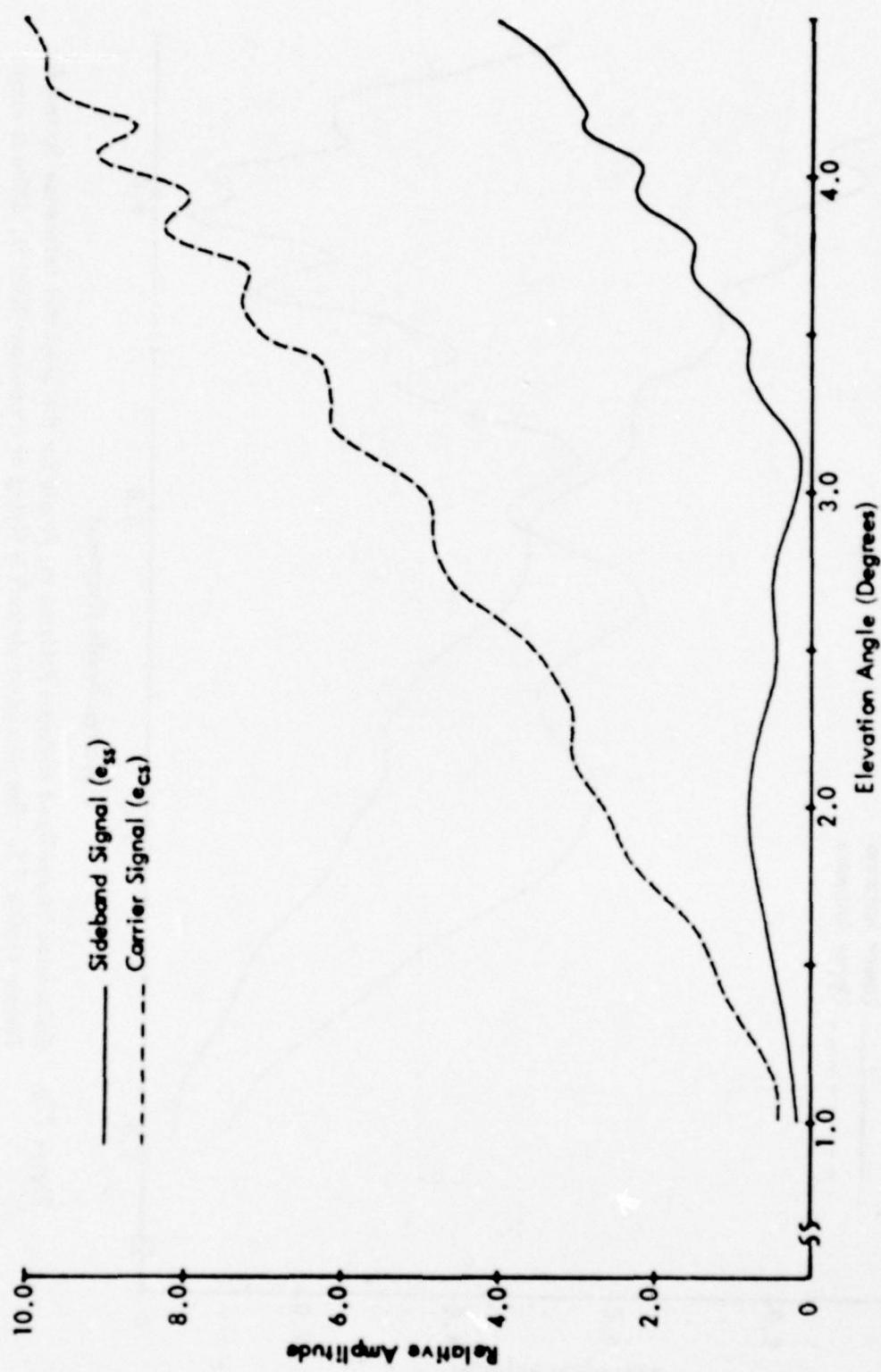
Figure 72f. Calculated Curves of Carrier and Composite Sideband Signals vs. Angle for the Sideband Reference Glide Slope for Terrain Profile #5. The simulated aircraft is flying at a constant 1000 ft. altitude above the runway centerline (extended).
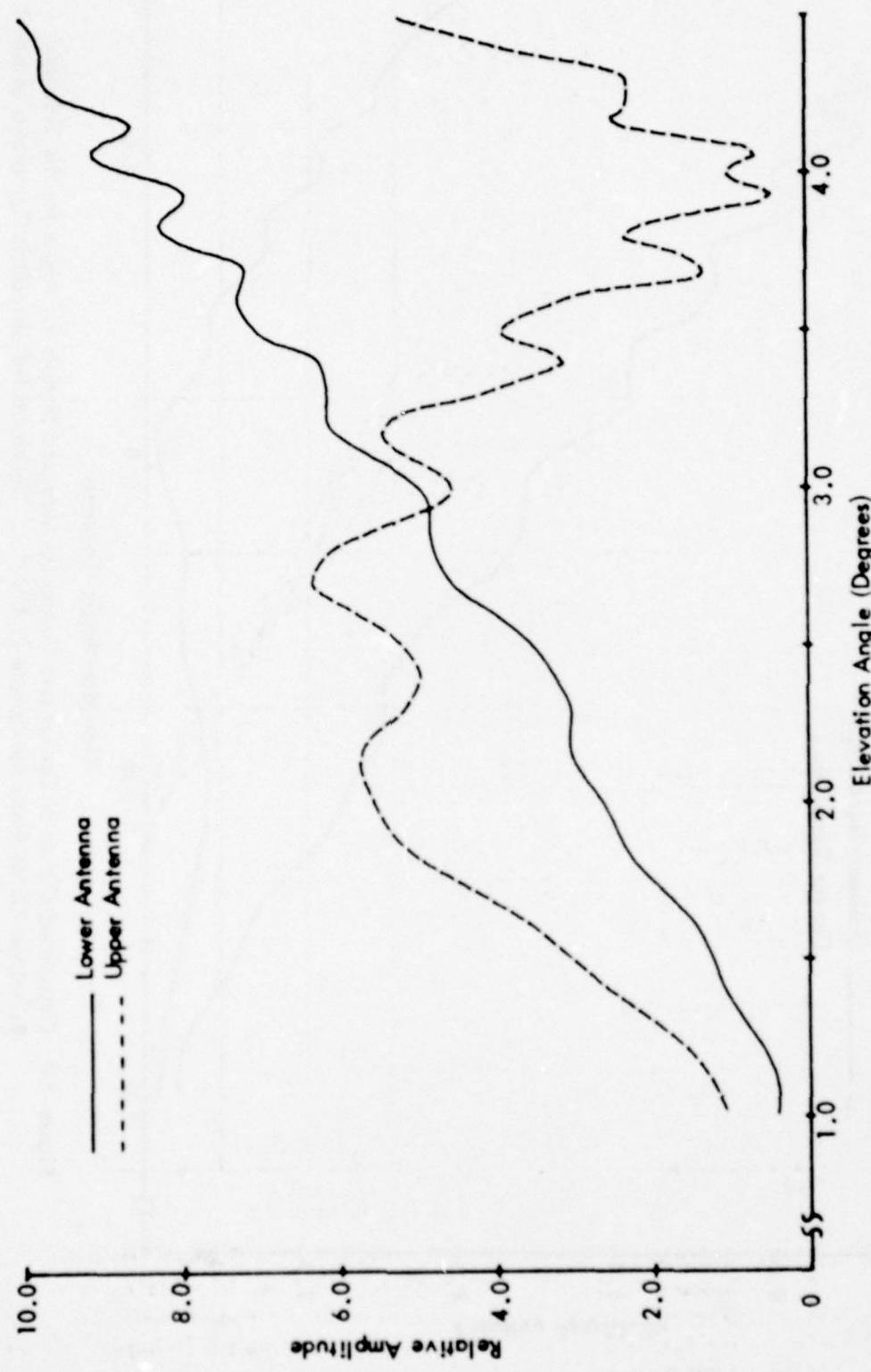
Figure 72g. Calculated Normalized Antenna Patterns vs. Angle for the Sideband Reference System for Terrain Profile #5. The simulated aircraft is flying at a constant 1000 ft. altitude above the runway centerline (extended).
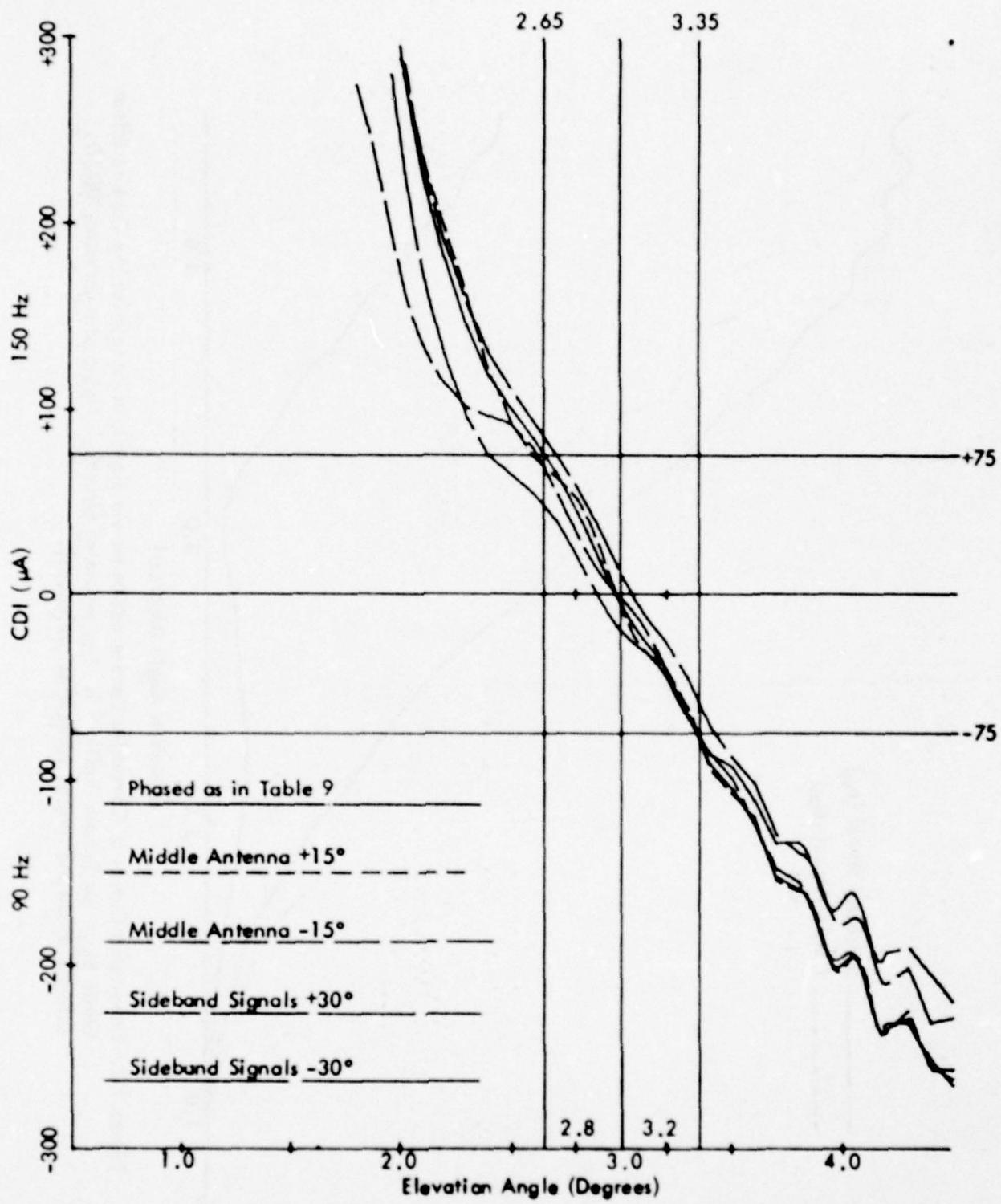
Figure 72h. Calculated Curves of CDI vs. Angle for the Capture Effect Glide Slope with the Normal Phasing (as Indicated in Table 9) and Dephased According to the Flight Inspection Manual Phase Verification Procedure for Terrain Profile #5. The simulated aircraft is flying at a constant 1000 ft. altitude above the runway centerline (extended).
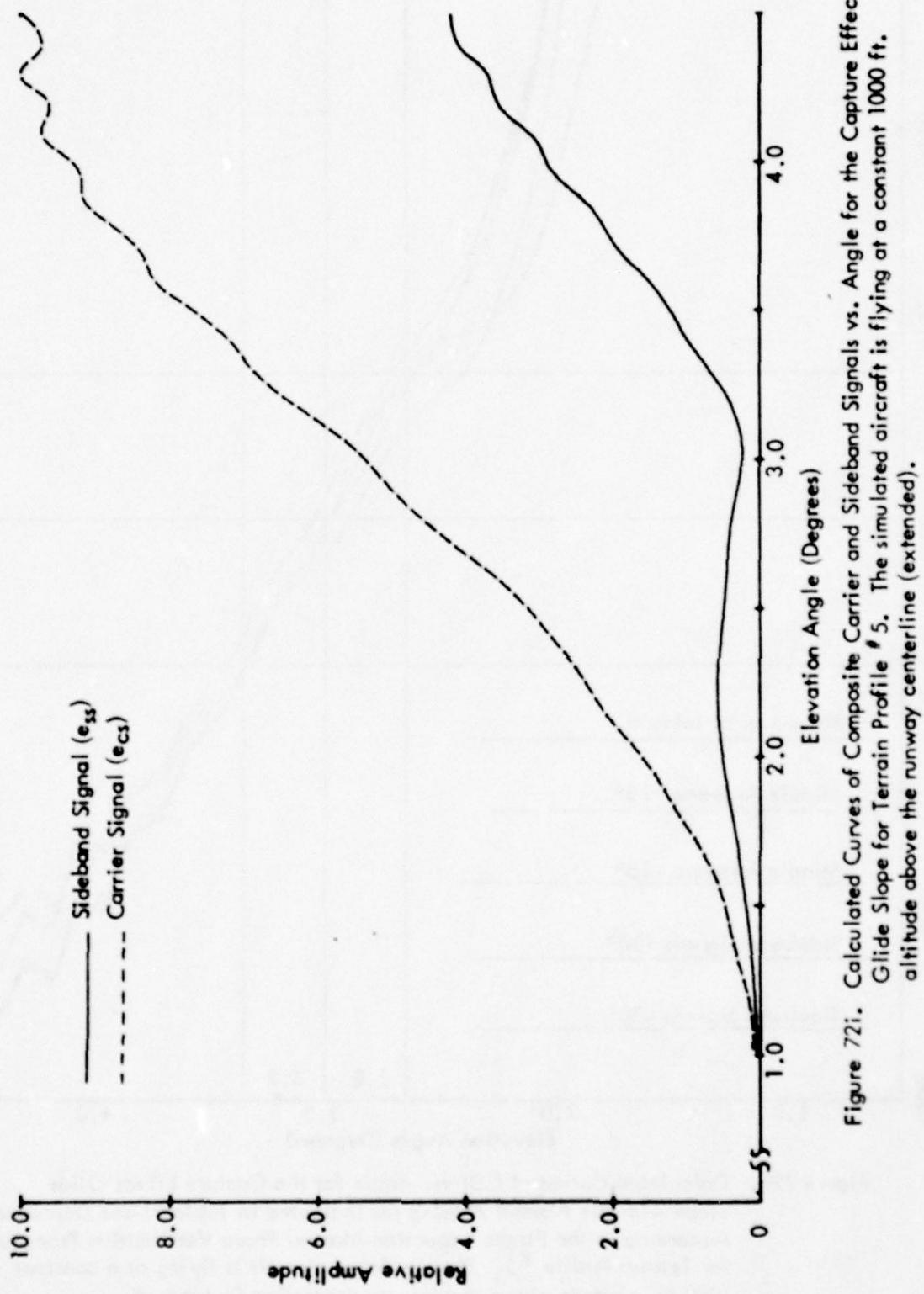
Figure 72i. Calculated Curves of Composite Carrier and Sideband Signals vs. Angle for the Capture Effect Glide Slope for Terrain Profile #5. The simulated aircraft is flying at a constant 1000 ft. altitude above the runway centerline (extended).

Figure 72j. Calculated Normalized Antenna Patterns vs. Angle for the Capture Effect and Null Reference Systems for Terrain Profile #5. The simulated aircraft is flying at a constant 1000 ft. altitude above the runway centerline (extended).

Lower Antenna
Middle Antenna (NR Upper)
Upper Antenna

Elevation Angle (Degrees)

Relative Amplitude

0.5°

8.2 ft.

1000 ft. — 2,750 ft. — 750 ft. — 750 ft.
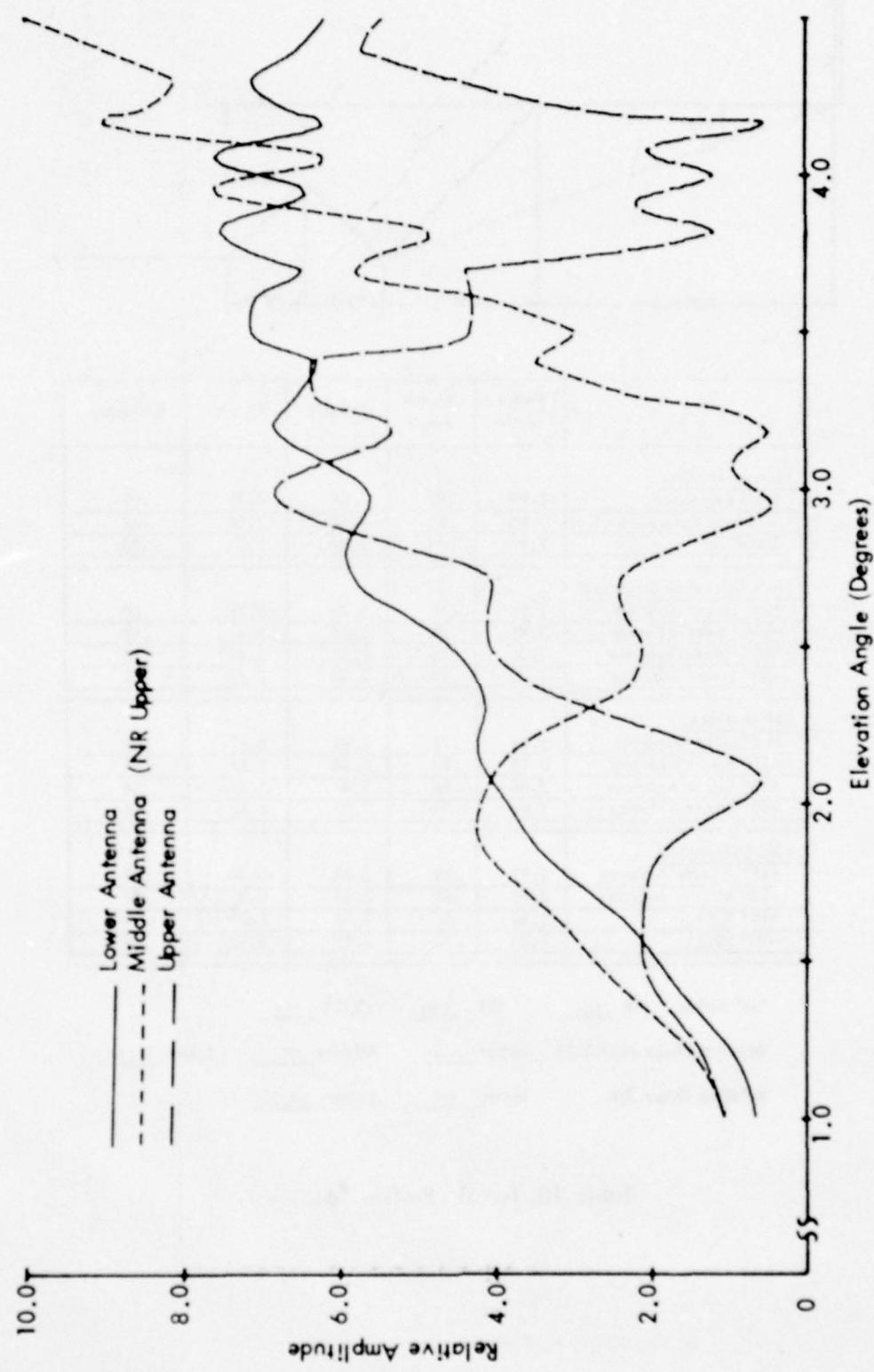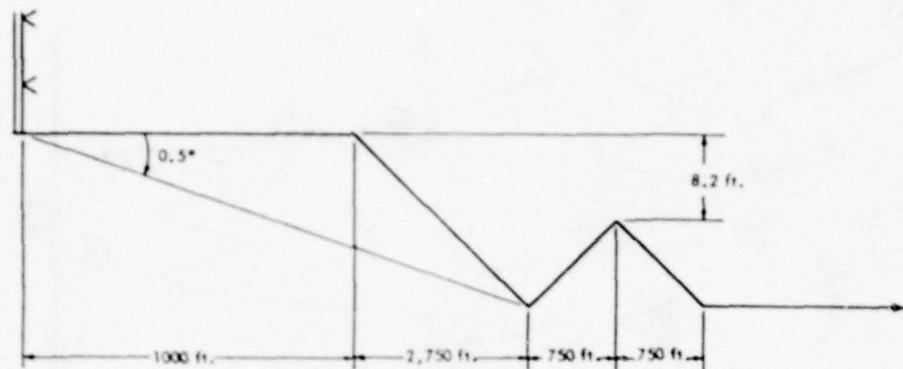
	Path Angle	Width Angle	+75 µA	-75 µA	Symmetry
Normal Phasing					
Null Reference	2.96	.70	2.69	3.39	.61
Sideband Reference	2.95	.70	2.68	3.38	.61
CEGS	2.98	.70	2.64	3.34	.52
Null Reference Dephased					
+15° Lower Antenna	2.97	.69	2.70	3.39	.60
-15° Lower Antenna	2.96	.80	2.61	3.41	.57
+30° Lower Antenna	3.00	.73	2.67	3.40	.55
-30° Lower Antenna	2.95	.99	2.46	3.45	.51
SBR Dephased					
+15° Lower Antenna	2.94	.71	2.66	3.37	.61
-15° Lower Antenna	2.92	.83	2.54	3.37	.54
+30° Lower Antenna	2.86	.86	2.47	3.32	.54
-30° Lower Antenna	2.84	1.00	2.32	3.32	.48
CEGS Dephased					
+15° Middle Antenna	2.97	.82	2.54	3.38	.48
-15° Middle Antenna	2.99	.67	2.67	3.35	.51
+30° SBO	2.90	.85	2.52	3.37	.54
-30° SBO	3.05	.75	2.67	3.43	.49

"A" Ratio: NR .286   SBR .290   CEGS .323

Relative Phase NR/CEGS   Upper 6.9°   Middle 0°   Lower -3.7°

Relative Phase SBR   Upper 0°   Lower -2.9°

Table 10. Terrain Profile #6.

-140-
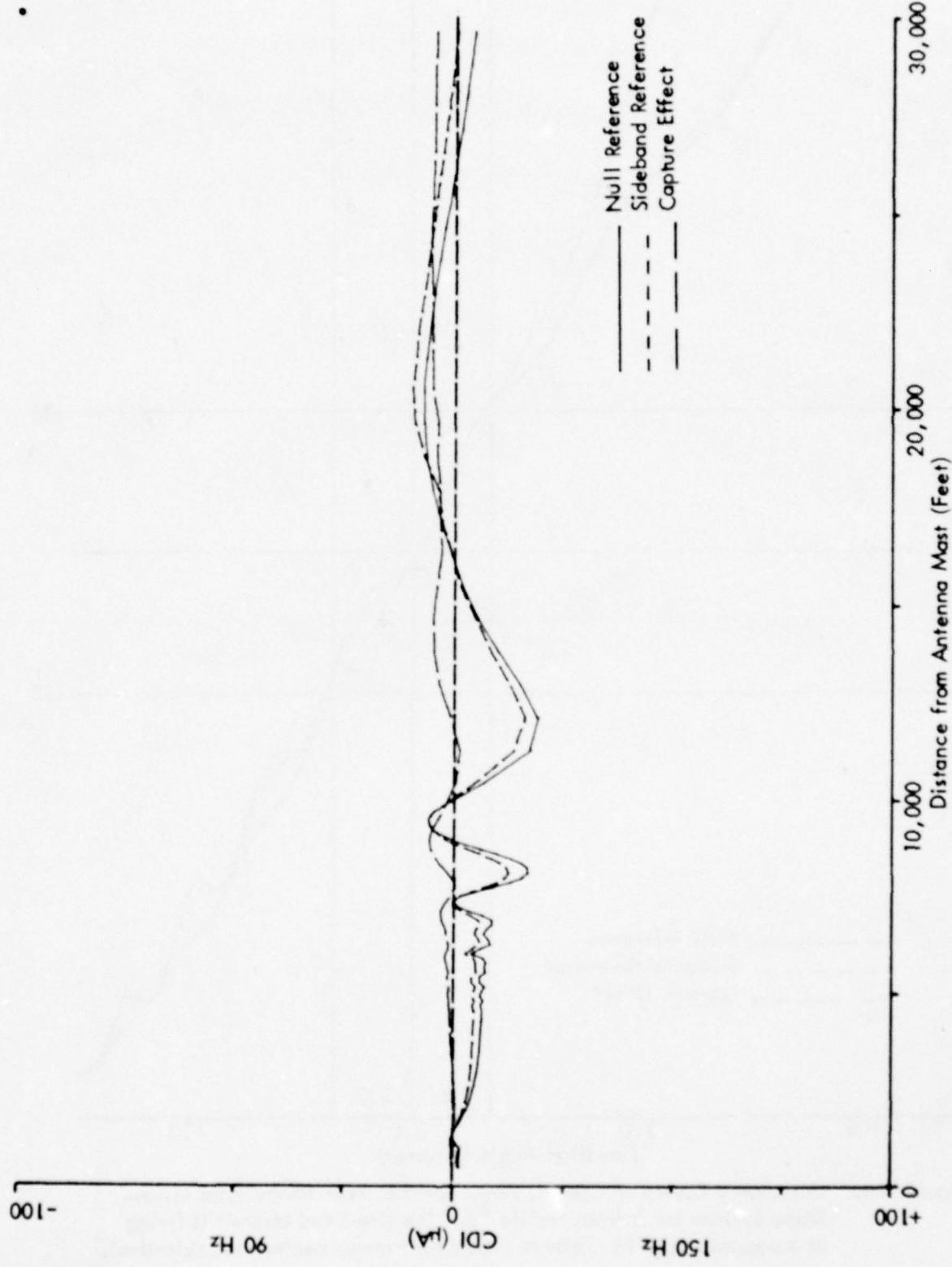
Figure 73a. Calculated Curves of CDI vs. Distance for the Three Image Type Glide-Slope Systems for Terrain Profile #6. The simulated aircraft is flying a constant 3.0 degree low approach over the runway centerline (extended).
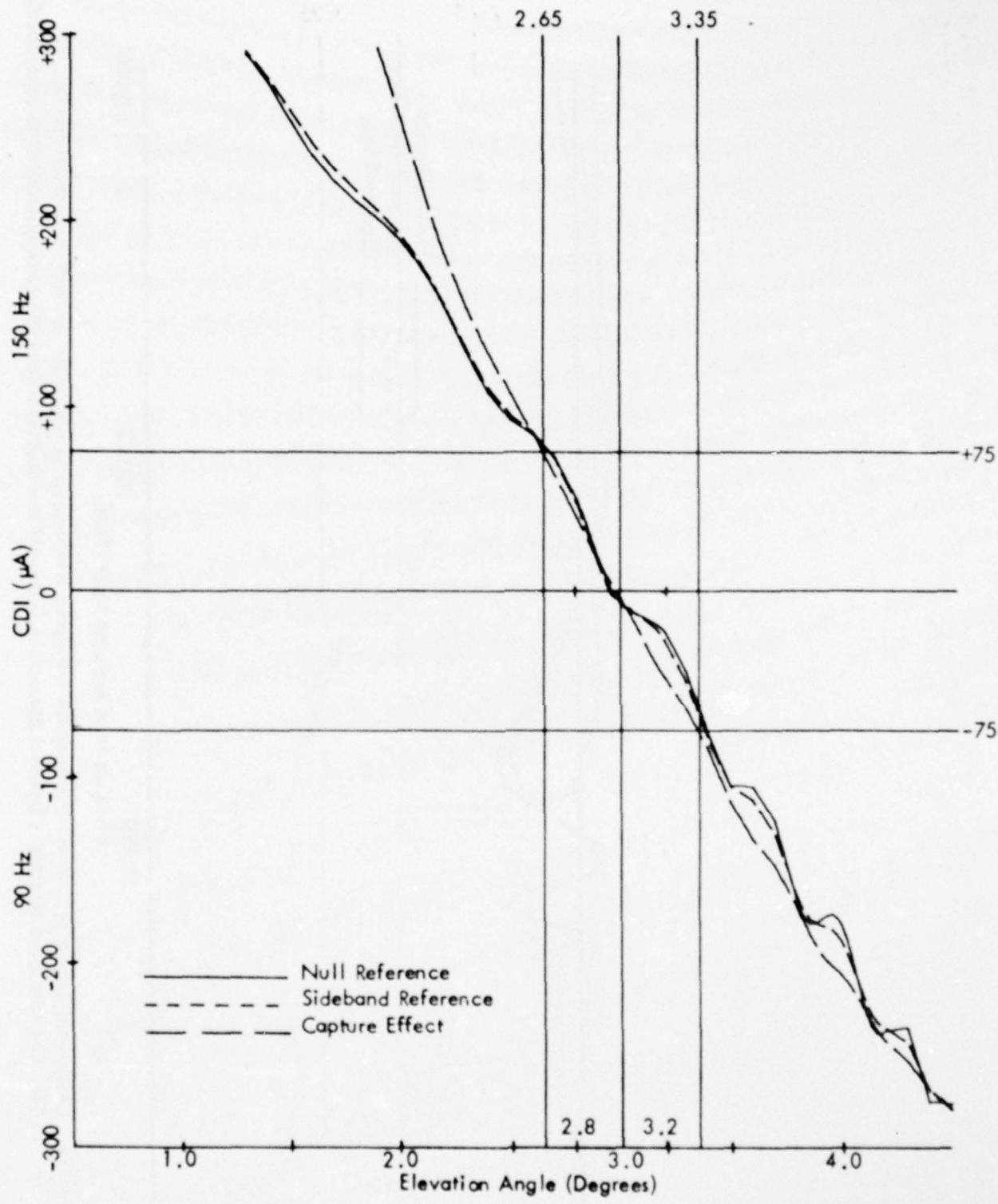
Figure 73b. Calculated Curves of CDI vs. Angle for the Three Image Type Glide-Slope Systems for Terrain Profile #6. The simulated aircraft is flying at a constant 1000 ft. altitude above the runway centerline (extended).

-142-
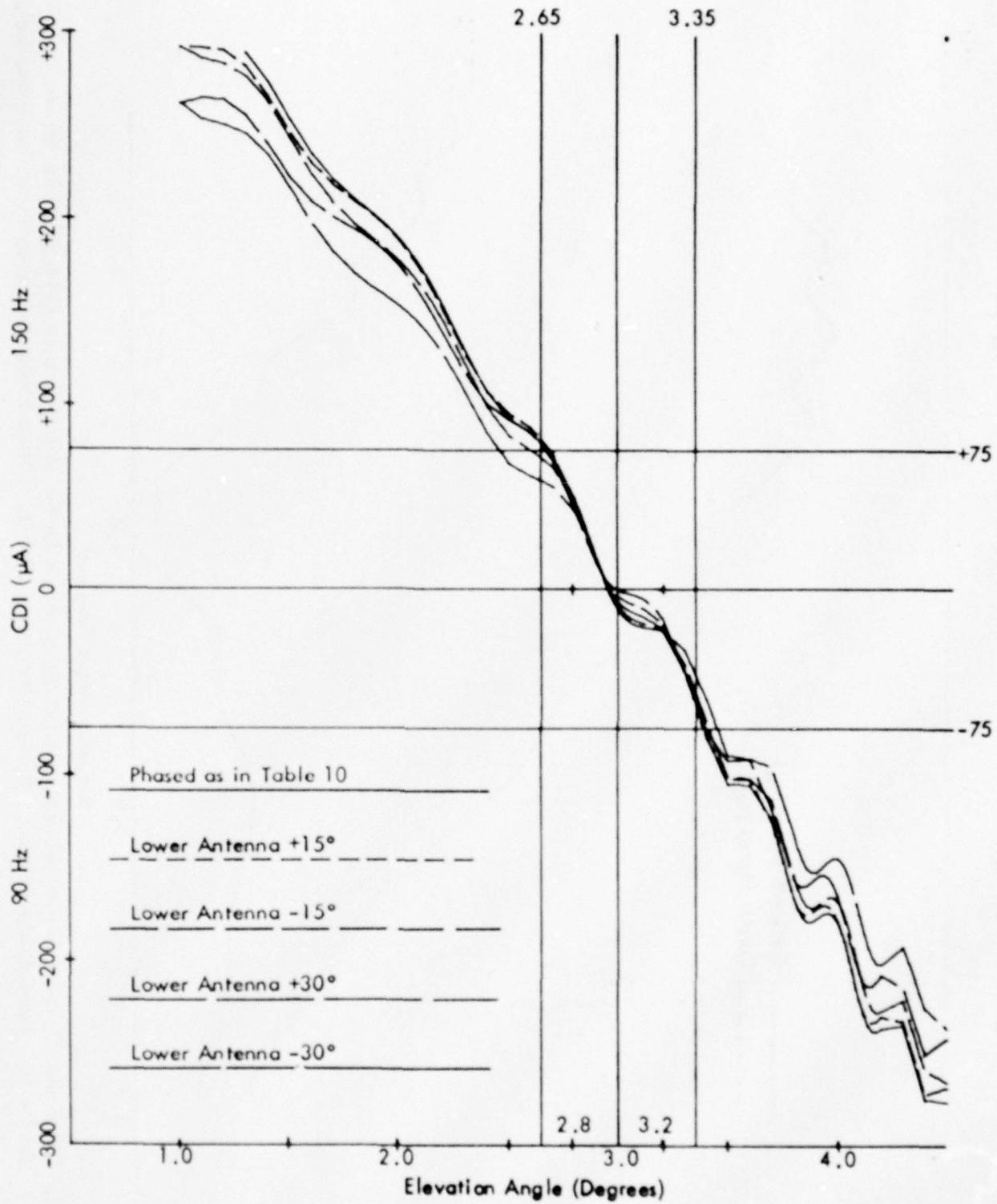
Figure 73c. Calculated Curves of CDI vs. Angle for the Null Reference Glide Slope with the Normal Phasing (as Indicated in Table 10) and Various Amounts of Dephasing for Terrain Profile #6. The simulated aircraft is flying at a constant 1000 ft. altitude above the runway centerline (extended).

-143-
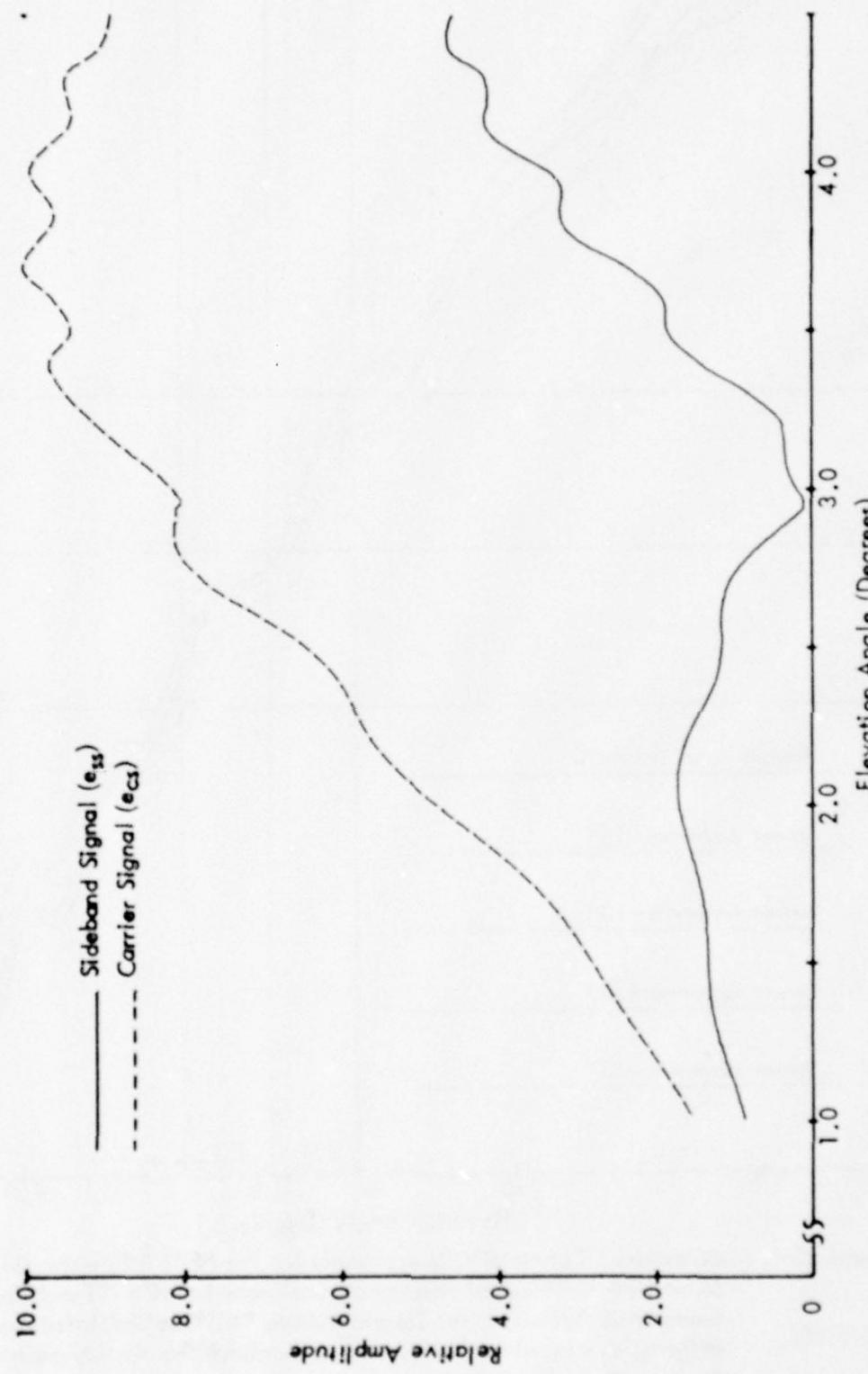
Figure 73d. Calculated Curves of Carrier and Sideband Signals vs. Angle for the Null Reference Glide Slope for Terrain Profile #6. The simulated aircraft is flying at a constant 1000 ft. altitude above the runway centerline (extended).

-144-
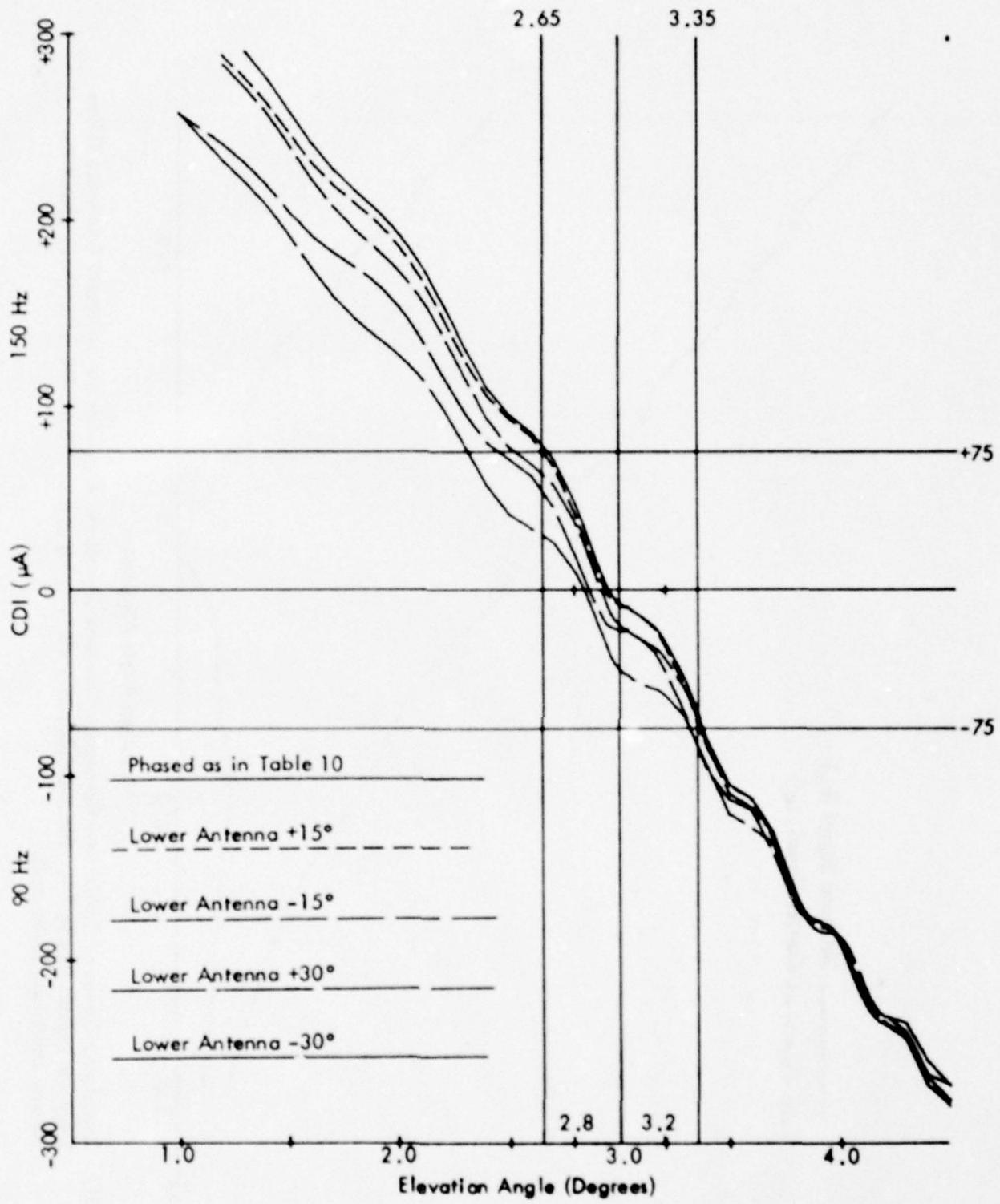
Figure 73e. Calculated Curves of CDI vs. Angle for the Sideband Reference Glide Slope with Normal Phasing (as Indicated in Table 10) and Various Amounts of Dephasing for Terrain Profile #6. The simulated aircraft is flying at a constant 1000 ft. altitude above the runway centerline (extended).

-145-
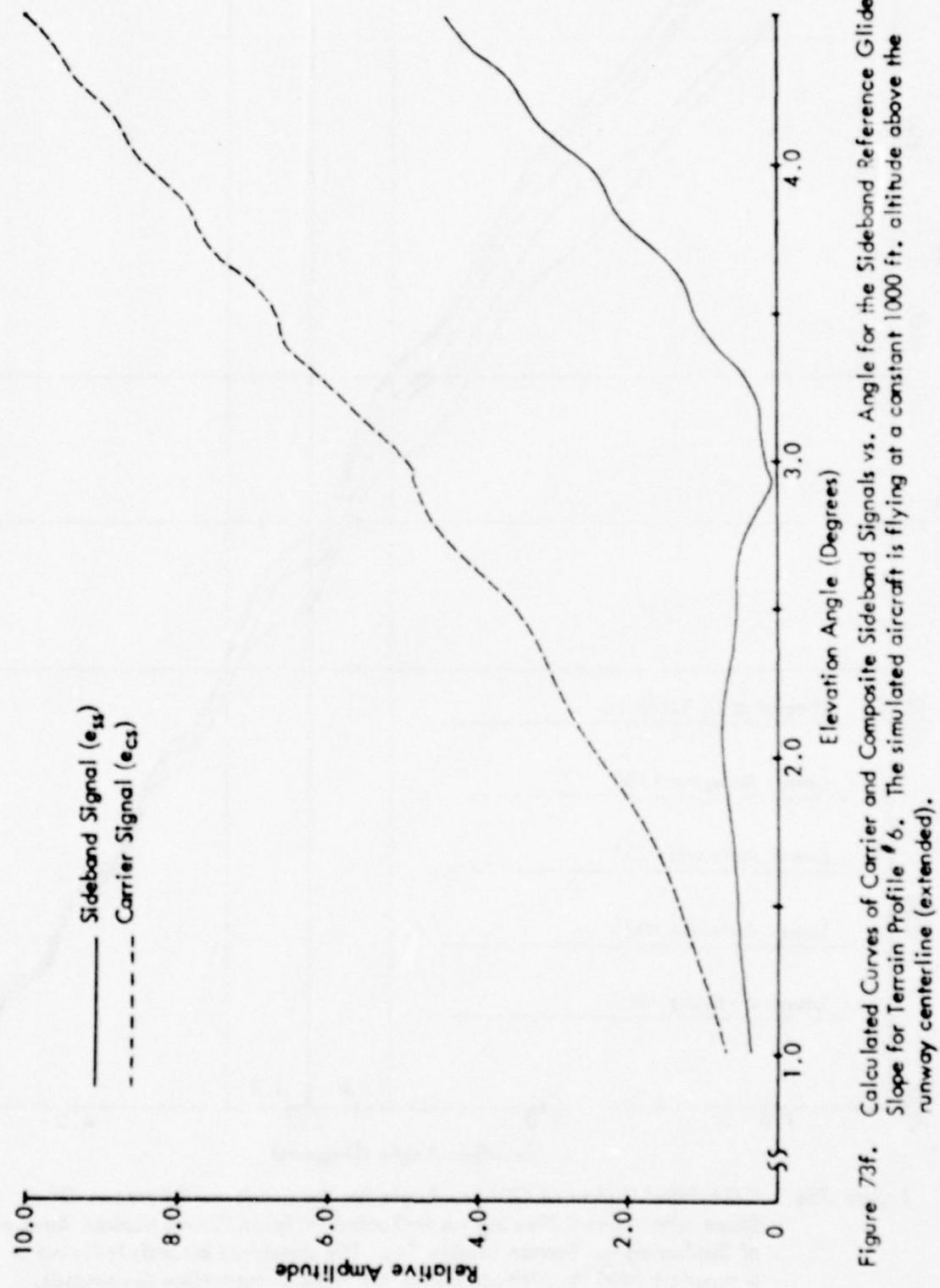
Figure 73f. Calculated Curves of Carrier and Composite Sideband Signals vs. Angle for the Sideband Reference Glide Slope for Terrain Profile #6. The simulated aircraft is flying at a constant 1000 ft. altitude above the runway centerline (extended).
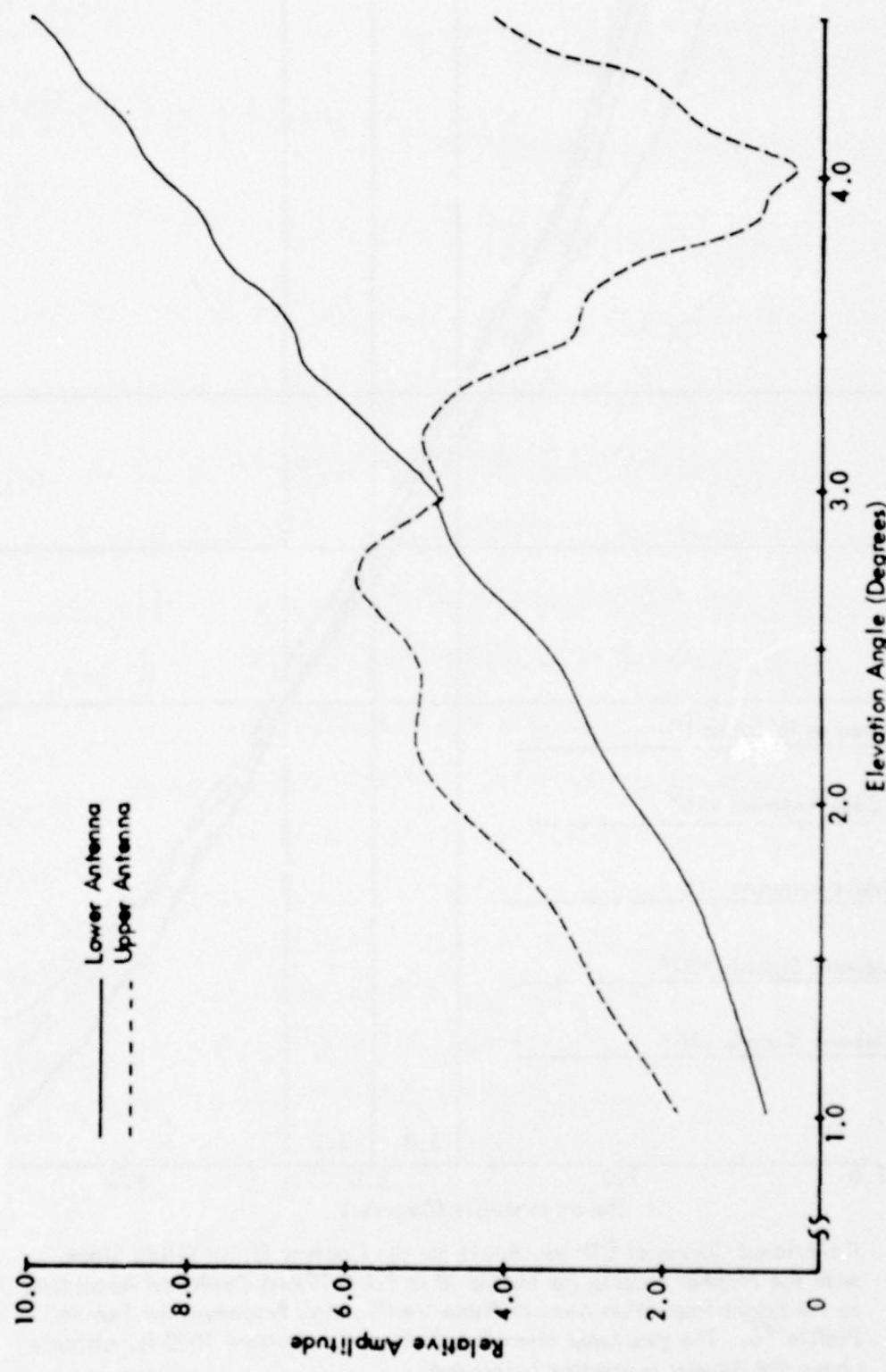
Figure 73g. Calculated Normalized Antenna Patterns vs. Angle for the Sideband Reference System for Terrain Profile #6. The simulated aircraft is flying at a constant 1000 ft. altitude above the runway centerline (extended).

-147-
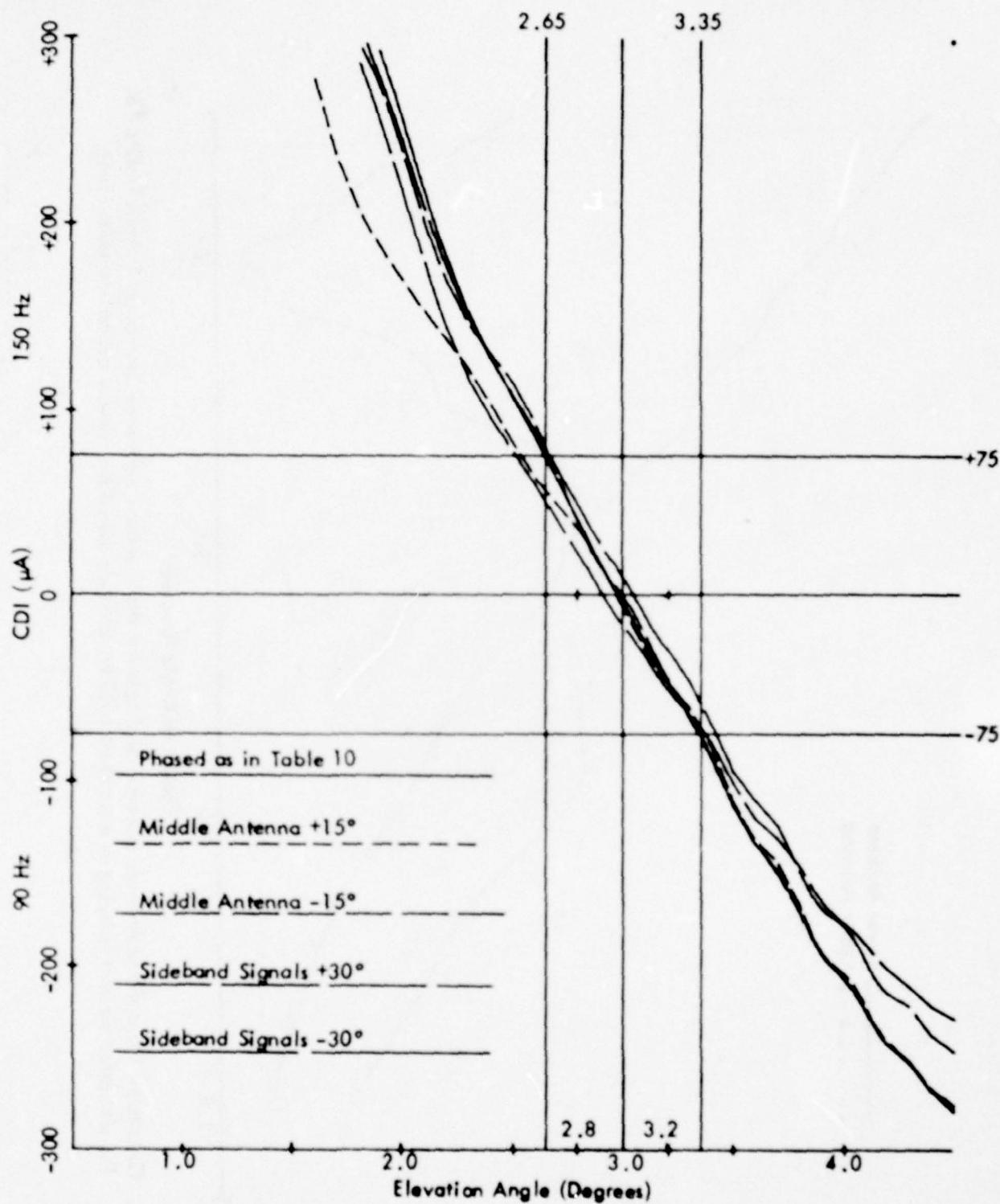
Figure 73h. Calculated Curves of CDI vs. Angle for the Capture Effect Glide Slope with the Normal Phasing (as Indicated in Table 10) and Dephased According to the Flight Inspection Manual Phase Verification Procedure for Terrain Profile #6. The simulated aircraft is flying at a constant 1000 ft. altitude above the runway centerline (extended).

-148-
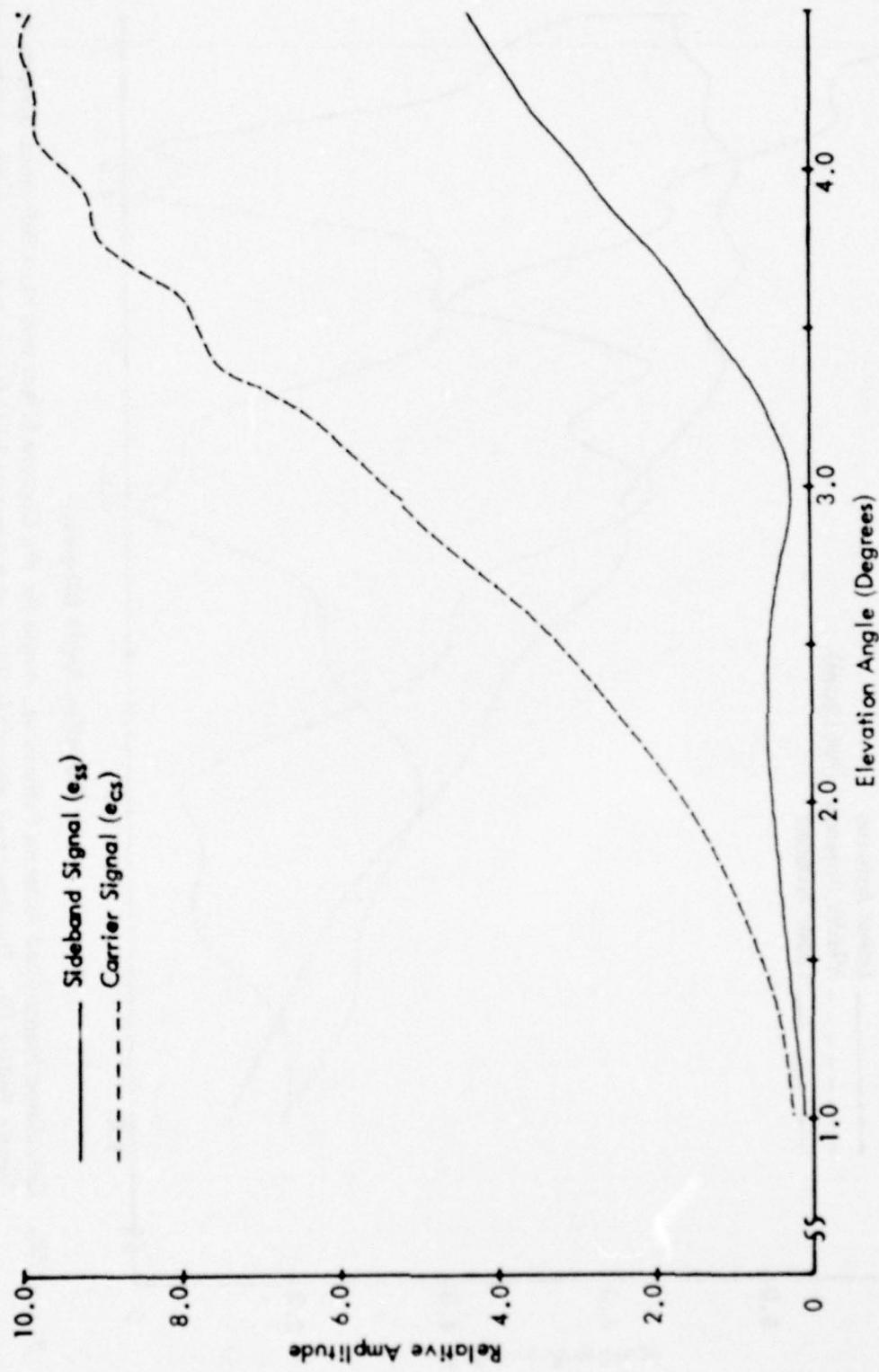
Figure 73i. Calculated Curves of Composite Carrier and Sideband Signals vs. Angle for the Capture Effect Glide Slope for Terrain Profile #6. The simulated aircraft is flying at a constant 1000 ft. altitude above the runway centerline (extended).

-149-
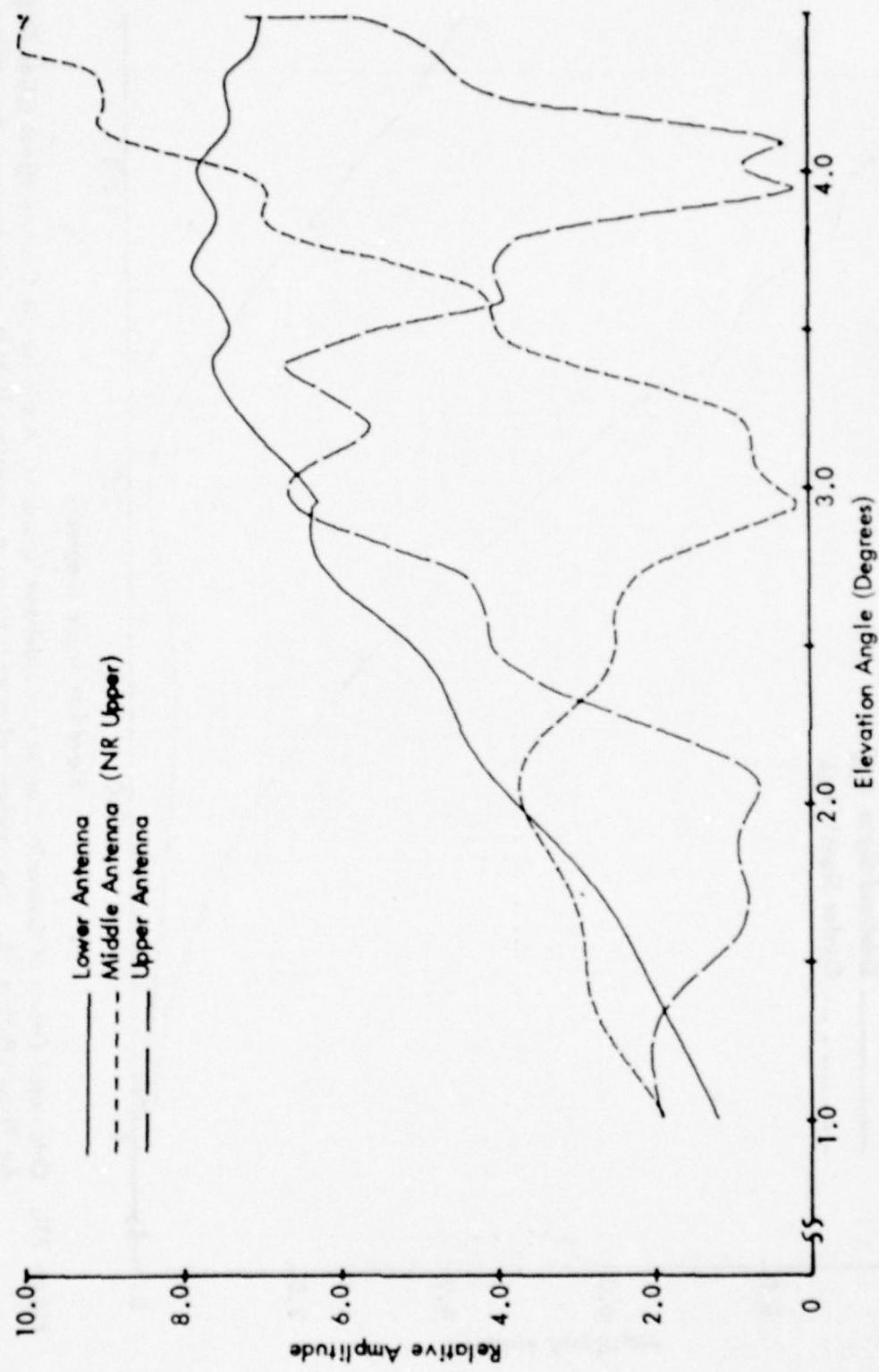
Figure 73j. Calculated Normalized Antenna Patterns vs. Angle for the Capture Effect and Null Reference Systems for Terrain Profile #6. The simulated aircraft is flying at a constant 1000 ft. altitude above the runway center-line (extended).

-150-

0.5°

8.2 ft.

3000 ft. — 750 ft. — 750 ft. — 750 ft.
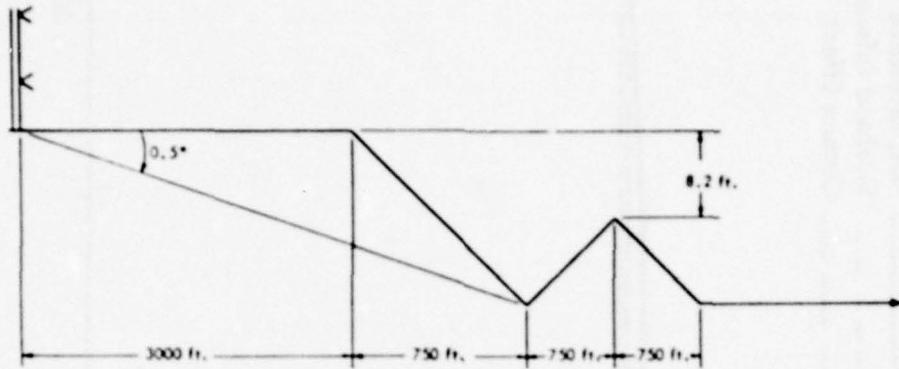
	Path Angle	Width Angle	+75 μA	-75 μA	Symmetry
Normal Phasing					
Null Reference	2.99	.70	2.63	3.33	.49
Sideband Reference	2.99	.70	2.64	3.34	.50
CEGS	3.01	.70	2.65	3.35	.49
Null Reference Dephased					
+15° Lower Antenna	3.00	.72	2.62	3.34	.48
-15° Lower Antenna	2.98	.74	2.61	3.35	.49
+30° Lower Antenna	3.10	.93	2.58	3.50	.44
-30° Lower Antenna	2.98	.84	2.54	3.38	.48
SBR Dephased					
+15° Lower Antenna	2.96	.72	2.60	3.31	.50
-15° Lower Antenna	2.95	.75	2.58	3.33	.50
+30° Lower Antenna	2.85	.86	2.40	3.26	.48
-30° Lower Antenna	2.85	.90	2.39	3.29	.48
CEGS Dephased					
+15° Middle Antenna	3.00	.75	2.61	3.36	.47
-15° Middle Antenna	3.01	.72	2.63	3.35	.47
+30° SBO	3.00	.81	2.59	3.40	.49
-30° SBO	3.01	.80	2.63	3.40	.49

"A" Ratio: NR .276   SBR .282   CEGS .302

Relative Phase NR/CEGS   Upper 0°   Middle 0°   Lower -0.4°

Relative Phase SBR   Upper 0°   Lower -.30°

Table 11. Terrain Profile #7.
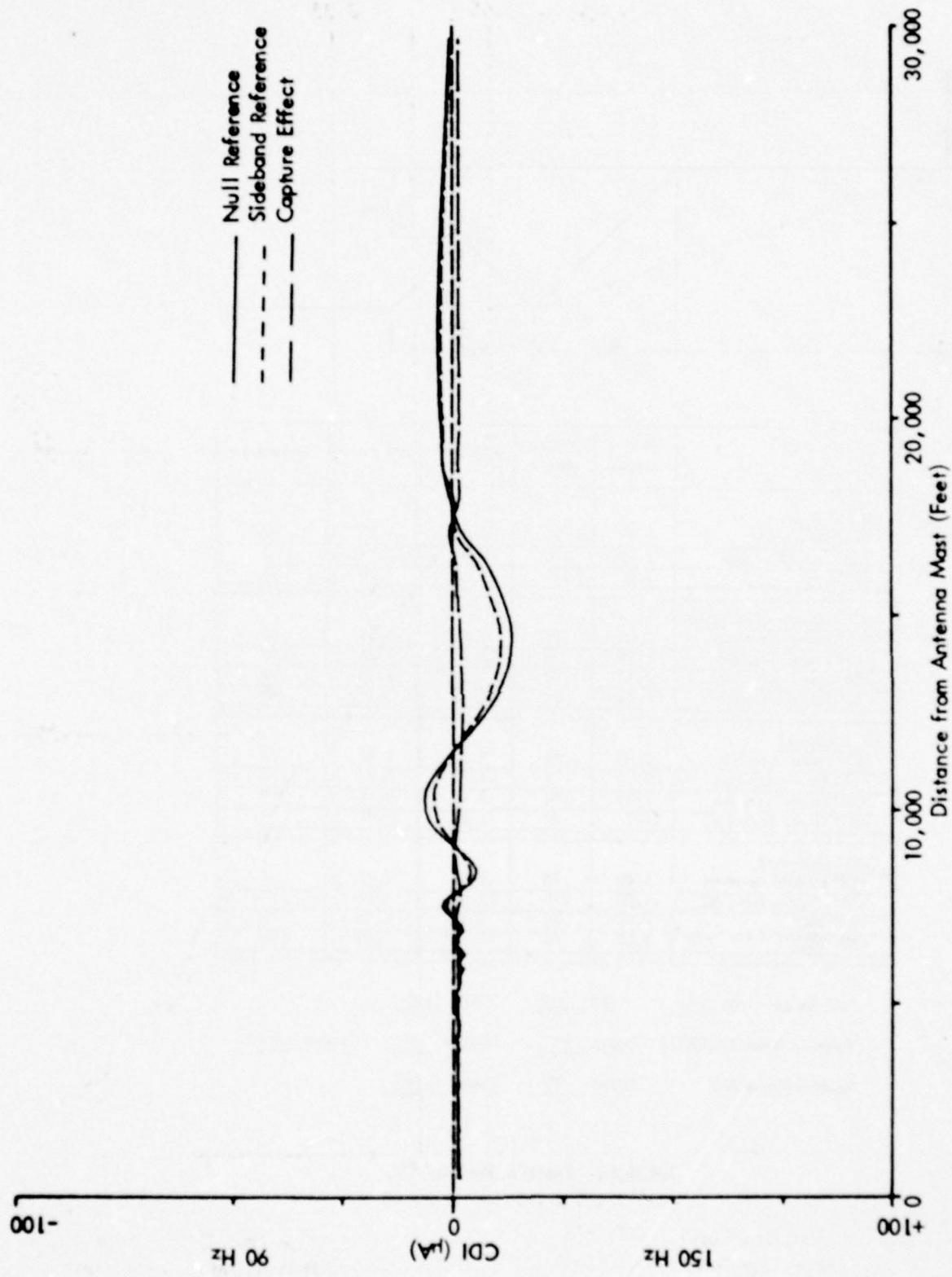
Figure 74a. Calculated Curves of CDI vs. Distance for the Three Image Type Glide-Slope Systems for Terrain Profile #7. The simulated aircraft is flying a constant 3.0 degree low approach over the runway centerline (extended).
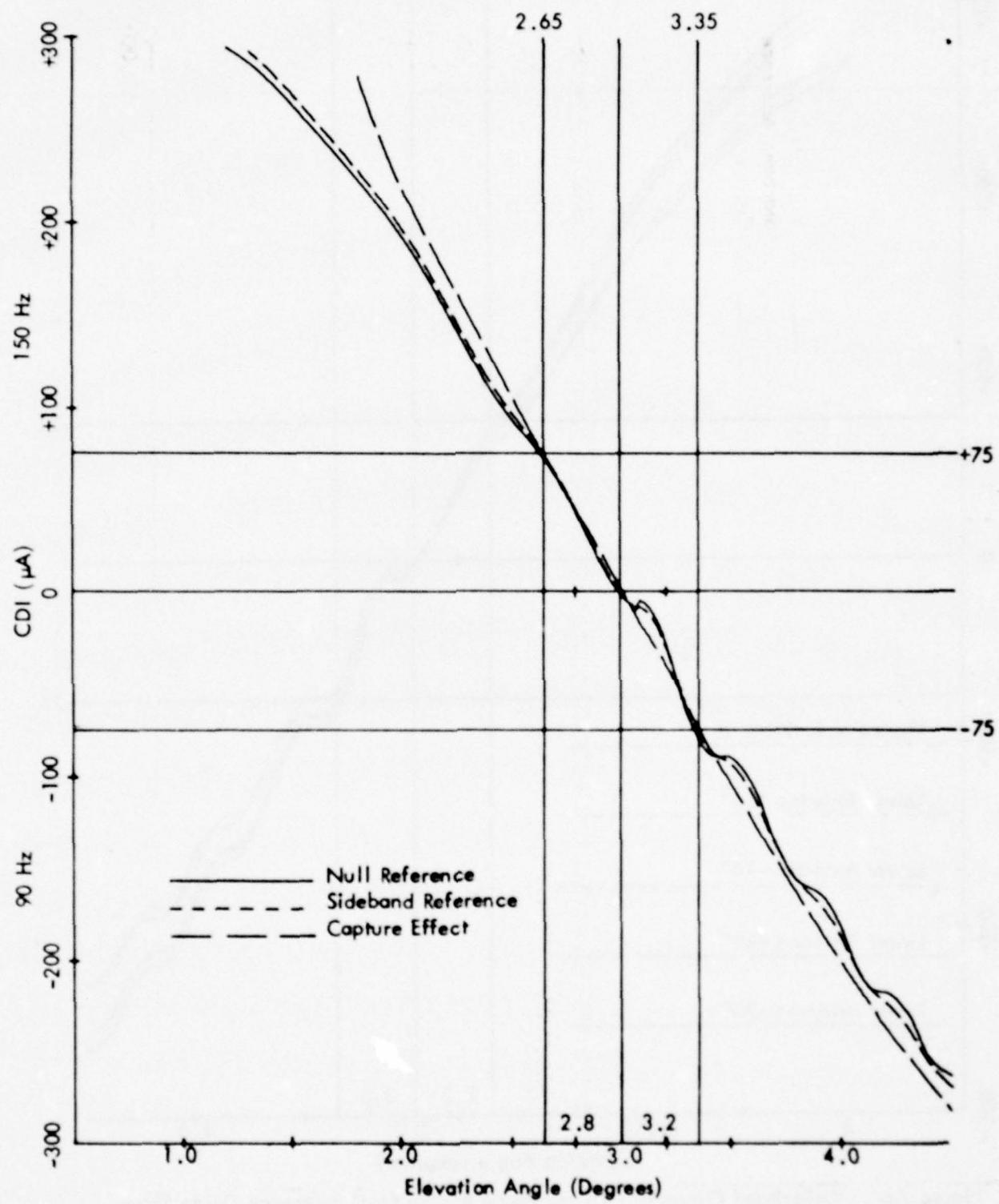
Figure 74b. Calculated Curves of CDI vs. Angle for the Three Image Type Glide-Slope Systems for Terrain Profile #7. The simulated aircraft is flying at a constant 1000 ft. altitude above the runway centerline (extended).
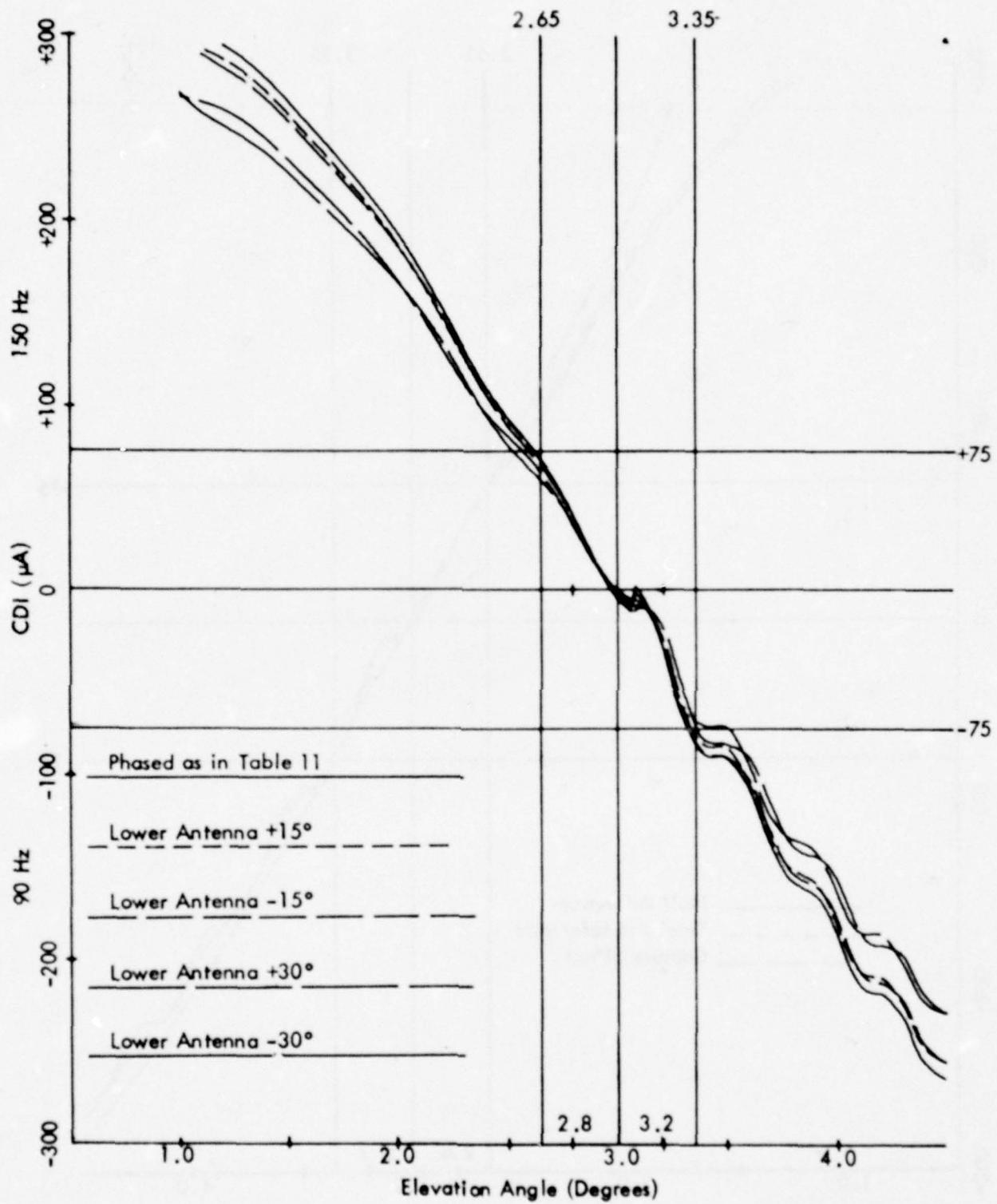
Figure 74c. Calculated Curves of CDI vs. Angle for the Null Reference Glide Slope with the Normal Phasing (as Indicated in Table 11) and Various Amounts of Dephasing for Terrain Profile #7. The simulated aircraft is flying at a constant 1000 ft. altitude above the runway centerline (extended).
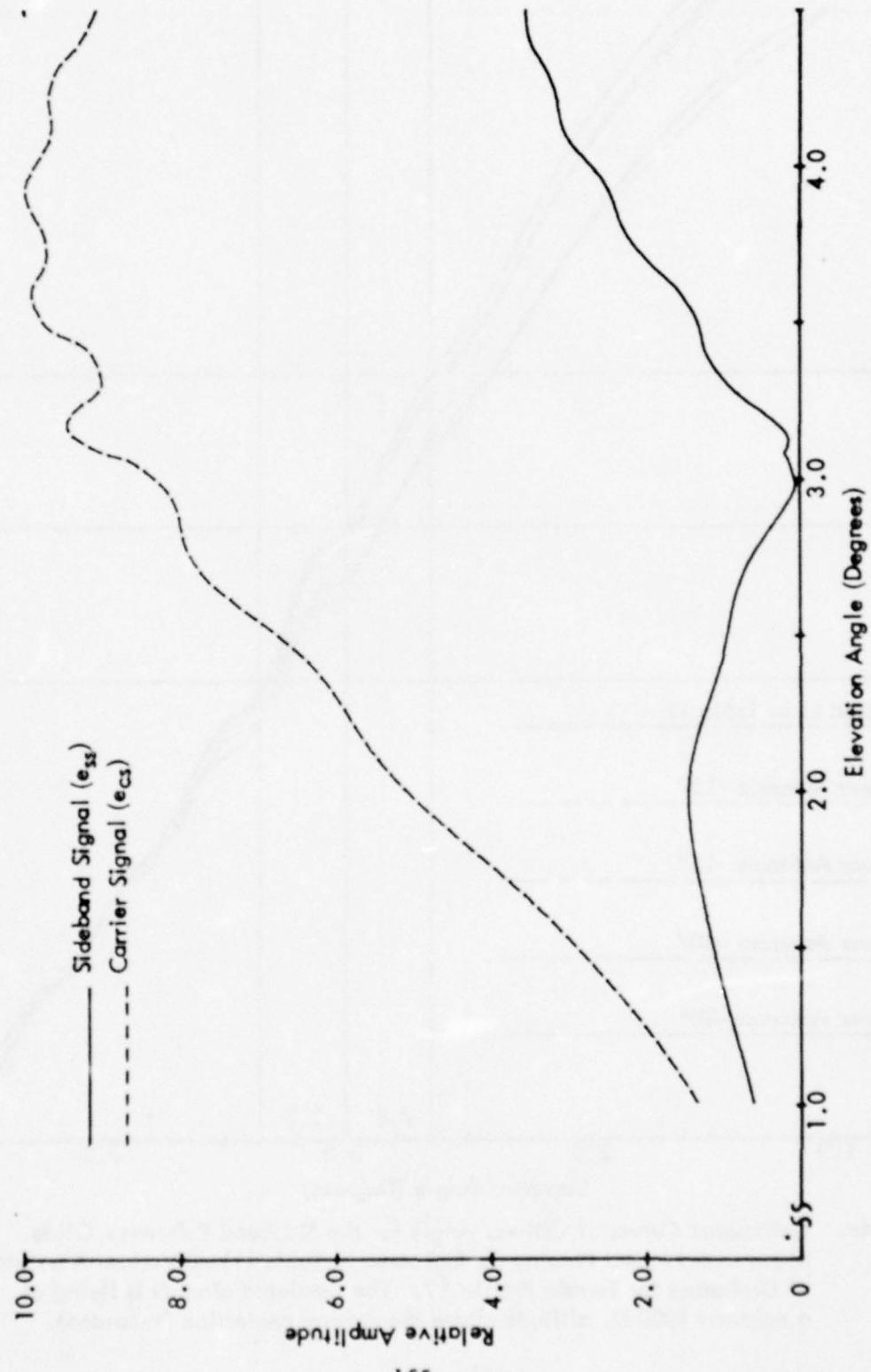
Figure 74d. Calculated Curves of Carrier and Sideband Signals vs. Angle for the Null Reference Glide Slope for Terrain Profile #7. The simulated aircraft is flying at a constant 1000 ft. altitude above the runway centerline (extended).
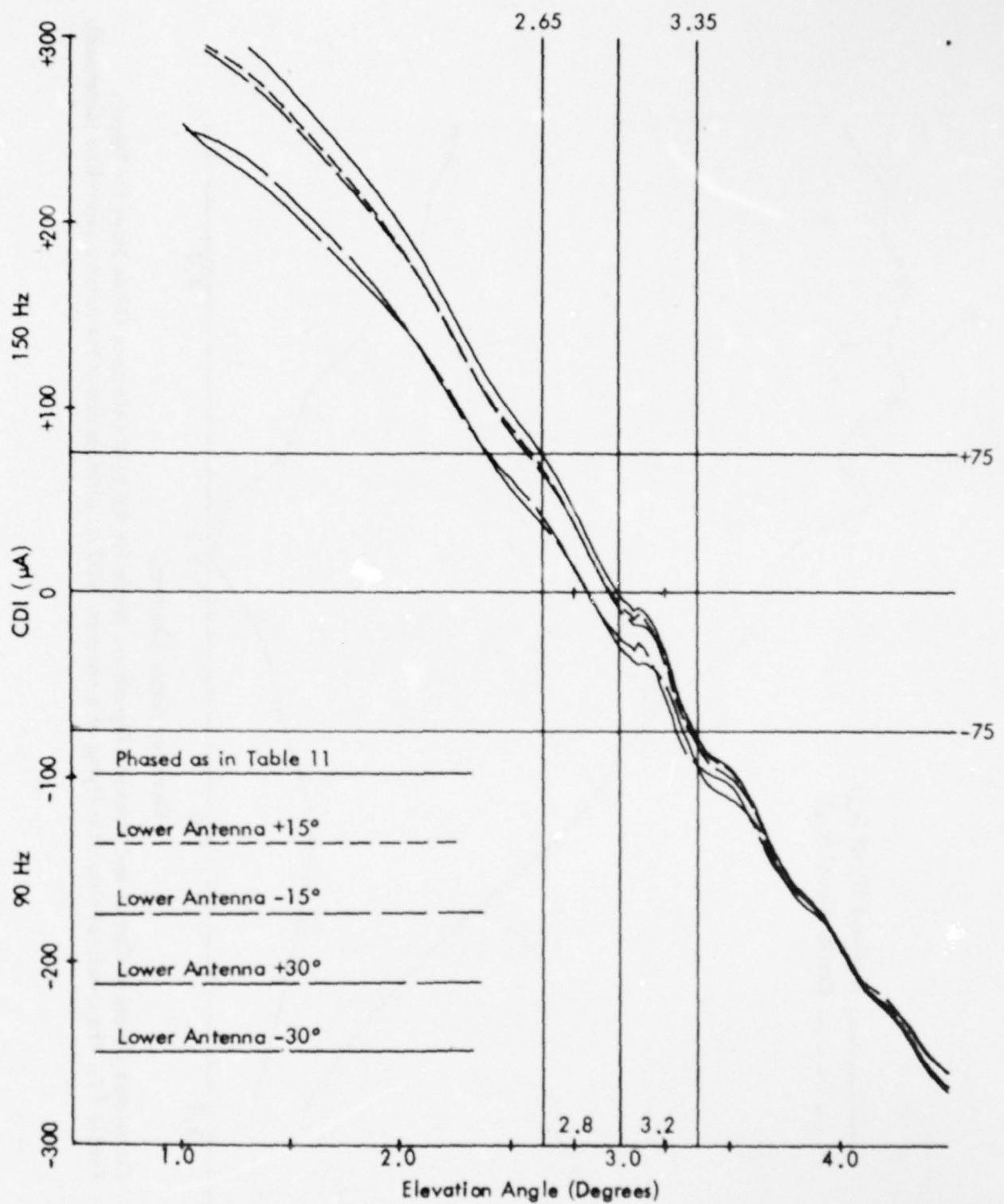
Figure 74e. Calculated Curves of CDI vs. Angle for the Sideband Reference Glide Slope with Normal Phasing (as Indicated in Table 11)and Various Amounts of Dephasing for Terrain Profile #7. The simulated aircraft is flying at a constant 1000 ft. altitude above the runway centerline (extended).
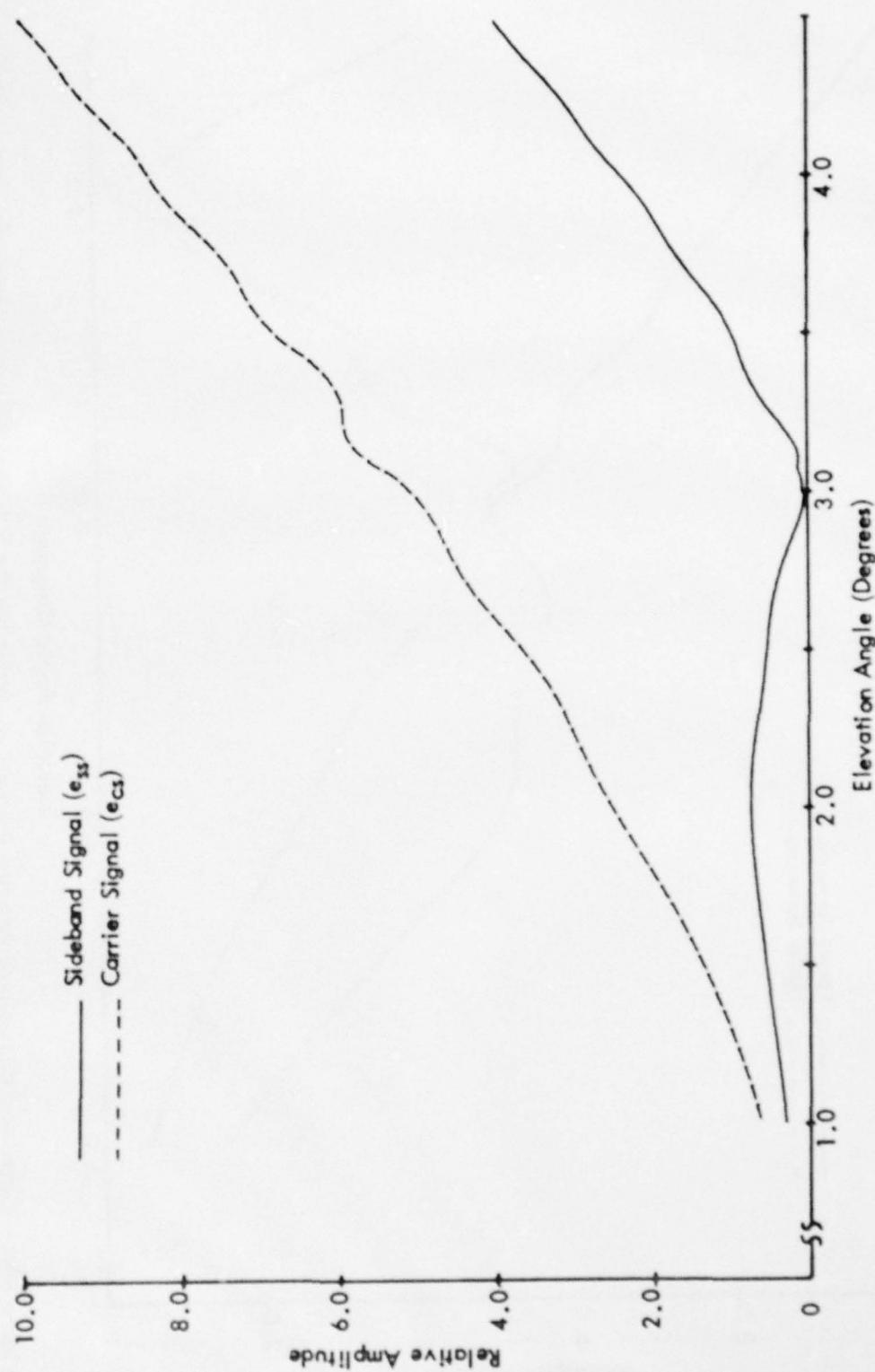
Figure 74f. Calculated Curves of Carrier and Composite Sideband Signals vs. Angle for the Sideband Reference Glide Slope for Terrain Profile #7. The simulated aircraft is flying at a constant 1000 ft. altitude above the runway center-line (extended).
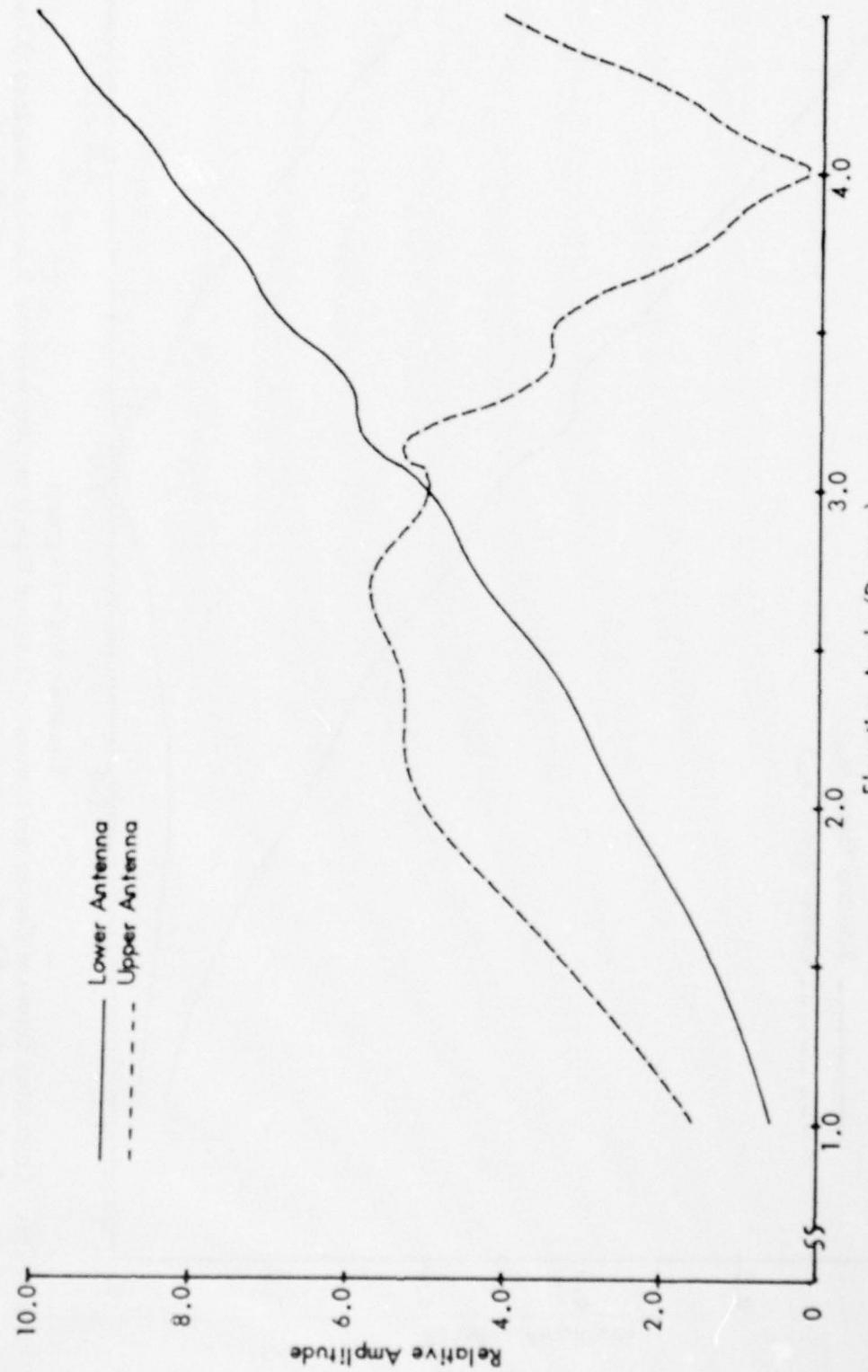
Figure 74g. Calculated Normalized Antenna Patterns vs. Angle for the Sideband Reference System for Terrain Profile #7. The simulated aircraft is flying at a constant 1000 ft. altitude above the runway centerline (extended).
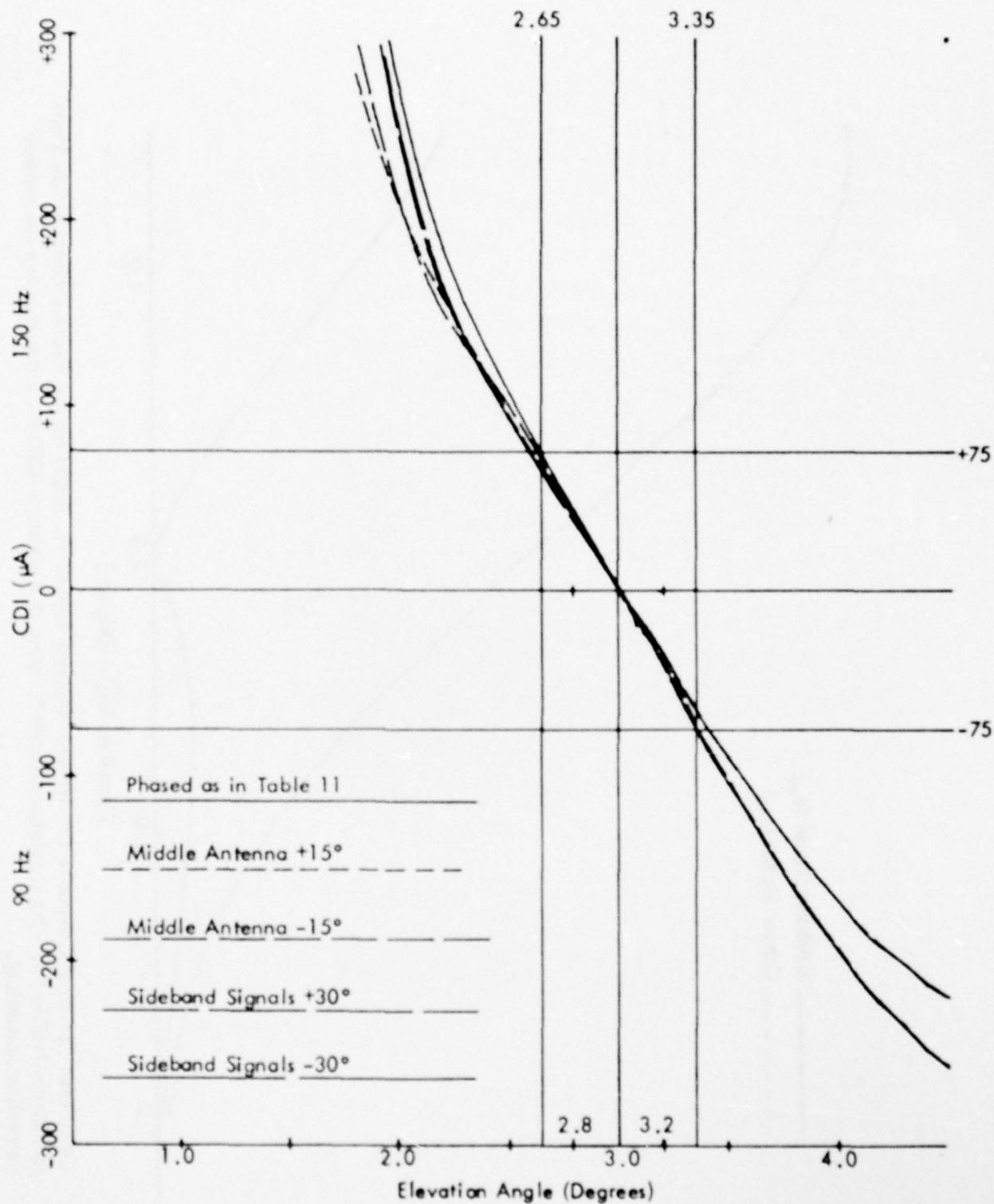
Figure 74h. Calculated Curves of CDI vs. Angle for the Capture Effect Glide Slope with the Normal Phasing (as Indicated in Table 11) and Dephased According to the Flight Inspection Manual Phase Verification Procedure for Terrain Profile #7. The simulated aircraft is flying at a constant 1000 ft. altitude above the runway centerline (extended).

-159-
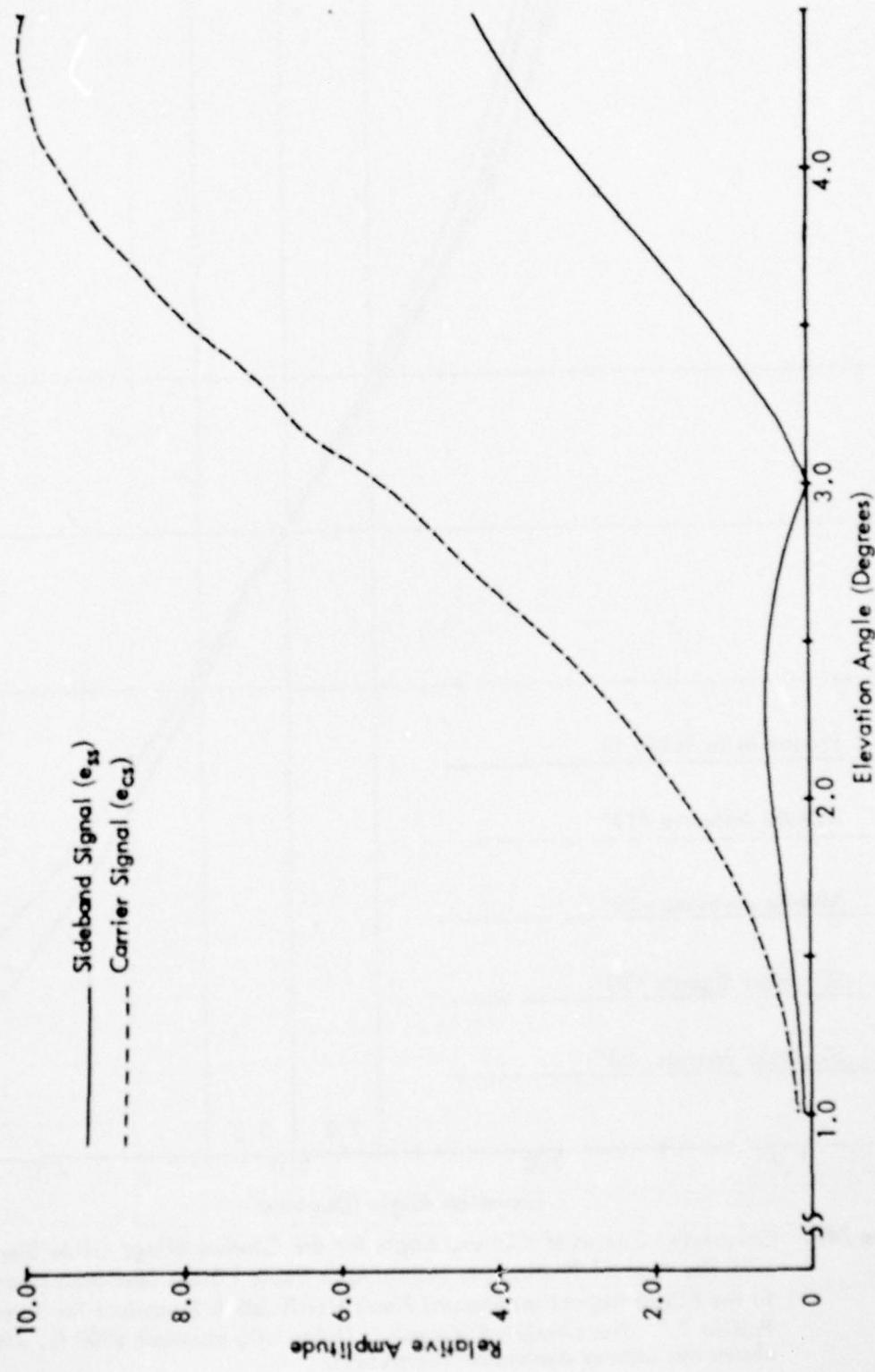
Figure 74i. Calculated Curves of Composite Carrier and Sideband Signals vs. Angle for the Capture Effect Glide Slope for Terrain Profile #7. The simulated aircraft is flying at a constant 1000 ft. altitude above the runway centerline (extended).
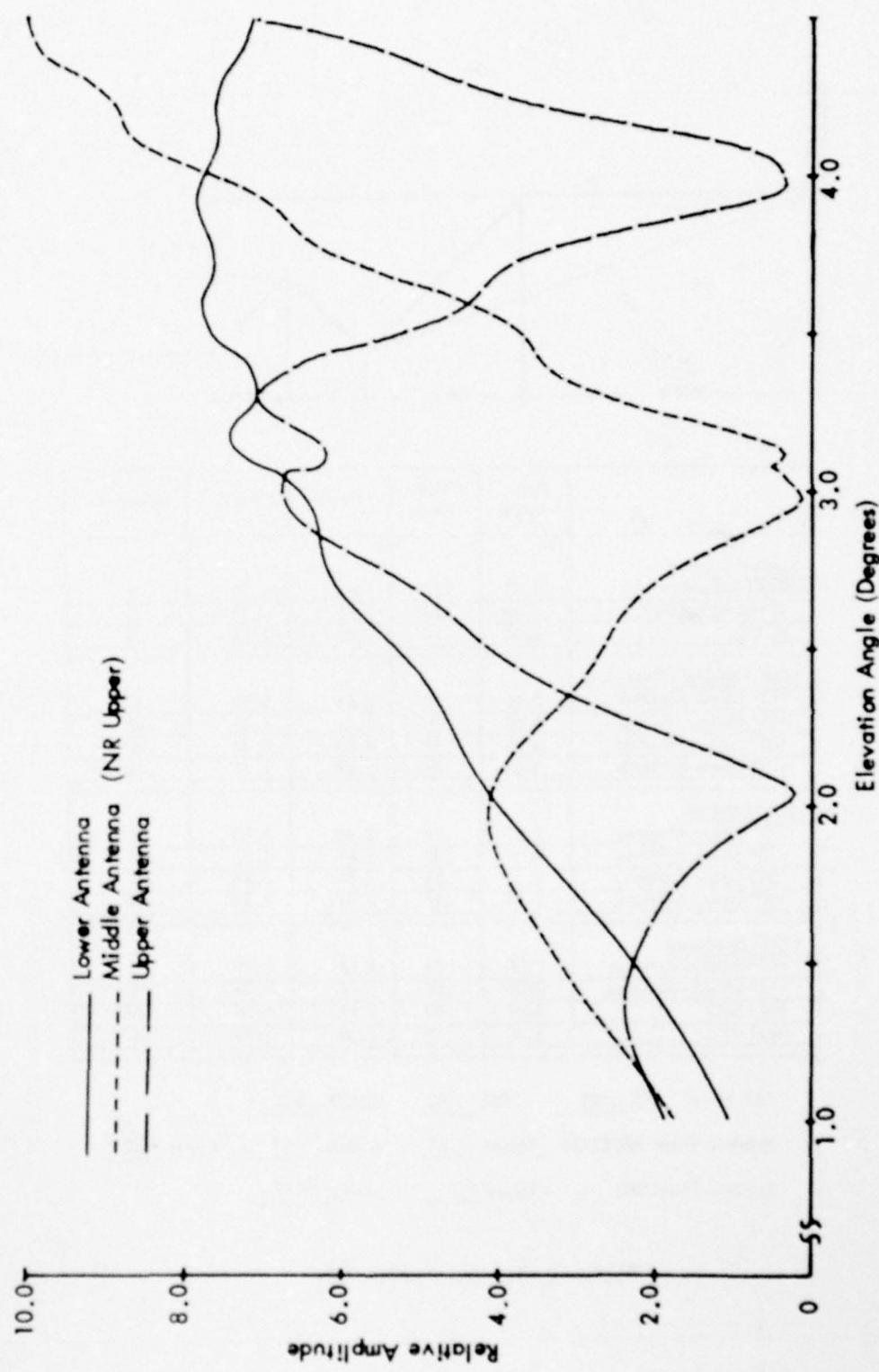
Figure 74j. Calculated Normalized Antenna Patterns vs. Angle for the Capture Effect and Null Reference Systems for Terrain Profile #7. The simulated aircraft is flying at a constant 1000 ft. altitude above the runway center-line (extended).
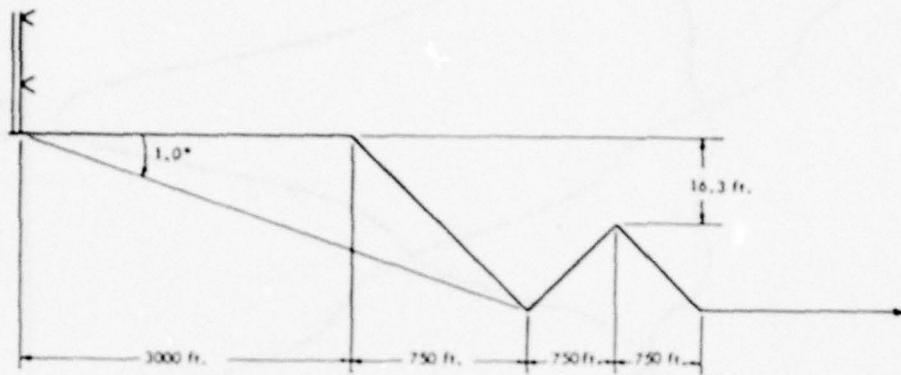
|	Path Angle	Width Angle	+ 75 µA	- 75 µA	Symmetry
Normal Phasing					
Null Reference	3.03	.70	2.65	3.35	.46
Sideband Reference	3.02	.70	2.65	3.35	.47
CEGS	3.01	.70	2.65	3.35	.50
Null Reference Dephased					
+15° Lower Antenna	3.03	.73	2.64	3.37	.47
-15° Lower Antenna	3.03	.72	2.64	3.36	.46
+30° Lower Antenna	3.02	.82	2.60	3.42	.48
-30° Lower Antenna	3.03	.81	2.60	3.41	.46
SBR Dephased					
+15° Lower Antenna	2.99	.72	2.60	3.33	.47
-15° Lower Antenna	2.99	.72	2.61	3.32	.47
+30° Lower Antenna	2.87	.80	2.44	3.24	.47
-30° Lower Antenna	2.85	.81	2.44	3.25	.50
CEGS Dephased					
+15° Middle Antenna	3.00	.73	2.63	3.36	.48
-15° Middle Antenna	3.00	.74	2.62	3.35	.48
+30° SBO	3.02	.80	2.61	3.42	.50
-30° SBO	3.00	.82	2.58	3.40	.50

"A" Ratio: NR .302   SBR .302   CEGS .302

Relative Phase NR/CEGS   Upper 2.2°   Middle 0°   Lower 0.3°

Relative Phase SBR   Upper 0°   Lower 0.1°

Table 12. Terrain Profile #8.
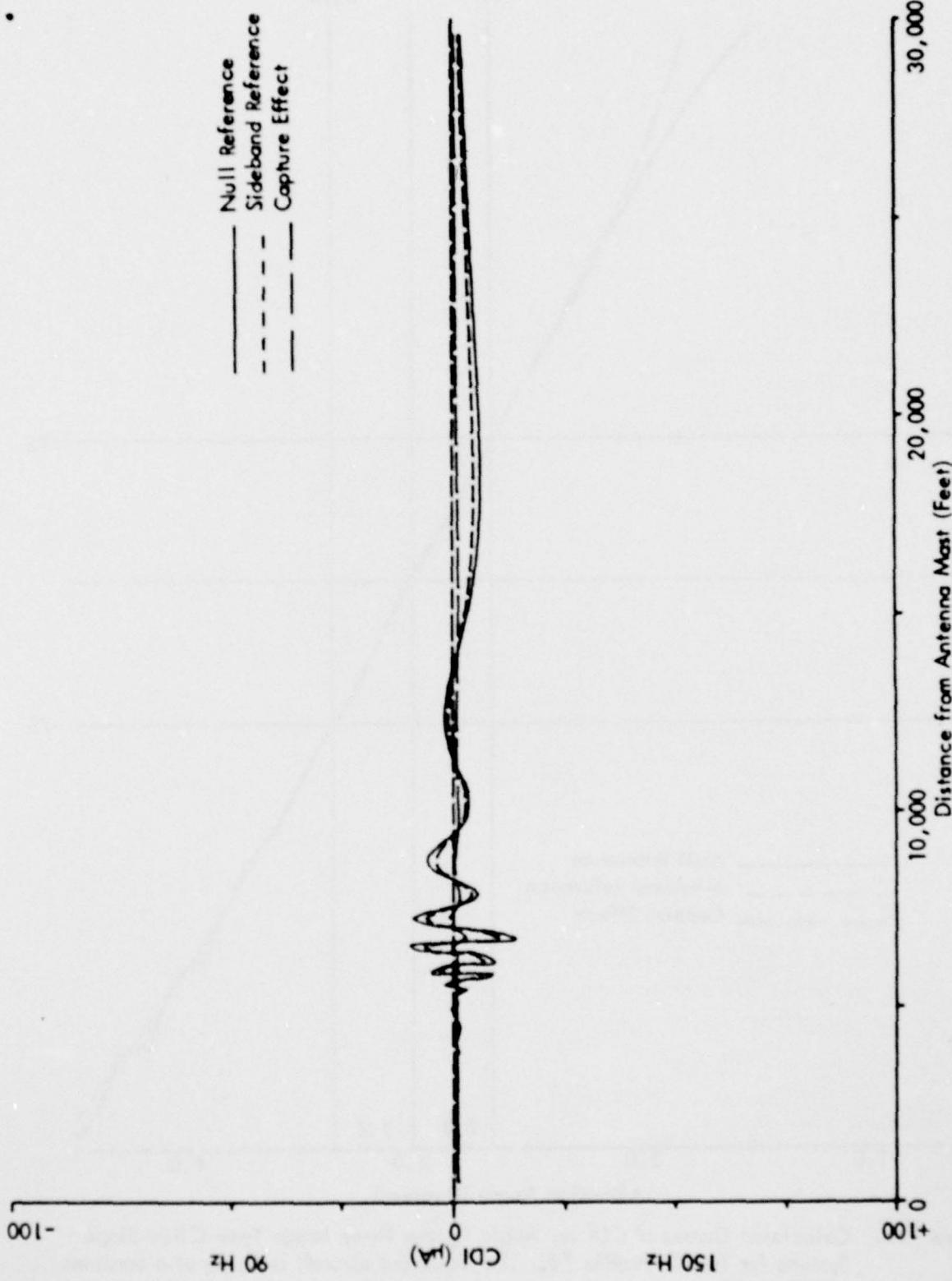
Figure 75a. Calculated Curves of CDI vs. Distance for the Three Image Type Glide Slope Systems for Terrain Profile #8. The simulated aircraft is flying a constant 3.0 degree low approach over the runway centerline (extended).

-163-
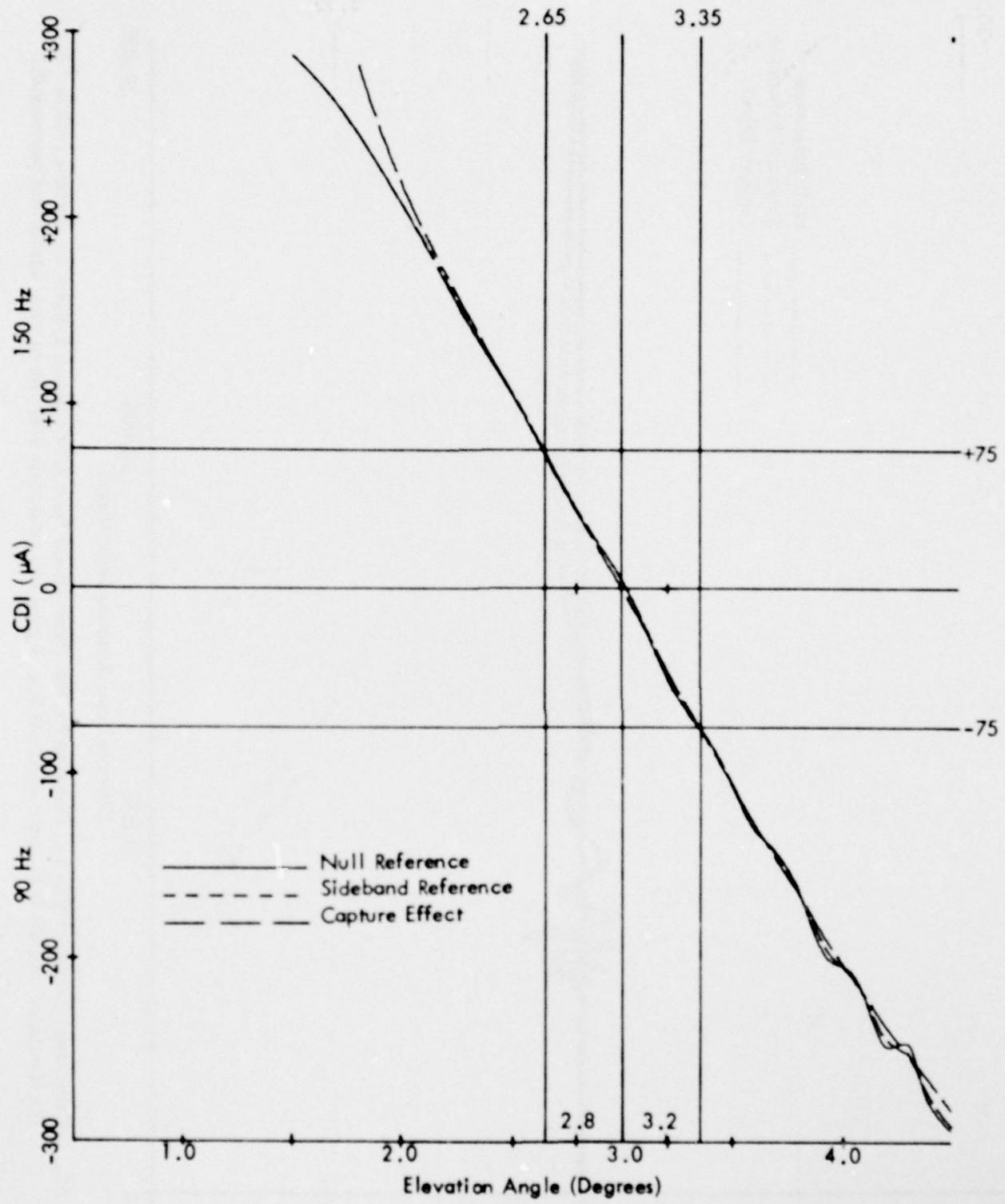
Figure 75b. Calculated Curves of CDI vs. Angle for the Three Image Type Glide-Slope Systems for Terrain Profile #8. The simulated aircraft is flying at a constant 1000 ft. altitude above the runway centerline (extended).

-164-
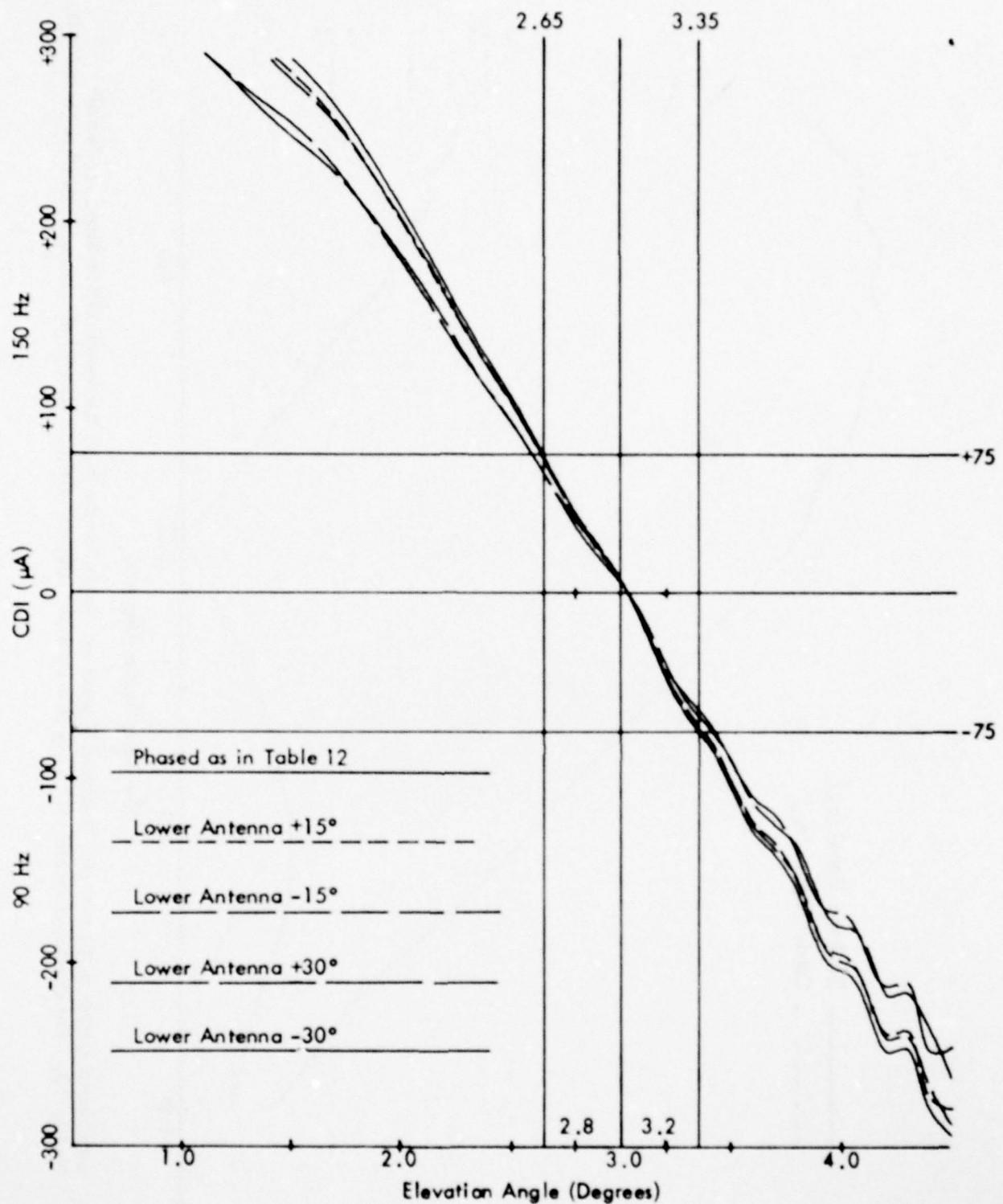
Figure 75c. Calculated Curves of CDI vs. Angle for the Null Reference Glide Slope with the Normal Phasing (as Indicated in Table 12) and Various Amounts of Dephasing for Terrain Profile #8. The simulated aircraft is flying at constant 1000 ft. altitude above the runway centerline (extended).
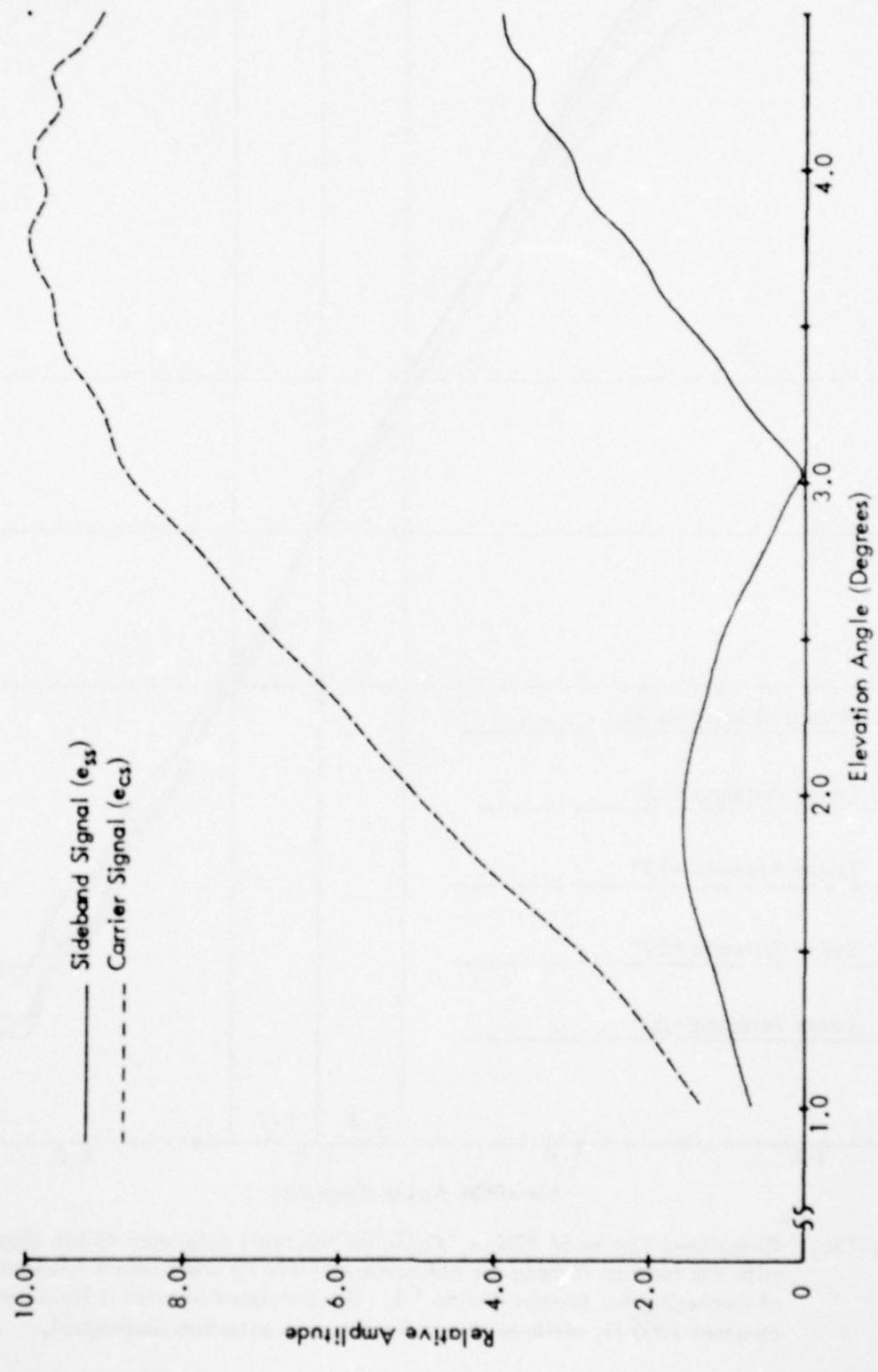
Figure 75d. Calculated Curves of Carrier and Sideband Signals vs. Angle for the Null Reference Glide Slope for Terrain Profile #8. The simulated aircraft is flying at a constant 1000 ft. altitude above the runway centerline (extended).
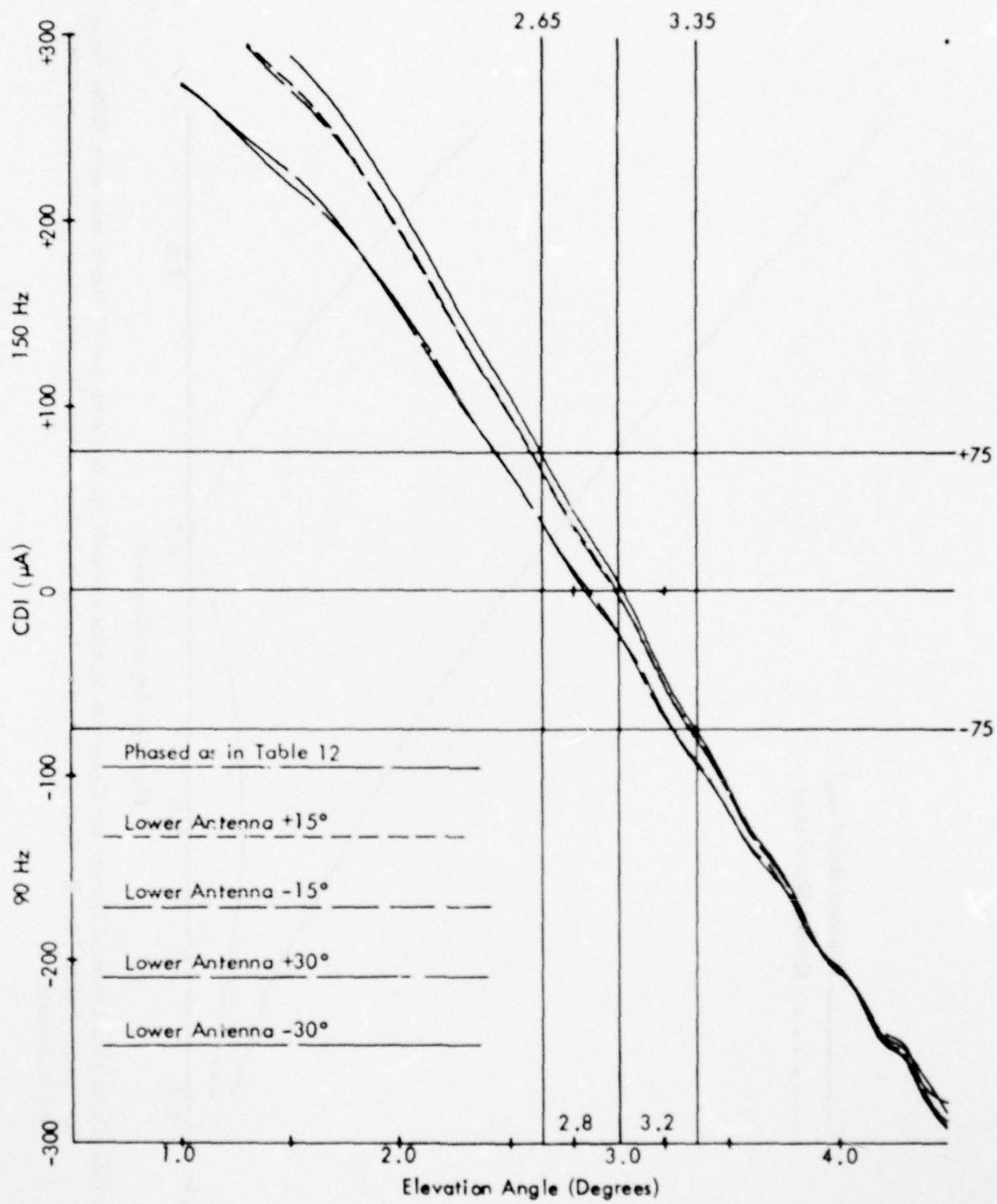
Figure 75e. Calculated Curves of CDI vs. Angle for the Sideband Reference Glide Slope with Normal Phasing (as Indicated in Table 12) and Various Amounts of Dephasing for Terrain Profile #8. The simulated aircraft is flying at a constant 1000 ft. altitude above the runway centerline (extended).
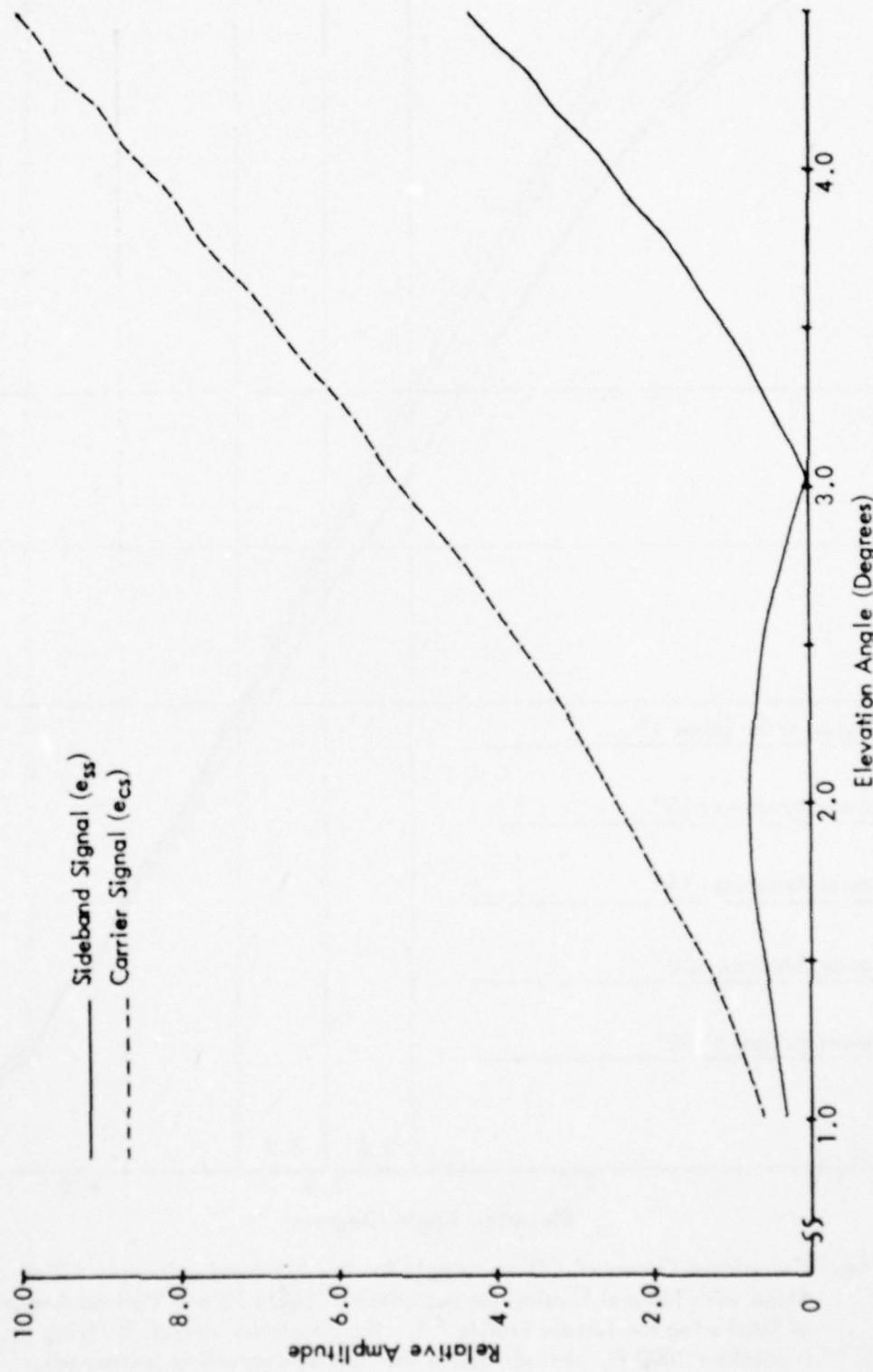
Figure 75f. Calculated Curves of Carrier and Composite Sideband Signals vs. Angle for the Sideband Reference Glide Slope for Terrain Profile #8. The simulated aircraft is flying at a constant 1000 ft. altitude above the runway center-line (extended).
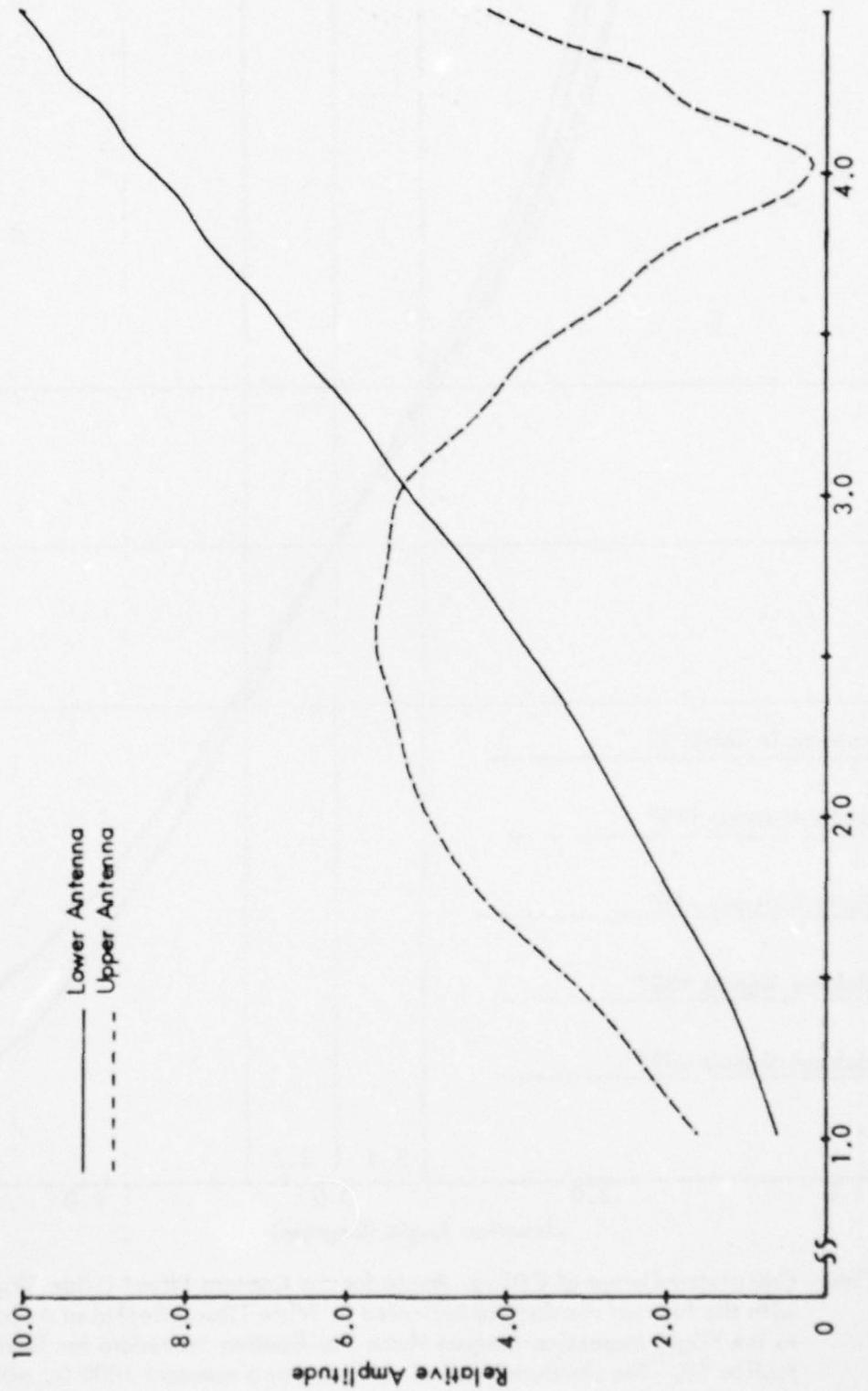
Figure 75g. Calculated Normalized Antenna Patterns vs. Angle for the Sideband Reference System for Terrain Profile #8. The simulated aircraft is flying at a constant 1000 ft. altitude above the runway centerline (extended).
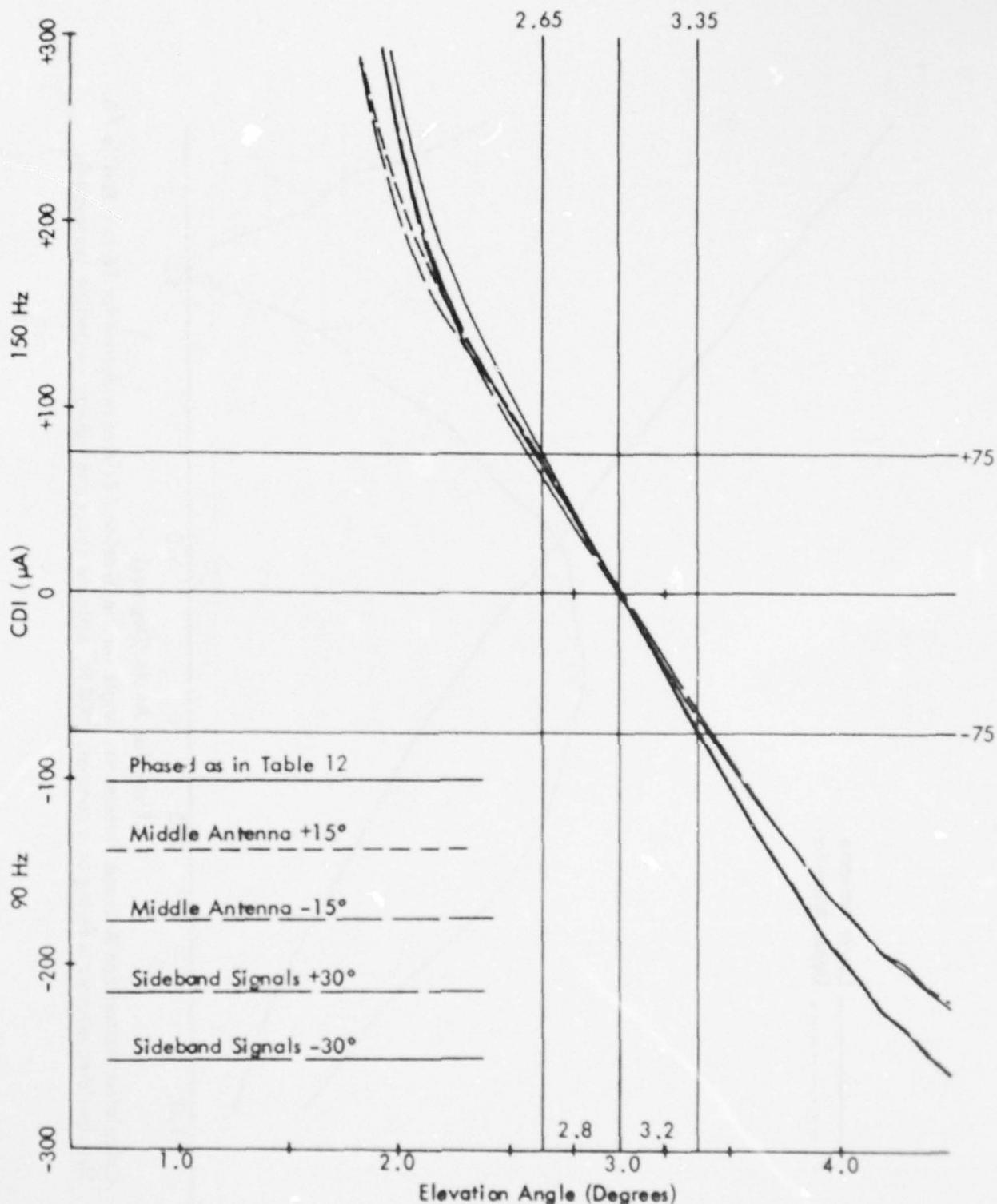
Figure 75h. Calculated Curves of CDI vs. Angle for the Capture Effect Glide Slope with the Normal Phasing (as Indicated in Table 12) and Dephased According to the Flight Inspection Manual Phase Verification Procedure for Terrain Profile #8. The simulated aircraft is flying at a constant 1000 ft. altitude above the runway centerline (extended).

-170-
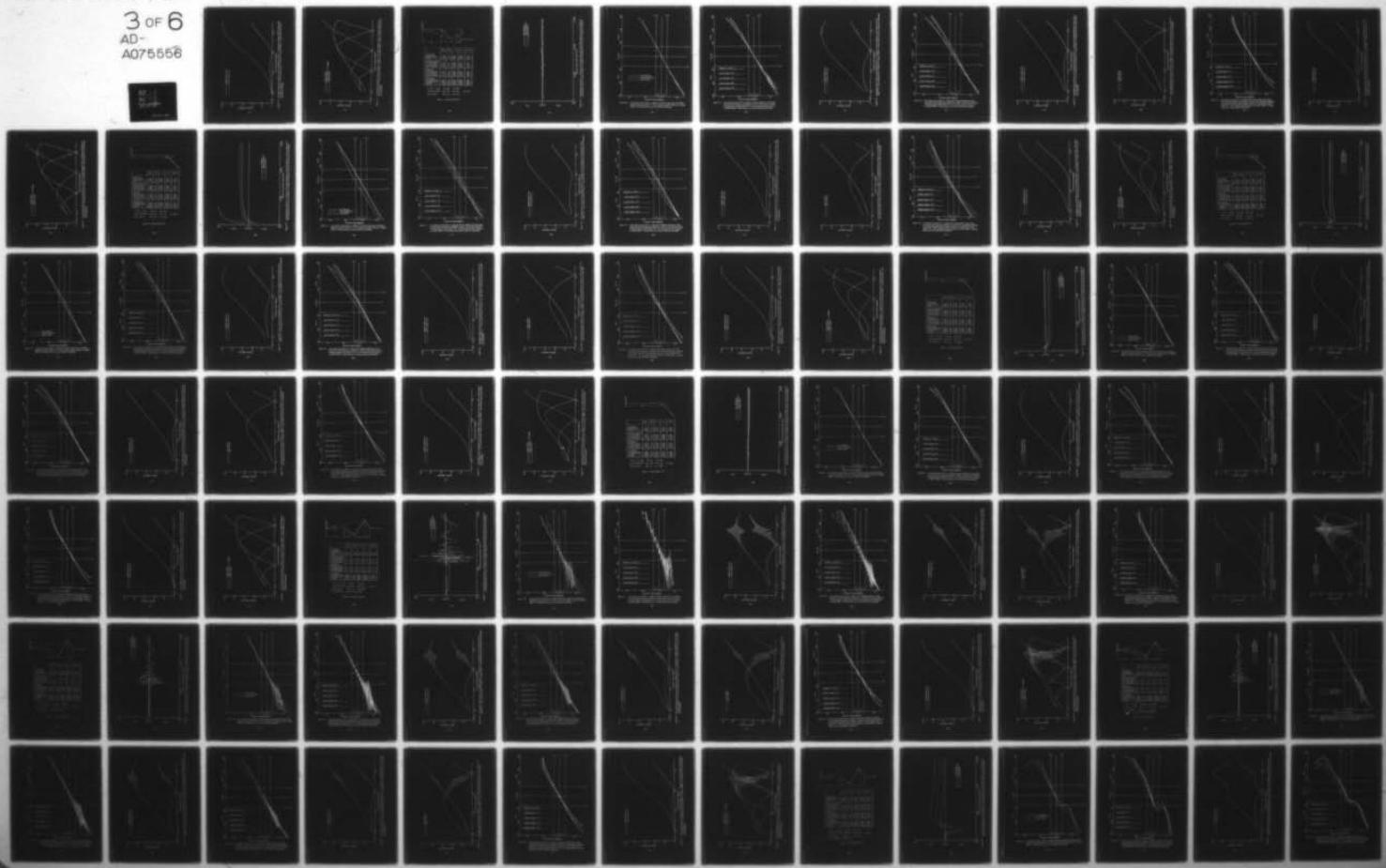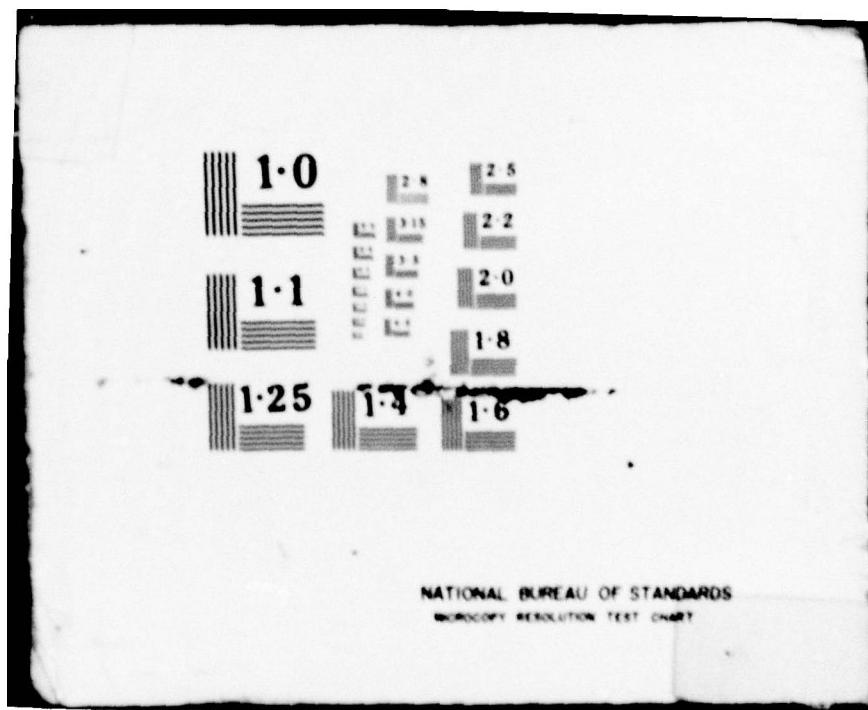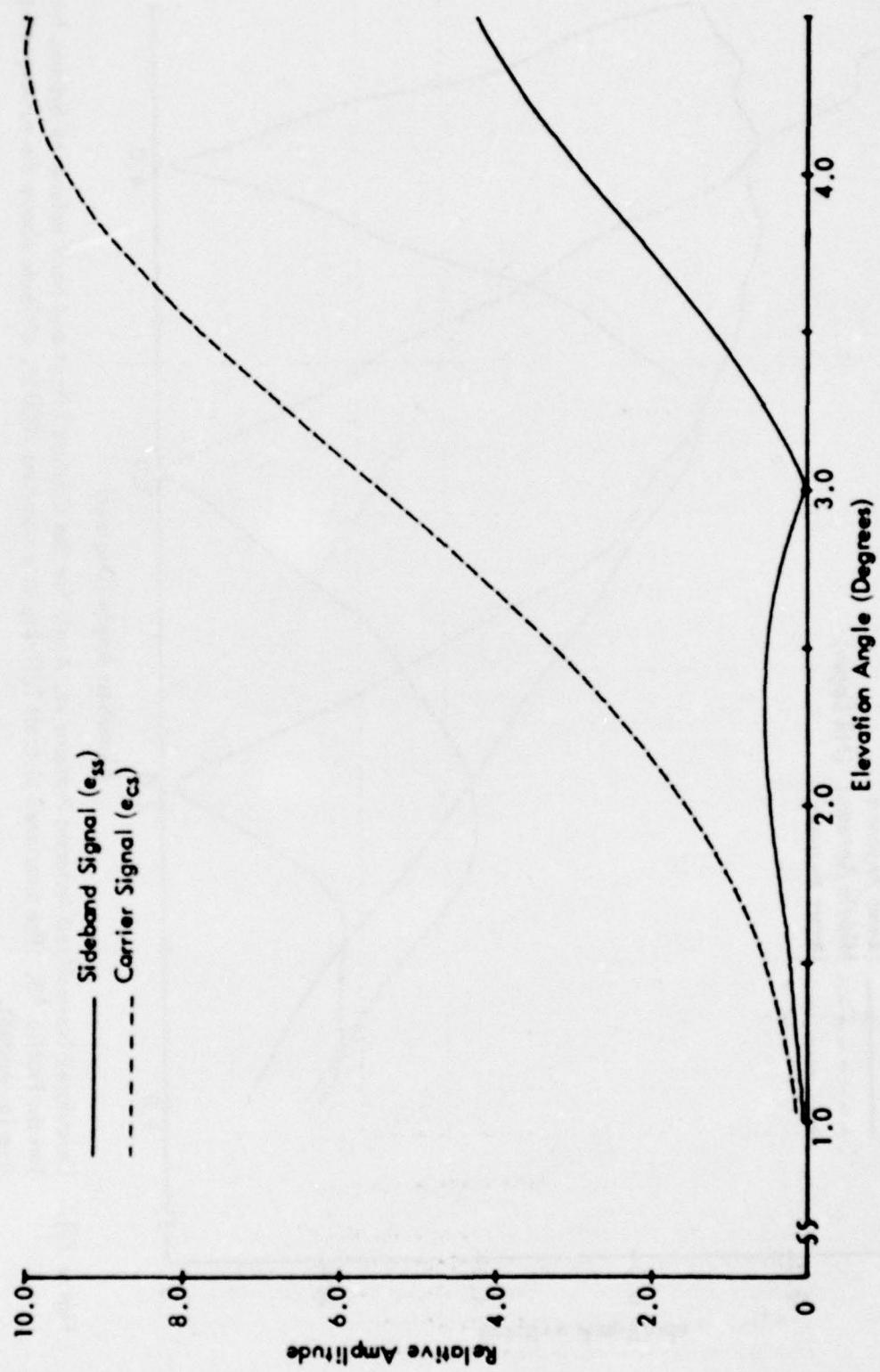
Figure 75i. Calculated Curves of Composite Carrier and Sideband Signals vs. Angle for the Capture Effect Glide Slope for Terrain Profile #8. The simulated aircraft is flying at a constant 1000 ft. altitude above the runway centerline (extended).

-171-
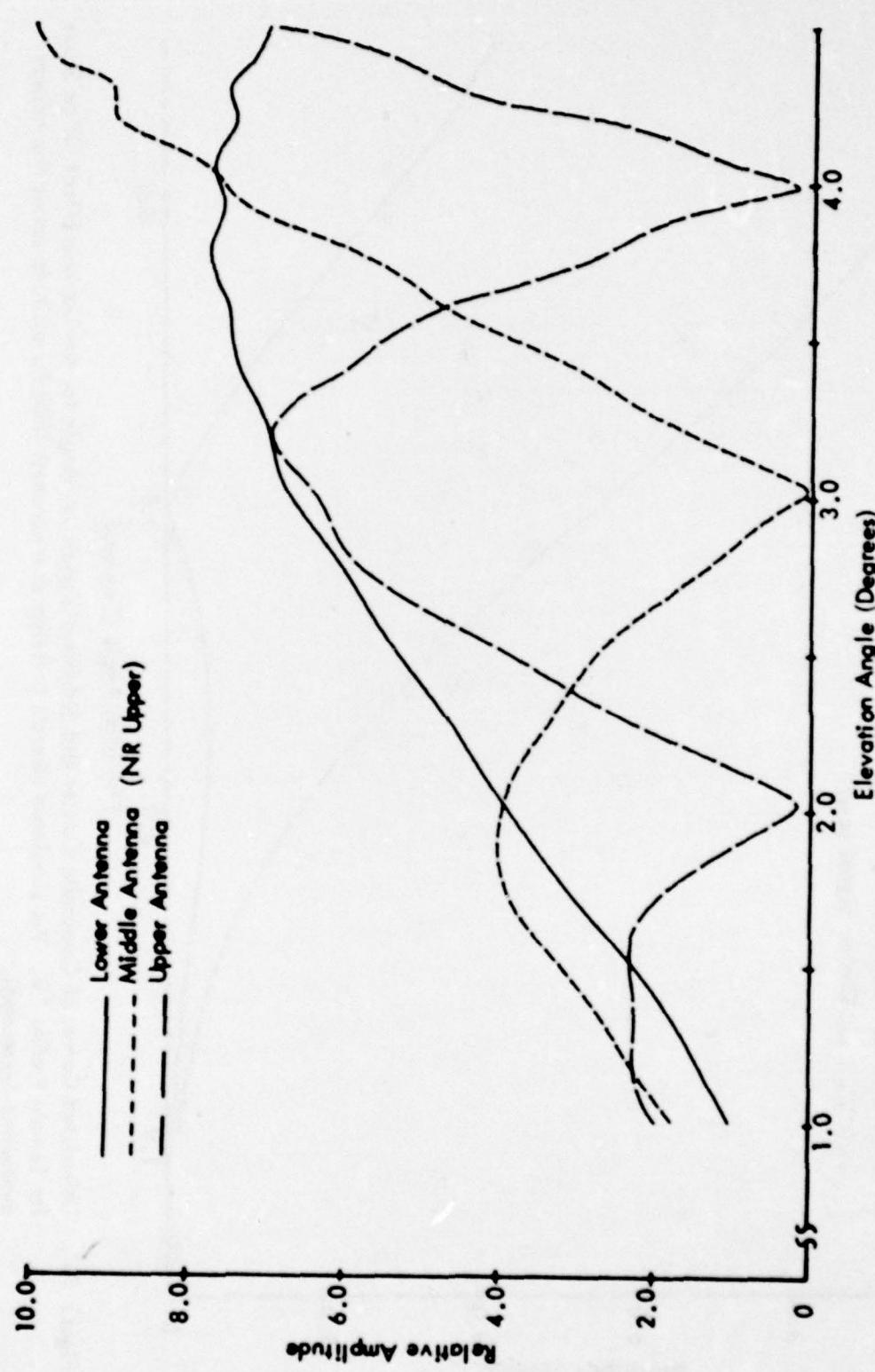
Figure 75j. Calculated Normalized Antenna Patterns vs. Angle for the Capture Effect and Null Reference Systems for Terrain Profile #8. The simulated aircraft is flying at a constant 1000 ft. altitude above the runway centerline (extended).

-172-
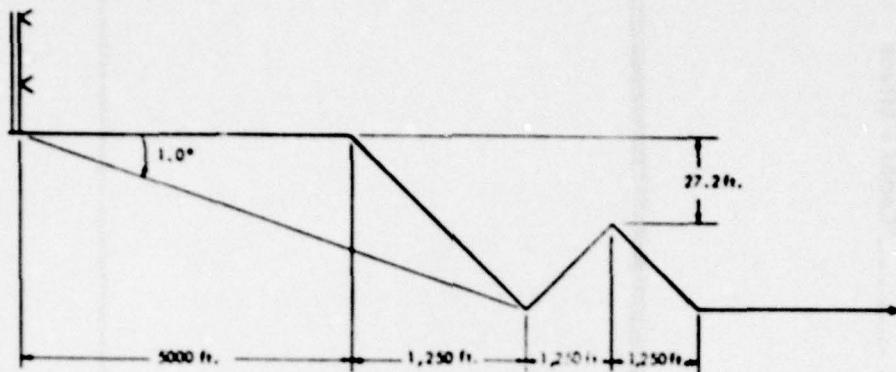
|	Path Angle	Width Angle	+75 µA	-75 µA	Symmetry
Normal Phasing					
Null Reference	2.99	.70	2.66	3.36	.52
Sideband Reference	3.00	.70	2.66	3.36	.51
CEGS	3.00	.70	2.65	3.35	.50
Null Reference Dephased					
+15° Lower Antenna	2.99	.73	2.64	3.37	.52
-15° Lower Antenna	3.00	.73	2.64	3.37	.51
+30° Lower Antenna	2.99	.83	2.59	3.42	.52
-30° Lower Antenna	3.00	.81	2.59	3.40	.50
SBR Dephased					
+15° Lower Antenna	2.96	.73	2.60	3.33	.50
-15° Lower Antenna	2.97	.73	2.60	3.34	.50
+30° Lower Antenna	2.85	.81	2.44	3.25	.49
-30° Lower Antenna	2.86	.80	2.46	3.26	.50
CEGS Dephased					
+15° Middle Antenna	3.01	.73	2.63	3.36	.48
-15° Middle Antenna	3.00	.74	2.62	3.36	.48
+30° SBO	3.02	.80	2.62	3.41	.50
-30° SBO	2.99	.82	2.58	3.40	.50

"A" Ratio: NR .303   SBR .303   CEGS .301

Relative Phase NR/CEGS   Upper -1.74°   Middle 0°   Lower +.7°

Relative Phase SBR   Upper 0°   Lower +.4°

Table 13.   Terrain Profile #9.
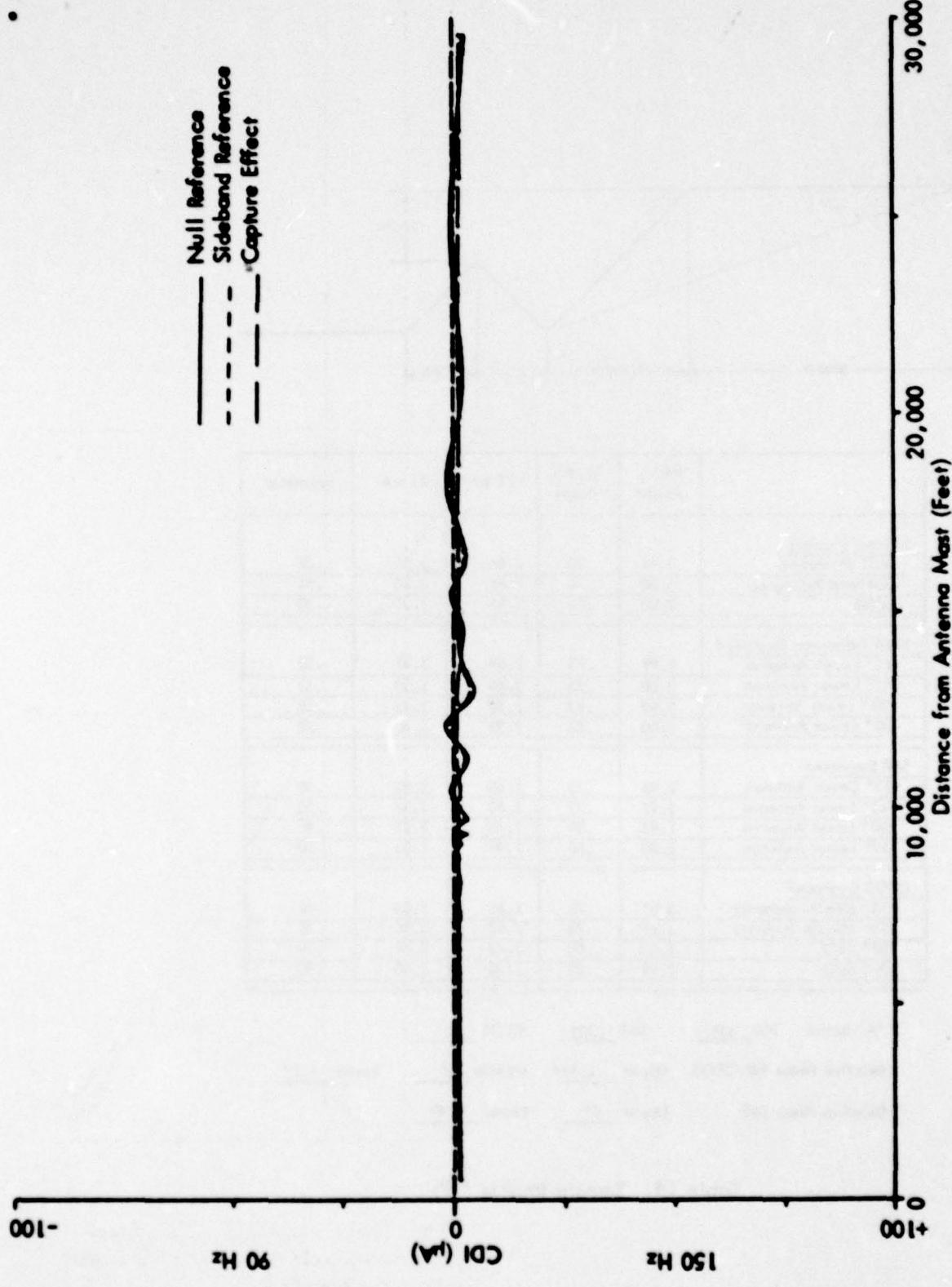
Figure 76a. Calculated Curves of CDI vs. Distance for the Three Image Type Glide-Slope Systems for Terrain Profile #9. The simulated aircraft is flying a constant 3.0 degree low approach over the runway centerline (extended).
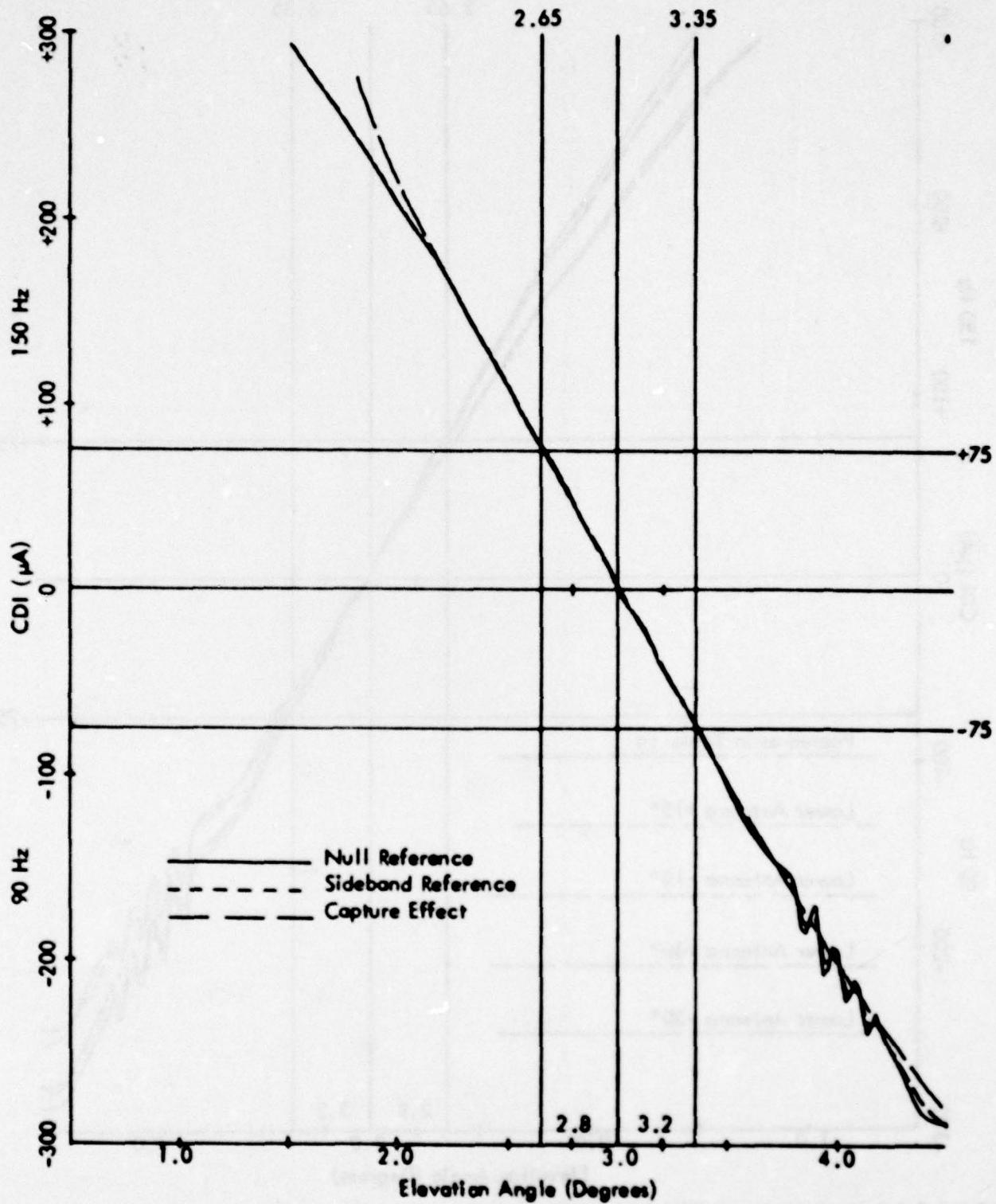
Figure 76b. Calculated Curves of CDI vs. Angle for the Three Image Type Glide-Slope Systems for Terrain Profile #9. The simulated aircraft is flying at a constant 1000 ft. altitude above the runway centerline (extended).
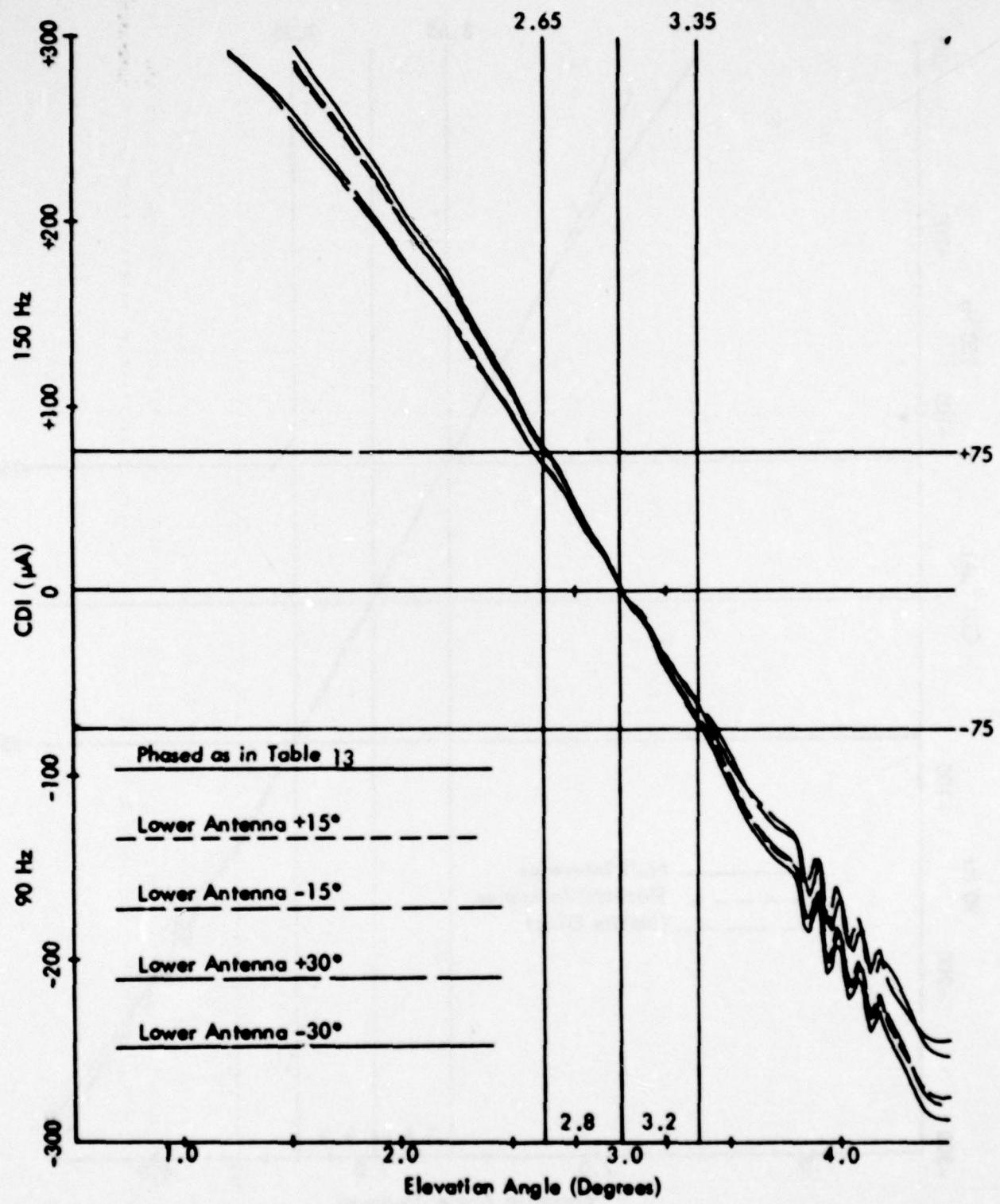
Figure 76c. Calculated Curves of CDI vs. Angle for the Null Reference Glide Slope with the Normal Phasing (as Indicated in Table 13) and Various Amounts of Dephasing for Terrain Profile #9. The simulated aircraft is flying at a constant 1000 ft. altitude above the runway centerline (extended).

-176-
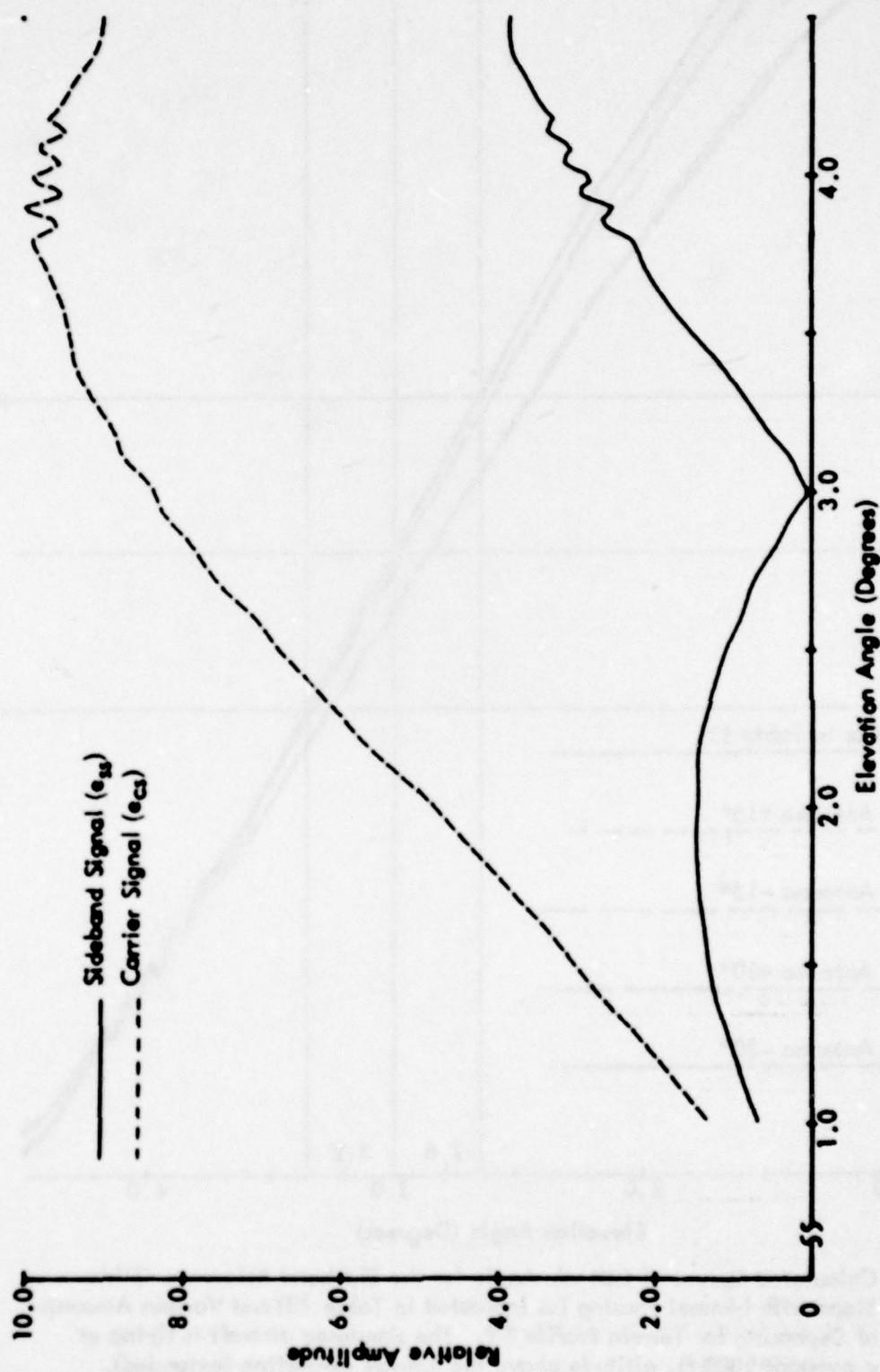
Figure 76d. Calculated Curves of Carrier and Sideband Signals vs. Angle for the Null Reference Glide Slope for Terrain Profile #9. The simulated aircraft is flying at a constant 1000 ft. altitude above the runway centerline (extended).
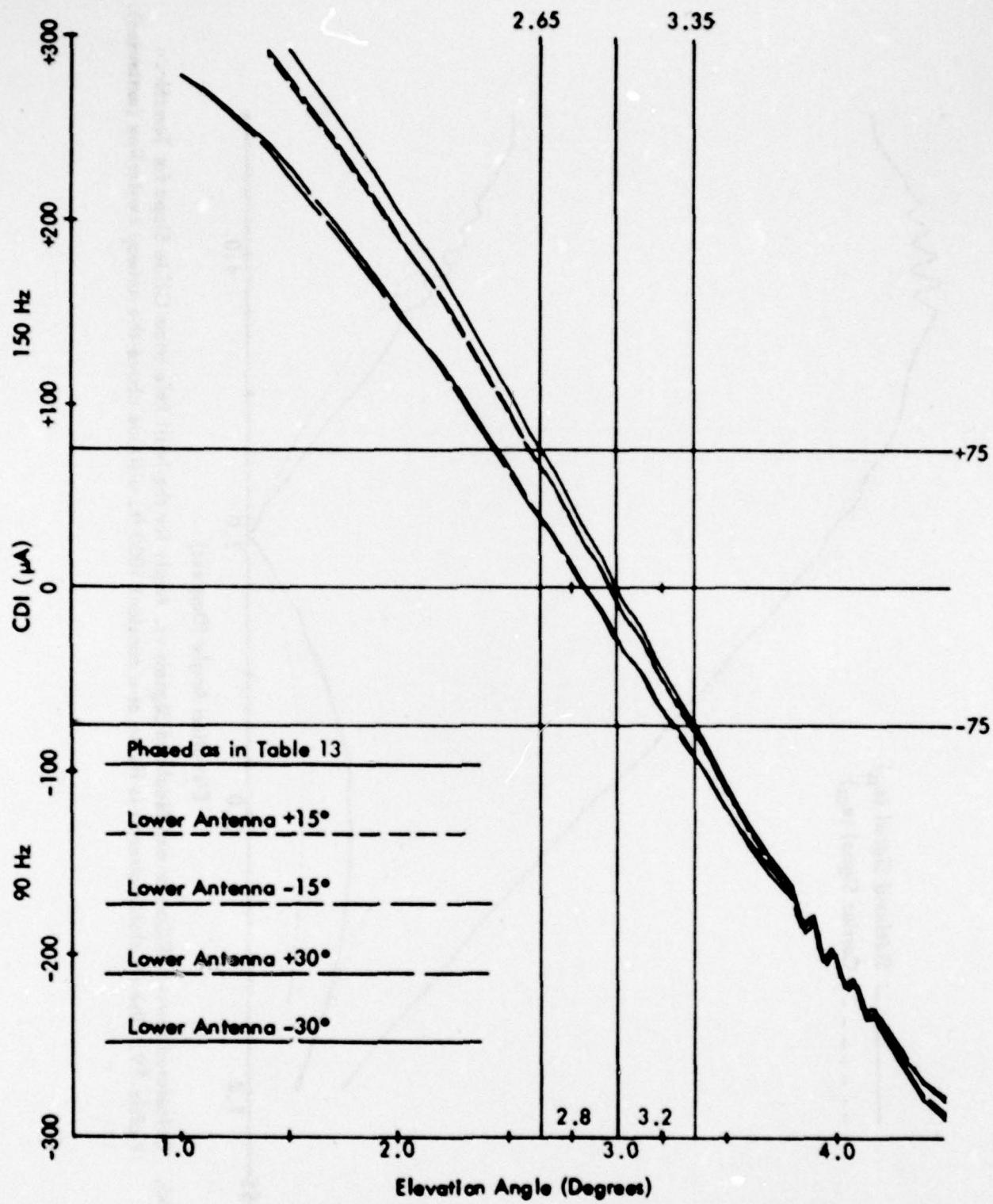
Figure 76e. Calculated Curves of CDI vs. Angle for the Sideband Reference Glide Slope with Normal Phasing (as Indicated in Table 13) and Various Amounts of Dephasing for Terrain Profile #9. The simulated aircraft is flying at a constant 1000 ft. altitude above the runway centerline (extended).

-178-
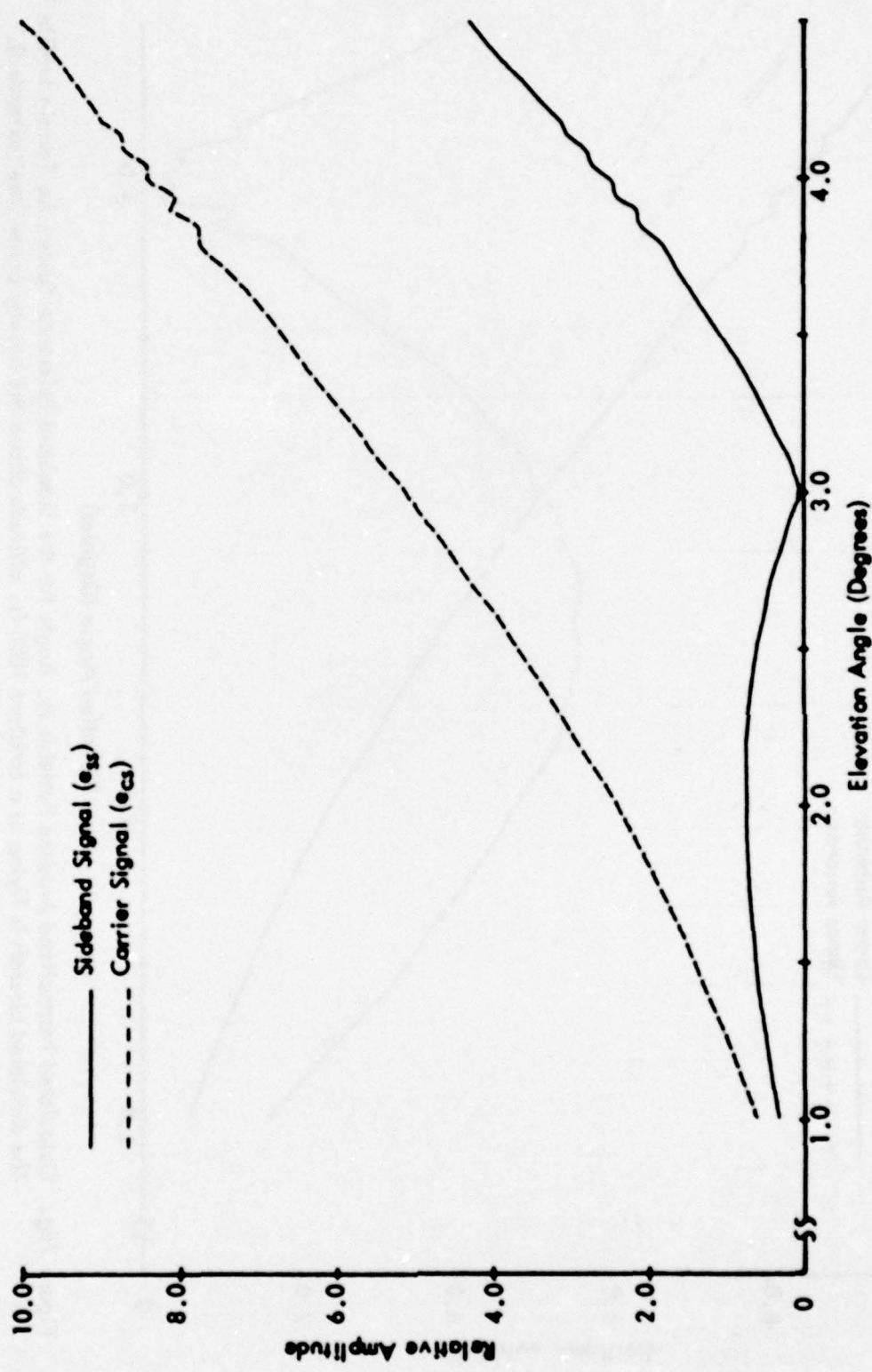
Figure 76f. Calculated Curves of Carrier and Composite Sideband Signals vs. Angle for the Sideband Reference Glide Slope for Terrain Profile ℓ9. The simulated aircraft is flying at a constant 1000 ft. altitude above the runway center-line (extended).
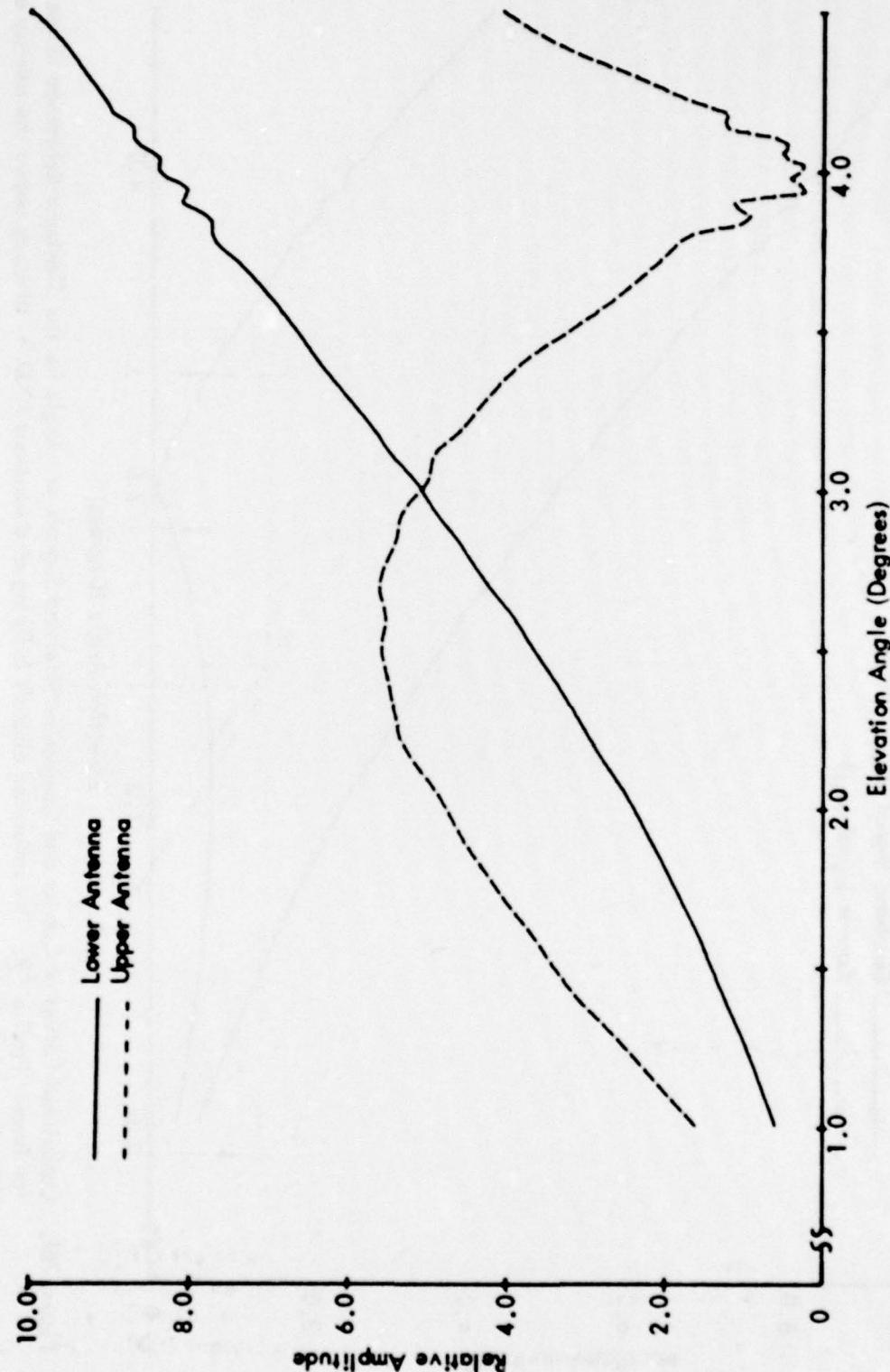
Figure 76g. Calculated Normalized Antenna Patterns vs. Angle for the Sideband Reference System for Terrain Profile #9. The simulated aircraft is flying at a constant 1000 ft. altitude above the runway centerline (extended).

-180-
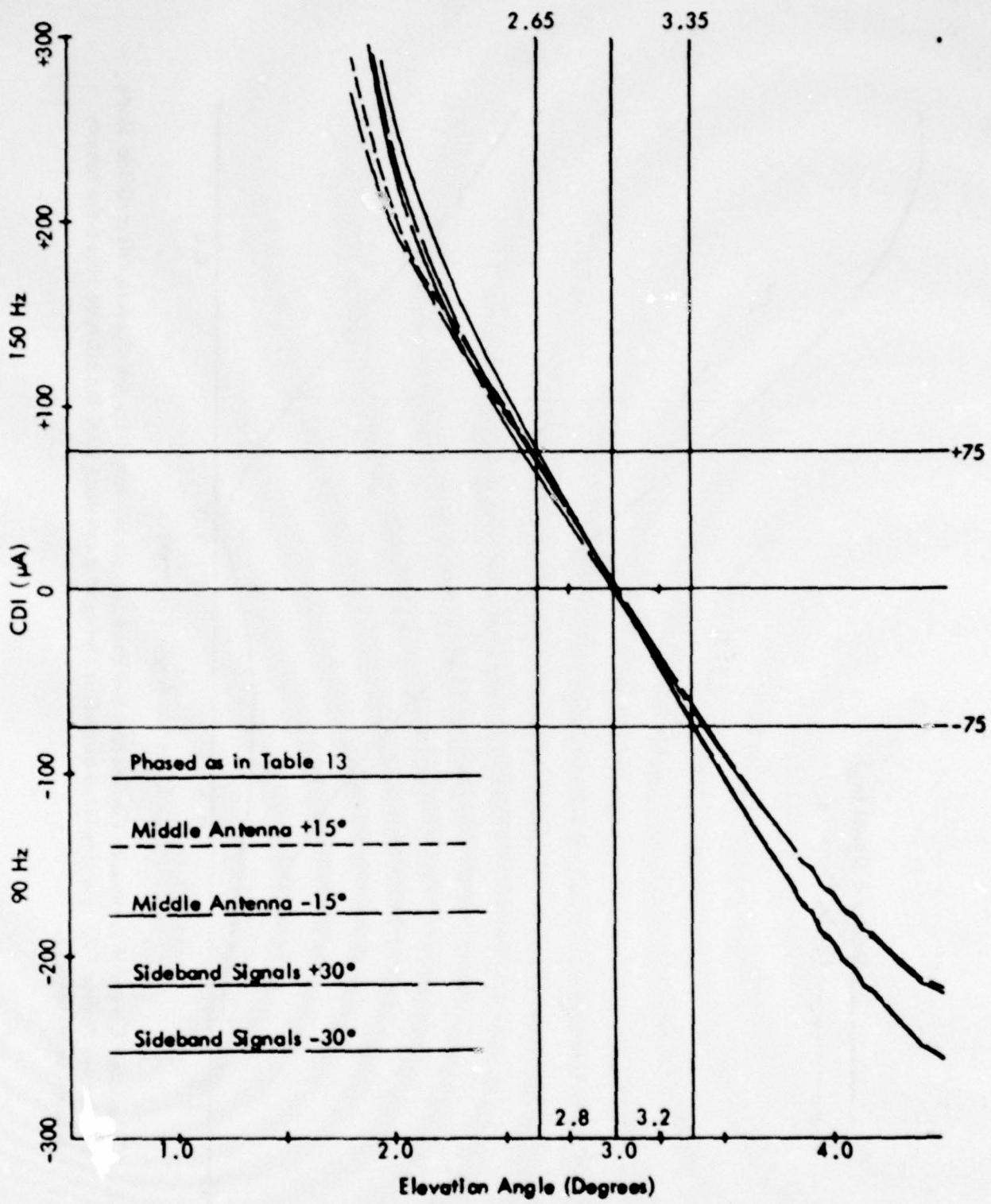
Figure 76h. Calculated Curves of CDI vs. Angle for the Capture Effect Glide Slope with the Normal Phasing (as indicated in Table 13) and Dephased According to the Flight Inspection Manual Phase Verification Procedure for Terrain Profile #9. The simulated aircraft is flying at a constant 1000 ft. altitude above the runway centerline (extended).

-181-
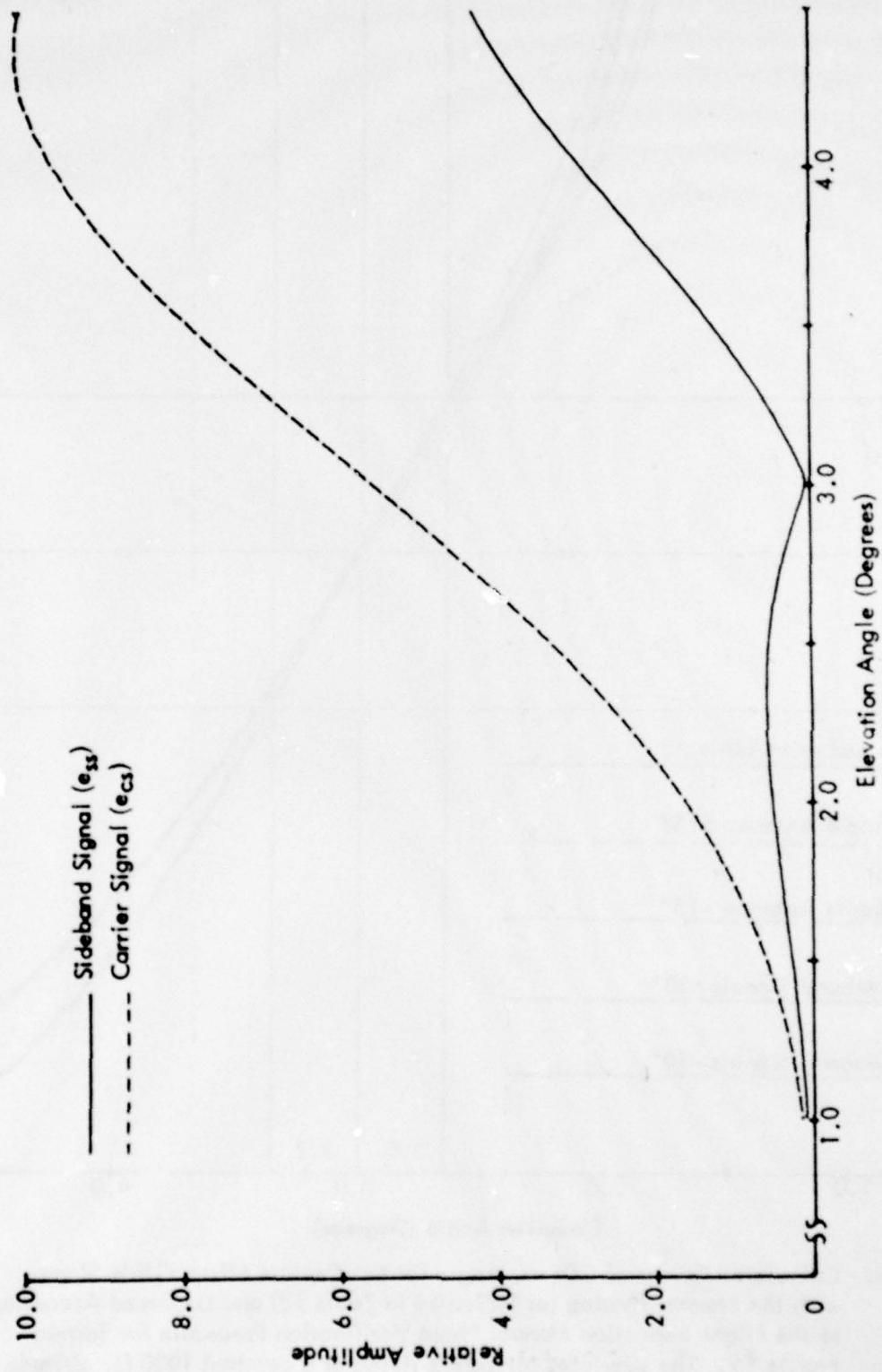
Figure 76i. Calculated Curves of Composite Carrier and Sideband Signals vs. Angle for the Capture Effect Glide Slope for Terrain Profile #9. The simulated aircraft is flying at a constant 1000 ft. altitude above the runway centerline (extended).

Figure 76j. Calculated Normalized Antenna Patterns vs. Angle for the Capture Effect and Null Reference Systems for Terrain Profile #9. The simulated aircraft is flying at a constant 1000 ft. altitude above the runway center-line (extended).

-183-
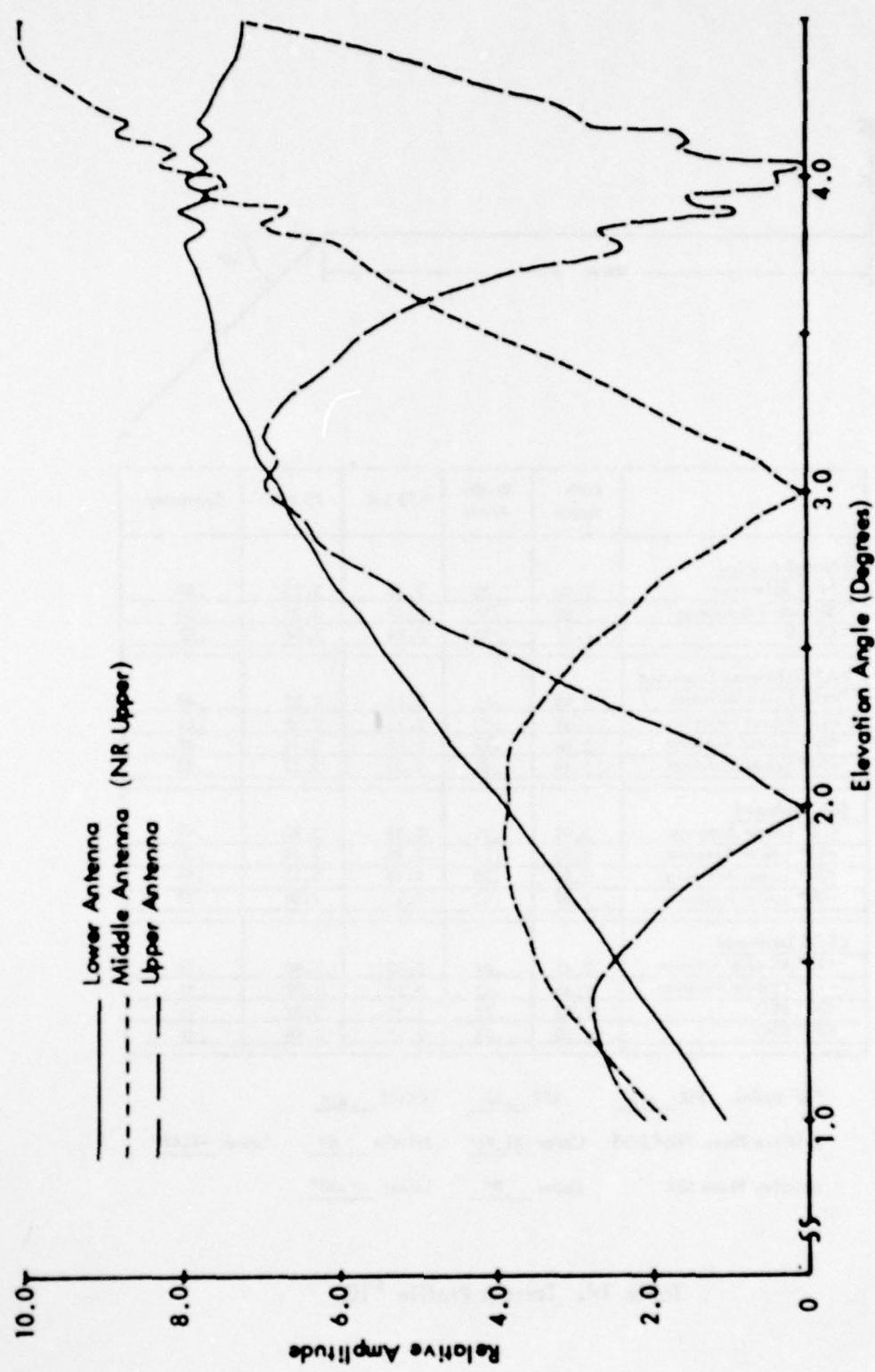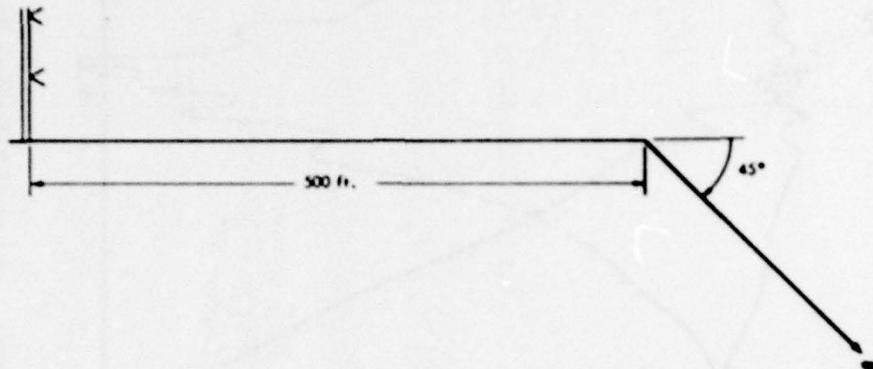
	Path Angle	Width Angle	+75 µA	-75 µA	Symmetry
Normal Phasing					
Null Reference	2.90	.70	2.54	3.25	.50
Sideband Reference	2.87	.70	3.51	3.21	.50
CEGS	2.57	.70	2.24	2.94	.52
Null Reference Dephased					
+15° Lower Antenna	2.98	.69	2.63	3.32	.49
-15° Lower Antenna	2.81	.75	2.43	3.19	.51
+30° Lower Antenna	3.06	.72	2.69	3.41	.48
-30° Lower Antenna	2.69	.86	2.28	3.14	.52
SBR Dephased					
+15° Lower Antenna	2.91	.71	2.55	3.26	.49
-15° Lower Antenna	2.73	.74	2.36	3.10	.50
+30° Lower Antenna	2.88	.78	2.48	3.25	.48
-30° Lower Antenna	2.47	.81	2.07	2.88	.51
CEGS Dephased					
+15° Middle Antenna	2.41	.84	2.00	2.85	.52
-15° Middle Antenna	2.68	.67	2.35	3.02	.51
+30° SBO	2.65	.72	2.30	3.02	.52
-30° SBO	2.50	.86	2.12	2.98	.56

"A" Ratio: NR .417   SBR .38   CEGS .455

Relative Phase NR/CEGS   Upper -31.72°   Middle 0°   Lower -9.66°

Relative Phase SBR   Upper 0°   Lower -7.68°

Table 14. Terrain Profile #10.
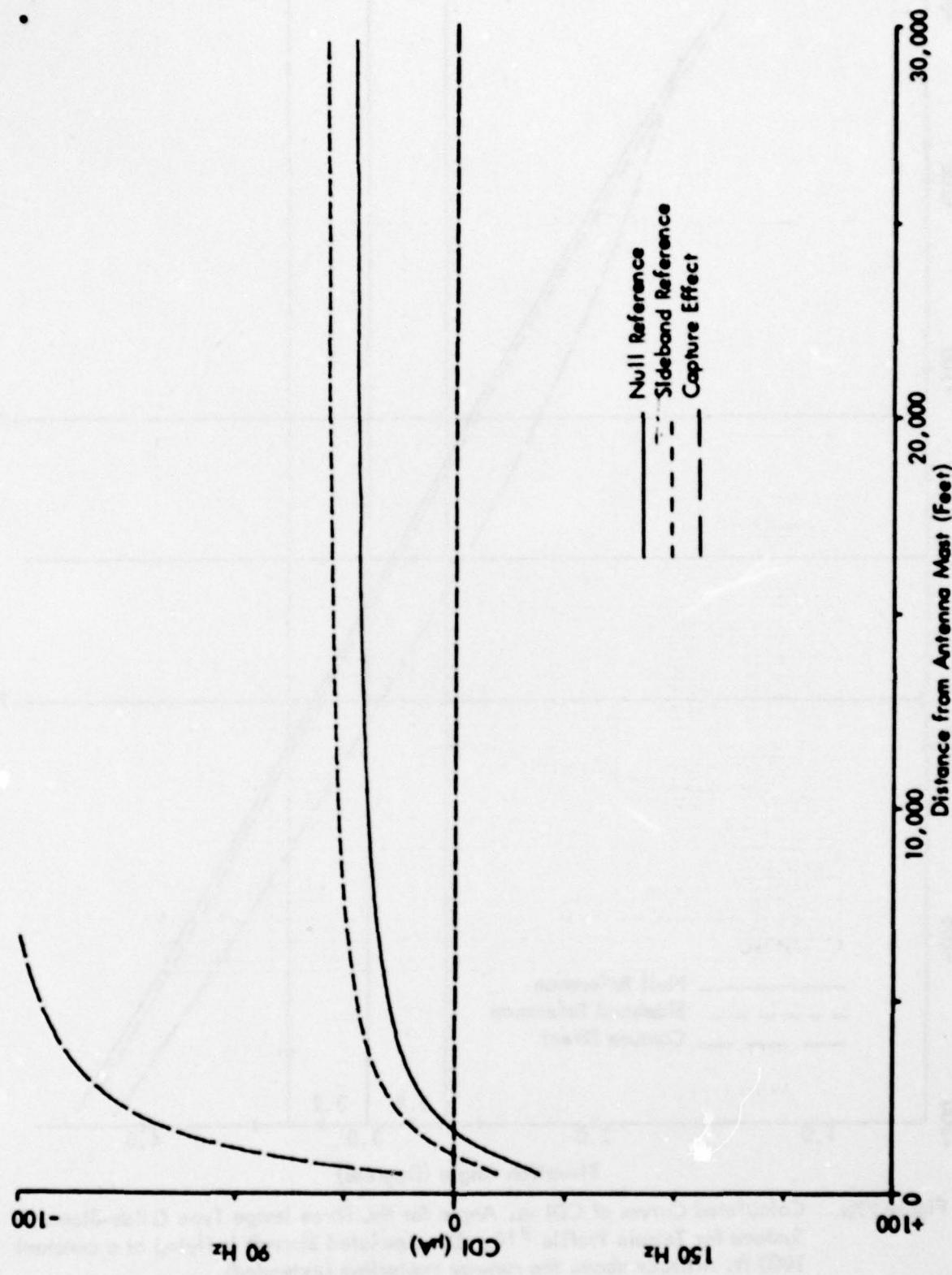
Figure 77a. Calculated Curves of CDI vs. Distance for the Three Image Type Glide Slope Systems for Terrain Profile #10. The simulated aircraft is flying a constant 3.0 degree low approach over the runway centerline (extended).

-185-
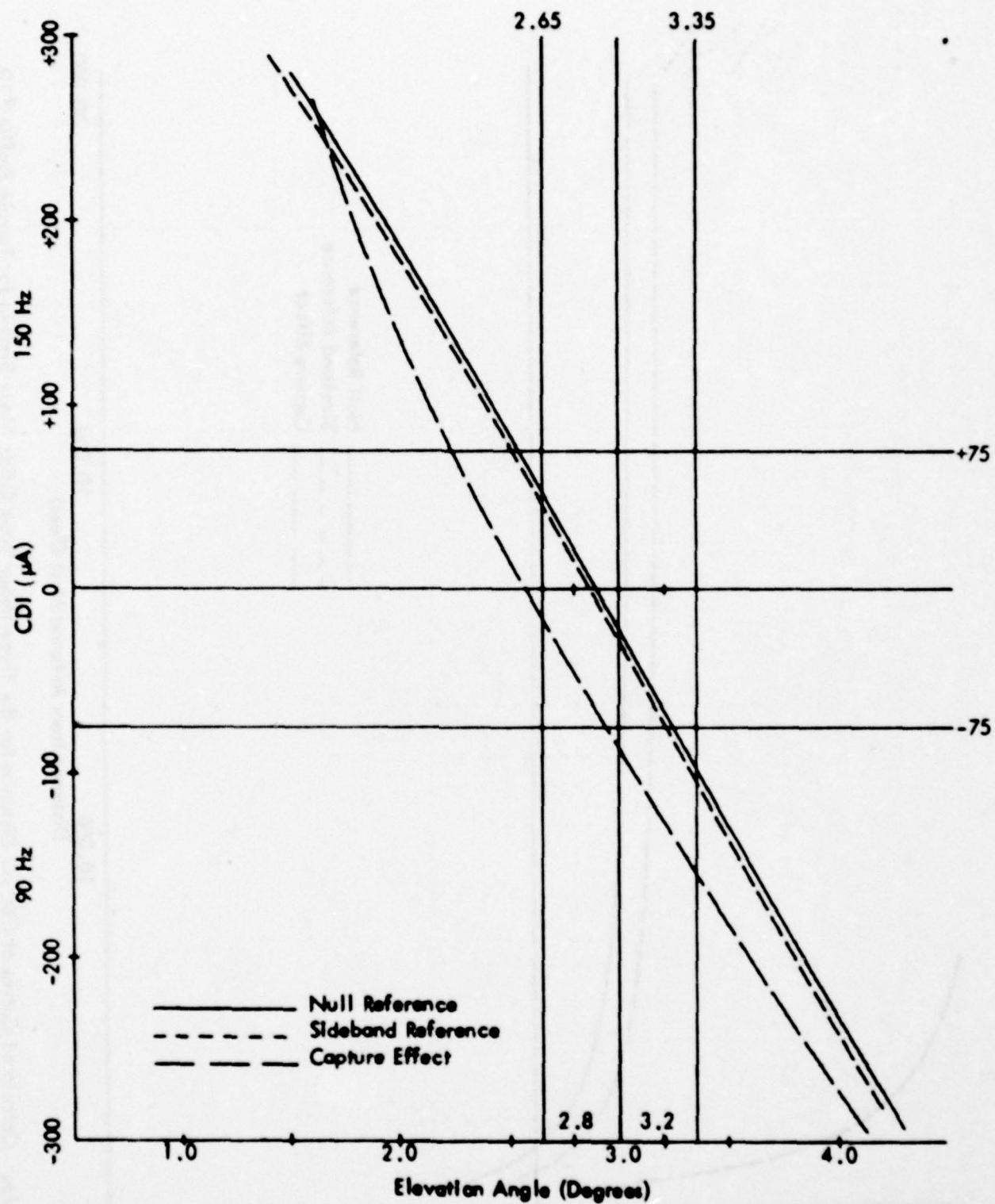
Figure 77b. Calculated Curves of CDI vs. Angle for the Three Image Type Glide-Slope Systems for Terrain Profile #10. The simulated aircraft is flying at a constant 1000 ft. altitude above the runway centerline (extended).
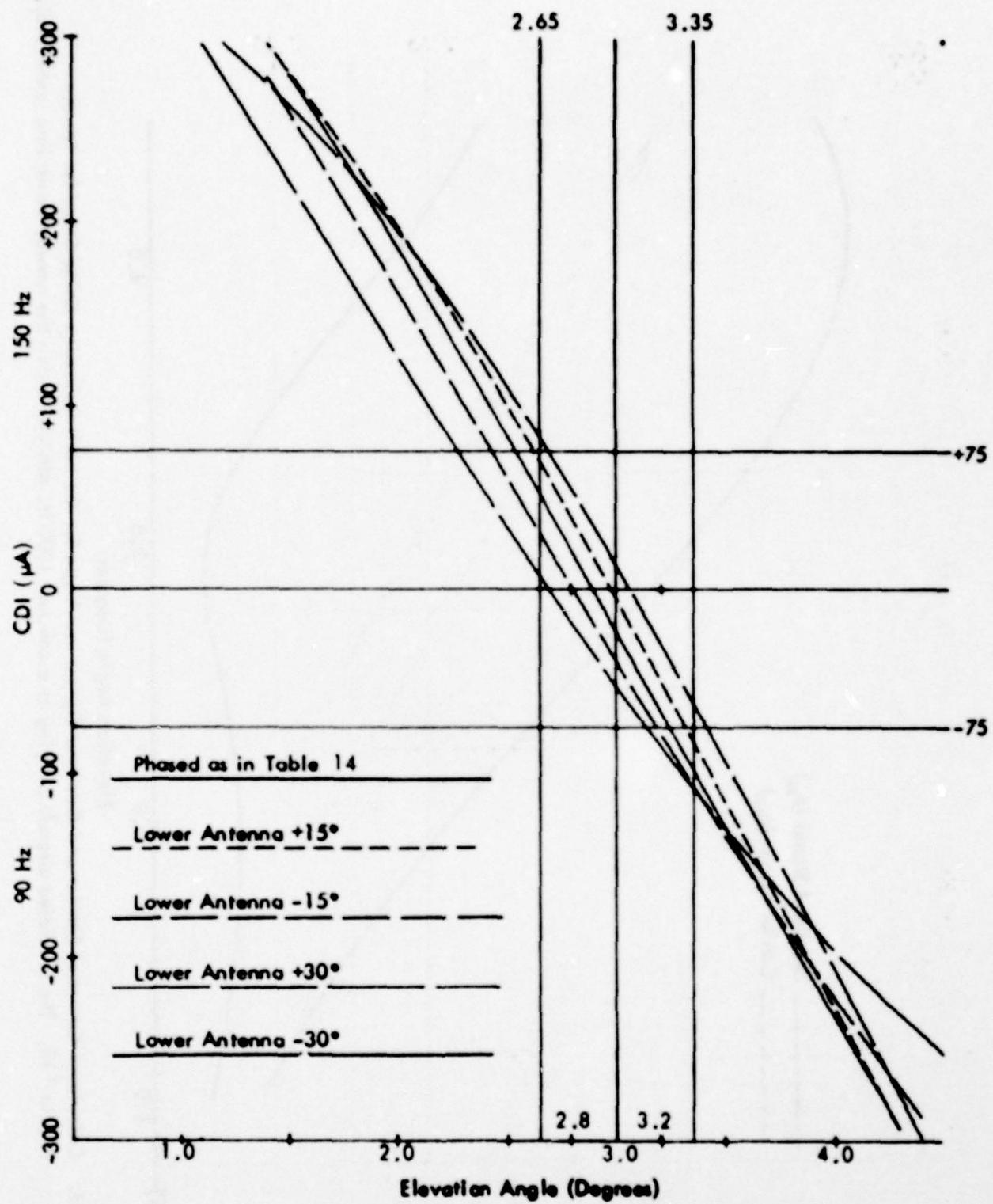
Figure 77c. Calculated Curves of CDI vs. Angle for the Null Reference Glide Slope with the Normal Phasing (as Indicated in Table 14) and Various Amounts of Dephasing for Terrain Profile #10. The simulated aircraft is flying at a constant 1000 ft. altitude above the runway centerline (extended).
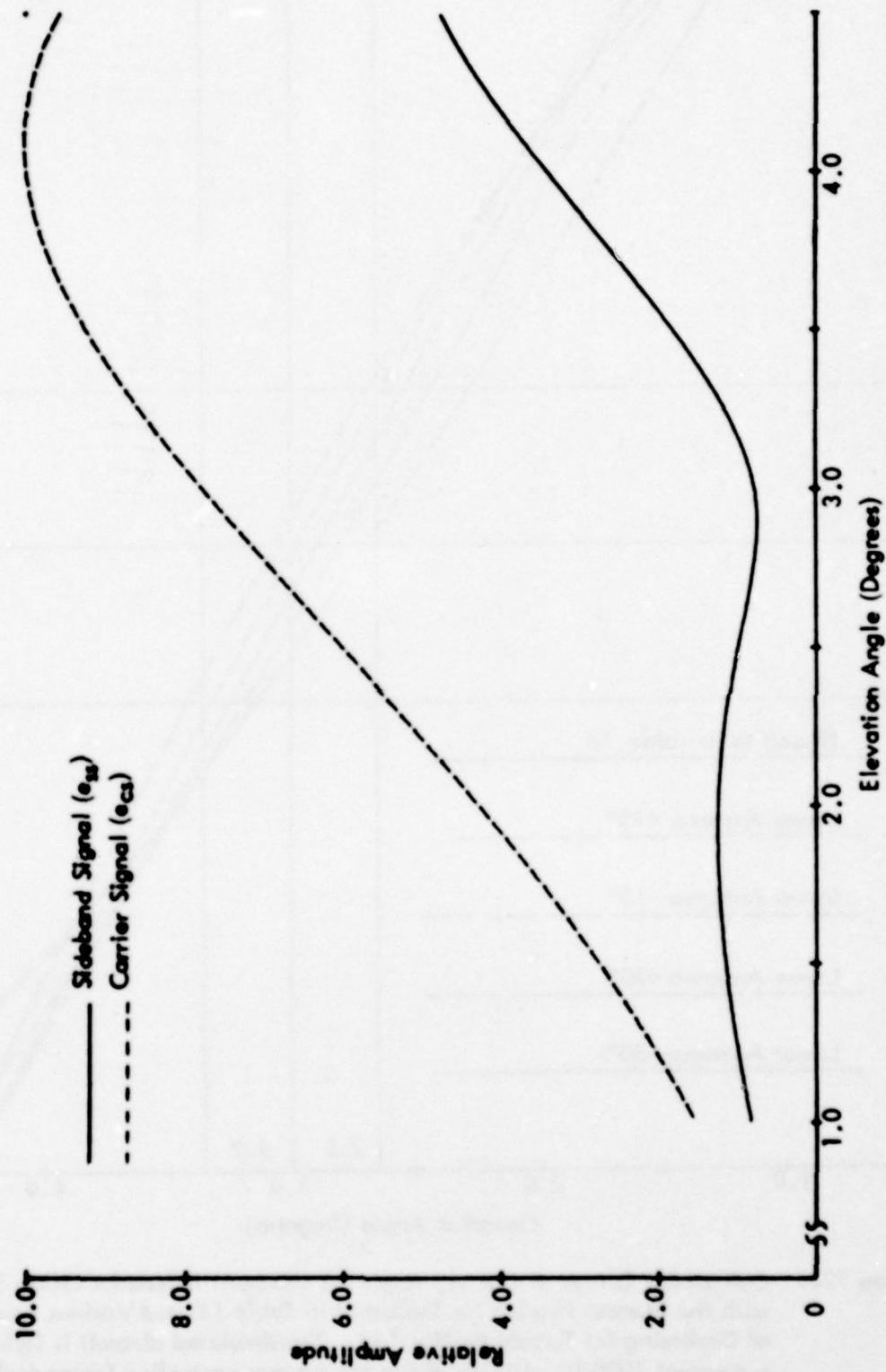
Figure 77d. Calculated Curves of Carrier and Sideband Signals vs. Angle for the Null Reference Glide Slope for Terrain Profile #10. The simulated aircraft is flying at a constant 1000 ft. altitude above the runway centerline (extended).
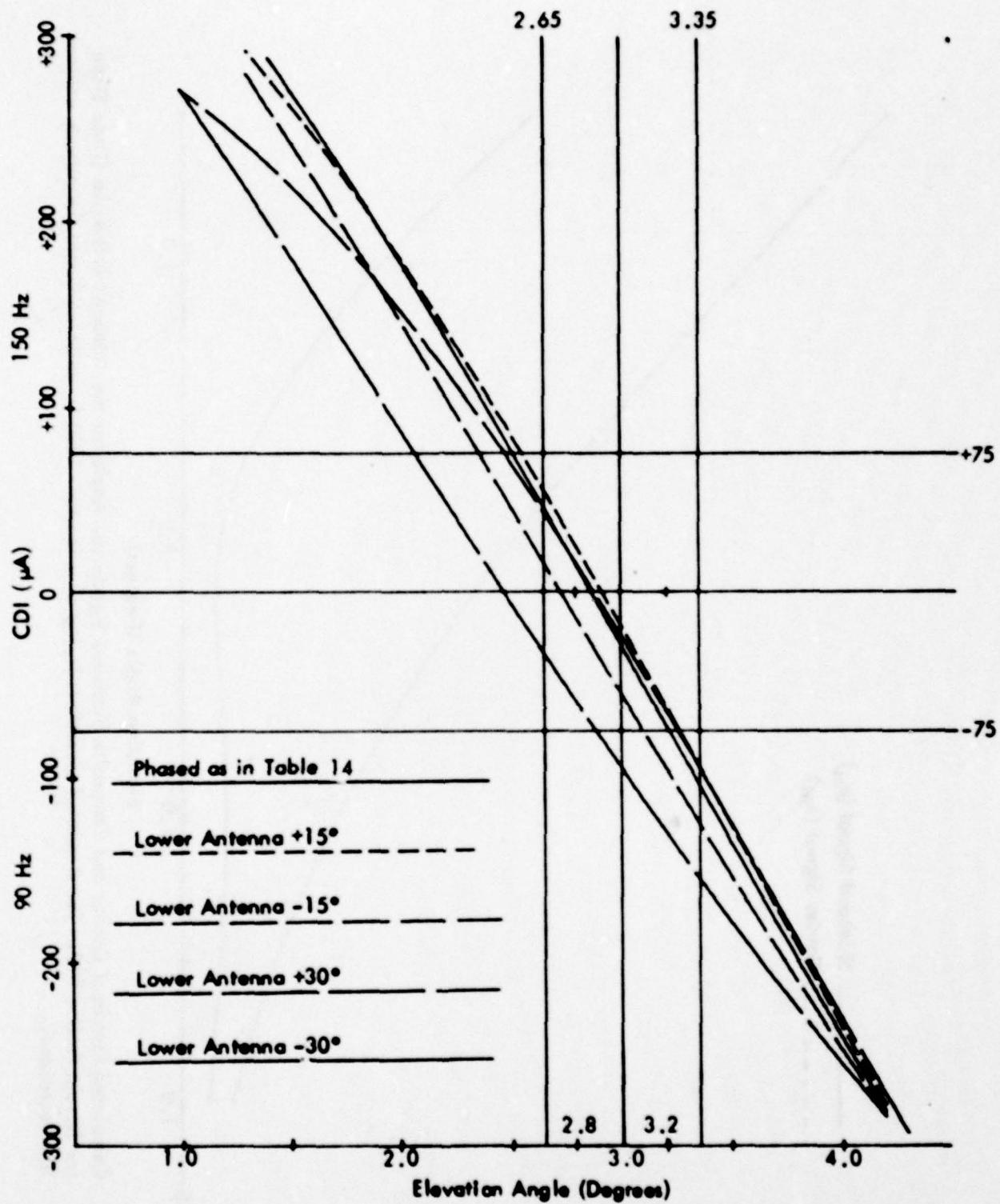
Figure 77e. Calculated Curves of CDI vs. Angle for the Sideband Reference Glide Slope with Normal Phasing (as Indicated in Table 14) and Various Amounts of Dephasing for Terrain Profile #10. The simulated aircraft is flying at a constant 1000 ft. altitude above the runway centerline (extended).
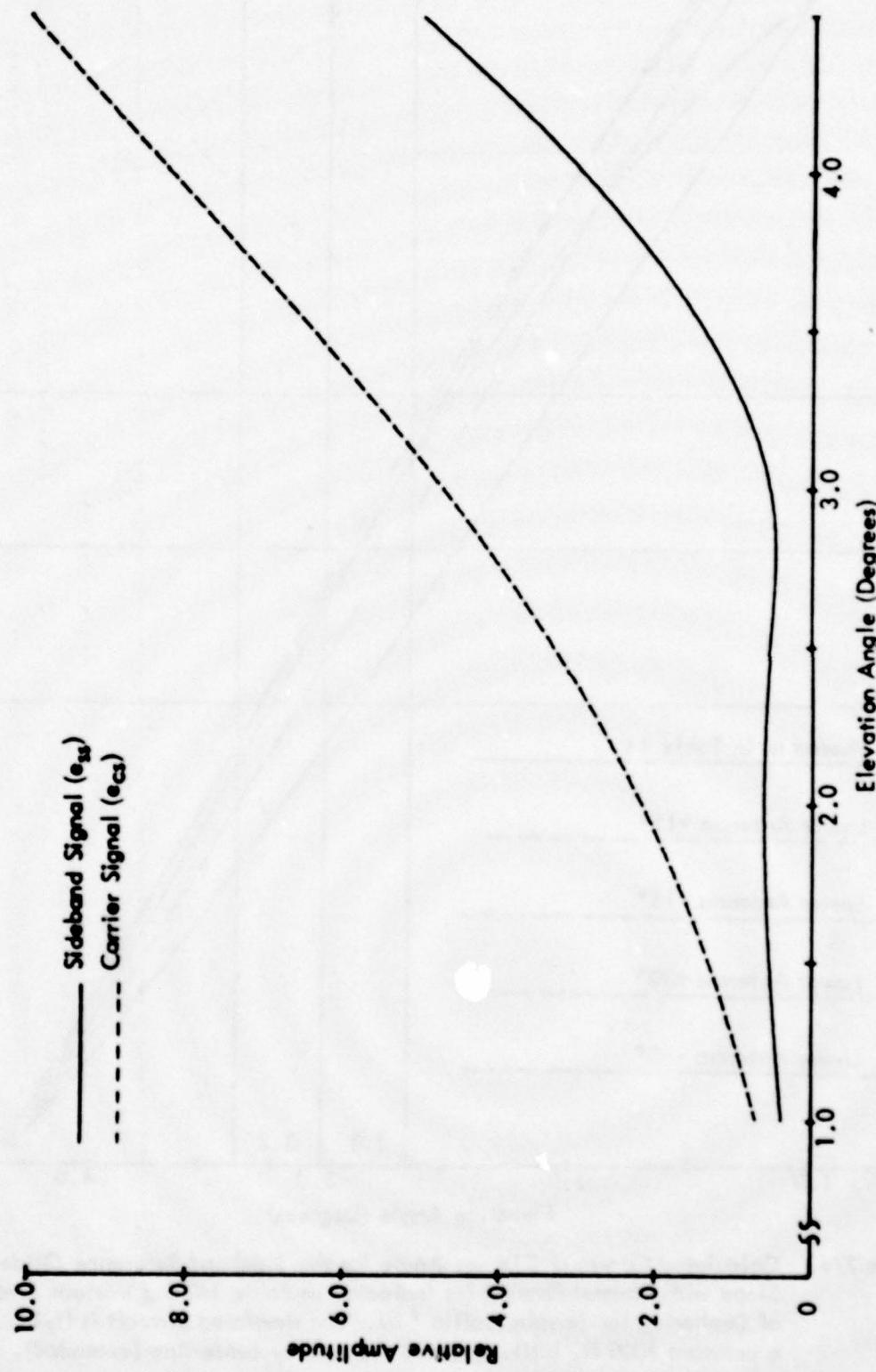
Figure 77f. Calculated Curves of Carrier and Composite Sideband Signals vs. Angle for the Sideband Reference Glide Slope for Terrain Profile #10. The simulated aircraft is flying at a constant 1000 ft. altitude above the runway centerline (extended).
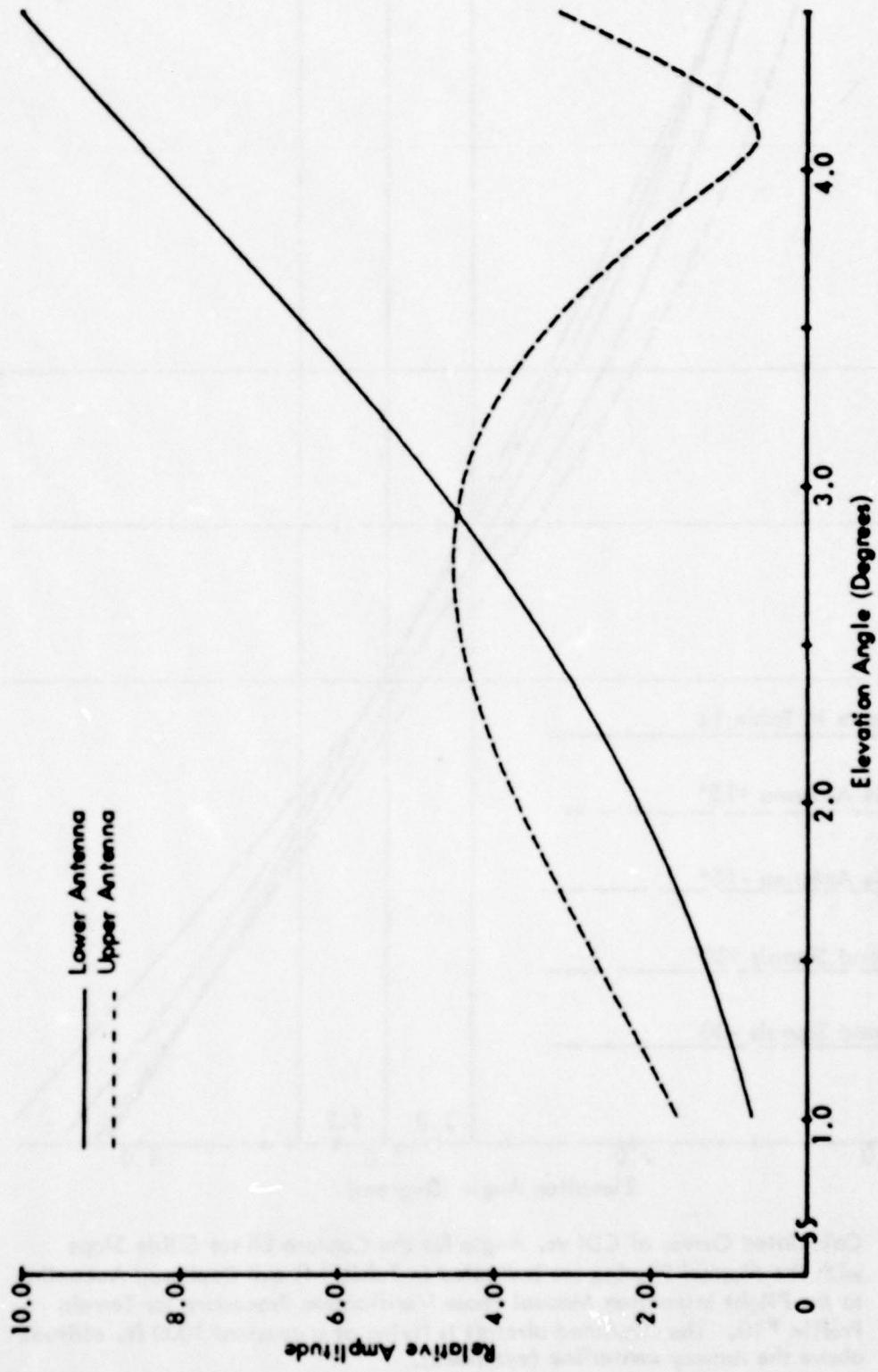
Figure 77g. Calculated Normalized Antenna Patterns vs. Angle for the Sideband Reference System for Terrain Profile #10. The simulated aircraft is flying at a constant 1000 ft. altitude above the runway centerline (extended).
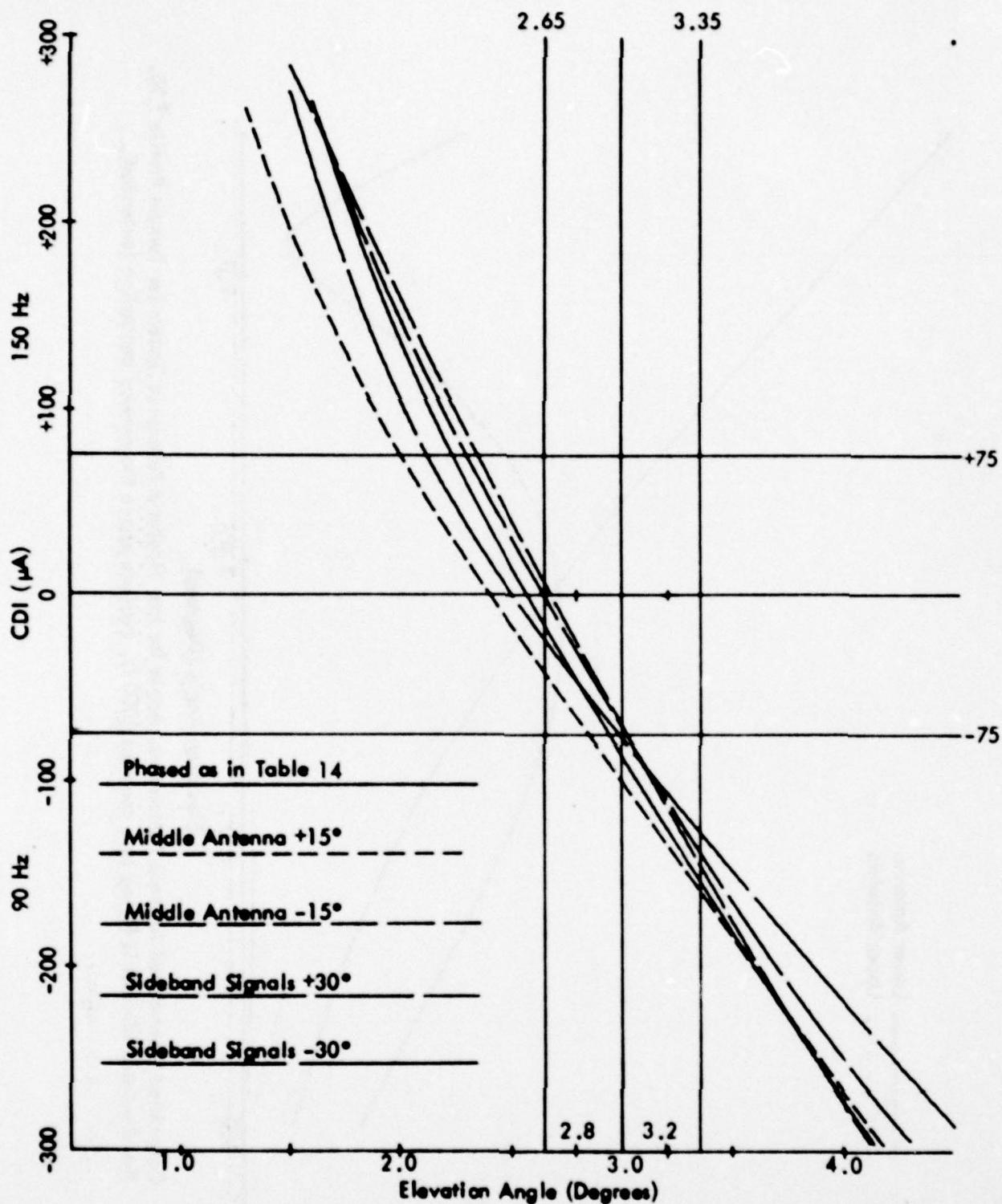
Figure 77h. Calculated Curves of CDI vs. Angle for the Capture Effect Glide Slope with the Normal Phasing (as Indicated in Table 14) and Dephased According to the Flight Inspection Manual Phase Verification Procedure for Terrain Profile #10. The simulated aircraft is flying at a constant 1000 ft. altitude above the runway centerline (extended).

Figure 77I. Calculated Curves of Composite Carrier and Sideband Signals vs. Angle for the Capture Effect Glide Slope for Terrain Profile #10. The simulated aircraft is flying at a constant 1000 ft. altitude above the runway centerline (extended).
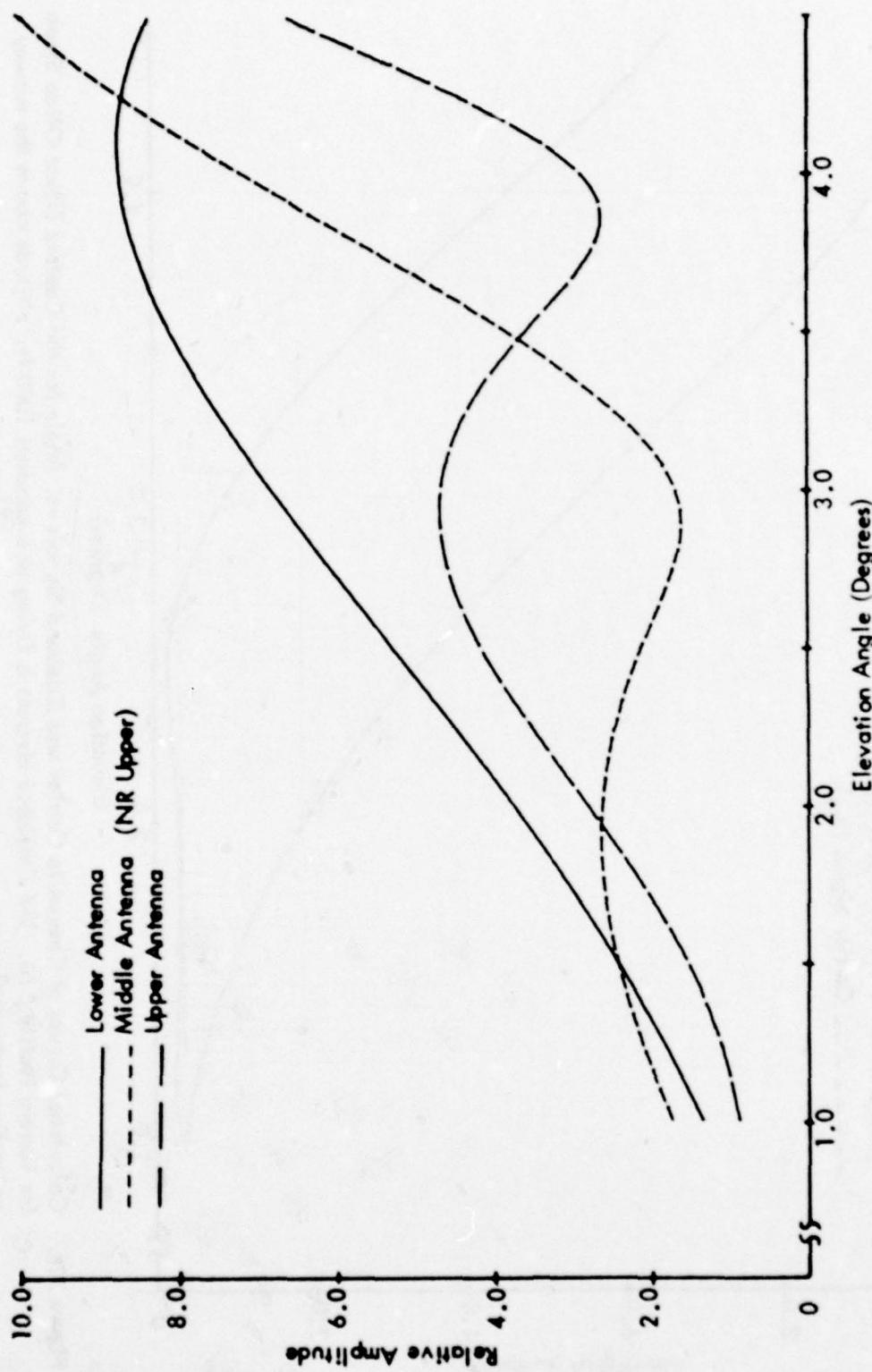
Figure 77i. Calculated Normalized Antenna Patterns vs. Angle for the Capture Effect and Null Reference Systems for Terrain Profile #10. The simulated aircraft is flying at a constant 1000 ft. altitude above the runway center-line (extended).

-194-

	Path Angle	Width Angle	+ 75 µA	-75 µA	Symmetry
Normal Phasing					
Null Reference	3.03	.70	2.67	3.37	.49
Sideband Reference	3.00	.70	2.64	3.34	.49
CEGS	2.88	.70	2.53	3.23	.50
Null Reference Dephased					
+15° Lower Antenna	3.07	.78	2.72	3.40	.48
-15° Lower Antenna	2.99	.77	2.60	3.37	.49
+30° Lower Antenna	3.11	.70	2.75	3.45	.48
-30° Lower Antenna	2.93	.92	2.47	3.39	.51
SBR Dephased					
+15° Lower Antenna	3.01	.70	2.65	3.35	.49
-15° Lower Antenna	2.90	.76	2.51	3.27	.49
+30° Lower Antenna	2.95	.76	2.55	3.31	.48
-30° Lower Antenna	2.68	.88	2.24	3.11	.50
CEGS Dephased					
+15° Middle Antenna	2.81	.89	2.33	3.22	.46
-15° Middle Antenna	2.93	.64	2.61	3.25	.50
+30° SBO	2.83	.80	2.43	3.23	.51
-30° SBO	2.94	.81	2.53	3.33	.49

"A" Ratio: NR .371   SBR .353   CEGS .370

Relative Phase NR/CEGS   Upper -5.9°   Middle 0°   Lower -6.0°

Relative Phase SBR   Upper 0°   Lower -4.6°

Table 15. Terrain Profile #11.
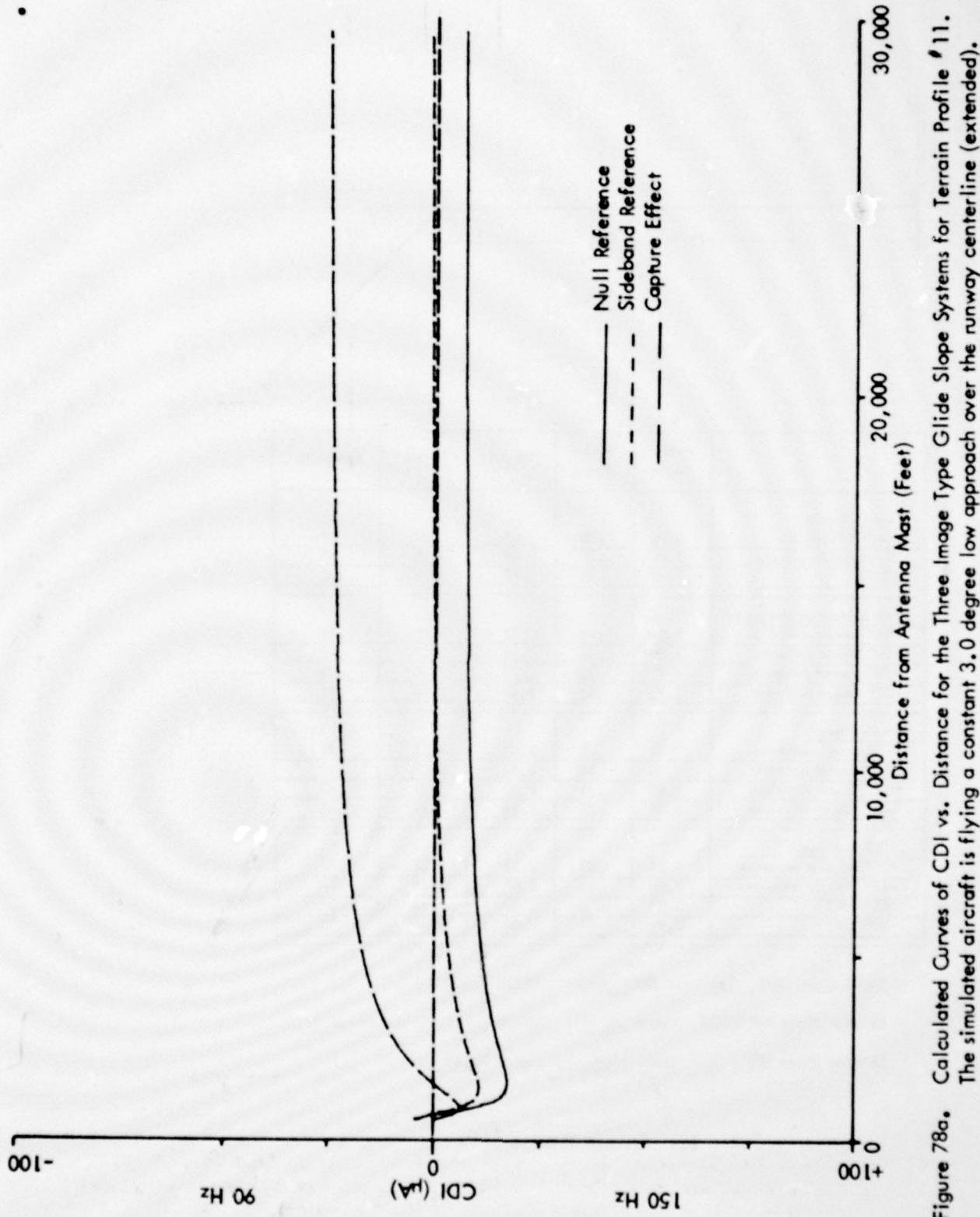
Figure 78a. Calculated Curves of CDI vs. Distance for the Three Image Type Glide Slope Systems for Terrain Profile #11. The simulated aircraft is flying a constant 3.0 degree low approach over the runway centerline (extended).
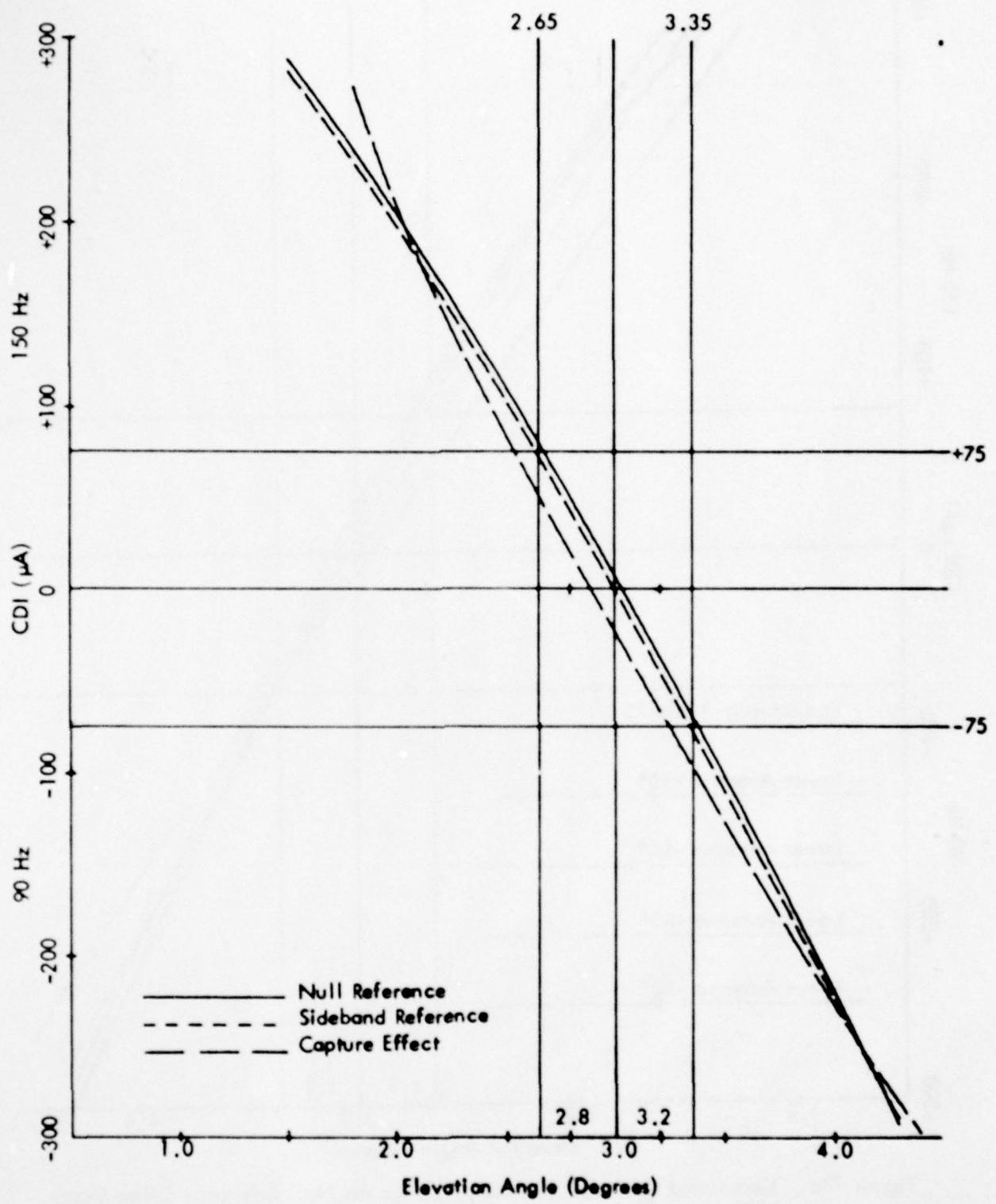
Figure 78b. Calculated Curves of CDI vs. Angle for the Three Image Type Glide-Slope Systems for Terrain Profile #11. The simulated aircraft is flying at a constant 1000 ft. altitude above the runway centerline (extended).

-197-
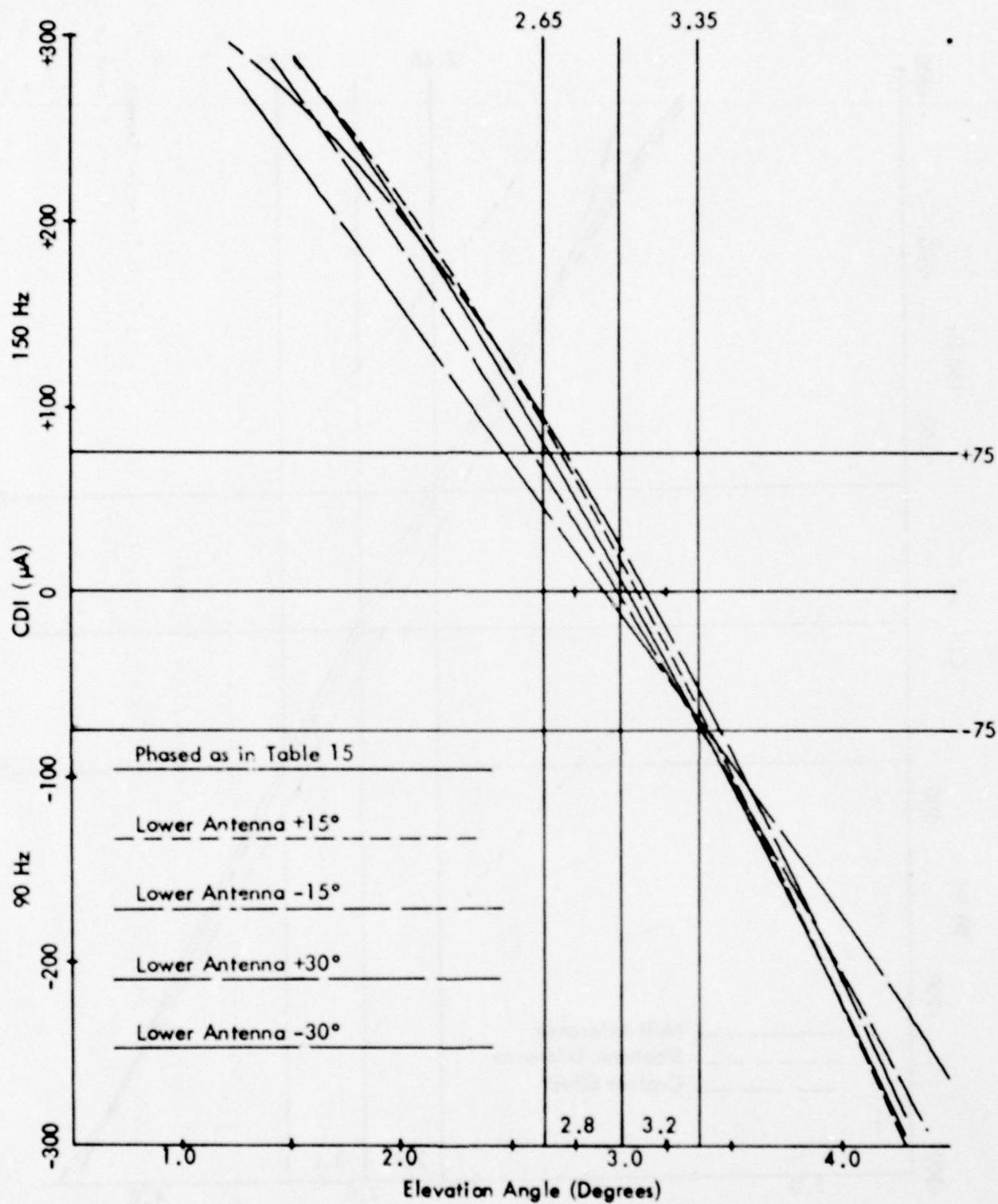
Figure 78c. Calculated Curves of CDI vs. Angle for the Null Reference Glide Slope with the Normal Phasing (as Indicated in Table 15) and Various Amounts of Dephasing for Terrain Profile #11. The simulated aircraft is flying at a constant 1000 ft. altitude above the runway centerline (extended).

-198-
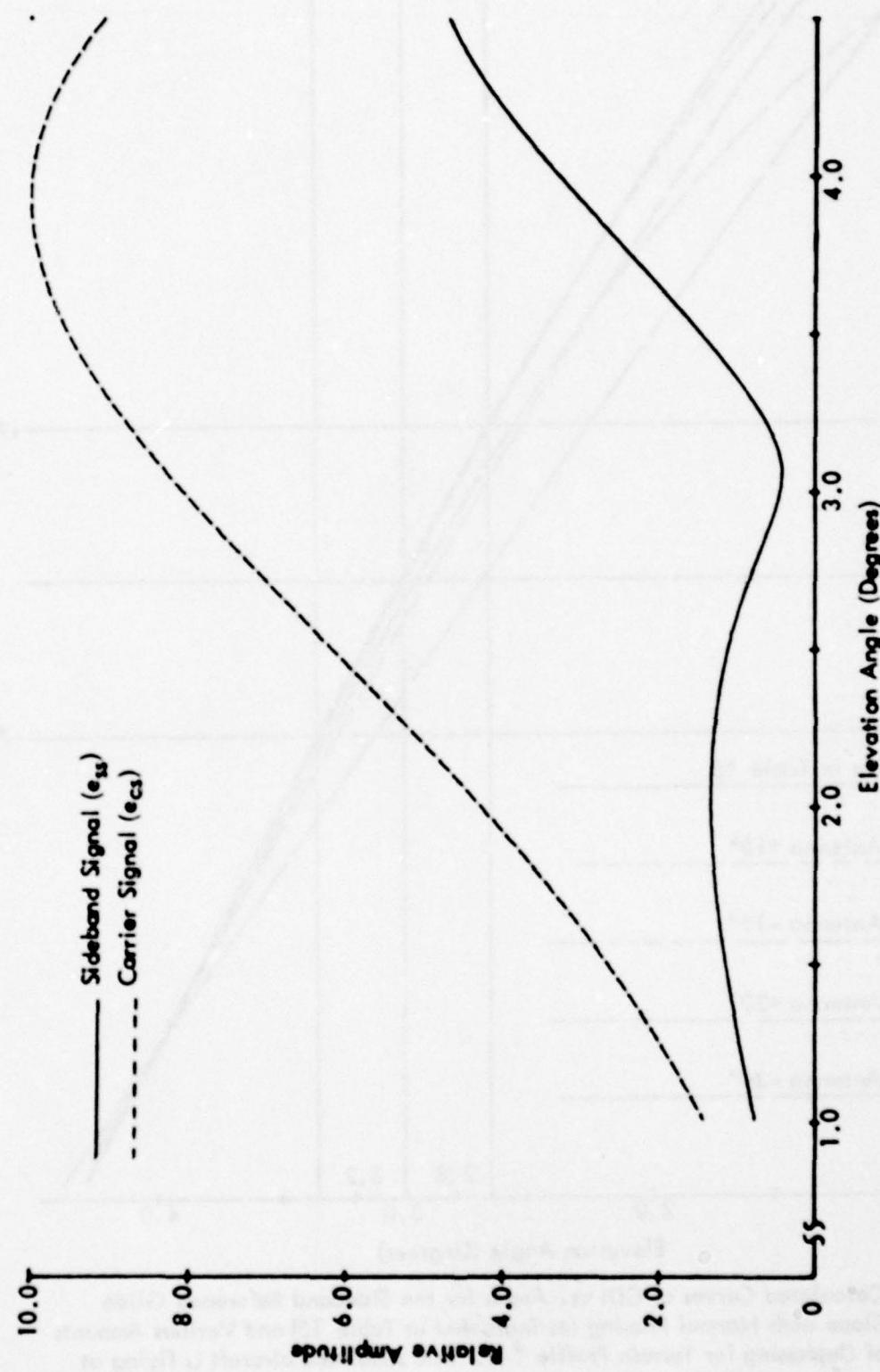
Figure 78d. Calculated Curves of Carrier and Sideband Signals vs. Angle for the Null Reference Glide Slope for Terrain Profile #11. The simulated aircraft is flying at a constant 1000 ft. altitude above the runway centerline (extended).
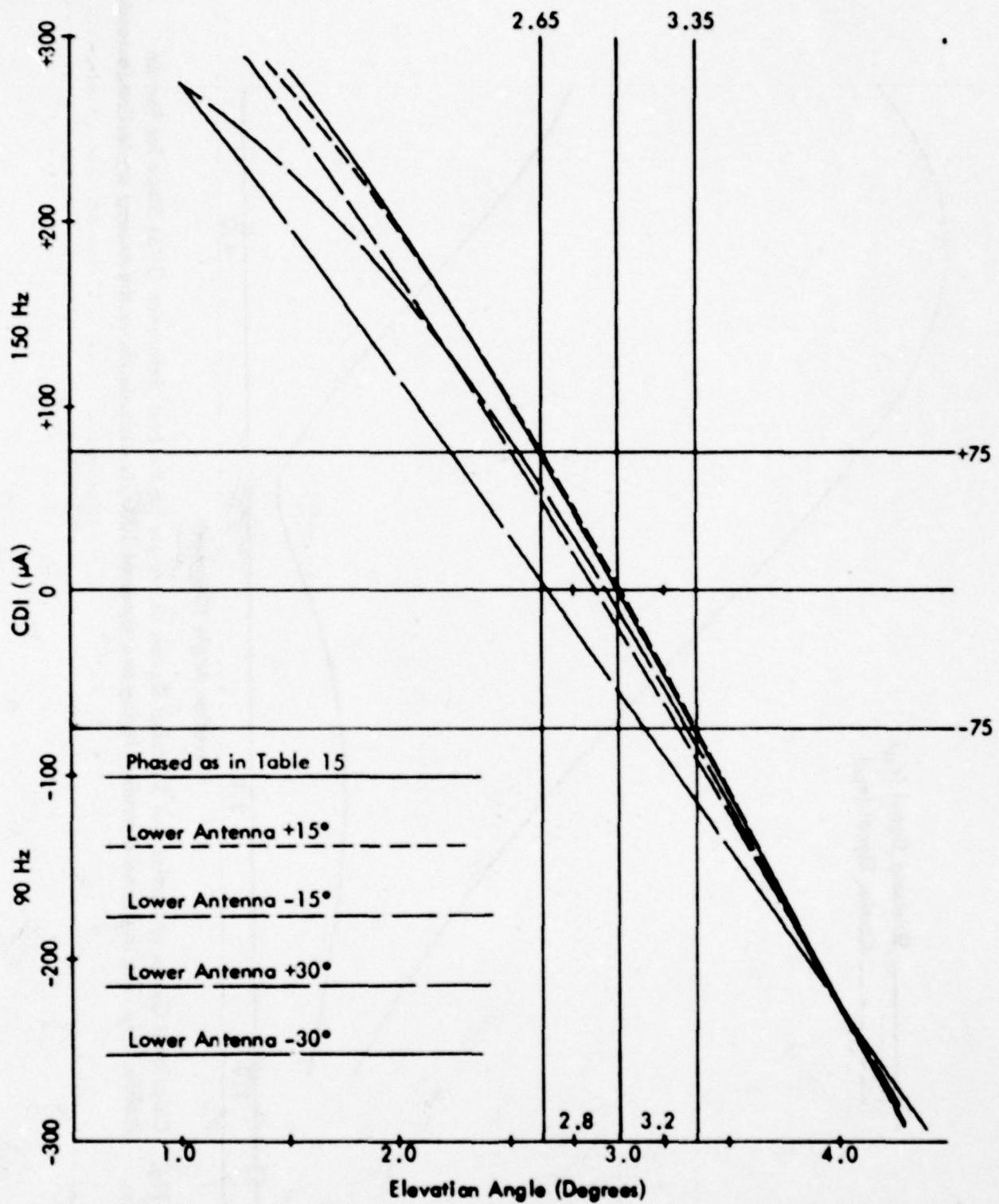
Figure 78e. Calculated Curves of CDI vs. Angle for the Sideband Reference Glide Slope with Normal Phasing (as Indicated in Table 15) and Various Amounts of Dephasing for Terrain Profile #11. The simulated aircraft is flying at a constant 1000 ft. altitude above the runway centerline (extended).

-200-
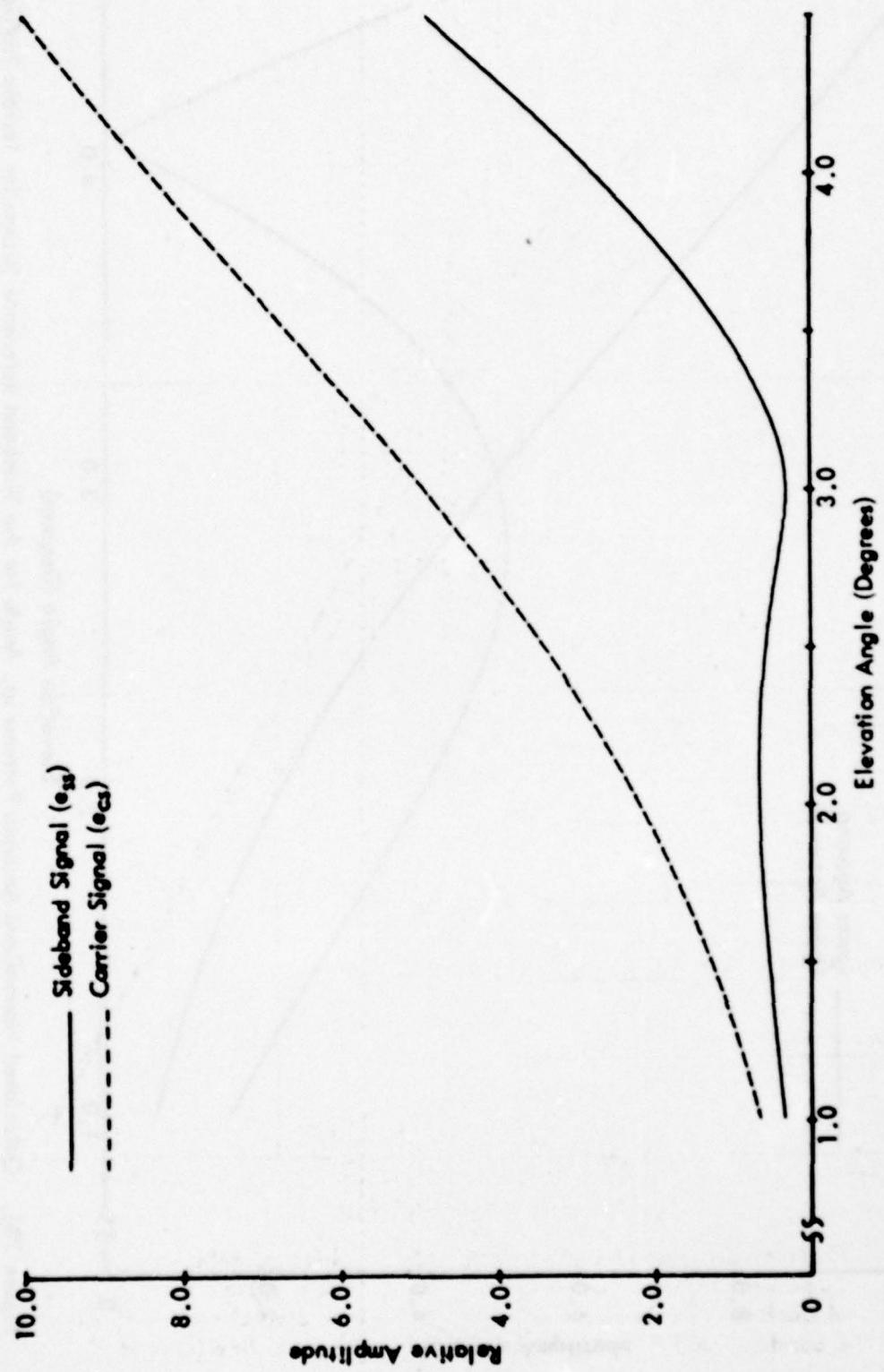
Figure 78f. Calculated Curves of Carrier and Composite Sideband Signals vs. Angle for the Sideband Reference Glide Slope for Terrain Profile #11. The simulated aircraft is flying at a constant 1000 ft. altitude above the runway centerline (extended).
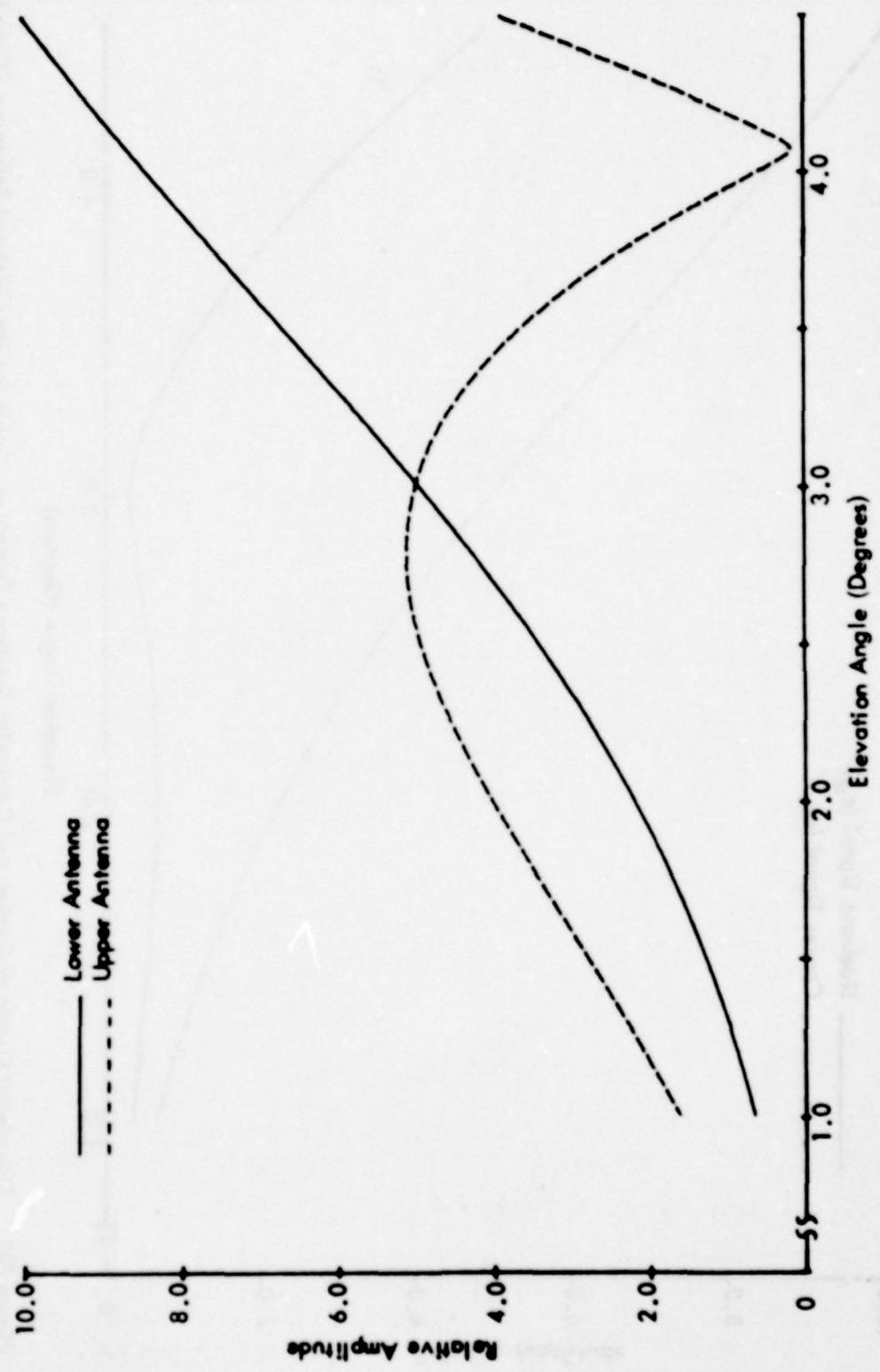
Figure 78g. Calculated Normalized Antenna Patterns vs. Angle for the Sideband Reference System for Terrain Profile #11. The simulated aircraft is flying at a constant 1000 ft. altitude above the runway centerline (extended).

-202-
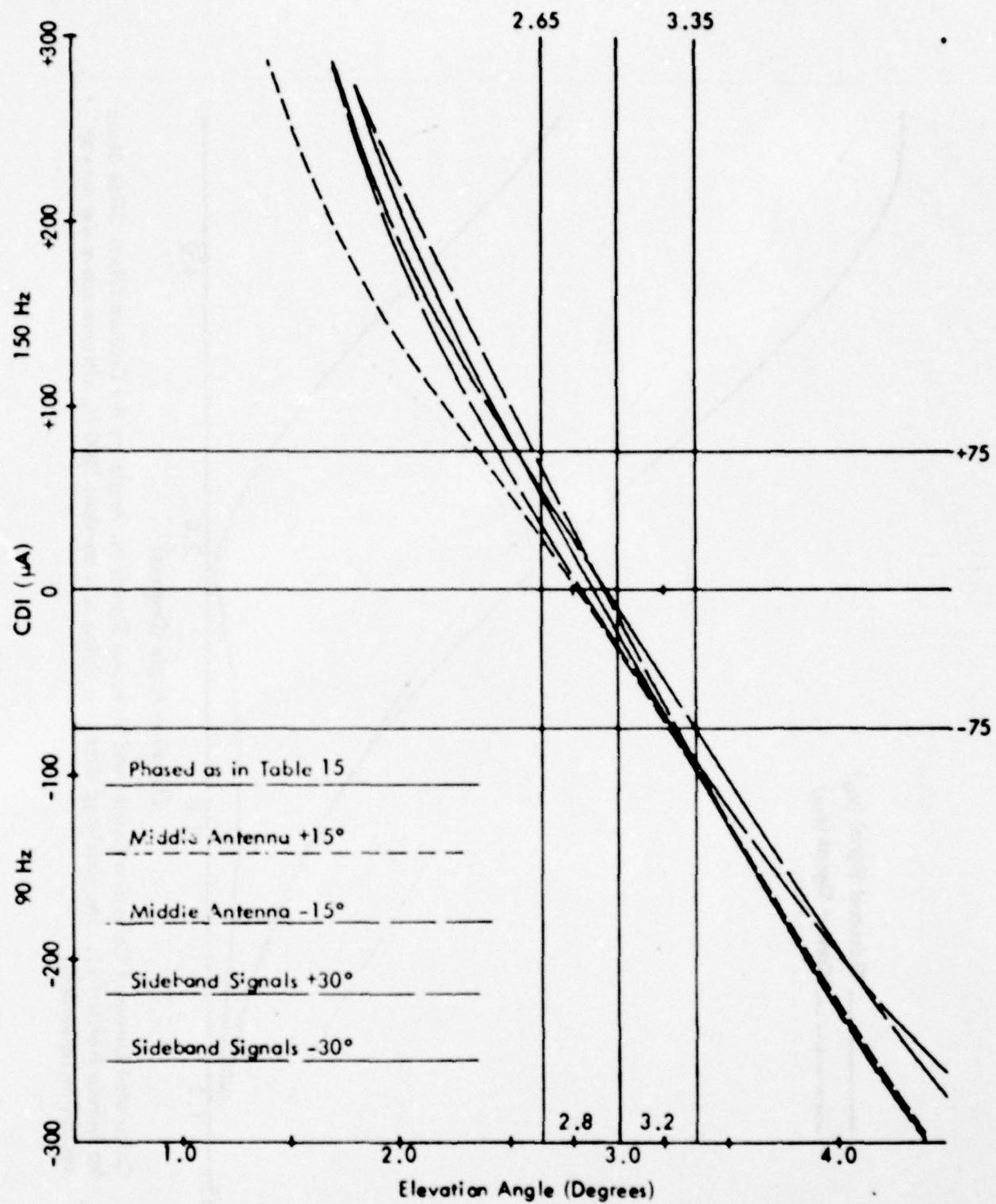
Figure 78h.   Calculated Curves of CDI vs. Angle for the Capture Effect Glide Slope
with the Normal Phasing (as Indicated in Table 15) and Dephased According
to the Flight Inspection Manual Phase Verification Procedure for Terrain
Profile #11.   The simulated aircraft is flying at a constant 1000 ft. altitude
above the runway centerline (extended).

-203-
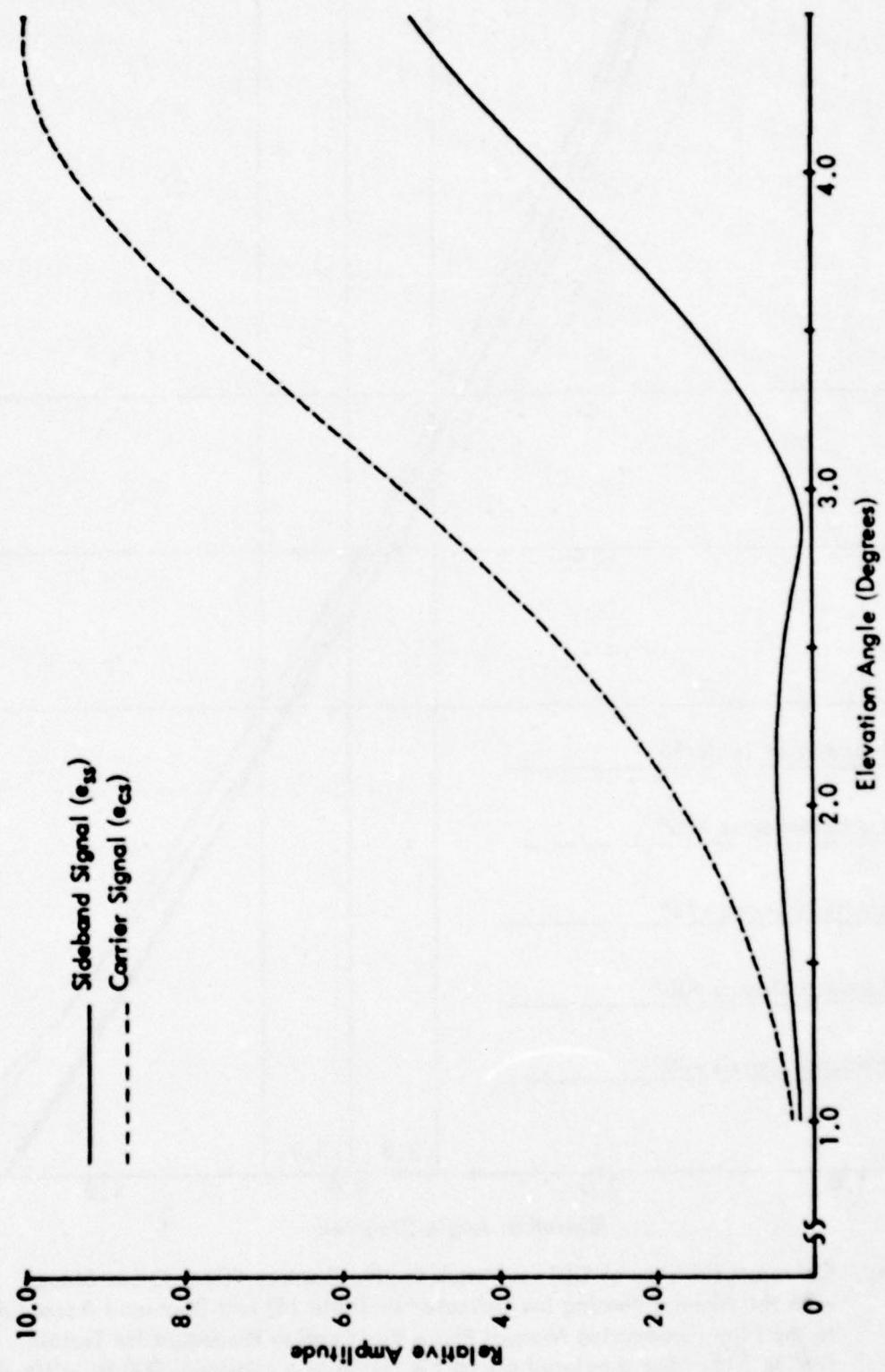
Figure 78I.   Calculated Curves of Composite Carrier and Sideband Signals vs. Angle for the Capture Effect Glide Slope for Terrain Profile #11.   The simulated aircraft is flying at a constant 1000 ft. altitude above the runway centerline (extended).
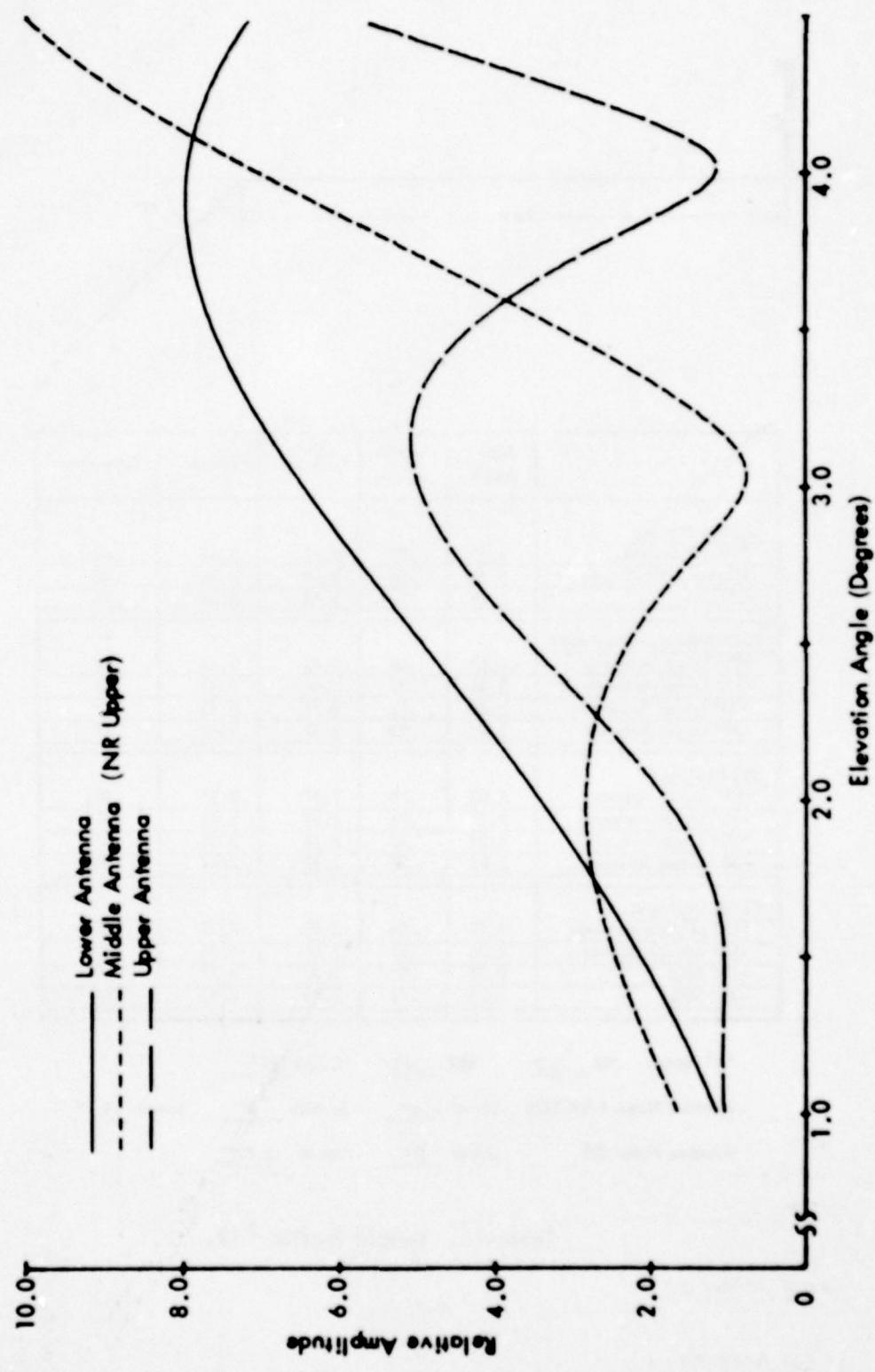
Figure 78j. Calculated Normalized Antenna Patterns vs. Angle for the Capture Effect and Null Reference Systems for Terrain Profile #11. The simulated aircraft is flying at a constant 1000 ft. altitude above the runway centerline (extended).

1000 ft. — 45°
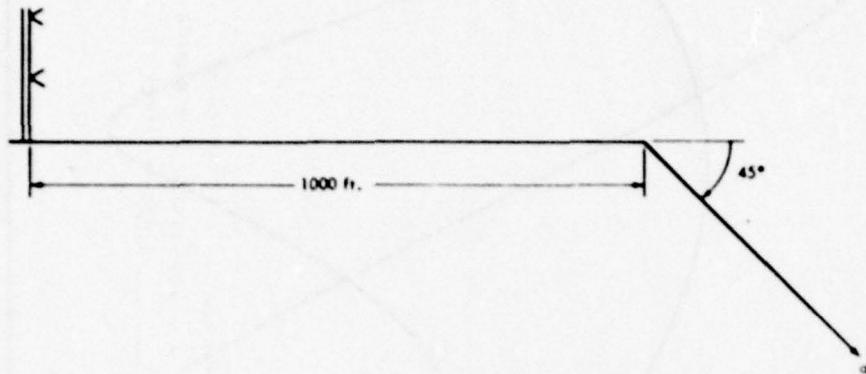
	Path Angle	Width Angle	+ 75 μA	-75 μA	Symmetry
Normal Phasing					
Null Reference	3.07	.70	2.71	3.41	.48
Sideband Reference	3.05	.70	2.68	3.38	.48
CEGS	2.99	.70	2.64	3.34	.49
Null Reference Dephased					
+15° Lower Antenna	3.08	.68	2.72	3.41	.48
-15° Lower Antenna	3.06	.77	2.66	3.43	.48
+30° Lower Antenna	3.09	.72	2.71	3.43	.47
-30° Lower Antenna	3.05	.92	2.57	3.49	.47
SBR Dephased					
+15° Lower Antenna	3.03	.70	2.67	3.37	.48
-15° Lower Antenna	2.99	.76	2.59	3.36	.48
+30° Lower Antenna	2.94	.77	2.54	3.31	.47
-30° Lower Antenna	2.82	.92	2.35	3.27	.48
CEGS Dephased					
+15° Middle Antenna	2.97	.84	2.51	3.35	.45
-15° Middle Antenna	3.00	.67	2.66	3.34	.49
+30° SBO	2.95	.85	2.52	3.37	.50
-30° SBO	3.04	.76	2.64	3.41	.48

"A" Ratio: NR .317   SBR .315   CEGS .332

Relative Phase NR/CEGS   Upper -.4°   Middle 0°   Lower -3.1°

Relative Phase SBR   Upper 0°   Lower -2.39°

Table 16. Terrain Profile #12.
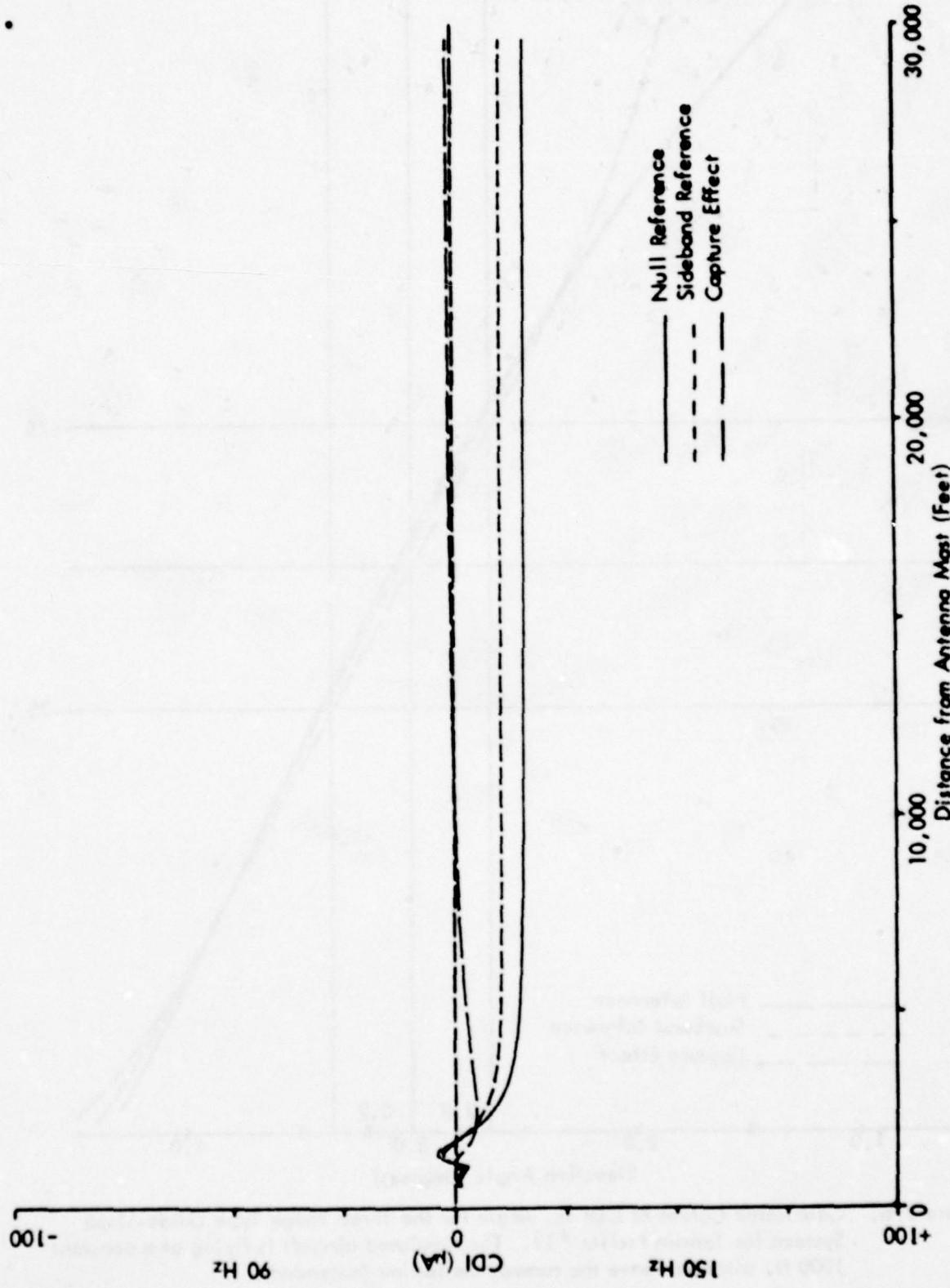
Figure 79a. Calculated Curves of CDI vs. Distance for the Three Image Type Glide Slope Systems for Terrain Profile #12. The simulated aircraft is flying a constant 3.0 degree low approach over the runway centerline (extended).
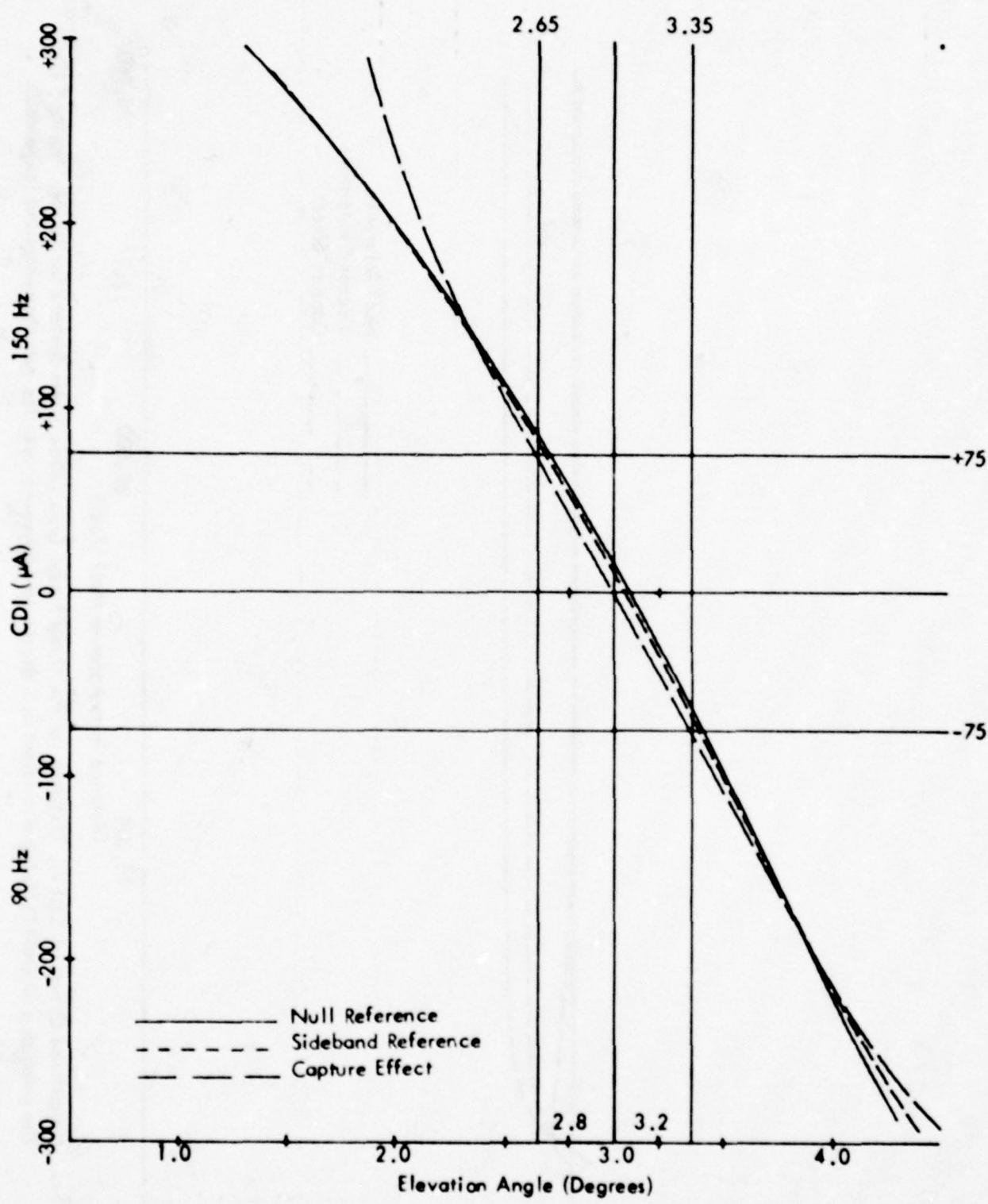
Figure 79b. Calculated Curves of CDI vs. Angle for the Three Image Type Glide-Slope Systems for Terrain Profile #12. The simulated aircraft is flying at a constant 1000 ft. altitude above the runway centerline (extended).
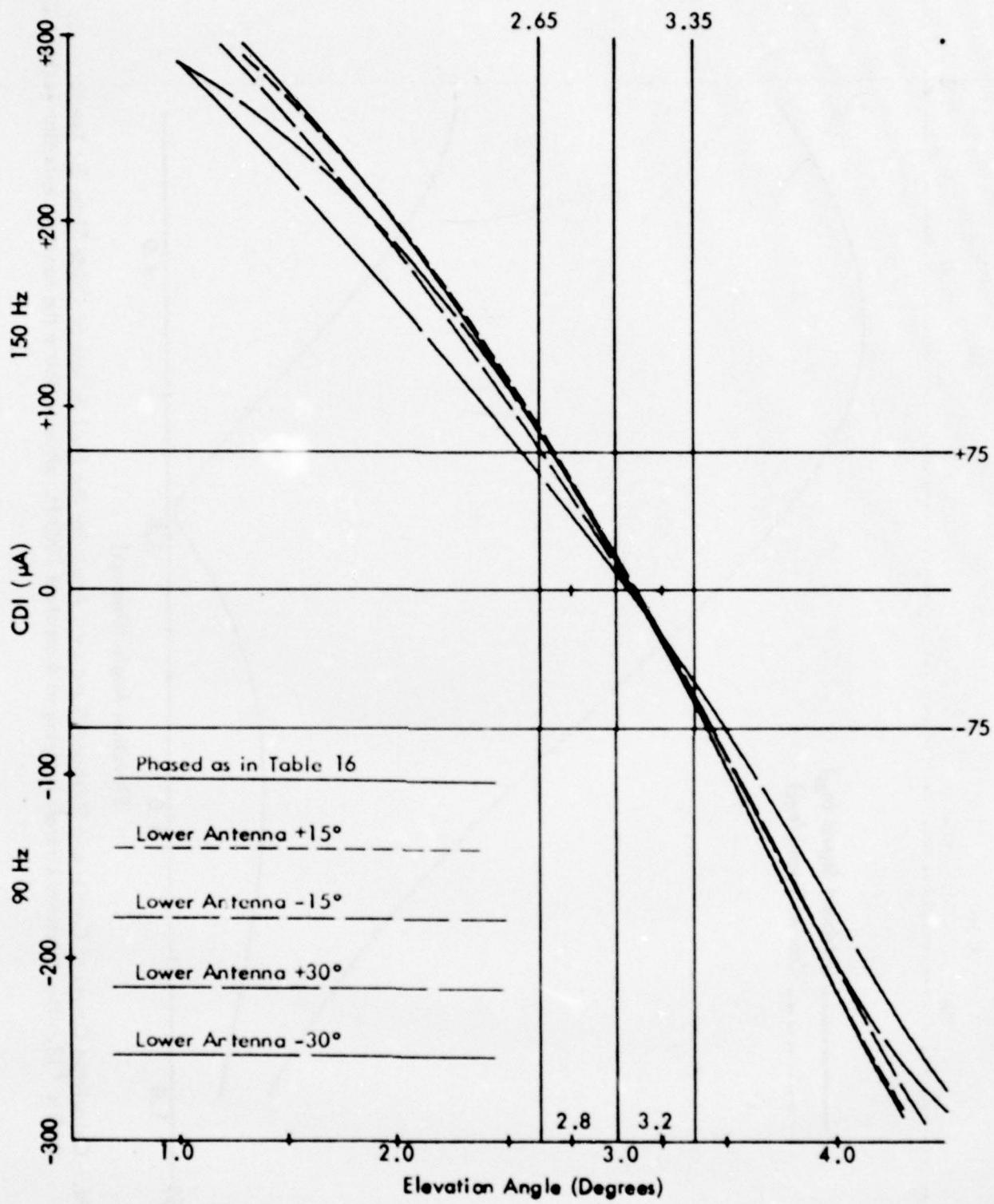
Figure 79c. Calculated Curves of CDI vs. Angle for the Null Reference Glide Slope with the Normal Phasing (as Indicated in Table 16) and Various Amounts of Dephasing for Terrain Profile #12. The simulated aircraft is flying at a constant 1000 ft. altitude above the runway centerline (extended).
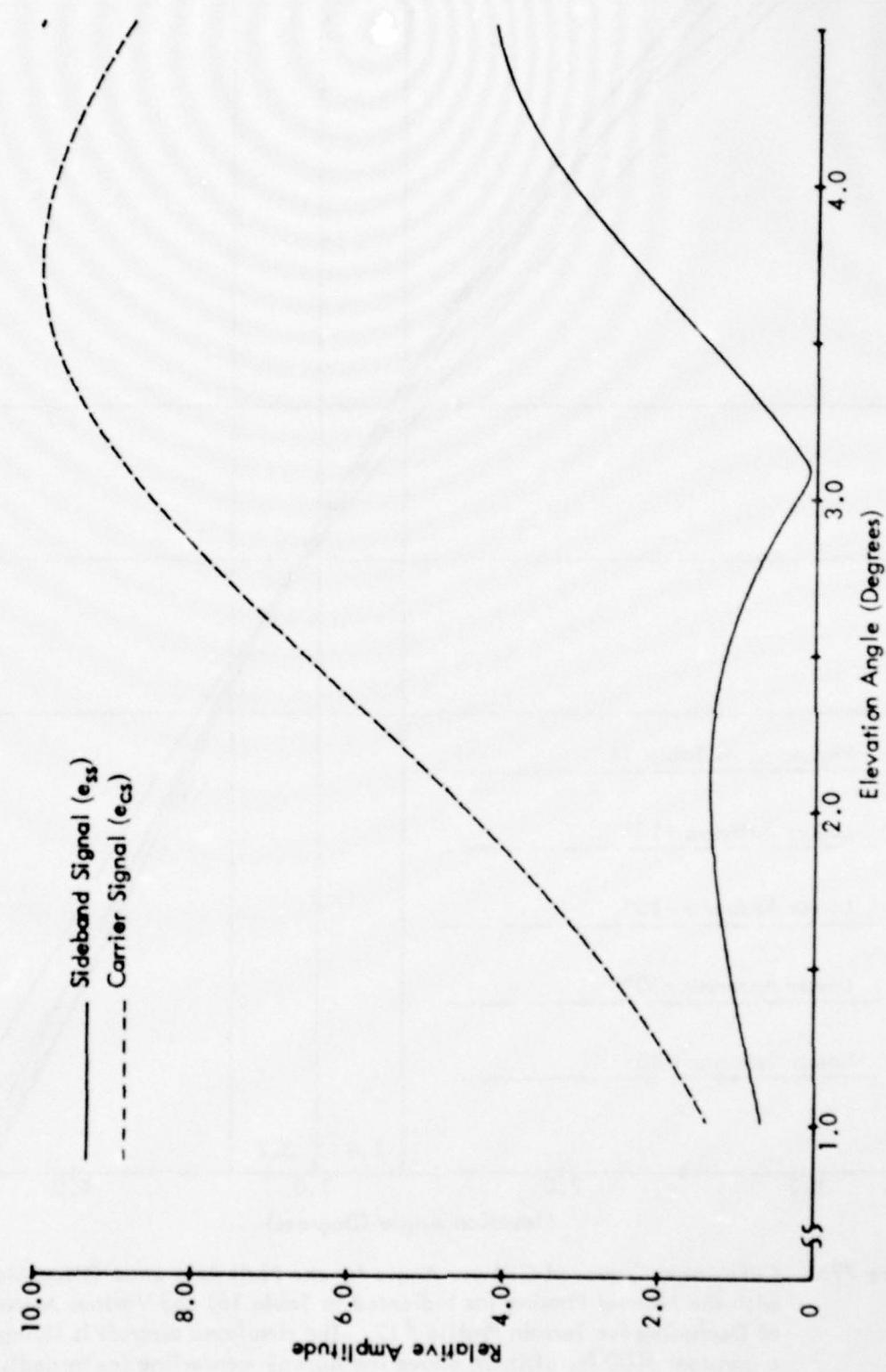
Figure 79d. Calculated Curves of Carrier and Sideband Signals vs. Angle for the Null Reference Glide Slope for Terrain Profile #12. The simulated aircraft is flying at a constant 1000 ft. altitude above the runway centerline (extended).
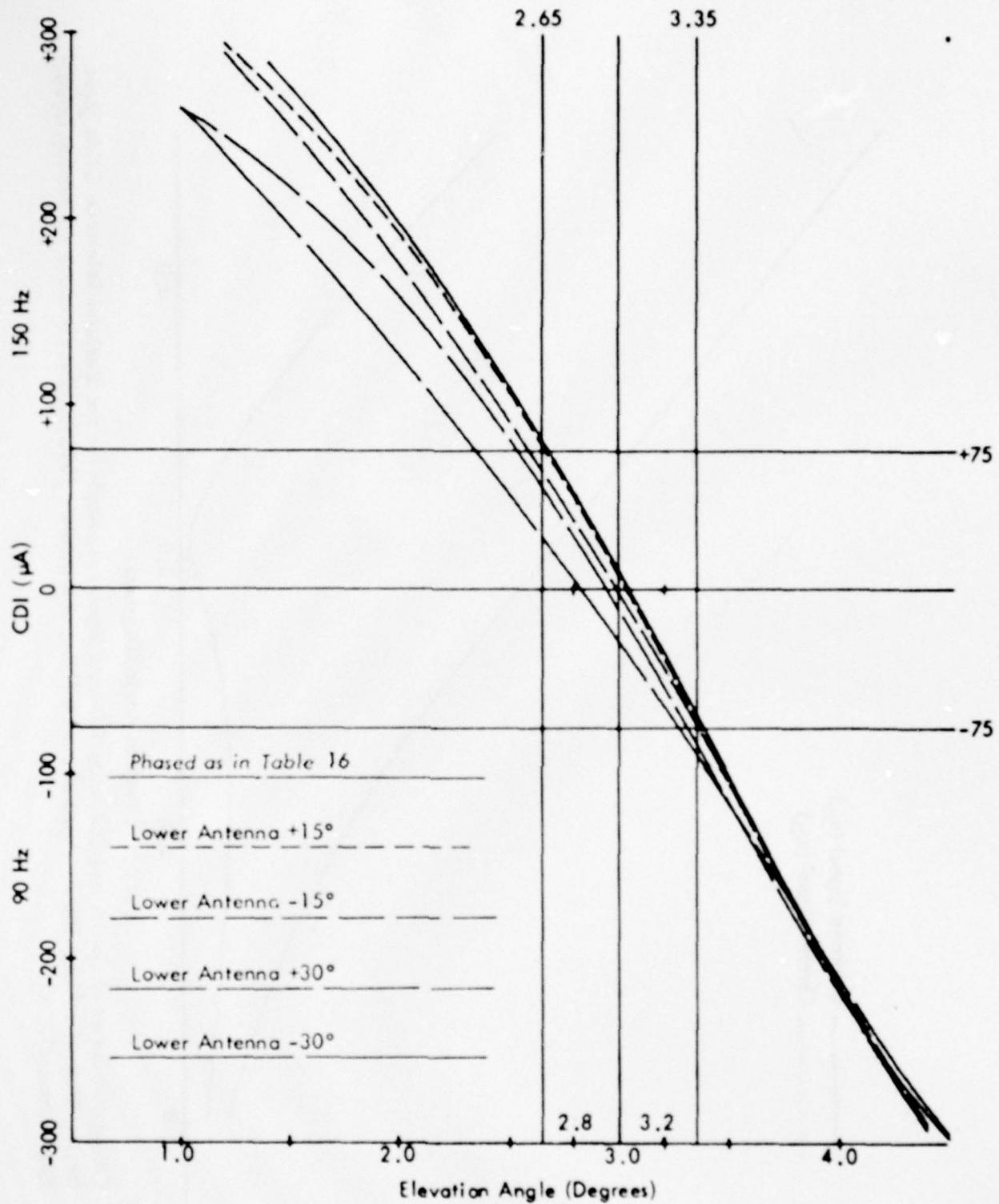
Figure 79e. Calculated Curves of CDI vs. Angle for the Sideband Reference Glide Slope with Normal Phasing (as Indicated in Table 16) and Various Amounts of Dephasing for Terrain Profile #12. The simulated aircraft is flying at a constant 1000 ft. altitude above the runway centerline (extended).

-211-

Sideband Signal (e_{ss})

Carrier Signal (e_{cs})

Relative Amplitude

10.0

8.0

6.0

4.0

2.0

0

1.0   2.0   3.0   4.0

Elevation Angle (Degrees)

Figure 79f.   Calculated Curves of Carrier and Composite Sideband Signals vs. Angle for the Sideband Reference Glide Slope for Terrain Profile #12. The simulated aircraft is flying at a constant 1000 ft. altitude above the runway center-line (extended).

-212-
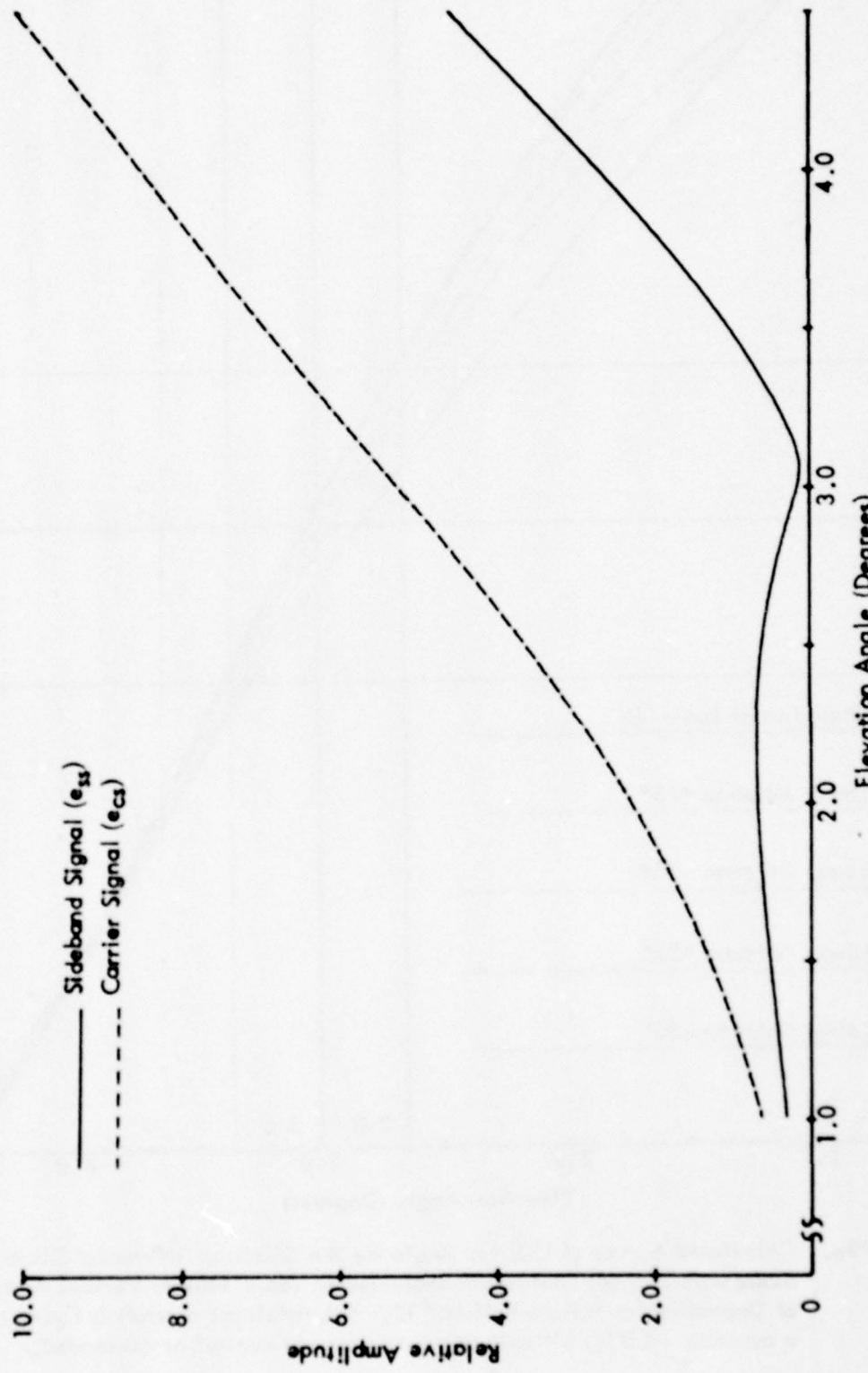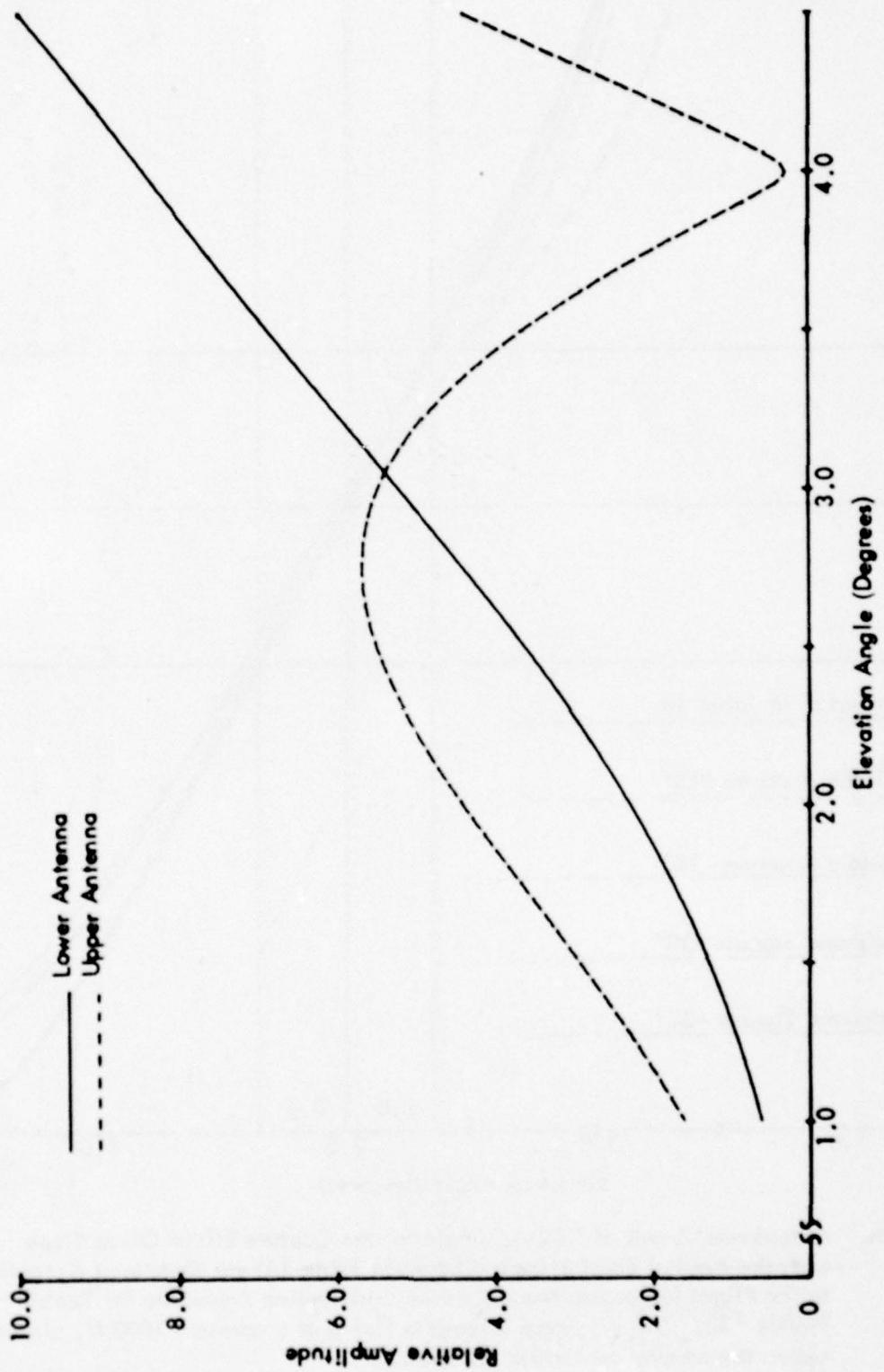
Figure 79g. Calculated Normalized Antenna Patterns vs. Angle for the Sideband Reference System for Terrain Profile #12. The simulated aircraft is flying at a constant 1000 ft. altitude above the runway centerline (extended).

-213-
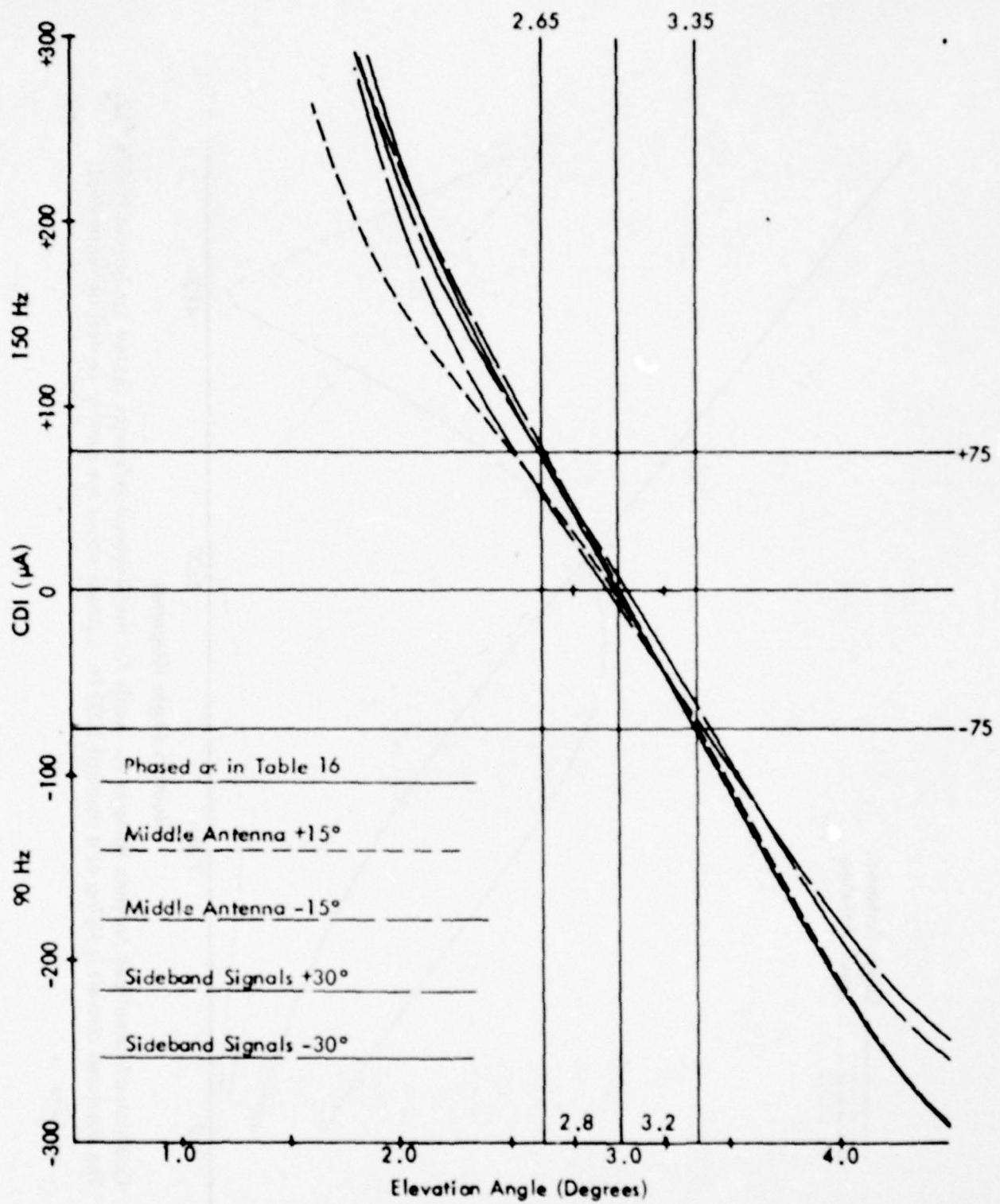
Figure 79h. Calculated Curves of CDI vs. Angle for the Capture Effect Glide Slope with the Normal Phasing (as Indicated in Table 16) and Dephased According to the Flight Inspection Manual Phase Verification Procedure for Terrain Profile #12. The simulated aircraft is flying at a constant 1000 ft. altitude above the runway centerline (extended).

-214-
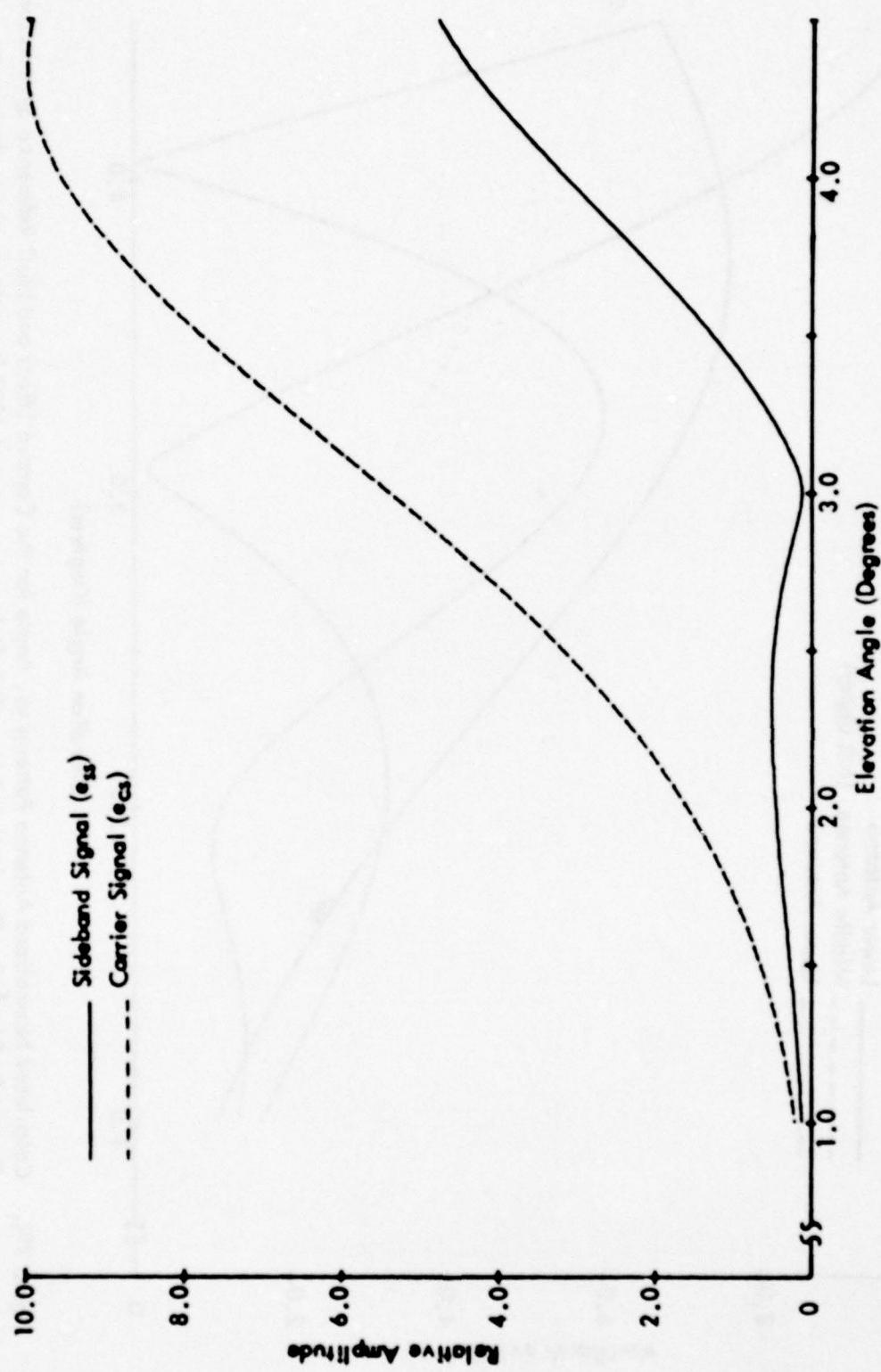
Figure 79i. Calculated Curves of Composite Carrier and Sideband Signals vs. Angle for the Capture Effect Glide Slope for Terrain Profile #12. The simulated aircraft is flying at a constant 1000 ft. altitude above the runway center-line (extended).

-215-
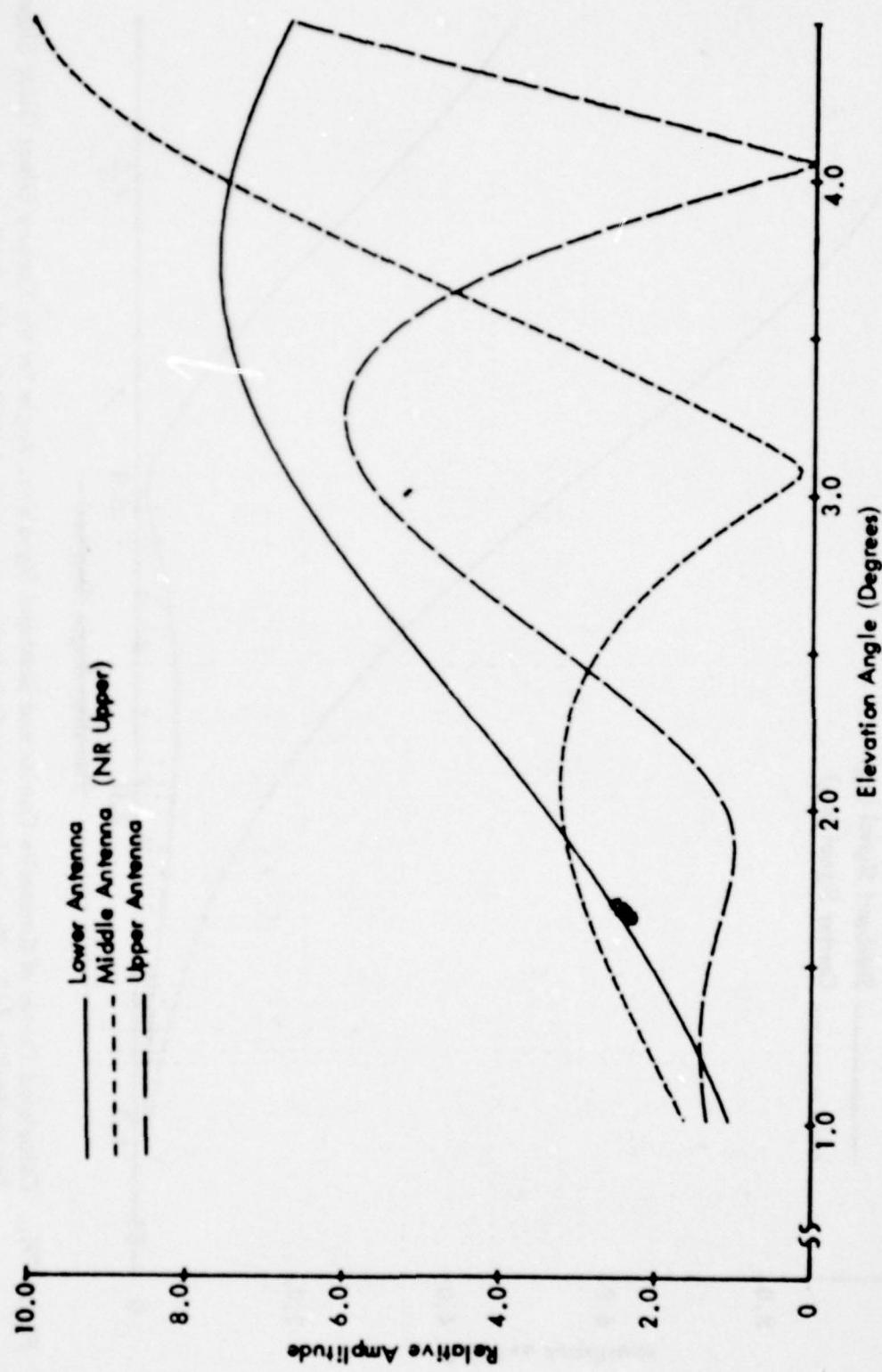
Figure 79i. Calculated Normalized Antenna Patterns vs. Angle for the Capture Effect and Null Reference Systems for Terrain Profile #12. The simulated aircraft is flying at a constant 1000 ft. altitude above the runway centerline (extended).

3000 ft.

45°
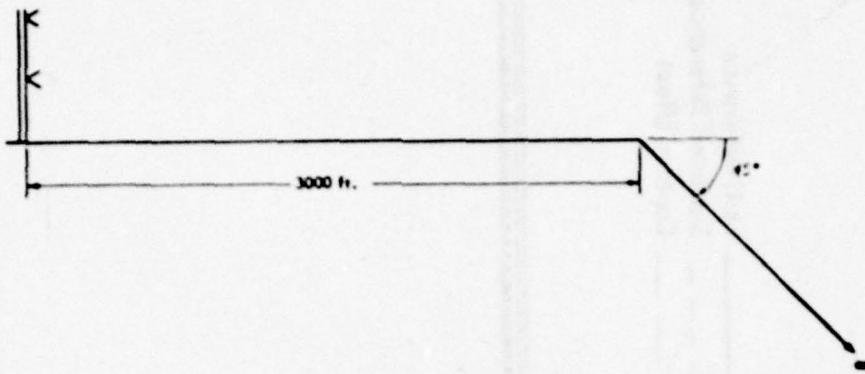
	Path Angle	Width Angle	+75 µA	-75 µA	Symmetry
Normal Phasing					
Null Reference	3.02	.70	2.65	3.34	.47
Sideband Reference	3.01	.70	2.65	3.35	.48
CEGS	3.00	.70	2.65	3.35	.50
Null Reference Dephased					
+15° Lower Antenna	3.01	.72	2.63	3.36	.47
-15° Lower Antenna	3.02	.73	2.63	3.36	.47
+30° Lower Antenna	3.01	.82	2.59	3.40	.48
-30° Lower Antenna	3.02	.81	2.58	3.40	.46
SBR Dephased					
+15° Lower Antenna	2.98	.73	2.60	3.32	.48
-15° Lower Antenna	2.98	.73	2.60	3.33	.47
+30° Lower Antenna	2.86	.82	2.43	3.25	.47
-30° Lower Antenna	2.86	.82	2.44	3.26	.49
CEGS Dephased					
+15° Middle Antenna	3.01	.73	2.62	3.36	.48
-15° Middle Antenna	3.00	.73	2.63	3.36	.49
+30° SBO	3.01	.80	2.61	3.41	.50
-30° SBO	3.00	.82	2.59	3.40	.50

"A" Ratio: NR .300   SBR .301   CEGS .302

Relative Phase NR/CEGS   Upper -1.46°   Middle 0°   Lower +0.4°

Relative Phase SBR   Upper 0°   Lower +0.2°

Table 17. Terrain Profile #13.
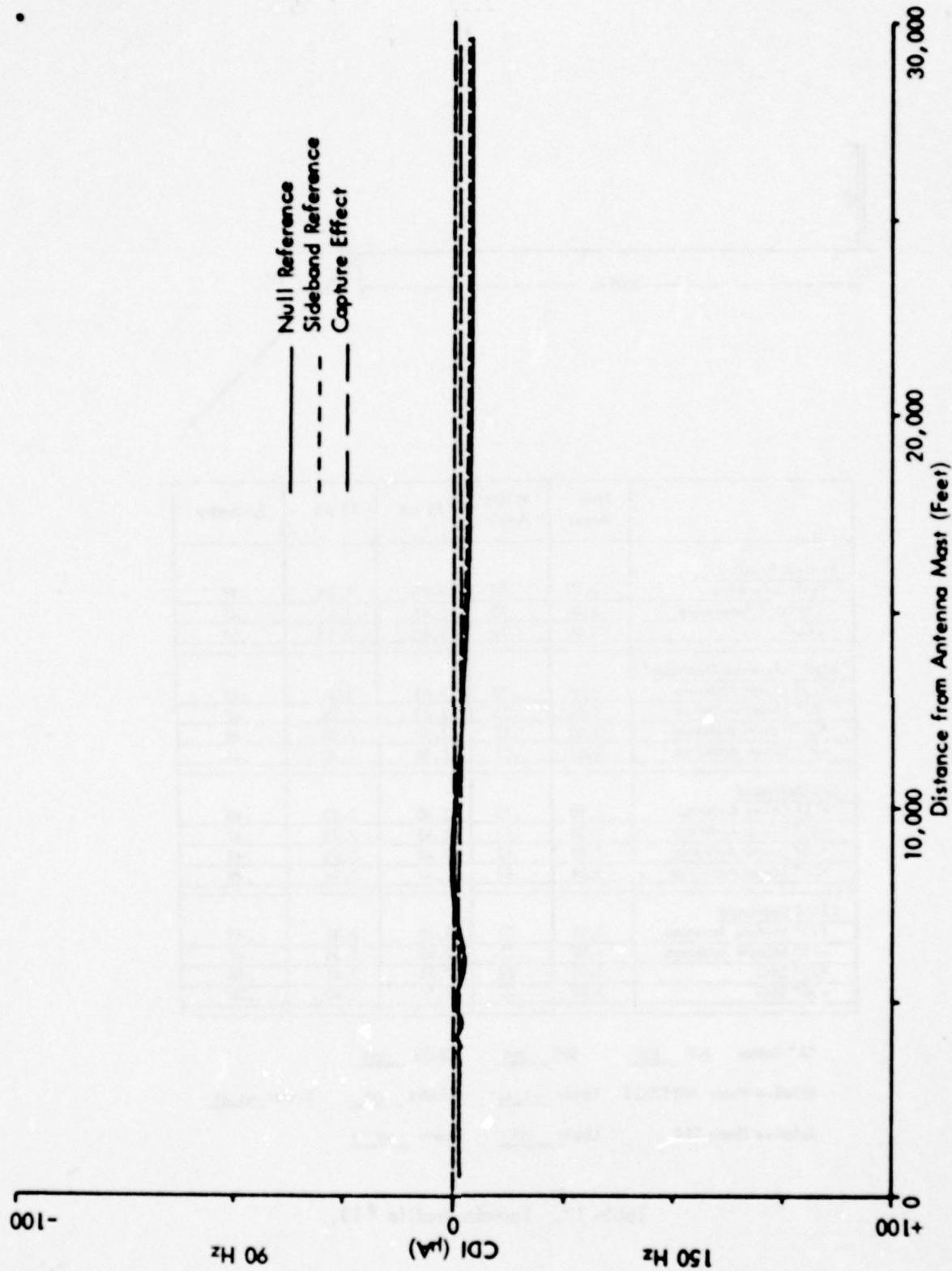
Figure 80a. Calculated Curves of CDI vs. Distance for the Three Image Type Glide Slope Systems for Terrain Profile #13. The simulated aircraft is flying a constant 3.0 degree low approach over the runway centerline (extended).
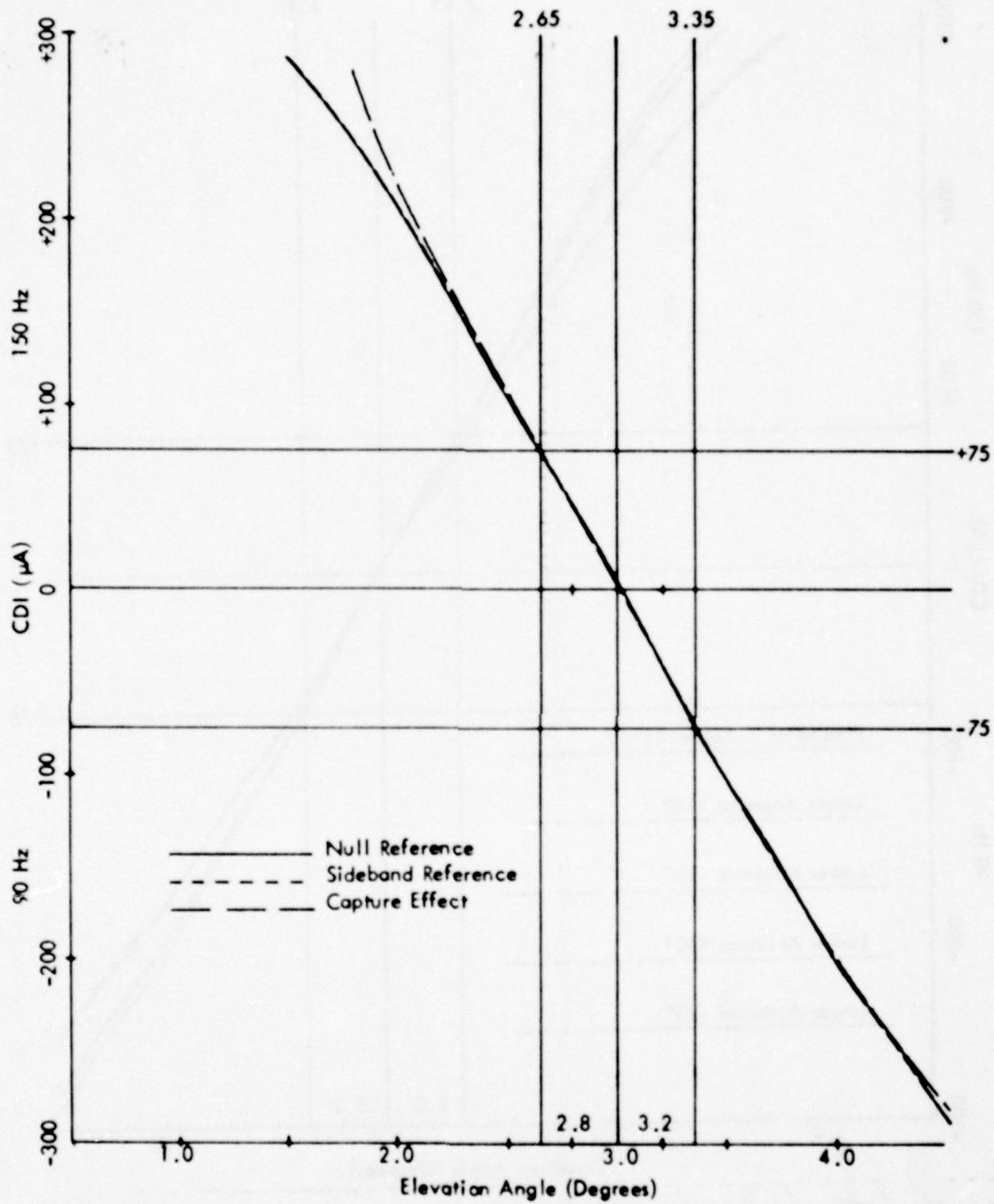
Figure 80b. Calculated Curves of CDI vs. Angle for the Three Image Type Glide-Slope Systems for Terrain Profile #13. The simulated aircraft is flying at a constant 1000 ft. altitude above the runway centerline (extended).
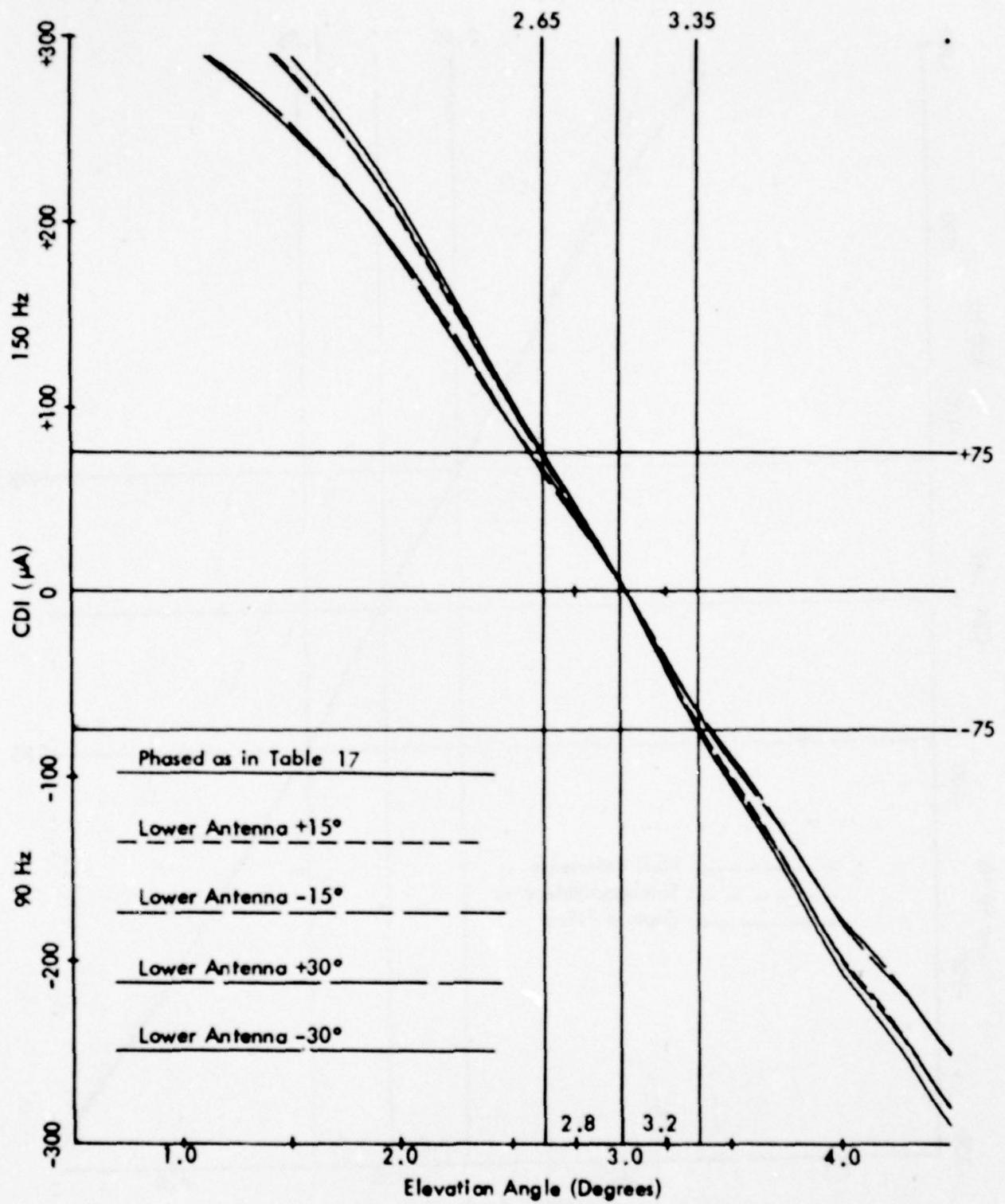
Figure 80c. Calculated Curves of CDI vs. Angle for the Null Reference Glide Slope with the Normal Phasing (as Indicated in Table 17) and Various Amounts of Dephasing for Terrain Profile #13. The simulated aircraft is flying at a constant 1000 ft. altitude above the runway centerline (extended).

-220-
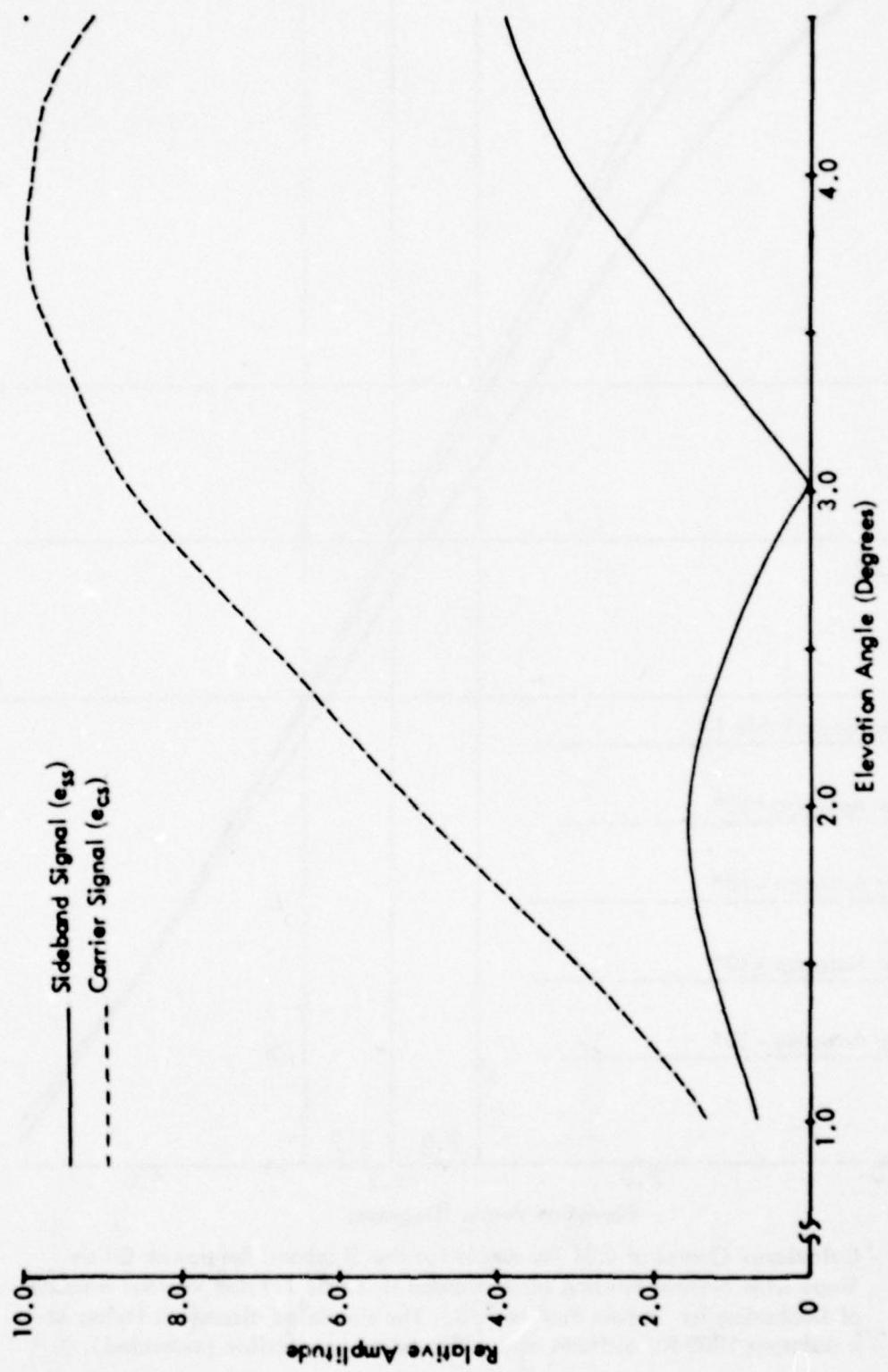
Figure 80d.   Calculated Curves of Carrier and Sideband Signals vs. Angle for the Null Reference Glide Slope for Terrain Profile #13.   The simulated aircraft is flying at a constant 1000 ft. altitude above the runway centerline (extended).

-221-
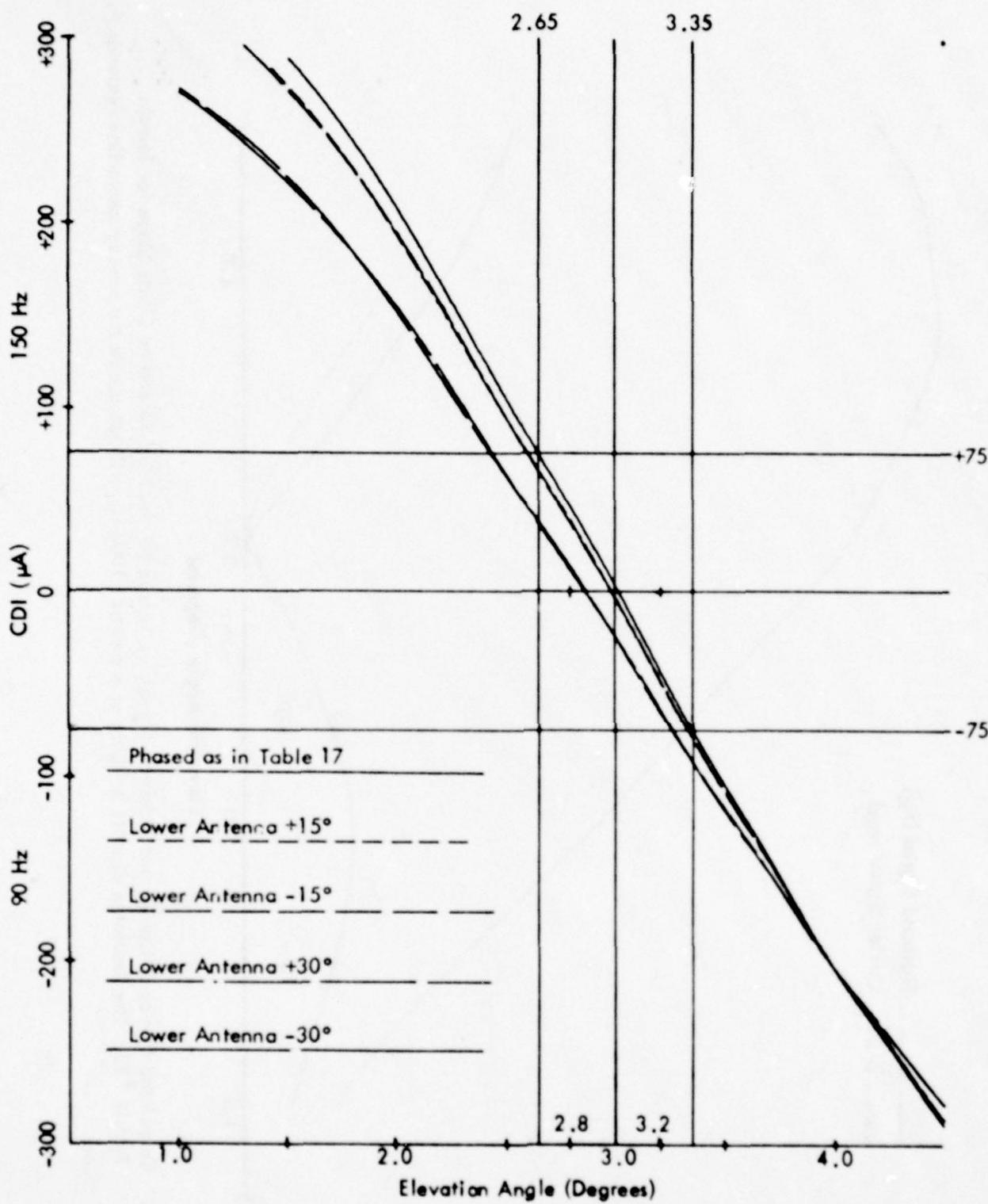
Figure 80e.   Calculated Curves of CDI vs. Angle for the Sideband Reference Glide
Slope with Normal Phasing (as Indicated in Table 17) and Various Amounts
of Dephasing for Terrain Profile #13.   The simulated aircraft is flying at
a constant 1000 ft. altitude above the runway centerline (extended).

-222-
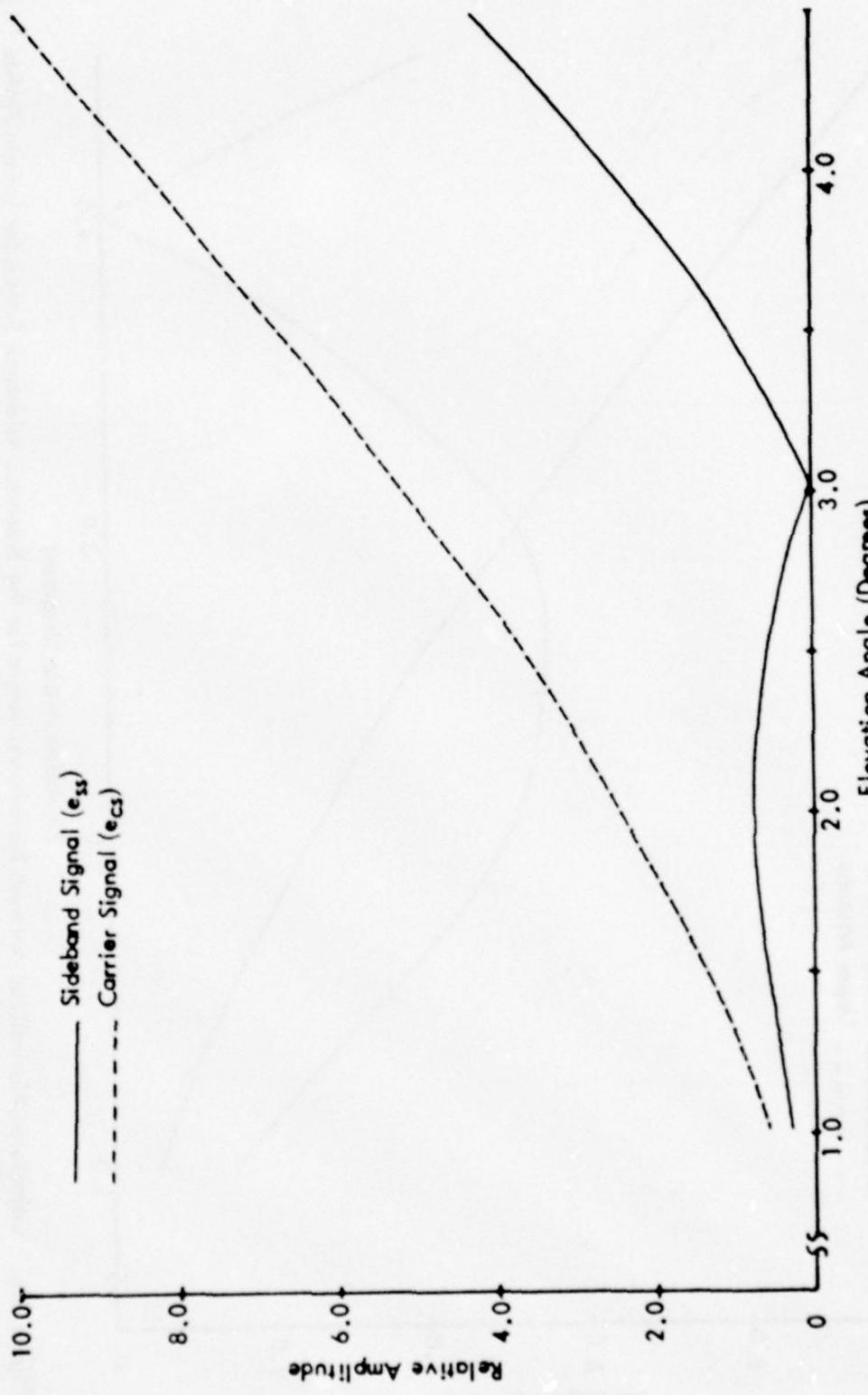
Figure 80f. Calculated Curves of Carrier and Composite Sideband Signals vs. Angle for the Sideband Reference Glide Slope for Terrain Profile #13. The simulated aircraft is flying at a constant 1000 ft. altitude above the runway centerline (extended).
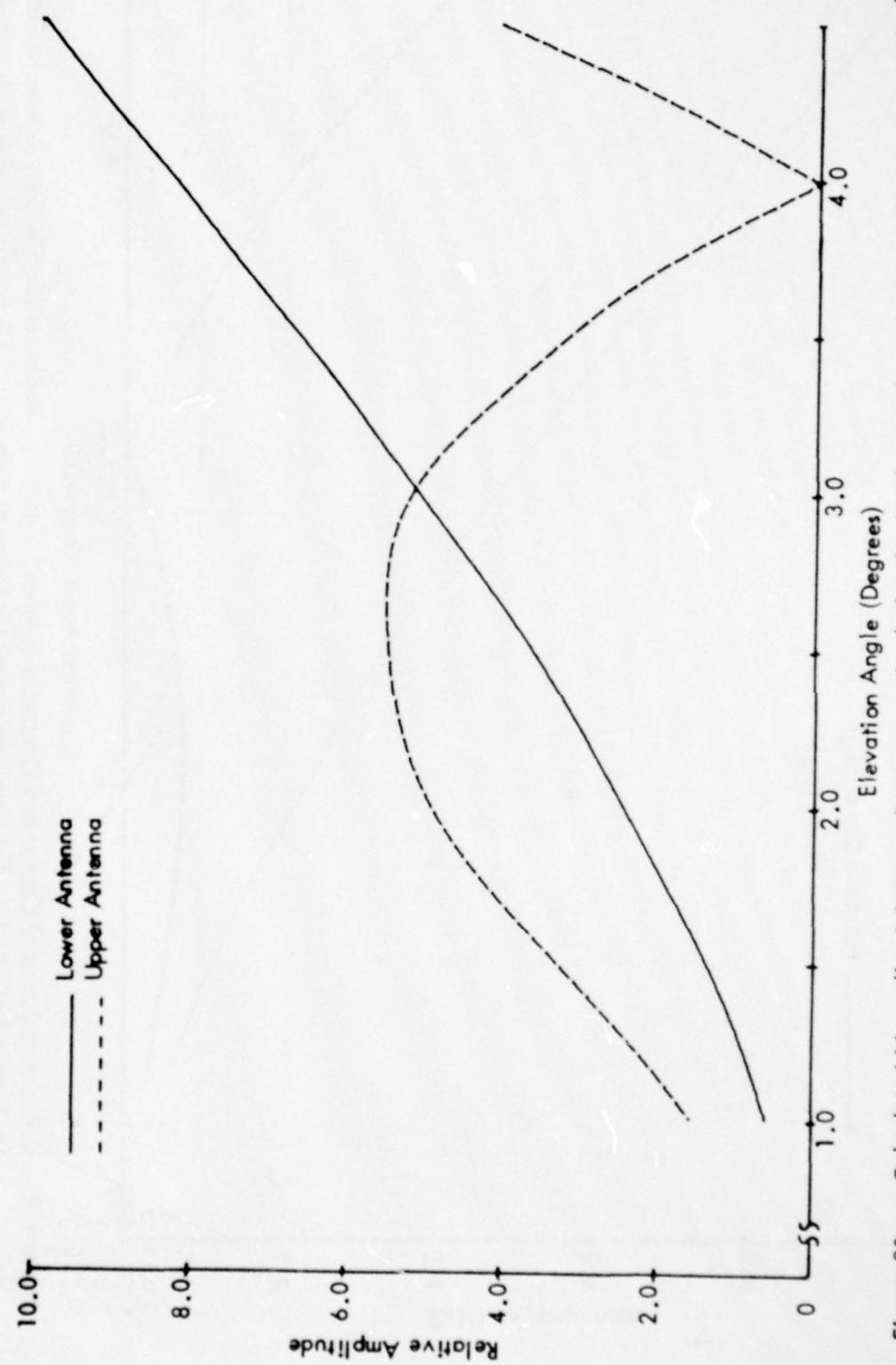
Figure 80g. Calculated Normalized Antenna Patterns vs. Angle for the Sideband Reference System for Terrain Profile #13. The simulated aircraft is flying at a constant 1000 ft. altitude above the runway centerline (extended).

-224-
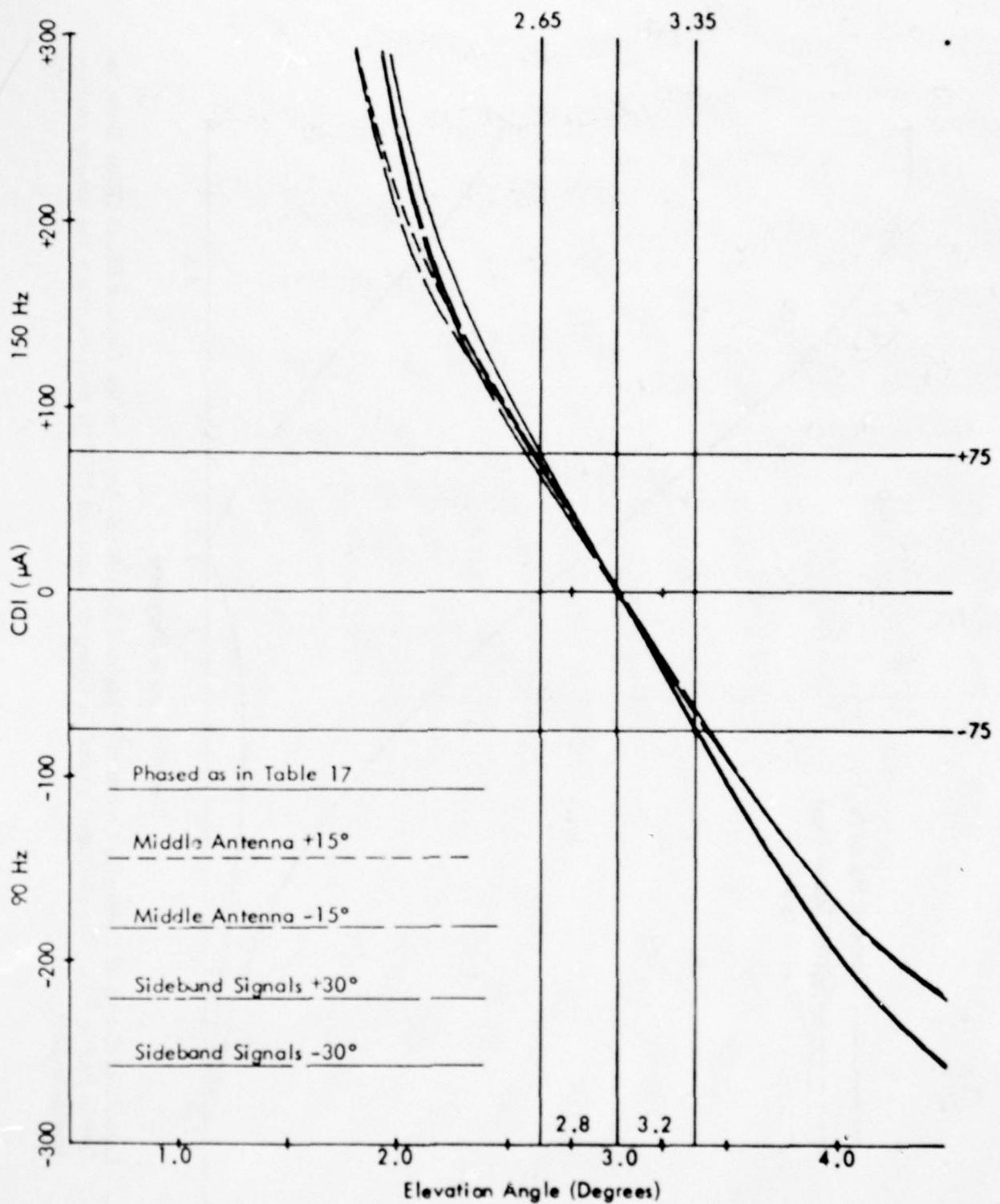
Figure 80h. Calculated Curves of CDI vs. Angle for the Capture Effect Glide Slope with the Normal Phasing (as Indicated in Table 17) and Dephased According to the Flight Inspection Manual Phase Verification Procedure for Terrain Profile #13. The simulated aircraft is flying at a constant 1000 ft. altitude above the runway centerline (extended).

-225-
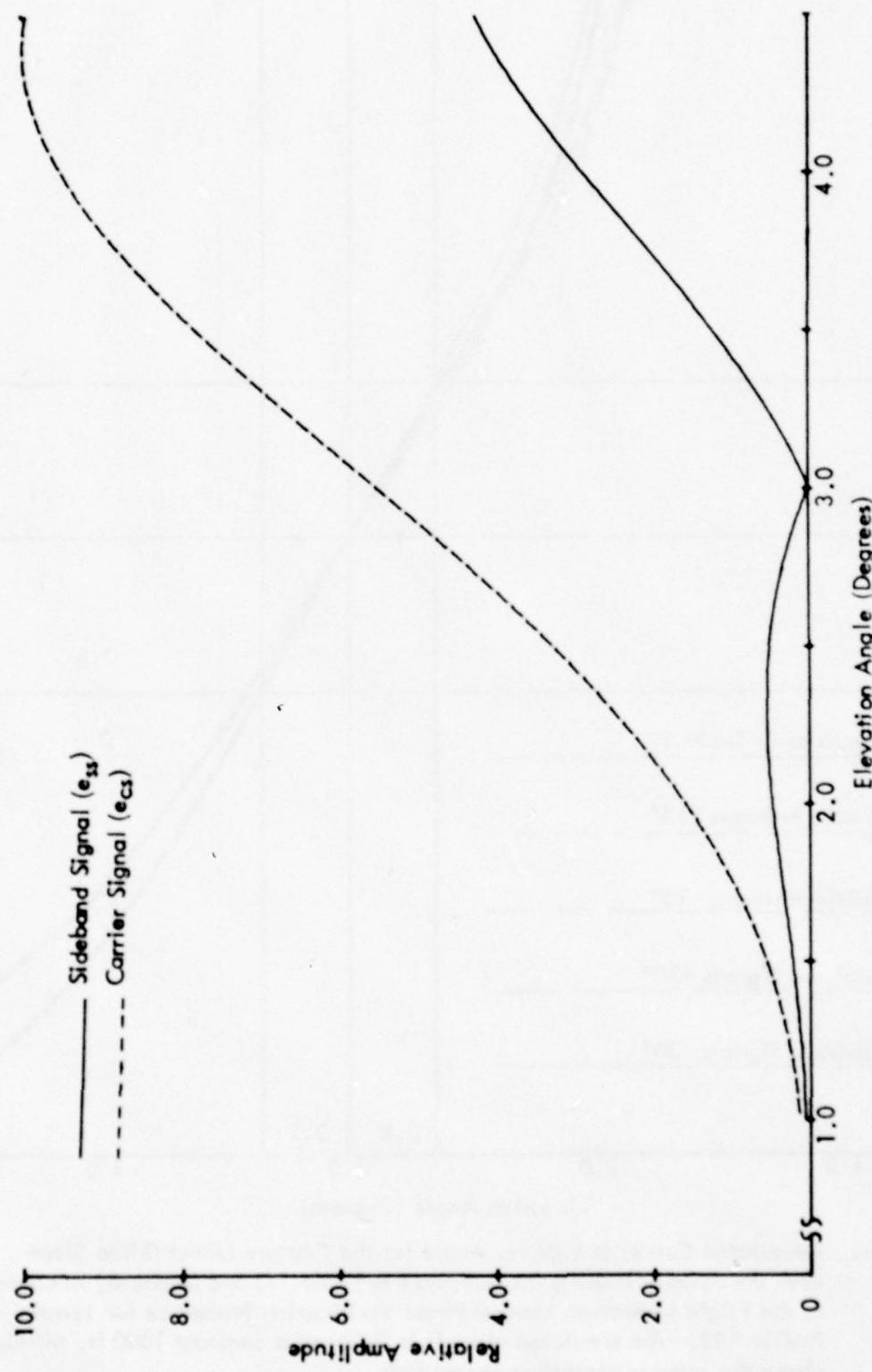
Figure 80i. Calculated Curves of Composite Carrier and Sideband Signals vs. Angle for the Capture Effect Glide Slope for Terrain Profile #13. The simulated aircraft is flying at a constant 1000 ft. altitude above the runway center-line(extended).
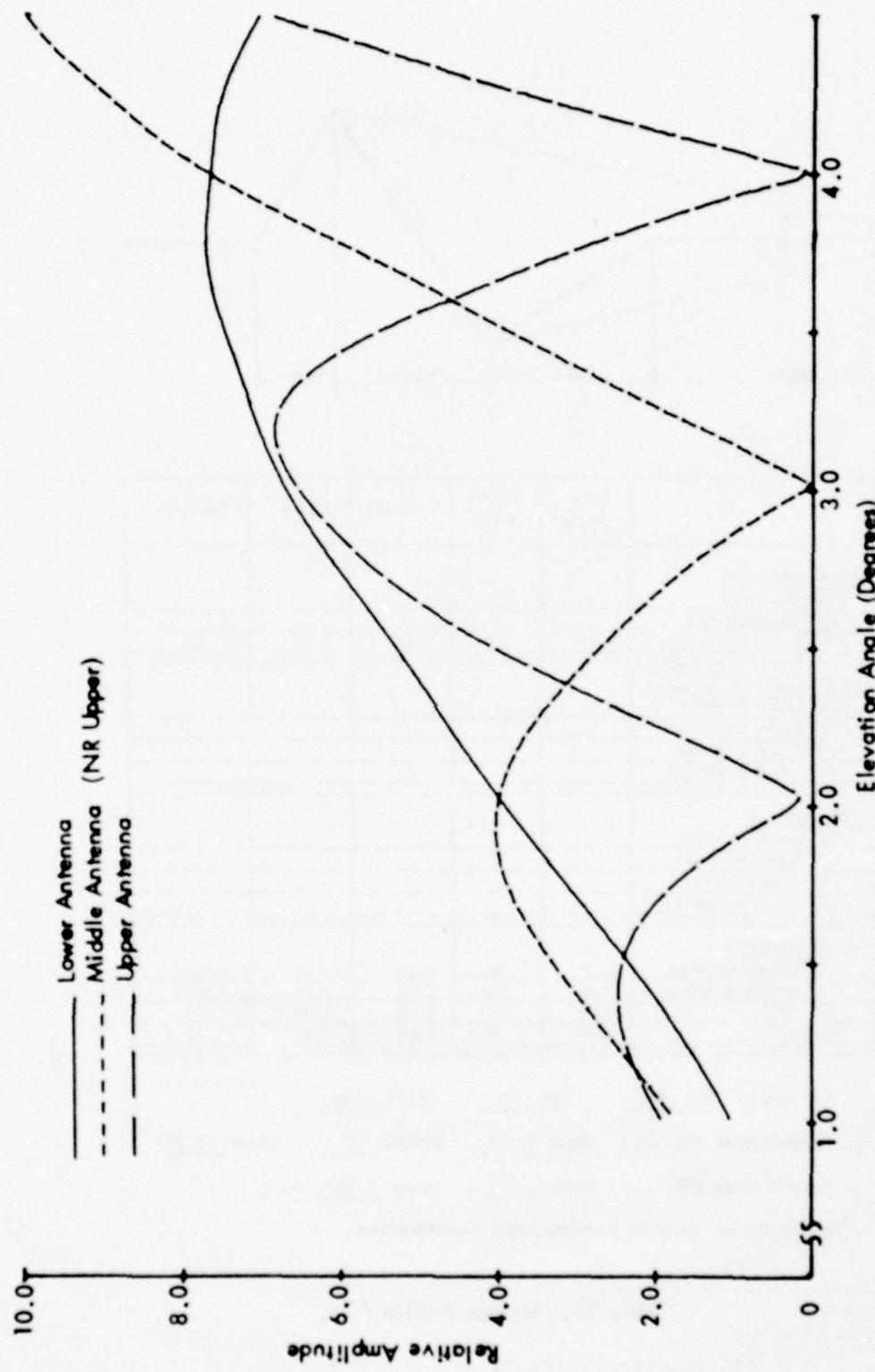
Figure 80j. Calculated Normalized Antenna Patterns vs. Angle for the Capture Effect and Null Reference Systems for Terrain Profile #13. The simulated aircraft is flying at a constant 1000 ft. altitude above the runway centerline (extended).
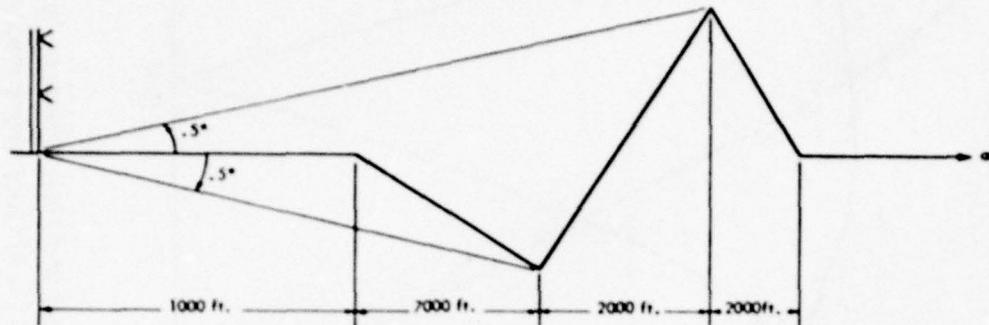
	Path Angle	Width Angle	+75 µA	-75 µA	Symmetry
Normal Phasing					
Null Reference					
Sideband Reference					
CEGS	2.99	.70	2.64	3.34	.50
Null Reference Dephased					
+15° Lower Antenna					
-15° Lower Antenna					
+30° Lower Antenna					
-30° Lower Antenna					
SBR Dephased					
+15° Lower Antenna					
-15° Lower Antenna					
+30° Lower Antenna					
-30° Lower Antenna					
CEGS Dephased					
+15° Middle Antenna	3.00	.86	2.55	3.40	.47
-15° Middle Antenna	2.98	.73	2.63	3.37	.53
+30° SBO	2.96	.87	2.53	3.40	.51
-30° SBO	3.02	.79	2.63	3.42	.51

"A" Ratio: NR .510   SBR .369   CEGS .320

Relative Phase NR/CEGS   Upper +3.3°   Middle 0°   Lower -2.2°

Relative Phase SBR   Upper 0°   Lower 3.88°

*NR and SBR Too Rough for Accurate Angle Determinations.

Table 18. Terrain Profile #14.

-228-
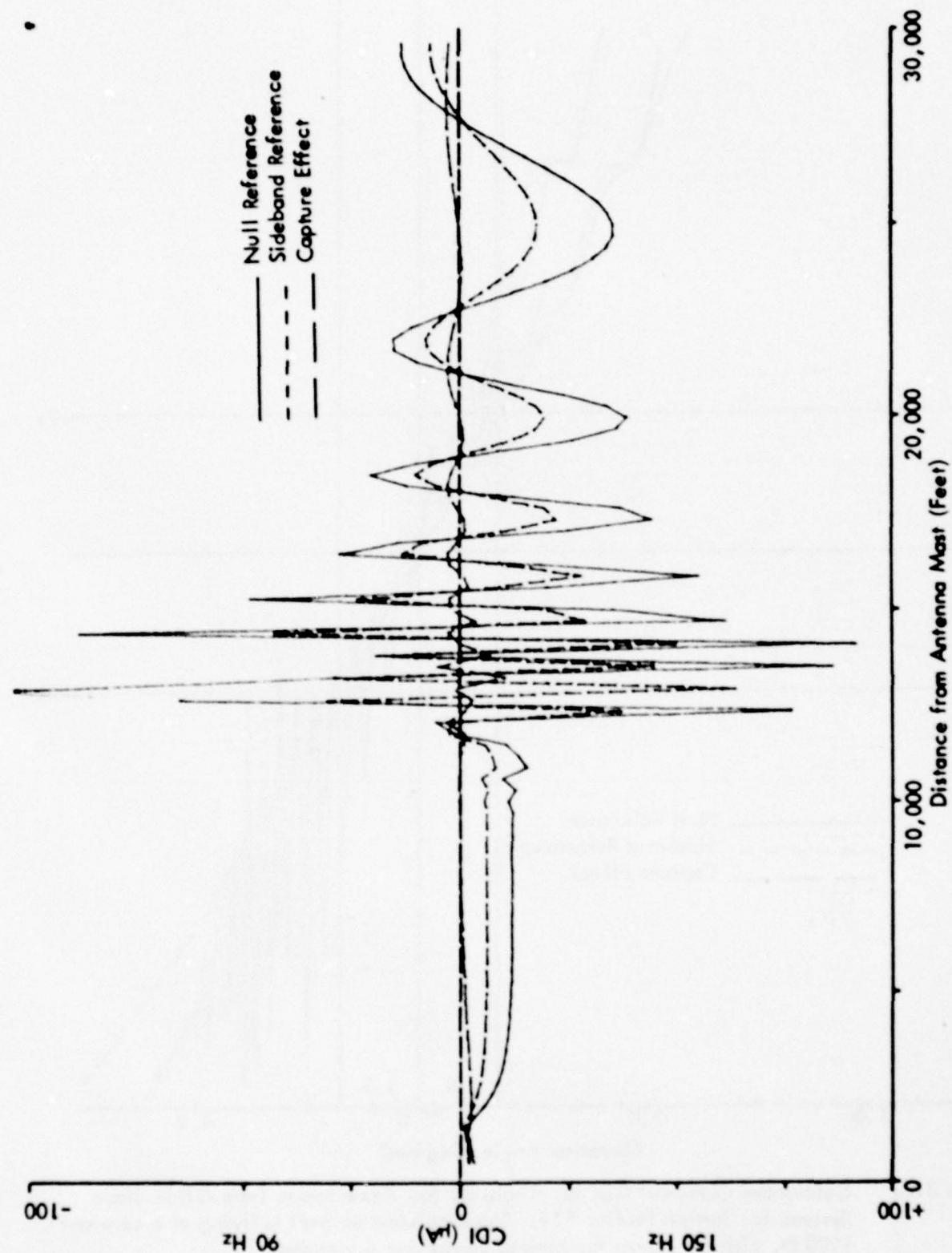
Figure 81a. Calculated Curves of CDI vs. Distance for the Three Image Type Glide Slope Systems for Terrain Profile #14. The simulated aircraft is flying a constant 3.0 degree low approach over the runway centerline (extended).
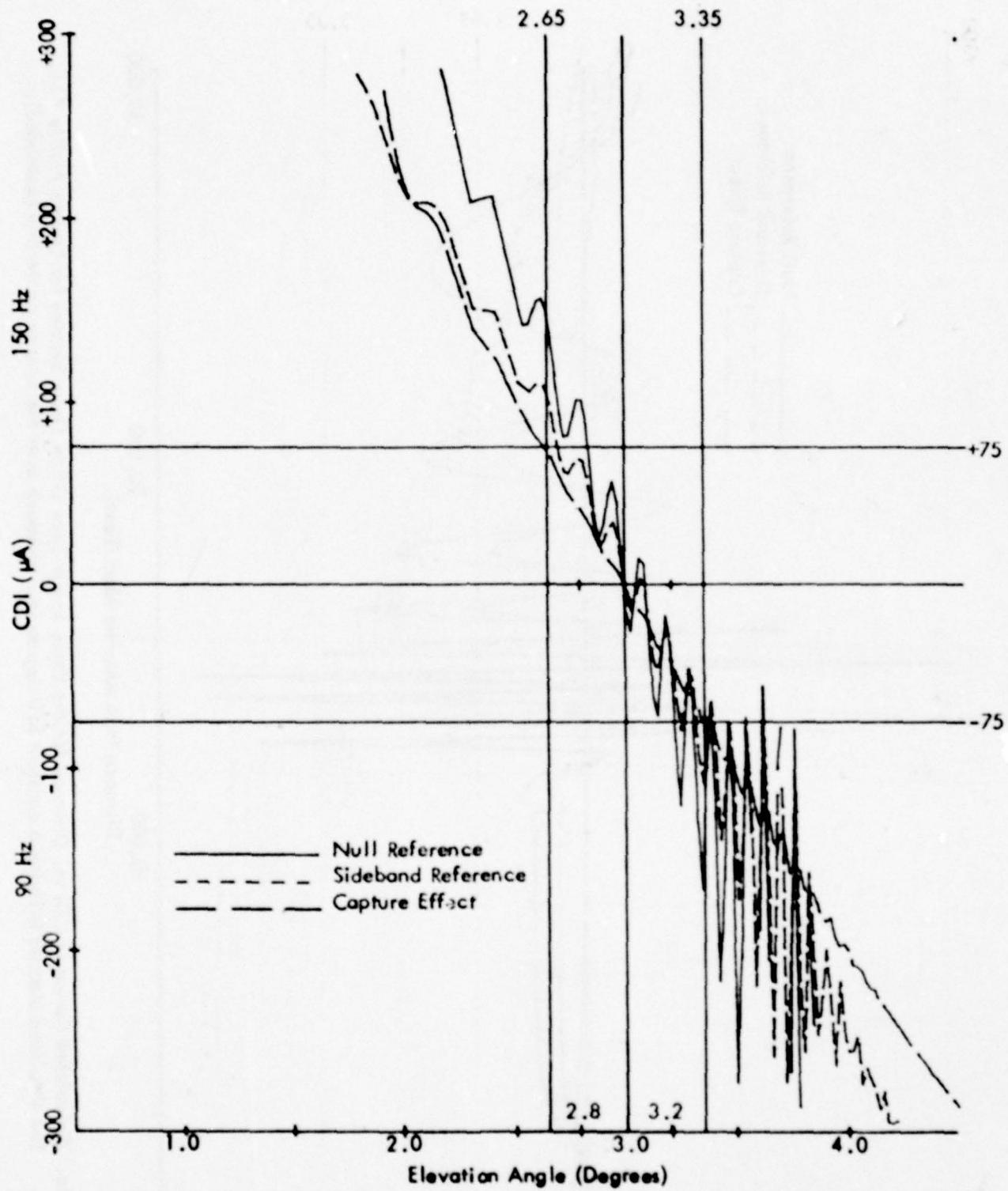
Figure 81b. Calculated Curves of CDI vs. Angle for the Three Image Type Glide-Slope Systems for Terrain Profile #14. The simulated aircraft is flying at a constant 1000 ft. altitude above the runway centerline (extended).
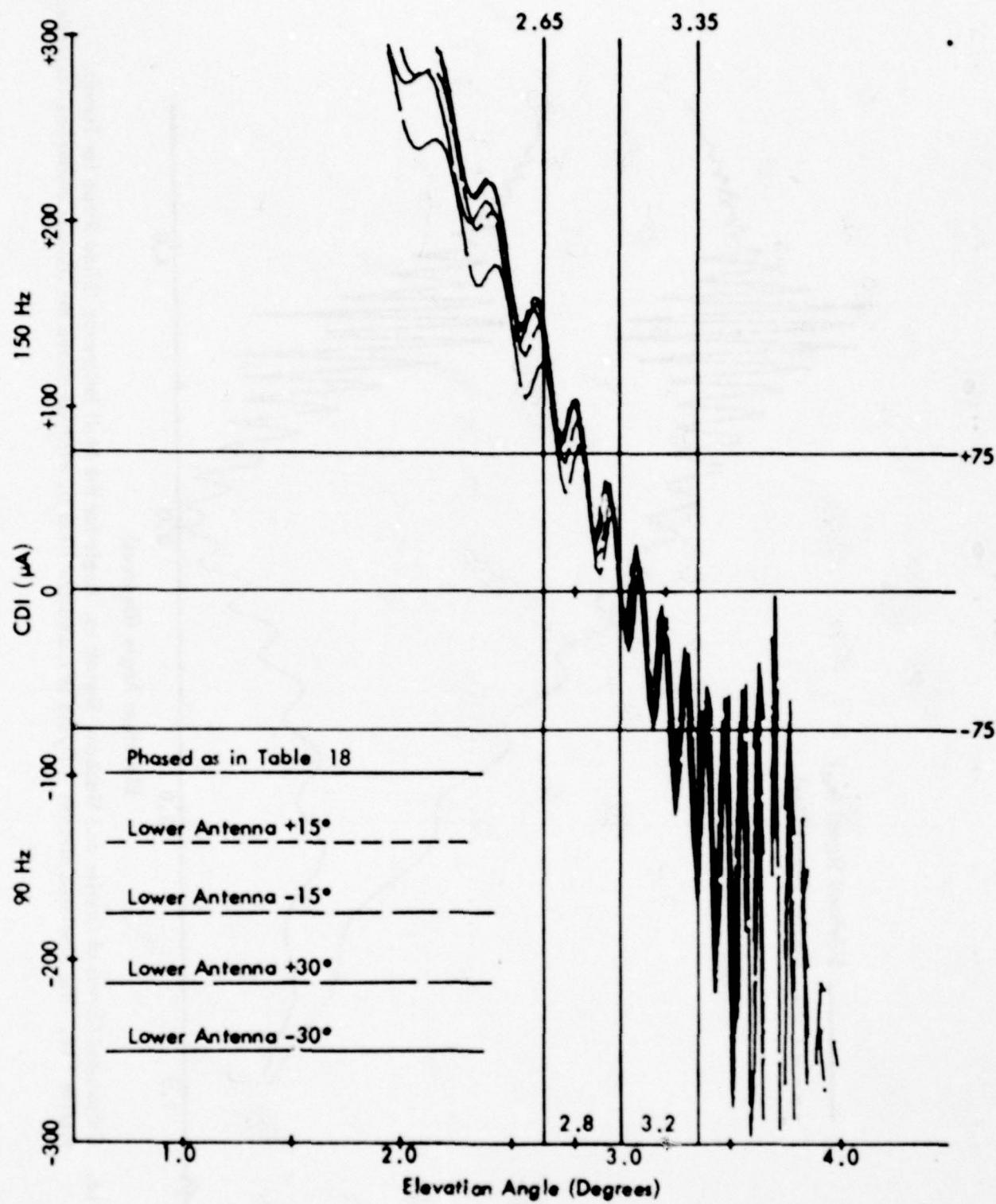
Figure 81c. Calculated Curves of CDI vs. Angle for the Null Reference Glide Slope with the Normal Phasing (as Indicated in Table 18) and Various Amounts of Dephasing for Terrain Profile #14. The simulated aircraft is flying at a constant 1000 ft. altitude above the runway centerline (extended).
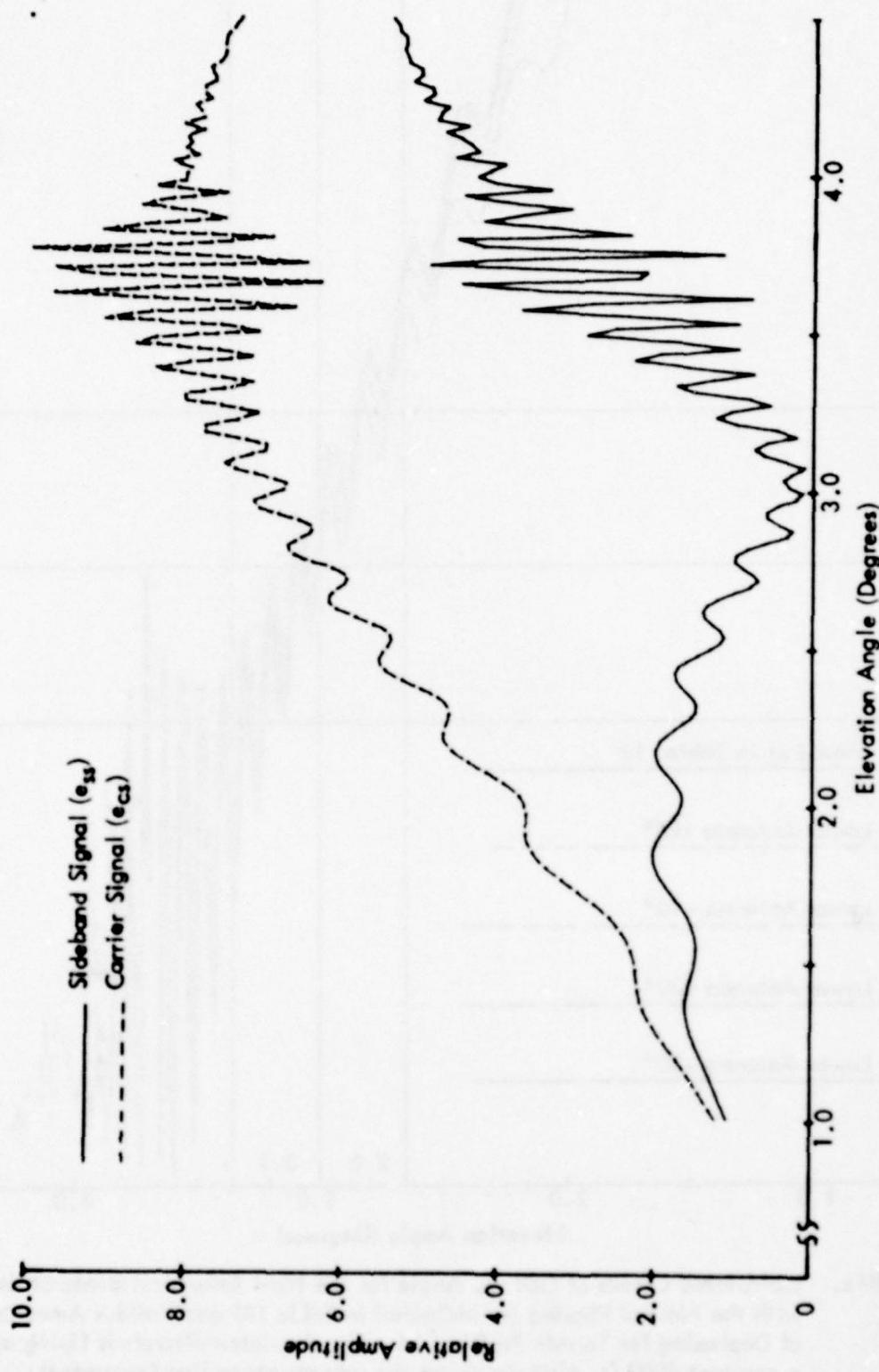
Figure 81d. Calculated Curves of Carrier and Sideband Signals vs. Angle for the Null Reference Glide Slope for Terrain Profile #14. The simulated aircraft is flying at a constant 1000 ft. altitude above the runway centerline (extended).

-232-
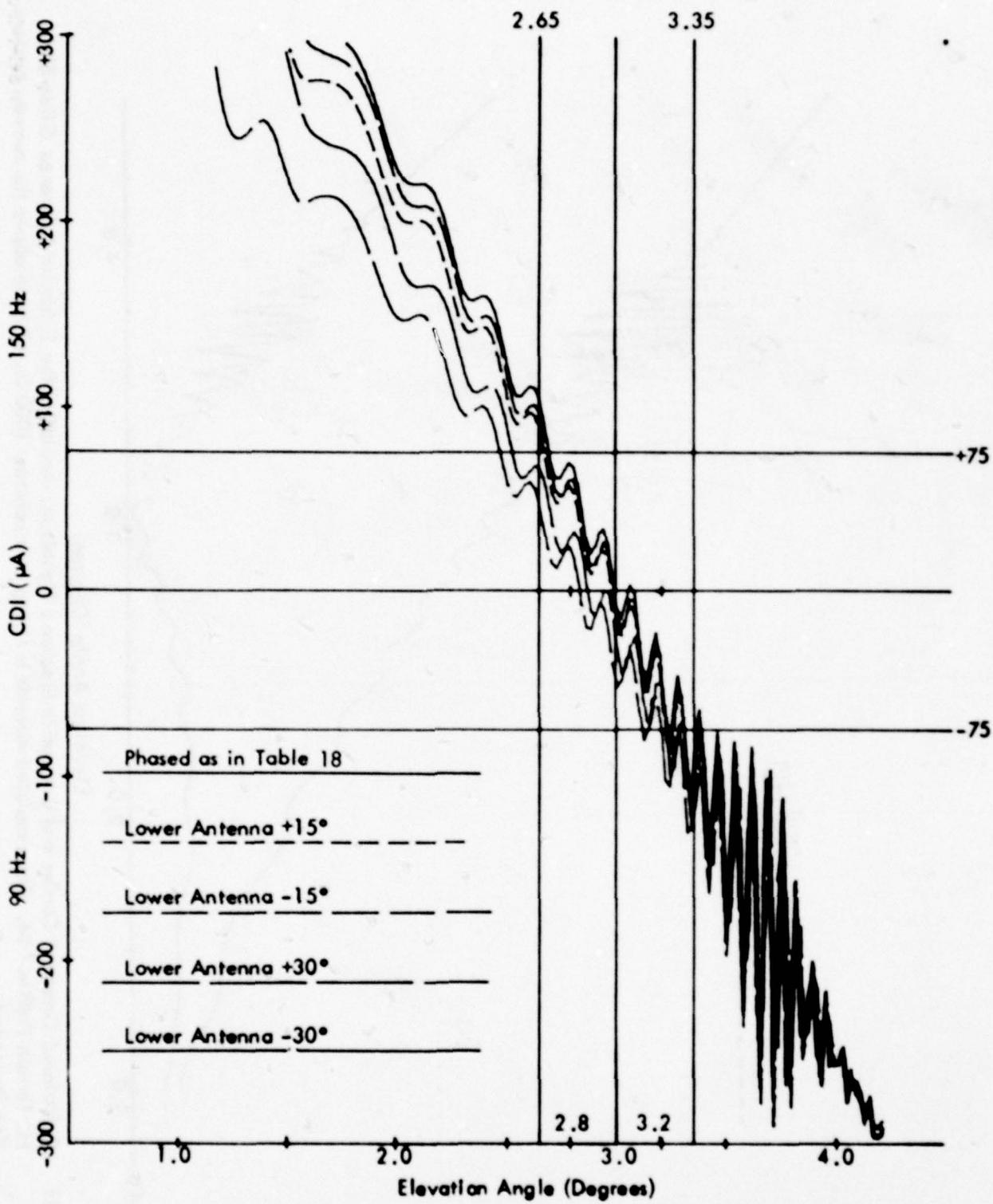
Figure 81e. Calculated Curves of CDI vs. Angle for the Sideband Reference Glide Slope with Normal Phasing (as Indicated in Table 18) and Various Amounts of Dephasing for Terrain Profile #14. The simulated aircraft is flying at a constant 1000 ft. altitude above the runway centerline (extended).
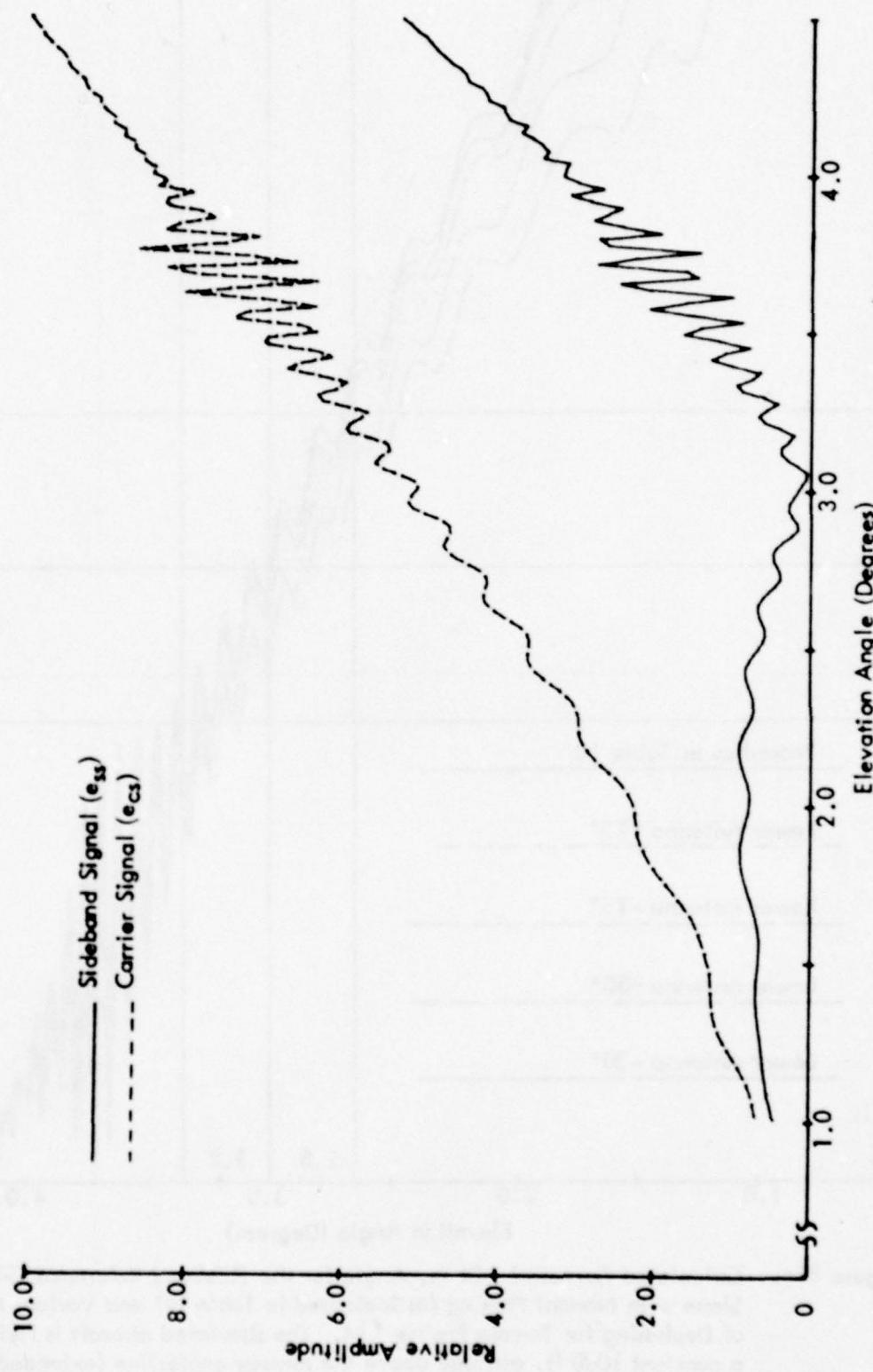
Figure 81f. Calculated Curves of Carrier and Composite Sideband Signals vs. Angle for the Sideband Reference Glide Slope for Terrain Profile #14. The simulated aircraft is flying at a constant 1000 ft. altitude above the runway center-line (extended).
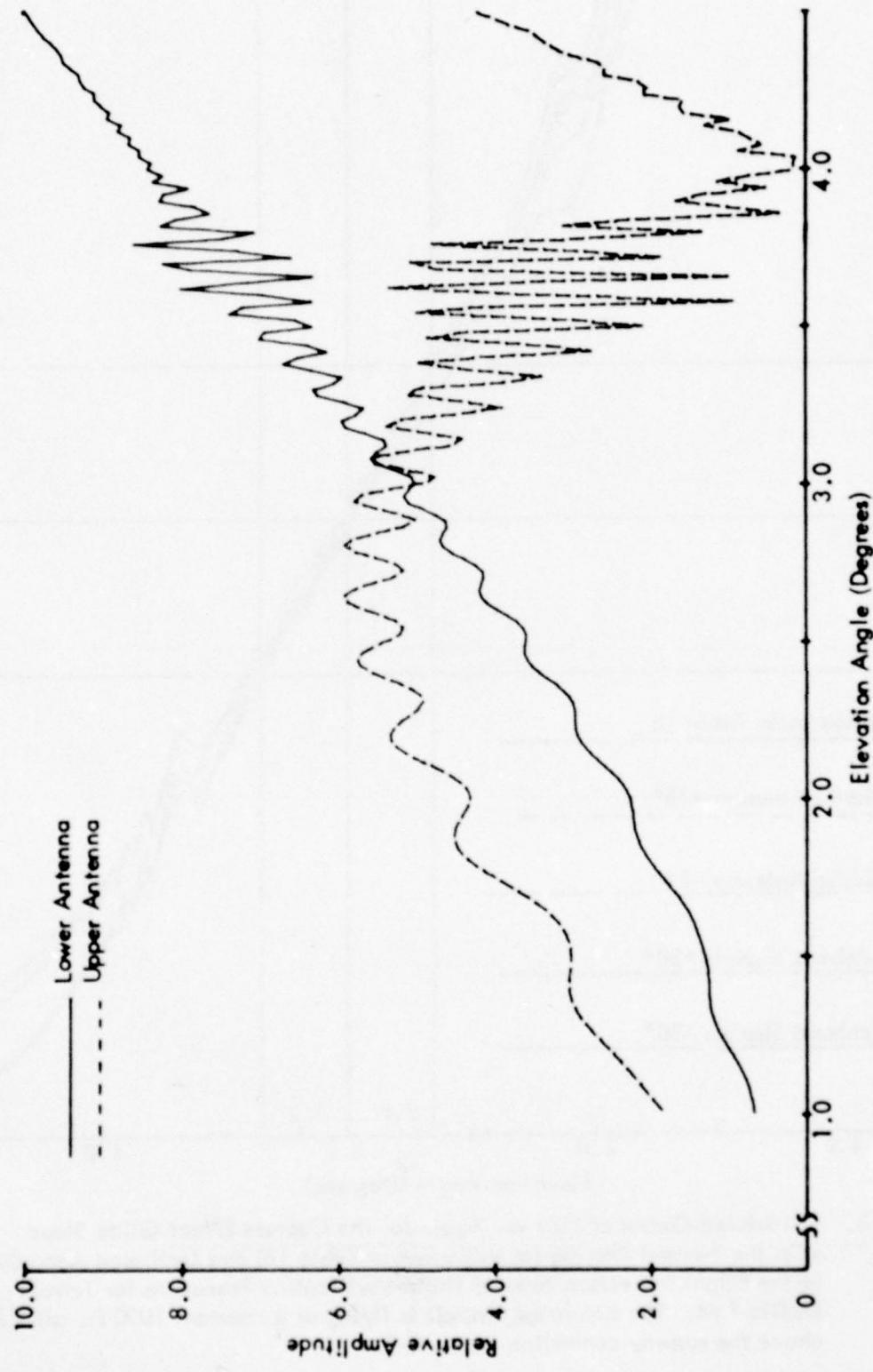
Figure 81g.   Calculated Normalized Antenna Patterns vs. Angle for the Sideband Reference System for Terrain Profile $\#14$.   The simulated aircraft is flying at a constant 1000 ft. altitude above the runway centerline (extended).

-235-
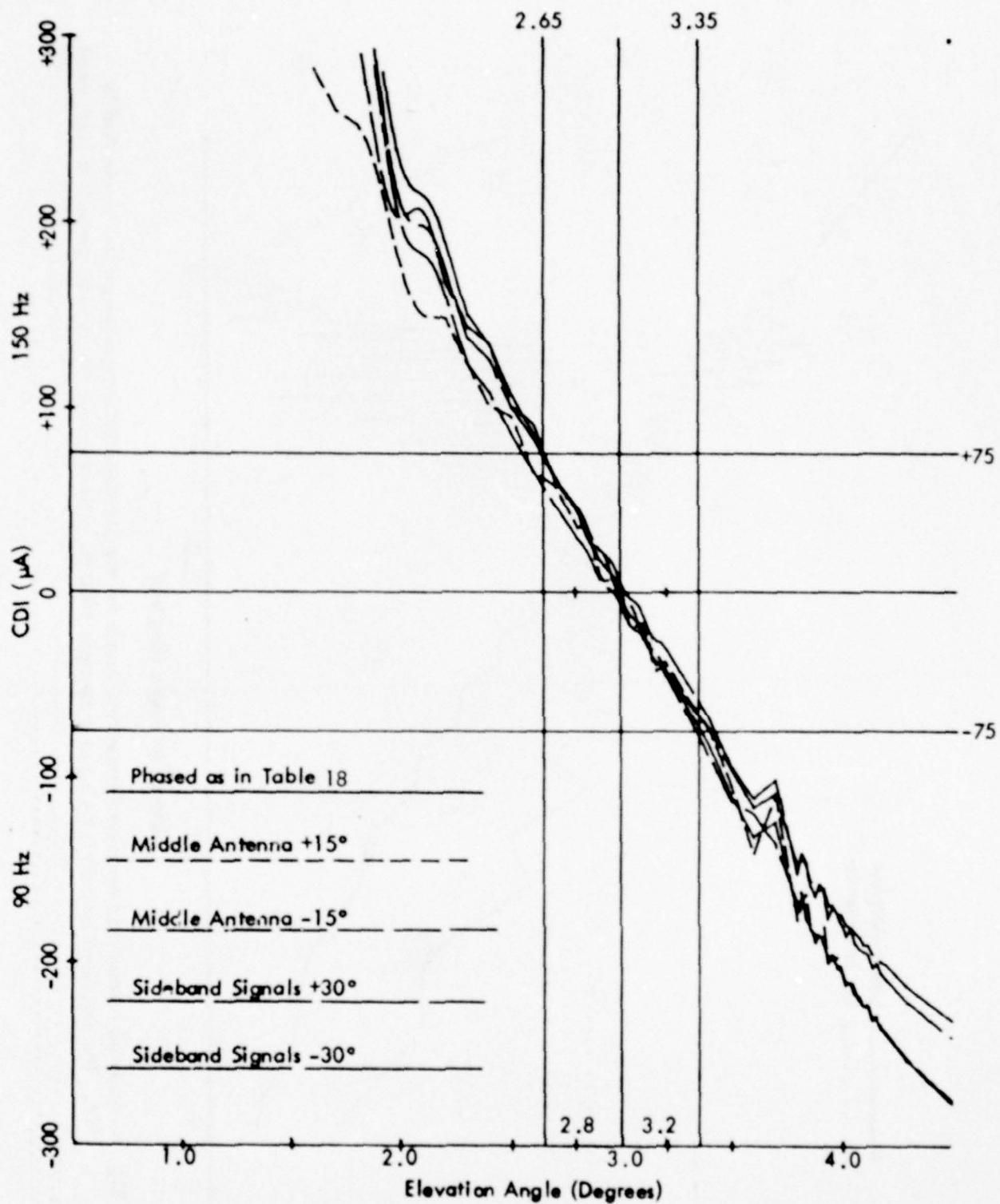
Figure 81h. Calculated Curves of CDI vs. Angle for the Capture Effect Glide Slope with the Normal Phasing (as indicated in Table 18) and Dephased According to the Flight Inspection Manual Phase Verification Procedure for Terrain Profile #14. The simulated aircraft is flying at a constant 1000 ft. altitude above the runway centerline (extended).
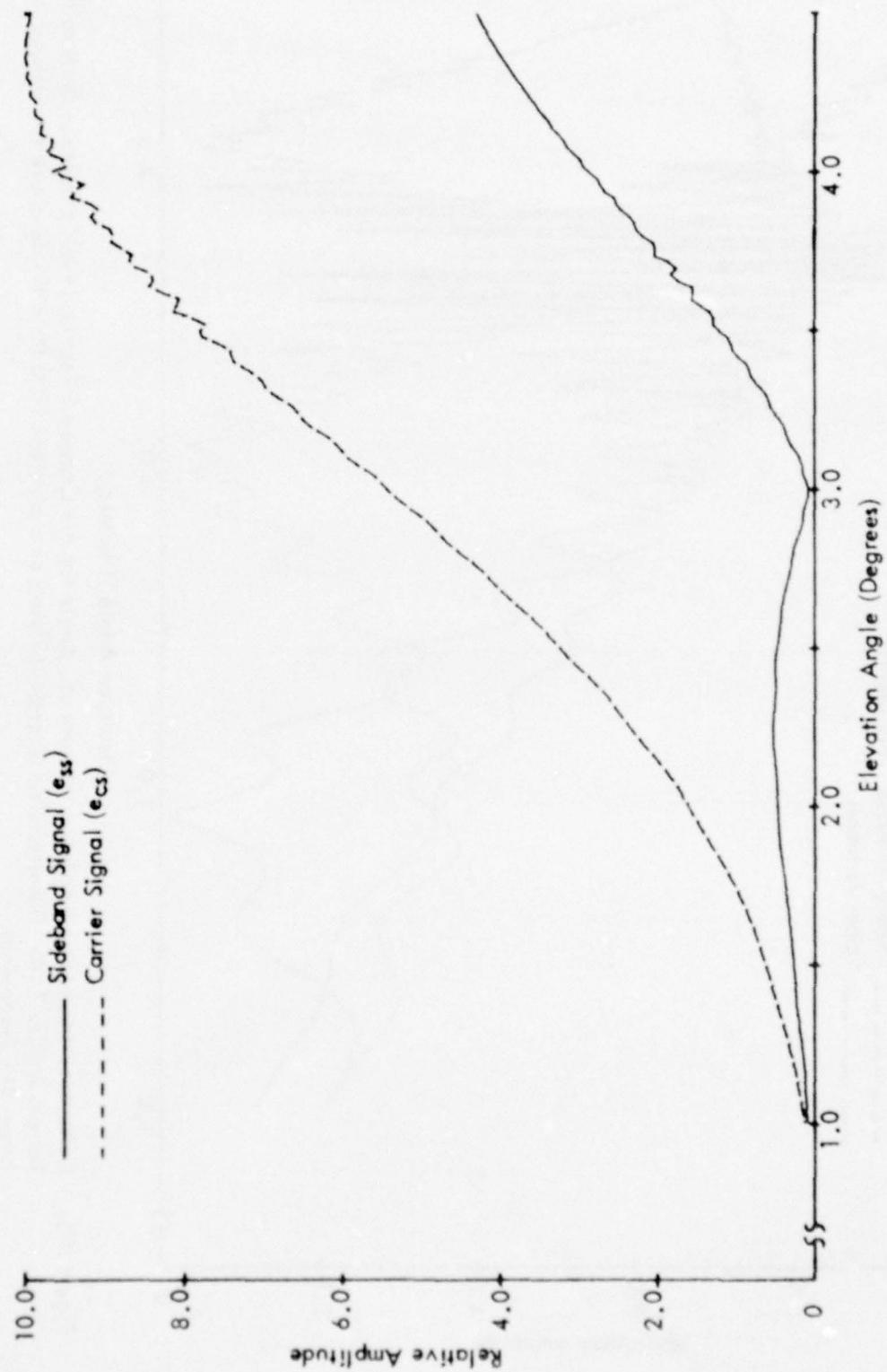
Figure 81i. Calculated Curves of Composite Carrier and Sideband Signals vs. Angle for the Capture Effect Glide Slope for Terrain Profile #14. The simulated aircraft is flying at a constant 1000 ft. altitude above the runway center-line (extended).

-237-
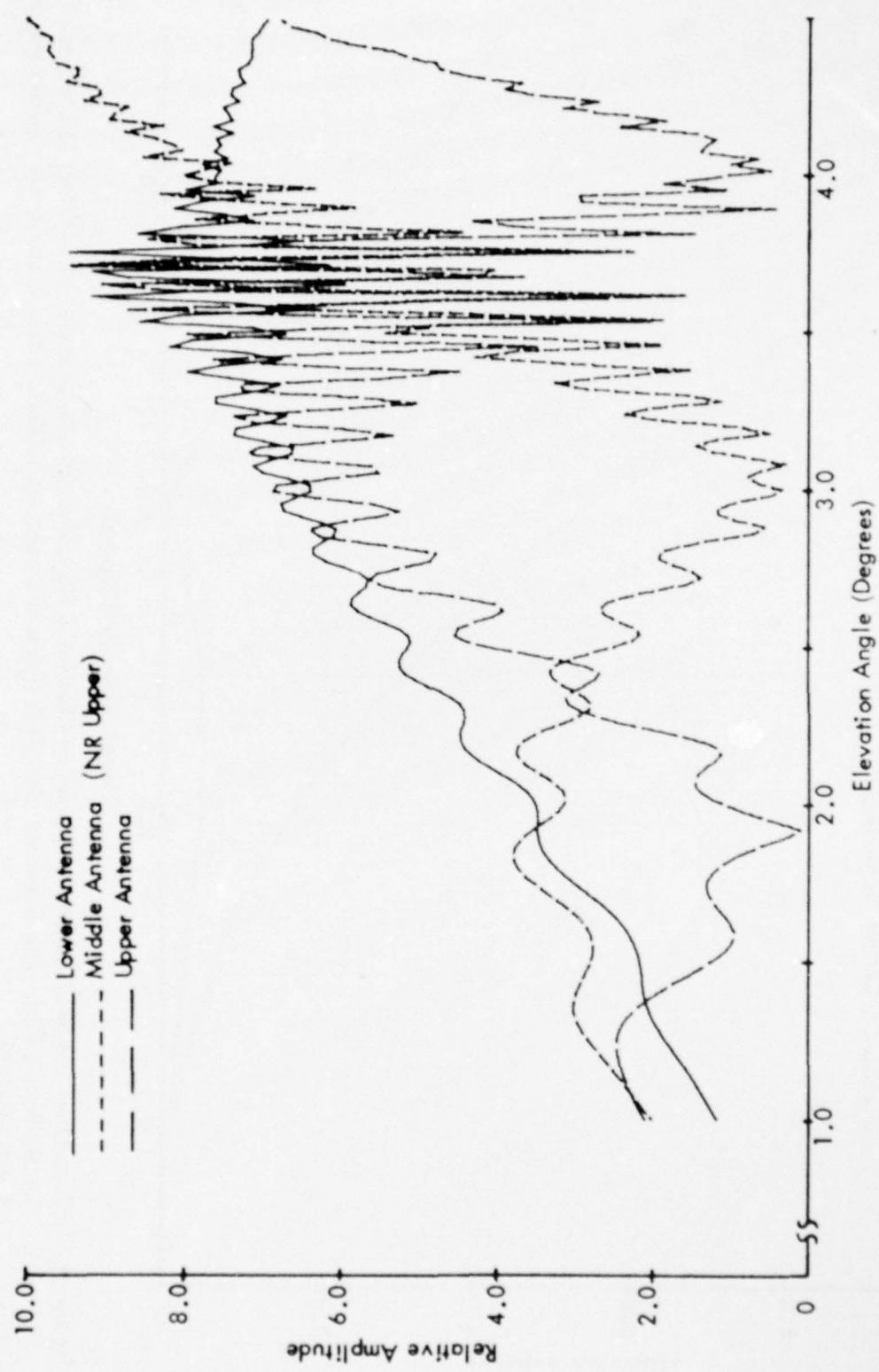
Figure 81j. Calculated Normalized Antenna Patterns vs. Angle for the Capture Effect and Null Reference Systems for Terrain Profile #14. The simulated aircraft is flying at a constant 1000 ft. altitude above the runway centerline (extended).

-238-
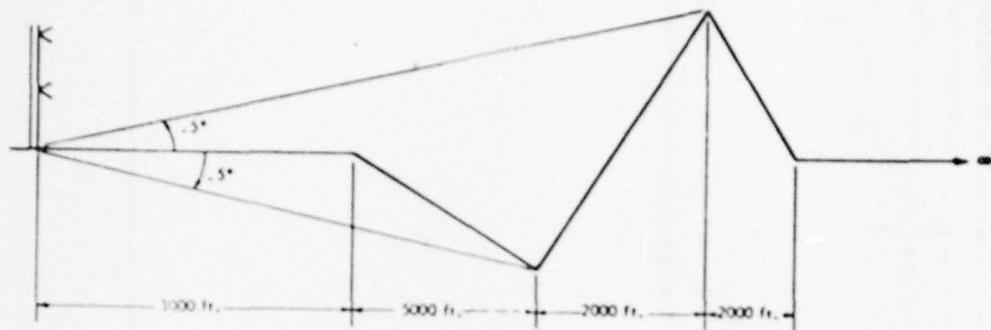
	Path Angle	Width Angle	+ 75 μA	- 75 μA	Symmetry
Normal Phasing					
Null Reference	2.99	.70	2.70	3.39	.57
Sideband Reference	2.99	.70	2.68	3.39	.56
CEGS	3.00	.70	2.65	3.35	.50
Null Reference Dephased					
+15° Lower Antenna					
−15° Lower Antenna					
+30° Lower Antenna					
−30° Lower Antenna					
SBR Dephased					
+15° Lower Antenna	2.97	.66	2.64	3.30	.51
−15° Lower Antenna	2.99	.70	2.68	3.38	.56
+30° Lower Antenna	2.82	.76	2.44	3.20	.50
−30° Lower Antenna	2.87	.78	2.52	3.30	.55
CEGS Dephased					
+15° Middle Antenna	3.01	.74	2.64	3.38	.50
−15° Middle Antenna	2.99	.71	2.64	3.35	.50
+30° SBO	3.02	.77	2.65	3.43	.52
−30° SBO	2.98	.83	2.57	3.40	.51

"A" Ratio: NR .376   SBR .339   CEGS .310

Relative Phase NR/CEGS   Upper −3.2°   Middle 0°   Lower 2.4°

Relative Phase SBR   Upper 0°   Lower +4.4°

*NR Too Rough for Accurate Angle Determinations.

Table 19. Terrain Profile #15.
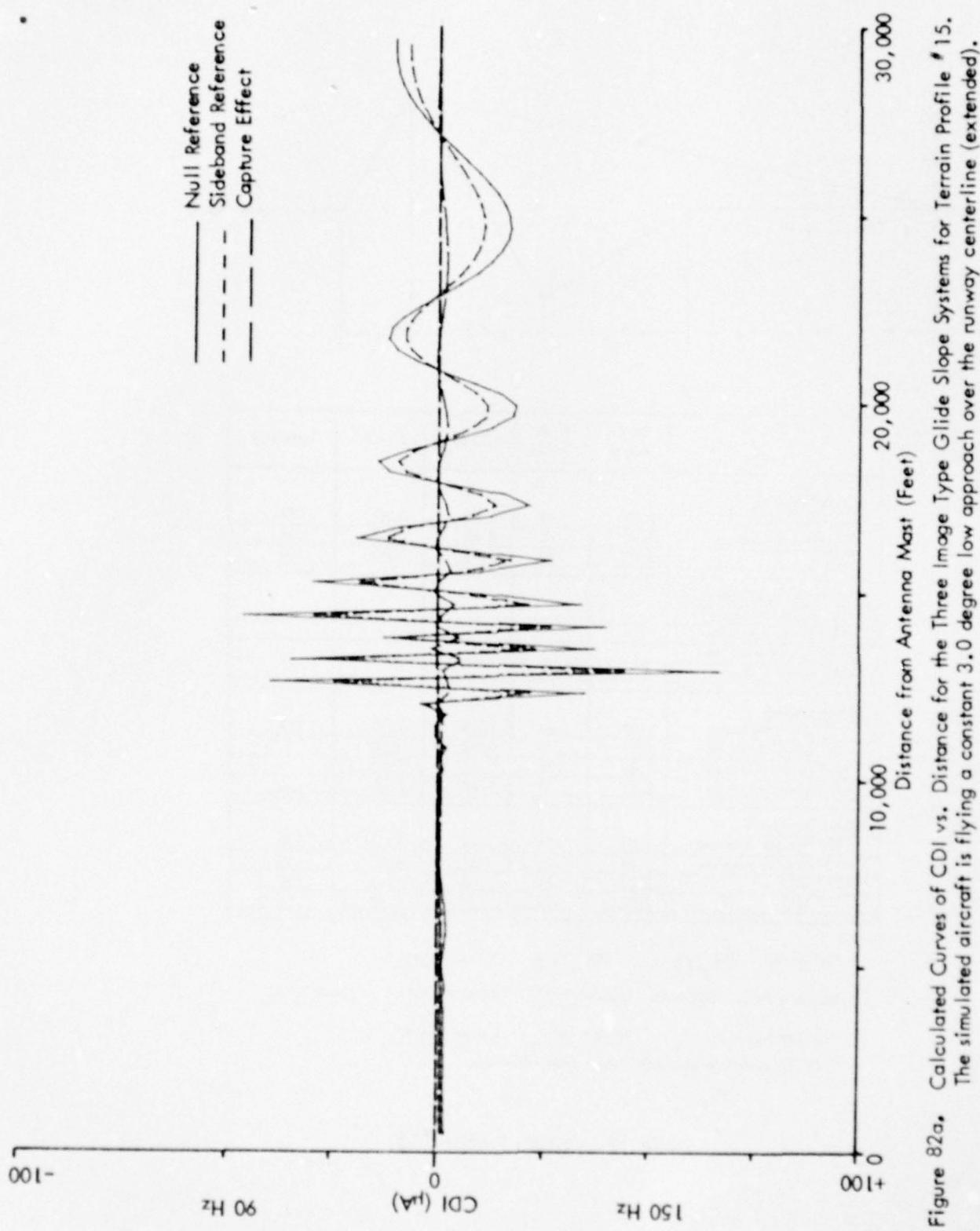
Figure 82a. Calculated Curves of CDI vs. Distance for the Three Image Type Glide Slope Systems for Terrain Profile #15. The simulated aircraft is flying a constant 3.0 degree low approach over the runway centerline (extended).

-240-
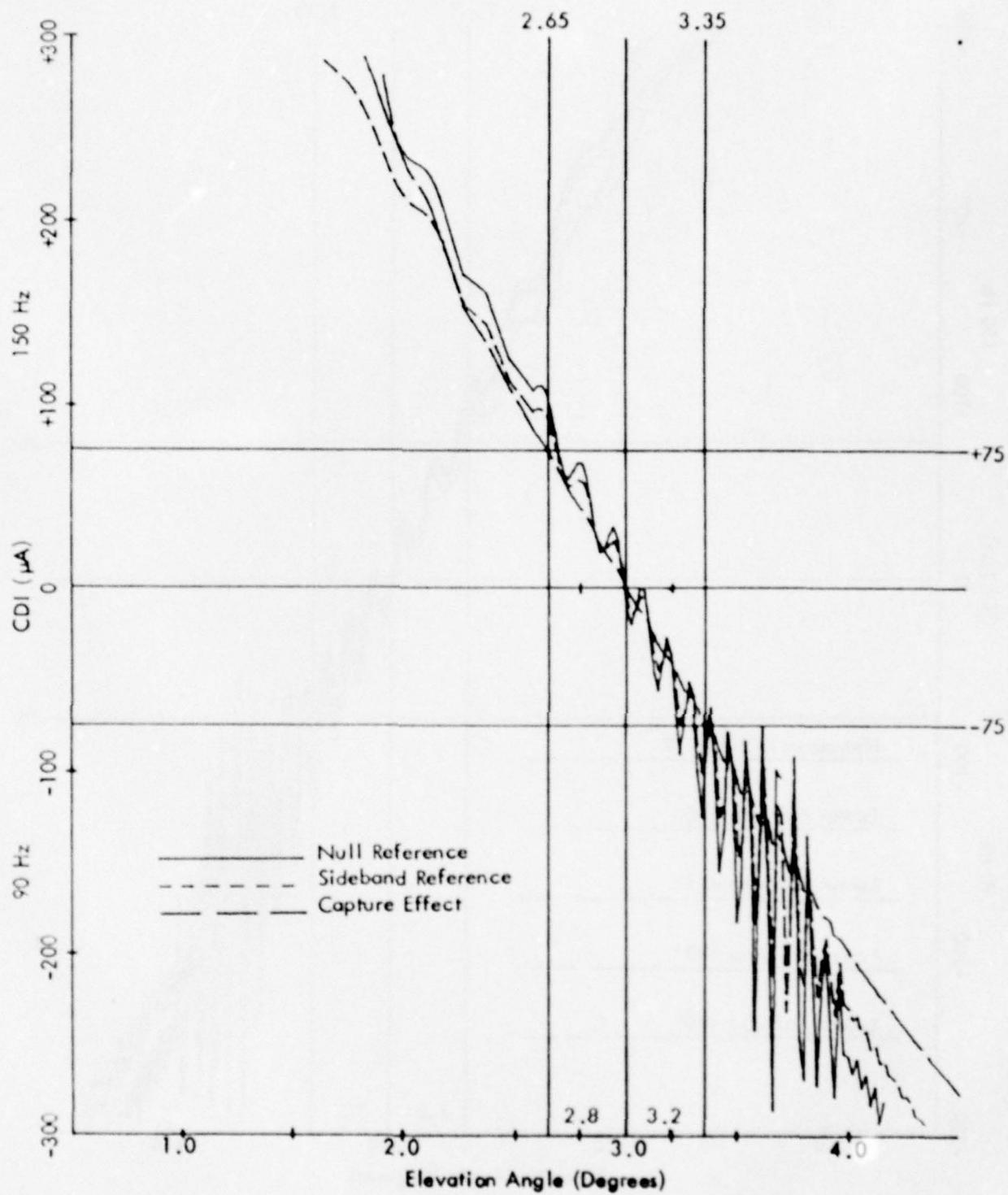
Figure 82b. Calculated Curves of CDI vs. Angle for the Three Image Type Glide-Slope Systems for Terrain Profile #15. The simulated aircraft is flying at a constant 1000 ft. altitude above the runway centerline (extended).

-241-
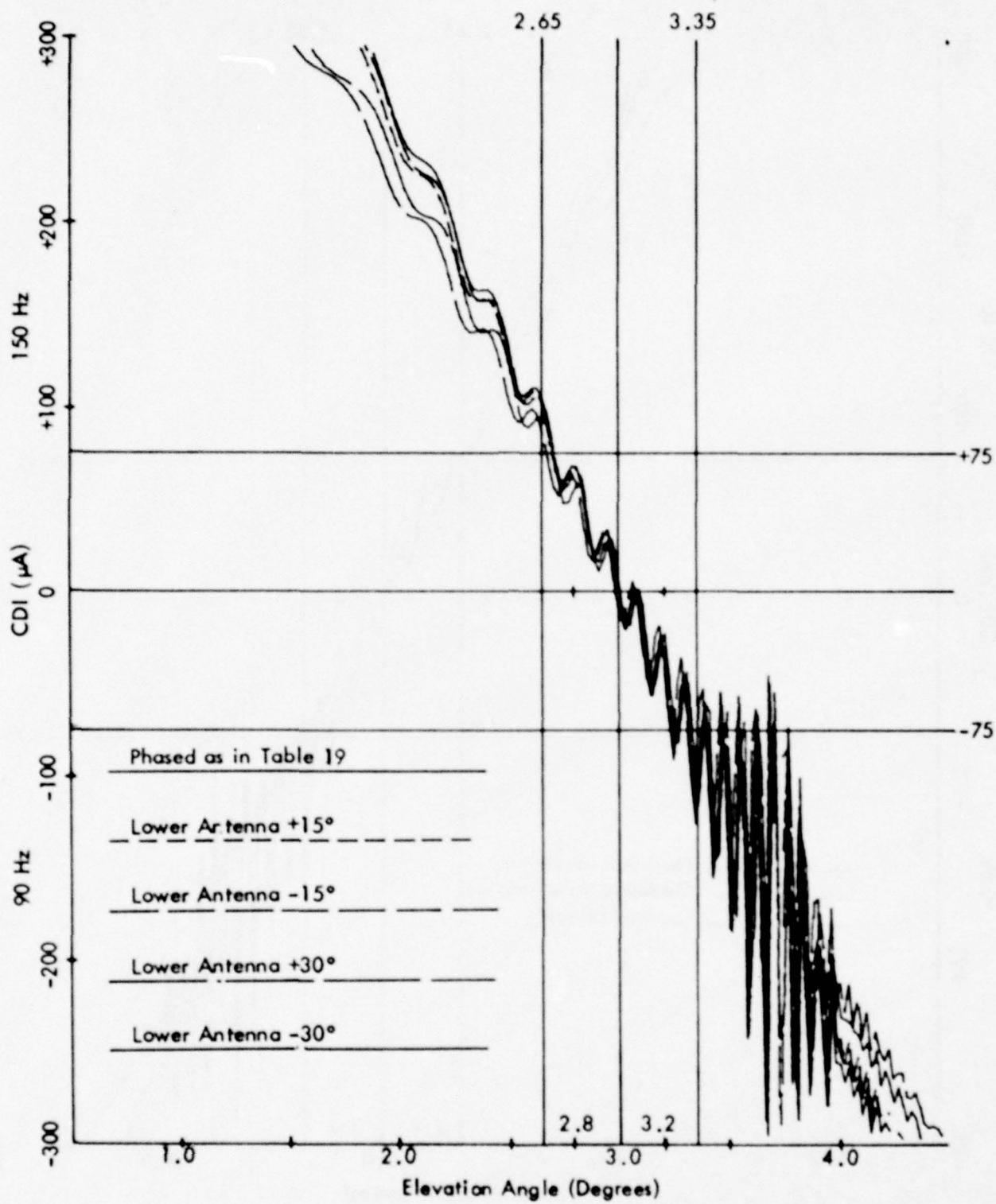
Figure 82c. Calculated Curves of CDI vs. Angle for the Null Reference Glide Slope with the Normal Phasing (as Indicated in Table 19) and Various Amounts of Dephasing for Terrain Profile #15. The simulated aircraft is flying at a constant 1000 ft. altitude above the runway centerline (extended).
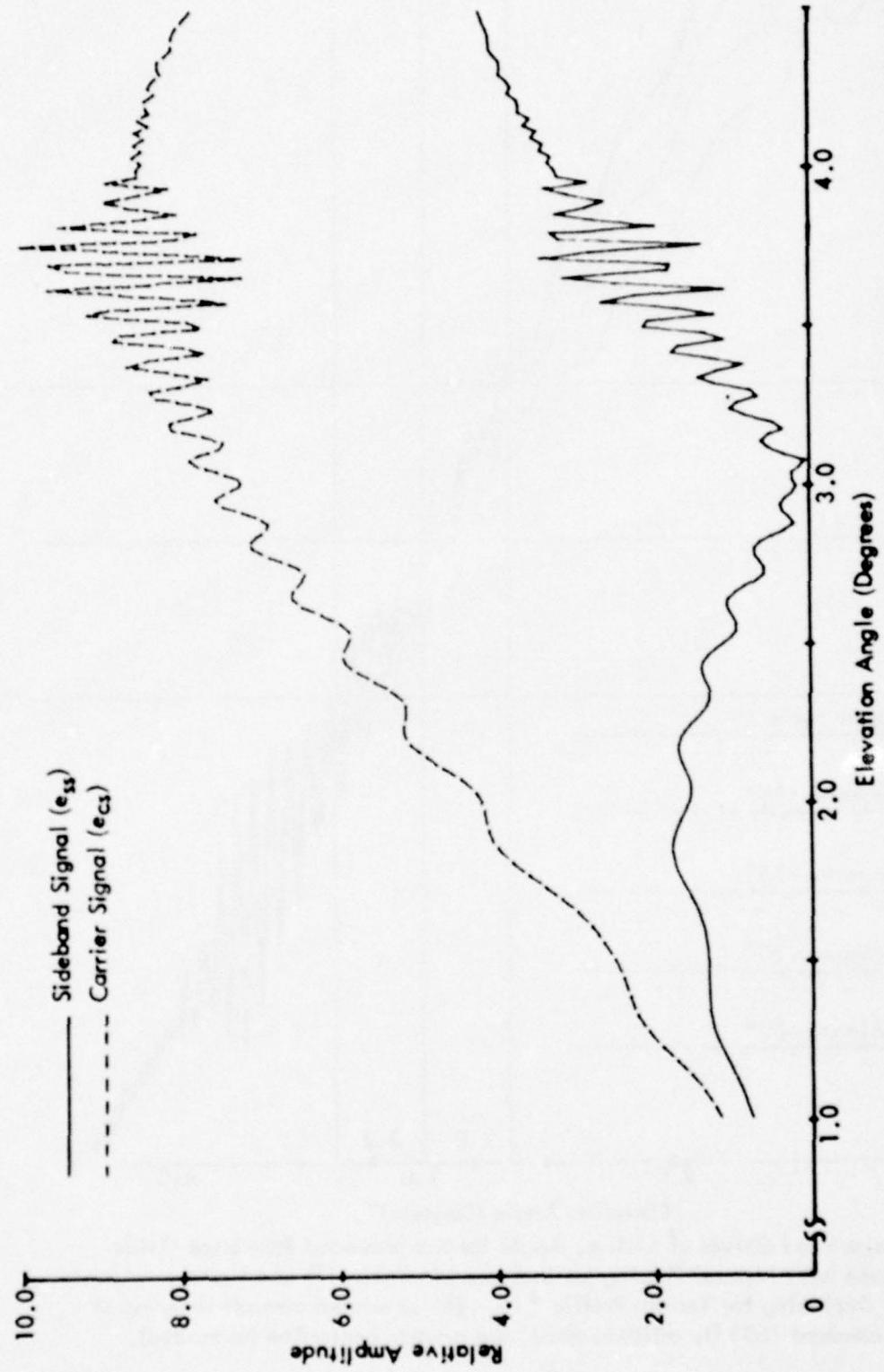
Figure 82d. Calculated Curves of Carrier and Sideband Signals vs. Angle for the Null Reference Glide Slope for Terrain Profile #15. The simulated aircraft is flying at a constant 1000 ft. altitude above the runway centerline (extended).
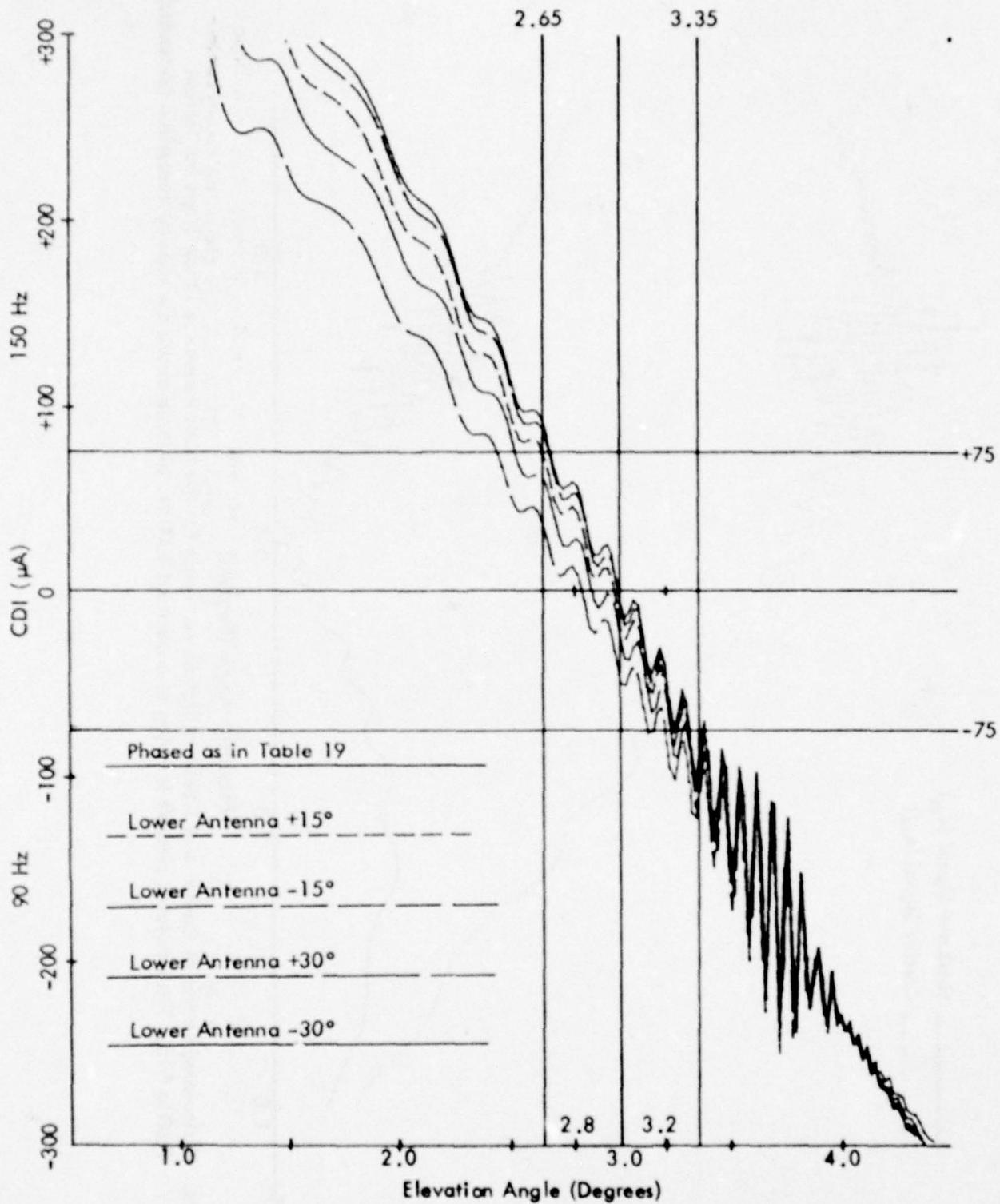
Figure 82e. Calculated Curves of CDI vs. Angle for the Sideband Reference Glide Slope with Normal Phasing (as Indicated in Table 19) and Various Amounts of Dephasing for Terrain Profile #15. The simulated aircraft is flying at a constant 1000 ft. altitude above the runway centerline (extended).
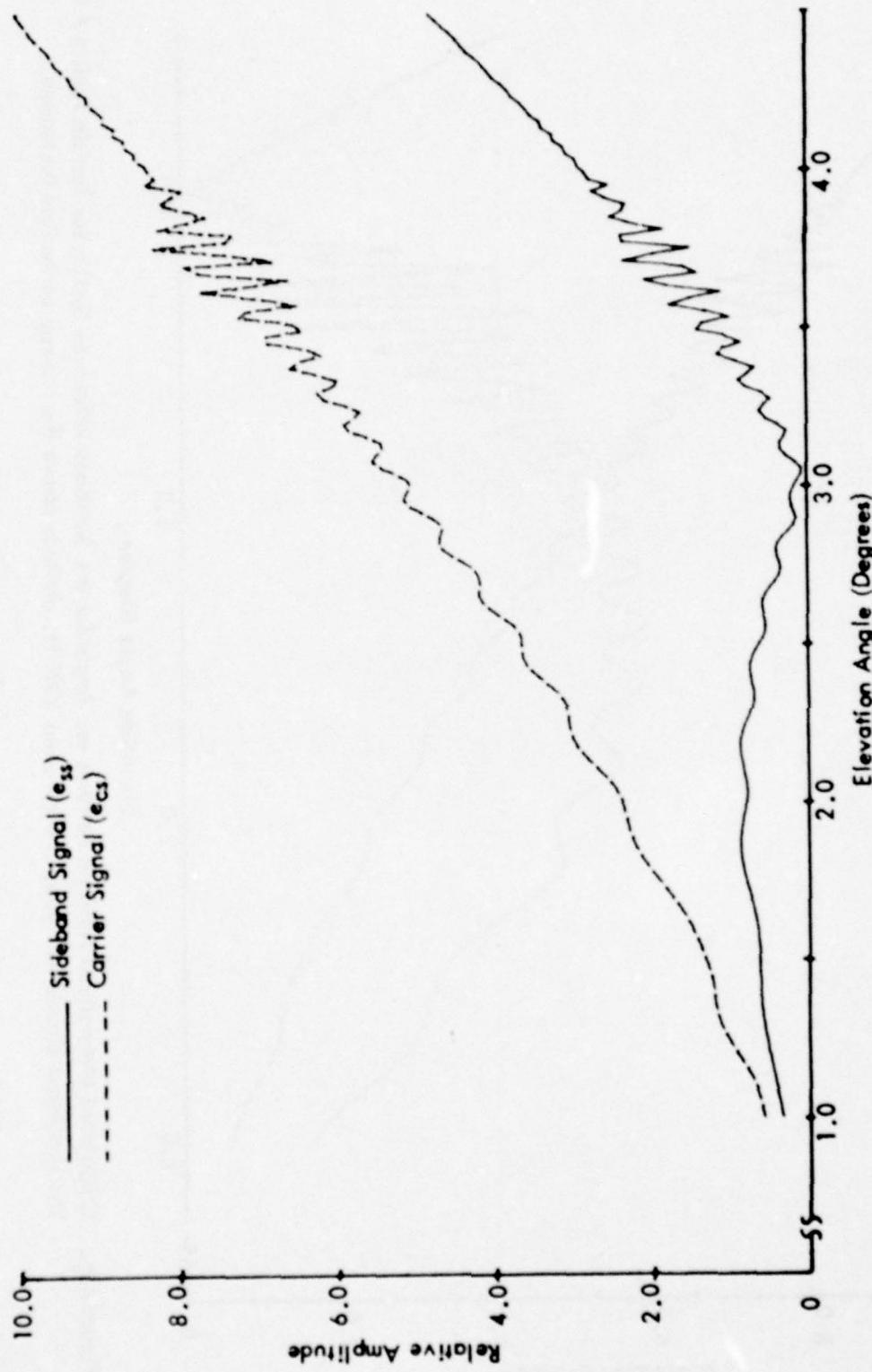
Figure 82f. Calculated Curves of Carrier and Composite Sideband Signals vs. Angle for the Sideband Reference Glide Slope for Terrain Profile #15. The simulated aircraft is flying at a constant 1000 ft. altitude above the runway center-line (extended).
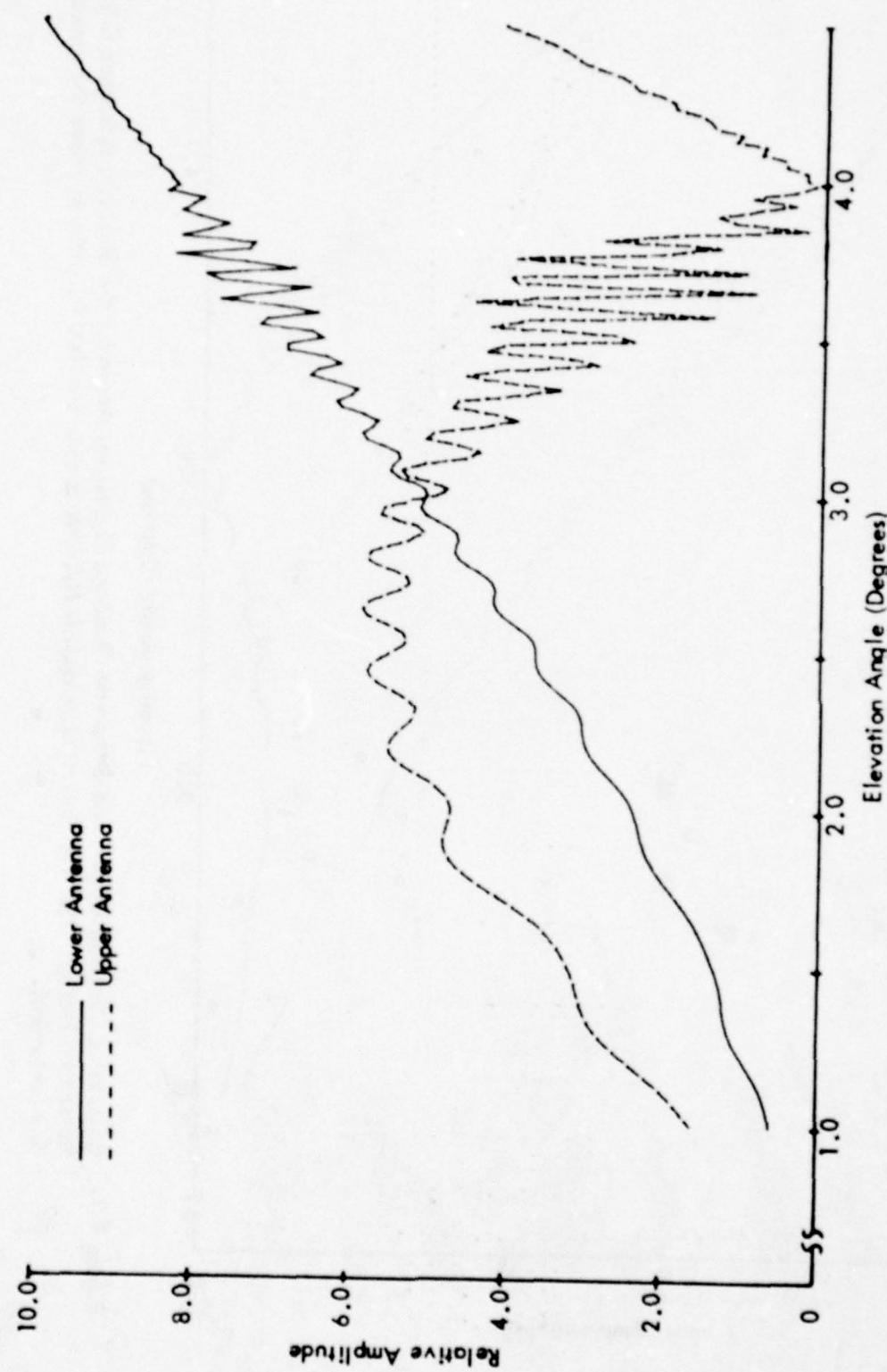
Figure 82g. Calculated Normalized Antenna Patterns vs. Angle for the Sideband Reference System for Terrain Profile #15. The simulated aircraft is flying at a constant 1000 ft. altitude above the runway centerline (extended).

-246-
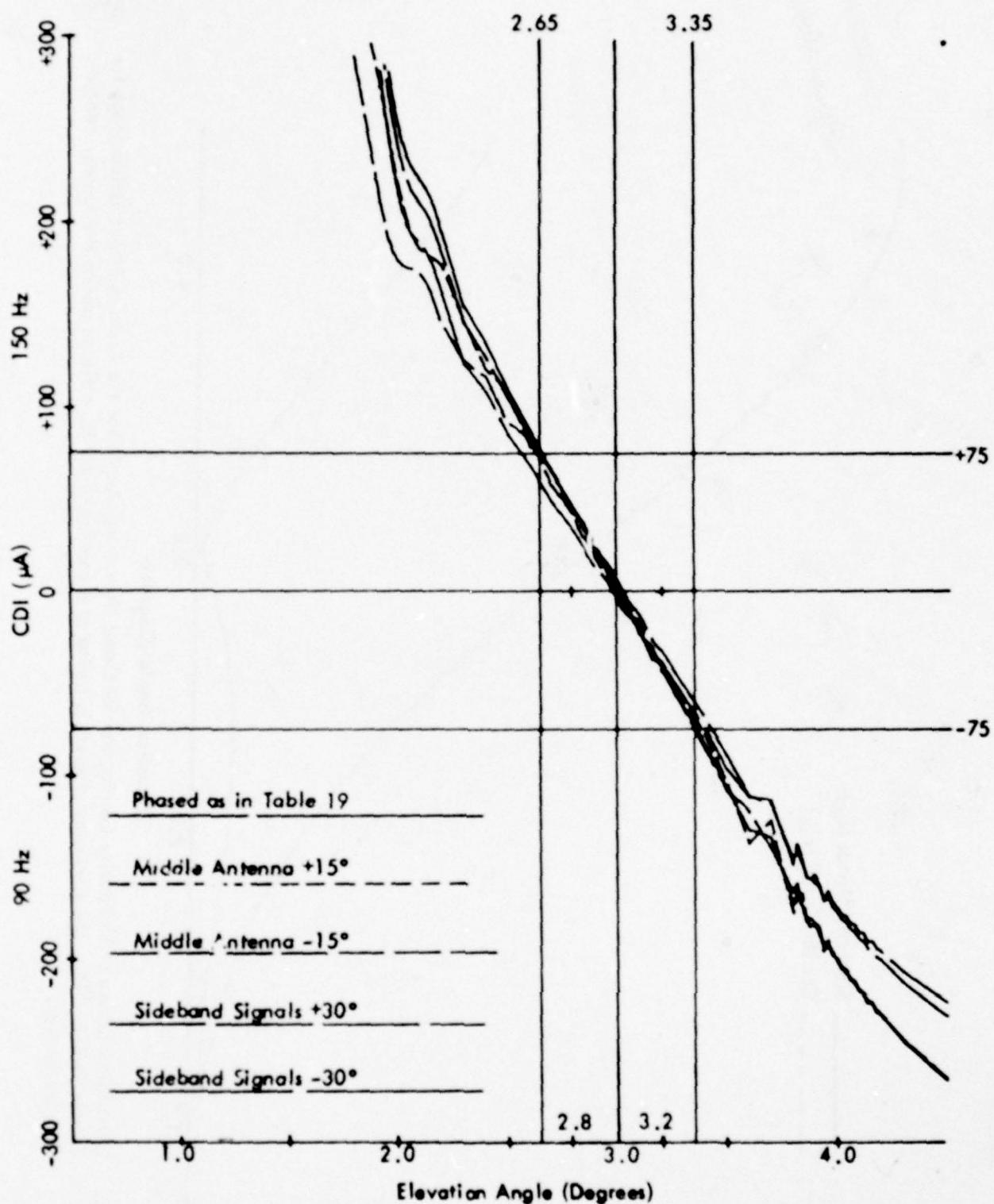
Figure 82h. Calculated Curves of CDI vs. Angle for the Capture Effect Glide Slope with the Normal Phasing (as Indicated in Table 19) and Dephased According to the Flight Inspection Manual Phase Verification Procedure for Terrain Profile #15. The simulated aircraft is flying at a constant 1000 ft. altitude above the runway centerline (extended).
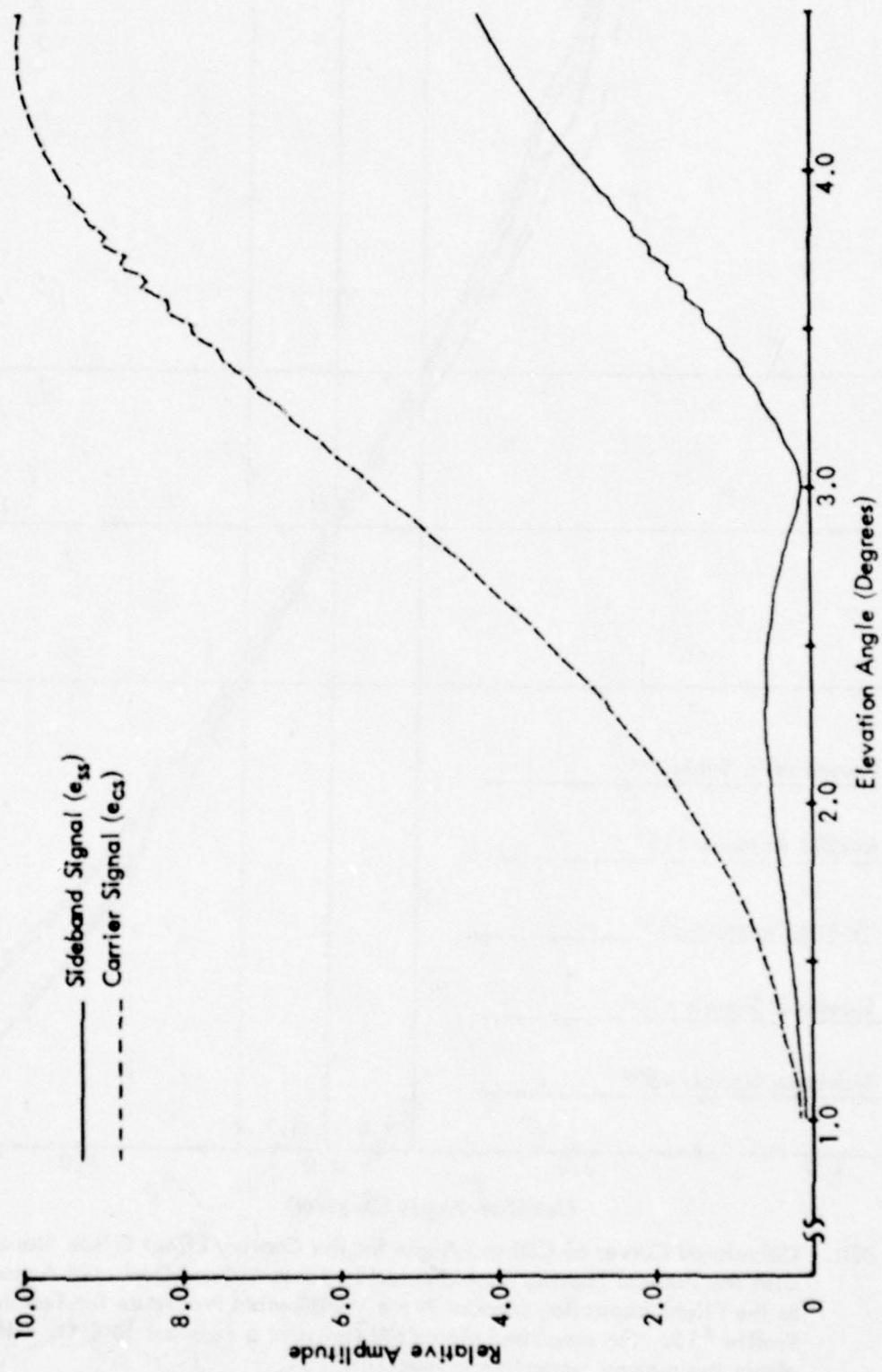
Figure 82i. Calculated Curves of Composite Carrier and Sideband Signals vs. Angle for the Capture Effect Glide Slope for Terrain Profile #15. The simulated aircraft is flying at a constant 1000 ft. altitude above the runway center-line (extended).
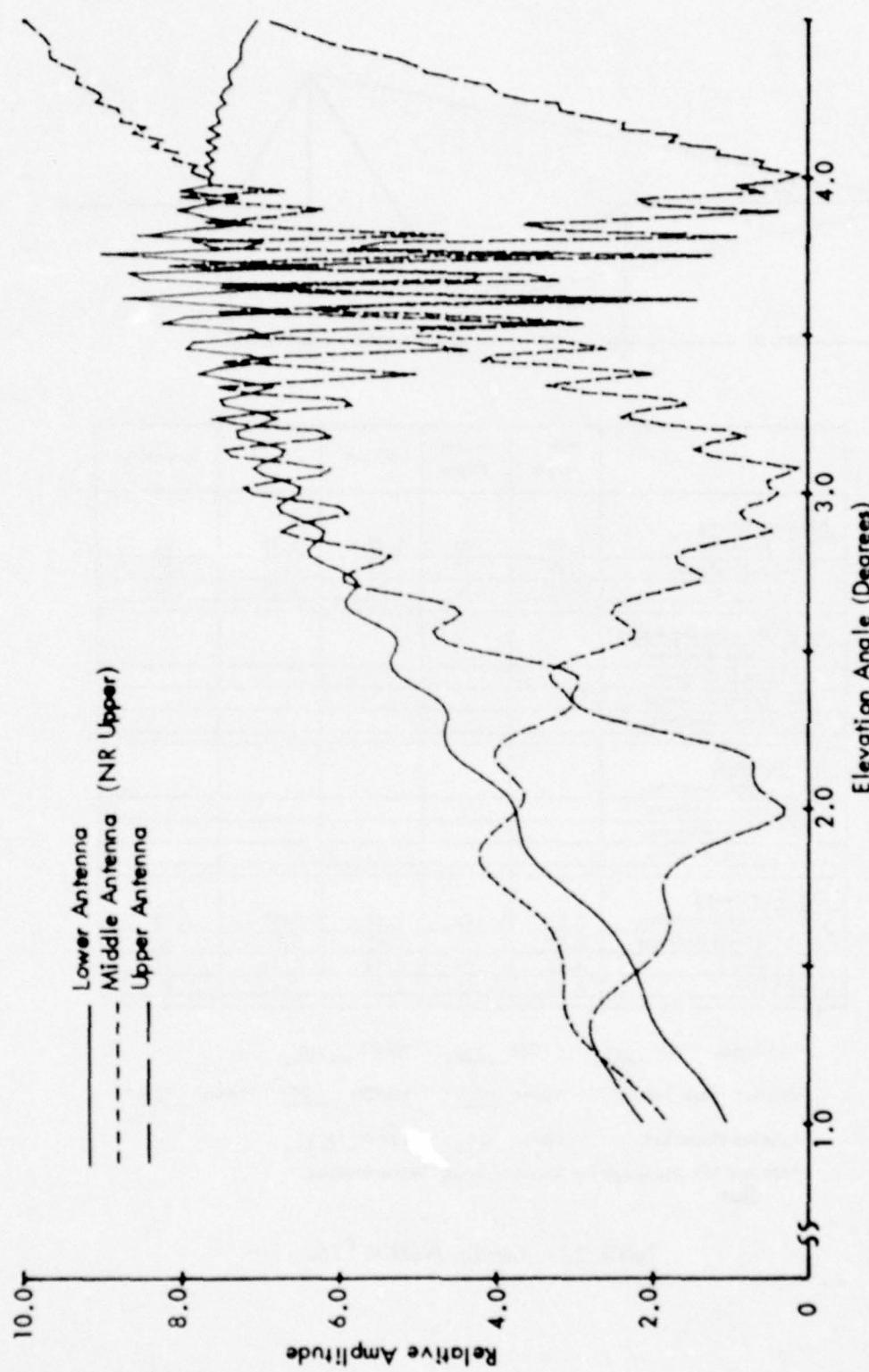
Figure 82j. Calculated Normalized Antenna Patterns vs. Angle for the Capture Effect and Null Reference Systems for Terrain Profile #15. The simulated aircraft is flying at a constant 1000 ft. altitude above the runway centerline (extended).

-249-
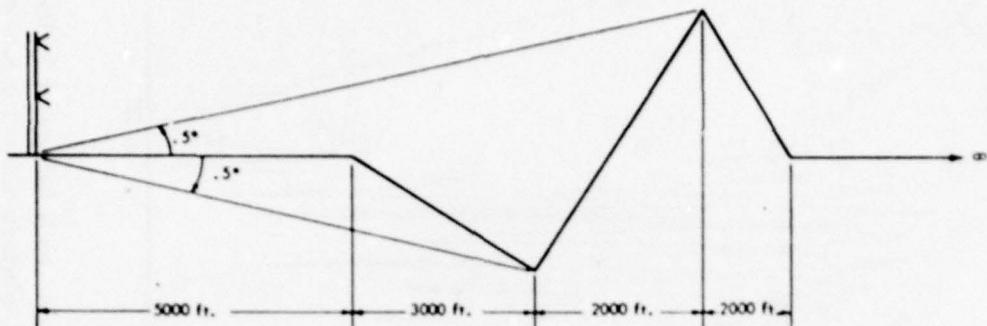
	Path Angle	Width Angle	+ 75 μA	- 75 μA	Symmetry
Normal Phasing					
Null Reference	2.99	.70	2.69	3.39	.57
Sideband Reference	2.99	.70	2.68	3.39	.56
CEGS	3.00	.70	2.65	3.35	.50
Null Reference Dephased					
+15° Lower Antenna					
-15° Lower Antenna					
+30° Lower Antenna					
-30° Lower Antenna					
SBR Dephased					
+15° Lower Antenna					
-15° Lower Antenna					
+30° Lower Antenna					
-30° Lower Antenna					
CEGS Dephased					
+15° Middle Antenna	3.01	.74	2.61	3.35	.50
-15° Middle Antenna	2.99	.71	2.61	3.39	.50
+30° SBO	3.03	.79	2.64	3.43	.51
-30° SBO	2.98	.83	2.57	3.41	.51

"A" Ratio: NR .343   SBR .330   CEGS .310

Relative Phase NR/CEGS   Upper -3.1°   Middle 0°   Lower +2.6°

Relative Phase SBR   Upper 0°   Lower +4.6°

*NR and SBR Too Rough for Accurate Angle Determinations.

Table 20. Terrain Profile #16.

-250-
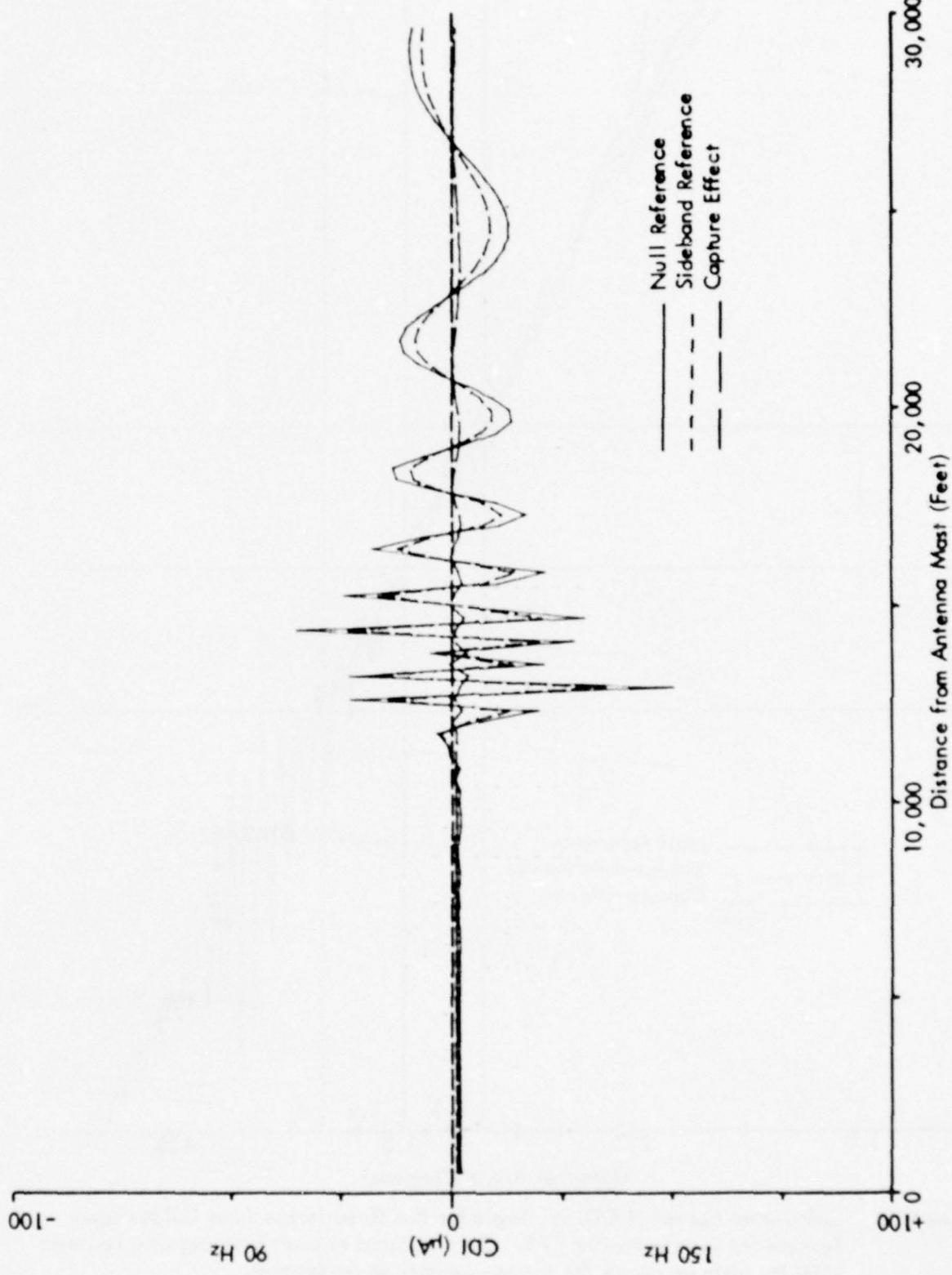
Figure 83a. Calculated Curves of CDI vs. Distance for the Three Image Type Glide-Slope Systems for Terrain Profile #16. The simulated aircraft is flying a constant 3.0 degree low approach over the runway centerline (extended).

-251-
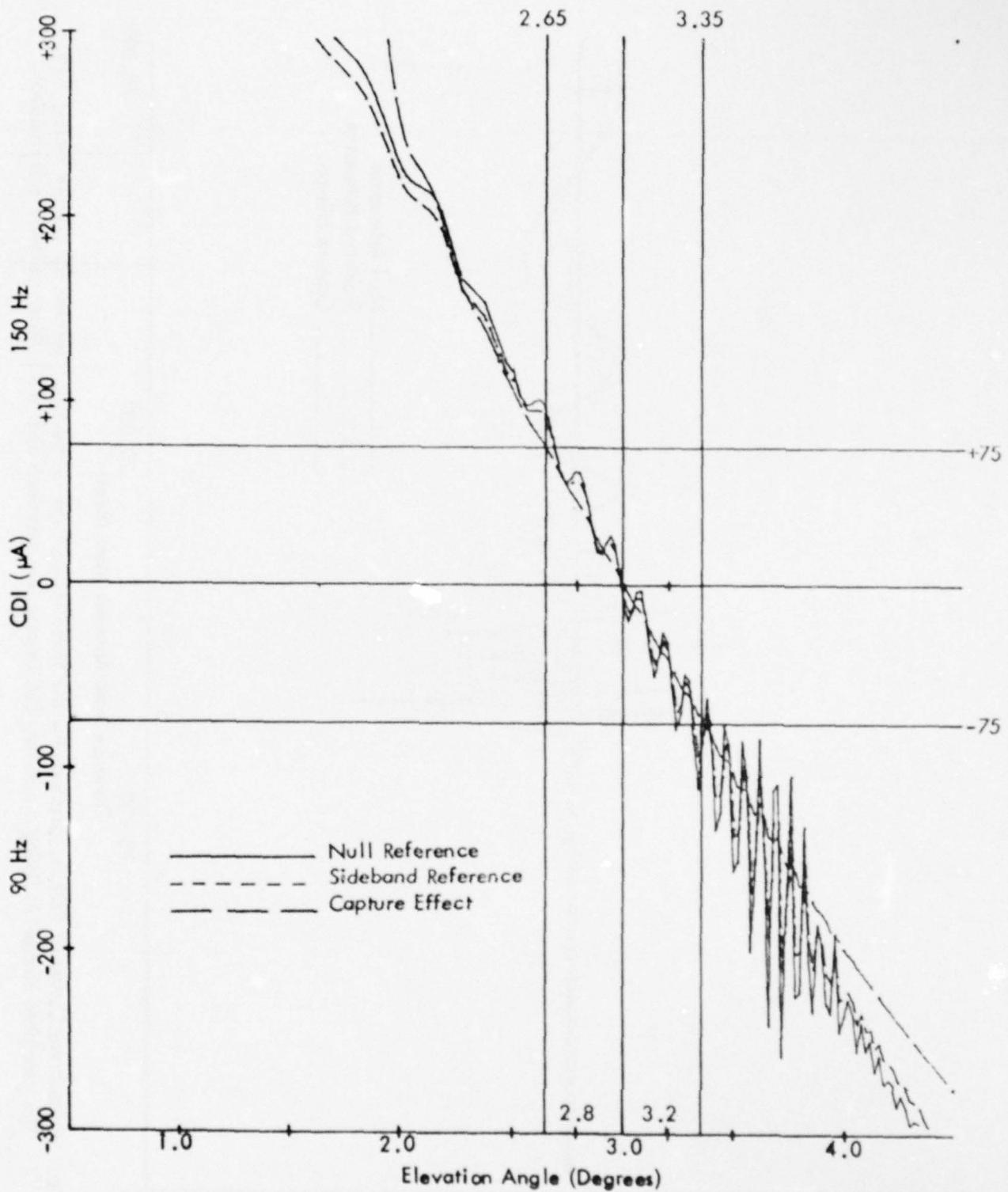
Figure 83b. Calculated Curves of CDI vs. Angle for the Three Image Type Glide-Slope Systems for Terrain Profile #16. The simulated aircraft is flying at a constant 1000 ft. altitude above the runway centerline (extended).
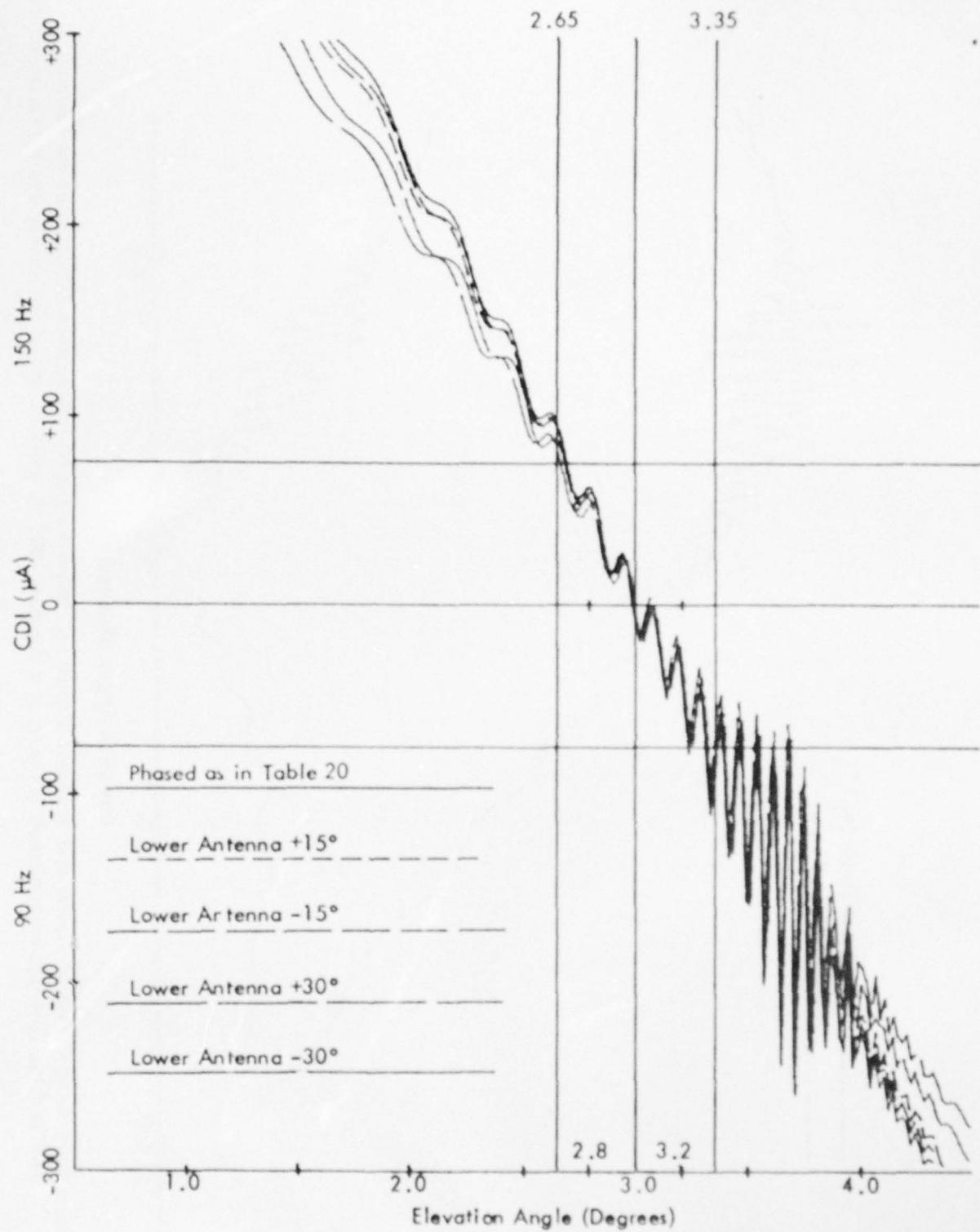
Figure 83c, Calculated Curves of CDI vs. Angle for the Null Reference Glide Slope
with the Normal Phasing (as Indicated in Table 20) and Various Amounts
of Dephasing for Terrain Profile #16. The simulated aircraft is flying at
a constant 1000 ft. altitude above the runway centerline (extended).
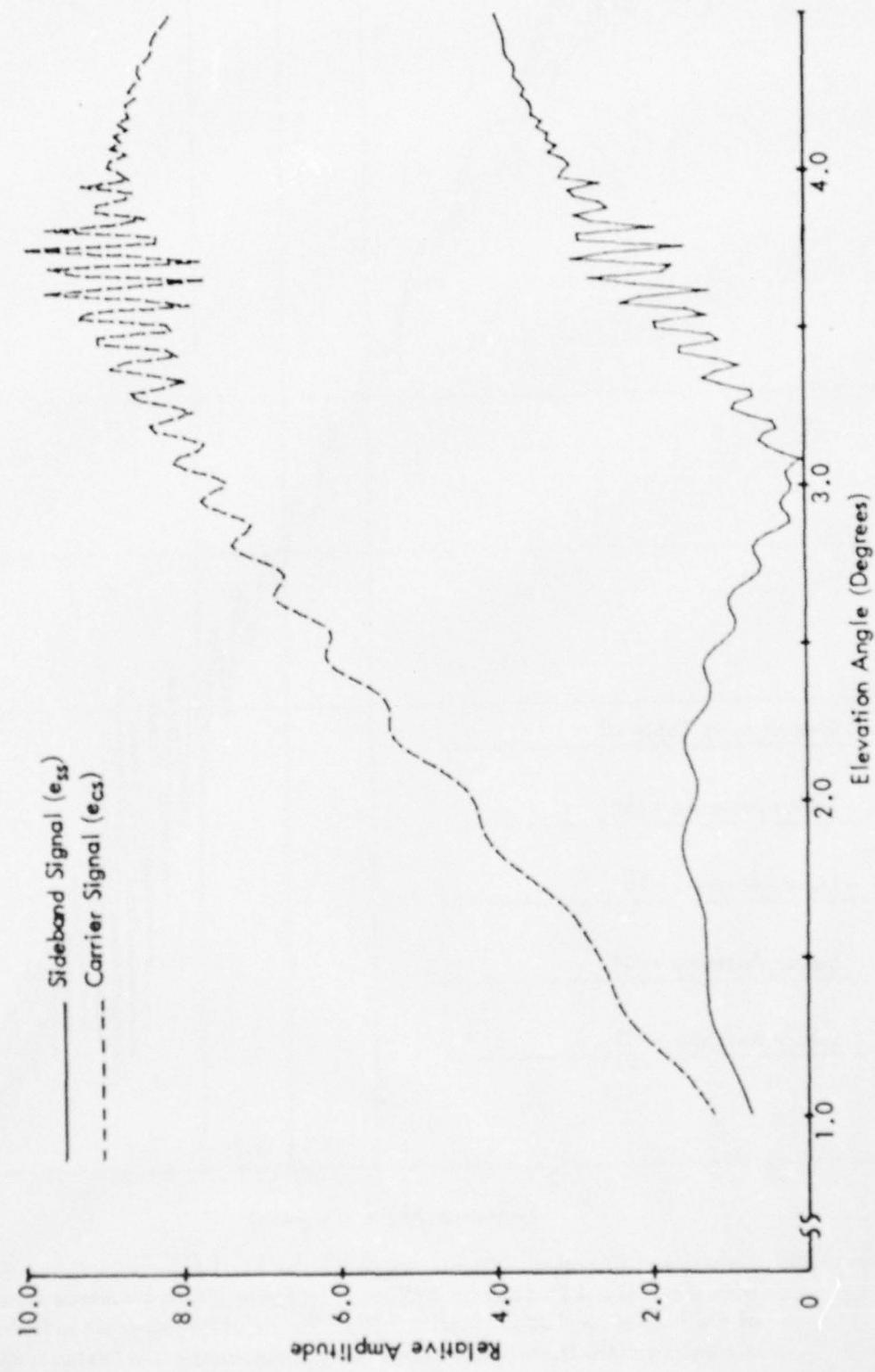
Figure 83d. Calculated Curves of Carrier and Sideband Signals vs. Angle for the Null Reference Glide Slope for Terrain Profile #16. The simulated aircraft is flying at a constant 1000 ft. altitude above the runway centerline (extended).

-254-
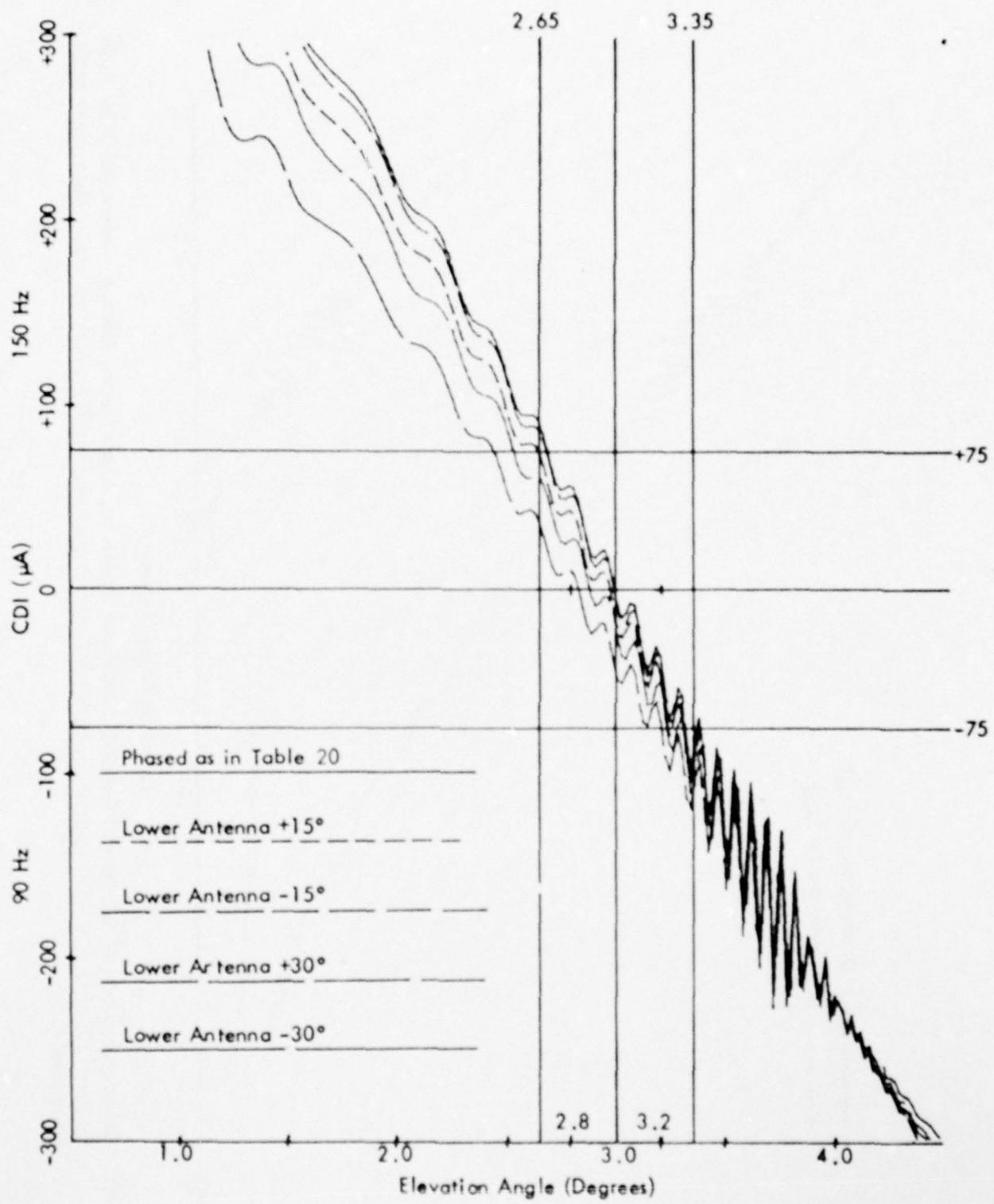
Figure 83e. Calculated Curves of CDI vs. Angle for the Sideband Reference Glide Slope with Normal Phasing (as Indicated in Table 20) and Various Amounts of Dephasing for Terrain Profile #16. The simulated aircraft is flying at a constant 1000 ft. altitude above the runway centerline (extended).
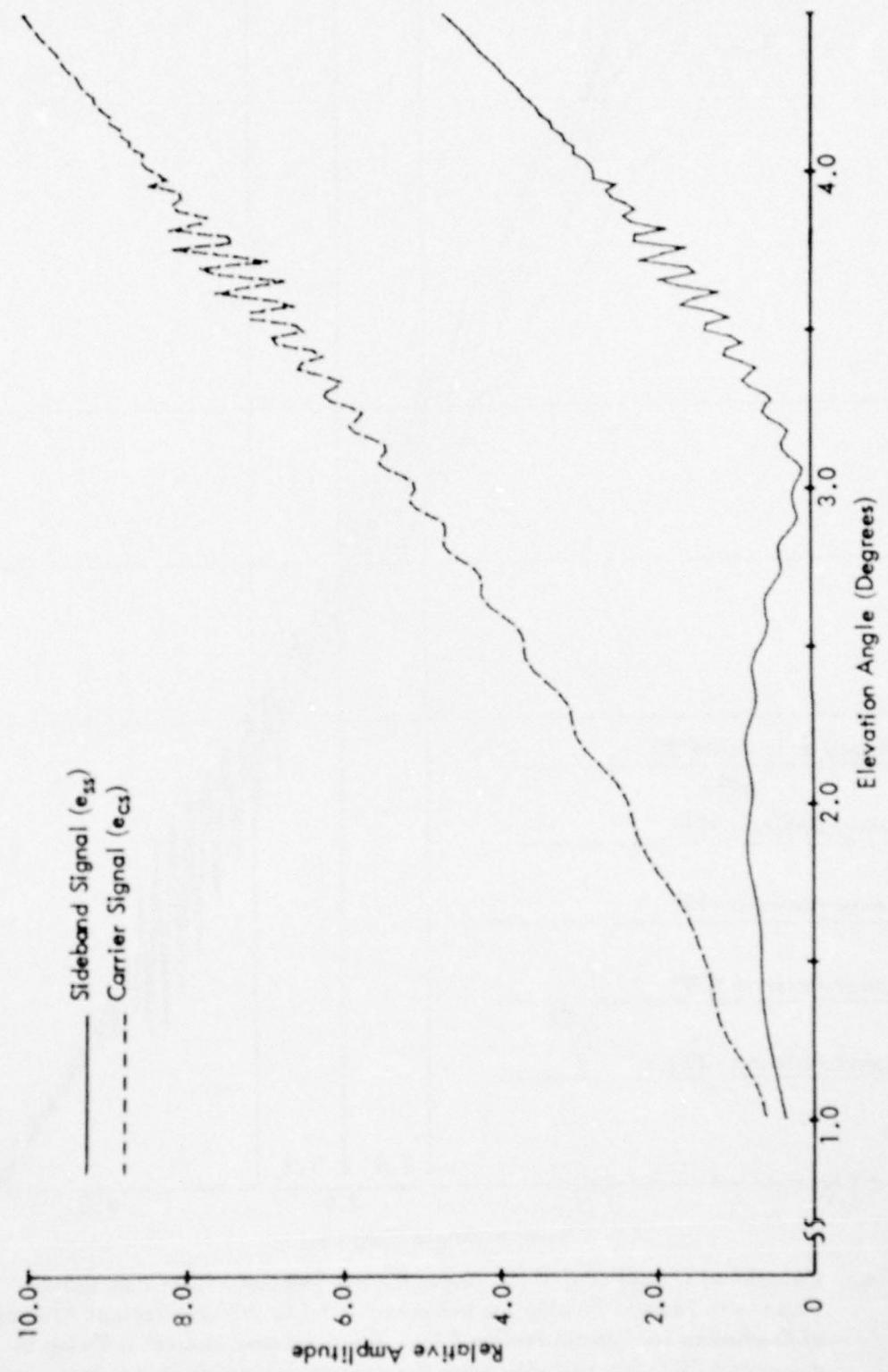
Figure 83f. Calculated Curves of Carrier and Composite Sideband Signals vs. Angle for the Sideband Reference Glide Slope for Terrain Profile #16. The simulated aircraft is flying at a constant 1000 ft. altitude above the runway center-line (extended).
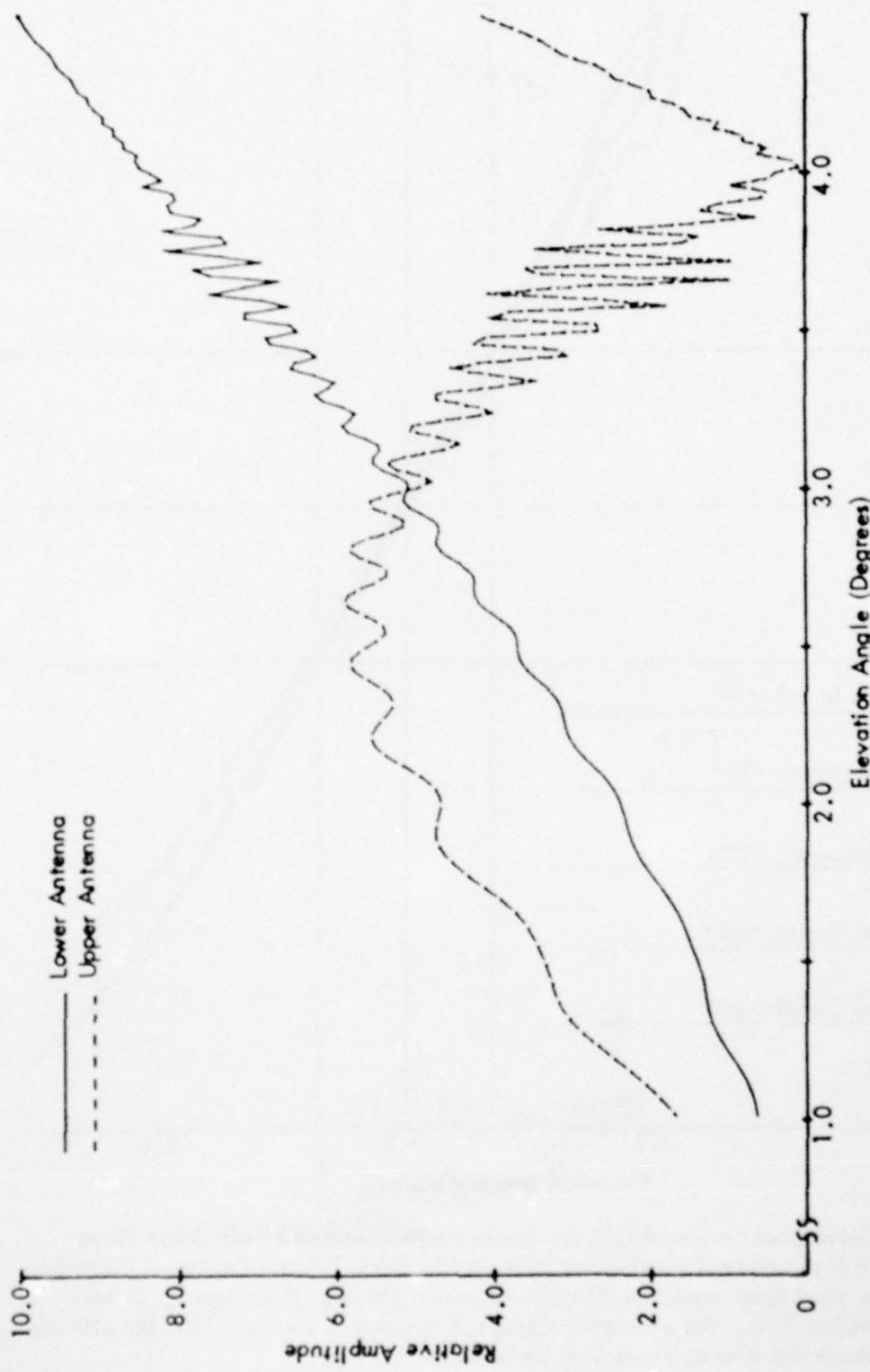
Figure 83g. Calculated Normalized Antenna Patterns vs. Angle for the Sideband Reference System for Terrain Profile #16. The simulated aircraft is flying at a constant 1000 ft. altitude above the runway centerline (extended).

-257-
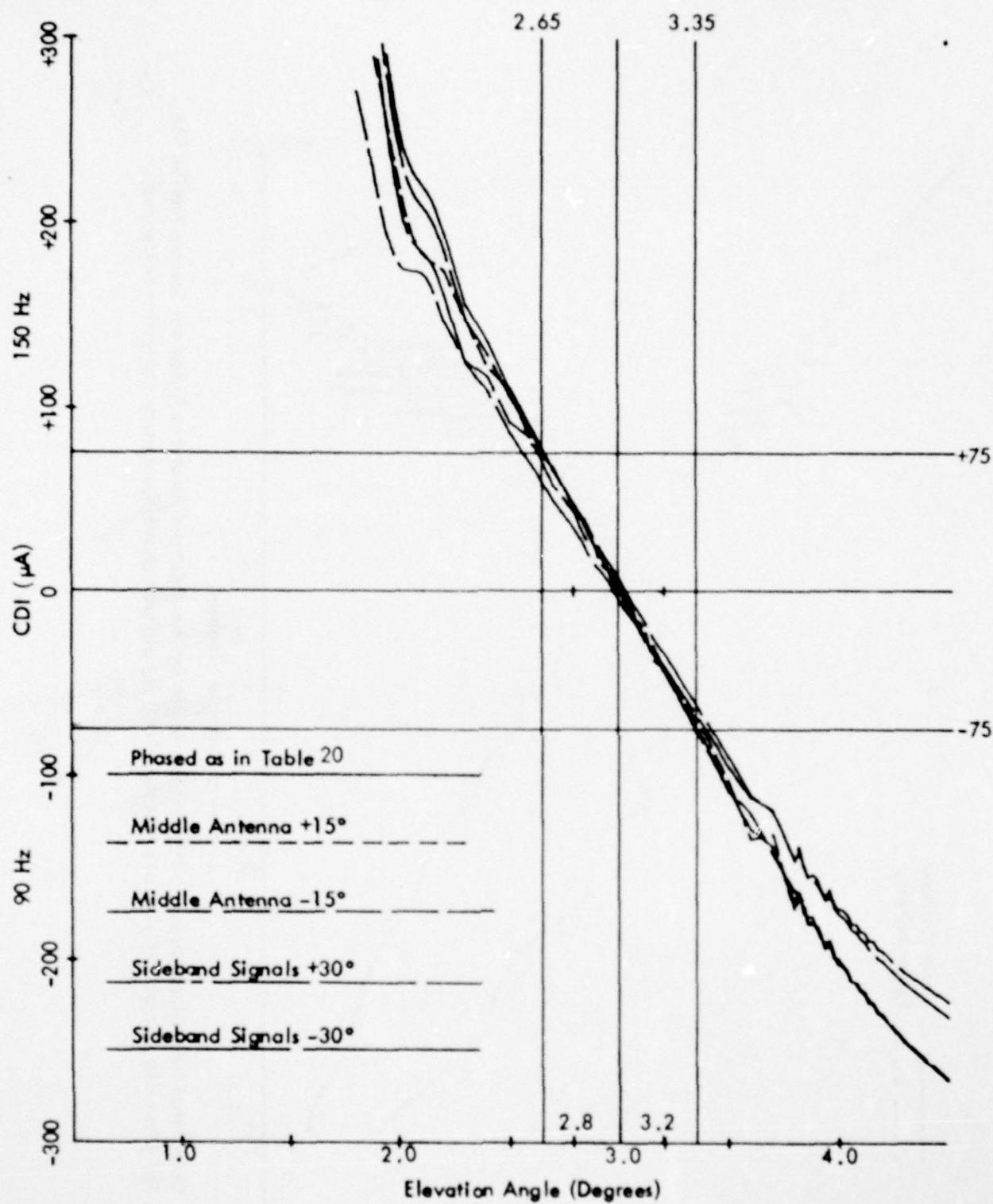
Figure 83h. Calculated Curves of CDI vs. Angle for the Capture Effect Glide Slope with the Normal Phasing (as Indicated in Table 20) and Dephased According to the Flight Inspection Manual Phase Verification Procedure for Terrain Profile #16. The simulated aircraft is flying at a constant 1000 ft. altitude above the runway centerline (extended).
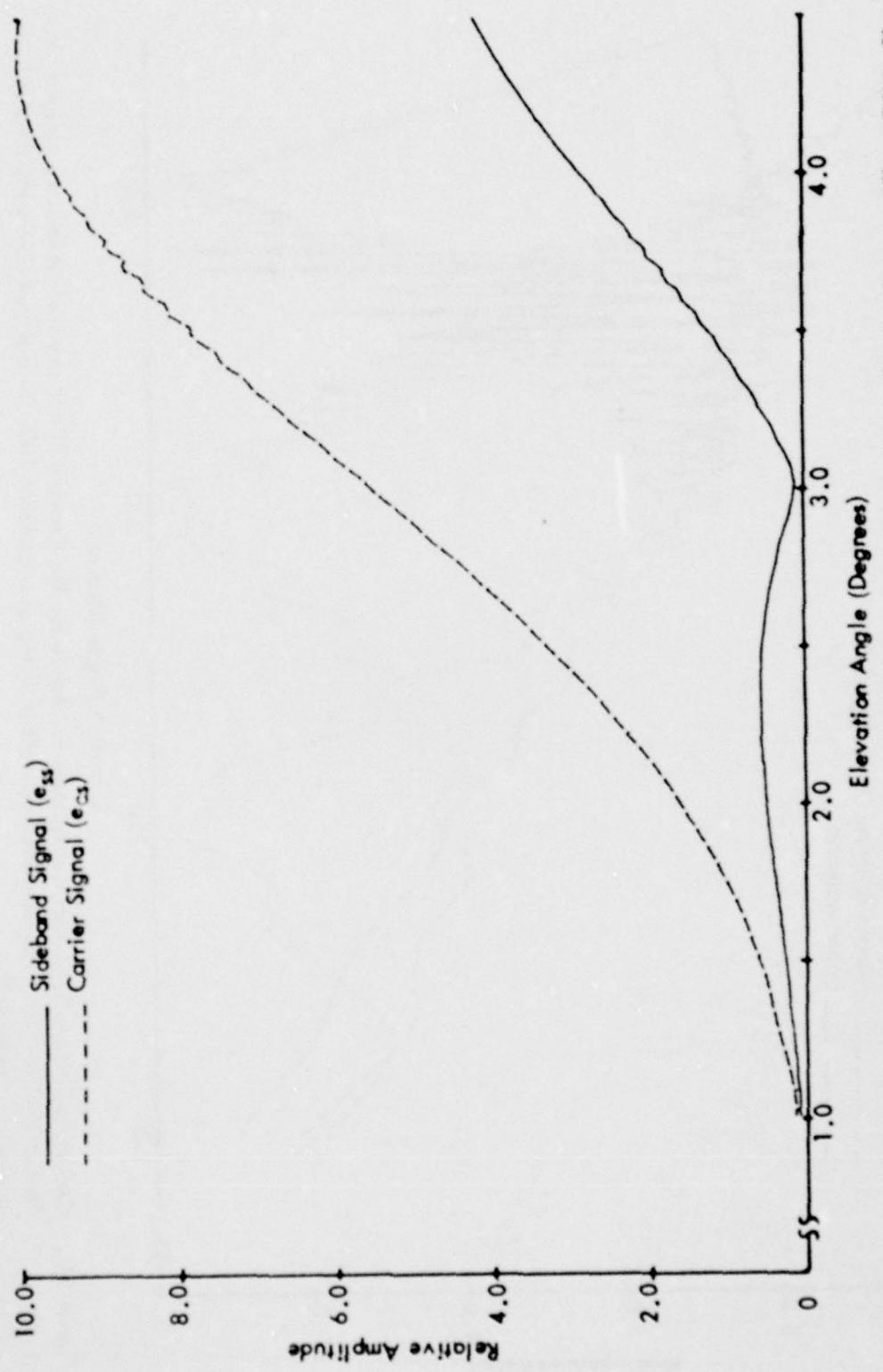
Figure 83i. Calculated Curves of Composite Carrier and Sideband Signals vs. Angle for the Capture Effect Glide Slope for Terrain Profile #16. The simulated aircraft is flying at a constant 1000 ft. altitude above the runway center-line (extended).

-259-
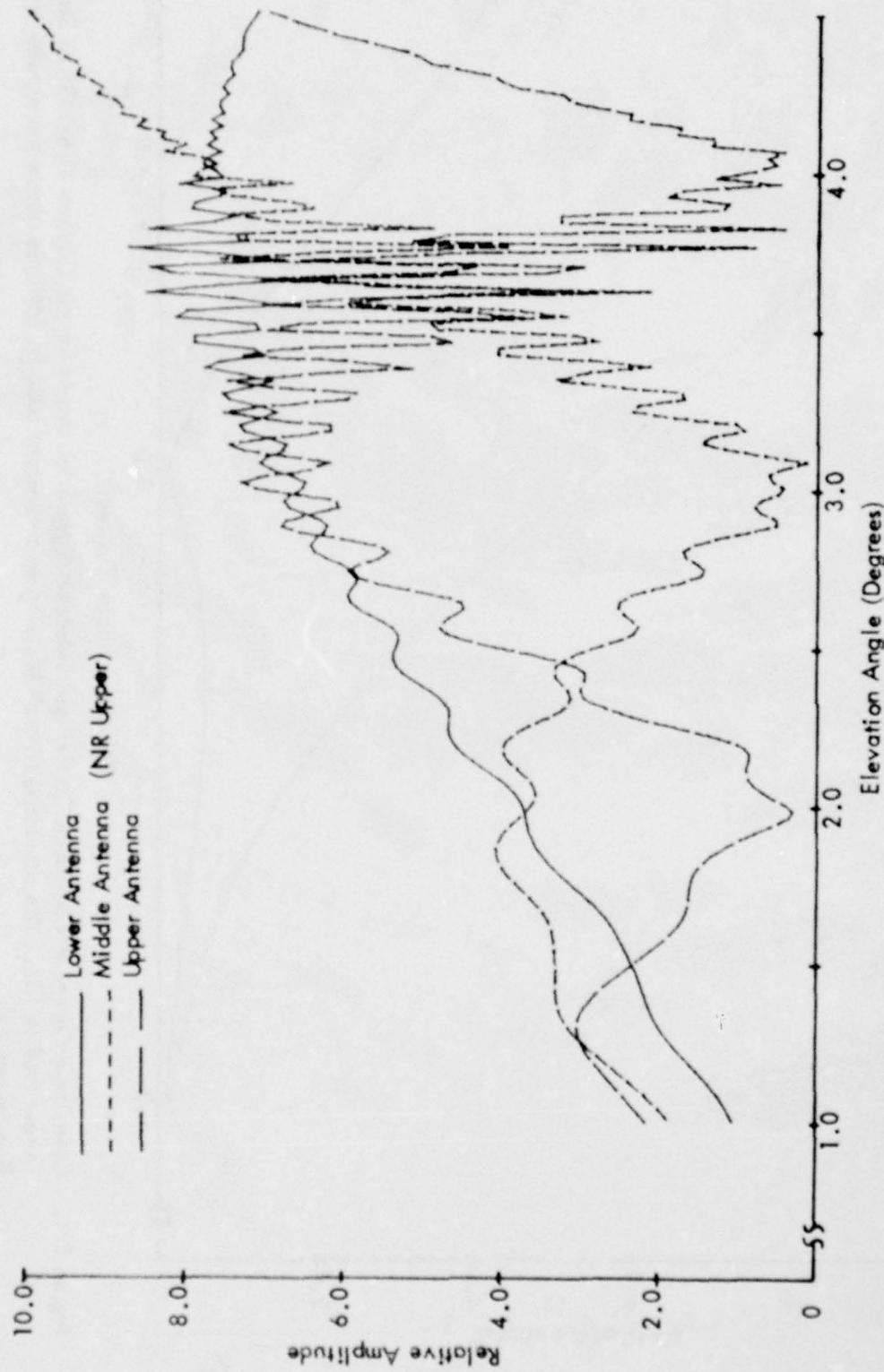
Figure 83j. Calculated Normalized Antenna Patterns vs. Angle for the Capture Effect and Null Reference Systems for Terrain Profile #16. The simulated aircraft is flying at a constant 1000 ft. altitude above the runway centerline (extended).

Lower Antenna
Middle Antenna (NR Upper)
Upper Antenna

Elevation Angle (Degrees)

Relative Amplitude
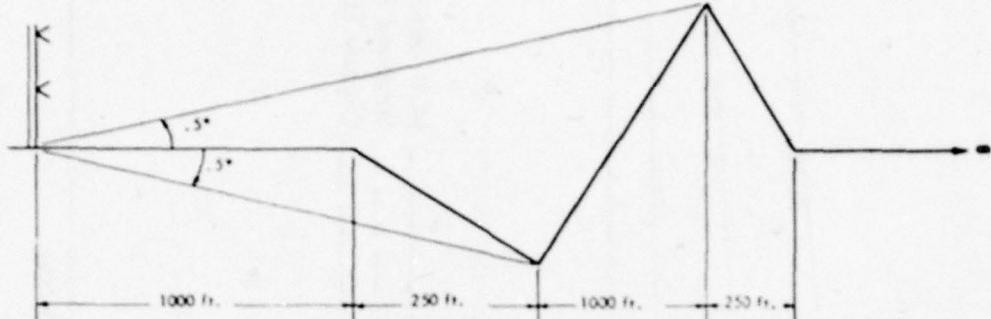
	Path Angle	Width Angle	+75 µA	-75 µA	Symmetry
Normal Phasing					
Null Reference	2.89	.46	2.67	3.12	.52
Sideband Reference	2.91	.70	2.61	3.31	.56
CEGS	2.96	.70	2.59	3.29	.47
Null Reference Dephased					
+15° Lower Antenna	2.87	1.11	2.63	3.73	.78
-15° Lower Antenna	2.91	.42	2.69	3.12	.49
+30° Lower Antenna	2.84	1.24	2.55	3.80	.77
-30° Lower Antenna	2.93	.42	2.70	3.13	.47
SBR Dephased					
+15° Lower Antenna	2.84	.79	2.50	3.29	.57
-15° Lower Antenna	2.93	.63	2.63	3.26	.52
+30° Lower Antenna	2.70	.82	2.28	3.10	.49
-30° Lower Antenna	2.90	.64	2.55	3.19	.45
CEGS Dephased					
+15° Middle Antenna	2.98	.60	2.66	3.26	.48
-15° Middle Antenna	2.94	.92	2.44	3.35	.45
+30° SBO	3.04	.69	2.68	3.36	.47
-30° SBO	2.85	.92	2.43	3.33	.53

"A" Ratio: NR .315*   SBR .260   CEGS .291

Relative Phase NR/CEGS   Upper -5.9°   Middle 0°   Lower +9.5°

Relative Phase SBR   Upper 0°   Lower +7.7°

*Could not be adjusted to 0.70° path width.

Table 21. Terrain Profile #17.
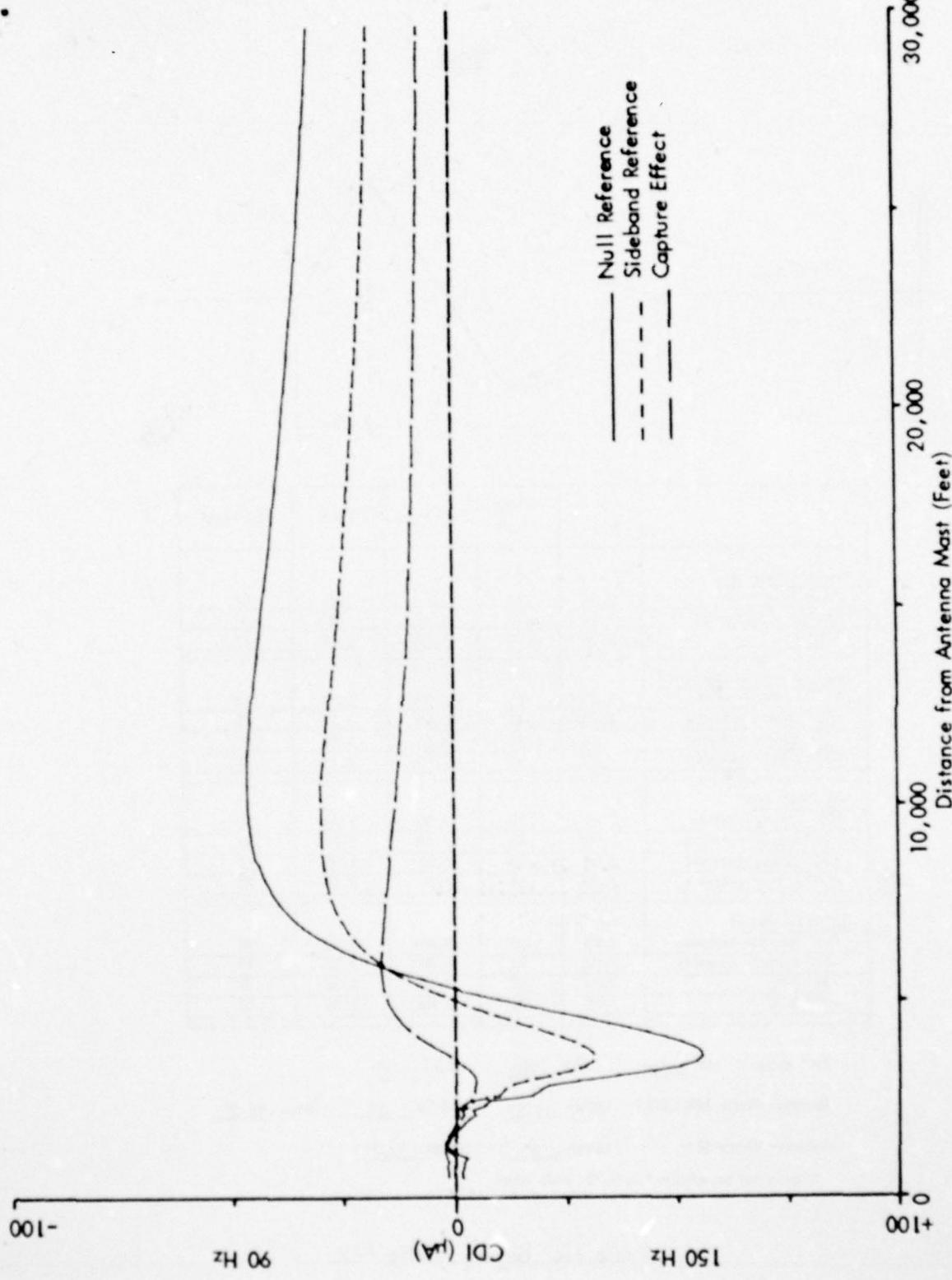
Figure 84a. Calculated Curves of CDI vs. Distance for the Three Image Type Glide Slope Systems for Terrain Profile #17. The simulated aircraft is flying a constant 3.0 degree low approach over the runway centerline (extended).
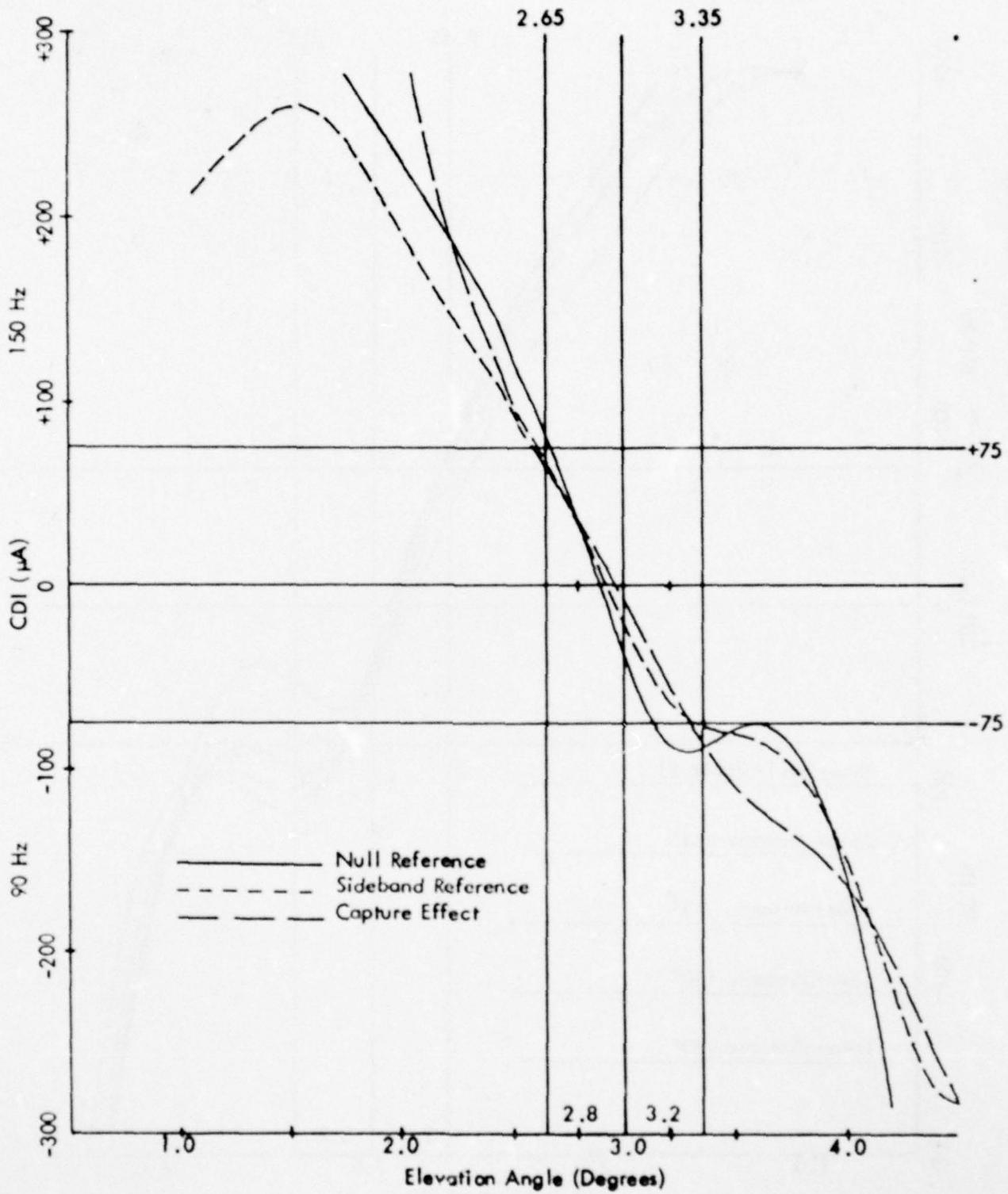
Figure 84b. Calculated Curves of CDI vs. Angle for the Three Image Type Glide-Slope Systems for Terrain Profile #17. The simulated aircraft is flying at a constant 1000 ft. altitude above the runway centerline (extended).

-263-
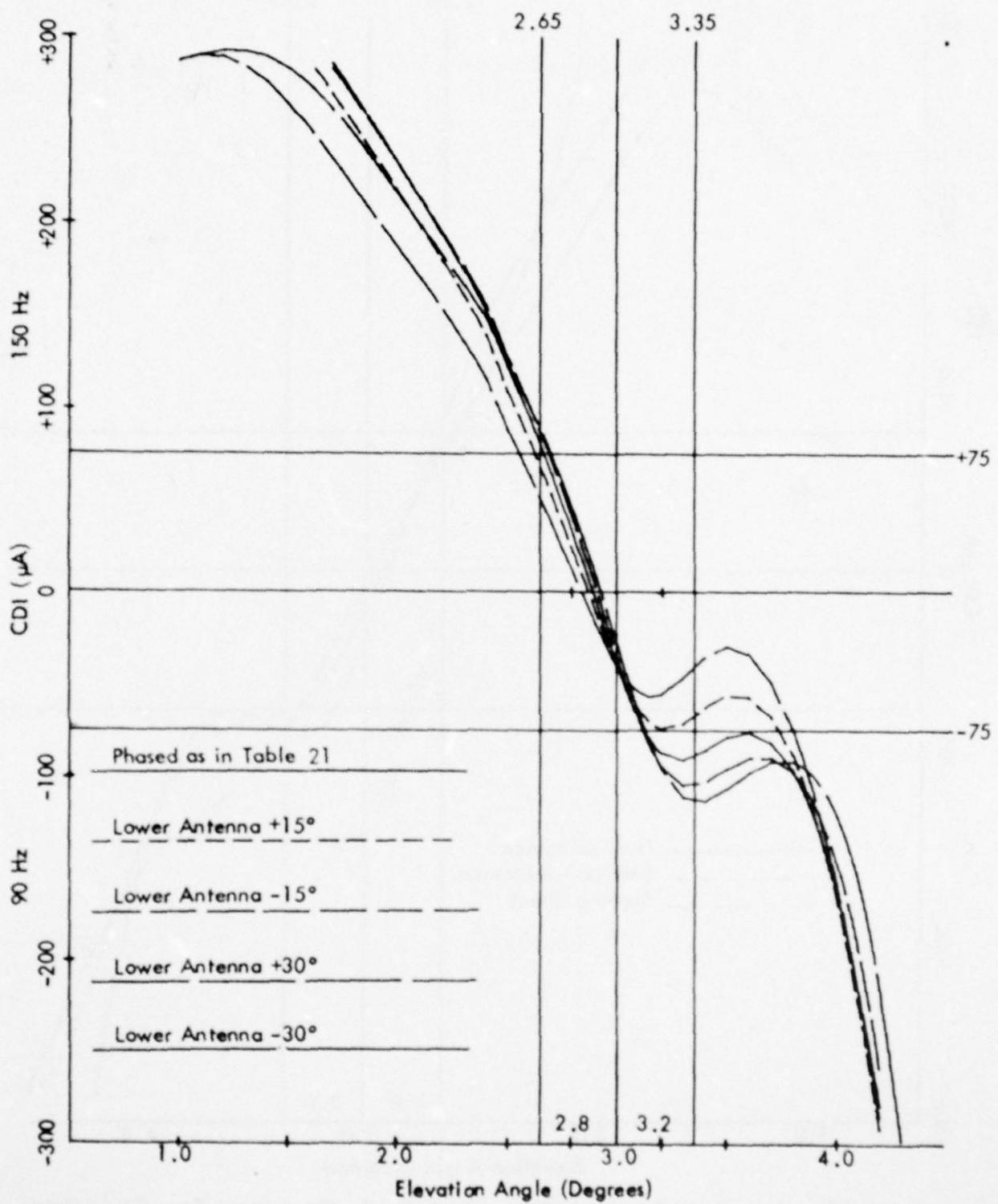
Figure 84c. Calculated Curves of CDI vs. Angle for the Null Reference Glide Slope with the Normal Phasing (as Indicated in Table 21) and Various Amounts of Dephasing for Terrain Profile #17. The simulated aircraft is flying at a constant 1000 ft. altitude above the runway centerline (extended).
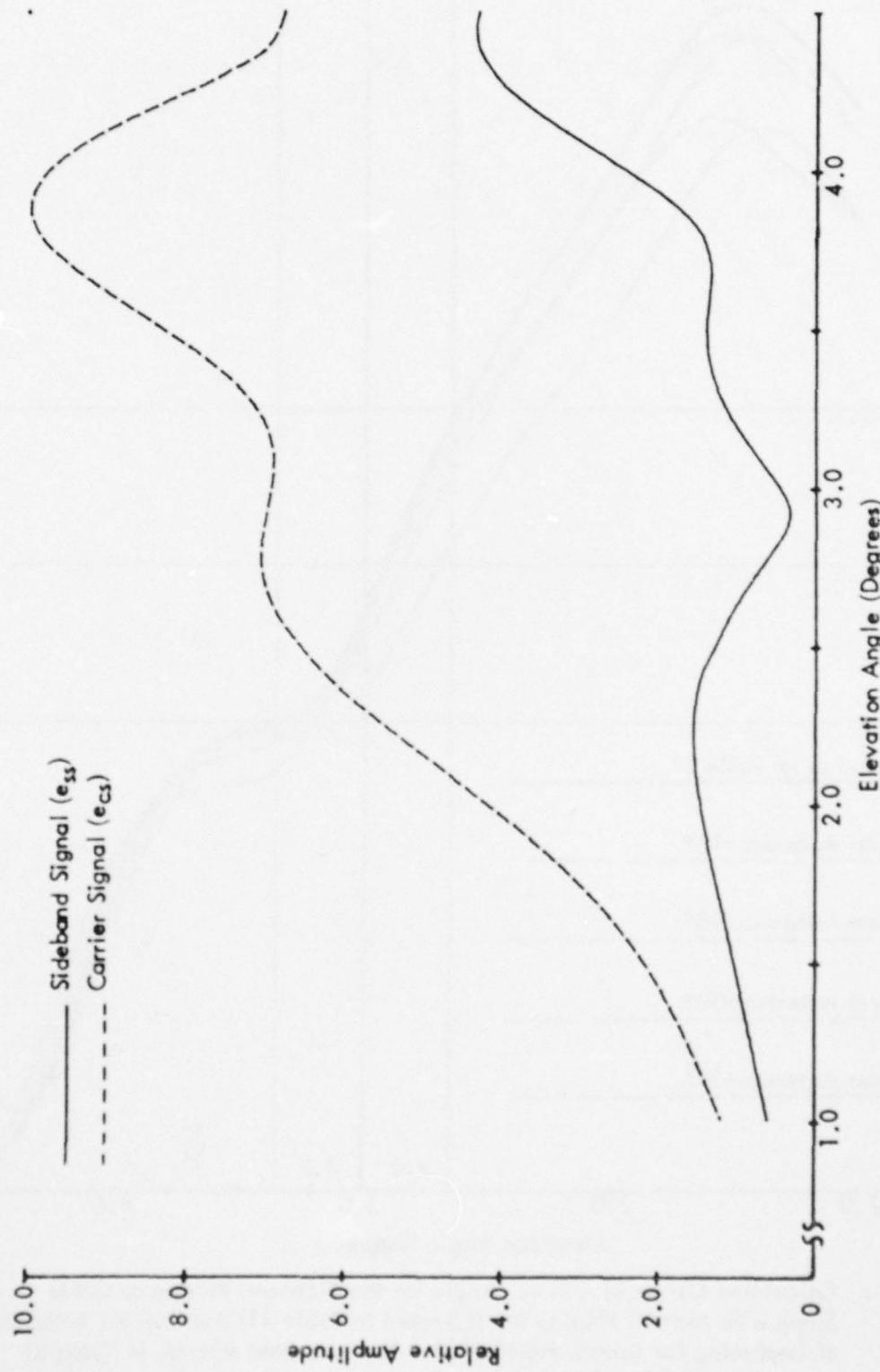
Figure 84d. Calculated Curves of Carrier and Sideband Signals vs. Angle for the Null Reference Glide Slope for Terrain Profile #17. The simulated aircraft is flying at a constant 1000 ft. altitude above the runway centerline (extended).
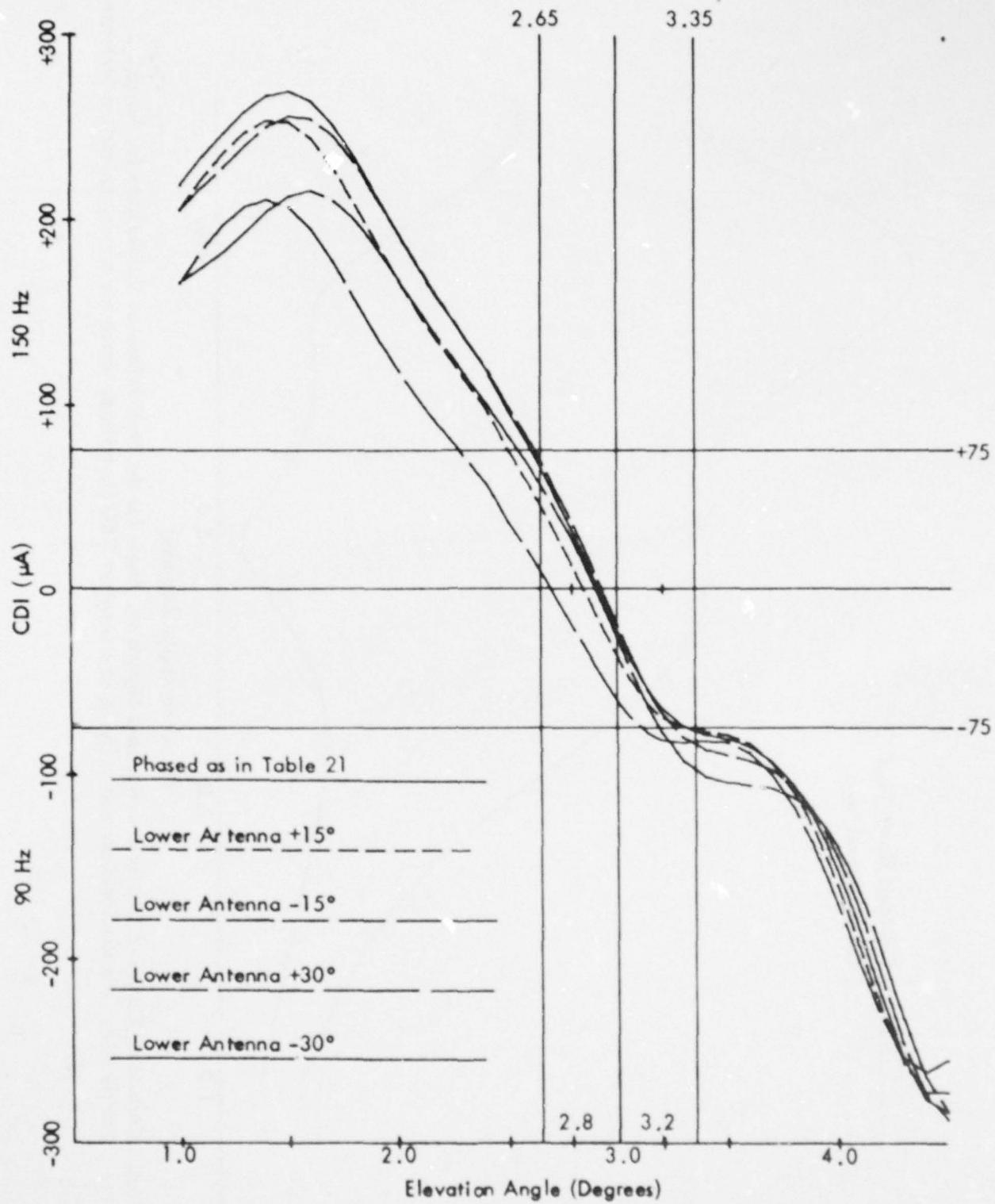
Figure 84e. Calculated Curves of CDI vs. Angle for the Sideband Reference Glide Slope with Normal Phasing (as Indicated in Table 21) and Various Amounts of Dephasing for Terrain Profile #17. The simulated aircraft is flying at a constant 1000 ft. altitude above the runway centerline (extended).

-266-

NATIONAL BUREAU OF STANDARDS
MICROCOPY RESOLUTION TEST CHART
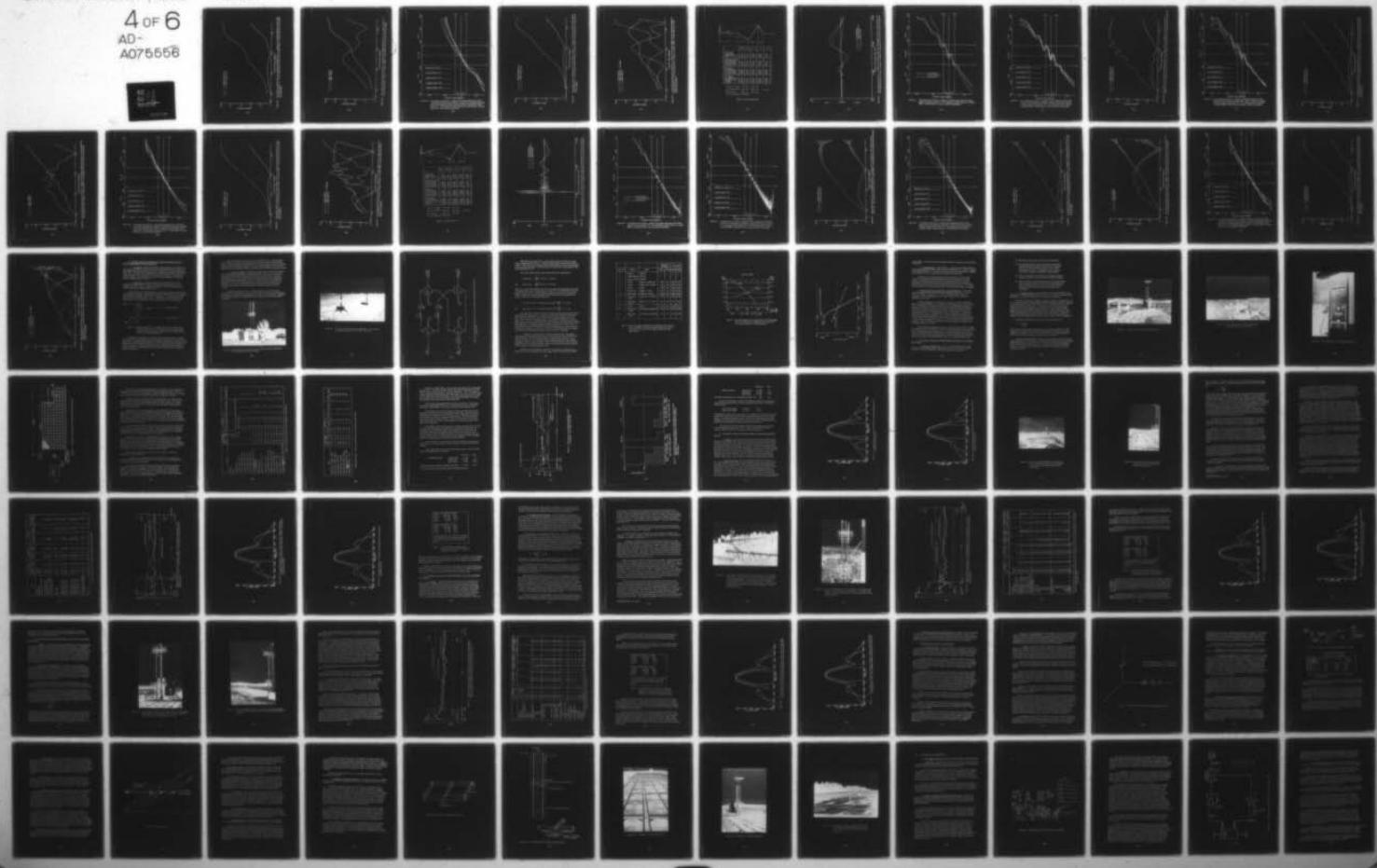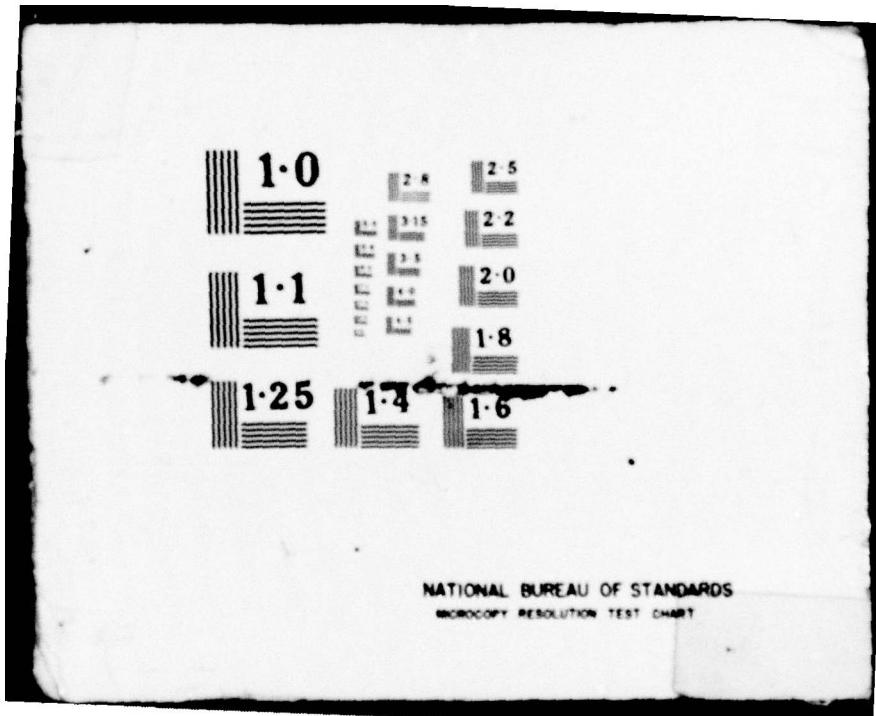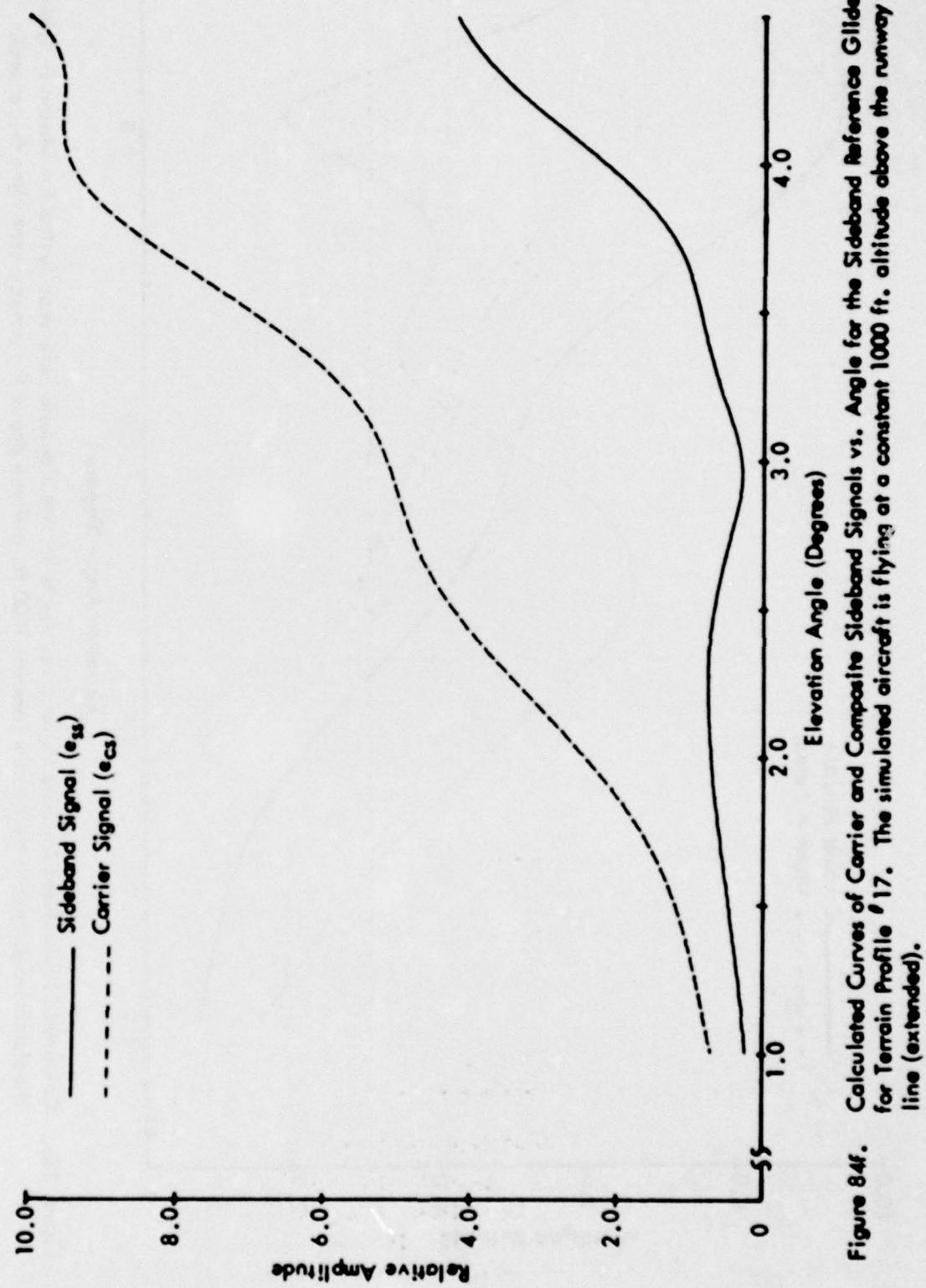
Figure 84f. Calculated Curves of Carrier and Composite Sideband Signals vs. Angle for the Sideband Reference Glide Slope for Terrain Profile #17. The simulated aircraft is flying at a constant 1000 ft. altitude above the runway centerline (extended).
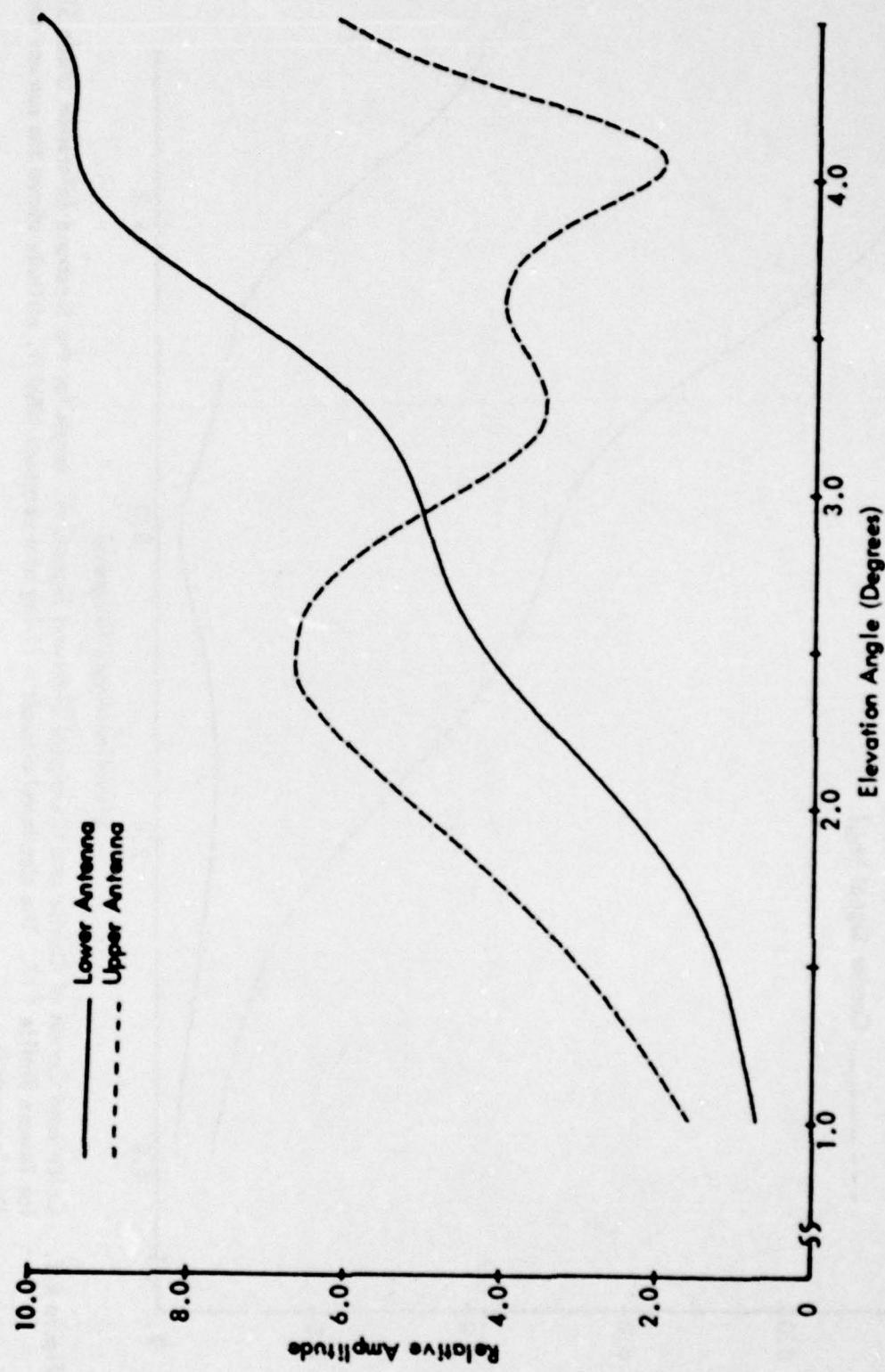
Figure 84g. Calculated Normalized Antenna Patterns vs. Angle for the Sideband Reference System for Terrain Profile #17. The simulated aircraft is flying at a constant 1000 ft. altitude above the runway centerline (extended).
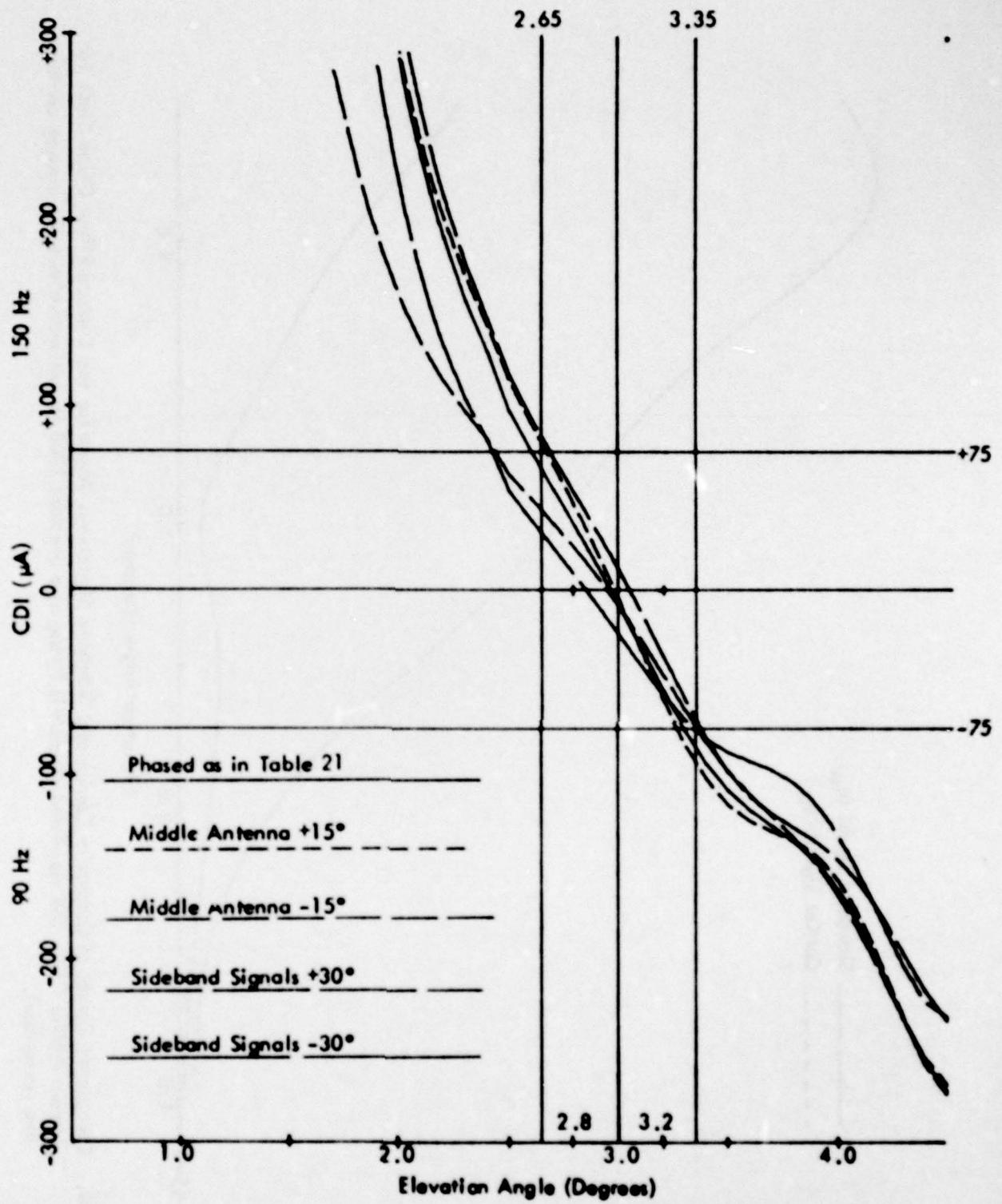
Figure 84h. Calculated Curves of CDI vs. Angle for the Capture Effect Glide Slope with the Normal Phasing (as Indicated in Table 21) and Dephased According to the Flight Inspection Manual Phase Verification Procedure for Terrain Profile #17. The simulated aircraft is flying at a constant 1000 ft. altitude above the runway centerline (extended).

-269-
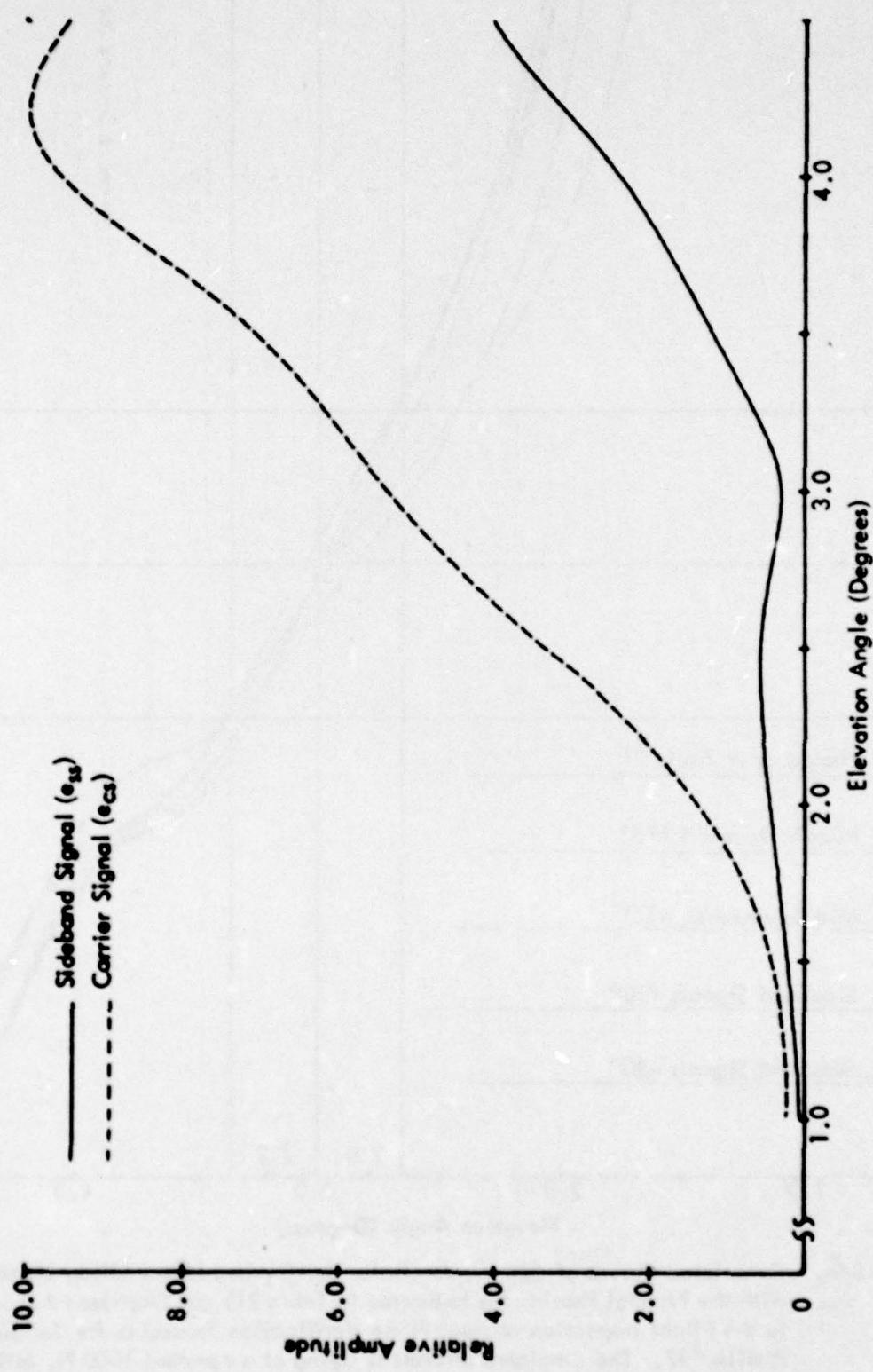
Figure 84i. Calculated Curves of Composite Carrier and Sideband Signals vs. Angle for the Capture Effect Glide Slope for Terrain Profile #17. The simulated aircraft is flying at a constant 1000 ft. altitude above the runway centerline (extended).
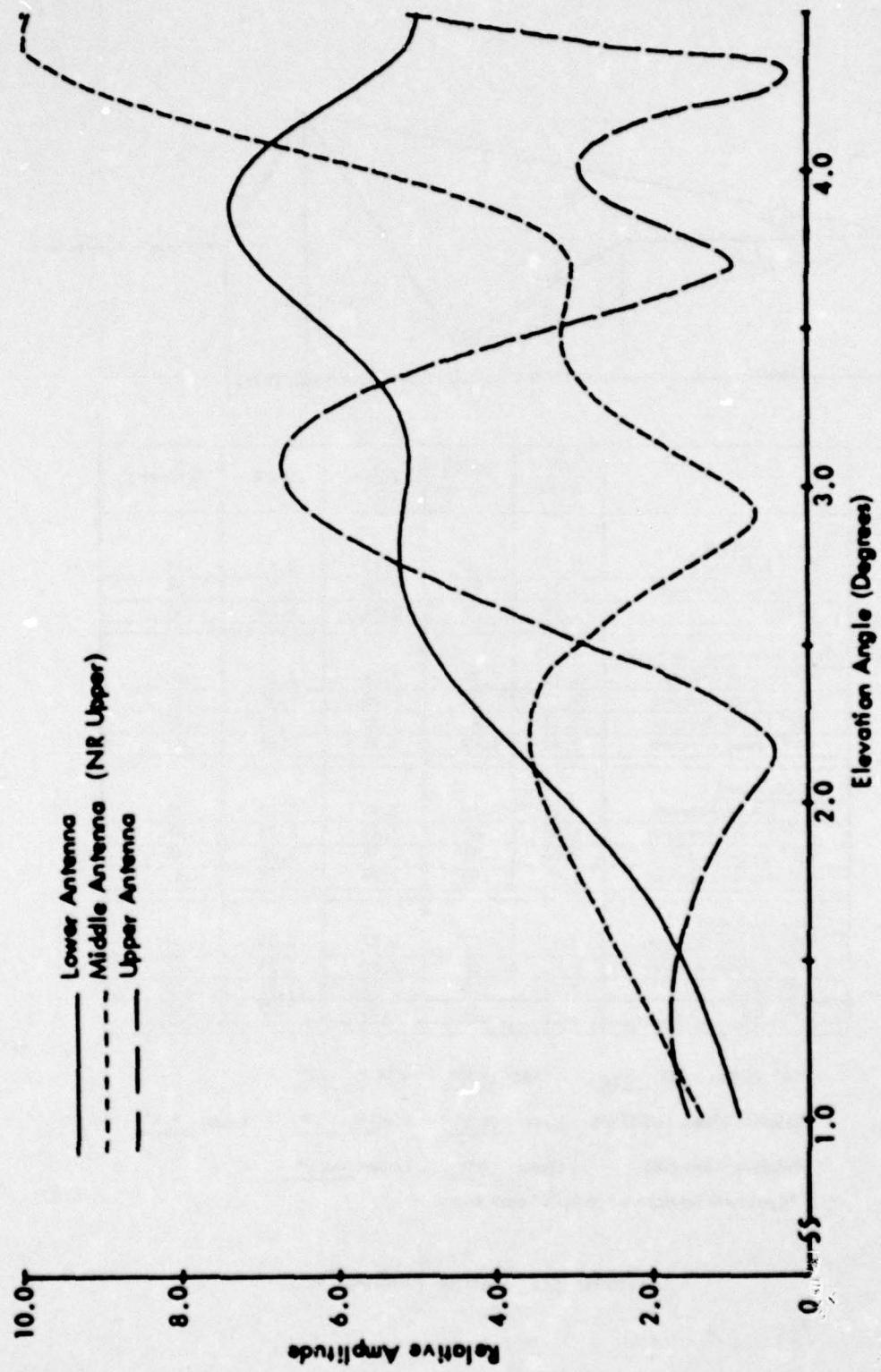
Figure 84j. Calculated Normalized Antenna Patterns vs. Angle for the Capture Effect and Null Reference Systems for Terrain Profile #17. The simulated aircraft is flying at a constant 1000 ft. altitude above the runway centerline (extended).

-271-
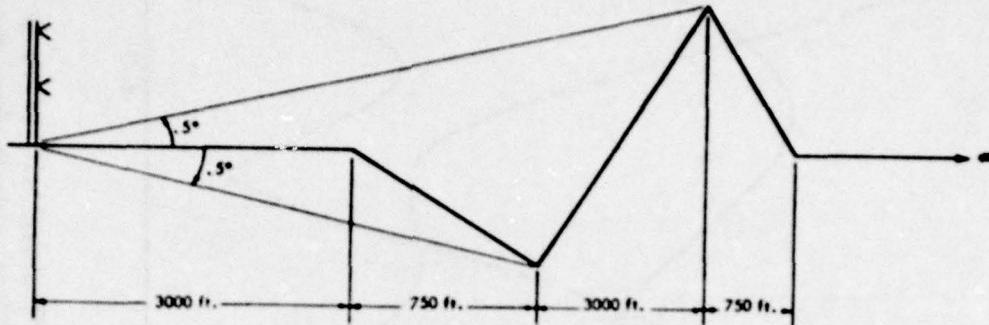
|	Path Angle	Width Angle	75 µA	75 µA	Symmetry
Normal Phasing					
Null Reference	3.16	.70	2.72	3.42	.37
Sideband Reference	3.11	.89	2.48	3.37	.29
CEGS	2.98	.70	2.64	3.34	.51
Null Reference Dephased					
+15° Lower Antenna	3.15	.78	2.72	3.50	.45
−15° Lower Antenna	3.17	.95	2.46	3.41	.25
+30° Lower Antenna	3.15	.85	2.70	3.55	.48
−30° Lower Antenna	3.18	1.09	2.45	3.55	.33
SBR Dephased					
+15° Lower Antenna	3.11	.89	2.46	3.36	.28
−15° Lower Antenna	2.90	.86	2.45	3.31	.48
+30° Lower Antenna	2.85	.89	2.38	3.28	.48
−30° Lower Antenna	2.87	.90	2.38	3.28	.45
CEGS Dephased					
+15° Middle Antenna	2.97	.77	2.57	3.35	.48
−15° Middle Antenna	3.03	.68	2.67	3.35	.47
+30° SBO	3.01	.79	2.62	3.41	.50
−30° SBO	2.96	.82	2.55	3.37	.50

"A" Ratio: NR .266   SBR .260°   CEGS .300

Relative Phase NR/CEGS   Upper −4.8°   Middle   0°   Lower +.4°

Relative Phase SBR   Upper   0°   Lower −4.0°

°Could not be adjusted to 0.70° path width.

Table 22. Terrain Profile #18.
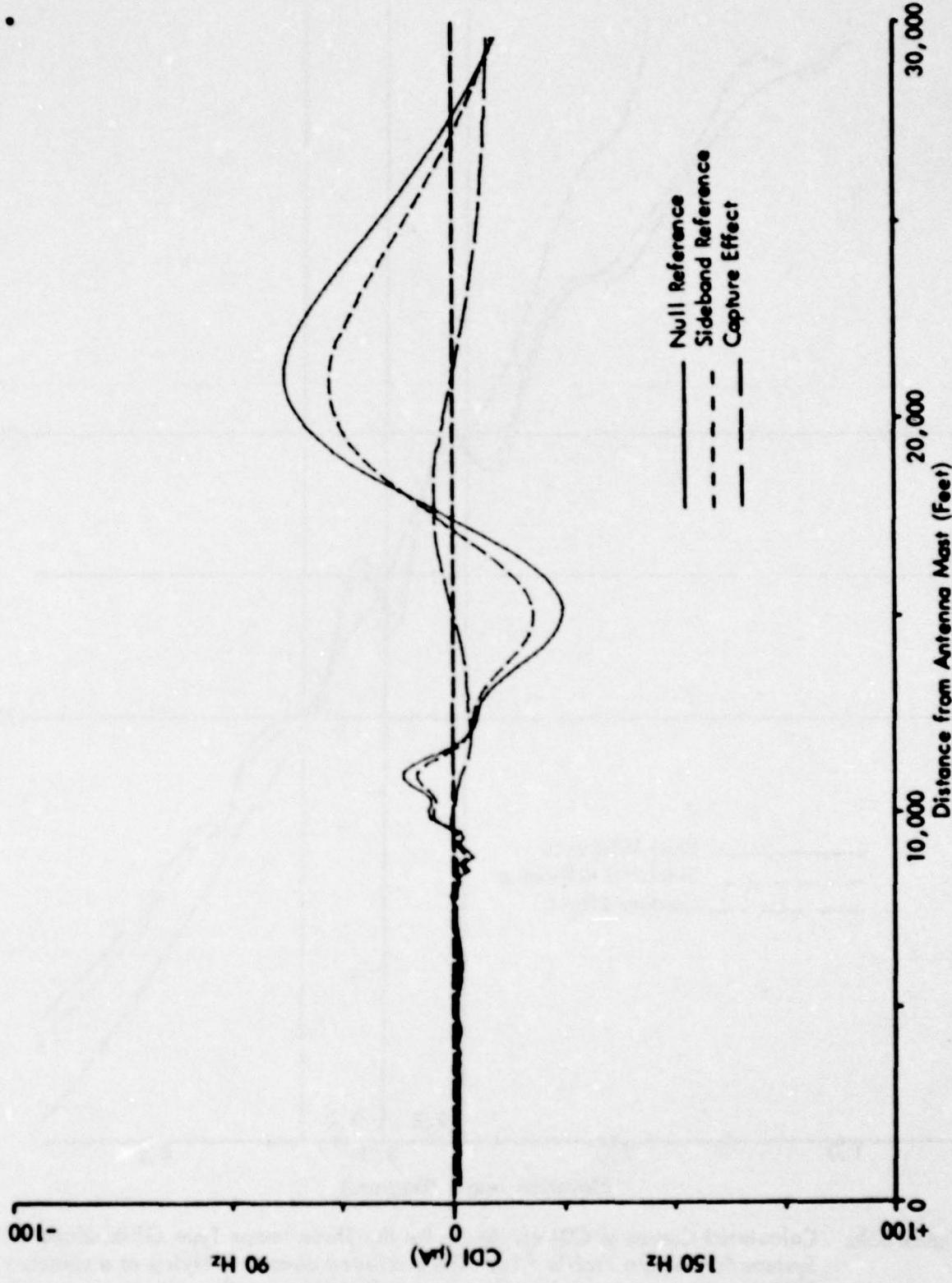
Figure 85b. Calculated Curves of CDI vs. Distance for the Three Image Type Glide-Slope Systems for Terrain Profile #18. The simulated aircraft is flying at a constant 3.0 degree low approach over the runway centerline (extended).

Figure 85b. Calculated Curves of CDI vs. Angle for the Three Image Type Glide-Slope Systems for Terrain Profile #18. The simulated aircraft is flying at a constant 1000 ft. altitude above the runway centerline (extended).

-274-
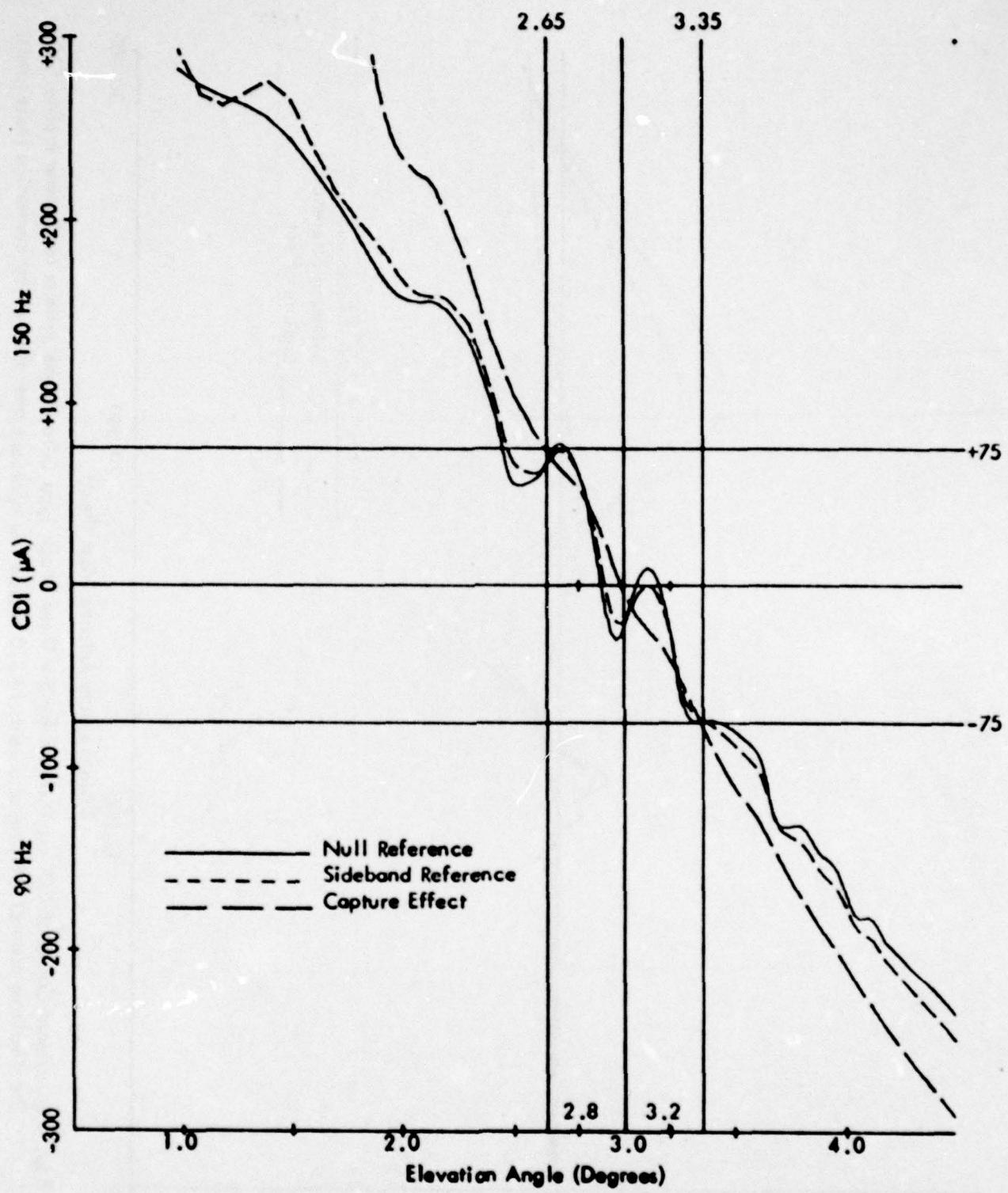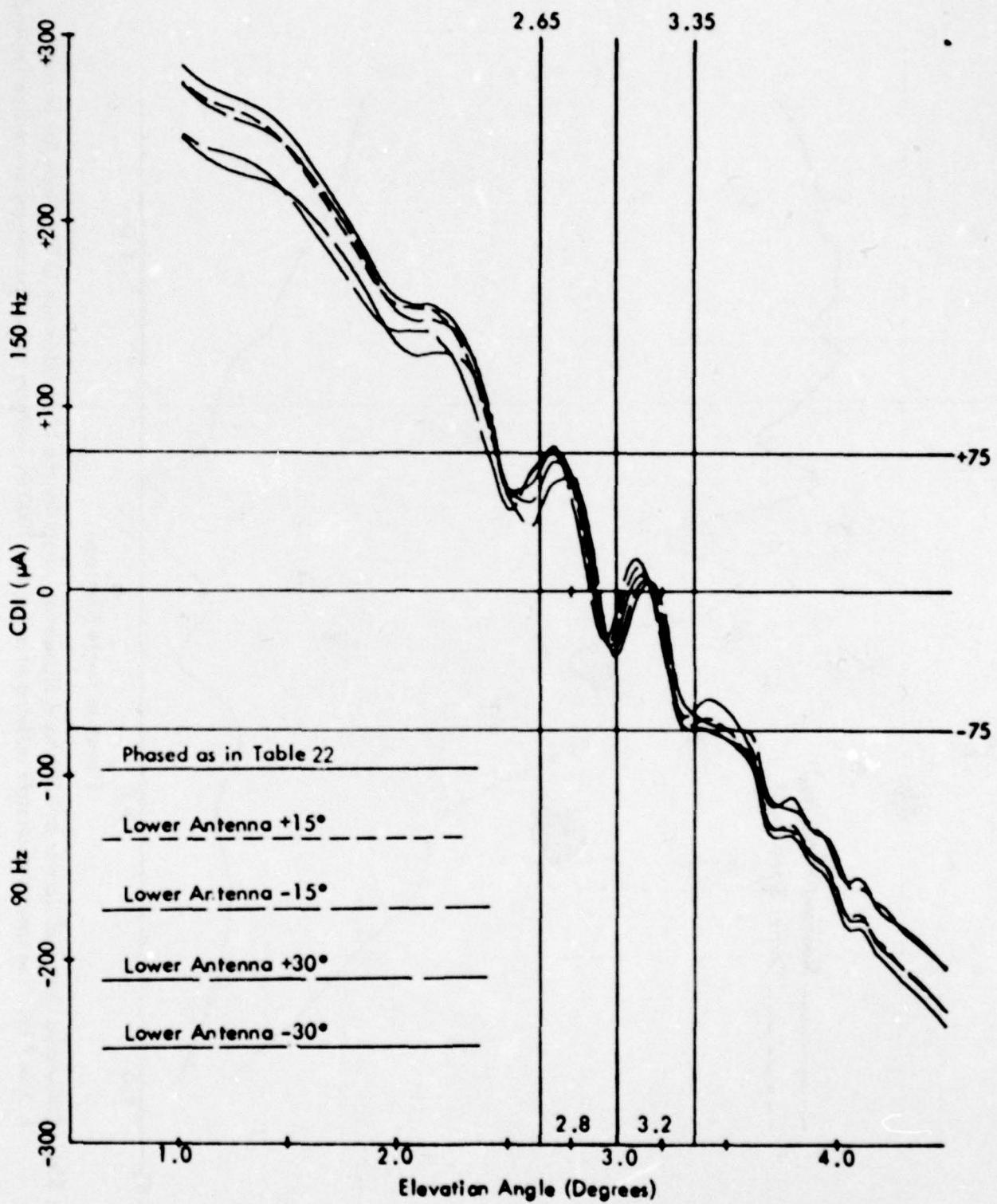
Figure 85c. Calculated Curves of CDI vs. Angle for the Null Reference Glide Slope with the Normal Phasing (as Indicated in Table 22) and Various Amounts of Dephasing for Terrain Profile #18. The simulated aircraft is flying at a constant 1000 ft. altitude above the runway centerline (extended).

-275-
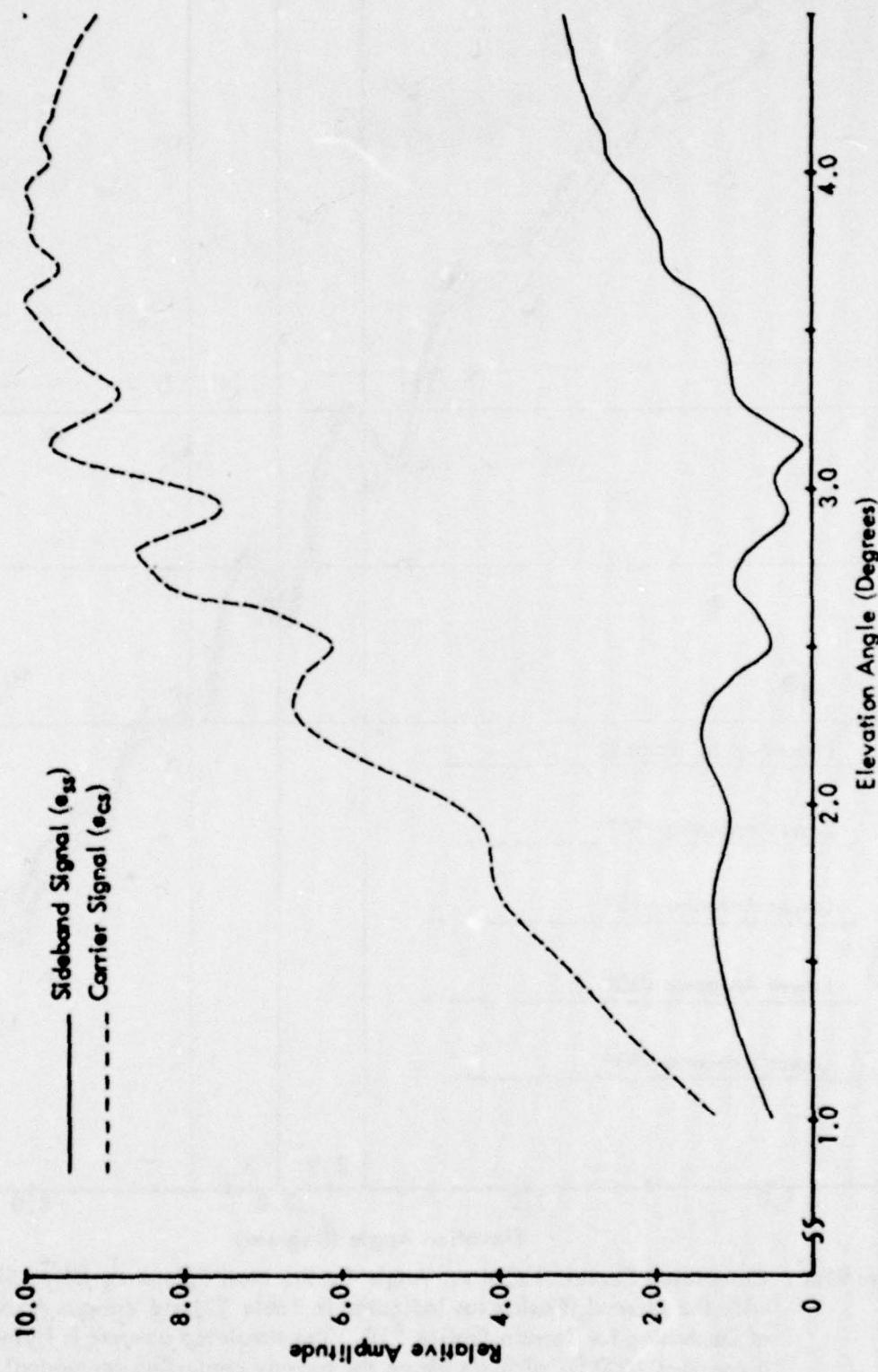
Figure 85d. Calculated Curves of Carrier and Sideband Signals vs. Angle for the Null Reference Glide Slope for Terrain Profile #18. The simulated aircraft is flying at a constant 1000 ft. altitude above the runway centerline (extended).
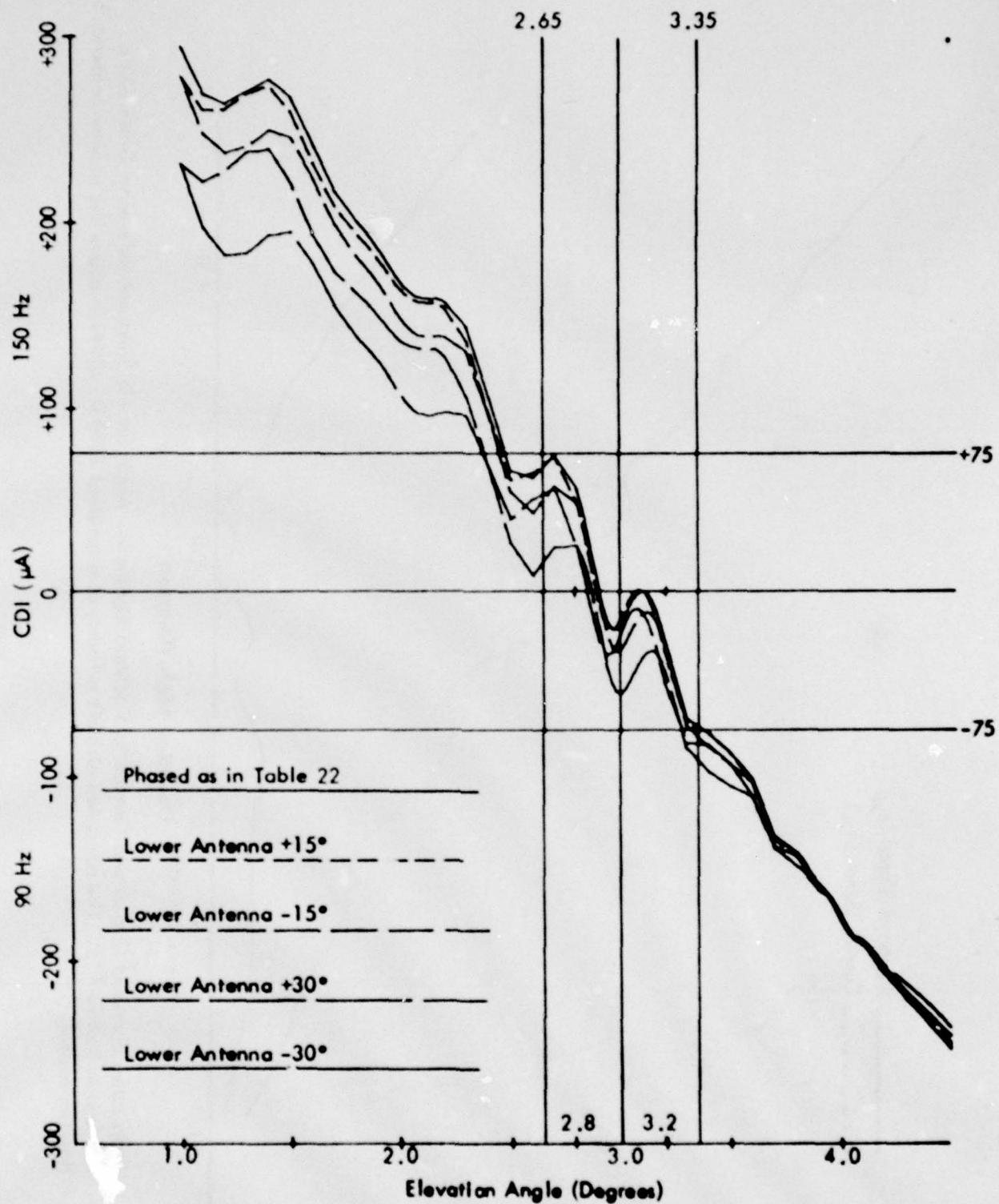
Figure 85e. Calculated Curves of CDI vs. Angle for the Sideband Reference Glide Slope with Normal Phasing (as Indicated in Table 22) and Various Amounts of Dephasing for Terrain Profile #18. The simulated aircraft is flying at a constant 1000 ft. altitude above the runway centerline (extended).

-277-
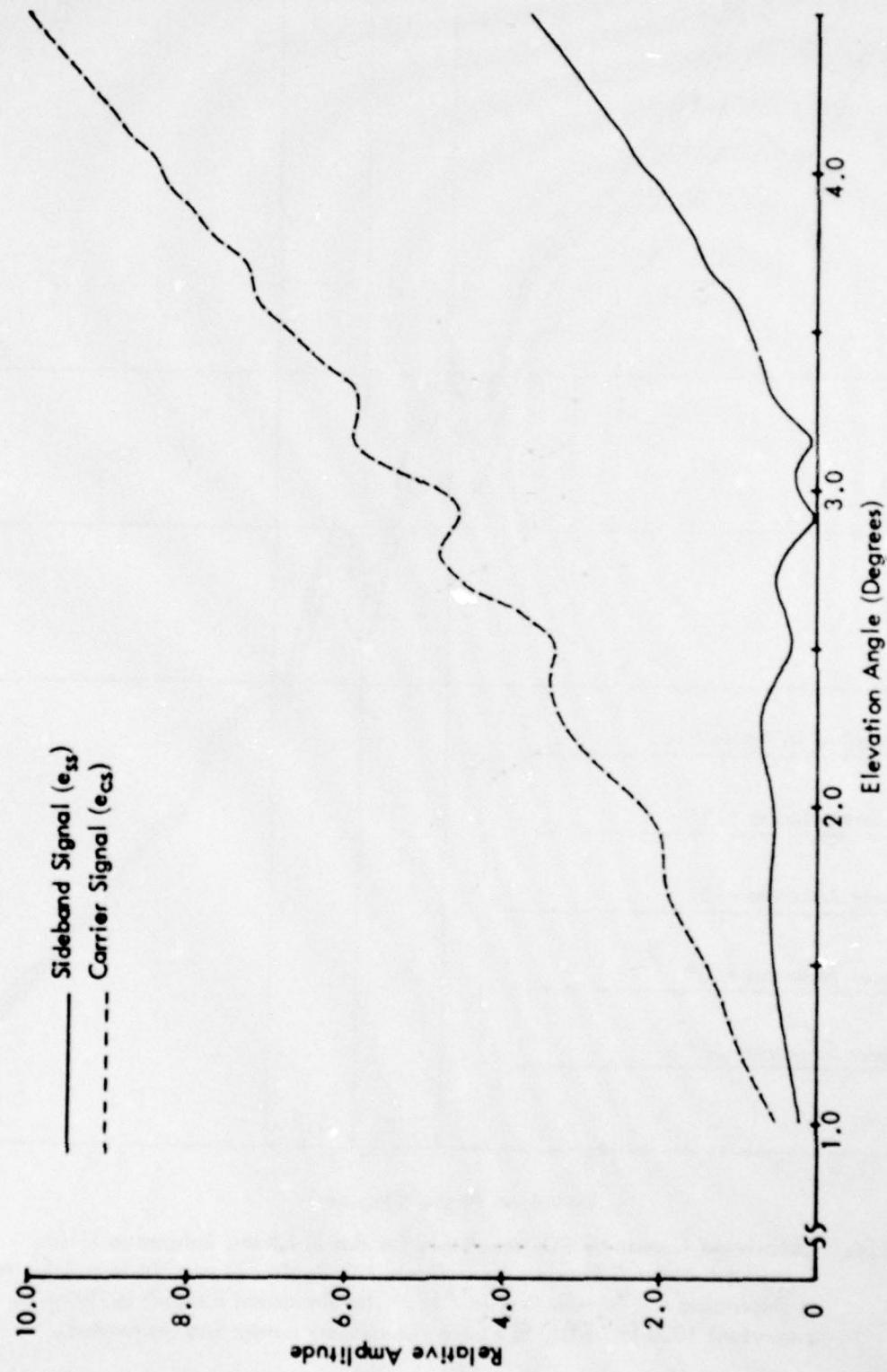
Figure 85f. Calculated Curves of Carrier and Composite Sideband Signals vs. Angle for the Sideband Reference Glide Slope for Terrain Profile #18. The simulated aircraft is flying at a constant 1000 ft. altitude above the runway centerline (extended).
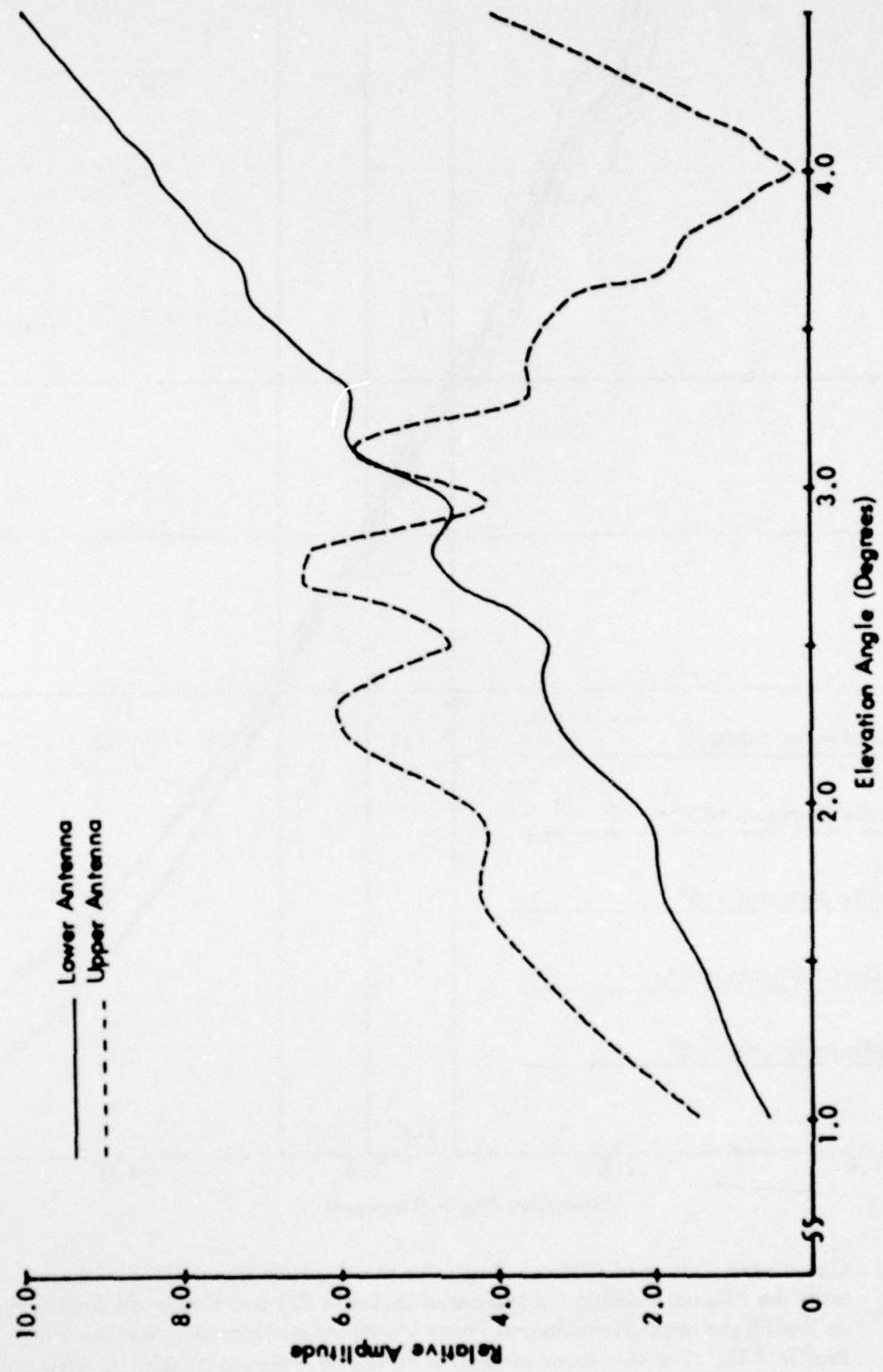
Figure 85g. Calculated Normalized Antenna Patterns vs. Angle for the Sideband Reference System for Terrain Profile #18. The simulated aircraft is flying at a constant 1000 ft. altitude above the runway centerline (extended).

-279-
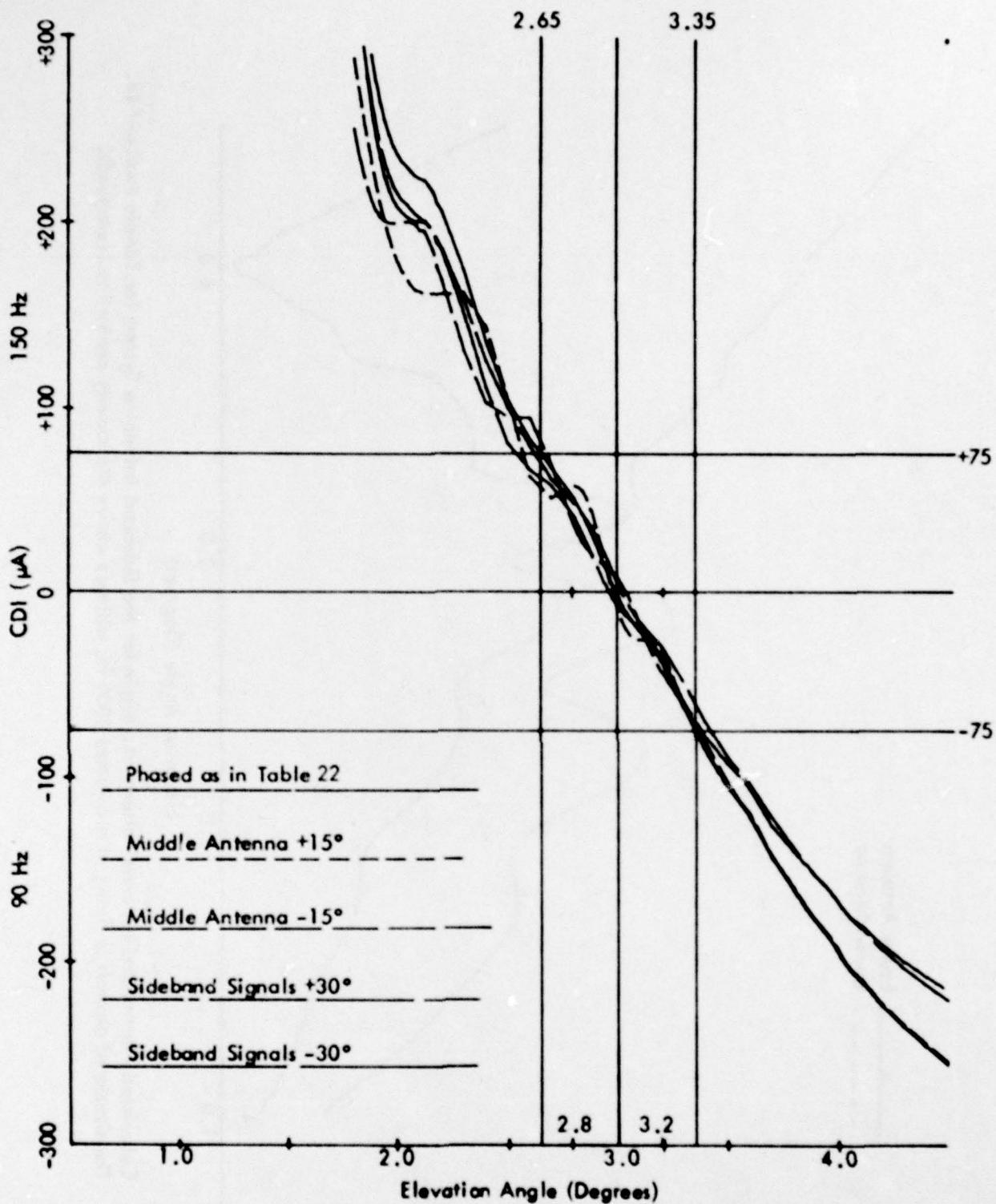
Figure 85h. Calculated Curves of CDI vs. Angle for the Capture Effect Glide Slope with the Normal Phasing (as Indicated in Table 22) and Dephased According to the Flight Inspection Manual Phase Verification Procedure for Terrain Profile #18. The simulated aircraft is flying at a constant 1000 ft. altitude above the runway centerline (extended).

-280-
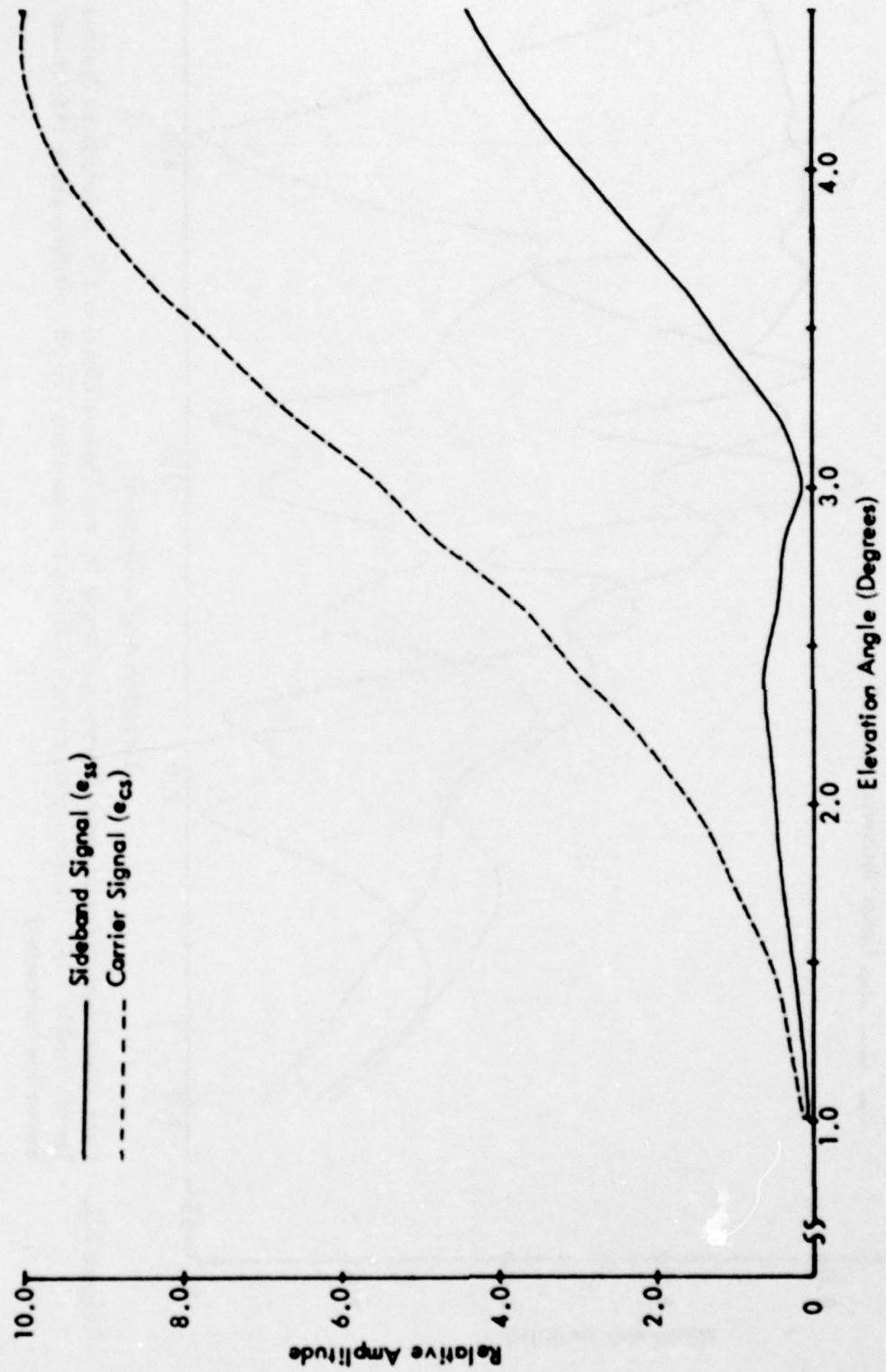
Figure 85i. Calculated Curves of Composite Carrier and Sideband Signals vs. Angle for the Capture Effect Glide Slope for Terrain Profile #18. The simulated aircraft is flying at a constant 1000 ft. altitude above the runway center-line (extended).

Figure 85j. Calculated Normalized Antenna Patterns vs. Angle for the Capture Effect and Null Reference Systems for Terrain Profile #18. The simulated aircraft is flying at a constant 1000 ft. altitude above the runway centerline (extended).

-282-
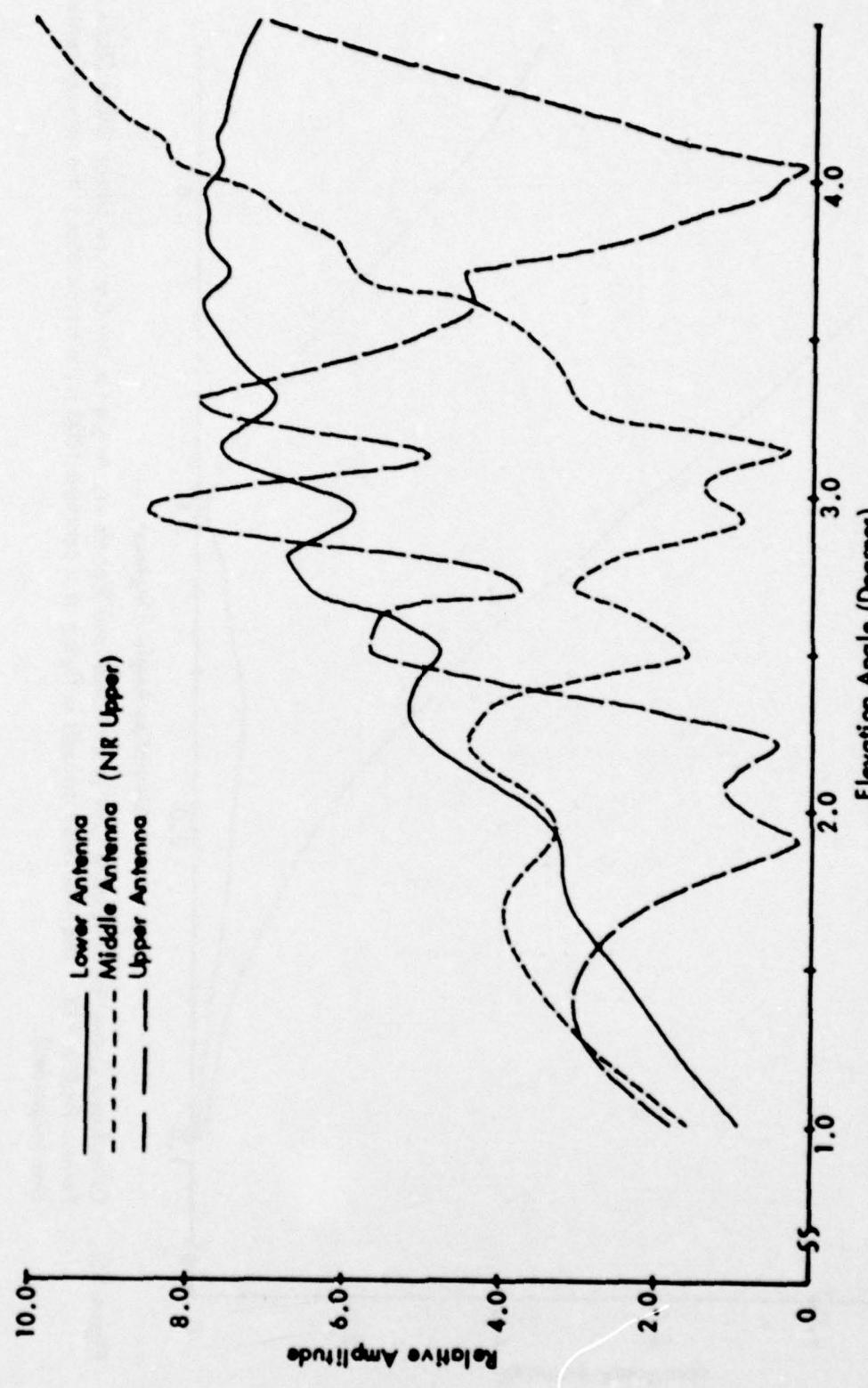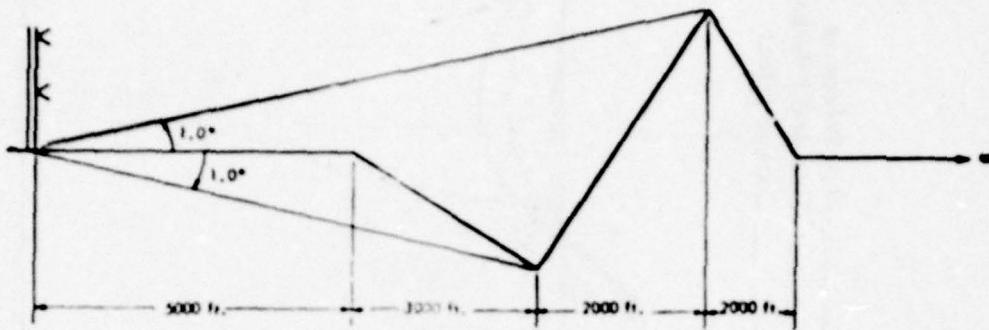
	Path Angle	Width Angle	+75 µA	-75 µA	Symmetry
Normal Phasing					
Null Reference	3.03	.77	2.65	3.42	.50
Sideband Reference	3.03	.69	2.65	3.33	.44
CEGS	3.00	.70	2.65	3.34	.49
Null Reference Dephased					
+15° Lower Antenna	3.03	.78	2.64	3.42	.50
-15° Lower Antenna	3.04	.76	2.66	3.42	.50
+30° Lower Antenna	3.03	.90	2.61	3.51	.54
-30° Lower Antenna	3.05	.78	2.65	3.43	.50
SBR Dephased					
+15° Lower Antenna	2.89	.73	2.59	3.32	.59
-15° Lower Antenna	3.03	.69	2.65	3.34	.44
+30° Lower Antenna	2.81	.87	2.32	3.19	.43
-30° Lower Antenna	2.90	.85	2.48	3.33	.50
CEGS Dephased					
+15° Middle Antenna	2.98	.68	2.66	3.35	.54
-15° Middle Antenna	3.00	.77	2.58	3.36	.46
+30° SBO	3.06	.77	2.67	3.44	.50
-30° SBO	2.92	.90	2.47	3.37	.50

"A" Ratio: NR .300°   SBR .296°   CEGS .310

Relative Phase NR/CEGS Upper -7.2°   Middle 0°   Lower +4.7°

Relative Phase SBR   Upper 0°   Lower +7.3°

°Could not be adjusted to 0.70° path width.

Table 23. Terrain Profile #19.
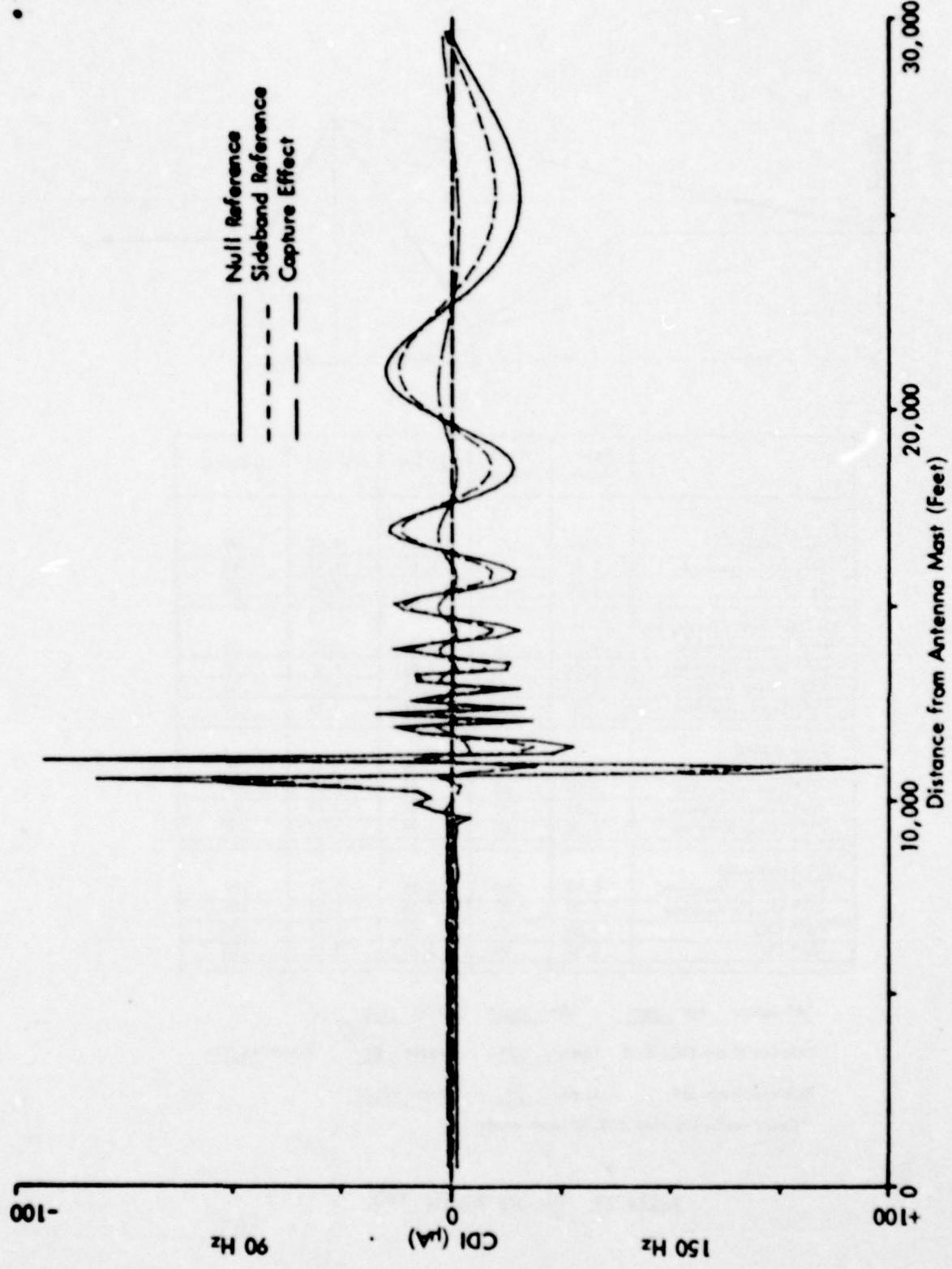
Figure 86a. Calculated Curves of CDI vs. Distance for the Three Image Type Glide Slope Systems for Terrain Profile #19. The simulated aircraft is flying at a constant 3.0 degree low approach over the runway centerline (extended).
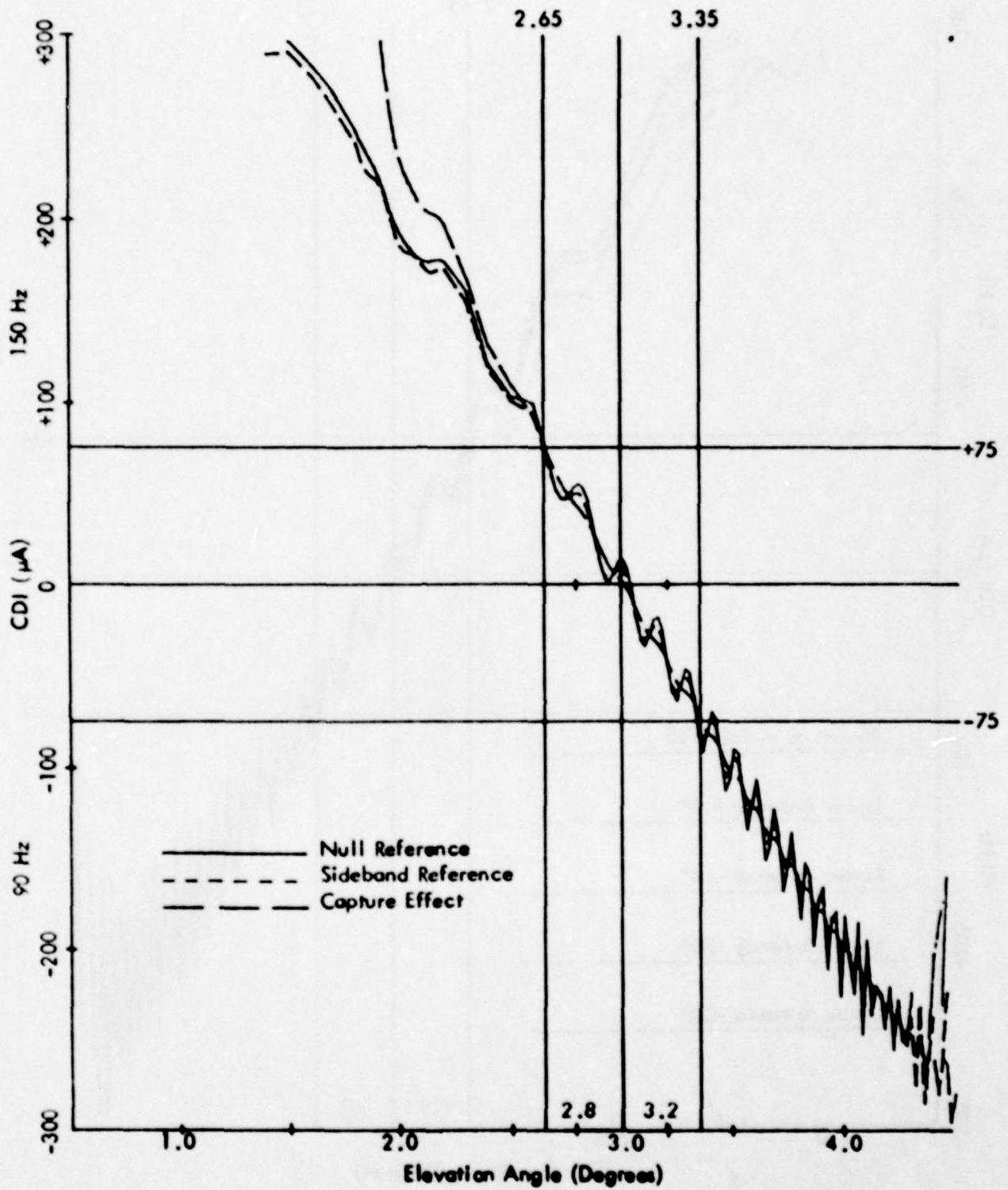
Figure 86b. Calculated Curves of CDI vs. Angle for the Three Image Type Glide-Slope Systems for Terrain Profile #19. The simulated aircraft is flying at a constant 1000 ft. altitude above the runway centerline (extended).
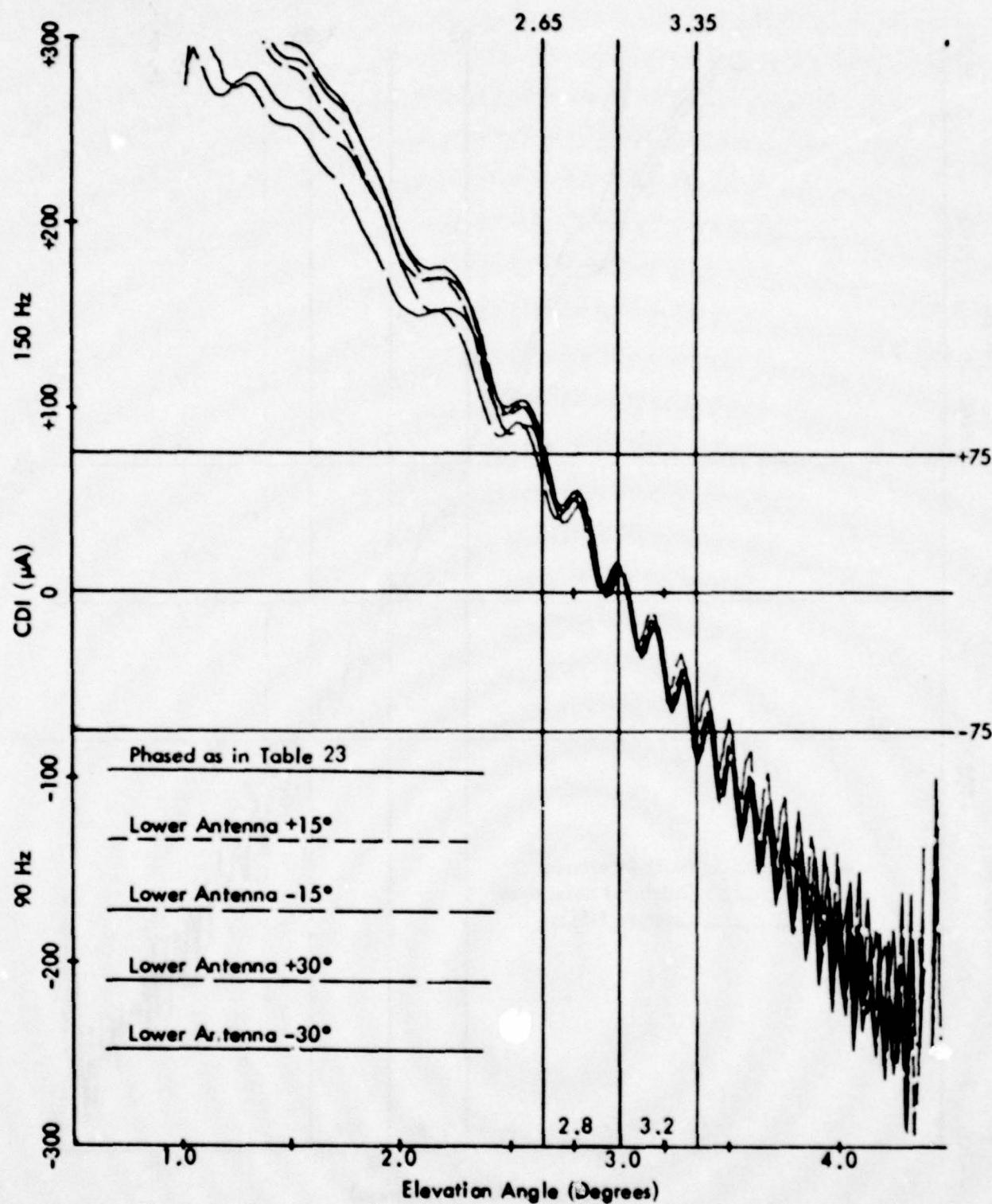
Figure 86c. Calculated Curves of CDI vs. Angle for the Null Reference Glide Slope with the Normal Phasing (as Indicated in Table 23) and Various Amounts of Dephasing for Terrain Profile #19. The simulated aircraft is flying at a constant 1000 ft. altitude above the runway centerline (extended).
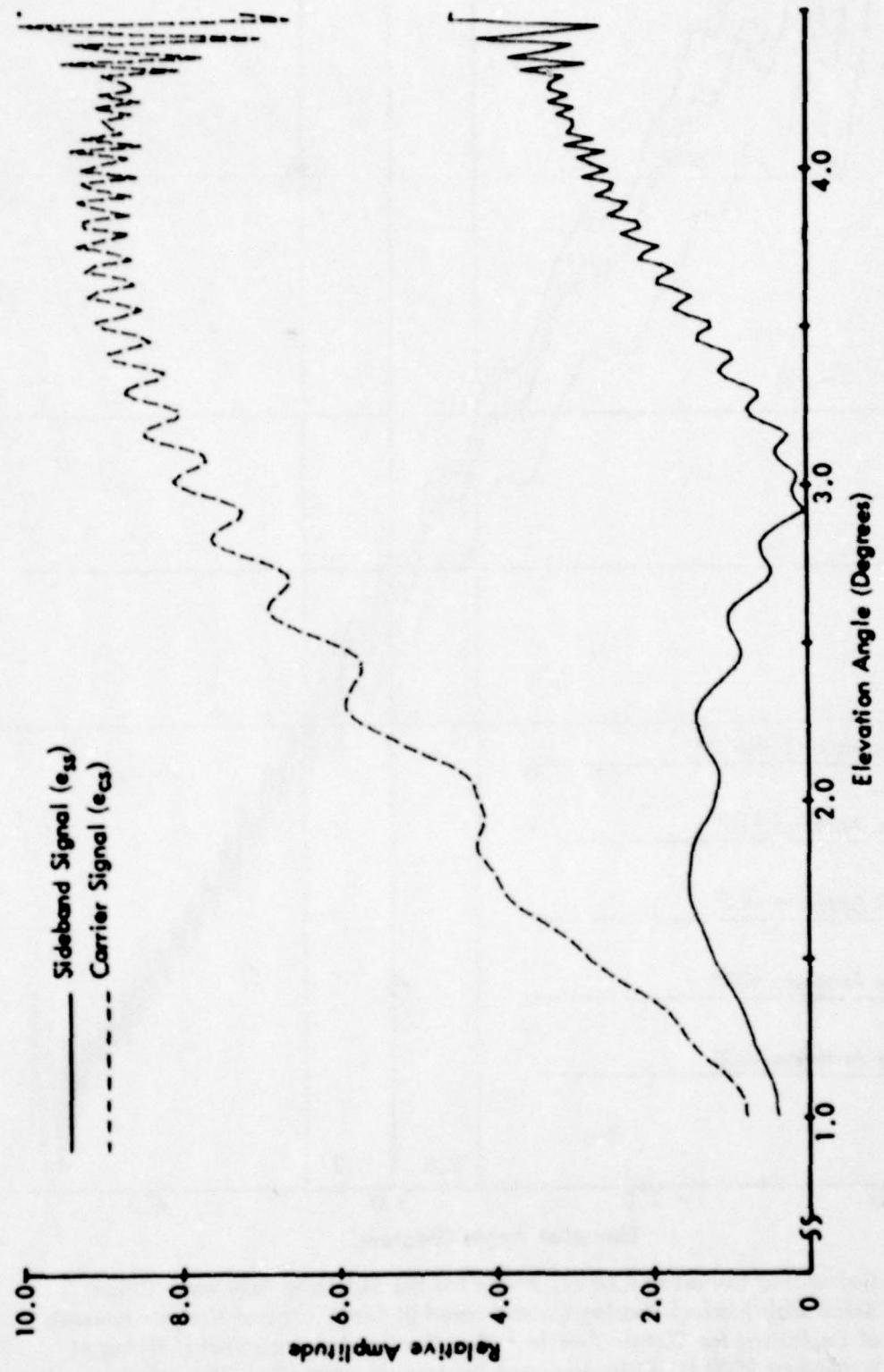
Figure 86d. Calculated Curves of Carrier and Sideband Signals vs. Angle for the Null Reference Glide Slope for Terrain Profile #19. The simulated aircraft is flying at a constant 1000 ft. altitude above the runway centerline (extended).
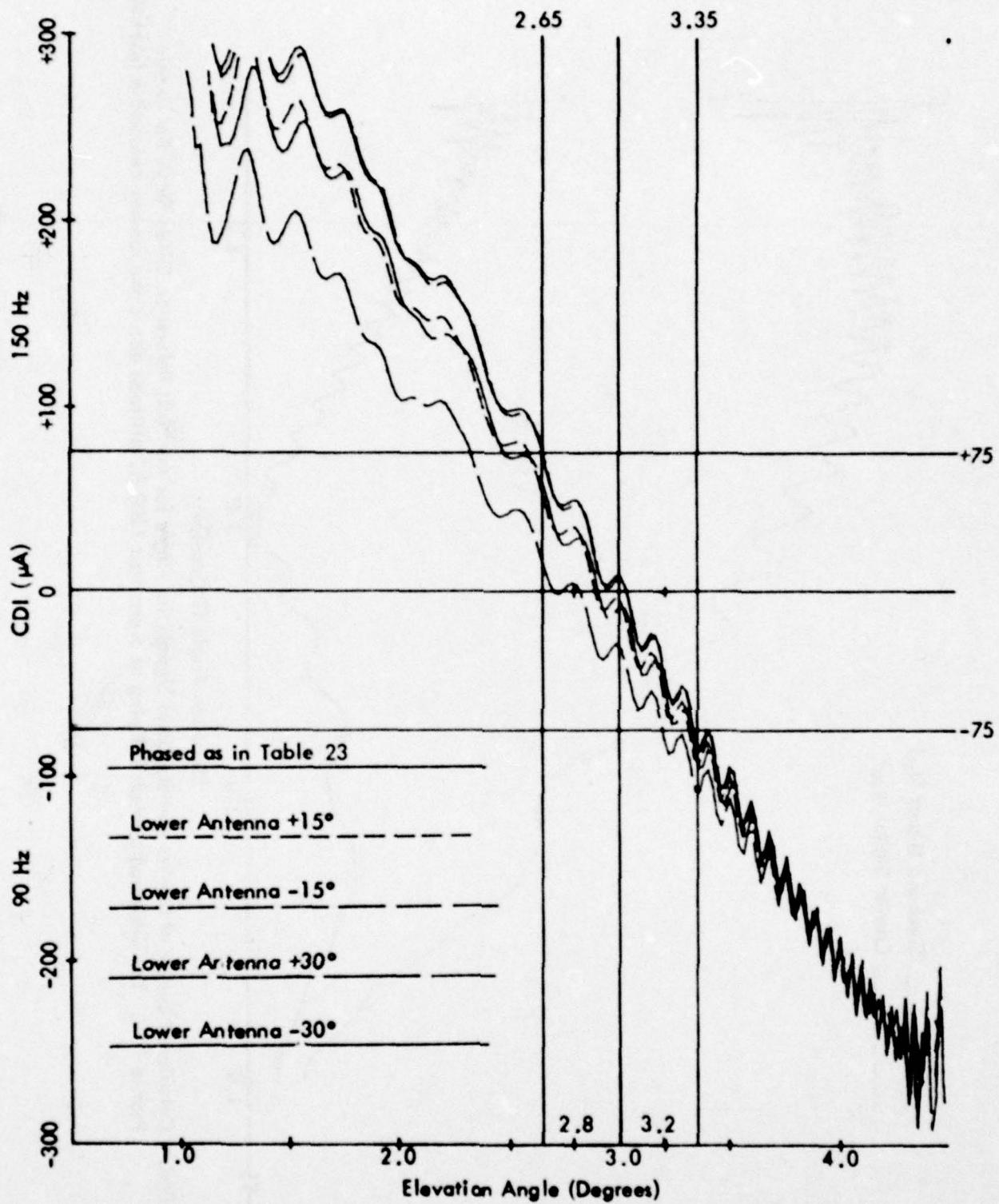
Figure 86e. Calculated Curves of CDI vs. Angle for the Sideband Reference Glide Slope with Normal Phasing (as Indicated in Table 23) and Various Amounts of Dephasing for Terrain Profile #19. The simulated aircraft is flying at a constant 1000 ft. altitude above the runway centerline (extended).
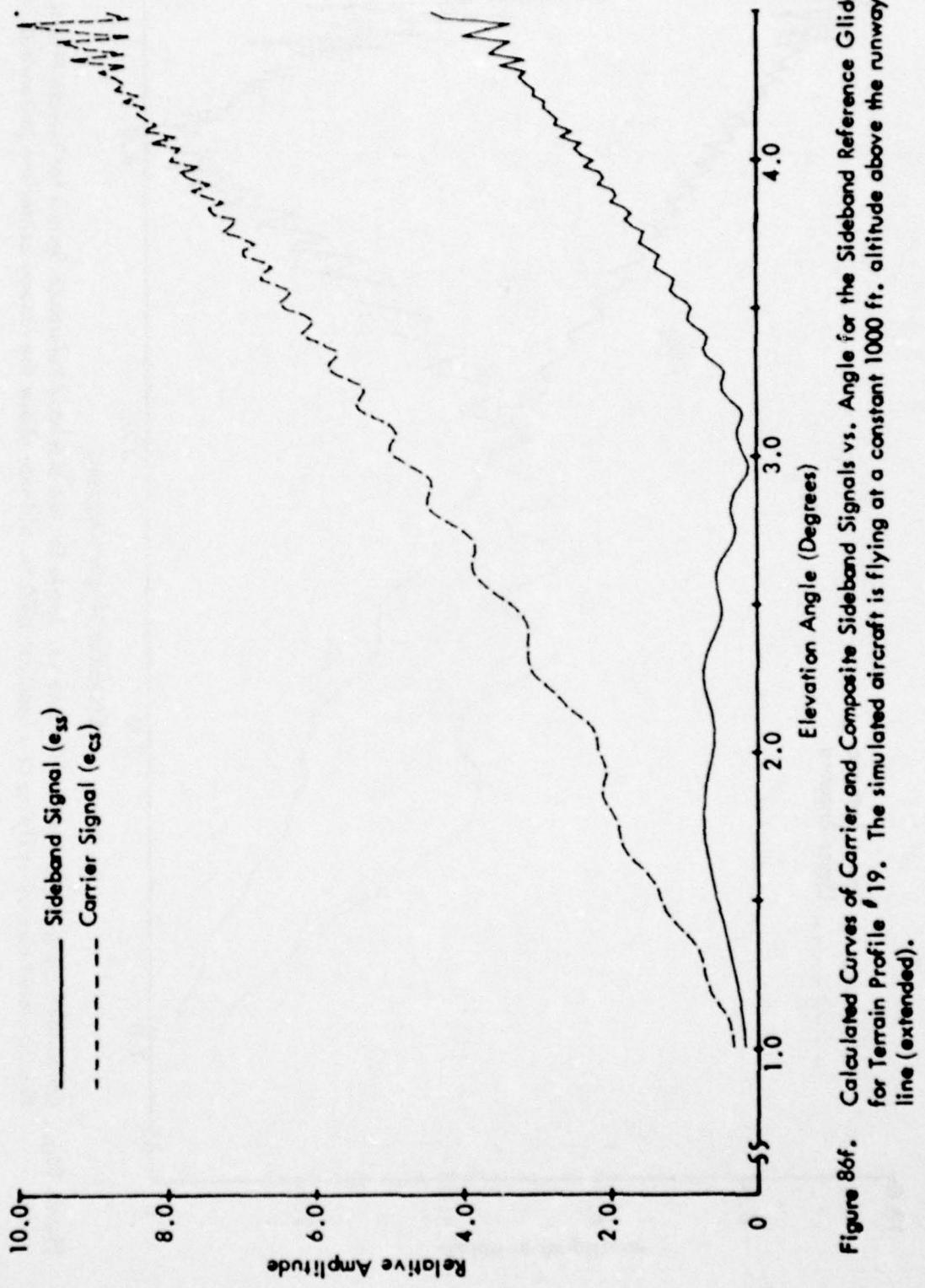
Figure 86f. Calculated Curves of Carrier and Composite Sideband Signals vs. Angle for the Sideband Reference Glide Slope for Terrain Profile #19. The simulated aircraft is flying at a constant 1000 ft. altitude above the runway centerline (extended).
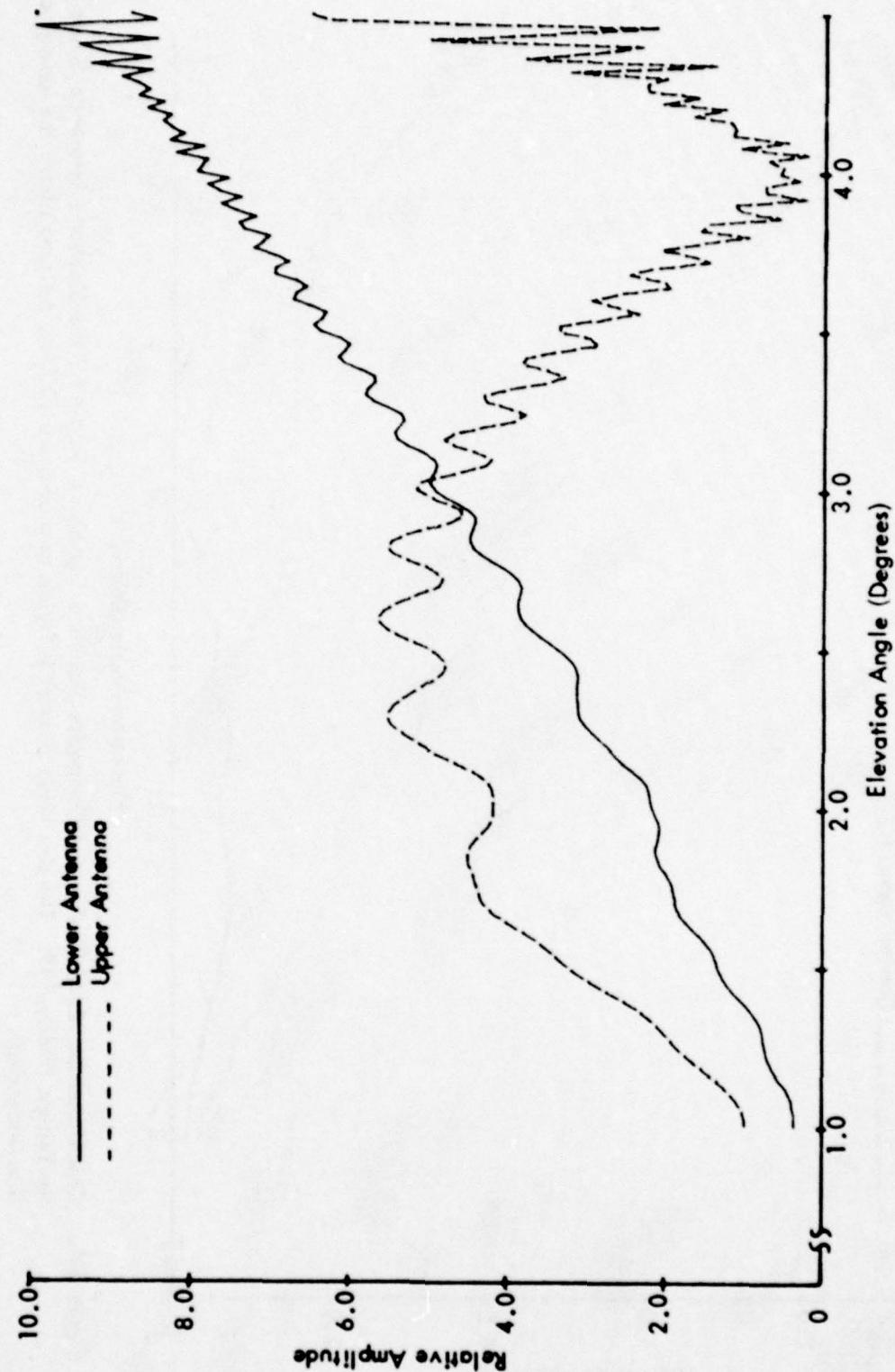
Figure 86g. Calculated Normalized Antenna Patterns vs. Angle for the Sideband Reference System for Terrain Profile #19. The simulated aircraft is flying at a constant 1000 ft. altitude above the runway centerline (extended).
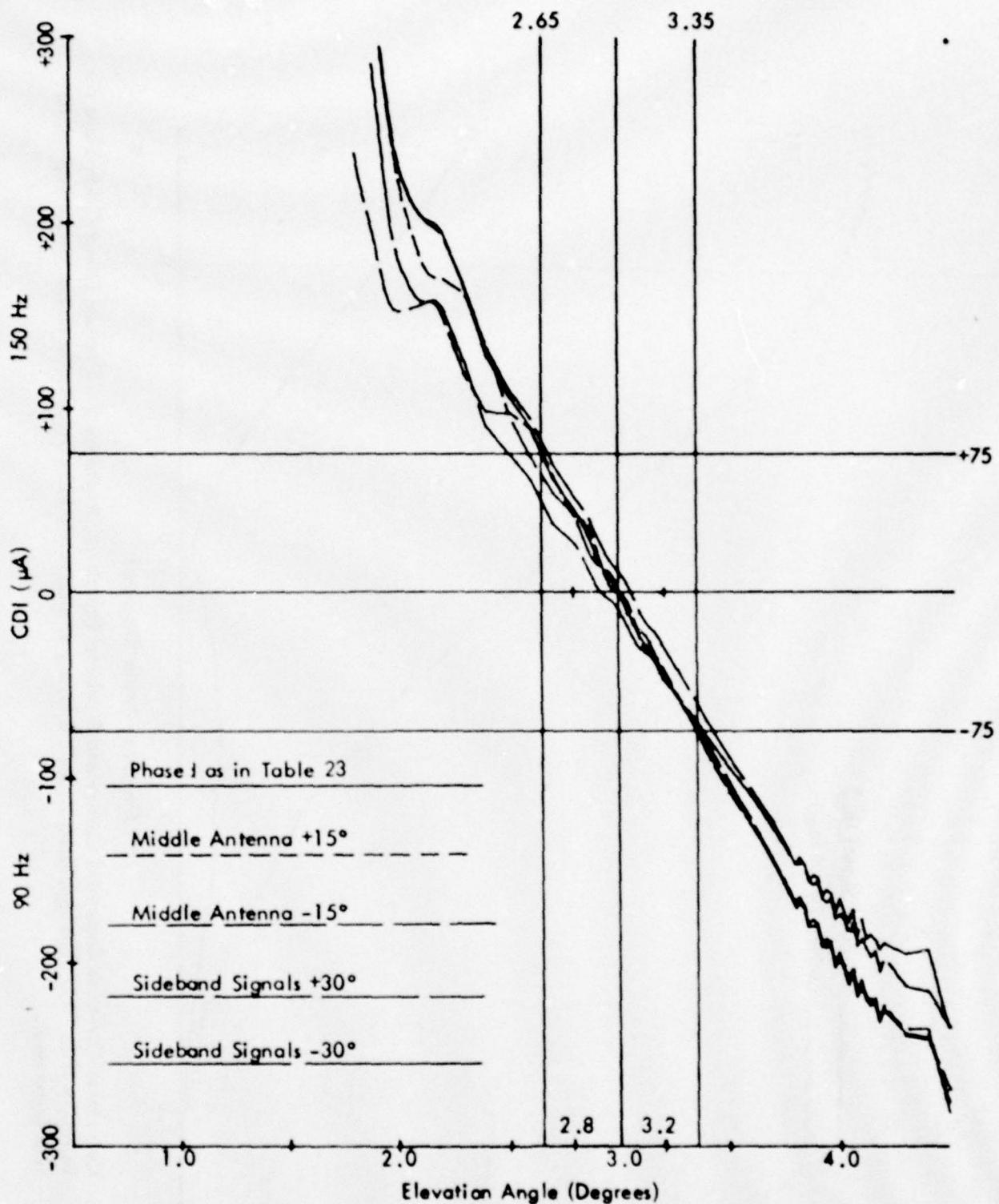
Figure 86h. Calculated Curves of CDI vs. Angle for the Capture Effect Glide Slope with the Normal Phasing (as Indicated in Table 23) and Dephased According to the Flight Inspection Manual Phase Verification Procedure for Terrain Profile #19. The simulated aircraft is flying at a constant 1000 ft. altitude above the runway centerline (extended).
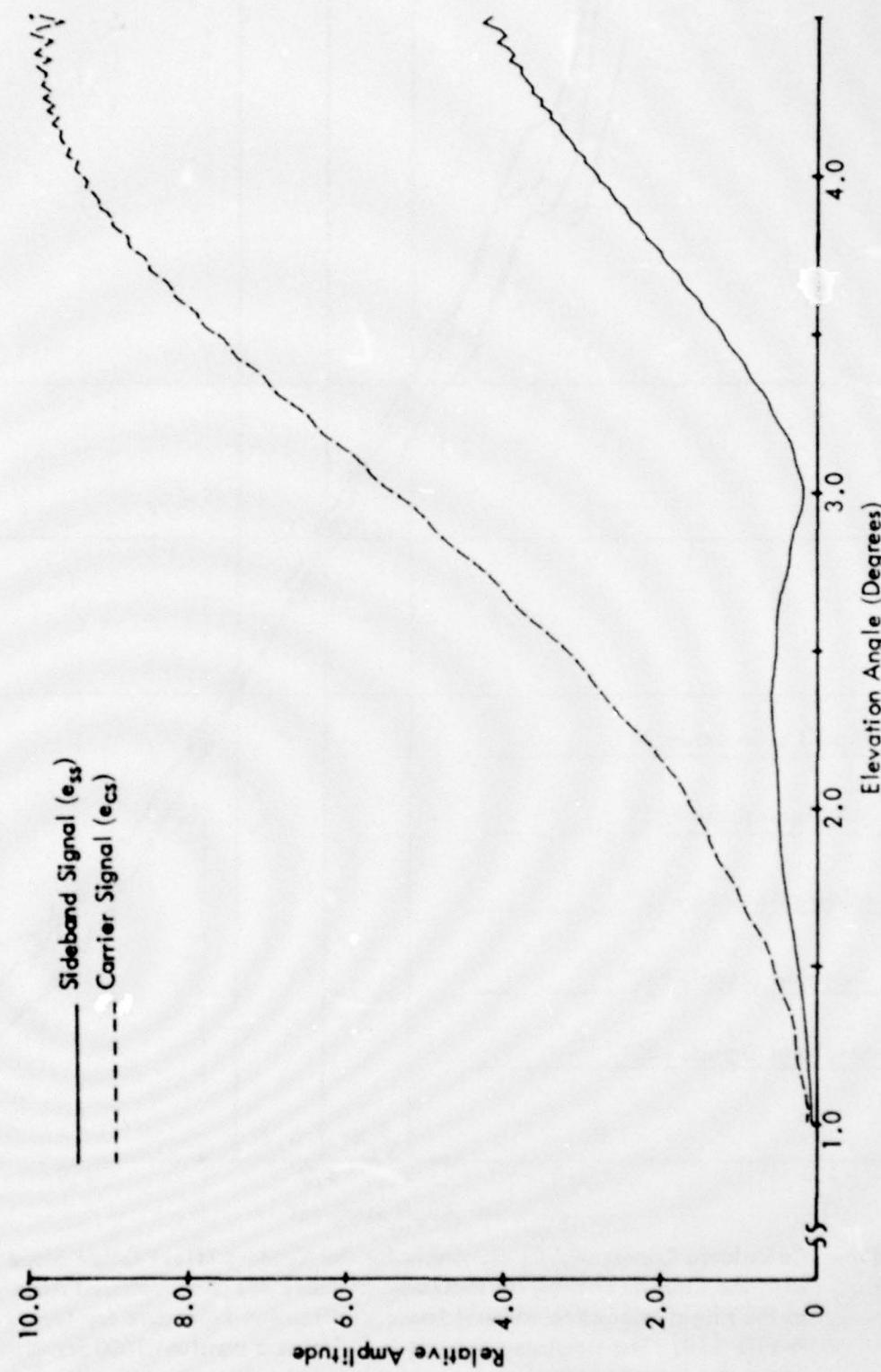
Figure 86i. Calculated Curves of Composite Carrier and Sideband Signals vs. Angle for the Capture Effect Glide Slope for Terrain Profile #19. The simulated aircraft is flying at a constant 1000 ft. altitude above the runway centerline (extended).
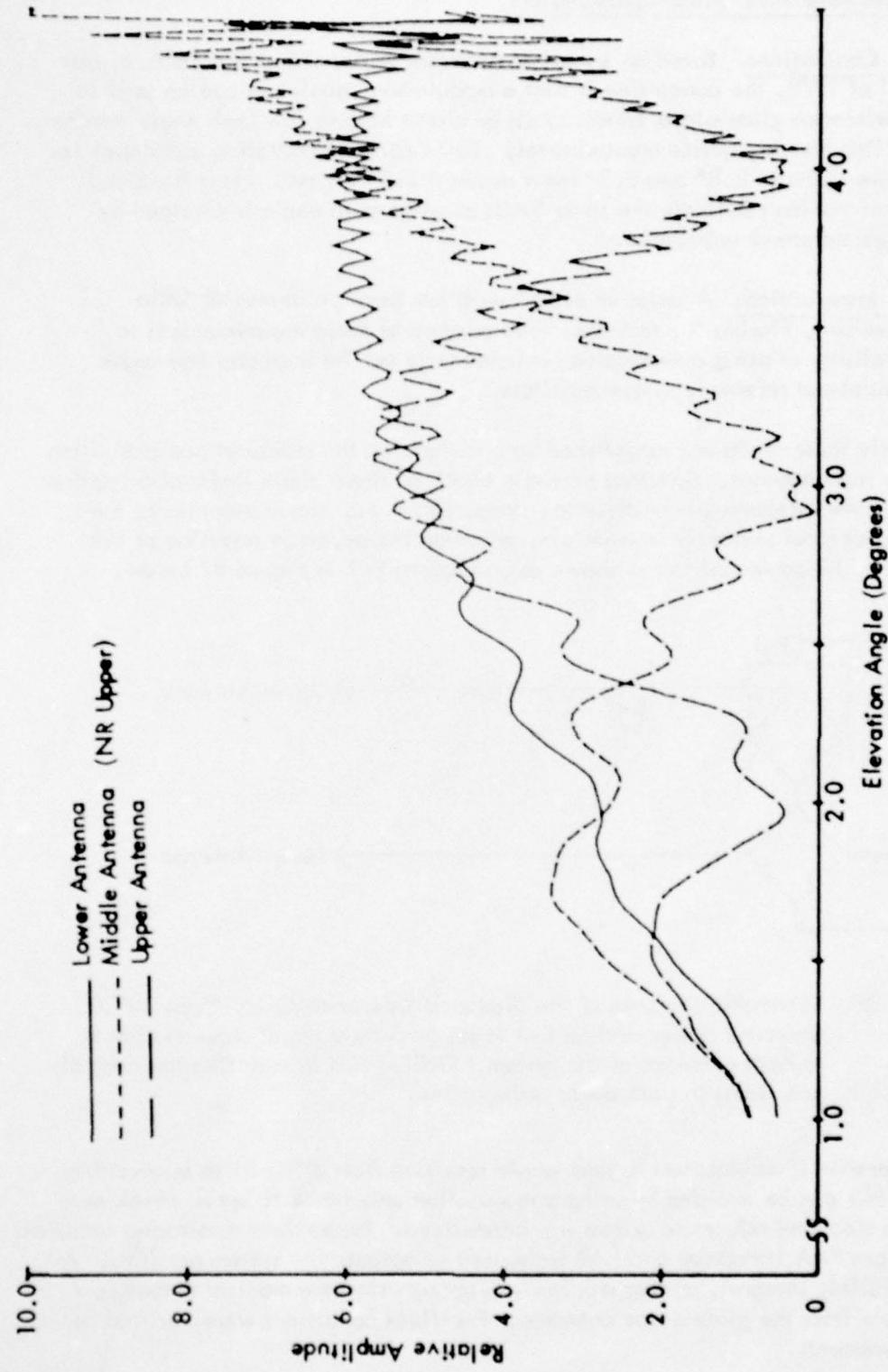
Figure 86j.   Calculated Normalized Antenna Patterns vs. Angle for the Capture Effect and Null Reference Systems for Terrain Profile #19. The simulated aircraft is flying at a constant 1000 ft. altitude above the runway centerline (extended).

D. The Use of Modulation Unbalance to Establish Path Angle Alarm Limits for the Sideband Reference Glide-Slope System.

1. Conclusions. Based on experimental work performed at the Tamiami test site in the Fall of 1978, the conclusion is that a modulation unbalance can be used in the sideband reference glide-slope system to set or check high or low path angle monitor alarm limits. This check requires approximately .050 DDM of modulation unbalance to reach path angle limits of 2.8° and 3.2° for a nominal 3.0° system. Near field and analog, integral monitors indicate the same limits as when path angle is changed by means of a sideband power unbalance.

2. Introduction. A series of experiments has been performed at Ohio University's Tamiami, Florida ILS test site. The purpose of these experiments is to establish the validity of using a modulation unbalance to set the high and low angle limits for the sideband reference system monitors.

Presently these limits are established by unbalancing the sideband power division to the system's two antennas. Required periodic check of these alarm limits also requires the changing of the sideband power division. Vagaries, i.e., inconsistencies in the power-splitting devices presently in wide use, preclude the accurate resetting of this power division. The power splitter is shown as component E-1 in Figure 87 below.
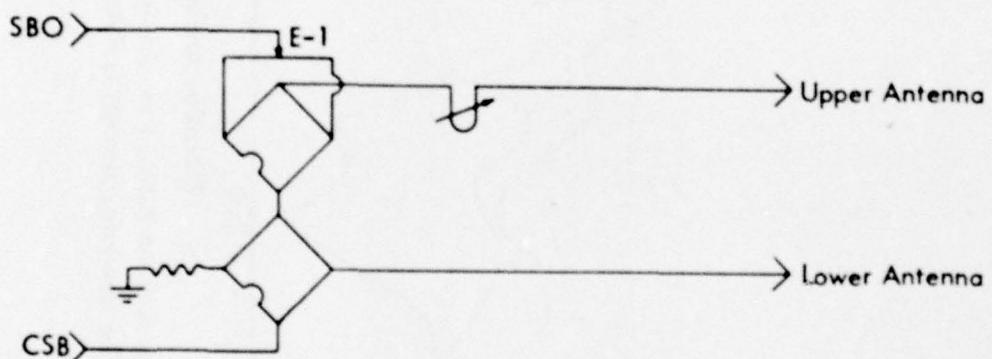
Figure 87. Schematic Diagram of the Sideband Reference Glide-Slope APCU. Sideband power divider E-1 is set to deliver equal sideband power to both antennas of the system. Difficulties in resetting the control can result in path angle ambiguities.

To determine if ambiguities in path angle resulting from difficulties in resetting this power splitter can be avoided by using a modulation unbalance to set or check path alarm limits, a sideband reference system was normalized. Near-field monitoring locations established as per FAA Handbook 6750.6B were used to operate the system monitors. As a check, a parallel, integral, analog monitor was set up using the monitor output port signals available from the glide-slope antennas. Far-field conditions were verified by airborne measurements.

Alarm limits for both sets of monitors were established by conventional methods with the high and low angle alarms determined by a suitable change in sideband power division. Broad and sharp path width alarms were set using a sideband power level change. Airborne checks verified these settings. The system was then brought into high and low angle alarm using a modulation unbalance and the far-field checked for proper path angles.

3. Discussion of Data. The SBR system established at Tamiami for these tests uses Wilcox Mark 1C transmitting and monitor equipment. The antennas used are APC Type FA-8976 glide-slope antennas positioned 7.09' (2.161m) and 21.27' (6.483m) above ground level as shown in Figure 88. Near-field monitor locations established as per 6750.6B were approximately 66' (20.1m) in front of the tower for the amplitude detector and 79' (24.1m) for the phase detector. These are shown in Figure 89. The detectors were located in the protective boxes at the base of each near-field probe with signal lines run back to the glide-slope hut to operate the system near-field monitors.

In addition to the conventional near-field monitoring, an integral analog monitor system was implemented. Signals available from the monitor port of the antennas were used for the integral analog RF recombining network shown in Figure 90. Alignment of the integral monitor was accomplished with a procedure outlined in Section 11B3 of this report.
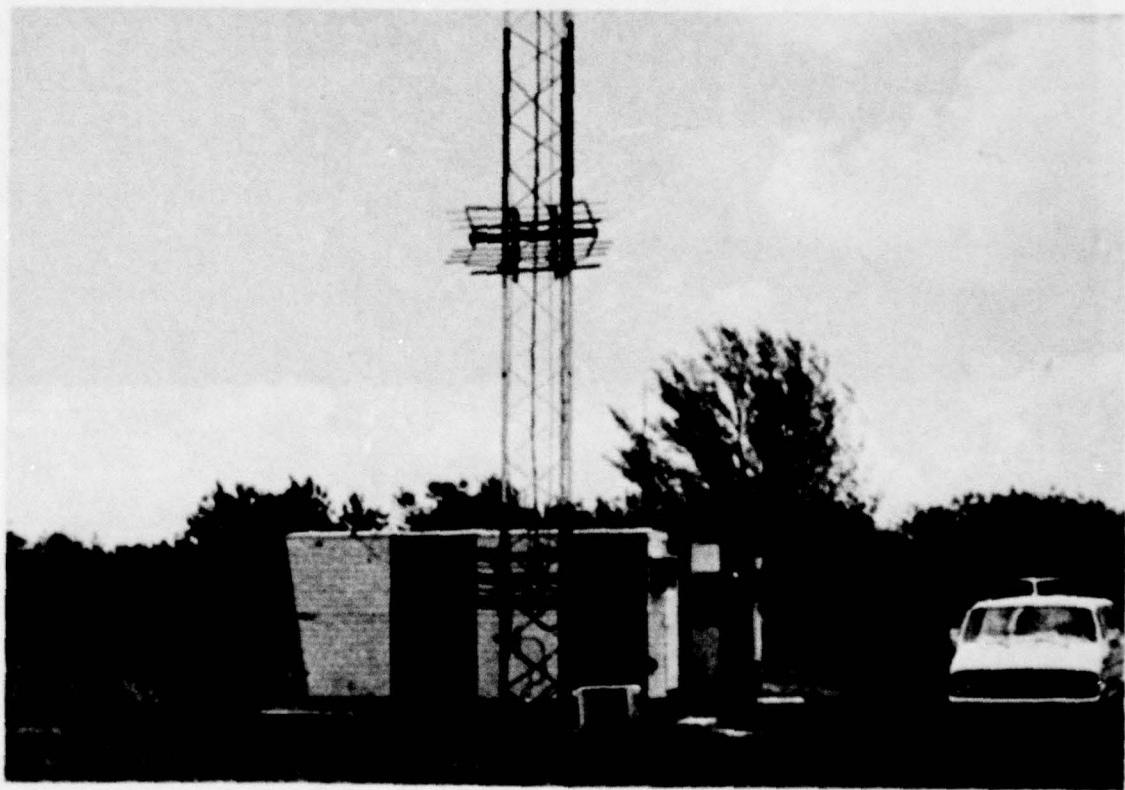
Figure 88. View of the Antenna System and Glide-Slope Hut Used for the SBR Tests at Ohio University's Tamiami Test Site.

-295-
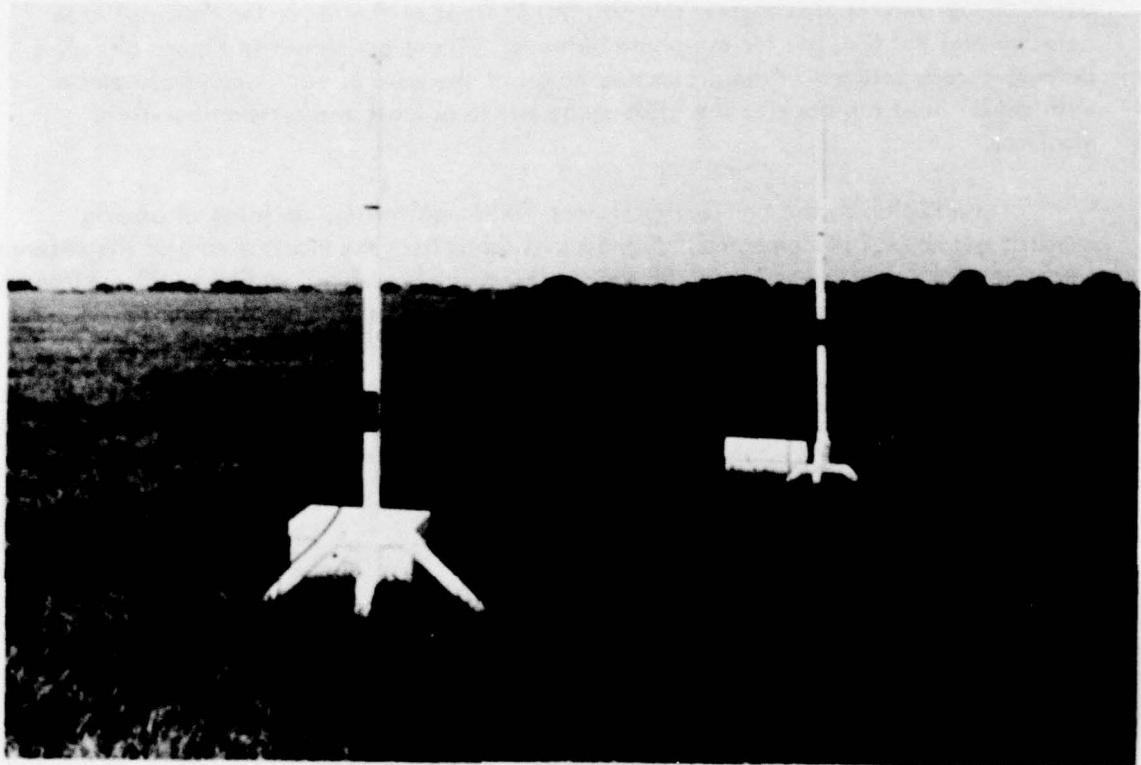
Figure 89.   The Near-Field Detectors for the SBR System.   Probe locations
are approximately 66' and 79' in front of the tower.
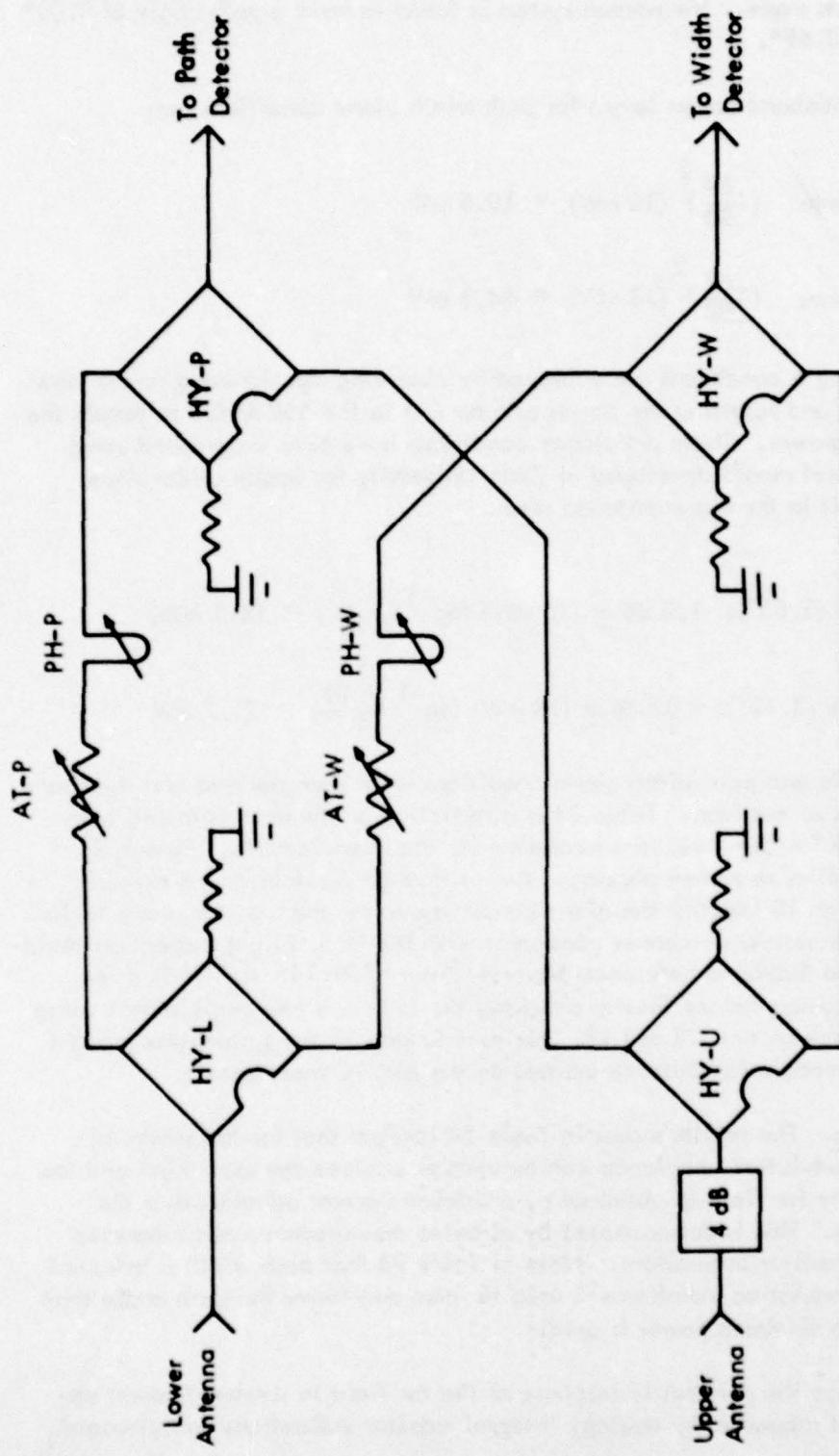
Figure 90. The RF Recombining Network for the Integral Analog Monitor Used During the Tamiami Tests.

This SBR system operates with a radiated carrier power of 2.0W and an upper antenna sideband power of 18 mW. An equal sideband power is delivered to the lower antenna. Both near-field and integral monitors were checked for normal indications and airborne measurements made. The normal system is found to have a path angle of 3.00° and a path width of 0.69°.

Calculated sideband power levels for path width alarm conditions are:

$$\text{Broad Alarm:} \quad (\frac{.69}{.90})^2 \ (18 \text{ mW}) = 10.6 \text{ mW}$$

$$\text{and} \quad \text{Sharp Alarm:} \quad (\frac{.69}{.50})^2 \ (18 \text{ mW}) = 34.3 \text{ mW}$$

High and low path angle conditions are achieved by observing the sideband power level in the upper antenna and resetting the power divider E-1 in the SBR APCU to obtain the proper unbalance of power. These unbalance conditions have been calculated using OUGS, a mathematical model developed at Ohio University for image glide-slope systems. Power levels in the upper antenna are:

$$\text{Low Angle (2.86°): } -1.0 \text{ dB } \underline{\text{or}} \ (18 \text{ mW}) \log^{-1} (\frac{-1.0}{10}) = 14.3 \text{ mW,}$$

$$\text{and} \quad \text{High Angle (3.12°): } +.82 \text{ dB } \underline{\text{or}} \ (18 \text{ mW}) \log^{-1} (\frac{+.82}{10}) = 21.7 \text{ mW}$$

The path angle and path width alarm conditions were then defined and the alarm limits set on both sets of monitors. Table 24 is a reduction of the data obtained from the 13 Pattern B (1000' AGL) level runs necessary for the measurements. Runs 1,2, and 3 were used to optimize system phasing. Runs 4 through 6 establish the normal system. Runs 7 through 10 identify the alarm conditions to set the monitor alarm limits. This is done in the conventional manner consistent with the U.S. Flight Inspection Hand-book OAP 8200.1 and Sideband Reference Manual Order 6750.34. Run 11 is a re-check of the normal system before finally checking the high and low angle alarms using a modulation unbalance on runs 12 and 13. For runs 12 and 13 the system was brought into alarm using the modulation balance control on the MK 1C modulator.

4. Results. The results shown in Table 24 confirm that for the sideband reference system a modulation unbalance can be used to achieve the same high and low angle conditions in the far field as obtained by a sideband power unbalance to the system's two antennas. This is demonstrated by airborne measurements and supported by analog, integral monitor indications. Note in Table 24 that path width is affected differently when a modulation unbalance is used to raise and lower the path angle than when an unbalance in sideband power is used.

Figure 91 shows the parametric response of the far field to sideband power un-balance. This data is supported by analog, integral monitor indications and airborne

-298-

			Measured in Far Field		Calculated	
Run No.	Purpose	Data	Angle	Width	Angle	Width
1	Equality	.003/90	--	--	--	--
2	C/SBO Phasing	.003/90	--	--	--	--
3	Upper Antenna	.002/90				
4	Normal	Pattern B, 1000' AGL	2.98	.64	3.00	0.70
5	Normal	P(SBO) 21mW →18mW	3.00	.69	3.00	0.70
6	Normal	Check	3.00	.69	3.00	0.70
7	Broad Alarm	P(SBO) → 9.2mW	2.99	.93	3.00	0.96
8	Sharp Alarm	P(SBO) → 35.0mW	3.00	.49	3.00	0.49
9	Low Angle Alarm	Upper Ant. → 14.9mW	2.83	.76	2.88	0.74
10	High Angle Alarm	Upper Ant. → 21.7mW	3.14	.63	3.16	0.63
11	Normal	Check	3.01	.69	3.00	0.70
12	Low Angle Alarm	.04/90 Mod Unbalance	2.85	.64	2.85	0.66
13	High Angle Alarm	.04/150 Mod Unbalance	3.16	.75	3.15	0.74

Table 24. Results of Airborne Measurements to Determine the Validity of Using a Modulation Unbalance to Set or Check High and Low Path Angle Alarm Limits on the Sideband Reference Glide-Slope System.
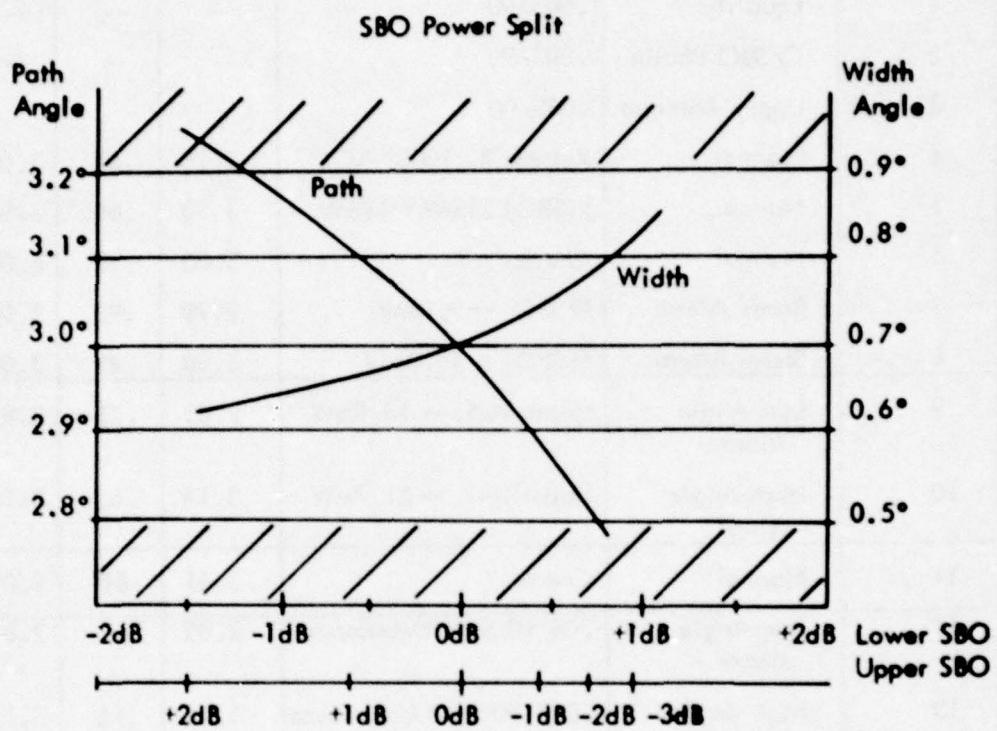
Figure 91. Parametric Response Data Generated by OUGS Indicating the Far-Field Response to Sideband Power Unbalance in the Sideband Reference Glide-Slope System.
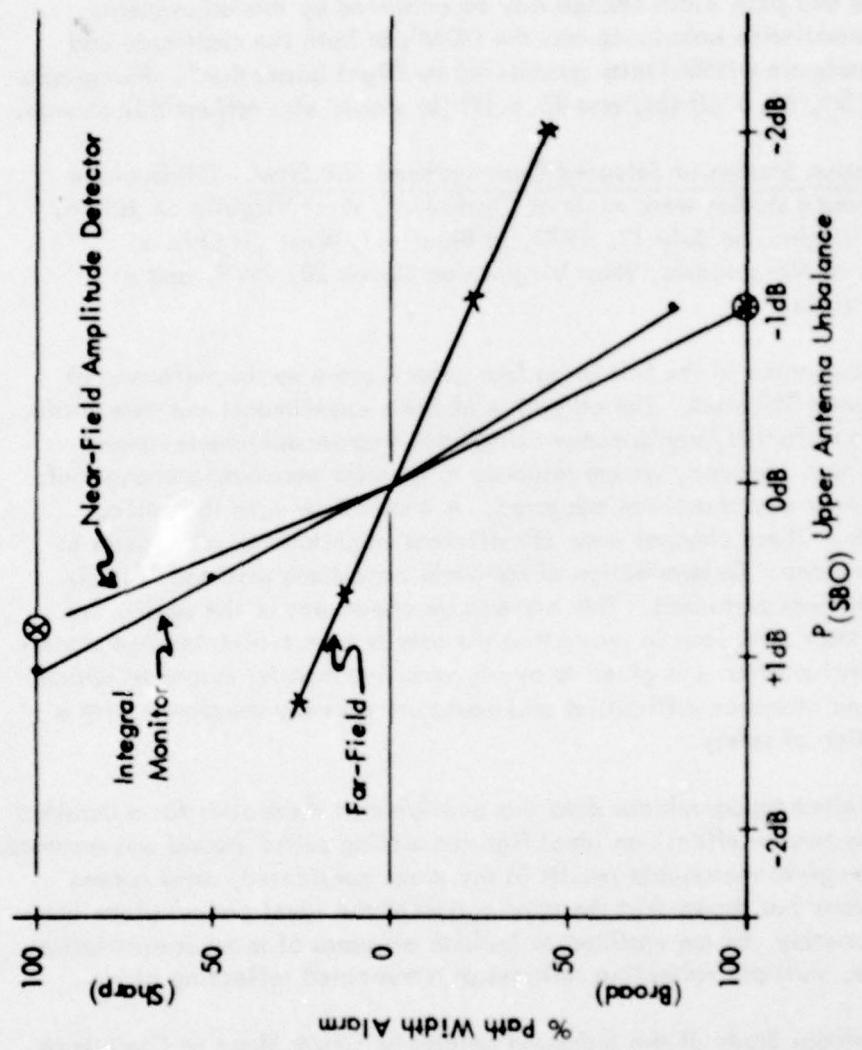
Figure 92. Graphical Results of the Path Width Integral Monitor and the Near-Field Amplitude Monitor Response to Sideband Power Unbalance to Achieve a Path Angle Change in the Sideband Reference Glide-Slope System.

measurements. The near-field amplitude detector response as measured is also indicated in Figure 92.

     5. <u>Recommendations</u>. Order 6750.34, "Maintenance of Sideband Reference Glide-Slope Equipment", should reflect the findings described here. Inasmuch as equipment configuration permits, a modulation unbalance should be substituted for a sideband power unbalance to set or check high and low path angle alarm limits.

     Accordingly, the following should be added to paragraph 115(3) of Order 6750.34: "In equipments capable of effecting a modulation unbalance of .040 or greater a path angle and path width change may be achieved by this adjustment. Ascertain that the modulation unbalance and the DDM's in both the amplitude and phase monitor channels are within limits established by flight inspection". Paragraphs 82.b.(2)(b), 82.c.(2), 83.b.(2)(b), and 83.c.(1)(b) should also reflect this change.

     E. <u>Perturbation Studies at Selected Commissioned SBR Sites</u>. Glide-slope and monitor performance studies were made at Clarksburg, West Virginia on July 6, 1978, at Roanoke, Virginia on July 17, 1978, at Bluefield, West Virginia on November 1, 1978, at Morgantown, West Virginia on March 28, 1979, and at Wheeling, West Virginia.

     The tests documented in the following four reports are a series performed at these five commissioned SBR sites. The objective of these experiments was three-fold. First, documentation of facility performance using FAA-independent measurement equipment was obtained. Second, system response to specific parametric changes of in-line signal amplitude and phase was measured. A comparison with theoretical predictions was made. These changes were of sufficient magnitude in some cases to bring the monitor to alarm. Determination of far-field conditions was made for all cases when the system was perturbed. This allowed an assessment of the sensitivity of the monitors and their adequacy in protecting the user from out-of-tolerance signals in space. Third, consideration was given to overly sensitive monitor responses which can easily produce maintenance difficulties and cause unnecessary shutdowns with a concomitant derogation of safety.

     Since insufficient topographical data was available at these sites for a detailed computer study of the terrain effect, an ideal flat conducting plane ground was assumed. While this assumption gives reasonable results in the cases considered, some recent work at Ohio University has shown that the application of the ideal ground plane concept cannot, unfortunately, be generalized to include all cases of snow accumulation such as, for example, multiple reflecting surfaces or a truncated reflecting plane.

     F. <u>Perturbational Study of the Sideband Reference Glide Slope at Clarksburg, West Virginia</u>.

     1. <u>Summary and Conclusions</u>. A series of perturbational tests have been conducted at the sideband reference (SBR) glide-slope facility at Clarksburg, West Virginia. As a result of these tests, the following conclusions are given:

(1) The facility was found to be within CAT I specifications.

(2) The near-field monitors used with the system are essentially fault detectors and not analogs of the far field. The phase monitor is overly sensitive and changes in the near-field environment can result in unnecessary facility shut-downs. The far field is essentially unaffected by these changes.

(3) The use of a somewhat short (83 electrical degrees) quadrature section at the facility is undesirable and should be corrected.

(4) The reluctance of maintenance personnel to alter sideband power division to check high and low angle alarm limits suggests that the use of fixed power dividers and line attenuators inserted specifically for alarm tests and changing mod balance be investigated.

2. Discussion of Data. System performance somewhat different from the theoretical for a flat site indicates that non-ideal terrain is present. Satisfactory topo maps were not available for making specific predictions for Clarksburg.

The ILS serves Runway 21 at Benedum Airport, Clarksburg. Equipment in use is an AIL Mark 1B system utilizing Meridan Type FAA-8021 dipole antennas. Figure 93 is a view of the facility from in front of the antennas. Figure 94 is a similar view looking out into the reflecting zone. The distance from the mast to the runway [250' (76.2m)] and the existence of a truncated ground plane [≈600' (≈183m)] suggest the need for the sideband reference system. Note the counterpoise in front of the array positioned 10 to 12 inches (25cm to 30cm) above ground. Figure 95 is a view of the transmitting equipment and the monitors. The amplitude and phase detectors are located approximately 93' (28m) and 120' (37m) in front of the antennas.

Utilizing the standard formula for the distance to the 360° point:

$$d = \frac{H^2 - h^2}{2B_p}$$

where H and h are the heights to the upper and lower antennas respectively in feet and B_p is the wavelength in feet at the operating frequency (approximately 2.964' (.9037m) at 332.0 MHz), the distance d to the 360° point with antenna heights of 25.8' (7.87m) and 8.7' (2.65m) is on the order of 99.5' (30.34m).

Noting that the counterpoise is effectively a raised ground plane and as such changes the effective antenna heights as viewed from the monitor detectors, the antenna heights referencing the counterpoise call for the 360° proximity point to be approximately 93.8' (28.60m) in front of the array. Accordingly, the amplitude monitor (located at the 360° point) at Clarksburg is located 93.3' (28.45m) in front of the array (see Figure 96).
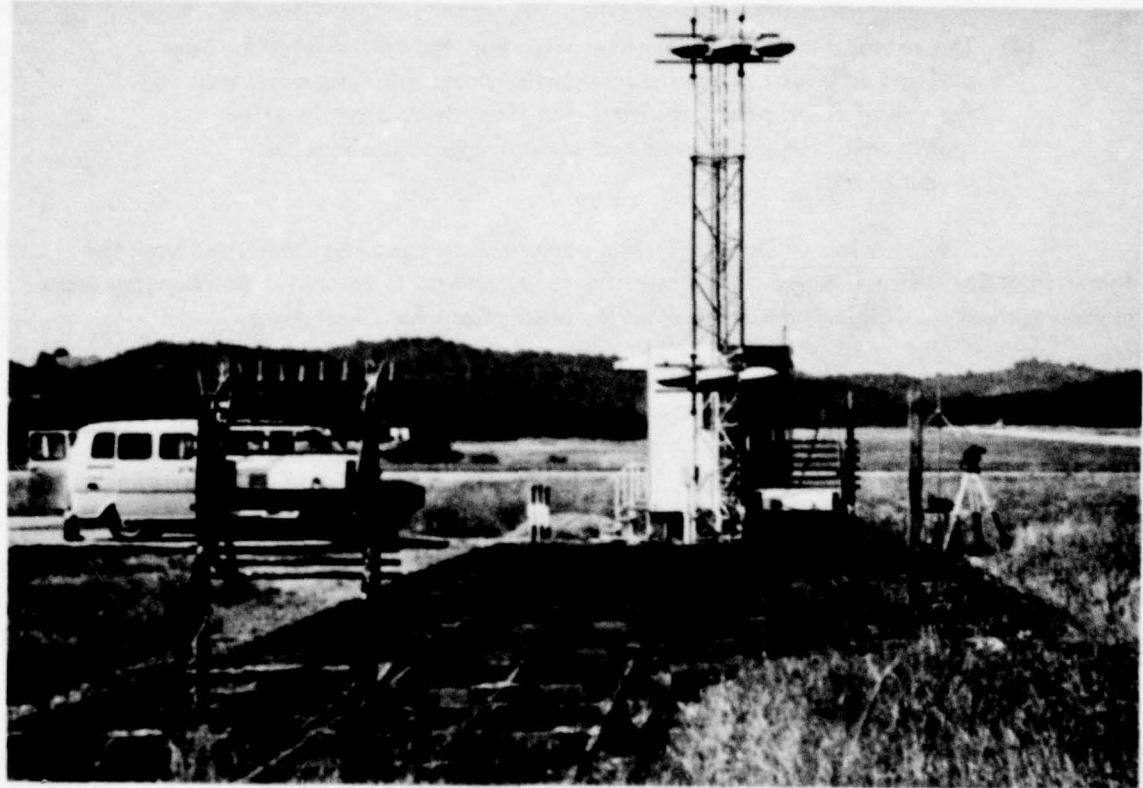
Figure 93.   Clarksburg, West Virginia Sideband Reference.

Figure 94. View of the Reflecting Zone from the Antenna
Position at Clarksburg, West Virginia.
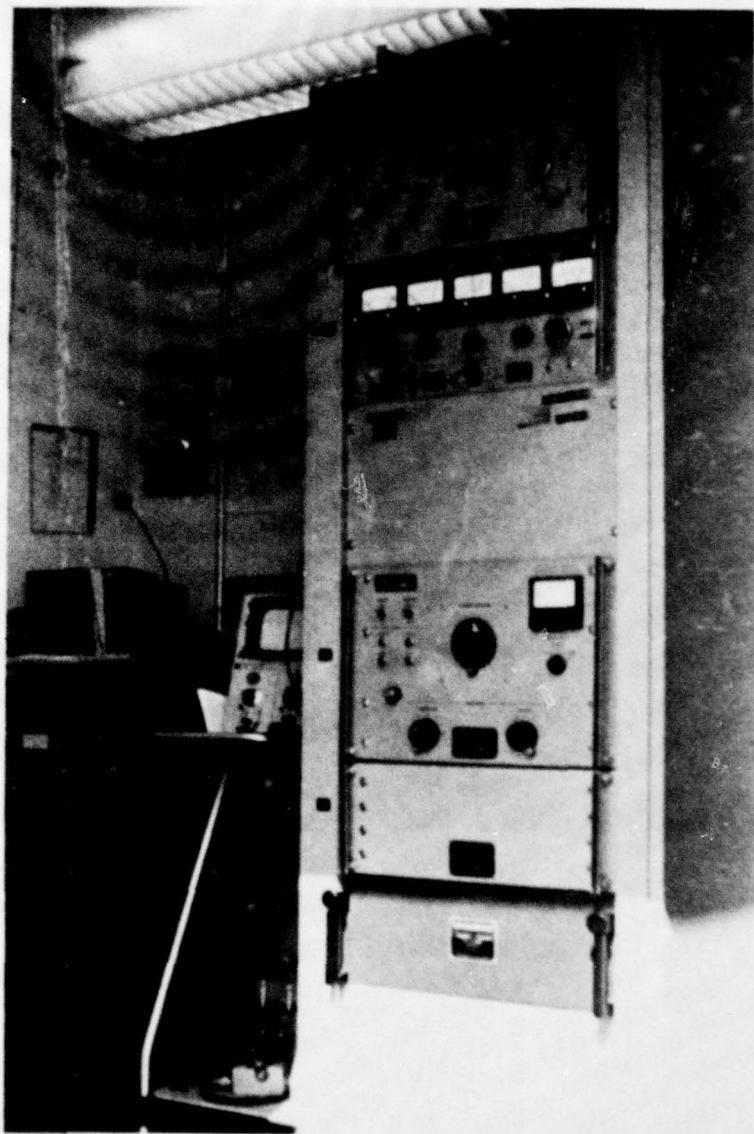
Figure 95. Mark 1B Equipment at Clarksburg, West Virginia.
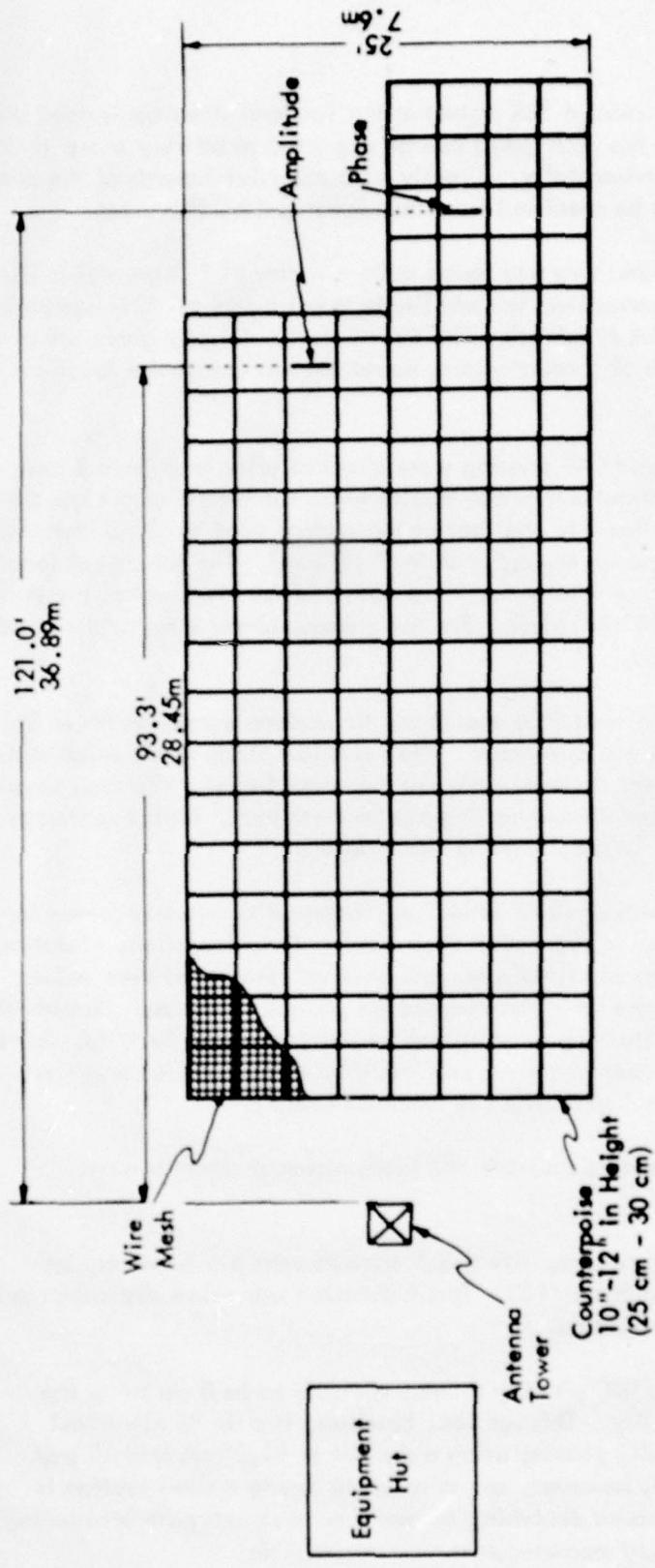
Figure 96. Dimensions of the Antenna Ground Screen and Detector Locations.

Work done on the experimental SBR system at the Tamiami site does indeed show that the calculated position for the 360° point can be expected to be very close [± 1' (±.3m)] to that point found experimentally. Clearly, the effective heights of the antennas for near-field calculations must be specified from the counterpoise, if present.

The phase monitor at Clarksburg was found to be a factor of 1.3 greater in distance from the transmitting antennas than the amplitude monitor probe. This compares to the factor of 1.3 given in FAA Handbook 6750.6B. Clearly, for any given set of antenna heights the introduction of a counterpoise moves the monitor probe locations closer to the antenna array.

Modulation, equality, and CSB phasing were checked prior to Pattern B and Pattern A flyability runs. A marked difference was noted in the length of the quadrature section in use at the Clarksburg facility and that of the section used by Ohio University ground crew. This difference was on the order of 5/8" (1.6cm). The electrical length of the section used by Ohio is known to be 91.2° at 332.0 MHz. This makes the section in use at Clarksburg very near 83° in length. For the purpose of these tests, the quadrature section from the facility was used.

The normal condition of the facility was found to produce a path/width of 3.10°/ 0.69°. A check of alarm limits was also made. High and low alarm limits established by a change in the sideband power division were not measured because site maintenance personnel preferred that the power divider setting not be disturbed. Their experience indicated a problem in resetting to precisely the same values.

Horizontal cuts of the path at 1000' (304.9m) (Pattern B's), were recorded for the perturbations which were line inserts rather than results of manipulations of station controls. Phasors and attenuators of suitable electrical length but set at zero values were inserted in the system and the far field checked for normal operation. Perturbations were then introduced without disturbing existing control settings at the facility. Removal of this hardware returned the system to normal as viewed by the near-field monitors (allowing for diurnal changes) and as verified by airborne checks.

After all flight measurement data were obtained, antenna currents were measured with hand-held probes.

3. Results. The airborne equality check showed zero μa; however, an antenna phasing checked showed 50 μa/150. This indication was space dependent and no change was made to antenna phasing.

An initial check of CSB/SBO phasing showed equality to be 0 μa using the quadrature section from the facility. This section, however, is only 83 electrical degrees. A check of the CSB/SBO phasing using a section of 91.2° showed 30 μa/ 90. As can be seen in Table 25, however, any misphasing due to a short section is not obvious, as symmetrical sideband dephasing caused a symmetrical path broadening. Table 25 is a summary of the flight measurements.

RUN	Calculated		Measured		% Phase Alarm	% Amp. Alarm
	Path Angle	Angle Width	Path Angle (°)	Path Width (°)		
Equality		0/90				
Mod		80%				
C/SB Phasing		0/90	(Insertion of OU section resulted in 30/90)			
Upper Antenna Phasing		50/150	(Space Dependent)			
Normal [1000' (300m) AGL]	-	-	3.10	.69	0	0
Normal [1000' (300m) AGL]	-	-	3.11	.67	0	0
Normal [1000' (300m) AGL]	-	-	3.11	.69	0	0
Normal [1500' (450m) AGL]	-	-	2.99	.69	0	0
Normal [1000' (300m) AGL after hardware]	3.10	0.70	3.05	.71	0	0
SBO Advanced 20°	3.10	0.79	2.91	.73	120	-
SBO Retarded 20°	3.10	0.79	3.20	.73	120	-
Upper Antenna -1 dB	2.98	0.78	2.90	.74	0	140
Upper Antenna -2 dB	2.86	0.83	2.80	.80	30	200+
Normal [1000' (304.9 m) AGL]	3.10	0.70	3.10	.69	0	0
Upper Antenna Advanced 10°	3.07	0.72	2.99	.69	75	0
Upper Antenna Retarded 10°	3.07	0.72	3.07	.69	75	50
Lower Antenna -1 dB	3.22	0.62	3.22	.67	0	80
Lower Antenna -2 dB	3.34	0.57	3.33	.54	30	200+
Normal [1000' (304.9m) AGL, P (SBO) ≈ 50mW]	3.10	0.70	3.11	.67	0	0

Table 25. Summary of Pattern B Runs at Clarksburg, West Virginia.

RUN	Calculated		Measured		% Phase Alarm	% Amp. Alarm
	Path Angle	Path Width	Path Angle (°)	Path Width (°)		
Broad Alarm (P (SBO) = 29mW)	3.10	0.91	3.10	.78	-	100
Sharp Alarm (P (SBO) = 80mW)	3.10	0.55	3.10	.65	-	100
Mod Inequality (.033/90)	2.94	0.65	2.88	.64	60	100
Mod Inequality (.045/150)	3.28	0.77	3.29	.68	0	100
Mod Inequality (.045/150 Rerun)	3.28	0.77	3.30	.65	0	100
Mod Inequality [.045/150, 1500' (300m) AGL]	3.13	0.77	3.15	.68	0	100
Normal [1800' (540m) AGL]	3.10	0.70	3.00	.67	0	0

Table 25(continued). Summary of Pattern B Runs at Clarksburg, West Virginia.

Pattern B's at 1000' (300 m) AGL revealed a path angle of 3.10° and a path width of 0.69°. A Pattern B at 1500' (450 m) AGL showed the angle to be 2.99°. This path angle change is also seen in the typical Pattern A. This is an example of where a single point measurement for path angle taken with a level run does not yield the most appropriate value for path angle. The Pattern A (low approach) will yield an actual path angle which is an average over an approximate three mile distance and, therefore, must be considered more representative.

The Clarksburg glide-slope structure is shown in Figure 97; it meets CAT I specifications reaching 90% of the limits. Pattern B's for all flight measurements were made at 1000' (300 m) AGL to minimize flight time and conserve fuel.

The near-field monitoring at Clarksburg is shown to be essentially a fault-detection type monitor and not a true analog of the far field. At no time did the far field go out-of-tolerance ($\pm 0.2°$ change in path or width) before reaching an alarm condition on either the amplitude or phase monitor. The alarms are quite conservative as can be seen by Table 25. Note the far-field path width during a check of the width alarm limits. This oversensitivity is even more apparent with upper antenna dephasing.

By inspecting Table 25 and Figure 98, one readily understands why the existing monitors must be regarded as fault detectors rather than analog sensors. For example, with 2 dB attenuation added to the lower antenna, the phase monitor shows 30% of alarm with the amplitude showing 200% while the far field has moved to approximately only 100% of tolerance. The existing sideband reference near-field monitors are in reality phase and amplitude detectors similar to integral monitors, but complicated by near-field ground plane affects.

Diurnal changes in nominal monitor values at Clarksburg are typically 30 to 50% of alarm, and reportedly do not give a problem in spite of the tight limits that exist.

Probe measurements using a hand-held probe and vector voltmeter yielded the following amplitude and phase data:

		Amplitude	Phase
LOWER ANTENNA	Center Dipole	- 6.5 dB	0°
	Left Dipole*	- 5.6 dB	+ 5.3°
	Right Dipole	-11.8 dB	+10.6°

Calculated composite effective amplitude and phase: + 1.9 dB   + 4.4°

* Left and right refer to the dipoles as seen from behind the array.
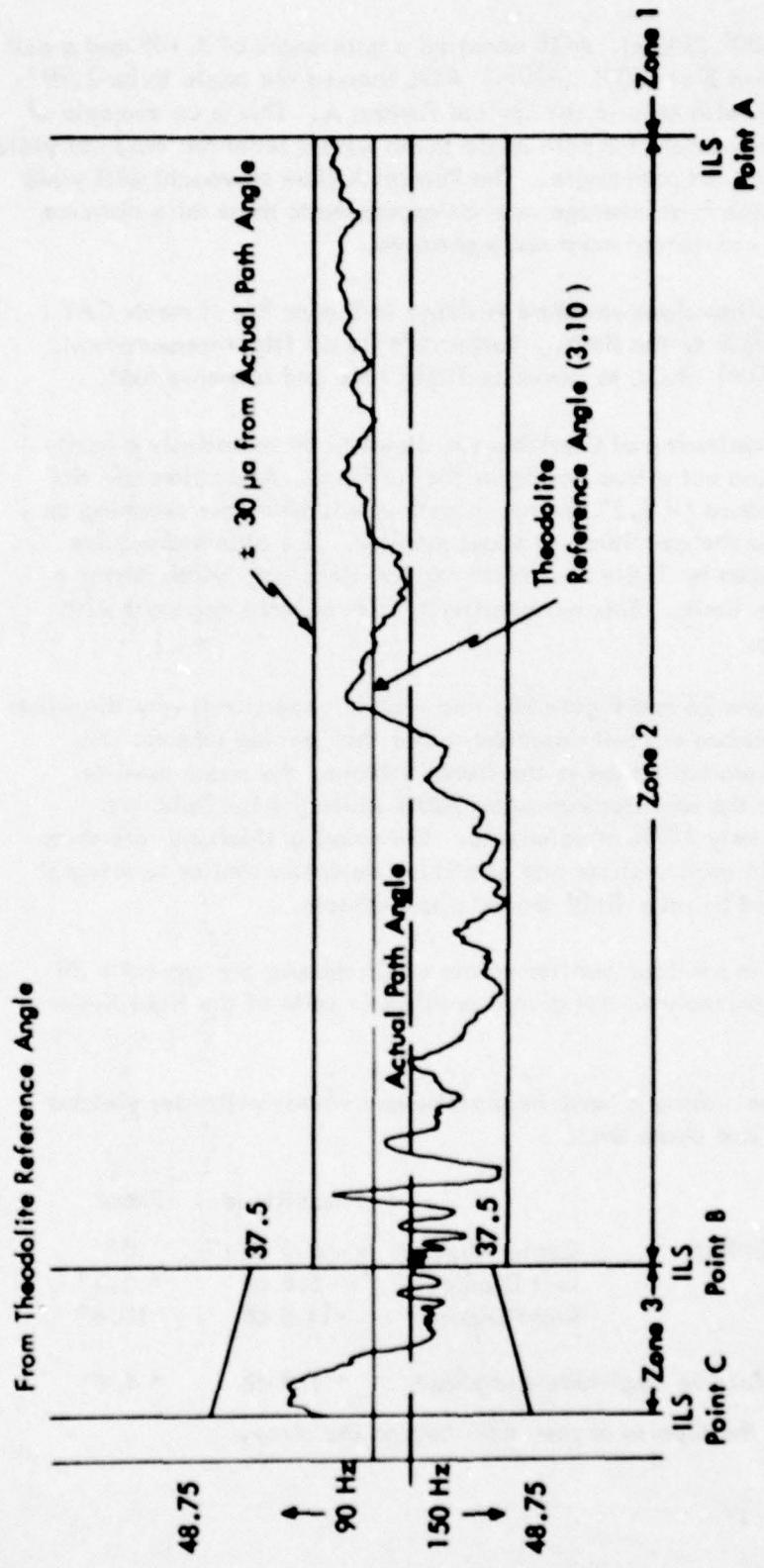
Figure 97. Path Structure of the Sideband Reference Facility at Clarksburg, West Virginia, July 1978.

-312-
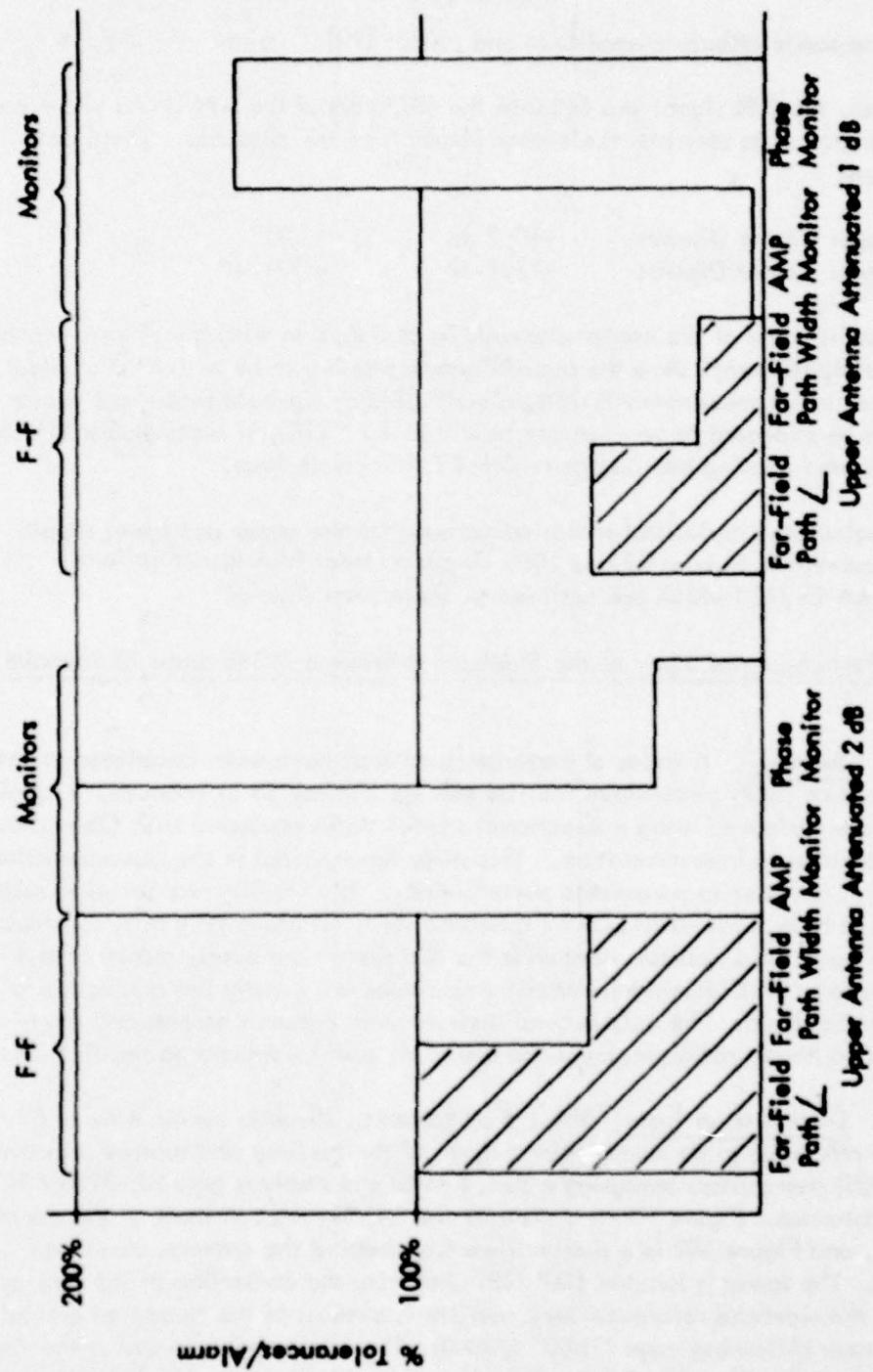
Figure 98. Near-Field Monitor and Measured Far-Field Response to Upper Antenna Attenuation in the Sideband Reference Glide Slope at Clarksburg, West Virginia.

		Amplitude	Phase
UPPER ANTENNA	Center Dipole	- 6.4 dB	0°
	Left Dipole	- 6.3 dB	- 9.8°
	Right Dipole	- 9.6 dB	- 4.5°

Calculated composite effective amplitude and phase: [10]   0 dB   - 2.5°

Further, the CSB signal was fed into the SBO port of the APCU and phase and amplitude measurements taken on the center elements of the antennas. These data were as follows:

Upper Center Dipole:	-10.2 dB	+ 50°
Lower Center Dipole:	-11.7 dB	- 131.4°

The difference in phase of the center elements in conjunction with the effective phase values for the dipole arrays show the overall system phasing to be within 5° of ideal phasing. Since phase measurements using a hand-held or jig-held probe and vector voltmeter can be expected to be accurate to within ± 2° [10], it seems reasonable to expect that ground phasing can reduce required flight check time.

The calculated horizontal radiation patterns for the upper and lower dipole arrays are presented in Figures 99 and 100. These do meet FAA specifications as given in FAA-E-2425 which are outlined on these same figures.

G. Perturbational Study of the Sideband Reference Glide Slope at Roanoke, Virginia.

1. Summary. A series of perturbational tests have been completed at the sideband reference (SBR) glide-slope facility serving Runway 33 at Roanoke, Virginia. These tests were performed using a Beechcraft Model V35A equipped with Ohio University Mini-Lab airborne instrumentation. This study has resulted in the documentation of the facilities response to parametric perturbations. The facility was found to respond predictably and to be well within CAT I specifications, reaching only 65% of tolerance. By nature the near-field monitors used with the SBR system are overly sensitive and essentially serve as fault detectors. Monitor responses are clearly not analogous to changes in the far field. The existence of non-standard antenna heights and (non-integer) antenna height ratio precludes the use of an equal sideband power division.

2. Discussion of Data. The ILS at Roanoke, Virginia serves Runway 33. The sideband reference glide slope located north of the taxiway and runway uses dual tube-type (TUS) transmitters operating a 333.2 MHz and employs type FA-8976 APC glide-slope antennas. Figure 101 is a view of the facility from in front of the transmitting antennas, and Figure 102 is a similar view from behind the antenna tower and counterpoise. The tower is located 600' (189.2m) from the centerline of the runway. The need for the sideband reference-type facility is a result of the truncated ground plane in the near reflecting zone (≈800' (240m)). The counterpoise in use at the Roanoke site is approximately 25' × 65' (7.6m × 19.8m) and is elevated from the immediate terrain
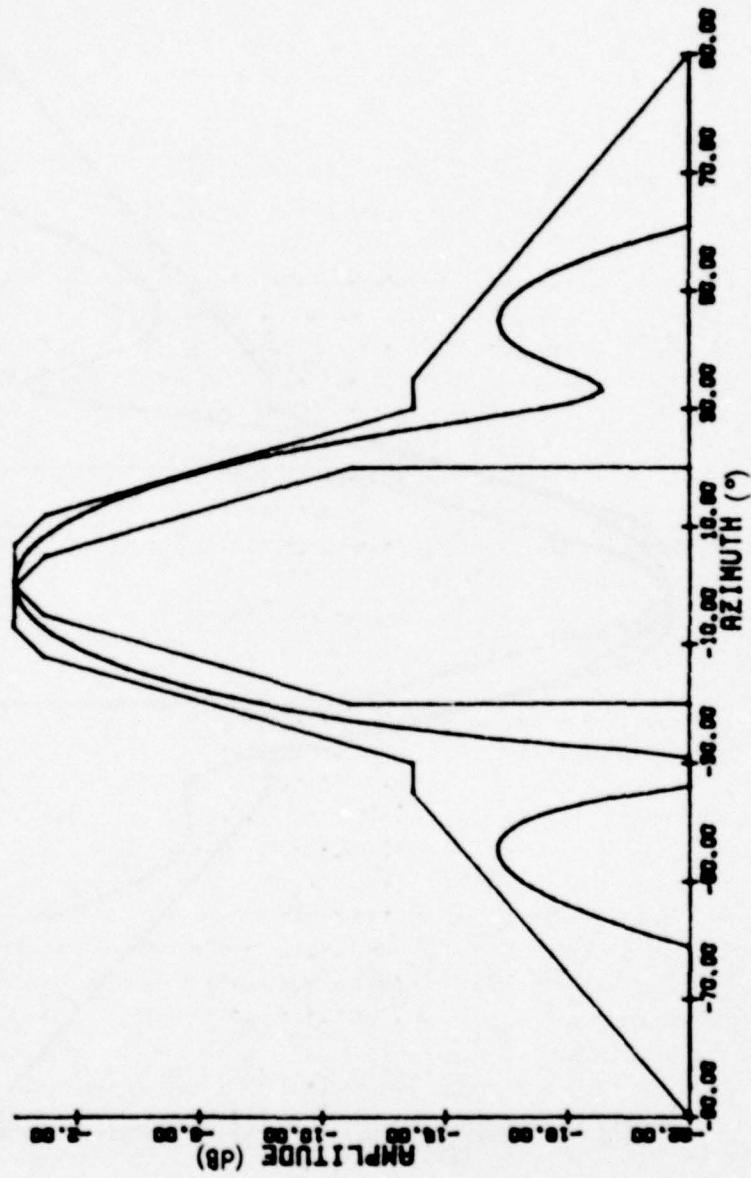
Figure 99. Calculated Horizontal Radiation Patterns for the Upper Dipole Array at Clarksburg, West Virginia.
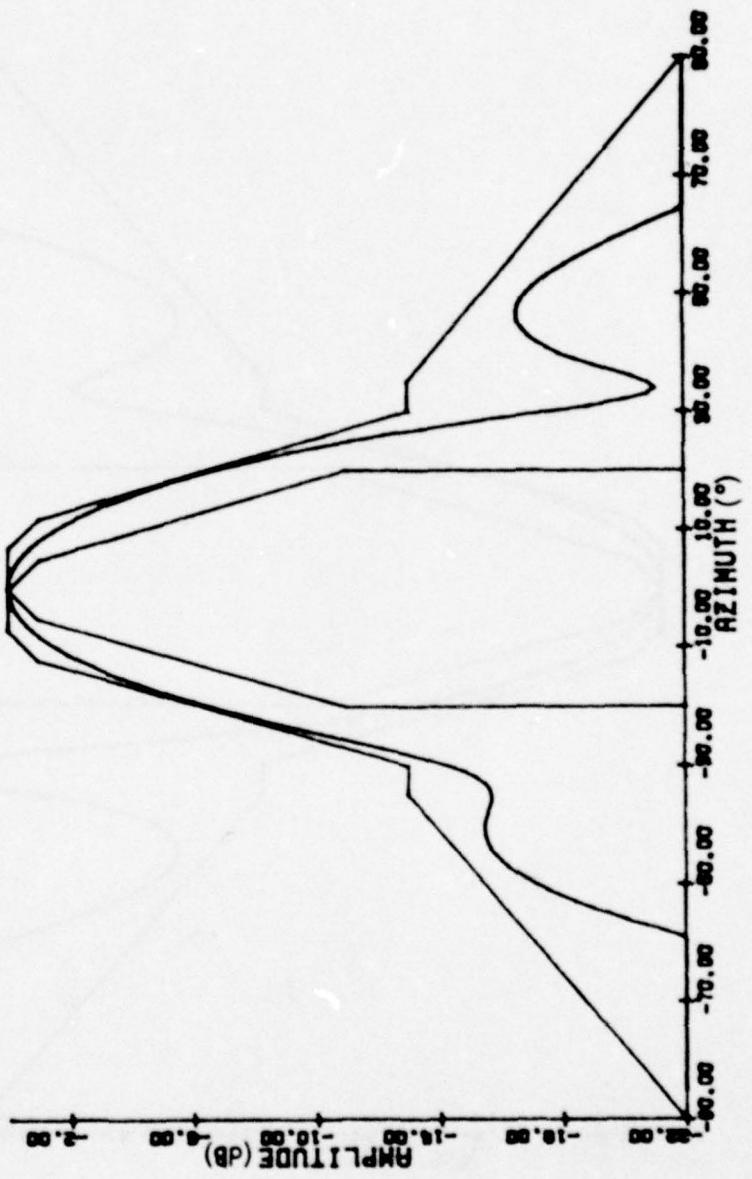
Figure 100. Calculated Horizontal Radiation Patterns for the Lower Dipole Array at Clarksburg, West Virginia.

Figure 101. A View of the Sideband Reference Glide-Slope
Facility at Roanoke, Virginia. The counterpoise
is an average of 14 inches (35cm) above the
local terrain.
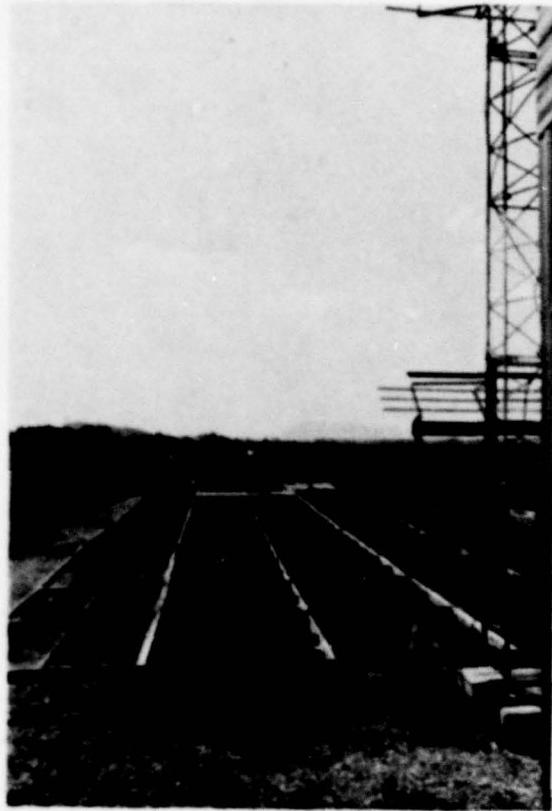
Figure 102. Near-Field Monitors and Counterpoise
at Roanoke, Virginia as Viewed from
Behind the Antenna Tower.

level 14" (35 cm). The antenna heights are 7.0' (2.13m) for the lower antenna and 19.5' (5.94m) for the upper. Using the standard formula for the distance to the 360° point:

$$d = \frac{H^2 - h^2}{2B_p}$$

where H and h are the heights in feet of the upper and lower antennas above effective ground (counterpoise), respectively, and B_p is the wavelength in feet in free space at the operating frequency. The calculated distance d then to the 360° point is 51.1' (15.58m). This is close to the actual location of the amplitude monitor at Roanoke, which is at 50.5' (15.39m). Accordingly, the phase monitor is located at 60.6' (18.46m) from the tower. This is a factor of 1.2 times that distance to the 360° point, which is in some disagreement with the factor of 1.3 stated in FAA Handbook 6750.6B. A factor of 1.2 is in agreement with that calculated by OUGS computer model.[*] This accuracy in predicting the distance to the 360° point and then to the phase monitor point reinforces the observation that a counterpoise between the antennas and the monitors effectively raises the ground plane for the monitors and that this can be used for near-zone calculations in a straightforward manner.

The departure of the measured results from the calculated results is, in part, due to an electrically short quadrature section in use at the facility. A check of the electrical length of this section with a vector voltmeter showed it to be approximately 82°. This section was used for the tests that are documented here.

Pattern B, or level runs on the glide slope and on localizer centerline, at 1000' (300m) AGL were used to determine the path angle and width. The facility was found to have a normal path/width of 3.03°/.81°. Sideband power level was changed -1.0 dB and +1.25 dB to bring the near-field monitor system to alarm for broad and sharp path width conditions, respectively. Alarm limits for high and low path angle conditions were not checked because site maintenance personnel preferred that the sideband power divider setting not be changed in the absence of FAA flight check.

With the normal facility conditions known and the path width alarm points checked, phasors and attenuators of suitable electrical length were inserted in-line and the normal condition rechecked. Phase and amplitude changes were then made to the system without disturbing station control settings. After all perturbations, the inserted devices were removed and the facility rechecked for a normal path and path width. It returned to 3.03°/.81°.

Antenna dipole currents were measured using a jig-held probe and vector voltmeter. The calculated horizontal radiation patterns for these measured antenna currents are presented.

3. Results. An airborne check of modulation equality showed 3 μa/150. Sideband phasing resulted in 2 μa/90 and upper antenna phasing check yielded 3 μa/90. Because the quadrature section in use at Roanoke is only 82° in length, the sidebands are dephased -8°.

---

[*] See Section IIA of this report.

Two Pattern B runs at 1000' (300m) AGL were used to establish the normal condition of the system at 3.03°/.81°. A single Pattern B run at 1500' (450m) AGL produced 3.05°/.72°. To conserve fuel and time, all subsequent Pattern B's were made at the lower altitude. Sharp and broad alarm conditions were produced with the appropriate changes in sideband power level. This resulted in path widths of .69° and .93°, respectively. The necessary hardware was then inserted in-line and a recheck of normal showed the system to again be 3.03°/.84°.

This check was then followed by a series of parametric perturbations. The results of these perturbations are given in Table 26. Note the asymmetrical response of the far-field path width to sideband dephasing. This is due, in part, to the short quadrature section. The calculated path angle and width in Table 26 is for a sideband reference facility with antenna heights and antenna currents as they were measured at Roanoke. Additionally, the computer model assumes ideal terrain; i.e., an infinite, flat, perfectly-conducting ground plane. In spite of the lack of sufficient topographic data providing a better description of the terrain, the calculated results shown in Table 26 are acceptable. Monitor responses to the perturbations are given in Table 26 as % of alarm. Clearly, the monitor response is non-analogue in nature and is not representative of the far-field conditions. At no time did the monitor fail to give an alarm indication when the far-field was out-of-tolerance.

Pattern A, or flyability runs made on an approach for landing and taken at the facility prior to any hardware insertion, show a path angle of 2.97°. Figure 103 is one of the flyability runs at Roanoke. The path clearly meets Category I specifications, reaching only 65% of tolerance limits.

Historically, the counterpoise in use at Roanoke has not provided the near-field monitors with adequate immunity from changes in the character of the ground below it. Technicians report moderate to heavy monitor sensitivity to changes in the moisture content of the ground. Inspection of the screen shows that electrical connections between two adjacent sections of screen are made only every 4-5' (1.2-1.5m). In general, this would not be considered adequate and influences from below the screen would be expected to be excessive. Connections on the counterpoise should reflect the common practice of reducing this dimension to 1/10 wavelength or less. Additionally, due to the horizontal polarization of the glide-slope antennas continuous sections of screen should lie with their long dimension perpendicular to the centerline of the runway on the supporting structure. This serves to further reduce the effects of discontinuities.

Probe measurements were made on the antennas with a jig-held probe and vector voltmeter. Normalized currents and the computed differential in amplitude and phase for the antennas is shown in Table 27.

Figures 104 and 105 are the calculated amplitudes as a function of azimuth for the upper and lower antennas, respectively. Figures 104 and 105 also show FAA specifications as given in FAA-E-2429. These specifications are not met principally

RUN	Calculated		Measured		% of Alarm		Far-Field
	Path (°) Angle	Path (°) Width	Path (°) Angle	Path (°) Width	Amplitude %	Phase %	% Tolerance
Equality	3/150						
SBO Phasing	2/90						
Upper Antenna Phasing	3/90						
Normal (1000' AGL)	3.03	.81	3.04	.82	0	0	0
Normal (1000' AGL)	3.03	.81	3.03	.83	0	0	0
Sharp Alarm (+1.25 dB)	3.04	.69	3.03	.70	100	0	55
Broad Alarm (-1.00 dB)	3.04	.93	3.02	.91	100	0	50
Normal (Hardware in)	3.03	.81	3.03	.84	0	0	0
SBO +20°	3.04	.85	3.04	.85	0	0	20
SBO -20°	3.04	.85	3.01	.94	0	120	44
Upper Antenna +20°	2.97	.85	3.04	.80	75	45	44
Upper Antenna +30°	2.87	.83	3.08	.74	67	79	76
Upper Antenna -20°	2.97	.85	2.87	.89	300	114	44
Upper Antenna -30°	2.87	.83	2.86	.84	375	121	76
Upper Antenna -1 dB	2.93	.89	2.98	.91	125	17	78
Upper Antenna -2 dB	2.80	.91	2.89	.81	350	32	106
Lower Antenna -1 dB	3.12	.72	3.08	.61	133	37	36
Lower Antenna -2 dB	3.21	.57	3.16	.61	300	61	77
Lower Antenna -3 dB	3.40	.52	3.37	.56	467	81	160
Mod Unbalance .024/90	2.96	.79	2.94	.72	110	31	36
Mod Unbalance .020/150	3.12	.83	3.11	.77	63	25	36
Normal	3.03	.81	3.03	.81	0	0	0

Table 26. Results of the Perturbational Testing at Roanoke, Virginia.
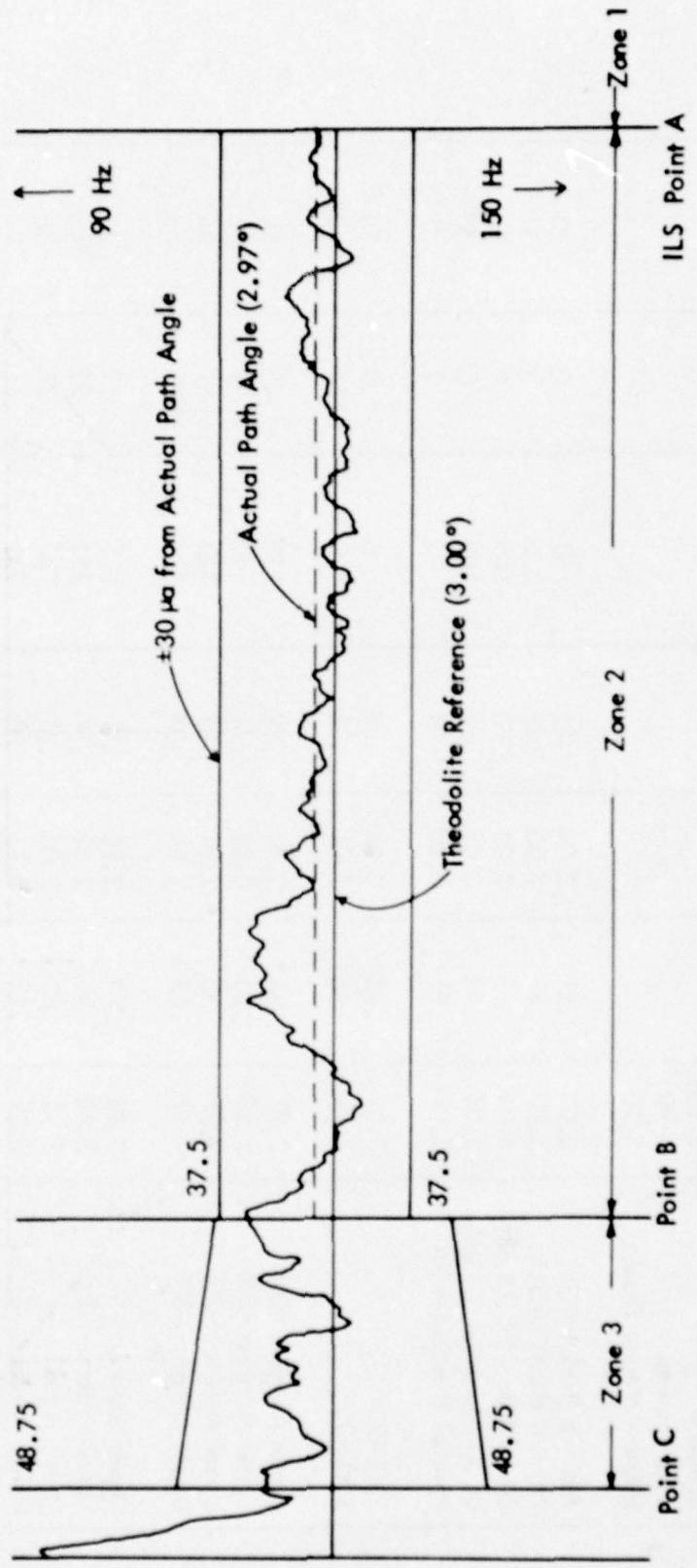
Figure 103. Pattern A Flyability Run Taken at Roanoke, Virginia During a Series of Perturbational Tests Conducted in July, 1978. The path meets Category I specifications reaching only 65% of tolerance limits.
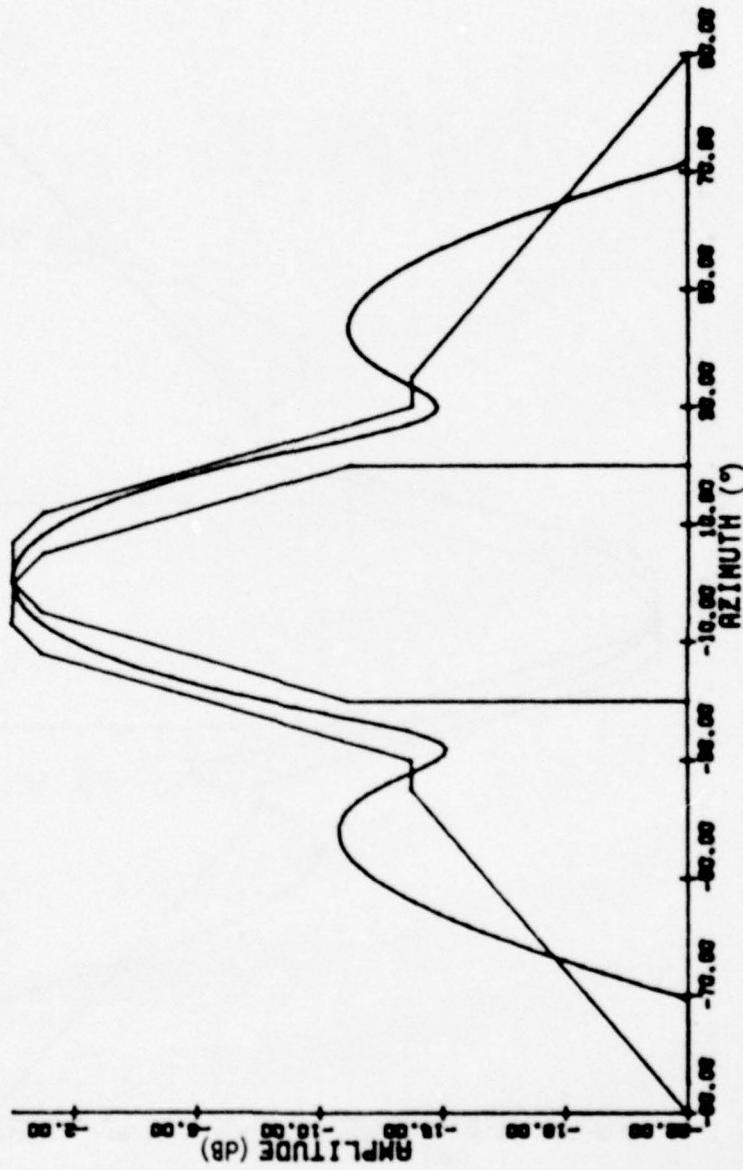
Figure 104. Calculated Amplitude vs. Angular Displacement for the Upper Antennas as Computed from Measured Dipole Currents at Roanoke, Virginia. The antennas are APC Type FA-8976.

Figure 105. Calculated Amplitude vs. Angular Displacement for the Lower Antenna at Roanoke, Virginia.

```
Lower Antenna Element Currents
Element      Amplitude     Phase
Center       -00.0 dB      -00.0°
Runway       -1.1 dB        33.0°
Outer        -0.6 dB        41.0°

Upper Antenna Element Currents
Element      Amplitude     Phase
Center       -00.0 dB      -00.0°
Runway       -0.9 dB        37.0°
Outer        -0.7 dB        43.0°

The Upper Antenna is -0.0 dB and 2.0 Degrees
with respect to the Lower Antenna when the
center element currents of both antennas are
equal.
```

Table 27. Calculated Effective Amplitude and
          Phase for Antenna Currents as Measured
          at Roanoke, Virginia.

because of a greater than usual phase advance and current amplitude in the two outboard elements. This situation presents no problems at the Roanoke site because the resulting side lobes do not illuminate any reflecting structures and, therefore, do not adversely affect the flyability of the path.

Further, a probe measurement shows that the upper antenna center element was +180° with respect to the same element in the lower antenna. The computed differential phase of +2° yields an overall measured upper antenna phasing of +182°. This is very close to both the ideal and the phasing indicated by the airborne check.

H. Perturbational Study of the Sideband Reference Glide Slope at Bluefield, West Virginia.

1. Summary. A series of perturbational tests has been completed at the sideband reference (SBR) glide-slope facility which serves Runway 23 at Bluefield, West Virginia. These tests were performed using a Beechcraft Model A36 equipped with Ohio University's Minilab instrumentation package. These tests have resulted in the documentation of the facility's response to parametric changes in the transmitting and antenna system. The facility is found to respond predictably to these perturbations. The normal condition of the system is found to be quite satisfactory and to be well within CAT I specifications, reaching only 60% of tolerance limits in zone 2. The inherent oversensitivity of the near-field monitor (phase) in common use

with the SBR system is evident from these data. Additionally, response for both the near-field phase and integral width monitor is found to be not analogous to far-field response. The monitors are, therefore, essentially serving as fault detectors.

2. Discussion of Data Acquisition. The ILS at Bluefield, West Virginia serves Runway 23. The facility utilizes Mark 1D transmitting and monitoring equipment and is located 250' (76.2m) from centerline on the north-west side of the runway. The transmitter operates at 332.6 MHz and employs Type FA-8976 APC glide-slope antennas. Figure 106 is a view of the facility from in front of the counterpoise area. Figure 107 is a similar view from behind the equipment building. The distance to the threshold is 1052' (320.6m). While this is a somewhat truncated ground plane, the deployment of the sideband reference system at Bluefield is a result of need for lower antenna heights and accommodation of the limited terrain available for mast location.

The counterpoise in use at Bluefield measures 20' x 100' (6.1m x 30.5m) and is elevated approximately 12" (31cm) above local terrain. The antenna heights used are 7.3' (2.22m) for the lower antenna and 21.53' (6.562m) for the upper. The monitoring for the system is near-field phase fed to the path channel and integral pickups for the width. This is standard for the Mark 1D equipment. Accordingly, there is only one monitor probe above the counterpoise. This phase monitor probe is located 3.25' (.991m) above the counterpoise and 74.8' (22.80m) in front of the antenna mast. Using the standard formula for the distance to the 360° point and given that the antenna heights above the counterpoise are approximately 6.0' (1.83m) and 20.2' (6.16m):

$$d = \frac{H^2 - h^2}{2B_p} = 62.86'$$

where H and h are the heights in feet of the upper and lower antennas, respectively, and B_p is the wavelength in free space at the operating frequency.

The distance to the phase monitor location should be a factor of 1.2 farther from the mast or 75.4' (22.98m). This compares favorably with the measured distance at Bluefield of 74.8' (22.80m). This is further demonstration of the fact that the counterpoise may be considered as simply a raised ground plane insofar as monitor probes in the near field are concerned.

Before any testing of the facility was done, or any perturbations introduced into the system, pattern A (flyability) and pattern B (level runs at 1000' (300m) AGL) runs were made to establish the normal condition. The pattern B showed a path/width of 3.07°/.69°. The pattern A showed an average in approach zone 2 of 3.03°. Suitable changes in sideband power (-2.17 dB and +1.8 dB) were used to establish broad and sharp alarm limits for the monitors. Two different methods were used to bring the system monitors to high and low angle alarm condition. First, the conventional approach using a change in the sideband power division was employed. Second, a change in modulation balance was used to effect a path-angle change to alarm limits.

With monitor alarm limits documented, a series of system perturbations were introduced. Monitor response, as well as far-field response, were recorded for each fault. These faults include sideband amplitude and phase and antenna amplitude and phase.

-326-

The introduction of these faults was facilitated by the use of suitable length lines containing the required phasor and attenuator. This hardware was inserted in-line and trimmed in electrical length to return the system monitors as closely as possible to normal. A check was then made of the far field to insure that any small changes to the path due to insertion losses, etc., are documented. After all perturbations were documented and the facility returned to normal, the far field was rechecked. The path/width was found to be 3.08°/.65°.

Dipole currents for the Type FA-8976 antennas were obtained using a jig-held probe and vector voltmeter. Calculated horizontal radiation patterns for these antennas based on the probe measurements are presented.

All of the flight data was collected using a radio telemetering theodolite as a reference. It was located consistent with the specification of the U.S. Flight Inspection Handbook, OA P 8200.1, paragraph 217.32.

3. Results. An airborne check of modulation equality showed zero micro-amperes. Carrier/sideband phasing produced 6 μa/150 Hz and a check of upper antenna phasing resulted in 43 μa/90 Hz. The pattern B, to establish the normal condition of the system, resulted in a path angle and width of 3.07°/.69°. A pattern A run showed the actual path angle in approach zone 2 to be 3.03°. Beginning at approximately one mile range, there is roughness which very likely is being produced by reflections from the up-slope identified in Figure 106. Additionally, the path is found to be well within CAT I specification reaching only 60% of tolerance limits. Figure 108 is a reproduction of the recorded differential trace obtained during this run.

Broad and sharp alarm conditions brought about by changes in sideband power level of -2.17 dB and +1.80 dB resulted in path widths of .82° and .55°, respectively. The monitor alarm limits were also checked for high and low path angle conditions. Changing the sideband power division by observing the sideband power in the upper antenna directional coupler is the conventional manner for changing path angle. Alarm limits established in this manner were 3.10° and 3.04°. These same alarm limits were achieved by a change in modulation balance. This approach resulted in path angles of 3.12° and 3.02°. It has been previously demonstrated that modulation unbalance can be used to establish or check the same high and low angle alarm limits for the sideband reference system that are obtained with an unbalance of sideband power.*

Following a check of alarm limits hardware suitable for effecting parametric changes in upper antenna attenuation and lower antenna phasing was inserted in-line and the normal condition of the system verified. An identical approach was also used to accomplish parametric changes in carrier-to-sideband phasing and lower antenna attenuation. A pattern B was run for every fault. The results of these runs are presented in Table 28. Data presented in Table 28 includes the measured path angle and width, the calculated path angle and width, and the percent of alarm for both the system monitors and the far field. The calculated path angle and width are a result of predictions made using the math model. Since adequate topographic data for the Bluefield site was

_____
* See Section IID of this report.

-327-
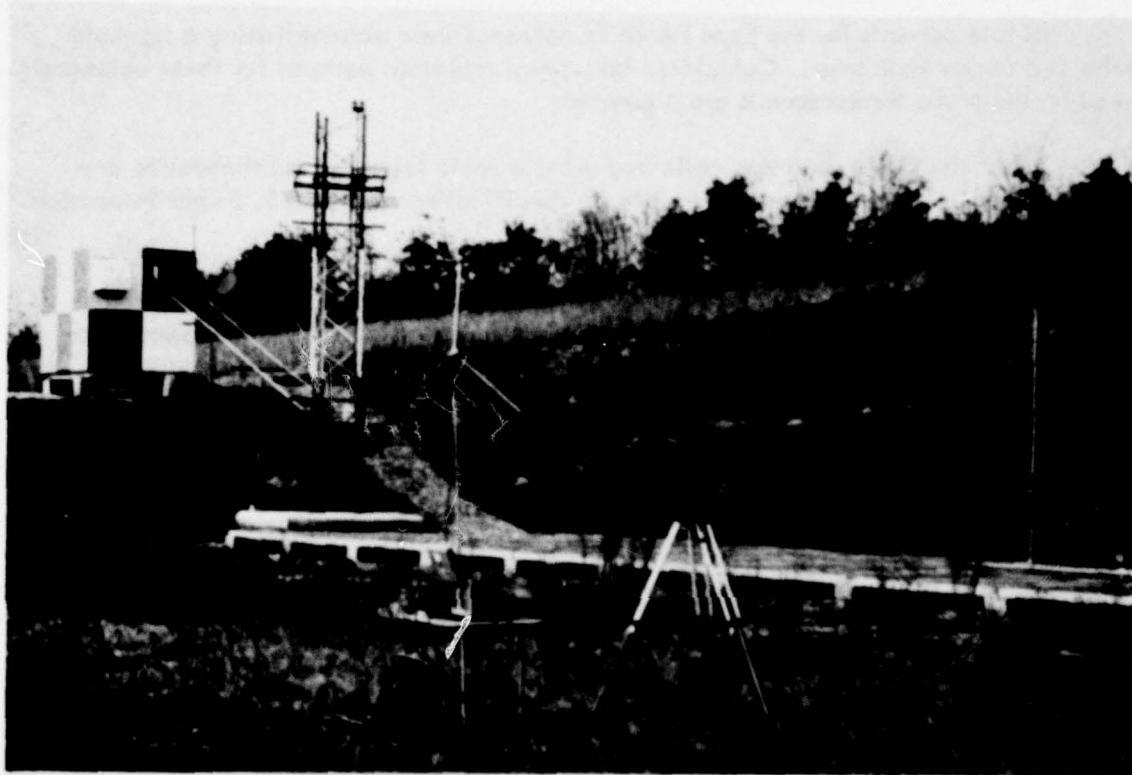
Figure 106. A View of the Sideband Reference Glide-Slope Facility at Bluefield, West Virginia. Limited terrain available for siting required the use of the sideband reference. The distance to centerline of Runway 23 is only 250 feet (76.5m). Note that there is a high embankment just to the north of the ground plane reflecting area. This area might be expected from an intuitive view to provide roughness in certain portions of the path.
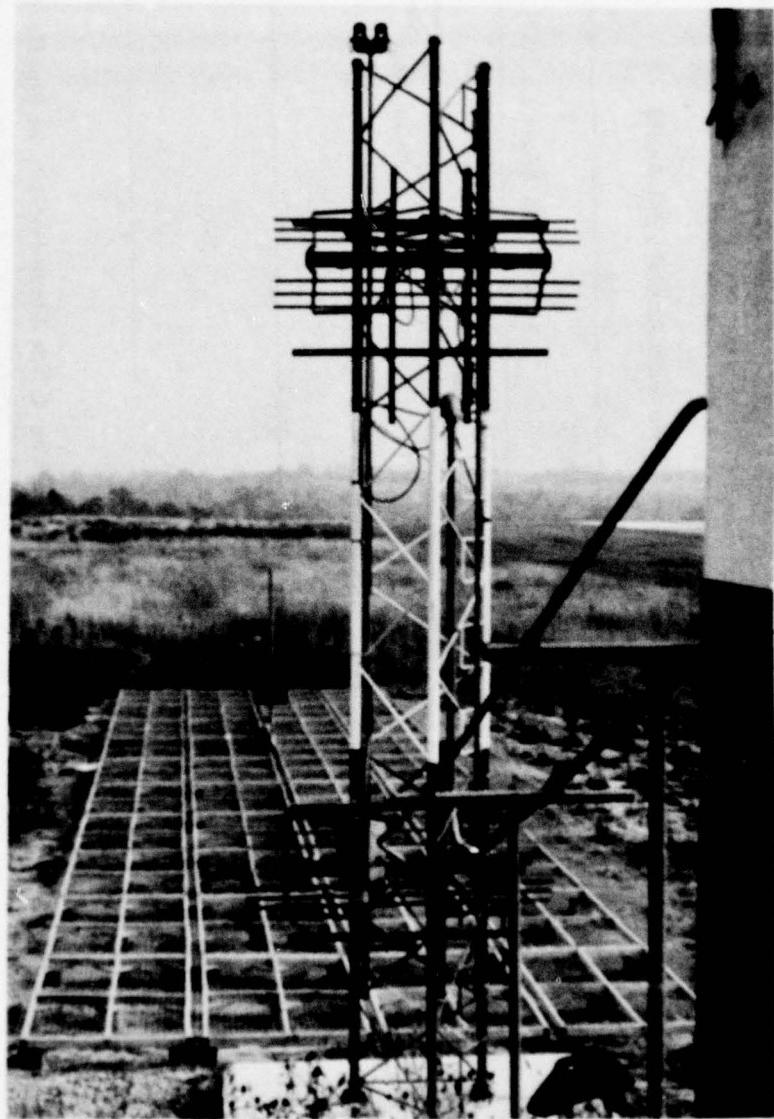
Figure 107. A View of the Antenna Mast and Counterpoise at Bluefield, West Virginia. The counterpoise is approximately 12" (30.5cm) above the ground and is well-constructed. Only a phase monitor is used in the near field.
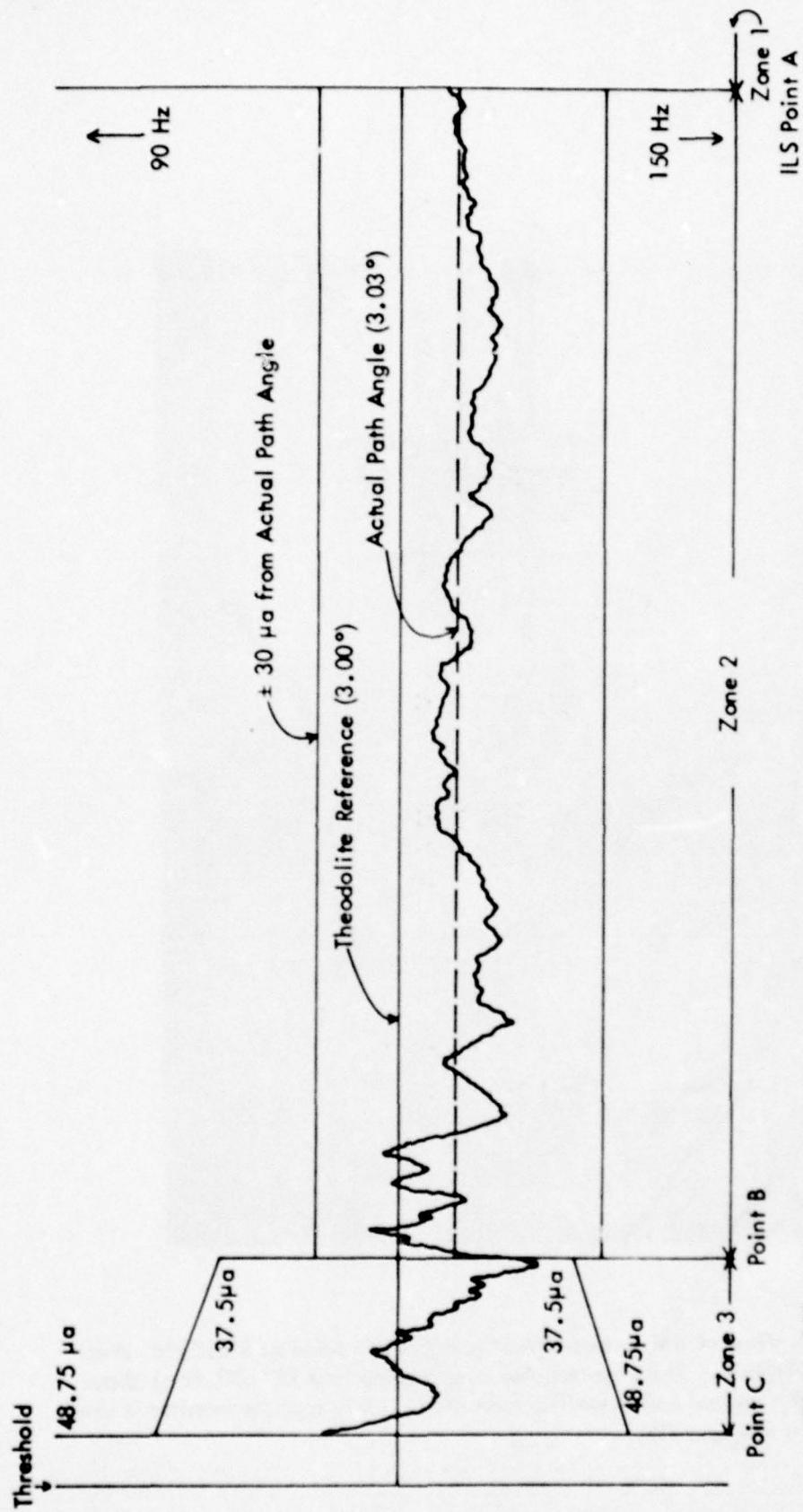
Figure 108. Pattern A Flyability Run Taken at the Sideband Reference Glide-Slope Facility at Bluefield, West Virginia in November 1978. The path meets CAT I specification reaching only 60% of tolerance limits.

Table 28. Results of the Perturbational Testing at the Bluefield, West Virginia Sideband Reference Glide Slope in November 1978.

	Measured		Calculated		Monitor % Alarm		Far Field % Alarm	
	∠ (°)	W (°)	∠ (°)	W (°)	Phase (%)	Width (%)	Path (%)	Width (%)
Equality	0							
SBO Phasing	6/150							
Upper Antenna Phasing	43/90							
Normal (B) (16.5mw)	3.07	.69	3.07	.69				
Normal (A)	3.03							
Broad (10mw, -2.17dB)	3.05	.82	3.07	.88	--	100	9	95
Sharp (25mw, +1.8 dB)	3.08	.55	3.07	.56	--	100	4	65
Hi∠(18.5mw, +.37 dB)	3.10	.60	3.11	.67	--	100	13	10
Lo∠(16.2mw, -.21 dB)	3.04	.62	3.04	.71	16	100	13	10
Lo∠(.016/90)mod unbal.	3.02	.69	3.01	.68	--	100	22	5
Hi∠(.029/150)mod unbal.	3.12	.67	3.18	.72	19	100	22	15
Normal (w/hardware)	3.04	.67	3.04	.67				
-1 dB UA	2.98	.75	2.92	.75	11	195	26	40
-2 dB UA	2.85	.95	2.84	.82	58	386	83	75
-3 dB UA	2.69	1.08	2.70	.88	135	576	154	105
LA +10°	3.02	.72	3.02	.68	100	81	9	5
+20°	2.96	.71	2.98	.70	128	200	35	15
+30°	2.86	.88	2.89	.78	180	367	79	55
-10°	3.07	.67	3.02	.68	100	29	13	5
-20°	3.05	.72	3.00	.70	287	100	4	15
-30°	3.00	.84	2.92	.78	468	224	18	55
Normal (w/hardware)	3.09	.60	3.09	.60				
SBO +10°	3.10	.65	3.09	.62	20	38	4	10
+20°	3.10	.68	3.09	.65	110	35	4	25
+30°	3.12	.77	3.09	.71	268	18	13	55
-10°	3.08	.60	3.09	.62	465	33	4	10
-20°	3.08	.70	3.09	.65	102	35	4	25
-30°	3.04	.72	3.09	.71	148	5	4	55
-1 dB LA	3.15	.57	3.19	.53	243	23	22	55
-2 dB LA	3.28	.51	3.29	.47	15	144	26	35
-3 dB LA	3.37	.44	3.35	.40	52	303	82	65
Normal	3.08	.65	3.07	.69	94	500	121	150

not available, an essentially ideal (i.e., perfectly conducting and infinite in extent) terrain had to be assumed for the computer model. This accounts for the departure of the calculated data from the measured results.

Clearly, the results in Table 28 show the monitor response of the system to be non-analogue in nature and not representative of far-field conditions. The monitors are oversensitive with respect to far-field changes. At no time did the monitors fail to indicate an alarm condition before the far field reached established tolerance limits.

Antenna currents were measured using a jig-held probe designed especially for the APC Type FA-8976 glide-slope antenna. The normalized currents for the antennas are given in Table 29.

Lower Antenna Element Currents		
Element	Amplitude	Phase
Center	-00.0 dB	-00.0°
Runway	+0.9 dB	24.0°
Outer	+1.9 dB	27.0°
Upper Antenna Element Currents		
Element	Amplitude	Phase
Center	-00.0 dB	-00.0°
Runway	+1.1 dB	26.5°
Outer	+1.1 dB	26.5°

The Upper Antenna is 0.5 dB, and 0.4 Degrees with respect to the Lower Antenna when the center element currents of both antennas are equal.

Table 29. The Calculated Effective Amplitude and Phase for Upper and Lower Antenna Currents as Measured at Bluefield, West Virginia.

Figures 109 and 110 are the calculated horizontal radiation patterns for the upper and lower antennas using the measured antenna dipole currents. Also shown on these figures are FAA specifications for glide-slope antennas as given in FAA-E-2429. These specifications are not met principally because of improper amplitude distribution across the dipole array. Current amplitudes for the outboard and runway elements should be 1 to 3 dB below that of the center element. This is not the case, as can be seen from Table 29.

Probe measurements also show that the center element of the upper antenna is +18.4° out of phase with respect to the lower antenna. The computed differential effective phase from Table 29 is +0.4°, resulting in a measured upper antenna phasing

Figure 109. Calculated Horizontal Radiation Pattern for the Upper Antenna (Type FA-8976 APC) at the Bluefield, West Virginia Sideband Reference Glide Slope.
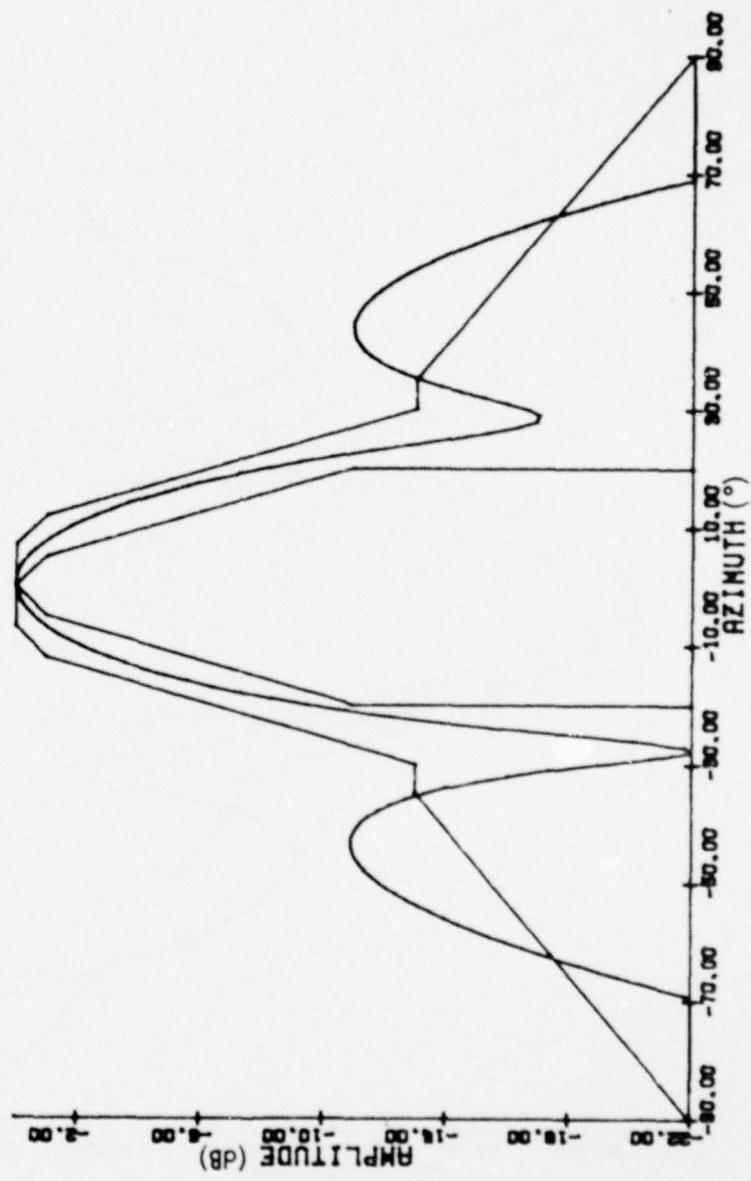
Figure 110. Calculated Horizontal Radiation Pattern for the Lower Antenna (Type FA-8976 APC) at the Bluefield, West Virginia Sideband Reference Glide Slope.

of +174.4°. This is certainly very close to ideal phasing (180°) and is a further demonstration that antenna phasing with the use of suitable probes and the vector voltmeter can be a viable set-up procedure.

I. Perturbational Study of the Sideband Reference Glide Slope at Morgantown, West Virginia.

1. Summary. A series of perturbational tests has been completed at the side-band reference (SBR) glide-slope facility at Morgantown, West Virginia. The airborne measurements were conducted in March 1979 using Ohio University's Minilab Mark 3 in a Beechcraft Model A36. One result of this study is the documentation of the facility response to parametric perturbations introduced into the system's transmitting equipment and antennas. The response of the system is predictable and is found to be well within CAT I specifications reaching only 40% of tolerance limits. The near-field monitoring scheme, which is typical of sideband reference facilities of this type, is found to be oversensitive and not analogous to changes in the far field. These monitors essentially serve as fault detectors.

2. Discussion of Data Acquisition. The Instrument Landing System at Morgantown, West Virginia serves Runway 18. The Mark 1D transmitting and monitoring equipment is located on the east side of the runway and is displaced 250' (76.2m) from runway centerline. Distance to threshold is 1100' (335.3m). Type FA-8976 APC glide-slope antennas are in use at the operating frequency of 329.9 MHz. Figure 111 is a view of the transmitting antennas and equipment shelter from the counterpoise area. Figure 112 is a view out into the reflecting zone from the counterpoise area with the AIL corner-reflector type monitor antennas.

The 1100' (335.3m) ground plane is certainly truncated; however, it is the limited terrain in the transverse direction that motivates to a great extent the use of the sideband reference system. Antenna heights are 7.75' (2.362m) and 22.67' (6.908m).

The sideband reference at Morgantown utilizes a counterpoise measuring 20' x 112' (6.1m x 37.2m) which is elevated from the local terrain an average of 10" (25 cm). The purpose of the counterpoise is to isolate the monitor probes from environmental changes, particularly those changes in the characteristics of the ground plane between the monitor probes and the transmitting antennas. Since the counterpoise can be viewed as a raised ground plane for the monitor probes, the distance d to the 360° point can be calculated using the standard formula:

$$d = \frac{H^2 - h^2}{2B_p}$$

where H and h are the heights of the upper and lower antennas, respectively, from the level of the counterpoise and B_p is the wavelength in feet at the operating frequency. The calculated distance of 71.9' (21.91m) compares with the measured distance to the amplitude monitor probe at Morgantown of 68.8' (20.97m). Accordingly, the phase detector position should be a factor of 1.2 farther from the antenna mast or at a distance of 86.3' (26.30m). This compares with a measured distance of 87.2' (26.58m).

-335-
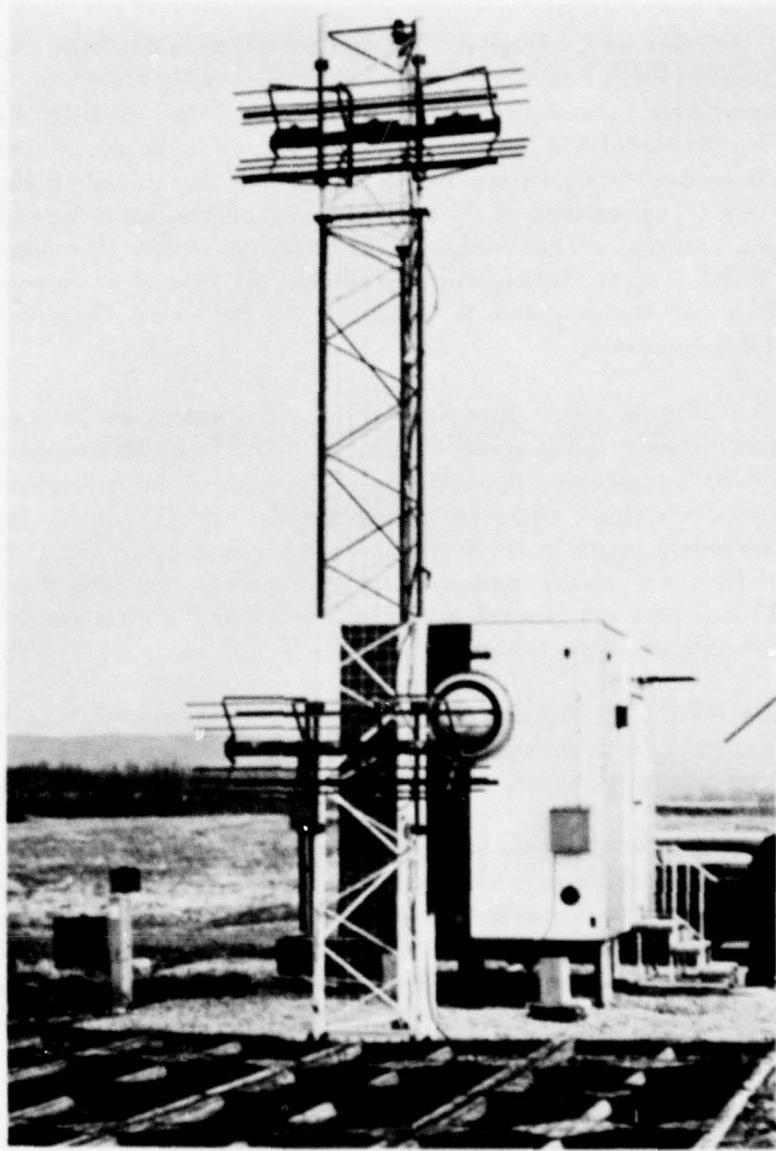
Figure 111. The Transmitting Antennas and Equipment Shelter at the Sideband Reference Facility at Morgantown, West Virginia. Mark 1B transmitting and monitoring equipment are in use.
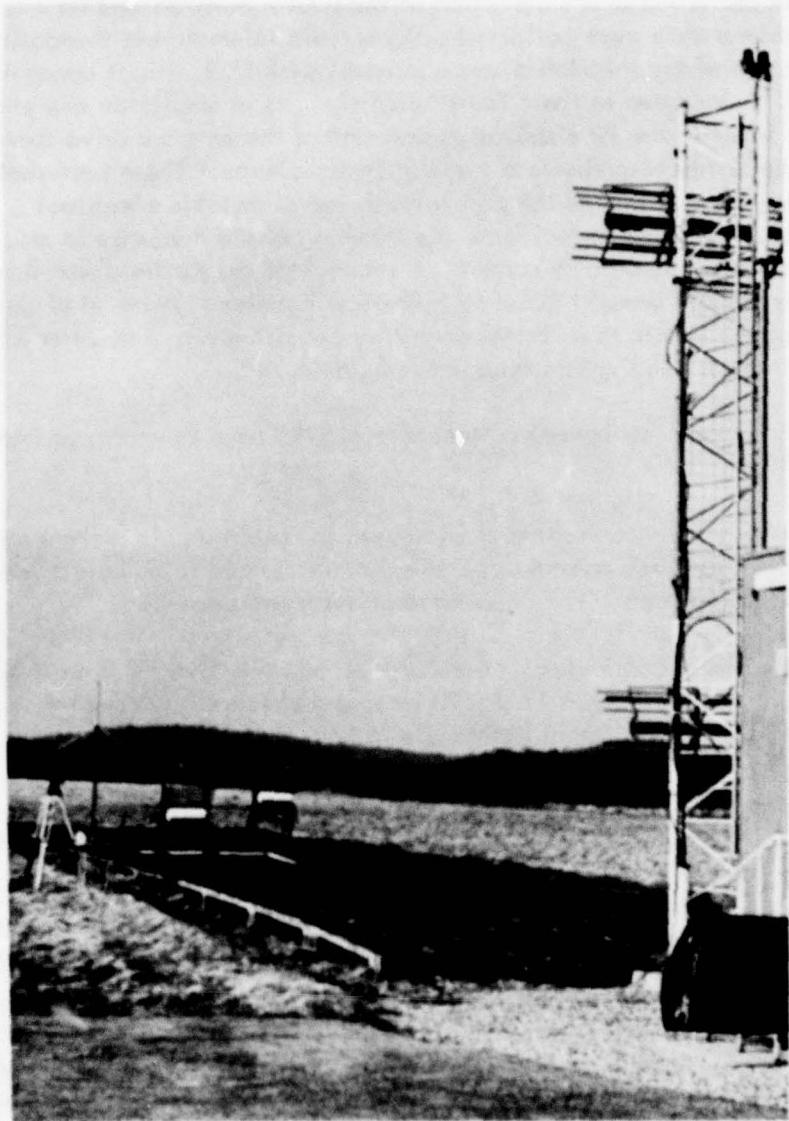
Figure 112. View of the Reflecting Zone in Front of the Transmitting Antennas and Counterpoise at Morgantown, West Virginia Sideband Reference Facility.

Prior to any testing of the facility, the normal conditions of the path angle and path width were determined with both pattern A runs (flyability) and pattern B runs at 1000' (300m) AGL.

With the monitor alarm limits established, a series of system perturbations was introduced. For each perturbation the condition of the system monitors and far field was determined. Airborne data were collected using a radio telemetering theodolite as a reference. Location of the theodolite was consistent with U.S. Flight Inspection Handbook OA P8200.1. Included in these faults were changes in amplitude and phase of the sidebands only input to the RF distribution unit and of the antenna drive currents. Also documented is the system response to a modulation unbalance. These perturbations were introduced by way of insertion of the proper hardware of suitable electrical length. A line stretcher was used to facilitate the trimming of the hardware to return system monitors as closely as possible to normal. A recheck of the far field was then made to document any change brought about by hardware insertion. Removal of the hardware and return of the system to a normal operating condition was done after all perturbations were checked. The system returned to 3.05°/.74°.

Calibration of airborne equipment is traceable to NBS through approved FAA Repair Station CO7-10.

A jig-held probe and vector voltmeter were used to obtain dipole current measurements for the FA-8976 glide-slope antennas. These data were used to calculate horizontal radiation patterns for the antennas. The calculated patterns are presented.

3. Results. The airborne check of modulation equality showed 3 μa/90 Hz. Carrier-to-sideband phasing resulted in 12 μa/90 Hz and a check of upper antenna phasing produced 10 μa/150 Hz. The actual path angle in zone 2 as established by the pattern A structure run was 3.01°. This path is also found to be well within CAT I specifications reaching only 40% of established tolerance limits. Figure 113 is the differential trace from this run. The path angle and path width as established by the pattern B runs at 1000' (300m) were 3.08°/.72°.

Broad and sharp alarm conditions produced by -1.25 dB and +1.18 dB changes in sideband power level resulted in measured values for path width of .83° and .64°, respectively. Monitor alarm limits for high and low angle conditions were established with a suitable change in sideband power unbalance. The far-field conditions for these limits were 3.14° and 2.98°. Path angle changes produced by a modulation unbalance are seen in Table 30 to result in a predictable response by the monitors. The results of all perturbations as well as normal runs and alarm conditions are presented in Table 30.

With alarm limits documented and the normal condition of the system determined, a series of perturbations was introduced. These include changes of in-line signal amplitude and phase. The response of both the system monitors and of the far field is presented in Table 30. Numbers are percent of alarm in the case of the monitors and as percent of tolerance limits in the case of the far field. Also presented in Table 30 are the measured airborne data and the calculated response of the far field. This calculated response has been generated by the computer model OUGS.
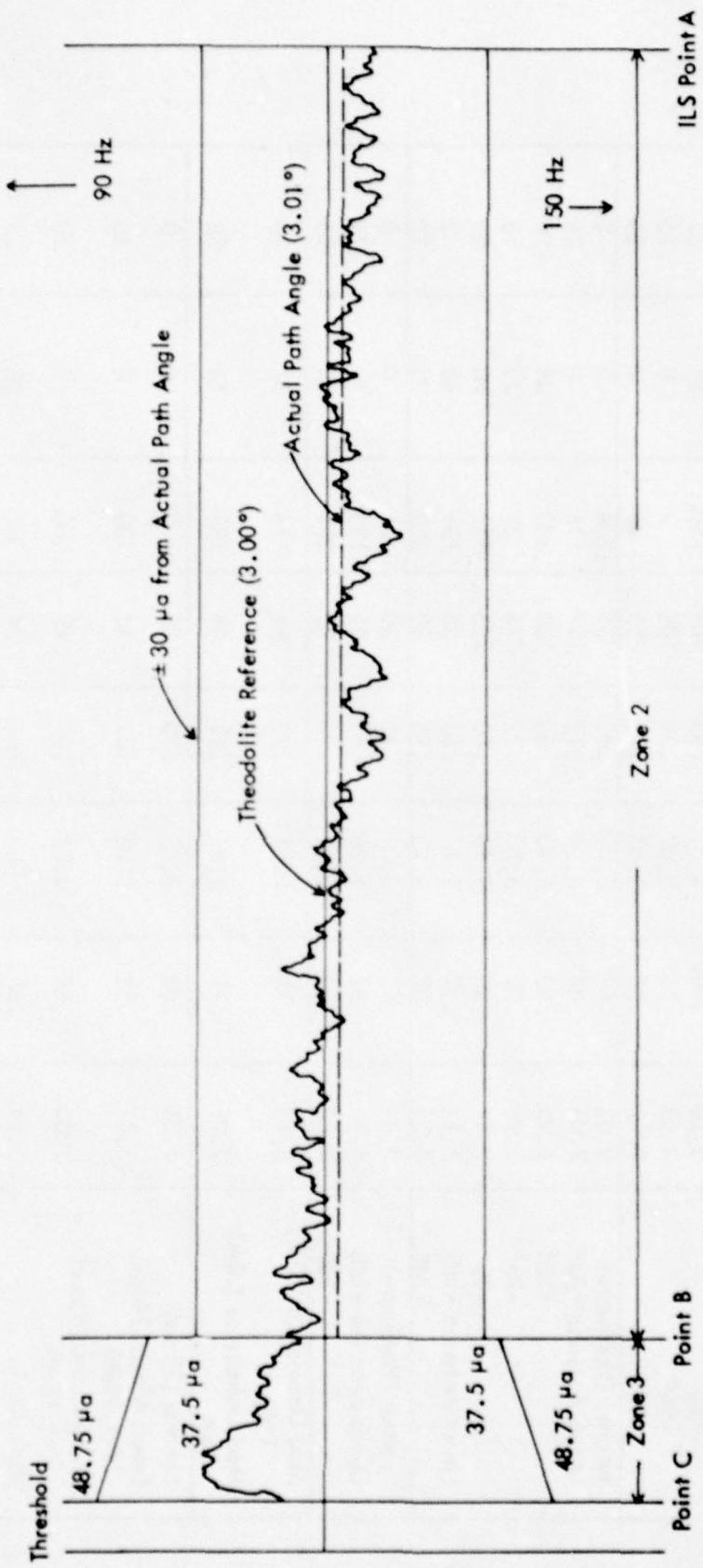
Figure 113. Pattern A Flyability Run Differential Amplifier Trace as Recorded at the Morgantown, West Virginia Sideband Reference Glide Slope by Ohio University in March 1979. The path meets CAT I specifications reaching only 40% of tolerance limits.

	Measured		Calculated		Monitor % Alarm		Far Field % Alarm	
	P (°)	W (°)	P (°)	W (°)	Phase	Amp	Path (±0.225°)	Width (±0.2°)
Equality	3 µa / 80 Hz							
SBO Phasing	12 µa / 90 Hz							
Upper Antenna Phasing	10 µa / 150 Hz							
Normal (Pattern A)	3.01							
Normal	3.08	.72						
Normal	3.11	.70						
Normal	3.08	.72	3.08	.72	0	0	--	--
Normal (Hardware)	3.03	.73	3.03	.73		4	0	0
SBO +20°	3.03	.79	3.03	.79	186	68	0	30
+30°	3.10	.90	3.03	.85	288	150	31	85
-20°	3.03	.76	3.03	.79	188	4	0	15
-30°	3.02	.77	3.03	.85	265	43	4	20
Normal (Hardware)	3.03	.69	3.03	.69	36	4	0	0
Upper Antenna +20°	3.04	.84	3.00	.72	198	114	4	75
+30°	2.93	.93	2.93	.80	328	250	44	120
-20°	2.98	.72	3.00	.72	176	36	22	15
-30°	2.87	.80	2.93	.80	223	132	70	55
Lower Antenna -1dB	3.12	.69	3.11	.63	35	121	40	0
-2dB	3.20	.55	3.23	.55	80	368	75	70
Normal (Hardware)	3.03	.75	3.03	.75	30	21	0	0
Upper Antenna -1dB	2.96	.81	2.92	.83	21	136	31	30
-2dB	2.83	.94	2.83	.90	29	275	88	95
Mod Unbalance (.040/150)	3.16	.71	3.19	.79	91	114	57	30
Mod Unbalance (.040/90)	2.91	.71	2.87	.71	28	100	53	30
Normal (32mw)	3.03	.70	3.03	.70	30	0	0	0
Broad Alarm (24mw) (-1.25dB)	3.03	.83	3.03	.81	41	100	0	65
Sharp Alarm (42mw) (+1.18dB)	3.05	.64	3.03	.61	48	100	9	30
High Angle	3.14	.65	--	--	74	82	48	25
Low Angle	2.98	.78	--	--	9	114	22	40
Normal	3.05	.74	--	--	38	32	0	20

Table 30. Results of Perturbational Testing Done by Ohio University at the Sideband Reference Facility at Morgantown, West Virginia in March 1979.

Note that the results in Table 30 show the monitor response of the system not representative of far-field conditions. The monitors are serving conservatively as fault detectors indicating alarm conditions before the far field reaches tolerance limits.

Dipole currents measured using a jig-held probe and a vector voltmeter were obtained for the Type FA-8976 APC glide-slope antennas. The normalized currents for the dipoles are presented in Table 31. [10]

Lower Antenna Element Currents		
Element	Amplitude	Phase
Center	-00.0 dB	-00.0°
Runway	-0.5 dB	27.4°
Outer	-0.5 dB	27.0°
Upper Antenna Element Currents		
Element	Amplitude	Phase
Center	-00.0 dB	-00.0°
Runway	0.3 dB	21.0°
Outer	0.3 dB	26.0°

The Upper Antenna is 1.4 dB, and -2.0 degrees with respect to the Lower Antenna when the center element currents of both antennas are equal.

Table 31. Calculated Effective Amplitude and Phase for the Upper and Lower Antennas of the Sideband Reference Glide Slope at Morgantown, West Virginia. The antennas are Type FA-8976 APC.

These measured currents result in the calculated horizontal radiation patterns given in Figures 114 and 115. FAA specifications for glide-slope antennas as given in FAA-E-2429 are also shown in these figures. The radiation patterns as calculated from measured data do not meet specifications because of insufficient taper in the amplitude distribution across the array. The runway and outer element amplitudes should be 1 to 3 dB below the center element.

Table 31 shows the antennas to have an effective differential phase of -2.0°. The measured upper-to-lower phasing using a vector voltmeter was +181° when viewed at the center elements of the antennas. The composite phasing of the upper antenna can be considered to be the algebraic sum of these values or +179°. Upper antenna phasing using the vector voltmeter and probe is seen to be a viable installation, maintenance, and set-up tool which can conserve flight time during commissioning or periodic flight checks.

-341-
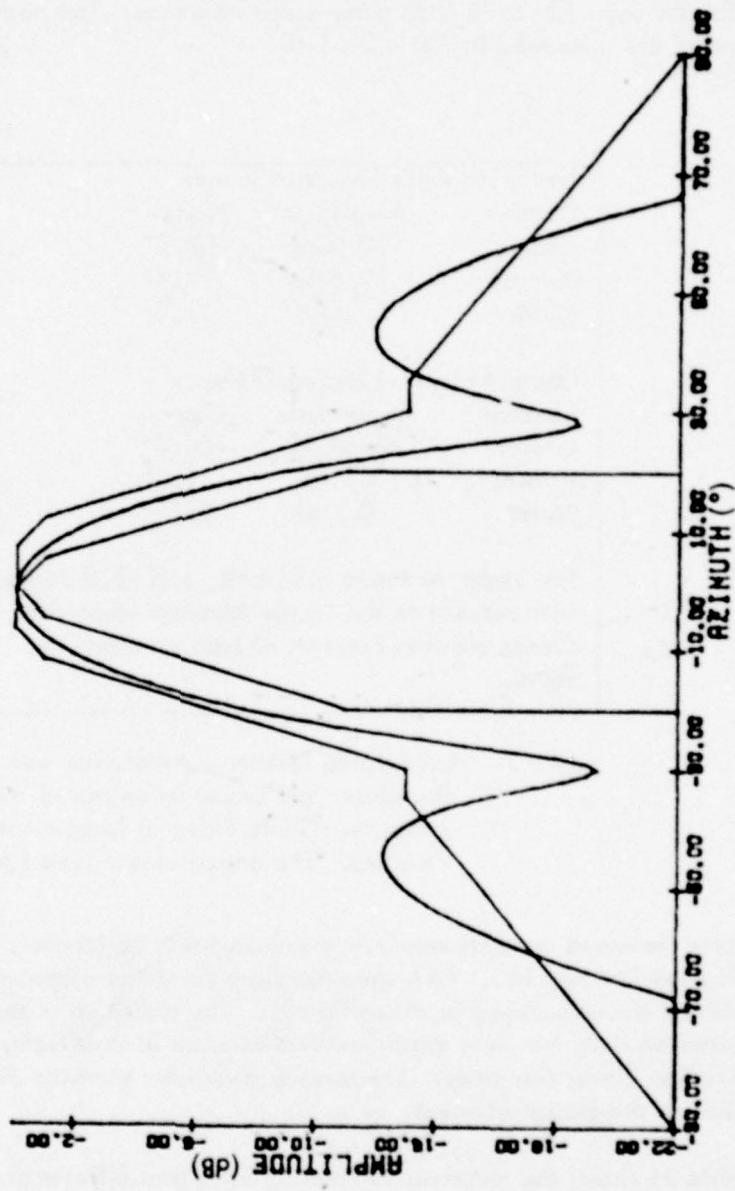
Figure 114. Calculated Horizontal Radiation Pattern for the Upper Antenna (Type FA-8976 APC) at the Morgantown, West Virginia Sideband Reference Glide Slope in March 1979.
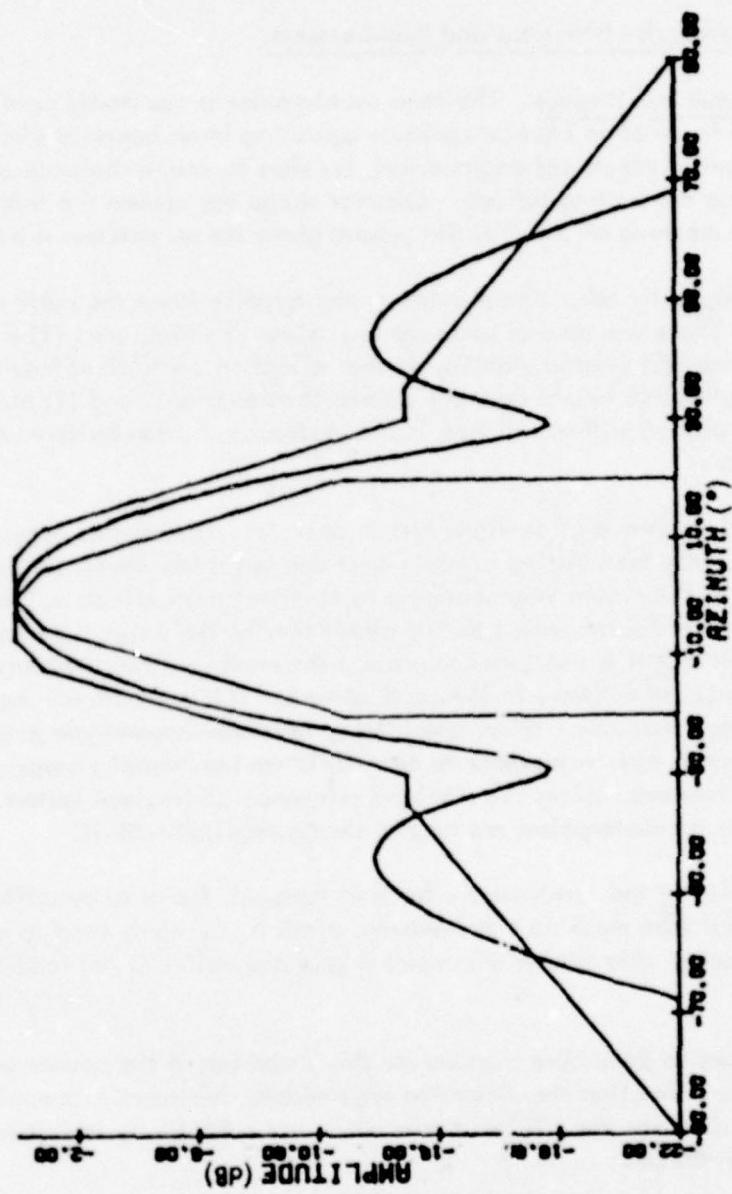
Figure 115. Calculated Horizontal Radiation Pattern for the Lower Antenna (Type FA-8976 APC) at the Morgantown, West Virginia Sideband Reference Glide Slope in March 1979.

J. Wheeling, West Virginia Sideband Reference. Numerous attempts were made to obtain data on sideband reference system performance at Wheeling, West Virginia. In spite of two visits to the site, weather and equipment difficulties prevented a complete systematic perturbational study from being completed. Partial data was obtained, but without the complete set an analysis of the system performance was not possible.

K. SBR Counterpoise Functions and Requirements.

1. Concept and Purpose. The term counterpoise is commonly used to mean a counterbalance or a force of an equal magnitude operating in an opposite direction. As applied in the context of electrical engineering, it refers to counterbalance of electrical charges provided by a conducting surface. Common usage has caused the term counterpoise to take on the meaning of an artificial ground plane for an antenna system.[11]

One might logically ask, Why provide a counterpoise when the earth itself can serve this purpose? There are several good reasons, some of which are: (1) a smoother surface may be desired, (2) greater stability in the reflection coefficient may be needed, (3) protection from effective height changes is sometimes required, and (4) elevation of the antenna may be desired without change in the vertical radiation pattern and the associated impedance.

The sideband reference glide-slope system operates with monitor detector probes within 80' (24.4m) of the transmitting antenna mast and but a few feet from the ground. This positioning makes the probes very sensitive to environmental effects. The monitor thus becomes sensitive to factors which do not affect the far-field signal performance. Experience has shown that it is necessary to protect the monitors from some environmental changes such as changes of moisture in the earth ground. This protection is best provided by installation of a counterpoise. When considering the three image-type glide slopes, the sideband reference is most vulnerable to near-field environmental changes. This section on counterpoises emphasizes the sideband reference glide-slope system and its monitoring, because counterpoises are nearly always required with it.

Since the value of the conductivity for most metals is found to be sufficiently high, galvanized steel wire mesh such as hardware cloth is commonly used to conserve cost and weight. Copper wire screen with needed grid dimensions is not readily available.

There is a need to determine a bound for the dimension of the counterpoise. From a theoretical consideration the dimension requirement decreases exponentially, such that at a given distance the effects of truncation are sufficiently low as to produce minimum undesirable effects.

In practice, therefore, it is common to find an area of steel wire mesh screening located specifically with respect to driven antenna elements to control and stabilize the vertical radiation patterns of VOR, ILS localizers, marker beacons, many glide slopes, and nondirectional beacons. The NDB antenna counterpoise, consisting of buried single conductors, may be more extensive but simpler due to wavelength considerations.

-344-

With respect to the contemporary sideband reference glide slope, the counterpoise becomes a reasonably well-defined object. It is employed to provide a stable environment for the monitor operation by eliminating effects of changes in ground characteristics on the signals arriving at the monitor probes approximately 75' (22.9m) in front of the transmitting antennas. Following is a discussion of details concerning deployment of counterpoises for application with the sideband reference glide slopes.

2. Theory. Consider a horizontal dipole antenna located in free space (see Figure 116). The electric current I is in the x-direction, thus yielding an omnidirectional electric field radiation pattern in the yz-plane. This field is normal to the yz-plane, and thus parallel to the xy-plane along the y-axis. If the xy-plane is made conducting, then this electric and magnetic field may be considered to be terminated by an electric and fictitious magnetic current respectively produced in the surface. These parasitic currents may be then considered as secondary sources producing their own radiated fields.

A simpler view may be that of considering the field to be reflected from the conducting surface. Optical principles may be applied to identify the regions of maximum radiation. Assumptions of perfect conductivity permit simplified calculations of radiation patterns.

Once the conducting plane has been established, obviously the omnidirectional field pattern has been altered. One common and convenient method of determining the resultant pattern is by the use of image theory. [12] This assumes the existence of a second antenna an equal distance below the ground plane with currents equal in magnitude but 180° out of phase with the principal source. The interference pattern calculated for the pair of two antennas is then considered to exist only in that portion of space above the ground plane. [13,14]

It should be evident from the drawing in Figure 116 that the efficiency involved in the reflection, i.e., reradiation process, is affected by the resistive (ohmic) loss affecting the electric current. Attenuation of this sheet current will obviously result in weaker fields being reradiated.

Further, it should be evident from the same drawing that the organization of the currents in the ideal ground is based on the orientation of the incident fields. Reradiation then is consistent with the vectors representing the incident fields. Should gaps or discontinuities in the conducting surface exist, the currents clearly must form or organize to be compatible with conducting paths. Should a current be prevented from flowing in the path consistent with the incident field, it will take an alternate path, thus producing a reflected field with changes in amplitude, phase and polarization from that which would be produced with the ideal reflector. The significance of this anomalous contribution is dependent, generally, on its magnitude. The magnitude is dependent on the relative size of the interrupting gap with respect to resonance (wavelength).

A worst-case type condition is where there are air gaps in the conducting surface with dimensions which are resonant at the frequency of the incident signal. If these slots are perpendicular to the flow of the electric sheet current normally established by the incident magnetic field, then a new current pattern will be set up. This, in effect,

Electric Sheet Current $J_{es} = \hat{n} \times \bar{H}$ amperes per m

Magnetic Sheet Current $J_{ms} = -\hat{n} \times \bar{E}$ volts per m
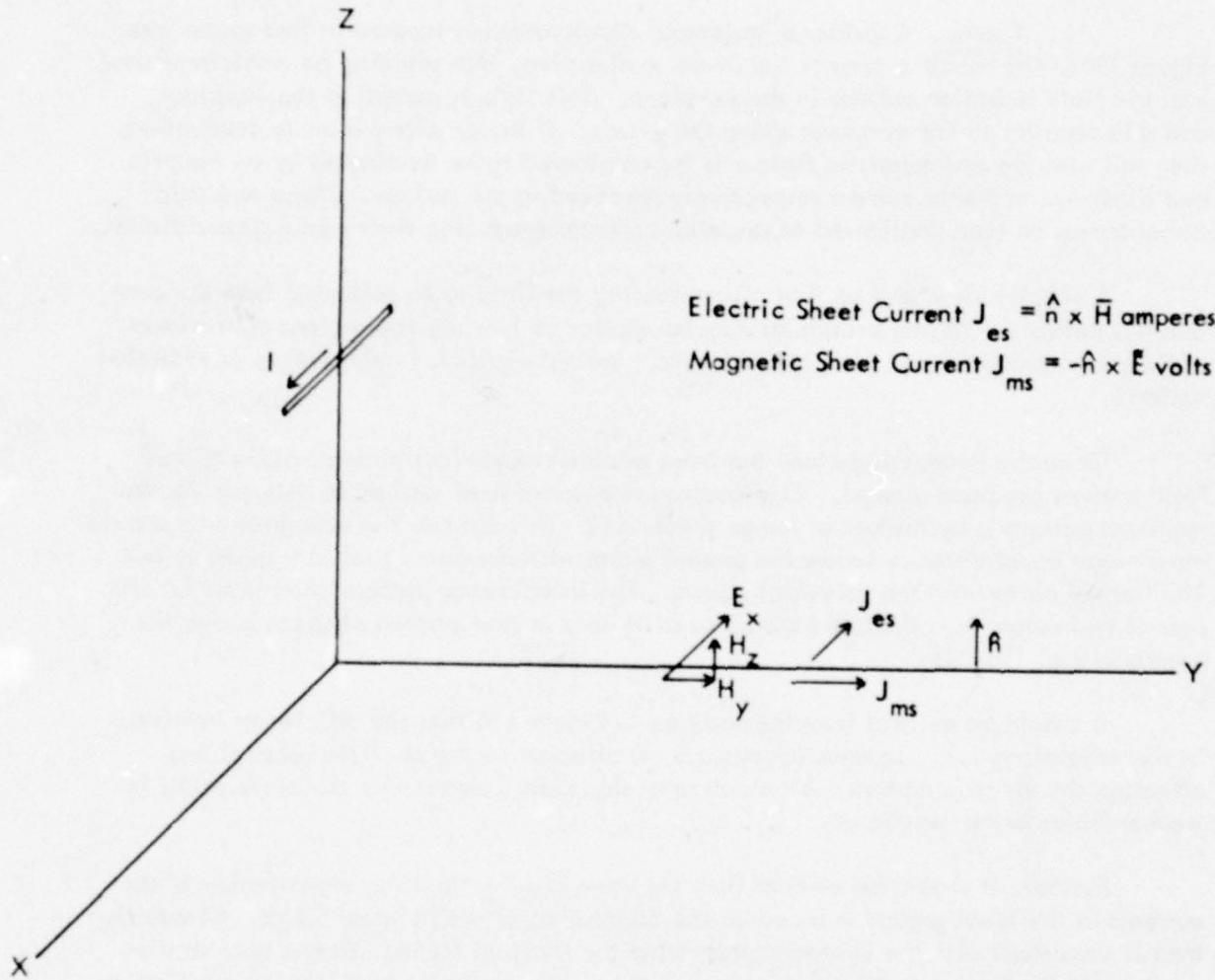
Figure 116. Dipole with Source Current, Fields, and Sheet Currents.

interrupts the current elements and reorganizes them into a new pattern. The resulting reradiated fields will have new patterns and polarizations. In practice, these would tend to be irregular and would produce considerable space variation in the signal. Should these slot dimensions formed by gappings and metal contacts be time varying (with wind or corrosion), then the space patterns would, of course, be time varying.

Corrosion can alter the conductivity and cause losses and less than optimum reflections. Moisture will produce other variations in ohmic losses.

3. Fabrication. When fabricating a counterpoise for a sideband reference system, it is important to keep in mind certain aspects of the theory just mentioned.

(a) Dimensions of Counterpoise. The magnitude and phase of the currents induced on the ground plane are related to the fresnel zones. [15] The currents which are principal contributors to the resultant radiated electromagnetic fields are located in what is termed the first fresnel zone. Therefore, it is necessary as a very minimum to contain this first fresnel area when the counterpoise is constructed. Because the counterpoise is at a different height than the earth ground, and edge effects may be a contribution to the field patterns, it is desirable to extend the counterpoise by 50 to 100%. An acceptable sideband reference counterpoise will have dimensions of 20 by 80' (6.1 x 24.4m), with the phase detector near the far edge from the transmitting antennas. Even with this size counterpoise, snow banks off the edges, for example, will be observed by the monitor detectors.

The use of corner reflector-type transmitting antennas reduces slightly the requirements on the size of the counterpoise for that appropriate for dipole antennas. No tests have been conducted; however, calculated patterns suggest that 10' (3.1m) of counterpoise may be eliminated immediately in front of the transmitting antennas when corner reflectors are used. The fresnel zone being centered nearer the monitor detector probes because of their low height also favors elimination of several feet of counterpoise near the transmitting mast. If a forward-looking, receiving antenna is used for the monitor probes then there is no need for counterpoise behind the probe antenna.

(b) Size of Wire Mesh or Spacing of Wires. The conductor which is effective in reflecting signal must be parallel to the electric field. This means that the conducting wires perpendicular to the reflecting conductors, such as exists in wire mesh fence material, are serving strictly as physical support members. It is important to note this distinction, viz, the controlling factor of the spacing S in Figure 117 is electrical and the controlling factor D is physical.

The allowable spacing S can be obtained from Table 32. If the spacing becomes too great, the reflection coefficient decreases in magnitude. With spacings greater than 18" (46cm) the reflector begins to produce lobing. A 1/10 wavelength spacing or less is usually needed to give satisfactory results in eliminating the effects of the earth. Wire mesh with 3" (8cm) spacing or less in the longitudinal direction is, therefore, recommended.

-347-
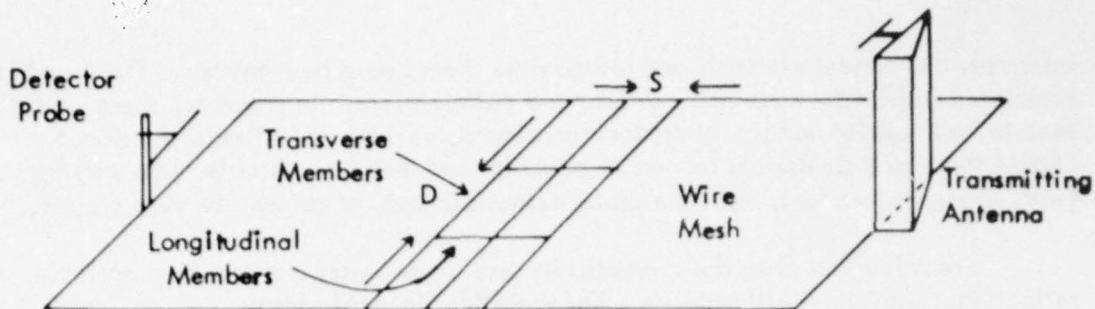
Figure 117. Counterpoise Layout for Sideband Reference System.

REFLECTION COEFFICIENT (Grazing Angle is 16 Degrees)				
No. 10 Wire Diameter		Spacing in λ	Amplitude	Phase Degrees
Inches	Millimeters			
0.102	2.55	0.100	0.9710	164.7
0.102	2.55	0.200	0.8441	147.8
0.102	2.55	0.300	0.6905	133.9
0.102	2.55	0.400	0.5495	123.3

Table 32. Reflection Coefficients Produced by No. 10 Wire with Various Spacings.

The lateral spacing D can be any value consistent with the mechanical requirements. When the conductors are run longitudinally, care should be taken to insure the laterally run conductors remain continuous.

The spacing of the longitudinal members may be any value. In fact, they may be eliminated altogether if transverse wires are stretched to be parallel to the electric field. If a wire mesh is used, care should be taken to insure that the transverse wire is continuous, thus avoiding the use of only twist connections for continuity. If a roll of wire screen is used, it is usually best from wire continuity considerations to run the stock transversely since the long wire elements are usually run lengthwise in the roll.

The basic concern should be to provide a continuous electric path transverse to the line from the transmitting antennas to the monitor detector probes. If sections of wire mesh are run longitudinally or parallel to this line, there is a strong burden then placed on the electrical ties from one section of the mesh to another. Ties tend to corrode in time leading to problems of instability.

(c) Spacing of Ties. When sections of chicken wire, hardware cloth or fencing are run in the longitudinal direction, it is important to tie (bond) these to neighboring sections so that an effectively continuous electrical wire exists in the transverse direction. To meet the electrical requirements, a bond should be made every 3" (8cm) (note Figure 118). These bonds must hold up against mechanical failure and corrosion. Use of solder and brazing, of course, adds heat and destroys existing corrosion protection on the wire. Care must be taken to restore this protection. The penalty for not doing so will be the vulnerability to intermittents and instability in the operation of the monitors.

(d) Conductivity. Obviously a perfectly-conducting material is ideal. Copper is excellent but expensive. The practical conducting element usually turns out to be steel with a conductivity of approximately 10^6 mhos per meter, compared with 6×10^7 for copper. Although this is not particularly good, experience has shown that it is adequate and good monitor operation can be maintained if approximately a #12 wire size is used.

(e) Height of Counterpoise. Even though the purpose of the counterpoise is to isolate the monitors from the environment, a complete isolation is not desired. One major reason is to detect the accumulation of snow. A few inches on a ground will usually affect the monitor detectors, but will not be evident on the far field. It is, therefore, desirable to set the height of the counterpoise 8 to 12" (20 to 31cm) above the earth such that when the snow passes through, builds up below, and possibly begins to rise above the conductors, the monitor will then alarm as the total snow on the far-field reflecting ground causing the path at the airplane to reach its tolerance. Should the counterpoise be at ground level, then the alarm would be premature because of the greater sensitivity of the monitor.

A wide mesh, as has been described, gives a lower reflection coefficient meaning that some of the electromagnetic energy penetrates through the mesh to the region below. Thus, should snow build up below a wide mesh screen, the monitor will begin to show effects before the accumulation is above the screen. A fine mesh, on the other hand, will be a better reflector, i.e., have a higher reflection coefficient, but it will collect snow rather than pass it to the earth below. As a result, the monitor responds excessively to that appropriate for predicting far-field conditions. The tradeoff is then between a wide mesh to let the snow through and a fine mesh to meet electrical requirements. The 3" (8cm) size is a good compromise.

Protection should be provided so that the monitor is at or near alarm with a total accumulation of 8" (20cm) of snow on the earth. [16] This means with a ground plane elevation of 8" (20cm), all of the snow falling through a 3" (8cm) mesh, a far-field tolerance will be reached when a few inches of snow rises above the mesh to give an alarm.
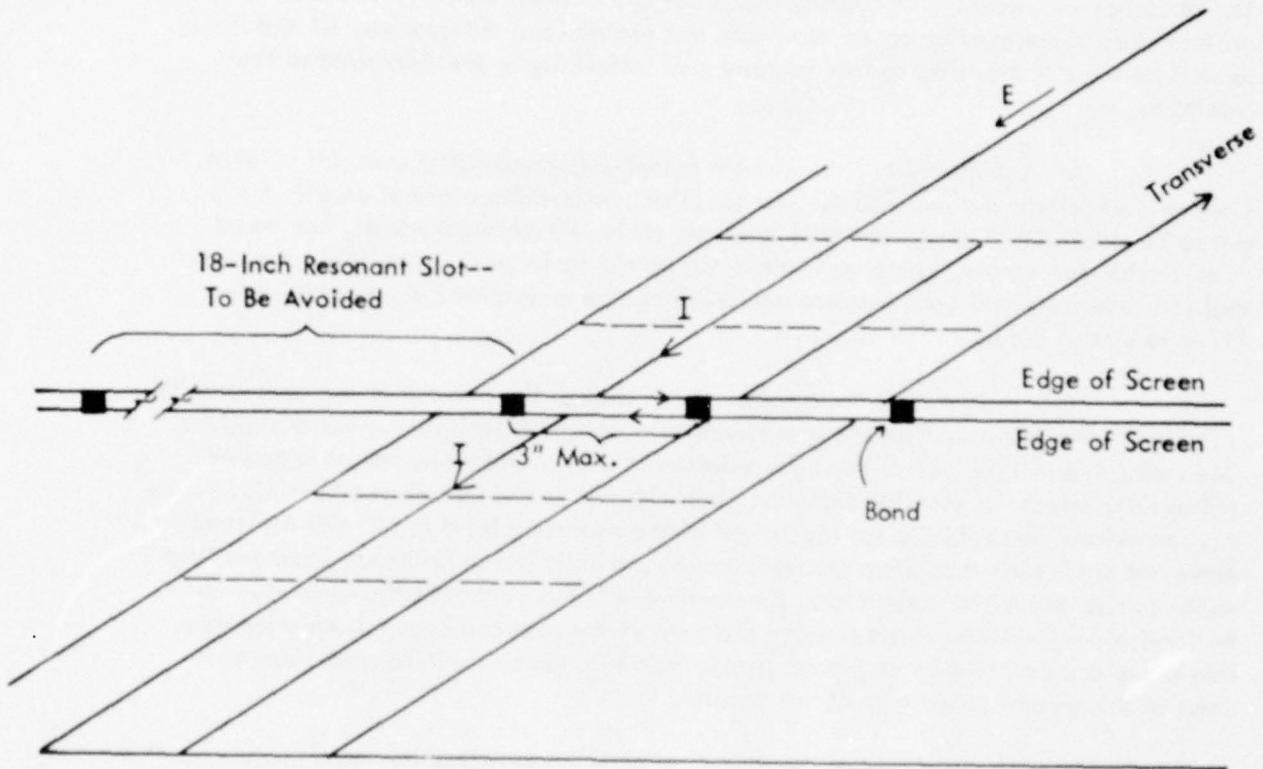
Figure 118. Bonding Requirements.

In some snow conditions the far-field tolerance has been reached with 8" (20cm) of snow on the ground plane. Serving the far field in general, however, it requires 12 to 15" (31 to 38cm) to reach far-field tolerance values. Protection usually has been for this latter, but an 8" (20cm) height should be adopted whenever practical.

The counterpoise serving as a ground should establish and control the images for the image antenna sideband reference system as seen by the monitors. The fact that the counterpoise is finite in extent means that it is not a complete control since some of the earth will also be reflecting signal to the probes.

From a theoretical standpoint, it is important to note that if the counterpoise is at resonant height above ground, say 9" (23cm), then it is conceivable that the area between the counterpoise edge and the earth might become a slot radiator should it be excited properly. This would produce an interference problem which could create observed path roughness on flight checks of the path structure. Earth grounding strips would not necessarily solve this problem. The best solution is to avoid exciting this probable radiator, i.e., avoid stray radiation from the hut and other assemblies.

(f) Smoothness. Since it is not possible to construct a perfectly smooth ground screen, some consideration must be given to allowable tolerances. First and foremost, the screen must be stable. Variations in the surface of the screen will produce changes at the monitor which are unrepresentative of the far field. Electrical requirements will be met and a satisfactory appearance obtained if a ±1" (2.54cm) tolerance is maintained over the surface area. Electrical tolerances will allow greater surface irregularities than this if they are invarient with respect to time and the monitors are adjusted to accommodate them.

(g) Ground Potential. The counterpoise, even though it is serving as a ground, does not need to be at a DC ground potential to serve its purpose from radio frequency, monitor considerations. There are other considerations, however, that make this DC grounding desirable, such as protection of personnel from shock hazard, lightning protection, and elimination of undesirable equipment grounding problems.

4. Conditions to Avoid. There are several items which, if not addressed, can provide significant problems in operating the sideband reference monitor system.

All factors which might prove variations of physical condition with time should be scrutinized. Physical stability is essential, because in most cases the electrical stability of the monitoring system will be critically dependent on it. Wooden, supporting forms which are frequently used should be made from lumber which has been pressure treated to resist insects, rot and decay. All metals used in the construction should be galvanized or treated with primers to prevent corrosion. Bonding points should be very carefully protected with paint, plastic sealers, or other coatings which resist sunlight and moisture.

Care should be taken to insure that no slot radiators have been created. For example, bonding every 36" (91cm) between longitudinally-run sections of wire mesh, invariably ends up producing gaps which are interrupting ground currents to form effective resonant slot antennas. Polarization of signals from these is horizontal and very effective in determining the sample acquired by the monitor probe. Adjusting the monitor initially compensates for this radiation but it is frequently unstable, thus producing monitor variations.

Hexagonal-configured chicken wire is undesirable because of the irregular current paths it produces.

5. Summary of Construction Suggestions. The ideal counterpoise is impossible to build. The following is a description of a practical counterpoise which should be of reasonable cost.

Fifty frames of pressure-treated 2 by 4 lumber stock are constructed with 4' by 8' (1.2m x 2.4m) dimensions (see Figure 119). A central cross brace is suggested to form 4' by 4' (1.2m x 1.2m) square areas. Farm fencing with 3" (8 cm) spacing in the width dimension on the screen roll is to be used and run continuously in the transverse direction covering 5 forms. Desirably the screen should have a 4' (1.2m) width to conform to the spacing of the form elements. The wire should be continuous lengthwise in the fencing roll. Twenty such transverse runs of the fencing on the forms will provide for a complete ground plane. With this configuration of fencing, there is no requirement for ties or bonding except for mechanical stability and attachment to the forms. Triangular corner braces should be used on the rectangular forms.

The forms are placed on 8" (20cm) high cement blocks supporting each corner and the central areas. Narrow walkways are provided in the central areas to provide access by maintenance personnel. These walkways should be painted, single 1 by 8 sheathing laid over areas which are provided additional concrete block support below. The surface area created for walkways should be minimized to prevent water, snow, and debris accumulation, and located aside of the major axis for the fresnel areas serving the monitor detectors. These suggestions are shown pictorially in Figure 120.

Many counterpoises have been built for sideband reference system use and are operating successfully. Figures 121a and b show examples of elevated counterpoises in current use. Figure 121c shows a crude counterpoise formed simply by placing wire mesh directly on the ground. Such a mechanization of a counterpoise does serve the basic electrical requirements, but is quite vulnerable to snow effects and to corrosion promoted by the moist ground.
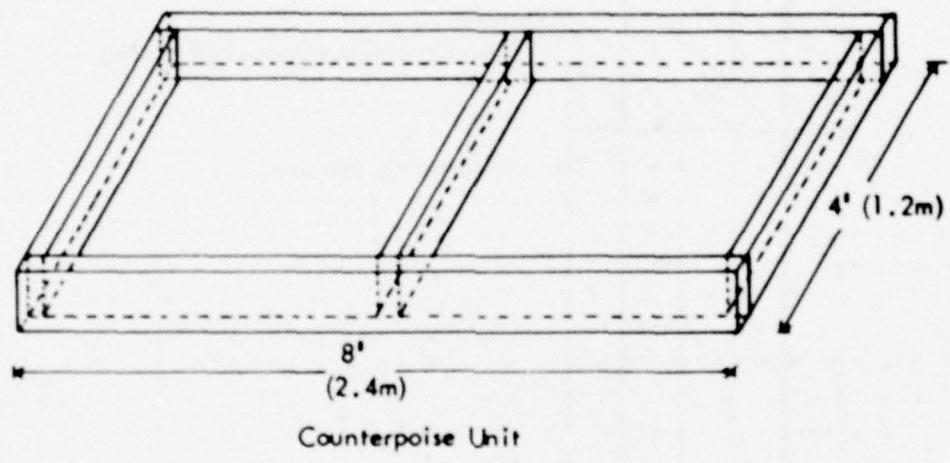
Counterpoise Unit

Figure 119. Basic Form for SBR Counterpoise Unit.
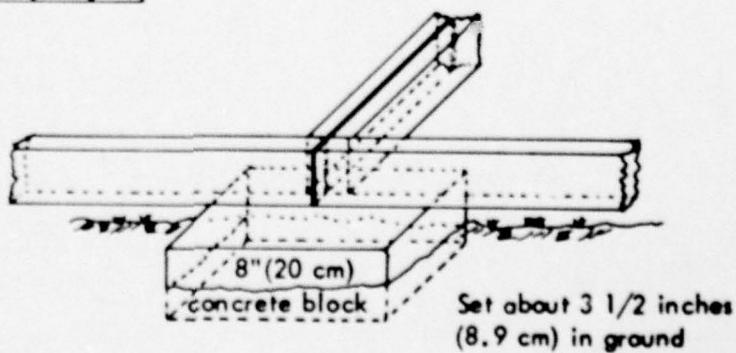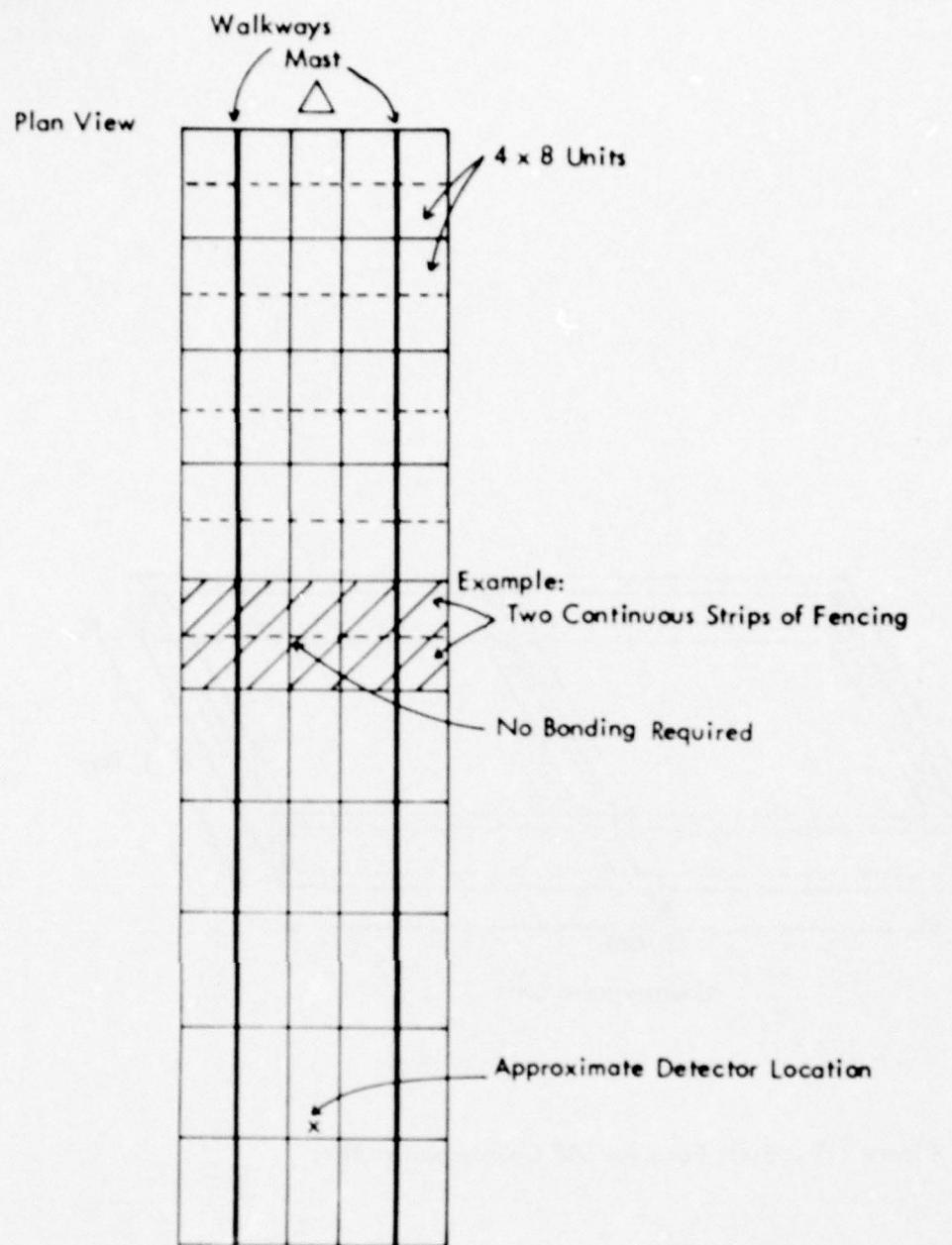
Figure 120. Counterpoise Plan for Sideband Reference System.
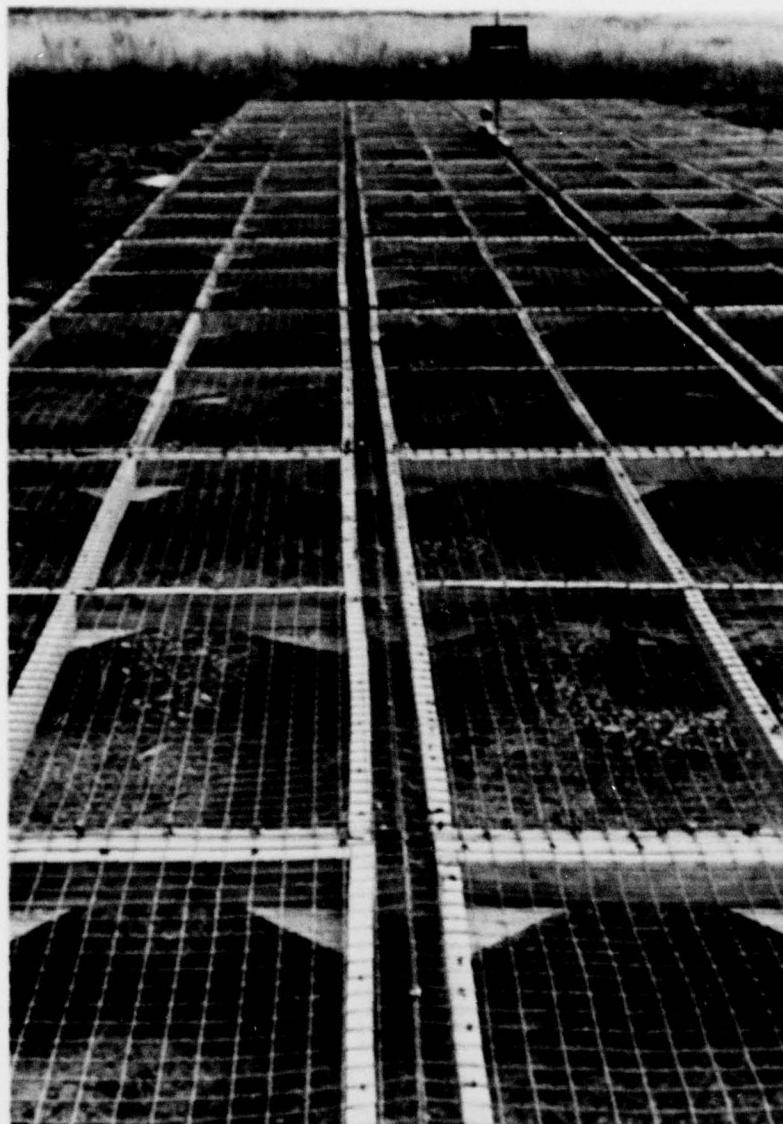
Figure 121a.   Photograph of Existing Counterpoise.
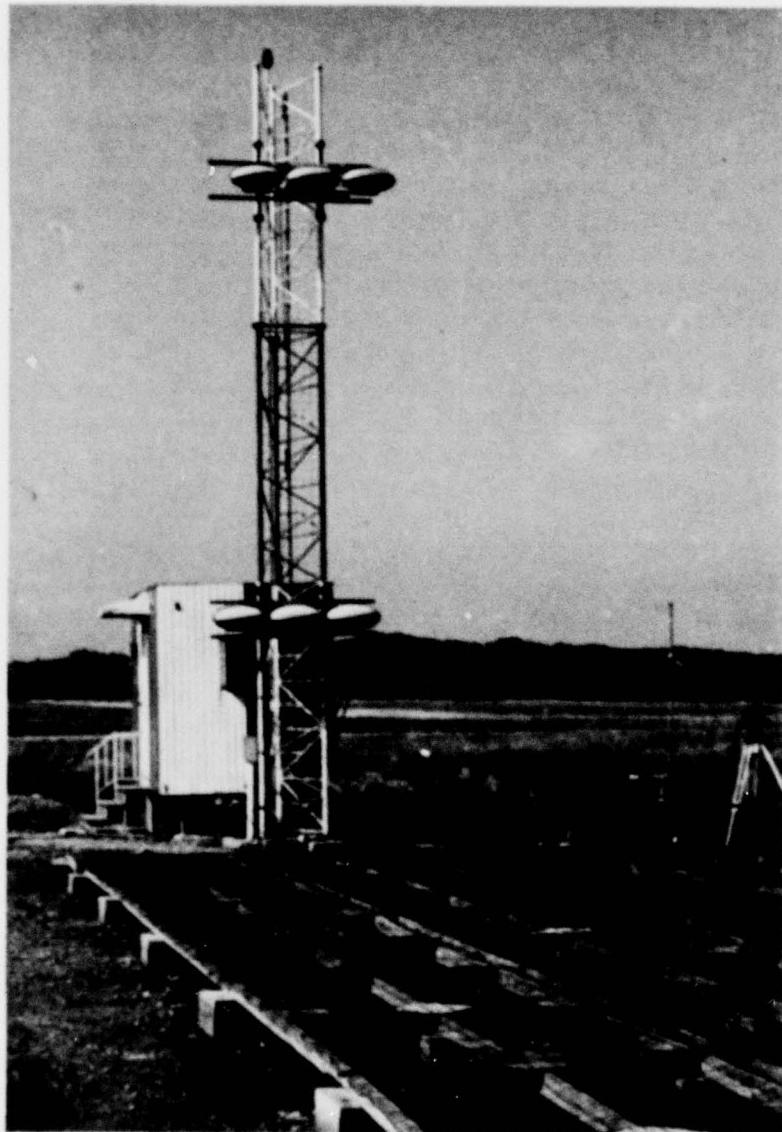
Figure 121b.   Photograph of Existing Counterpoise.

Figure 121c. Photograph of Existing Counterpoise. This is an example of conducting mesh laid directly on the earth. This obviously is at a site where no snow is expected.

III. ILS ANOMALY INVESTIGATIONS

A. Investigation of a Deficiency in the FA-5723 Clearance Transmitter Monitor.

1. Introduction. Modifications of the FA-5723 clearance transmitter monitor have been designed and implemented. These changes permit the monitor to respond properly to all fault conditions in the transmitter and load termination.

The FA-5723 clearance transmitter is a self-monitoring system that is designed for operation in a capture effect, glide-slope system. The self-monitoring capability is essential in the clearance transmitter since its output is intentionally canceled in, and thus not seen by, the capture effect system monitor. Therefore, in order to maintain system integrity, the clearance transmitter output must stay within given tolerances or an alarm must be indicated by the clearance transmitter.

It has been discovered that the monitor of the FA-5723 clearance transmitter does not adequately respond to certain fault conditions. Specifically, tuning capacitors on the transmitter output (C740, C751, and C763) can be detuned and/or the output transistor (Q710) can be shorted so as to drive the output power to less than one-fourth watt without the system indicating alarm.

2. RF Level and Load Termination Monitoring Circuitry. The FA-5723 internally monitors four components of its output signal: (1) modulation percentage, (2) frequency lock (AFC), (3) RF level, and (4) load termination. Modulation percentage and frequency monitor functions have been shown to perform adequately and are not discussed here.

An RF level detector is used on the final stage of the RF amplifier to provide an analog of the output power (see Figure 122). This detector consists of components C759, CR701, CR702, R727, C765, C767, and R729. The RF input for the detector circuit is from a tap on inductor L717 and is coupled to a voltage doubler/detector which provides a voltage to pin E of the RF module that is intended to be an analog of the output voltage.

Experimental data shows that the output of this detector does not provide an analog of the output for certain conditions such as detuning the output trimmer capacitors. In fact, it appears that the detector output follows the voltage on the previous amplifier stage with greater accuracy than it follows the final output. A possible explanation for this is that the detector coupling to the final is not tight (RF coupling is made through a 1.0 pF capacitor) and there is a good deal of RF within the RF module that could be coupled to the detector through stray capacitance. The reason that the FA-5723 does not alarm when the output is detuned is that the RF detector used to measure the output power is captured by signals other than the desired output signal.
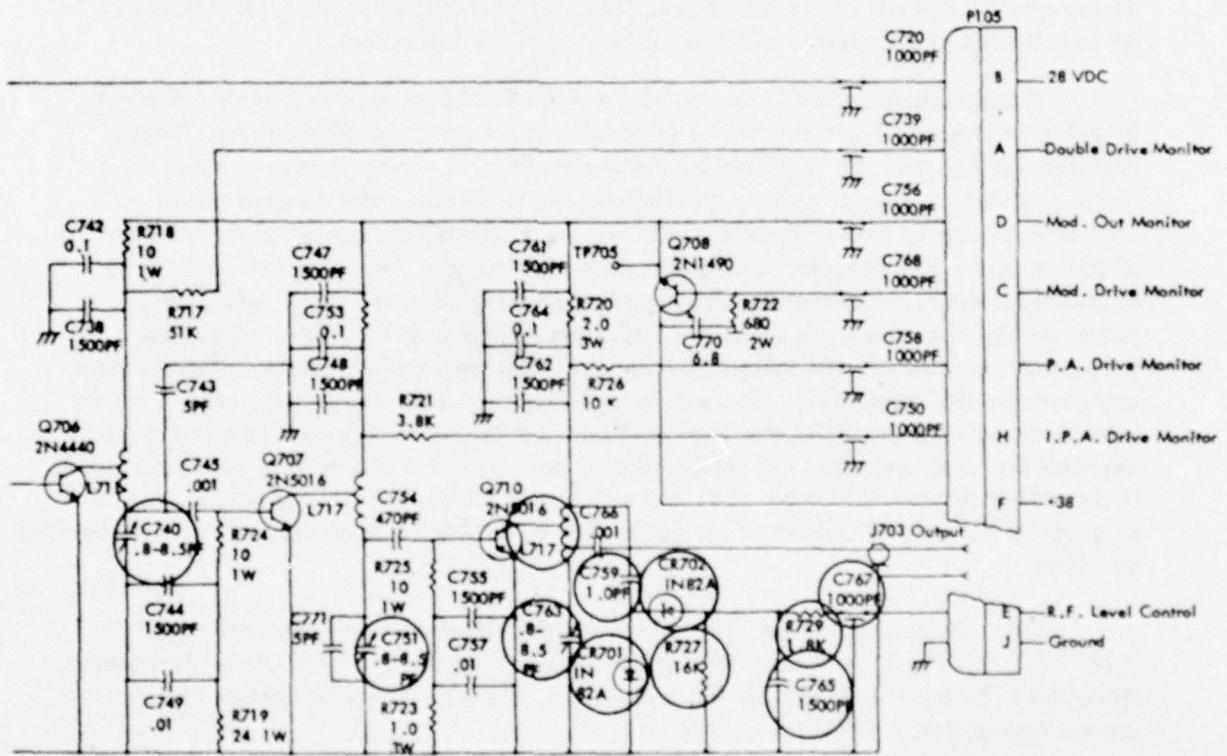
Figure 122. Output Section of FA-5723 with RF Level Detector.

The Load Termination Monitor (LTM) is itself an RF detector located approxi-
mately 90 electrical degrees beyond the RF level detector. It was assumed that out-
of-tolerance VSWR would cause one of these monitors to show a decrease in signal
sufficient to result in an alarm. Experiments showed that the LTM-RF level combination
could easily be fooled and it was dropped as a solution even though the LTM sensitivity
could be improved sufficiently to permit it to respond to nulls if they occurred at its
location.

3. Modification. Several modification design concepts have been evaluated
to determine the one that is most feasible in terms of: (1) meeting monitoring require-
ments, (2) requiring minimal circuit alterations to existing equipment, (3) not changing
transmitter set-up procedures, (4) component availability, and (5) cost. The selected
design qualifies in all of the above areas and has been shown to work effectively in
an installation at Lafayette, Indiana as well as in the laboratory.

As previously stated, the monitor network has been observed to be deficient
in detecting certain fault conditions in power output and load termination. These
deficiencies can both be rectified by the installation of a bi-directional coupler,
along with interfacing circuitry, on the transmitter output. The forward power
port of this coupler is used to provide an analog of the output power to the monitor
circuitry; since this detector is external to the RF module, its operation will not be
hindered by the RF interference affecting the existing detector. The reflected
power port of the coupler is used as a load termination sensor. If the transmitter
is properly terminated, the reflected power will be low, and an improper termination
anywhere on the transmission line will result in a high reflected power. The required
interface circuitry amplifies the analog of forward power so as to emulate the existing
detector and also compares the reflected port output with a presettable threshold value;
if the reflected port output exceeds that value, a transmission gate is actuated so as
to cause the analog of output power going to the monitor to go to zero volts, thus causing
an alarm.

This monitoring scheme allows for the monitoring of load termination and RF
level solely by the RF level monitor which obviates the need for the LTM. However,
since the LTM is not adjusted by the technician, there need not be any change in
set-up procedures.

A schematic diagram of the interface between the bi-directional coupler and
the monitor circuitry is shown in Figure 123. Power for this interface comes from the
clearance transmitter power supply; the interface requires -15 volts and uses 15 milli-
amperes of current. As seen in Figure 123, the incident output of the coupler is amplified
before being fed to the transmission gate. The resistors that determine voltage gain,
R_1 and R_2, have been selected so as to provide the same levels as does the existing
detector. The reflected output of the coupler is fed to a comparator. When the re-
flected port voltage is less negative than the reference voltage, which is set by the
potentiometer, the output of the operational amplifier will be at ground potential.
A ground on the transmission gate control line will cause the gate to appear as a

-360-
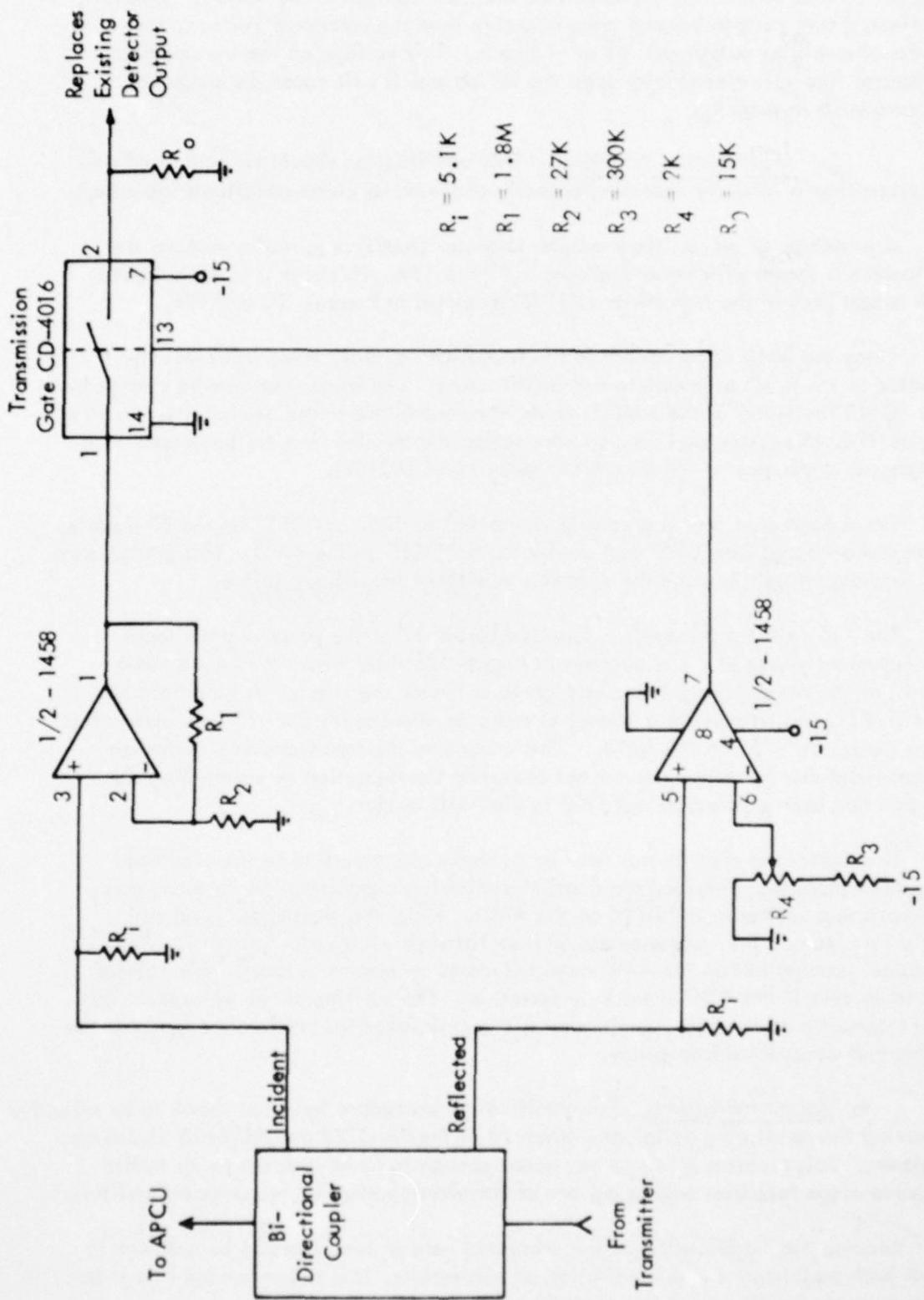
Figure 123. Schematic Diagram of Bi-Directional Coupler/Monitor Interface.

$R_i = 5.1K$

$R_1 = 1.8M$

$R_2 = 27K$

$R_3 = 300K$

$R_4 = 2K$

$R_0 = 15K$

closed switch thus connecting the amplified incident voltage to the output. Should the reflected port voltage become more negative than the reference voltage, the operational amplifier output will be at -15 volts. This voltage on the transmission gate control line will electrically open the switch which will cause the output to go to zero volts through R_o.

(a) Modification Procedure. This modification should be performed only on a system that is initially operating properly and with no alarm conditions indicated.

A prototype of an auxiliary monitor detector (AMD) required to perform the modification is shown with cover removed in Figure 124. This unit is to be installed on the output jack of the transmitter (XJ102) as shown in Figures 125 and 126.

Once the AMD is connected to the transmitter output, three wires must be connected to the AMD to complete the modification. The black ground wire connected to the "GND" terminal of the AMD is to be attached to the transmitter chasis. As shown in Figure 125, this is accomplished by connecting the terminal lug on the ground wire to the chassis screw nearest the transmitter output port (XJ102).

The orange wire that is presently connected to C767 or "DET" on the RF module is to be disconnected from C767 and connected to "DET" on the AMD. This orange wire should be long enough to make the connection without requiring a splice.

The -15 volts for the AMD is supplied by pin 17 of the power supply board which is presently unused. The pointers in Figure 126 show where a wire connects to pin 17 of the power supply board and where it leaves the chasis. A hole has been drilled (9/23") and fitted with a gromet to make an opening for the -15 volt wire. This wire connects to "-15" on the AMD. This completes the modification installation. The transmitter can be restored to normal operating configuration by connecting the cable that had been connected to XJ102 to the AMD output.

The transmitter monitor can now be calibrated as specified in the clearance transmitter handbook. The load termination monitoring capability can be evaluated by connecting a voltmeter to "DET" on the AMD. When the transmitter is on and properly terminated, the voltmeter should read between -1.0 and -5.0 volts. With an improper termination on the AMD output (such as an open or a short), this voltage will drop to zero if the AMD is working correctly. The shorting of the voltage on this line to ground for an improper termination is the only functional difference between the modified and unmodified transmitter.

4. Recommendations. This modification procedure has been shown to be effective in removing the monitoring deficiency observed in the FA-5723 and FA-8633 clearance transmitters. This problem is felt to be serious enough to be of concern to air traffic using glide-slope facilities employing one of the aforementioned clearance transmitters.

Because the modification design presented here is considered to be optimum in terms of both performance and installation considerations, it is recommended that it be applied to every facility using the clearance transmitters in question.

1·0   2·8   2·5

3·15   2·2

3·5   2·0

1·1   1·8

1·25   1·4   1·6

NATIONAL BUREAU OF STANDARDS
MICROCOPY RESOLUTION TEST CHART
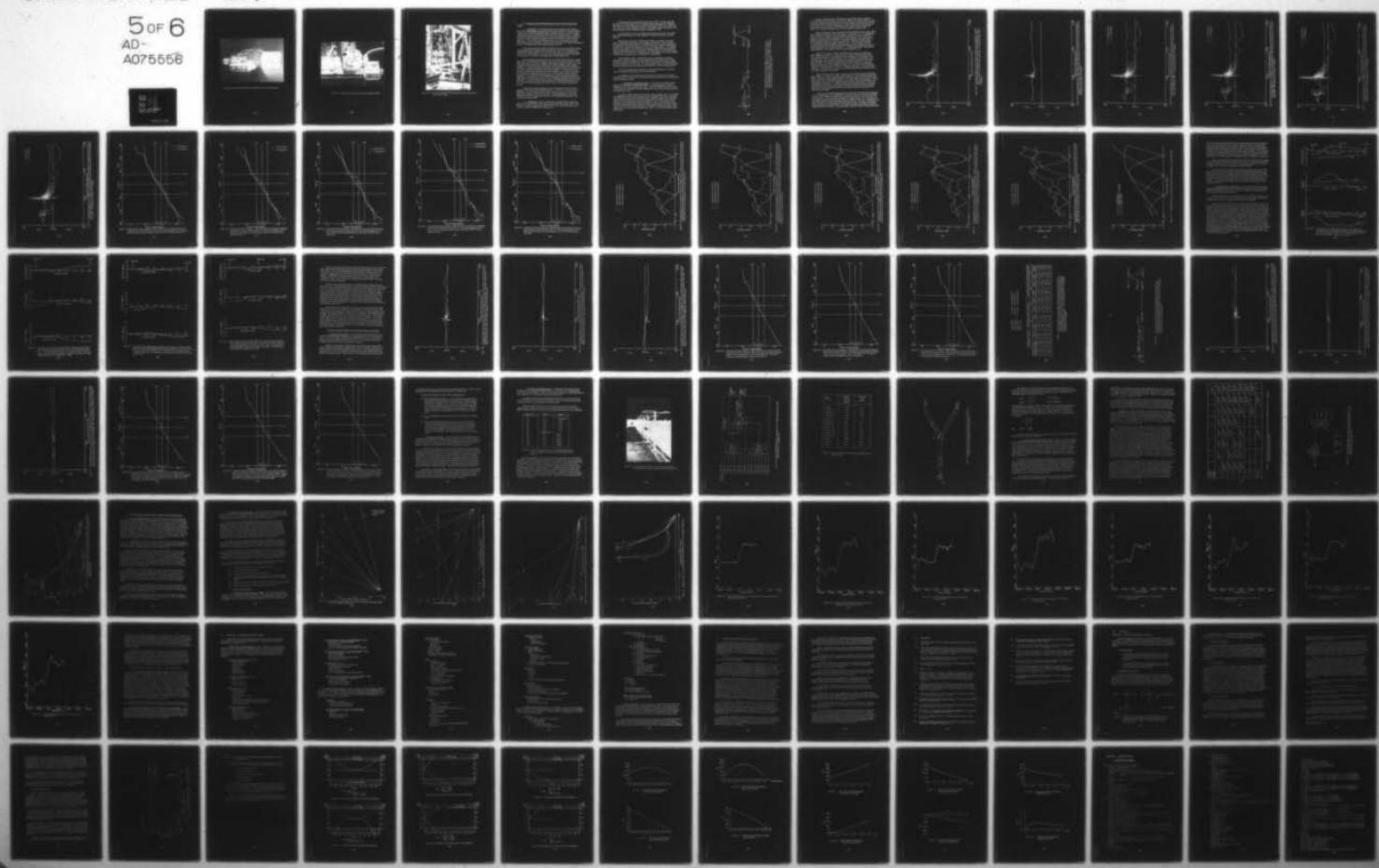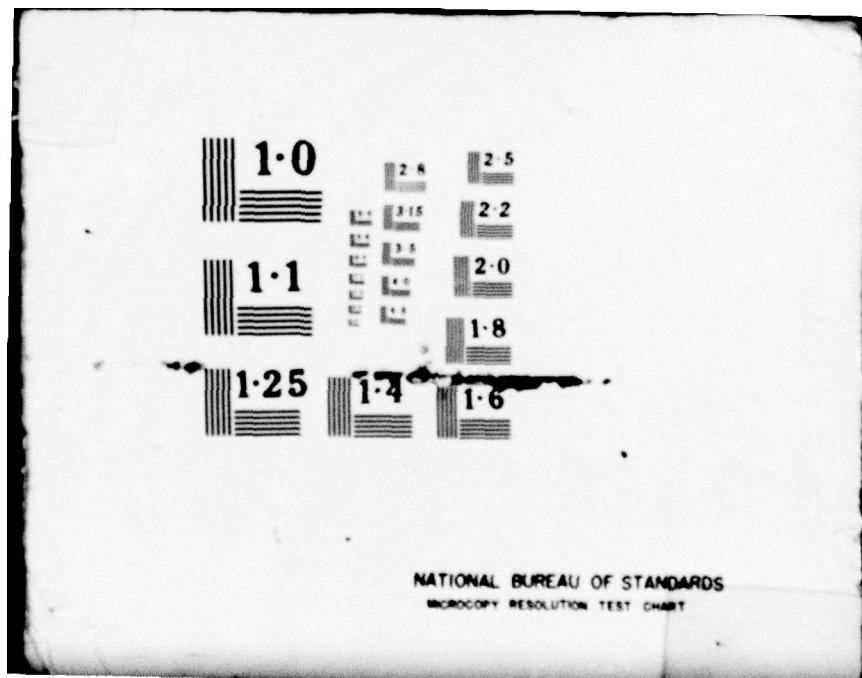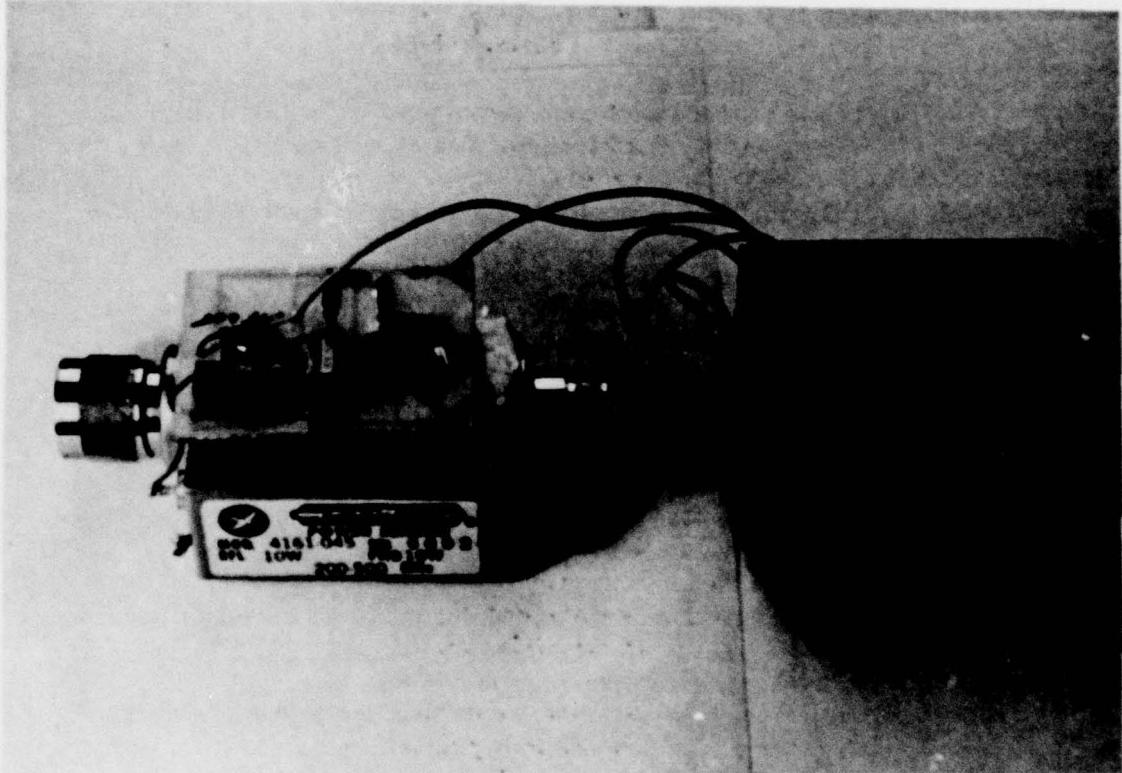
Figure 124. Auxiliary Monitor Detector (AMD) Shown with Cover Removed.
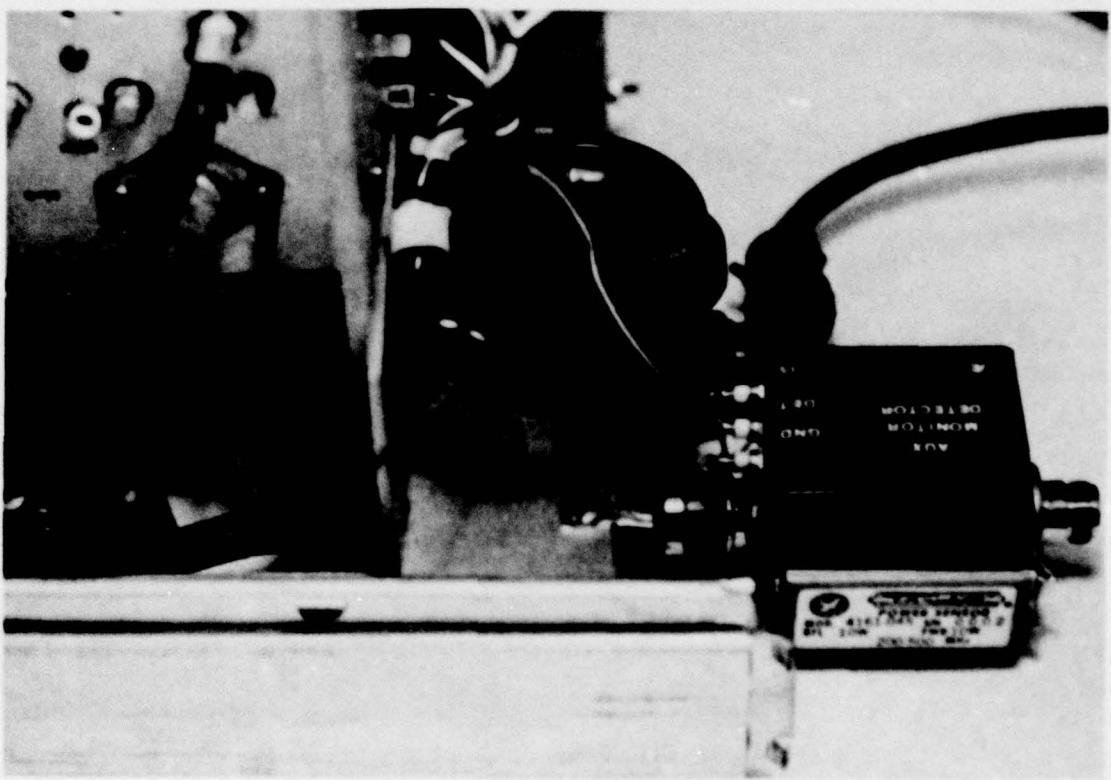
Figure 125. Picture of Installed Auxiliary Monitor Detector (AMD).
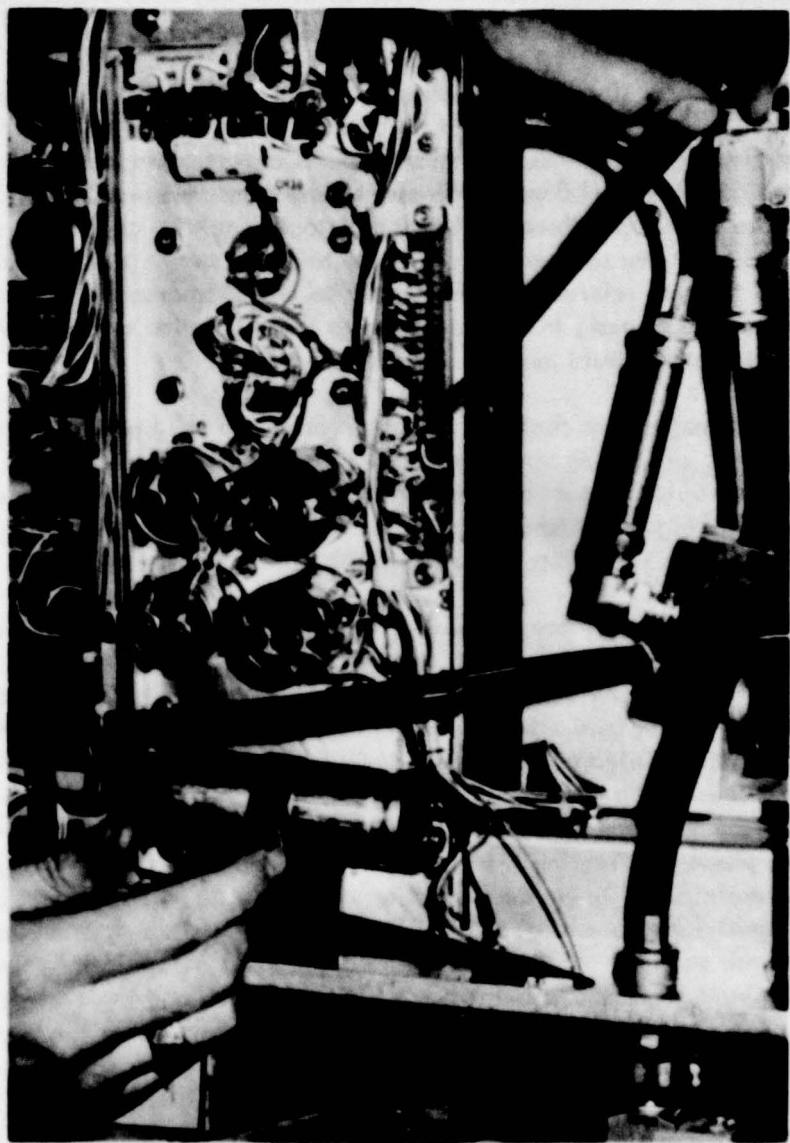
Figure 126. Picture of Completed Modification Showing Connection to the
-15 Volt Power Supply.

B. **Investigation of Glide-Slope Performance at Runway 22L, Boston Logan Airport.**

1. **Conclusions.** The results obtained from the computer model indicate that a null reference glide slope installed at the present location will not meet Category I tolerances. The flyability roughness (80 microamperes excursion in zone2) and poor crossovers observed by the FAA [17] are confirmed by the computed results. In addition, calculations indicate that tidal effects will cause the path angle to change by approximately 0.2° and the symmetry to change from 44/56 to 19/81 as the tide varies from high to low. Thus, the null reference system would be out of tolerance due to both tidal changes and path roughness, in contradiction to the prediction made by Westinghouse that a null reference system would perform satisfactorily. [18]

The computed results also confirm FAA observations on the capture effect system. The computations show, depending upon the tide level, that the path angle for the capture effect system would be as much as 0.26° below that for a null reference system with the same antenna heights. Also, the calculated path angle variation from high to low tide was 0.11°, which is in close agreement with FAA observations.

The computed results indicate, however, that despite these difficulties a capture effect system will perform within Category I tolerances at the present location, with the path angle, width, and symmetry changes compensated by tightened monitor limits. The computed flyability of the capture effect system indicates roughness within Category I tolerances. It should be pointed out that even when properly phased the system may not be within the guidelines of the phase verification procedure. This will not, however, prevent the system from performing within CAT I tolerances, as no airborne tolerances are imposed by the phase verification test. [19] The calculations indicate that good clearances will be maintained under the dephasing conditions imposed during phase verification. Computations were also made with the glide-slope antennas moved 1000' (300m) back from their present location. Since no detailed topographic information was available, it was assumed that the terrain between this location and the present one is flat. The results indicate performance similar to that with the system at the present location.

It should be mentioned that preliminary results reached by the same authors in December 1978 showed somewhat different results. The reason is that the accurate topographic information upon which this report is based was not yet available, and approximate topographic information was used. The large differences in the results obtained indicate the importance of obtaining accurate topographic data upon which to apply the computer model.

2. **Introduction.** The work reported here was prompted by the anomalous behavior of the capture effect glide slope at Runway 22L, Boston Logan Airport. This behavior was caused in part by tidal variations of 14 feet in the reflecting zone, and in part by a steep hill 9000' from the antenna mast.

Westinghouse Electric conducted a siting survey in 1974. In their report they state that "It is recommended that a null reference glide-slope antenna be installed to serve RWY 22L at Logan International Airport" since except for traffic on a nearby taxi-way, "There are no other derogations or terrain irregularities which would prevent a null reference glide slope from attaining Category I performance." [18]

On November 18, 1977 a null reference glide slope was installed. The system did not pass flight check due to severe roughness in zone 2 and very poor cross-over behavior.

Between April and August of 1978 several attempts were made to install and phase a capture effect system so as to meet Category I tolerances. Several problems were encountered, including difficulty in phasing, difficulty in repeating measurements, and difficulty in aligning the middle antenna null with the path angle. It soon became evident to the engineer involved that the changing path angles and widths correlated in time with tidal changes in the reflecting zone. This observation, while providing some understanding of the difficulties, indicated that the siting problem was unusually complex in that at one site uneven terrain was combined with tidal effects.

When significant delays in obtaining the accurate topographic information developed, a preliminary report based upon approximate terrain information was made and sent to the FAA on December 4, 1978. The results contained in this report showed the severe roughness in zone 2 for the null reference system, but did not show the capture effect path angle as being well below the angle of the RF null for the middle antenna.

The accurate topographic information was obtained on February 16, 1979 and serves as the basis for the computed results contained herein.

An explanation of the techniques used to obtain the calculations is contained in Reference [20]. All results for this memorandum were calculated using the Geometrical Theory of Diffraction option.

3. Comparison with Measured Results. In this section calculations will be presented with the systems configured (as closely as is possible based on available in-formation) as they were during the flight checks. This will establish the accuracy of the modeling results, and hopefully provide explanations of the anomalous behavior observed during the flight checks.

The terrain profile used in the calculations is shown in Figure 127. It is a straight line approximation of the data provided by the new topographic information. The signi-ficant differences between this profile and the less accurate one used in the preliminary report are the downslope just in front of the antennas, the small hill at the far side of the bay, and the height and location of the large hill. Also, it should be pointed out that the two-dimensional profile neglects the terrain which does not lie directly in front of the antennas and that the actual ground is not smooth but covered with houses, trees, roads, etc. which tend to reduce the reflections. Both will tend to reduce the accuracy of the results.

-367-
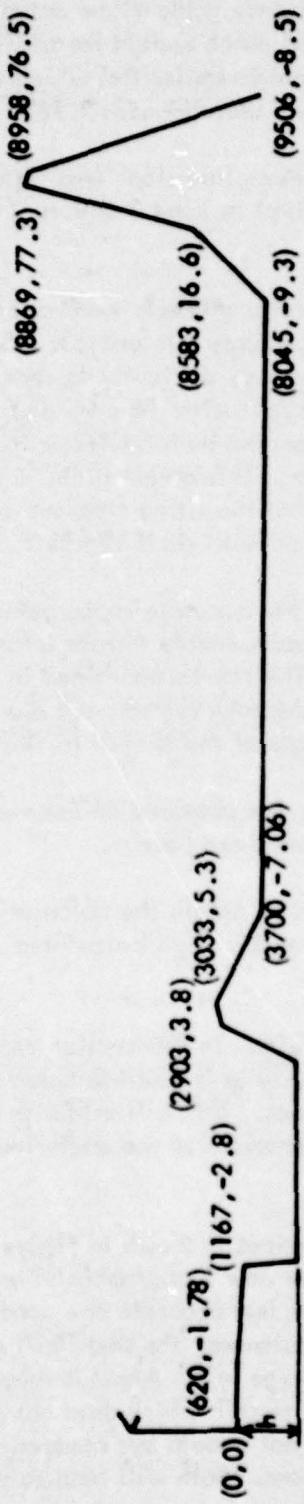
Figure 127. Straight-Line Terrain Profile for Reflecting Zone of Boston Logan 22L Glide Slope Used to Obtain Results in this Report. Based on aerial photogrammetry and ground survey data supplied by Henderson Aerial Survey Company of Columbus, Ohio.

All calculations in Figures 128 through 143 were made for antenna heights of 14.13' (4.307m), 28.26' (8.614m), and 42.39' (12.920m). The computer model was used to simulate airborne phasing at mean tide with the result being a 6.8° phase retard for the lower antenna and a 3.0° phase advance for the upper antenna, both with respect to the currents in the middle antenna. These phasing values were also used for Figures 128 through 143, and agree reasonably well with those reported in Reference [17].

Figures 128 through 132 are calculated centerline flyability for both capture effect and null reference systems for various tide levels. In Reference [17] it was reported that when tested the null reference system exhibited structure excursions of over 80 micro-amperes, and peak-to-peak excursions of over 130 microamperes. While the tide level for these measurements was not specified, examination of Figures 128 through 132 in-dicate reasonable agreement with the measured values. The capture effect flyability was measured to be within Category II tolerances [17], and this too agrees with the calculated capture effect flyability of Figures 128 through 132, providing path reference angle is adjusted to the average path angle (i.e., approximately 2.85°). Thus the cal-culated flyability results agree well with the results reported in [17].

Figures 133 through 137 contain calculated values of CDI versus angle for a 1600' (490m) elevation level run above the runway centerline for both capture effect and null reference systems. The measured results in Reference [17] include poor cross-over behavior for the null reference system, with a path angle of approximately 3.16°, while the capture effect system was reported having a good crossover, but with a path angle of 2.80°. No information regarding the tide level was given, but examining Figure 134 (high-mean tide) and Figure 135 (mean tide), one finds almost precisely the same results, with the exception that the null reference path angle is calculated slightly (.07°) low. This difference is, however, only slightly greater than the tolerance usually associated with airborne measurements.

Figures 138 through 142 contain calculated curves of relative signal strength from each antenna versus angle for the terrain profile of Figure 127 with each antenna fed equal power. These calculations would correspond to the AGC voltage of an ideal receiver with the aircraft flying at 1600' (490m) elevation level run above the runway centerline. Figure 143 contains similar curves for an ideally flat ground site and ideal antenna heights, and is included for comparison. It is evident that the antenna pattern structure is very much affected by the uneven terrain, and the point might be made here that the capture effect system does an amazing job of producing a good crossover despite the roughness of the separate antenna patterns.

One of the most disturbing features of the measurement results reported in Reference [17] was the measurement of a composite RF null from the upper and lower antennas at both 2.30 and 2.58°. Referring to Figure 143, this should occur at 3.0°, where the upper and lower antenna patterns have the same amplitude but opposite phase. For an explanation of this measured result, examine the patterns of Figures 138-142. Note that in comparison with Figure 143, the relative amplitude of the upper antenna signal is increased and the lower antenna decreased in the region near 2.5°, causing the relative amplitudes to be approxi-mately equal and out-of-phase. More specifically, referring to Figure 139 (high-mean tide)

-369-
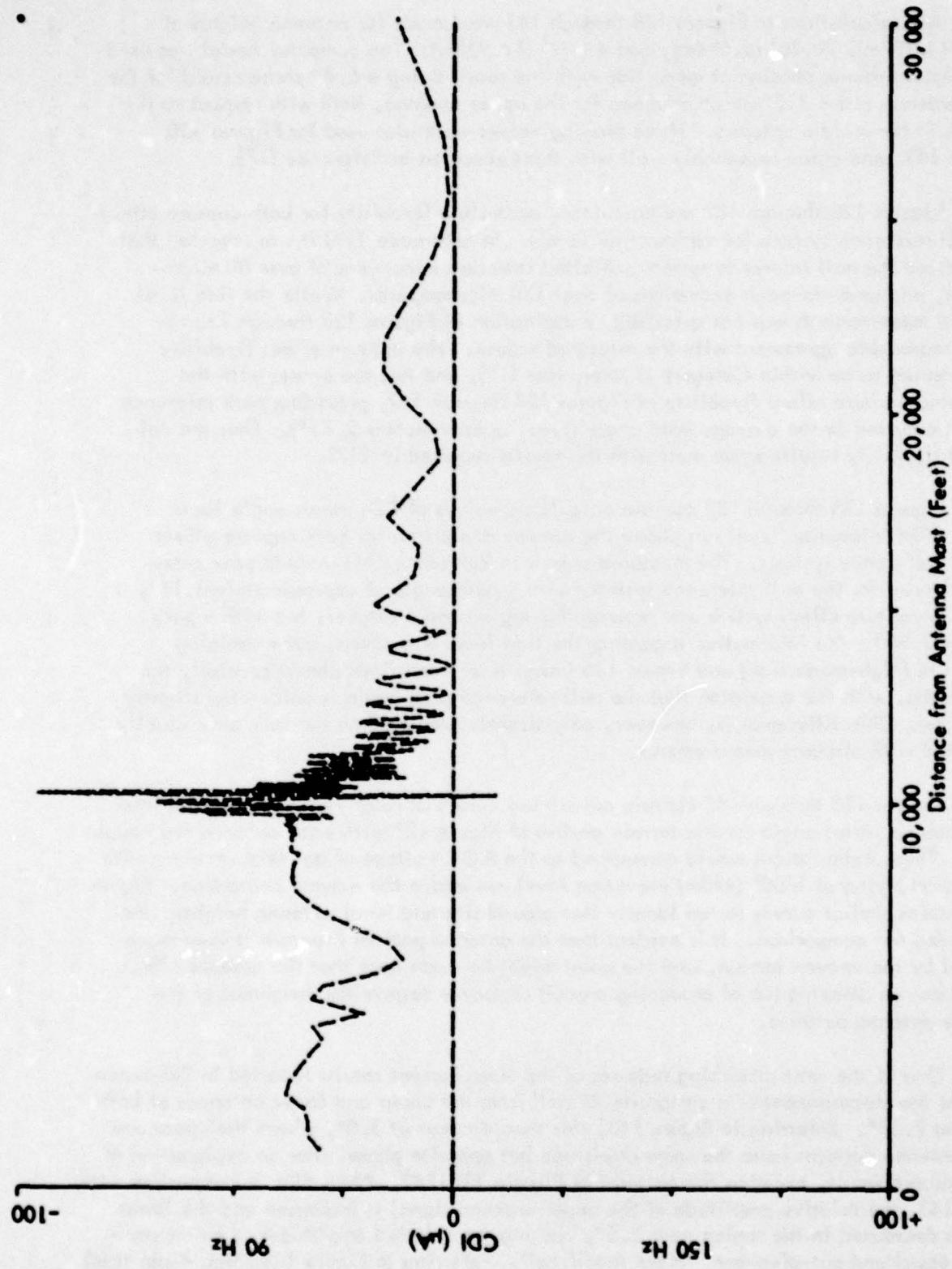
Figure 128a. Calculated Flyability for Null Reference Glide Slope for the Terrain Profile of Fig. 127 with Antenna Heights of 14.13, 28.26, and 42.39 feet and a Tidal Distance h (see Fig. 127) of 6.24 feet (high tide). The reference glide angle is 3.0 degrees.
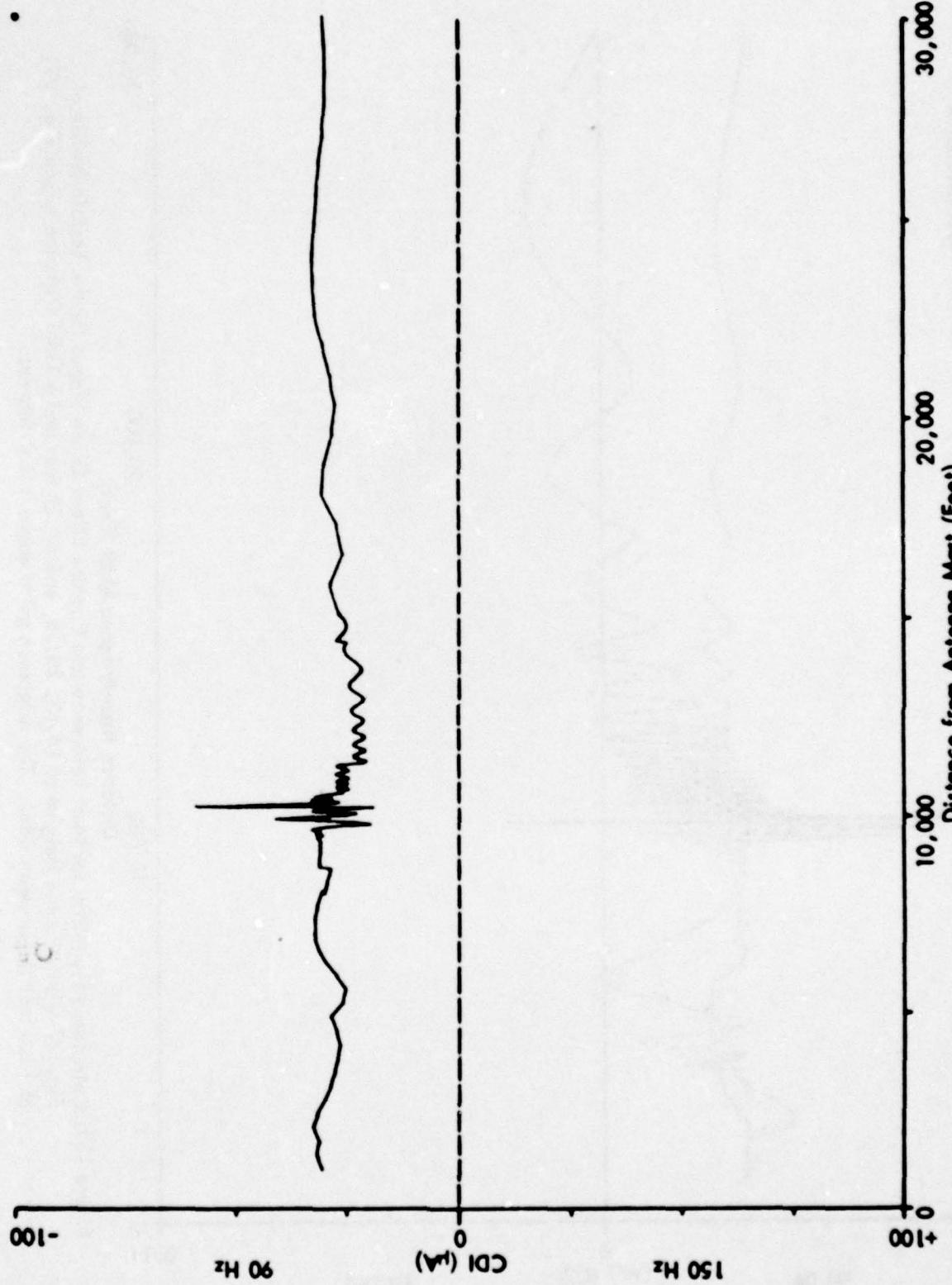
Figure 128b. Calculated Flyability for Capture Effect Glide Slope for the Terrain Profile of Fig. 127 with Antenna Heights of 14.13, 28.26, and 42.39 feet and a Tidal Distance h (See Fig. 127) of 6.24 feet (high tide). The reference glide angle is 3.0 degrees.
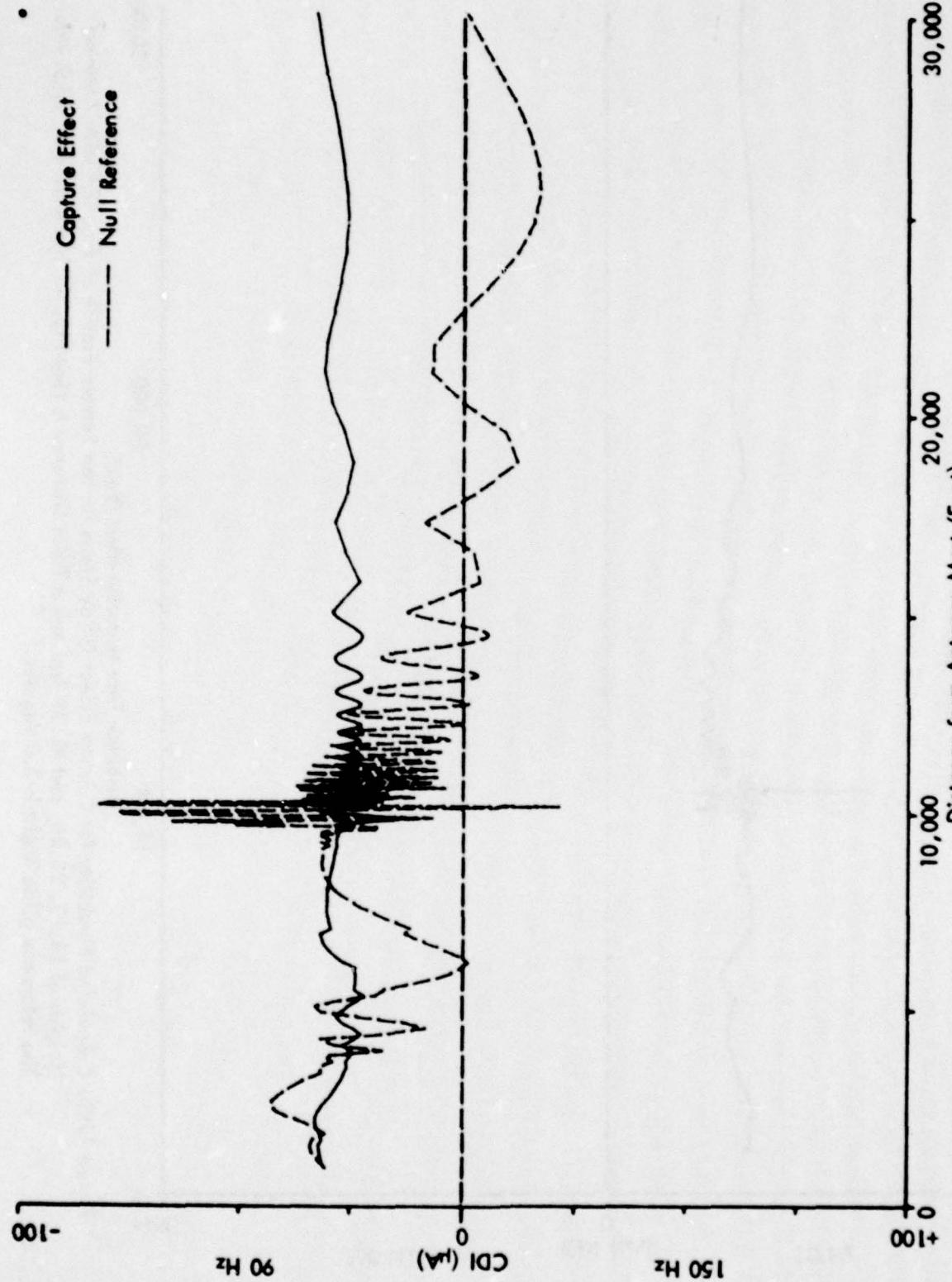
Figure 129. Calculated Flyability for Null Reference and Capture Effect Glide Slopes for the Terrain Profile of Fig. 127 with Antenna Heights of 14.13, 28.26, and 42.39 feet and a Tidal Distance h (see Fig. 127) of 10.0 feet (high-mean tide). The reference glide angle is 3.0 degrees.
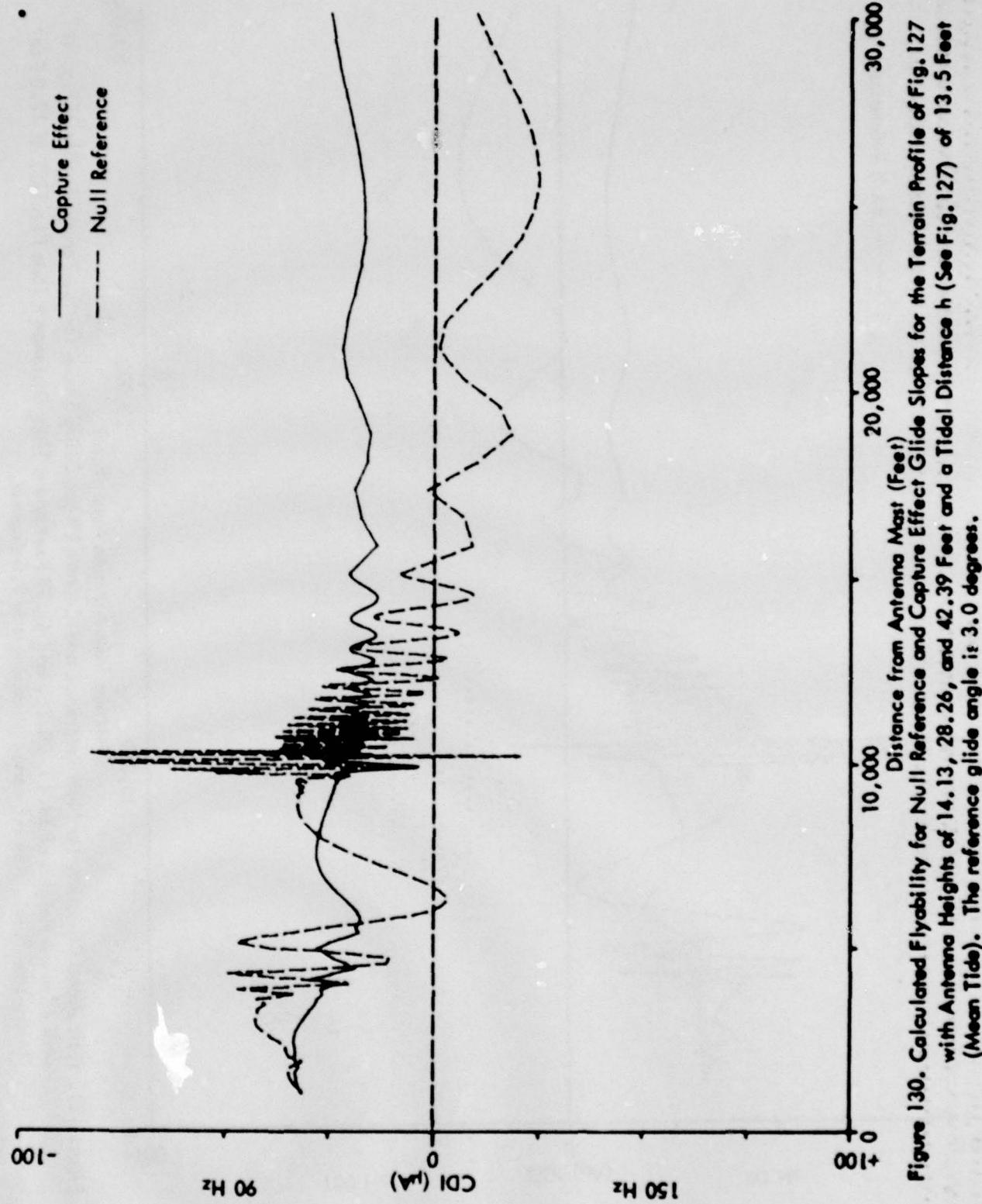
Figure 130. Calculated Flyability for Null Reference and Capture Effect Glide Slopes for the Terrain Profile of Fig. 127 with Antenna Heights of 14.13, 28.26, and 42.39 Feet and a Tidal Distance h (See Fig. 127) of 13.5 Feet (Mean Tide). The reference glide angle is 3.0 degrees.

-373-
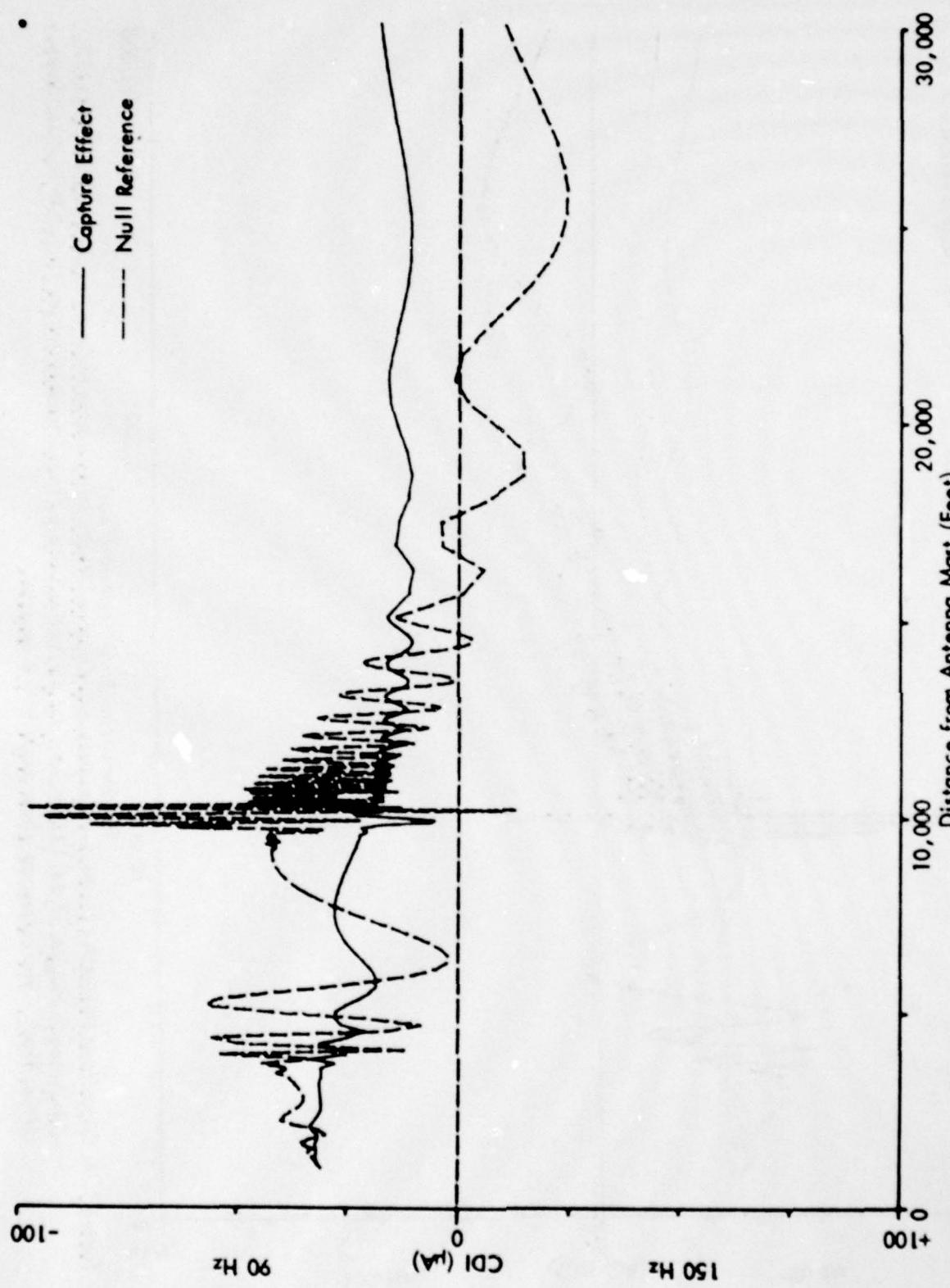
Figure 131. Calculated Flyability for Null Reference and Capture Effect Glide Slopes for the Terrain Profile of Fig. 127 with Antenna Heights of 14.13, 28.26, and 42.39 Feet and a Tidal Distance h (See Fig. 127) of 17.0 Feet (Mean–Low Tide). The reference glide angle is 3.0 degrees.
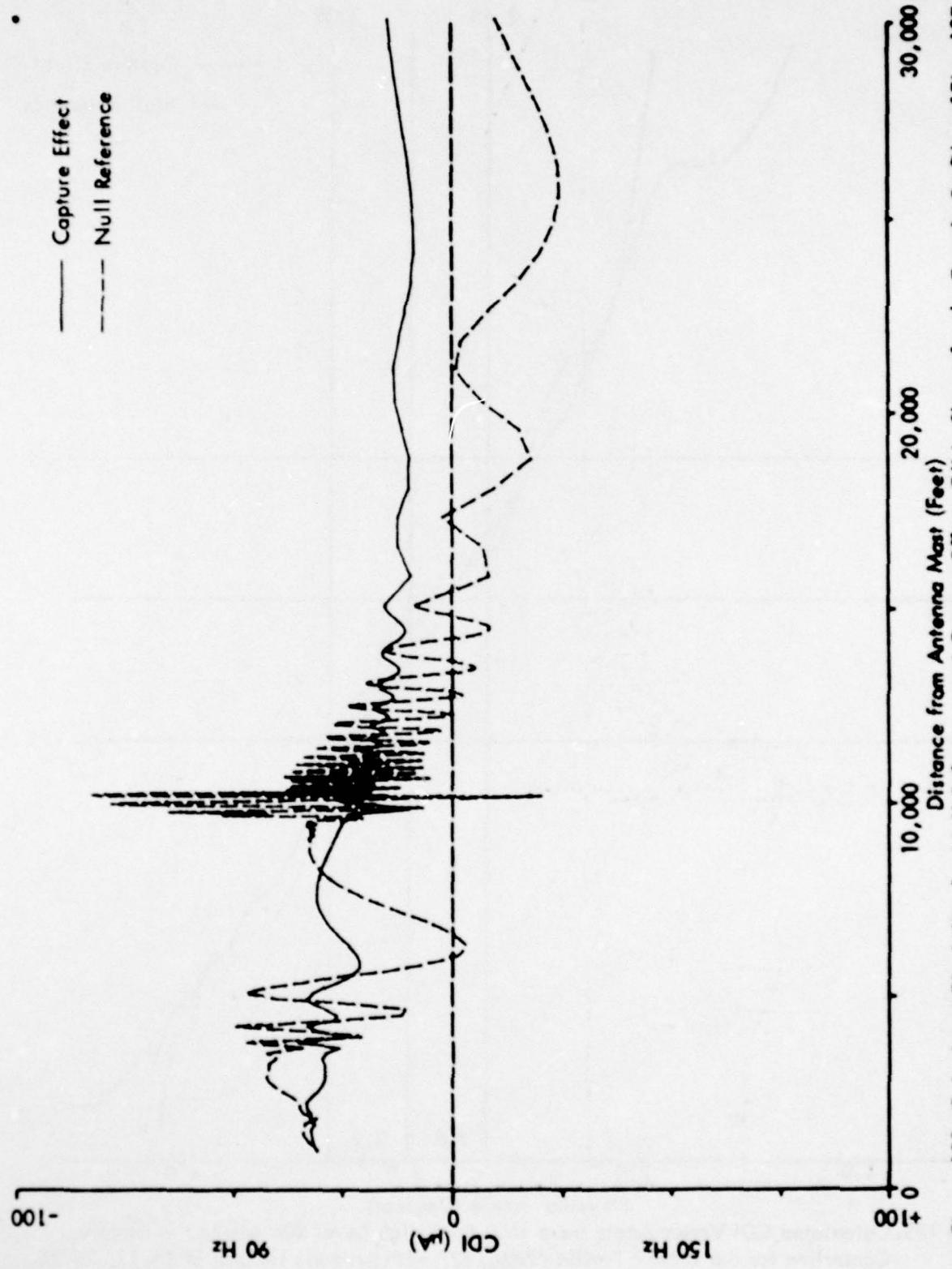
Figure 132. Calculated Flyability for Null Reference and Capture Effect Glide Slopes for the Terrain Profile of Fig. 127 with Antenna Heights of 14.13, 28.26, and 42.39 Feet and a Tidal Distance h (See Fig.127) of 20.24 Feet (Low Tide). The reference glide angle is 3.0 degrees.
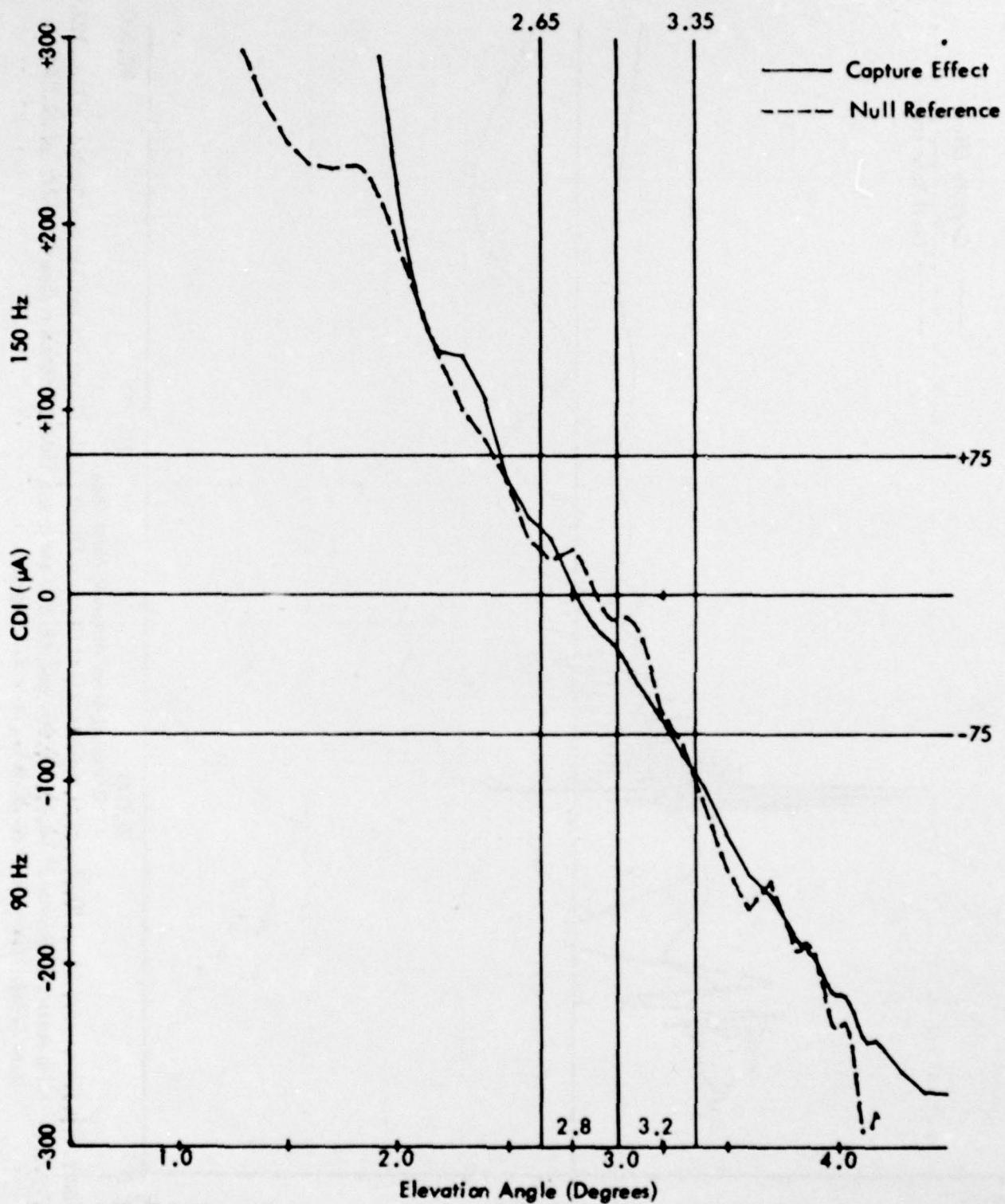
Figure 133. Calculated CDI Versus Angle for a 1600 Foot High Level Run Above the Runway Centerline for the Terrain Profile of Fig. 127 with Antenna Heights of 14.13, 28.26, and 42.39 Feet and a Tidal Distance h (See Fig. 127) of 6.24 Feet (High Tide).
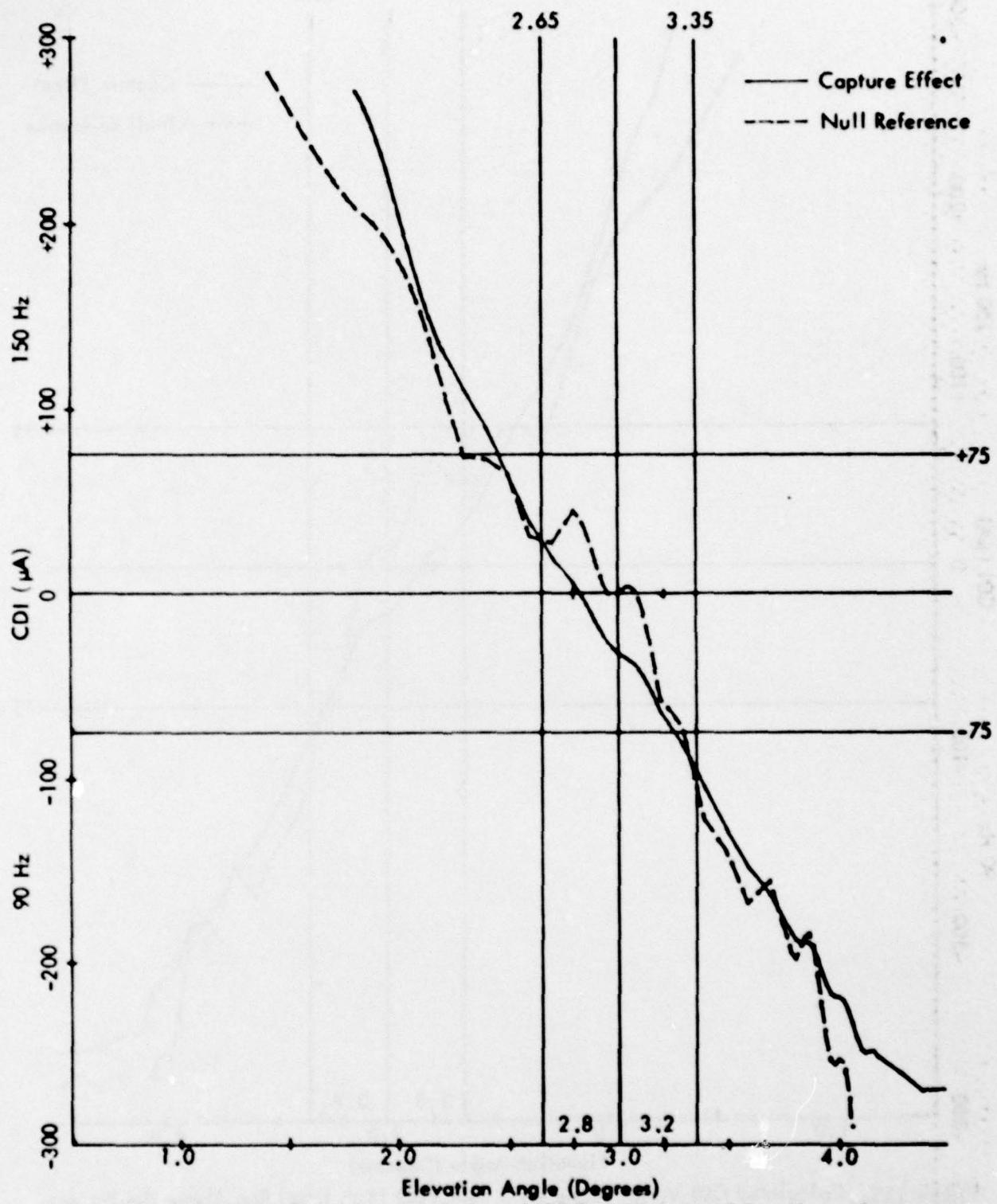
Figure 134. Calculated CDI Versus Angle for a 1600 Foot High Level Run Above the Runway Centerline for the Terrain Profile of Fig. 127 with Antenna Heights of 14.13, 28.26, and 42.39 Feet and a Tidal Distance h (See Fig. 127) of 10.0 Feet (High-Mean Tide).

-377-
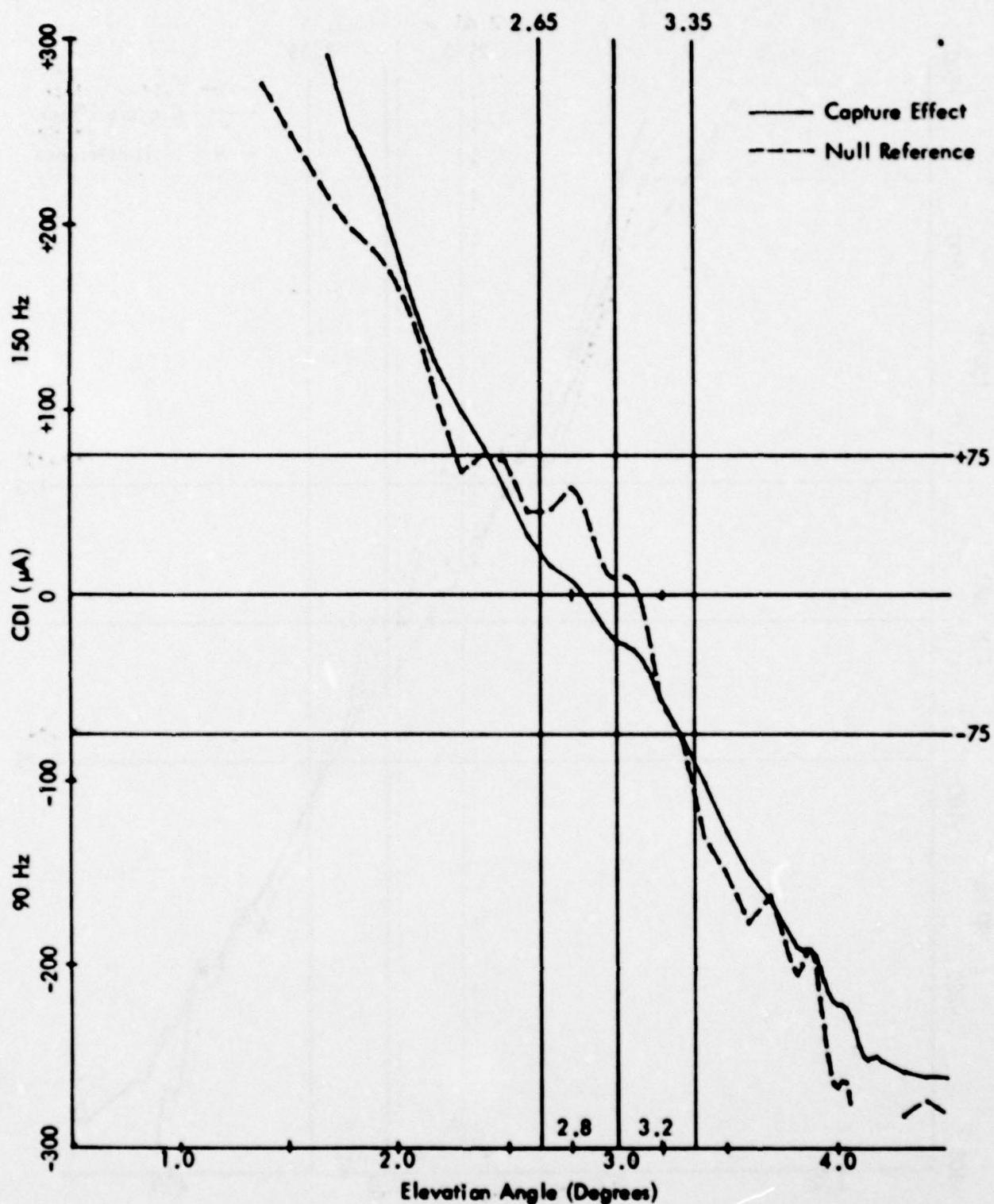
Figure 135. Calculated CDI Versus Angle for a 1600 Foot High Level Run Above the Runway Centerline for the Terrain Profile of Fig. 127 with Antenna Heights of 14.13, 28.26, and 42.39 Feet and a Tidal Distance h (See Fig. 127) of 13.5 Feet (Mean Tide).
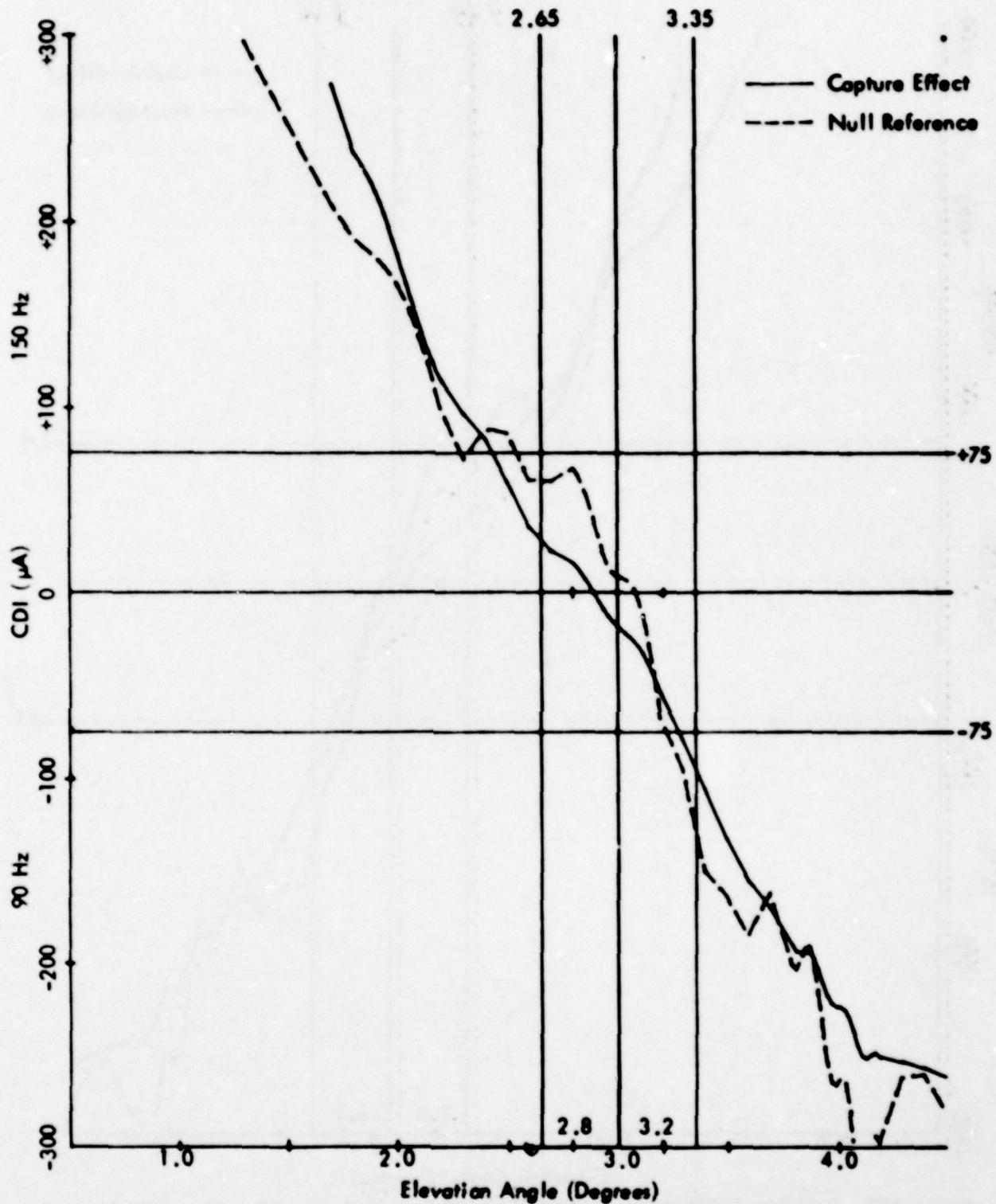
Figure 136. Calculated CDI Versus Angle for a 1600 Foot High Level Run Above the Runway Centerline for the Terrain Profile of Fig. 127 with Antenna Heights of 14.13, 28.26, and 42.39 Feet and a Tidal Distance h (See Fig. 127) of 17.0 Feet (Mean-Low Tide).
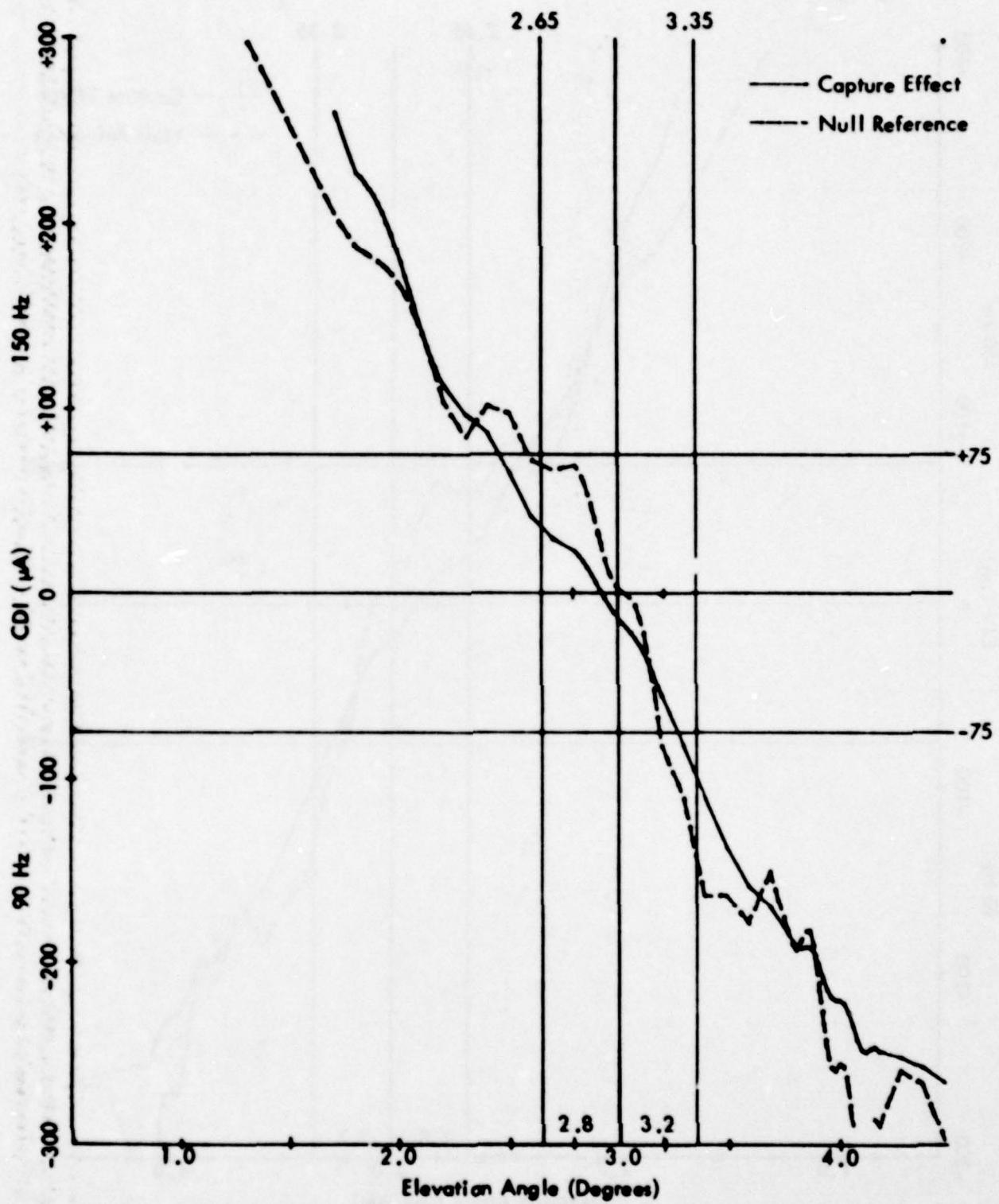
Figure 137. Calculated CDI Versus Angle for a 1600 Foot High Level Run Above the Runway Centerline for the Terrain Profile of Fig. 127 with Antenna Heights of 14.13, 28.26, and 42.39 Feet and a Tidal Distance h (See Fig. 127) of 20.24 Feet (Low Tide).
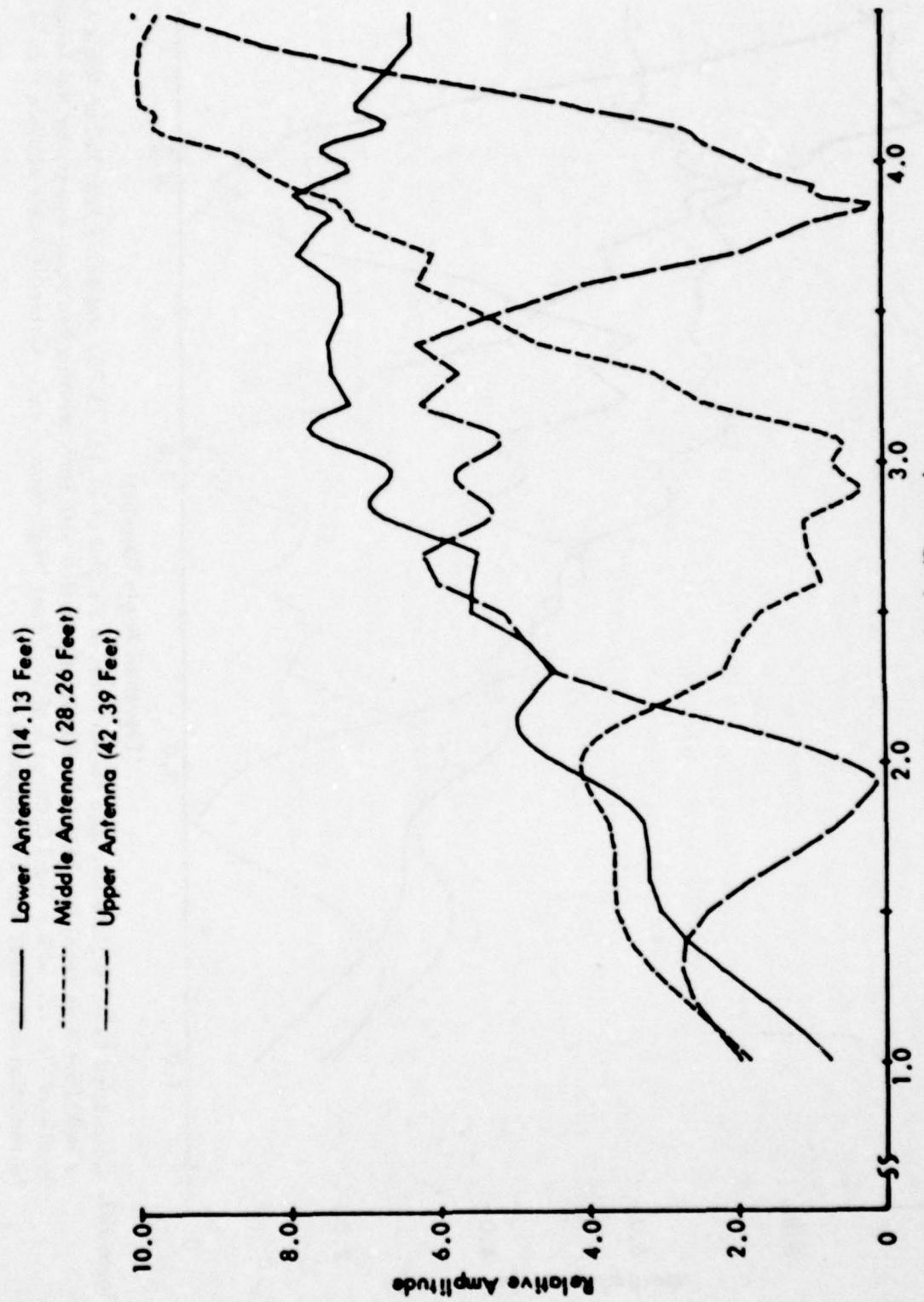
Figure 138. Calculated Relative Field Strengths for Antennas at Heights of 14.13, 28.26, and 42.39 Feet Versus Angle for a 1600 Foot High Level Run Above the Runway Centerline with Each Antenna Fed Equal Power, for the Terrain Profile of Fig. 127 with a Tidal Distance h of 6.24 Feet (High Tide).

Lower Antenna (14.13 Feet)
Middle Antenna (28.26 Feet)
Upper Antenna (42.39 Feet)
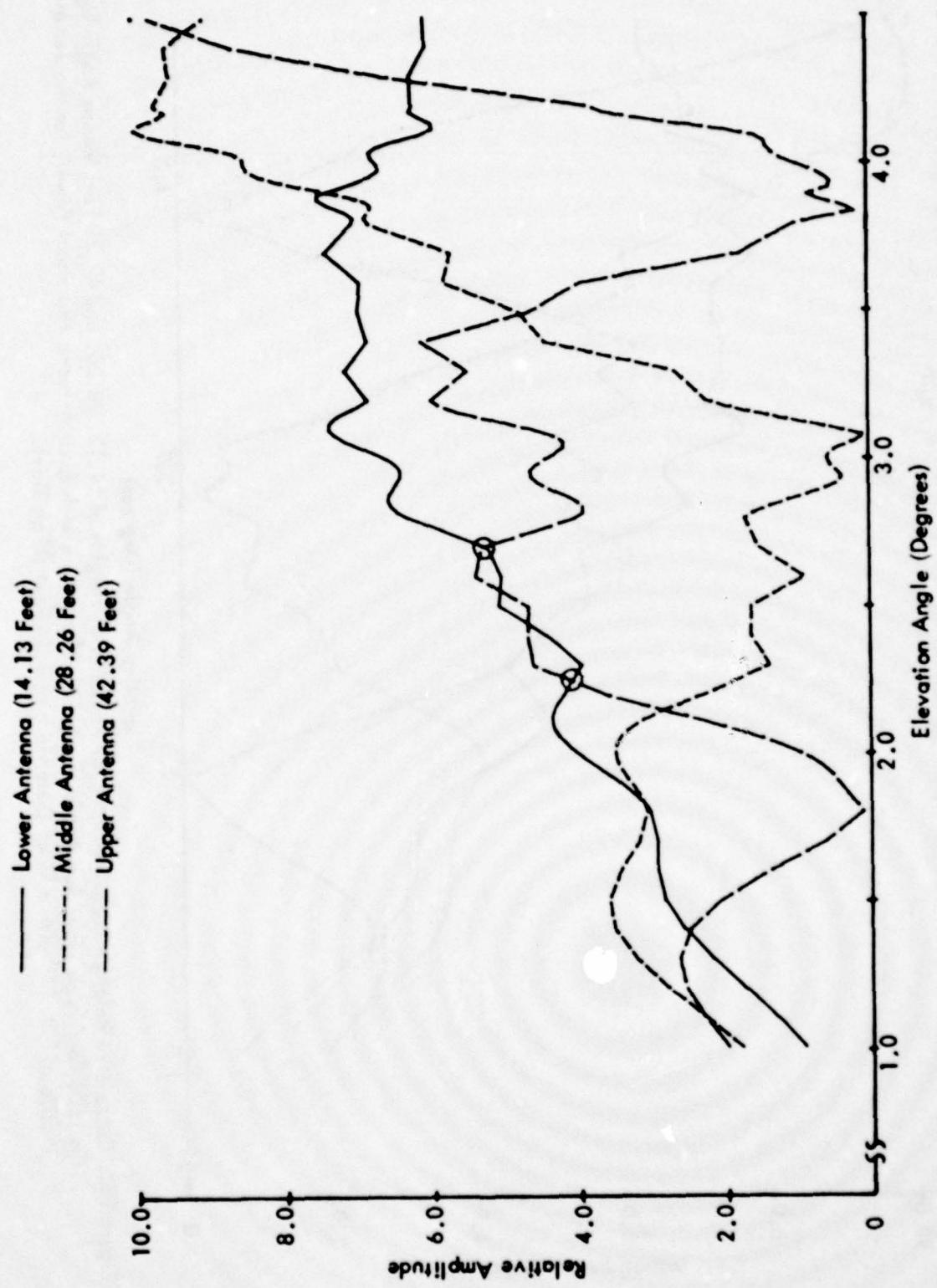
Figure 139. Calculated Relative Field Strengths for Antennas at Heights of 14.13, 28.26, and 42.39 Feet Versus Angle for a 1600 Foot High Level Run Above the Runway Centerline with Each Antenna Fed Equal Power, for the Terrain Profile of Fig. 127 with a Tidal Distance h of 10.0 Feet (High-Mean Tide). Circles indicate possible rf nulls for radiation from upper and lower antennas.
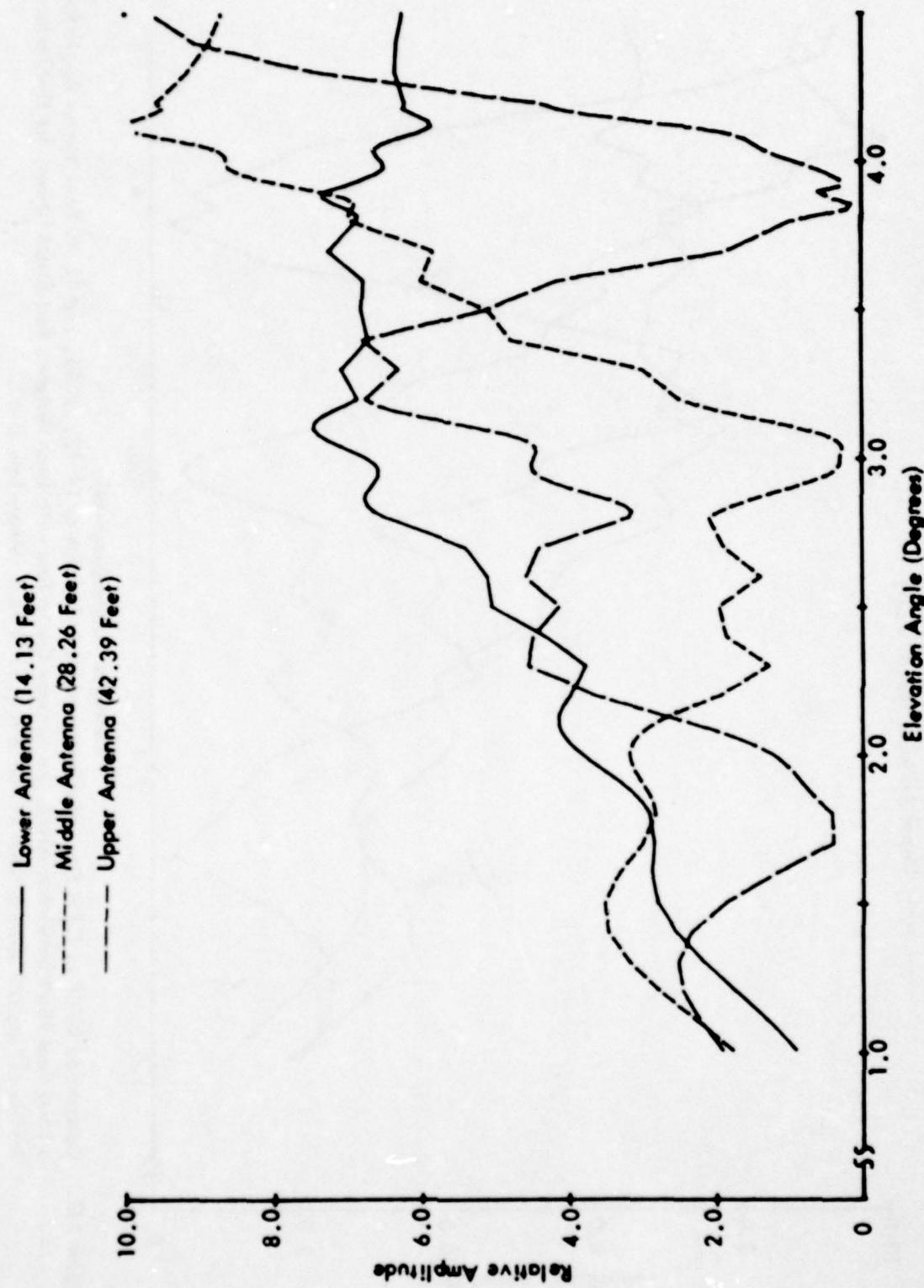
Figure 140. Calculated Relative Field Strengths for Antennas at Heights of 14.13, 28.26, and 42.39 Feet Versus Angle for a 1600 Foot High Level Run Above the Runway Centerline with Each Antenna Fed Equal Power, for the Terrain Profile of Fig. 127 with a Tidal Distance h of 13.5 Feet (Mean Tide).

-383-
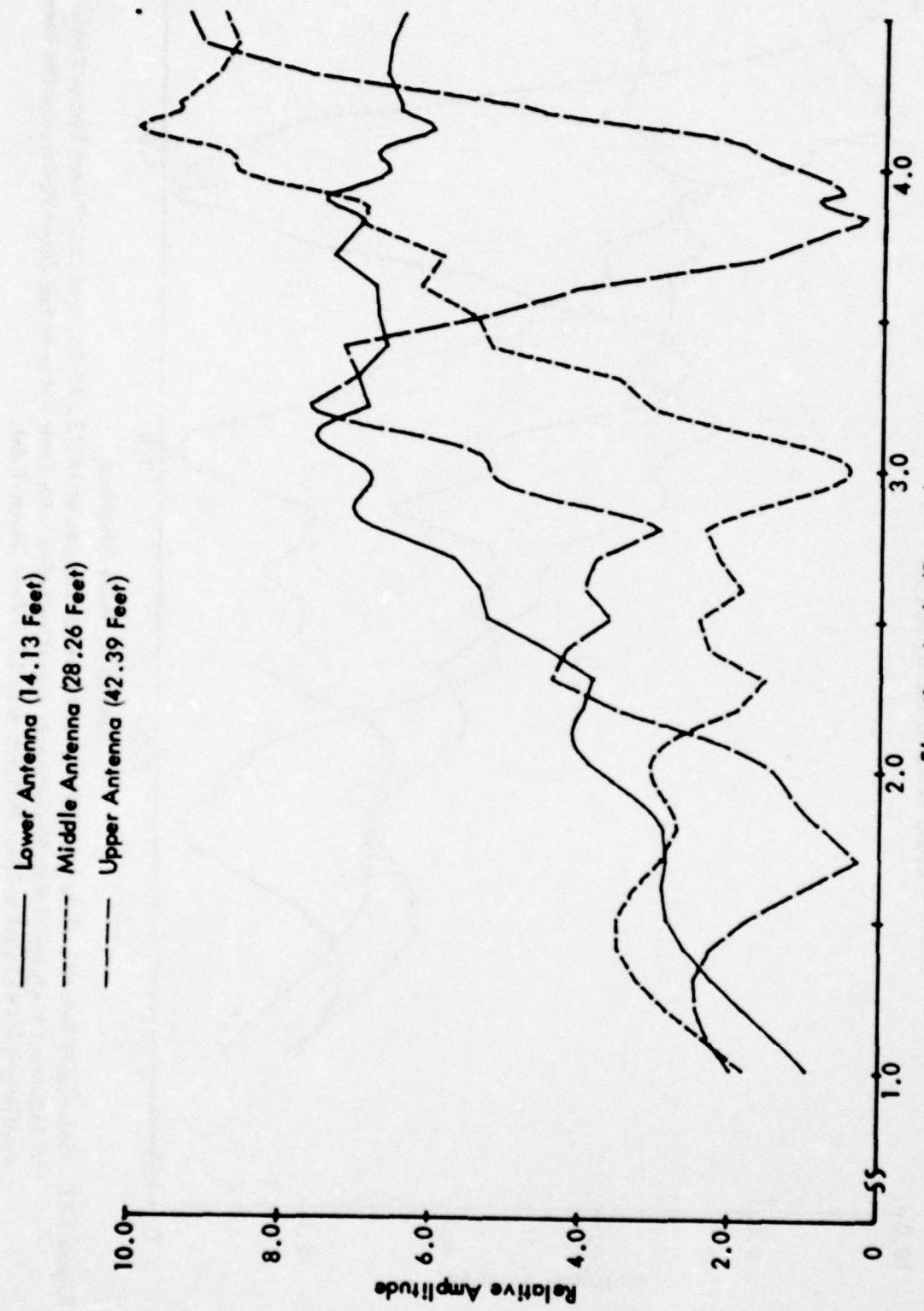
Figure 141. Calculated Relative Field Strengths for Antennas at Heights of 14.13, 28.26, and 42.39 Feet Versus Angle for a 1600 Foot High Level Run Above the Runway Centerline with Each Antenna Fed Equal Power, for the Terrain Profile of Fig. 127 with a Tidal Distance h of 17.0 Feet (Mean-Low Tide).
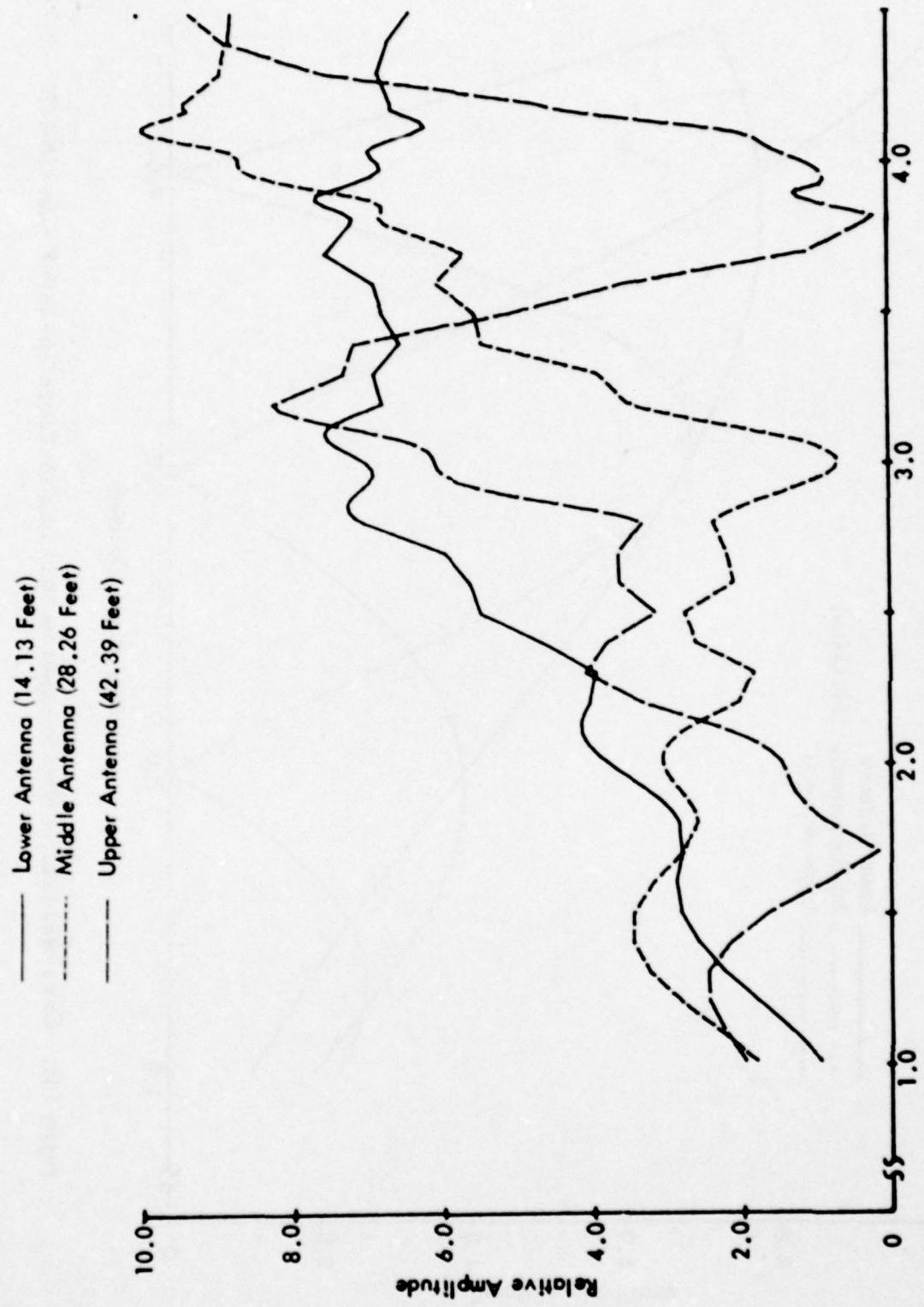
Figure 142. Calculated Relative Field Strengths for Antennas at Heights of 14.13, 28.26, and 42.39 Feet Versus Angle for a 1600 Foot High Level Run Above the Runway Centerline with Each Antenna Fed Equal Power, for the Terrain Profile of Fig. 127 with a Tidal Distance h of 20.24 Feet (Low Tide).
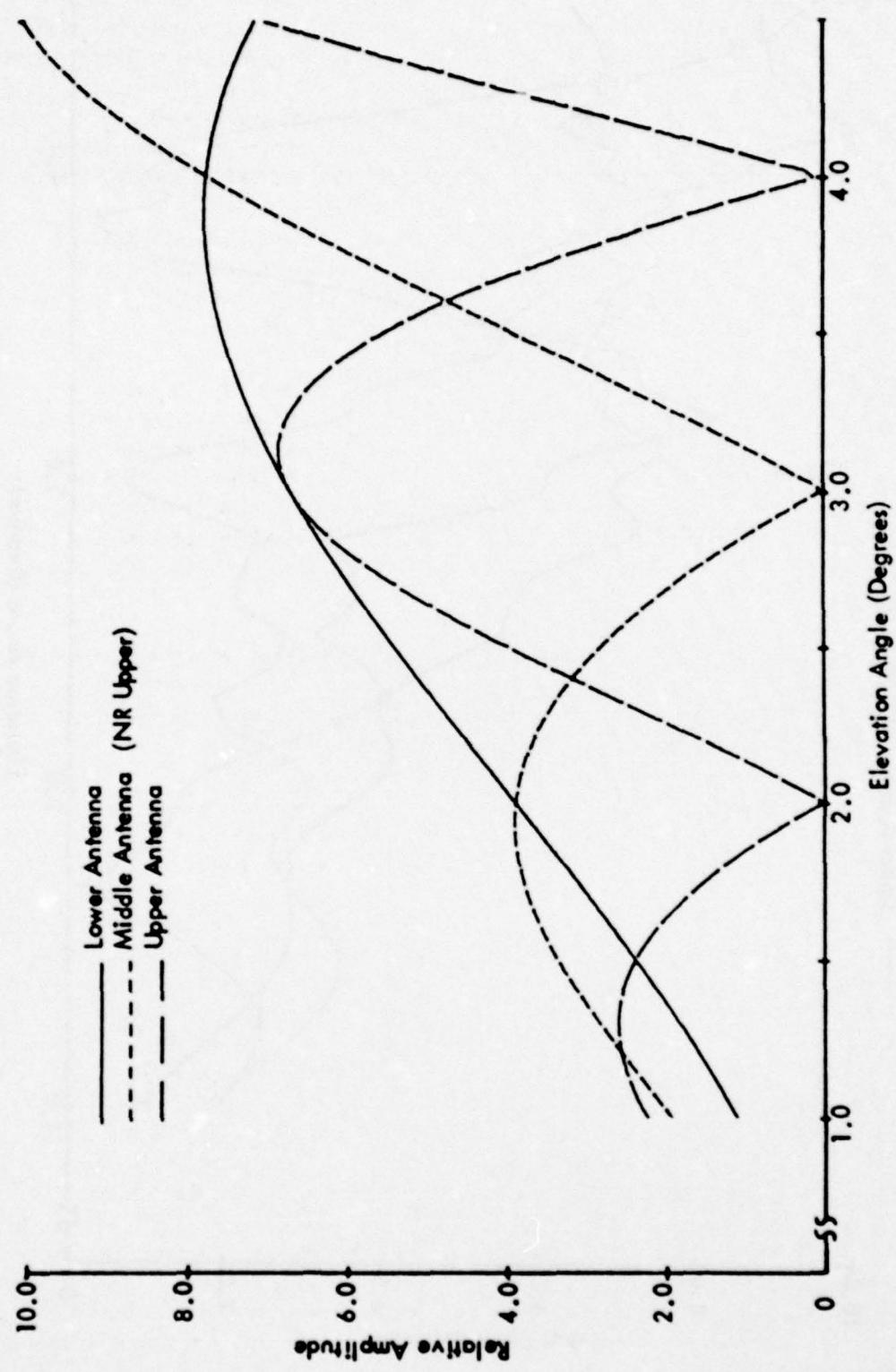
Figure 143. Calculated Relative Field Strengths for Ideal Case for Comparison with Figures 138-142.

curves, two points where the upper and lower antenna signals have the same amplitude are circled, and these points lie very near the measured values of 2.30 and 2.58°. These equal amplitude points will correspond to RF nulls, with the null depth depending on the relative phasing between the two signals. (The two equal amplitude points in between may not have produced deep nulls due either to changes in relative phasing, or to errors in the amplitude calculations which caused the two curves to cross over one another when in actuality, this was not the case.) Thus the strange RF null locations are apparently due to perturbations in the antenna patterns caused by the uneven terrain.

Finally, Figure 144 contains a graphic summary of the calculated data contained in Figures 128 through 142 (and other calculations as well). Note that the path angle change from high to low tide calculated for the capture effect system is .11°, which corresponds very closely with the measured value of .09°. [20]

To summarize, the calculated results obtained using the more accurate terrain profile agree very well with those actually observed during flight measurements. The poor crossovers and flyability roughness for the null reference system and the smoother flyability results for the capture effect system were evident in the calculations. Also, the measured path angle change due to tidal variations agreed closely with the calculations. In addition, the measured RF nulls at 2.30 and 2.58° agree with the calculations, and are explained as deformations in the vertical antenna patterns caused by the uneven terrain.

4. Recommendations and Predictions. In this section recommended antenna heights and phasing will be given for the system sited both at the present location and displaced 1000' (300m) from the present location, and predictions of performance for the recommended configurations are made.

After consideration of the poor performance of the null reference system as discussed in the previous section, it is recommended that a capture effect system be used at these sites, and only this system will be discussed in the following.

Figures 145, 146, and 147 contain calculated values of path angle, width, and symmetry as a function of tide level for various system phasing and A ratio values. The antenna heights are fixed for these 3 figures at values which give a 3.0° path angle for a tide level near mean tide. In Figure 145 the system is phased using simulated airborne phasing, and the A ratio adjusted to yield a 0.7° path width at mean tide. This result was not considered satisfactory due to the poor symmetry and large path angle variation at low tide. In an attempt to improve this performance, the relative antenna phasing was adjusted (on a trial-and-error basis) so as to improve the low tide symmetry and path angle variation. The results are indicated in Figure 146. This result, however, has a low average path width, so the sideband power was reduced to give the results shown in Figure 147. These results predict a path angle between 2.96 and 3.04°, path width between 0.60 and 0.72, and path symmetry between .52 and .43, as the tide changes. All of these parameters are within Category I tolerances, and the system should be capable of assured Category I performance with appropriate tightening of monitor alarm limits. The system parameters given in Figure 147 are those recommended if the system is to be installed at the present location.
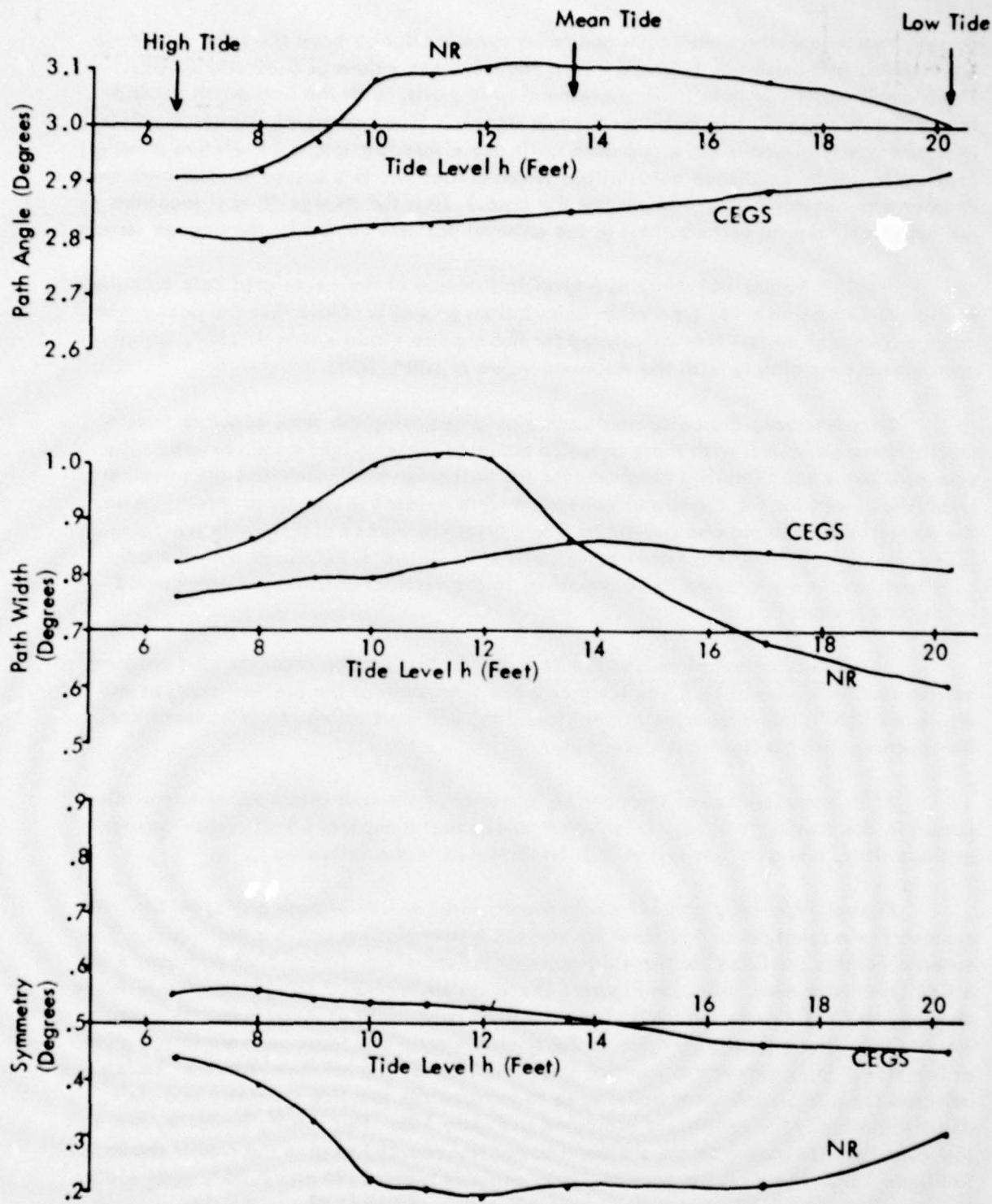
Figure 144. Calculated Values of Path Angle, Path Width, and Symmetry for Capture Effect and Null Reference Systems for Various Tidal Distances h for the Terrain Profile of Fig. 127. The antenna heights are 14.13 28.26, and 42.39 feet, and the A ratio is .300.
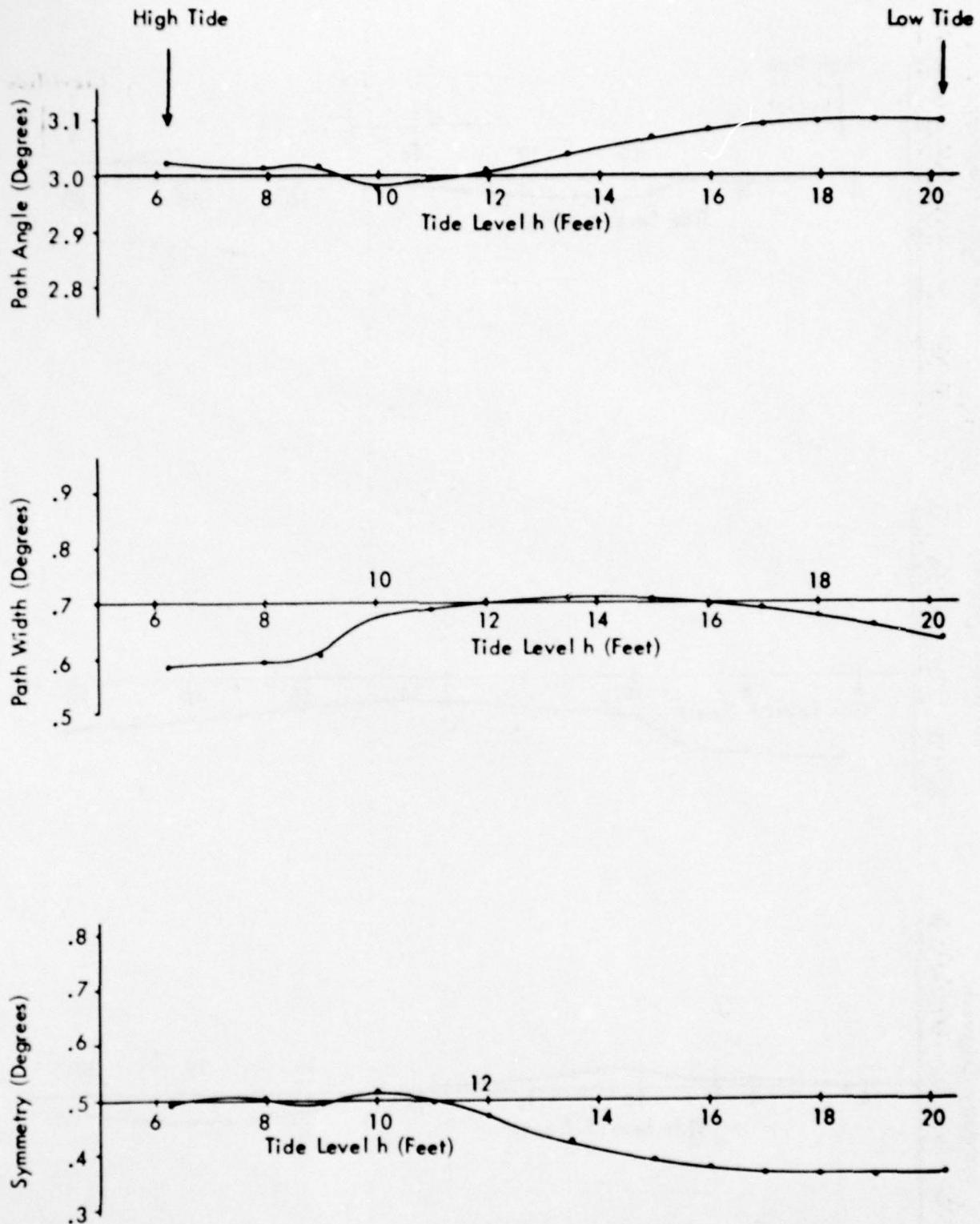
Figure 145. Calculated Values of Path Angle, Path Width, and Symmetry for a Capture Effect System for Various Tidal Distances h for the Terrain Profile of Fig. 127.   The antenna heights are 13.45, 26.9, and 40.35 feet. The lower antenna is phase retarded 6.8 degrees with respect to the middle, the upper antenna advanced 3.1, and the A ratio is .392.

-389-
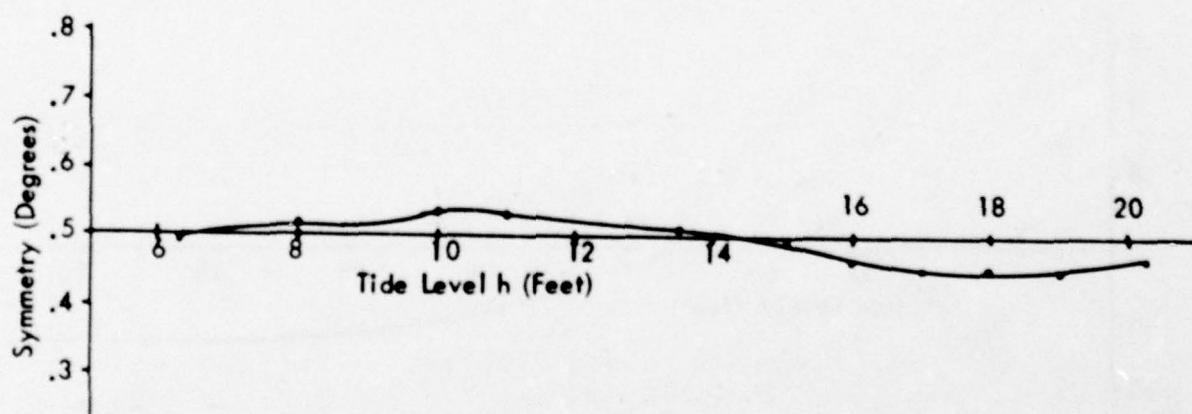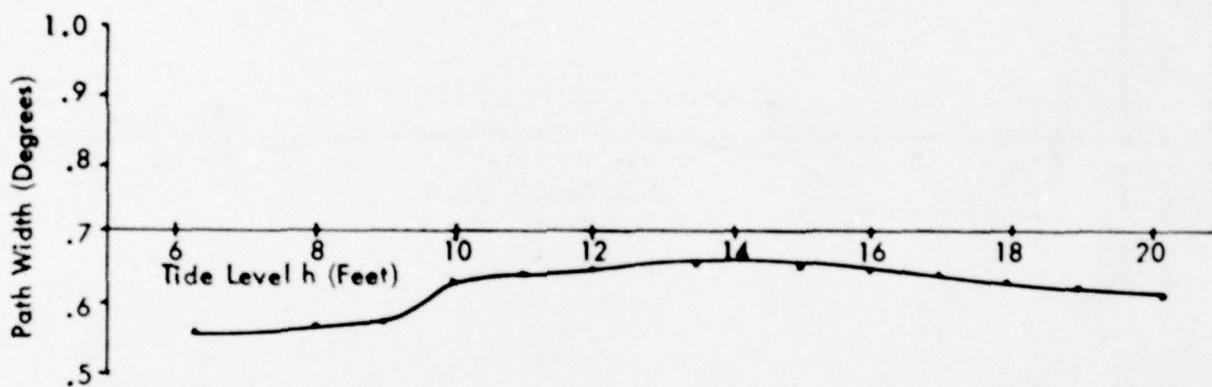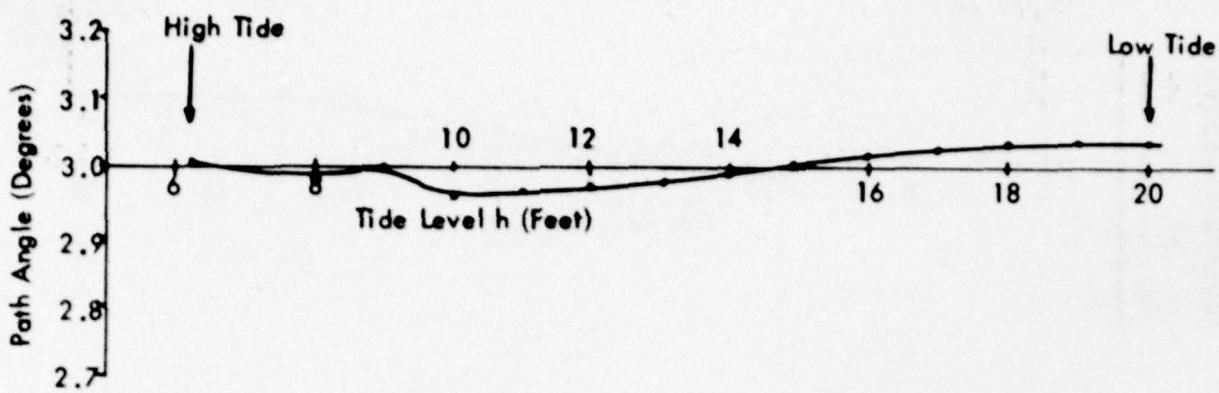
Figure 146. Calculated Values of Path Angle, Path Width, and Symmetry for a Capture Effect System for Various Tidal Distances h for the Terrain Profile of Fig. 127. The antenna heights are 13.45, 26.9, and 40.35 feet. The lower antenna is phase retarded 6.8 degrees with respect to the middle, the upper antenna advanced 20.0, and the A ratio is .392.
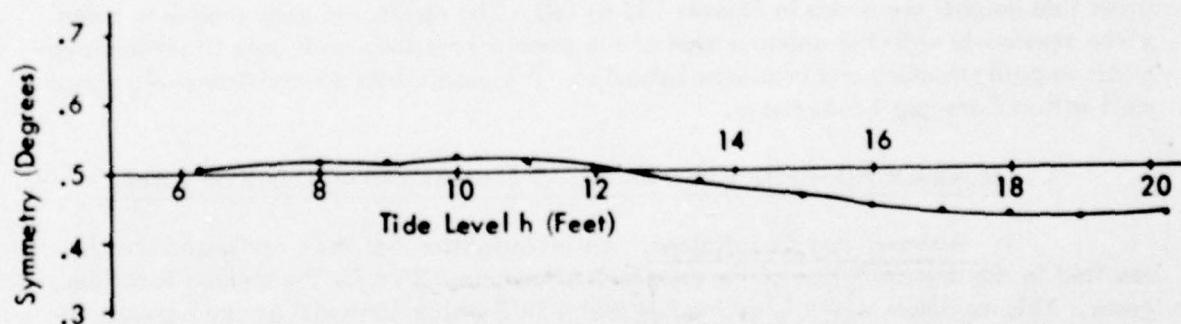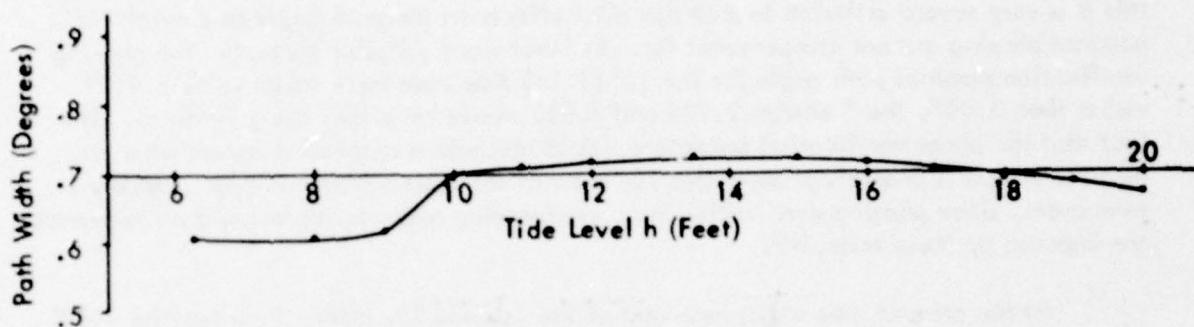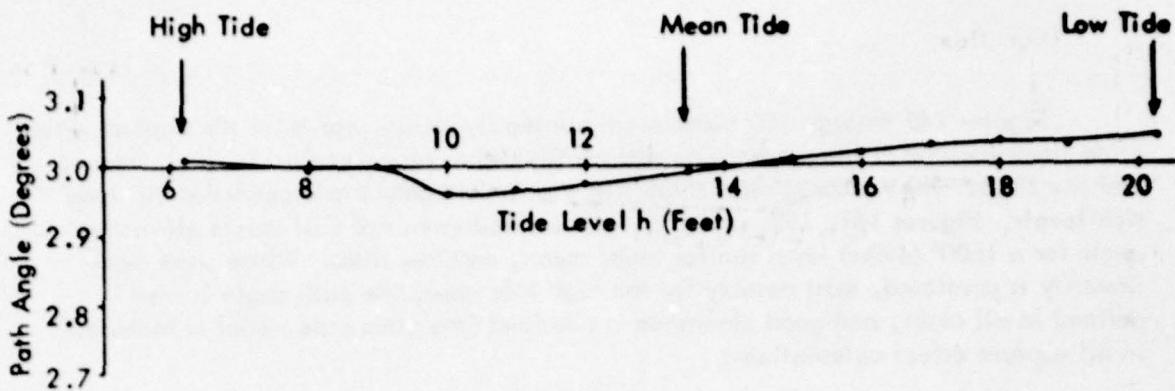
Figure 147. Calculated Values of Path Angle, Path Width, and Symmetry for a Capture Effect System for Various Tidal Distance h for the Terrain Profile of Fig. 127. The antenna heights are 13.45, 26.9, and 40.35 feet. The lower antenna is phase retarded 6.8 degrees with respect to the middle, the upper antenna advanced 20.0, and the A ratio is .360.

Figures 148 through 150 contain calculated flyability results for the capture effect glide slope located at the present site and configured as recommended for high, mean, and low tides. The results predict flyability within Category I tolerances for all three tide levels. Figures 151, 152, and 153 are predicted values of CDI versus elevation angle for a 1600' (490m) level run for high, mean, and low tides. While some non-linearity is predicted, most notably for the high tide case, the path angle is well defined in all cases, and good clearance is obtained (the clearance signal is included in all capture effect calculations).

Table 33 contains tabulated results of a simulated phasing verification exercise for 4 tide levels. The entries marked with an asterisk (*) would be outside the recommended limits for a nominal path width and symmetry of 3.00 and 0.70°, respectively. Note that this is a very severe criterion in that the tidal effects on the path angle and width for nominal phasing are not compensated for. In other words, if, for example, the phasing verification nominal path angle for the 10' (3.1m) tide case were taken to be 2.959° rather than 3.00°, the * entries 2.924 and 2.866 would be within the guidelines. The fact that the phase verification procedure would indicate a misphased system when in fact the system is properly phased does not prevent the system from meeting Category I tolerances, since phasing verification is an engineering and support test and no tolerances are imposed by these tests. [19]

At the present time a displacement of the Runway 22L glide-slope facility 1000' (300m) back from the current location is being considered. In the event that this move is made, the following predictions of performance are included. These predictions cannot be made with complete confidence, however, since the additional 1000' (300m) of terrain included in the reflecting zone was not included in the terrain mapped. For the purpose of these predictions, this terrain was assumed to be flat and horizontal. The resulting terrain profile is shown in Figure 154. Predicted flyability and level run crossovers for three tide heights are given in Figures 155 to 160. The results are very similar to those given previously with the antenna mast at the present location, with only slight improvements in path structure and crossover behavior. The predictions do indicate performance well within Category I tolerances.

C. Maximum Allowable VSWR for the 15-Element V-Ring Localizer Array.

1. Summary and Conclusions. An investigation has been performed that has resulted in the determination of the maximum allowable VSWR for the V-Ring localizer array. This maximum VSWR is defined as that VSWR which can exist at any antenna in the array and produce effects on the far-field that result in no more than 25% of the theoretically allowable far-field tolerances being consumed.

To begin, the assumption is made that the entire array has some average VSWR across it and that a single antenna is deteriorating. Since, in general, nothing is known about the angle of the reflection coefficient that results in a given VSWR (as might be measured with a thru-line wattmeter), the model was manipulated to determine the worst case for this reflection angle. This worst case is the most damaging to the far field and
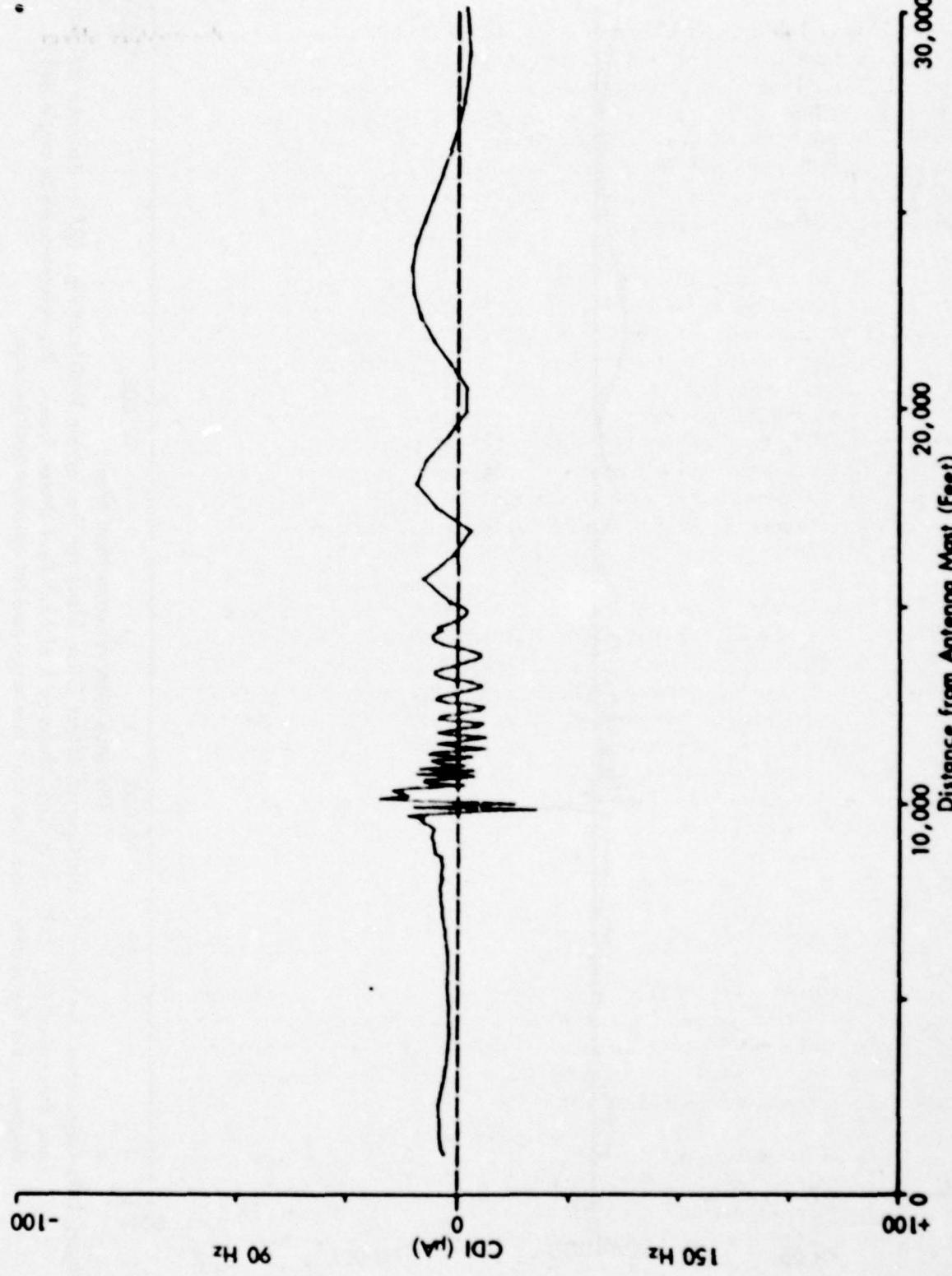
Figure 148. Calculated Flyability for the Capture Effect Glide Slope for the Terrain Profile of Fig. 127 for Antenna Heights and Phasing of Fig. 147 and a Tidal Distance h of 6.24 Feet (High Tide). The reference glide angle is 3.0 degrees, and the system conditions are those suggested for optimum performance.
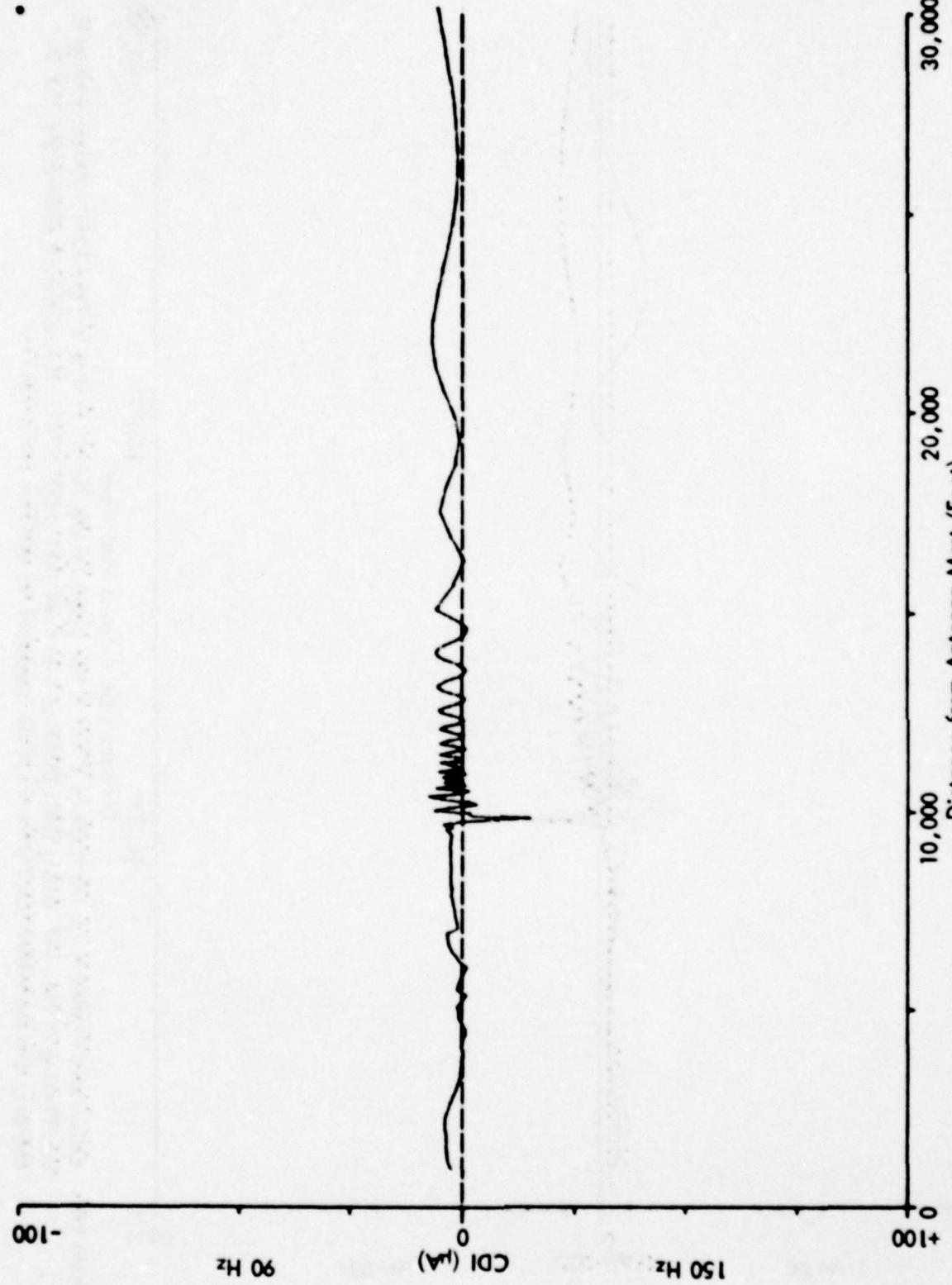
Figure 149. Calculated Flyability for the Capture Effect Glide Slope for the Terrain Profile of Fig. 127 for Antenna Heights and Phasing of Fig. 147 and a Tidal Distance h of 13.5 Feet (Mean Tide). The reference glide angle is 3.0 degrees, and the system conditions are those suggested for optimum performance.
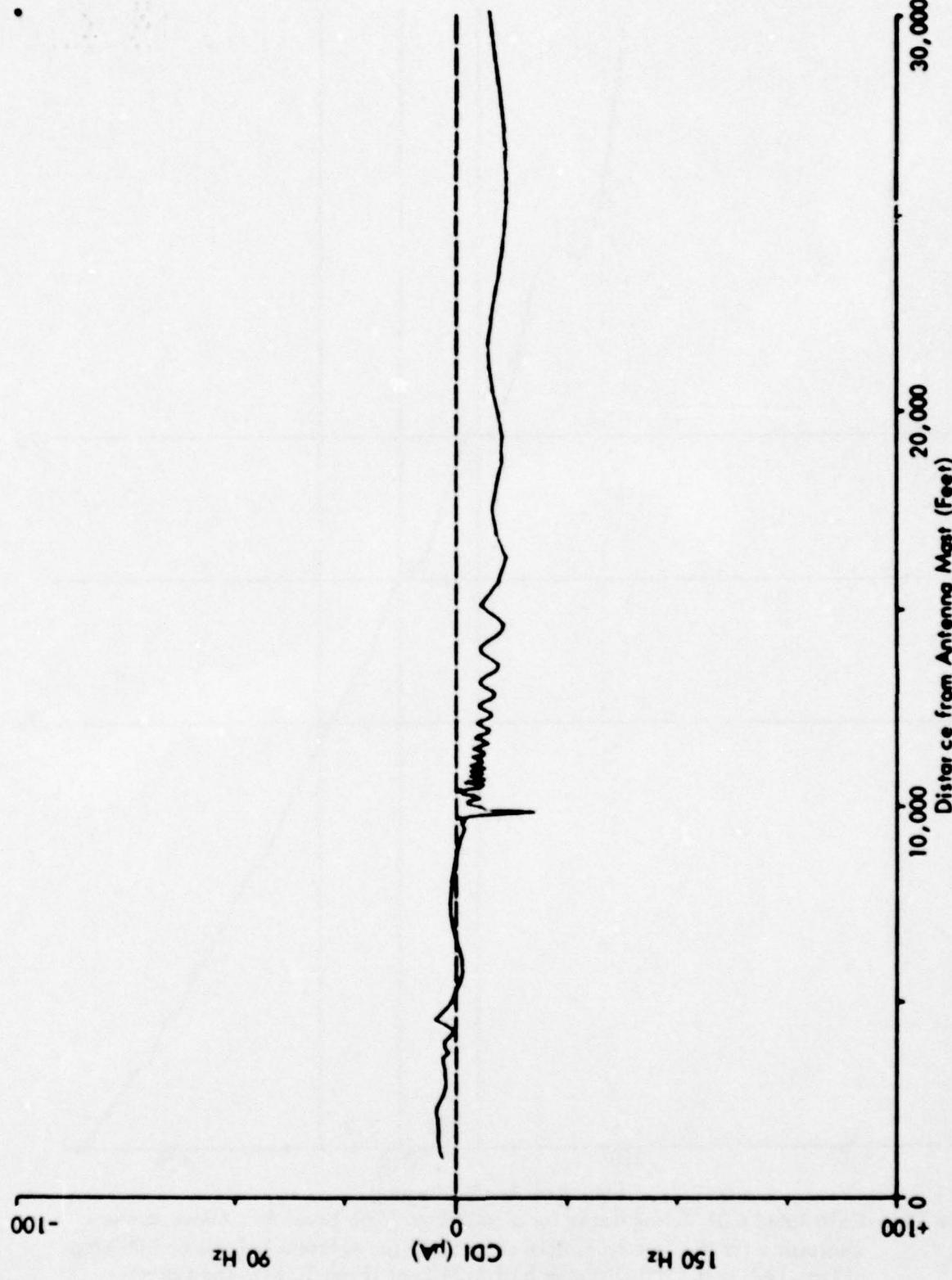
Figure 150. Calculated Flyability for the Capture Effect Glide Slope for the Terrain Profile of Fig. 127 for Antenna Heights and Phasing of Fig. 147 and a Tidal Distance h of 20.24 Feet (Low Tide). The reference glide angle is 3.0 degrees, and the system conditions are those suggested for optimum performance.
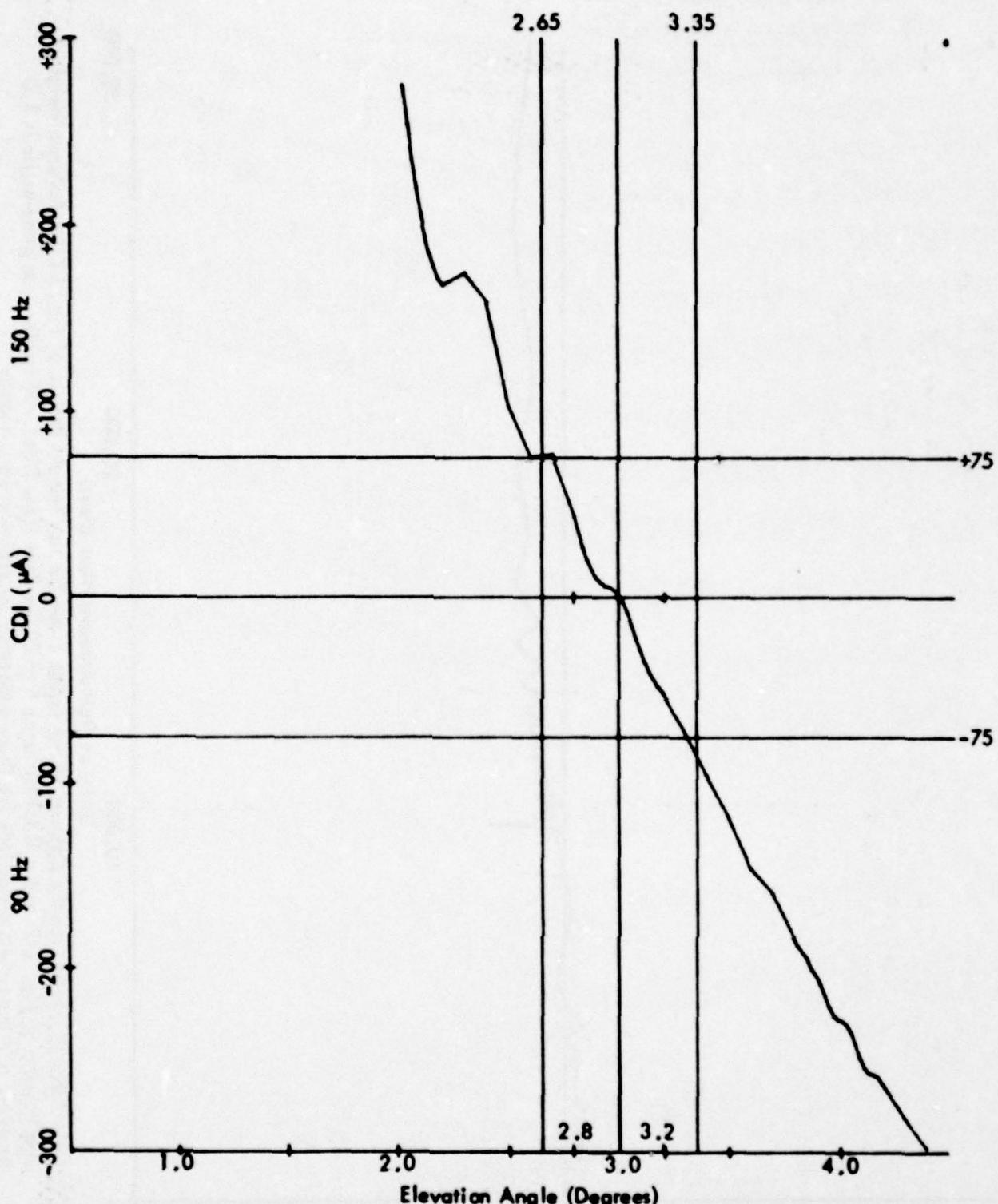
Figure 151. Calculated CDI Versus Angle for a 1600 Foot High Level Run Above Runway Centerline for the Terrain Profile of Fig. 127 for Antenna Heights and Phasing of Fig. 147 and Tidal Distance h of 6.24 Feet (High Tide). The system conditions are those suggested for optimum performance.

-396-
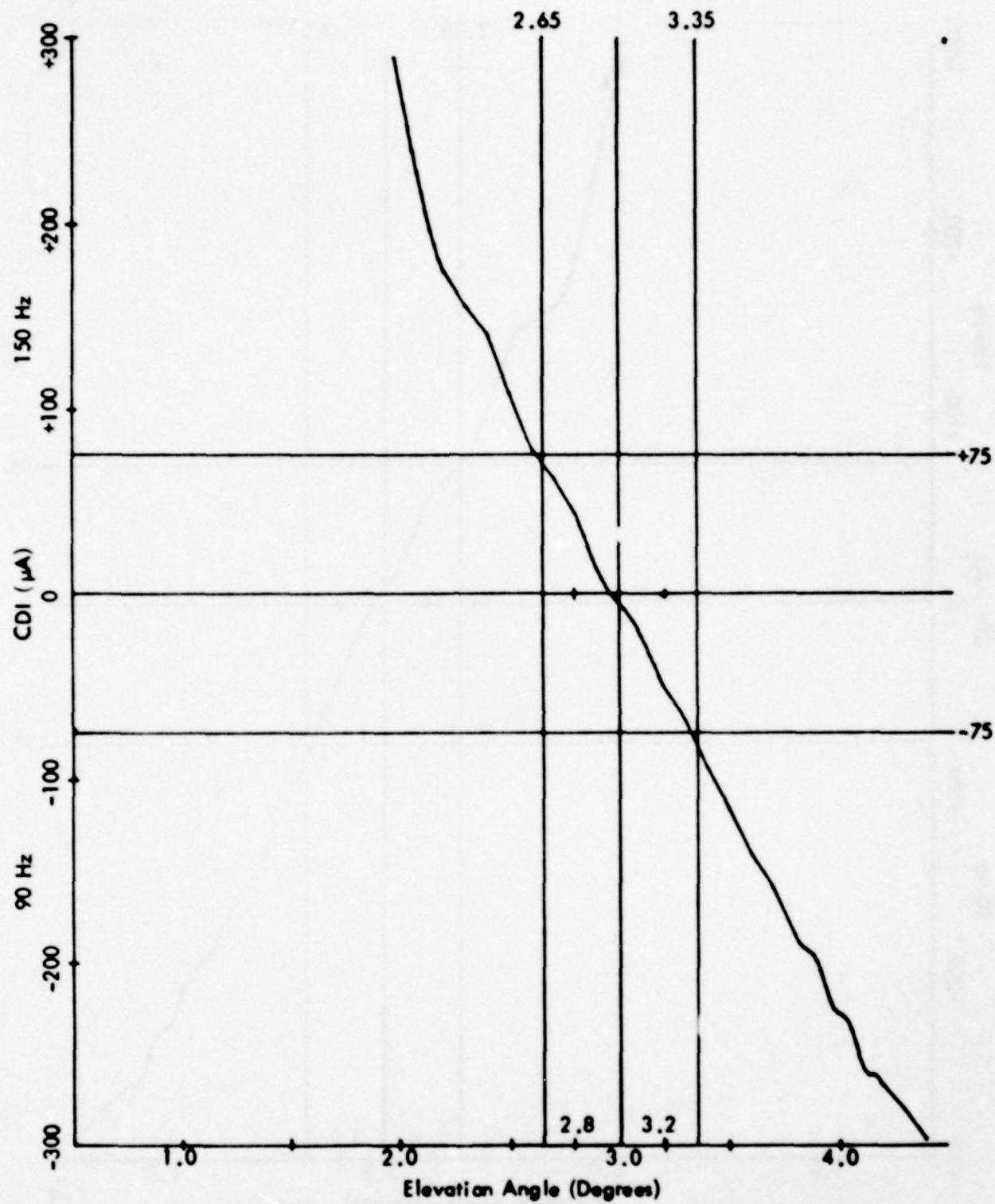
Figure 152. Calculated CDI Versus Angle for a 1600 Foot High Level Run Above Runway Centerline for the Terrain Profile of Fig. 127 for Antenna Heights and Phasing of Fig. 147 and Tidal Distance h of 13.5 Feet (Mean Tide). The system conditions are those suggested for optimum performance.
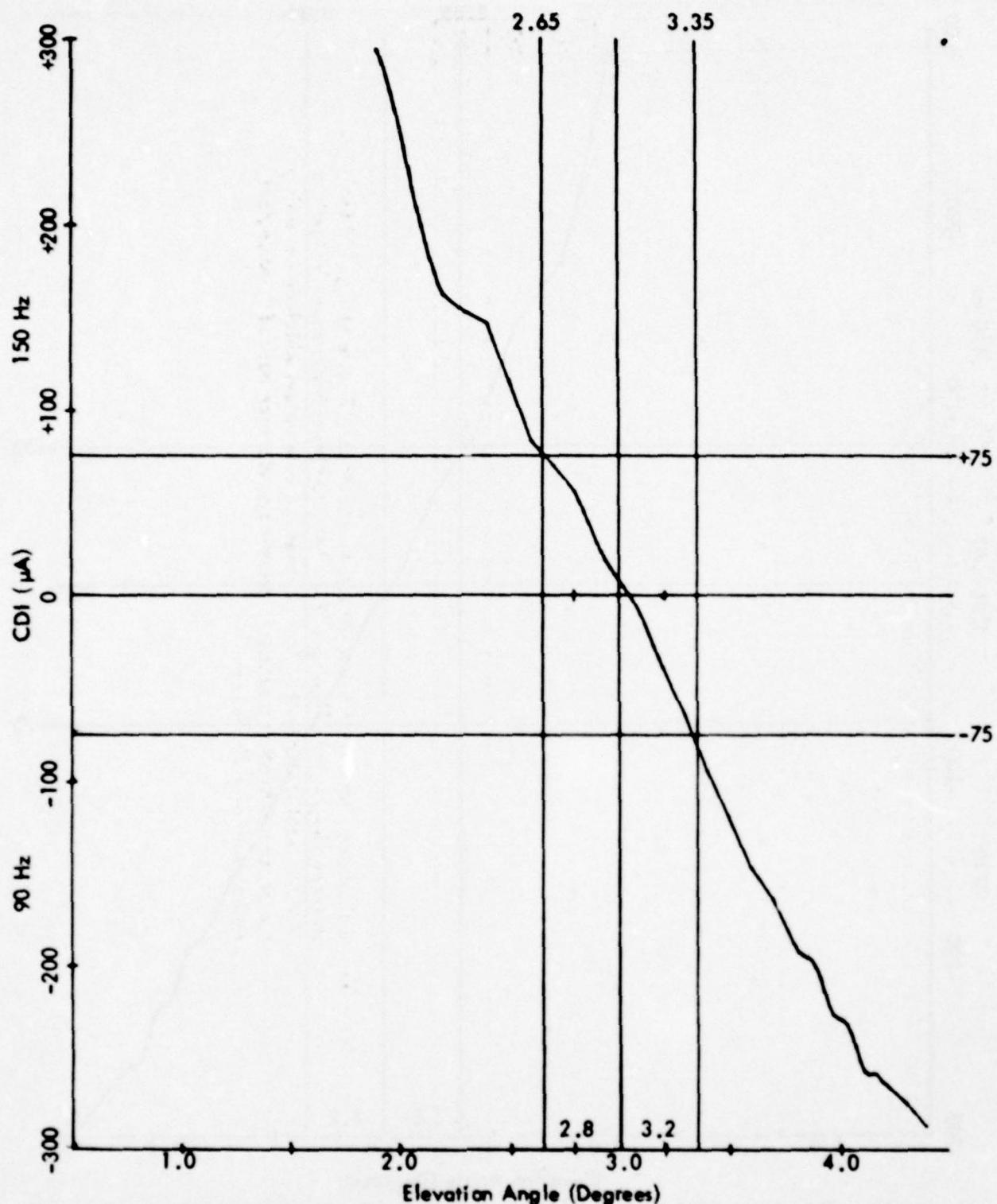
Figure 153. Calculated CDI Versus Angle for a 1600 Foot High Level Run Above Runway Centerline for the Terrain Profile of Fig. 127 for Antenna Heights and Phasing of Fig. 147 and Tidal Distance h of 20.24 Feet. The system conditions are those suggested for optimum performance.

-398-

Lower Antenna 13.45 Feet, Phase Retarded 6.8°

Middle Antenna 26.90 Feet, Phase Reference

Upper Antenna 40.35 Feet, Phase Advanced 20°

A Ratio .360

TIDE (h) (Wrt Mast)	NOMINAL VALUES		DEPHASING MIDDLE ANTENNA				DEPHASING MAIN SIDEBAND PHASOR			
			15°		-15°		30°		-30°	
	PATH ANGLE	PATH WIDTH	PATH ANGLE	PATH WIDTH	PATH ANGLE	PATH WIDTH	PATH ANGLE	PATH WIDTH	PATH ANGLE	PATH WIDTH
6 Ft	3.006	0.604	2.942*	0.777	3.024	0.560*	2.857*	0.797	3.070	0.666
10 Ft	2.959	0.695	2.924*	0.802	3.001	0.568*	2.866*	0.789	3.099	0.700
12 Ft	2.972	0.714	2.932*	0.844	3.004	0.566*	2.868*	0.808	3.114*	0.700
20 Ft	3.041	0.671	3.098*	0.864	3.002	0.570*	2.907	0.813	3.133*	0.615

Table 33. Calculated Phase Verification Results for the Terrain Profile of Fig. 127 for Antenna Heights and Phasing of Fig. 147 (Optimum Performance Values) for Various Tidal Distances h. The * entries indicate values which do not satisfy the phase verification procedure, assuming a reference path of 3.00 degrees and a width of 0.70 degrees.

-399-
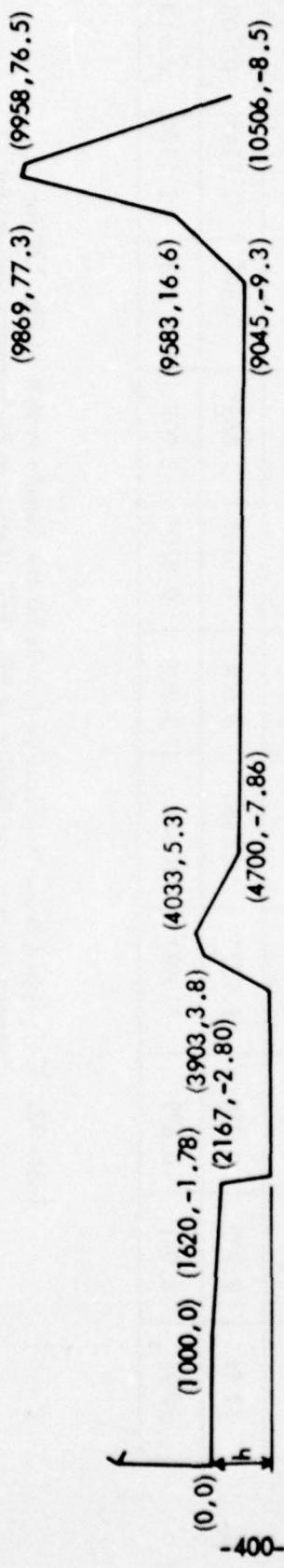
Figure 154. Terrain Profile for the Boston 22L Glide Slope Reflecting Zone But with the Glide Slope Antennas Displaced 1000 Feet from the Current Location. The additional terrain included (with respect to Fig. 127) was not measured, but is assumed to be flat and horizontal.
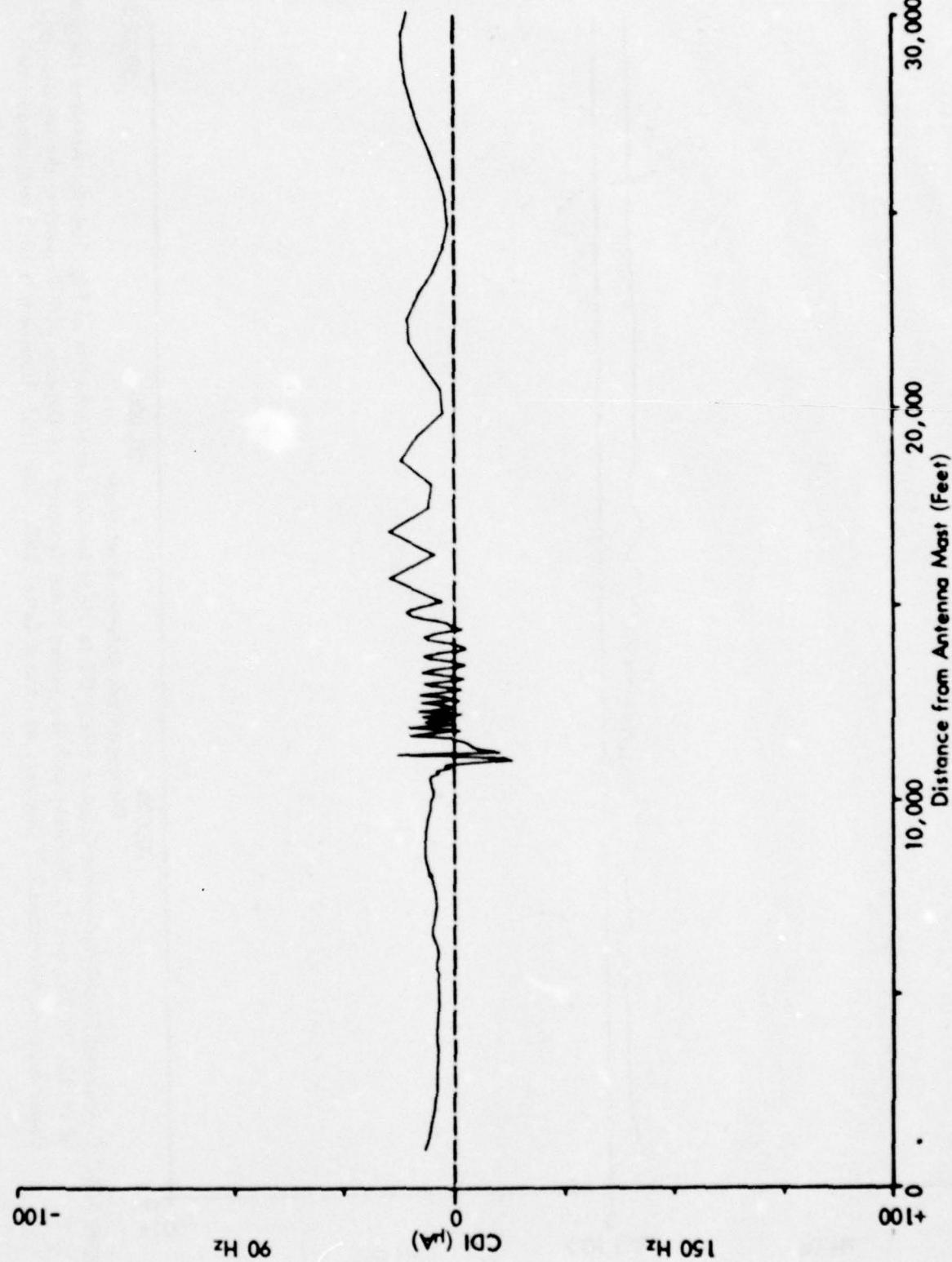
Figure 155. Calculated Flyability for the Capture Effect Glide Slope for the Terrain Profile of Fig. 154 for Antenna Heights of 14.13, 28.26, and 42.39 Feet, with the Lower Phase Retarded 4.1 Degrees with Respect to the Middle, and Upper Antenna Advanced 2.0 Degrees, and the A Ratio .295. The tidal distance h is 6.24 feet (high tide).
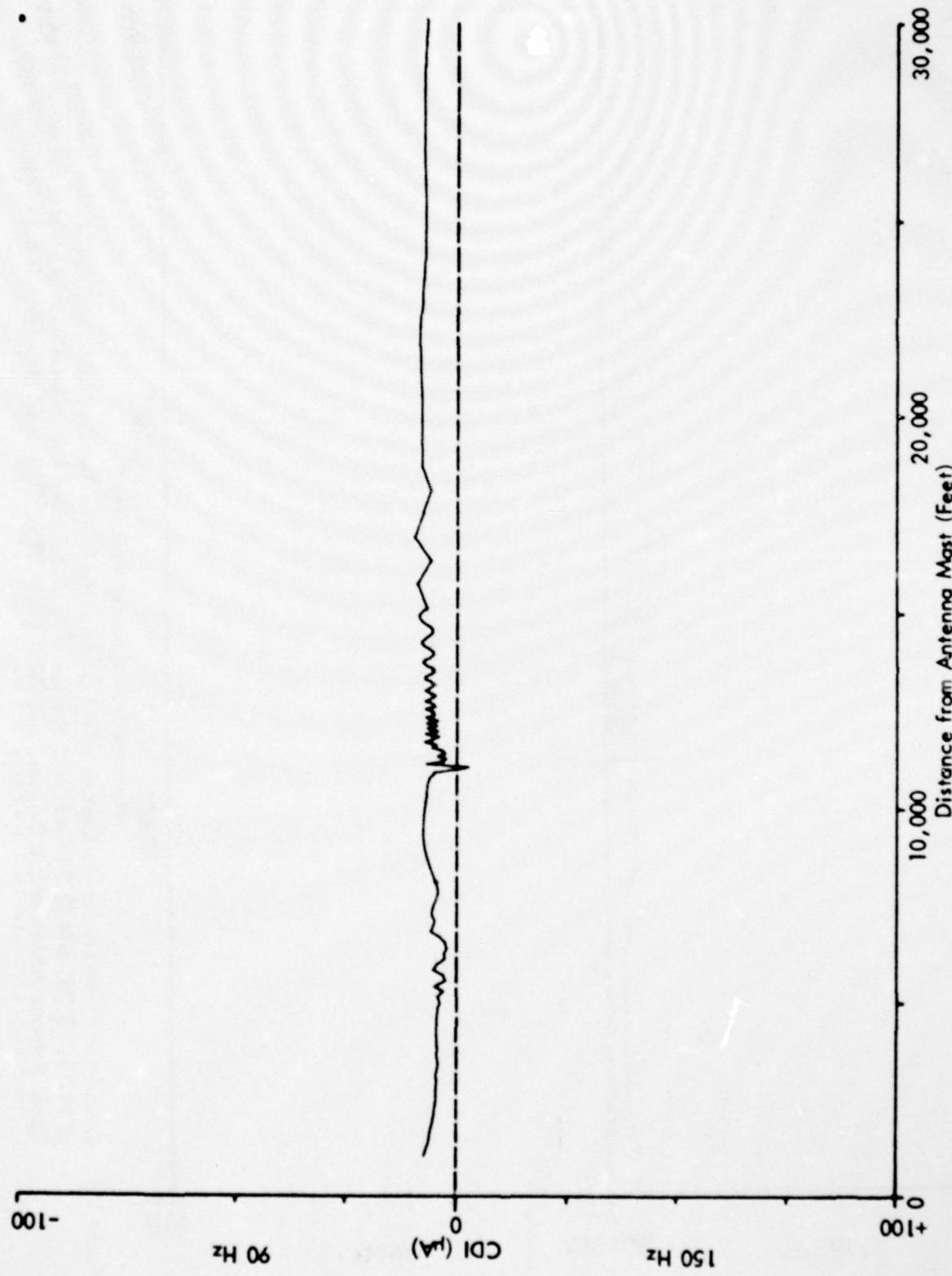
Figure 156. Calculated Flyability for the Capture Effect Glide Slope for the Terrain Profile of Fig. 154 for Antenna Heights of 14.13, 28.26, and 42.39 Feet, with the Lower Phase Retarded 4.1 Degrees with Respect to the Middle, and Upper Antenna Advanced 2.0 Degrees, and the A Ratio .295. The tidal distance h is 13.5 feet (mean tide).

Figure 157. Calculated Flyability for the Capture Effect Glide Slope for the Terrain Profile of Fig. 154 for Antenna Heights of 14.13, 28.26, and 42.39 Feet, with the Lower Phase Retarded 4.1 Degrees with Respect to the Middle, and Upper Antenna Advanced 2.0 Degrees, and the A Ratio .295. The tidal distance h is 20.24 feet (low tide).

-403-
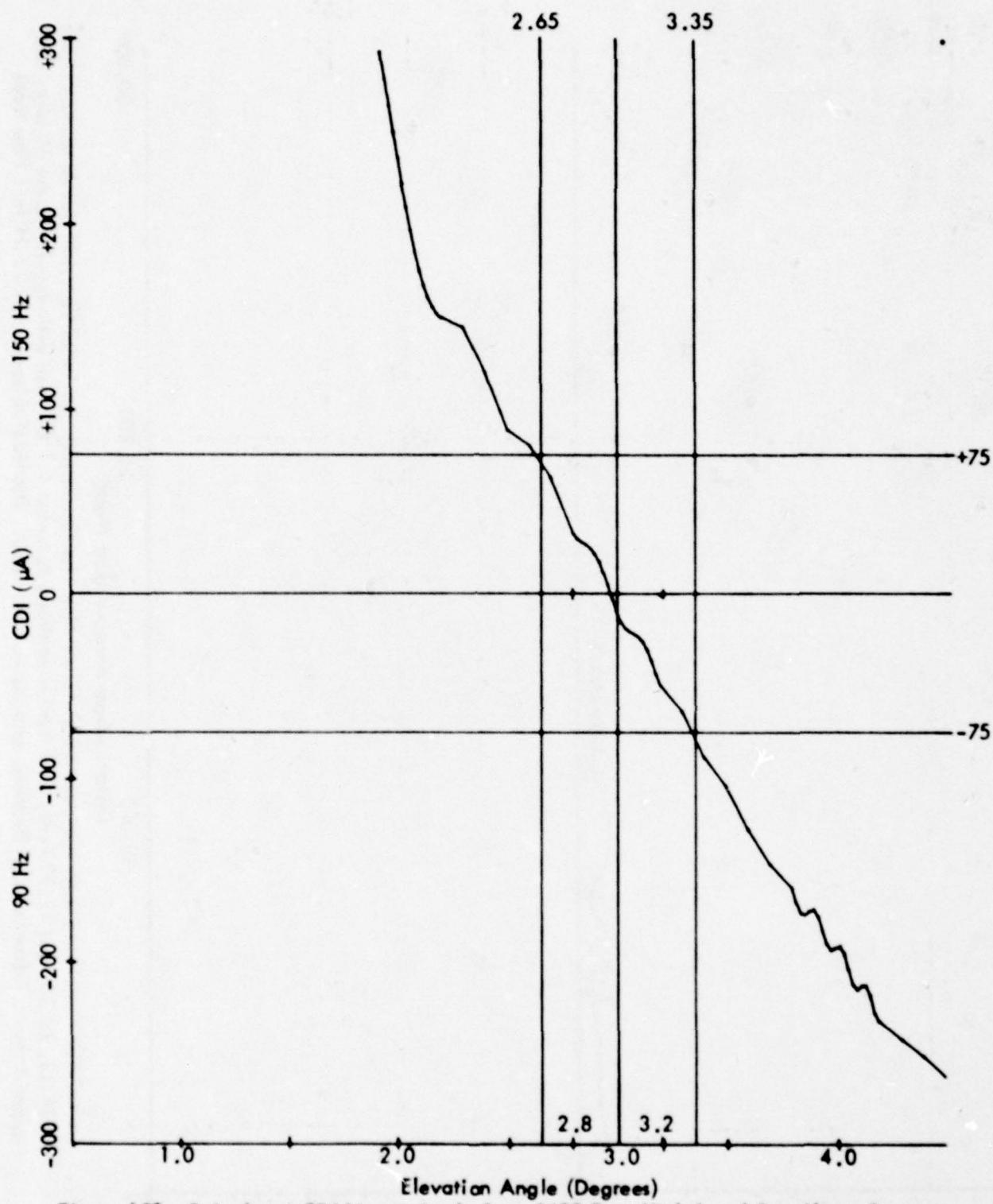
Figure 158. Calculated CDI Versus Angle for a 1600 Foot High Level Run Above Runway Centerline for the Terrain Profile of Fig. 154 for Antenna Heights of 14.13, 28.26, and 42.39 Feet, with the Lower Antenna Phase Retarded 4.1 Degrees with Respect to the middle, and Upper Advanced 2.0 Degrees, and the A Ratio .295. The tidal distance h is 6.24 feet (high tide).
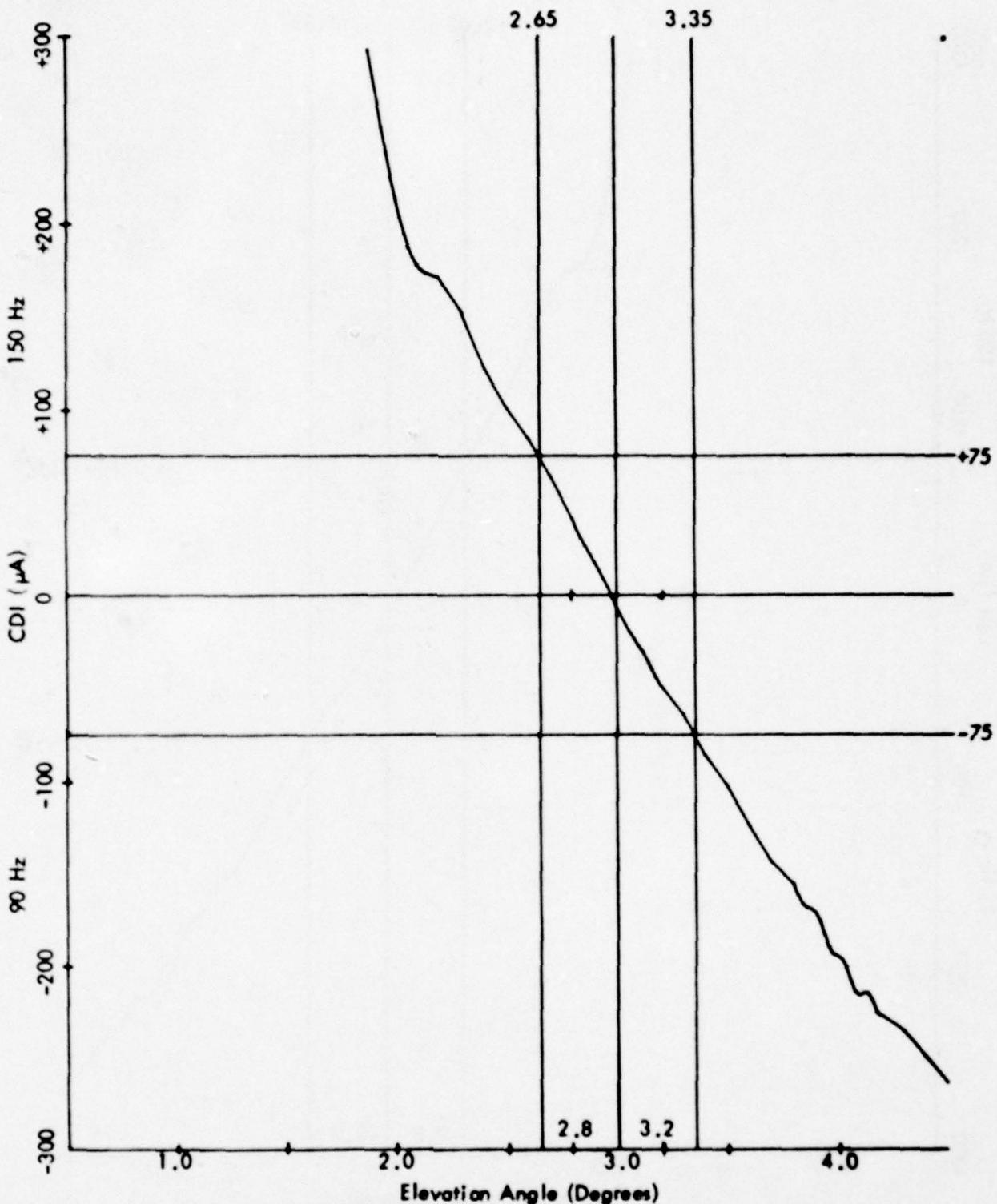
Figure 159. Calculated CDI Versus Angle for a 1600 Foot High Level Run Above Runway Centerline for the Terrain Profile of Fig. 154 for Antenna Heights of 14.13, 28.26, and 42.39 Feet, with the Lower Antenna Phase Retarded 4.1 Degrees with Respect to the Middle, and Upper Advanced 2.0 Degrees, and the A Ratio .295. The tidal distance he is 13.5 feet (mean tide).
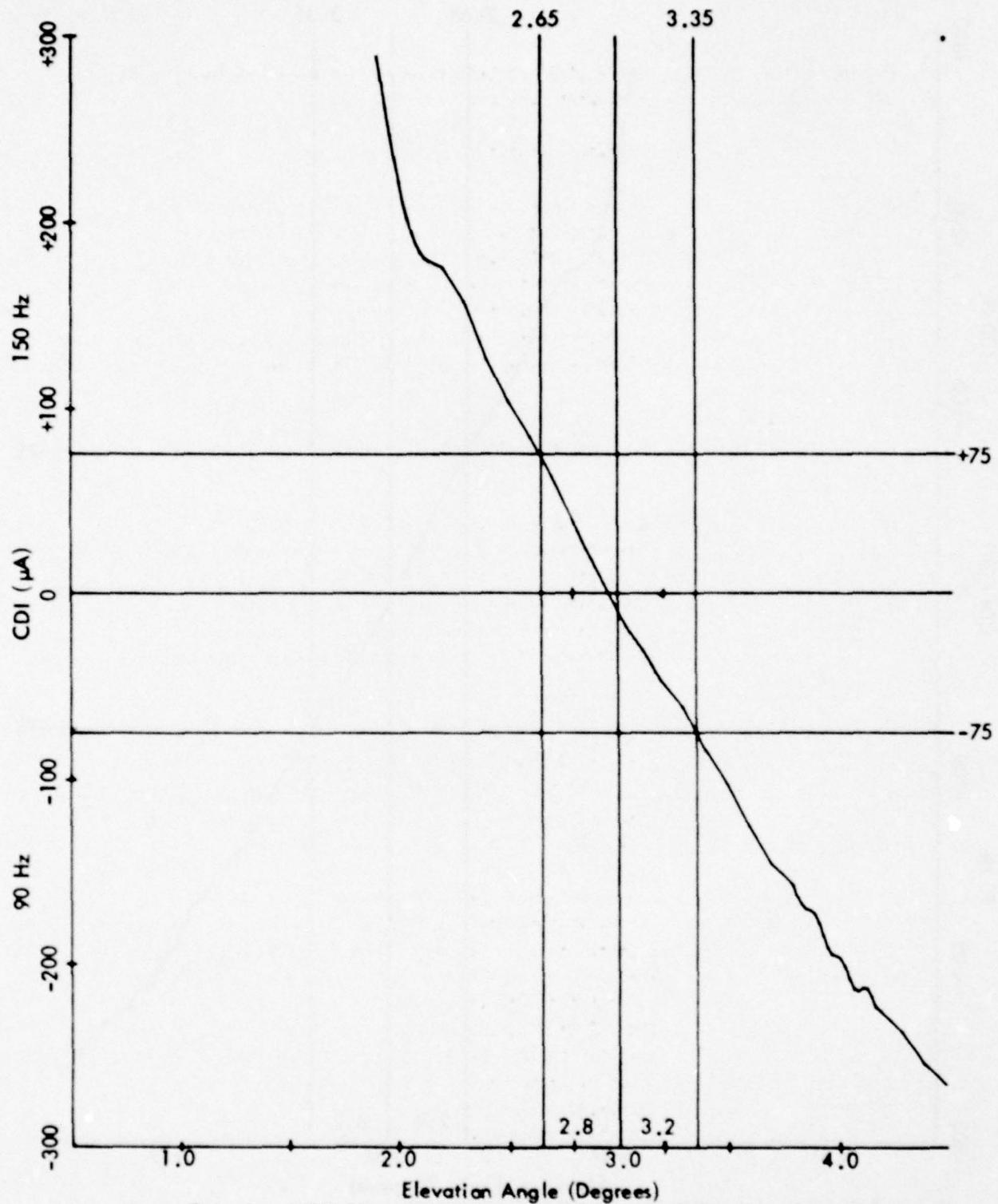
Figure 160. Calculated CDI Versus Angle for a 1600 Foot High Level Run Above Runway Centerline for the Terrain Profile of Fig. 154 for Antenna Heights of 14.13, 28.26, and 42.39 Feet, with the Lower Antenna Phase Retarded 4.1 Degrees with Respect to the Middle, and Upper Advanced 2.0 Degrees, and the A Ratio .295. The tidal distance h is 20.24 feet (low tide).

is where the reflections are at an angle of 0° on both sides of the array. A best, or least damaging case is where reflections on both sides are at an angle of 90°.

The conclusions reached as a result of this investigation are:

(1) For the identified worst case, i.e., where the reflection coefficients on both sides of the V-Ring array are at an angle of 0°, the entire array can deteriorate to a VSWR of 1.175:1. Given an average condition (VSWR) of the entire array better than this value, the maximum tolerable VSWR for any single element is greater than 1.175:1 and is given in Figure 165. This is absolute worst case and means that every antenna has a reflection coefficient angle that is more damaging to the far field than any other angle.

(2) For the identified best case the entire array can deteriorate to a VSWR of 1.43:1.

(3) The operating tolerance for the V-Ring array as given in 6750.15A is 1.25:1 and this provides adequate protection for all cases of complex reflections from the antennas, given that no more than 25% of far-field tolerances should be consumed by the existing VSWR. The identified maximum allowable VSWR is for that absolute worse case and is not representative of conditions which can be expected to exist on any given array.

2. Introduction and Purpose. The purpose of the work documented herein is to determine and document the maximum allowable VSWR that can be present in the 15-element V-Ring localizer array. The VSWR existing on the array and with any particular element of the array is considered to be tolerable if the effect on the far field is such that no more than 25% of the theoretically allowable tolerance is consumed.

A 15-element V-Ring array was set up at Ohio University's Tamiami test site for the purpose of validating the operation of computer model OULOC, a Fortran program to predict the response of the V-Ring array to various system faults. Far-field course, width and clearance were calculated based on currents derived from jig-held antenna probe measurements. For purposes of this work OULOC is modified to model also the RF distribution network, the characteristics of which determine the redistribution of reflected powers in the array. A series of complex faults was introduced into the antenna array and the effects on the far-field radiation pattern measured with Ohio University's Mini-lab instrumentation in a Beechcraft Model A36. These measured effects were then compared to the effects predicted by OULOC. Correlation was within experimental error.

Accordingly, a series of parametric runs with the model yields the maximum VSWR that can be tolerated in that element. This maximum VSWR is a function not only of the position of the antenna in the array but also of the condition of the rest of the array. For this reason the results of this work show that one must know the general condition (VSWR) of the entire array and the position of the antenna in question.

3. **Discussion of Experimental Data**. A 15-element V-Ring localizer array has been set up and operated at Ohio University's Tamiami test site. Proper operation of the array was established by airborne check using Ohio University's Minilab instrumentation. Figure 161 is a view of the V-Ring array at the test site.

A schematic diagram for the Type FA-8040 distribution unit used with the array is shown in Figure 162. The complete distribution unit also has a monitoring section but this was not used with the array setup at the Tamiami site.

The array elements were set up with the proper spacing on the pad and the antenna feedline lengths trimmed for maximum suppression of parasitics. With antenna feedline lengths optimized, the following probe measurements across the array were taken:

Antenna No.	CSB(°)	SBO(°)
E1	-2.2	0.0 (Reference)
E2	+1.8	+4.4
E3	-0.8	+1.8
E4	-1.8	+1.8
E5	-5.0	-2.8
E6	+0.6	+3.2
E7	+4.2	+0.8
E8	0.0 (Reference)	-
E9	+3.8	+181.0
E10	+2.6	+184.5
E11	-4.8	+177.5
E12	-1.0	+183.0
E13	+0.5	+184.0
E14	+1.2	+184.5
E15	-1.6	+180.0

Table 34. Phase Measurements Taken with a Jig-Held Antenna Probe on the 15-Element V-Ring Localizer Array at the Tamiami Test Site.

With the array operating normally, the carrier-plus-sidebands and the sidebands-only powers were 9.6W and 265mV, respectively. An airborne check of the normal system showed the course to be on centerline and the width to be 4.0°. A series of complex faults was introduced into the feedlines of antennas E7, E9, E10, and E11 and the far field checked. The faults were inserted at the bulkhead N-Type connector at the feed of the V-Ring antenna element. A phase delay of 17° was added to the antenna being faulted because of the hardware necessary for the fault insertion. Physically, the faults were shorted and open stubs attached to a "tee" in the line. The results of this series of faults are given in Table 35. The faults listed in Table 35 are identified as an electrical length, as a short or an open, and as the antenna faulted. Figure 163 shows the electrical equivalent of the faulted case.
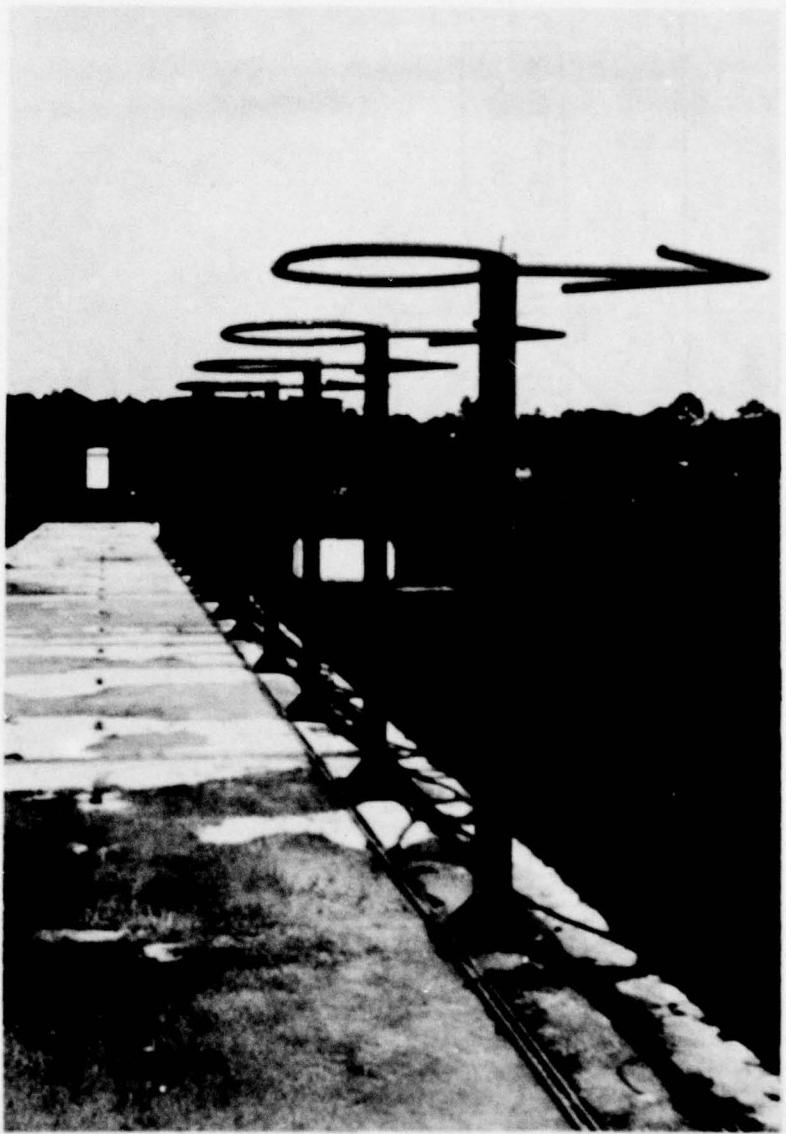
Figure 161. V-Ring Localizer Array Set Up at the Tamiami Test Site
for Validation of Computer Model OULOC, December 1978.
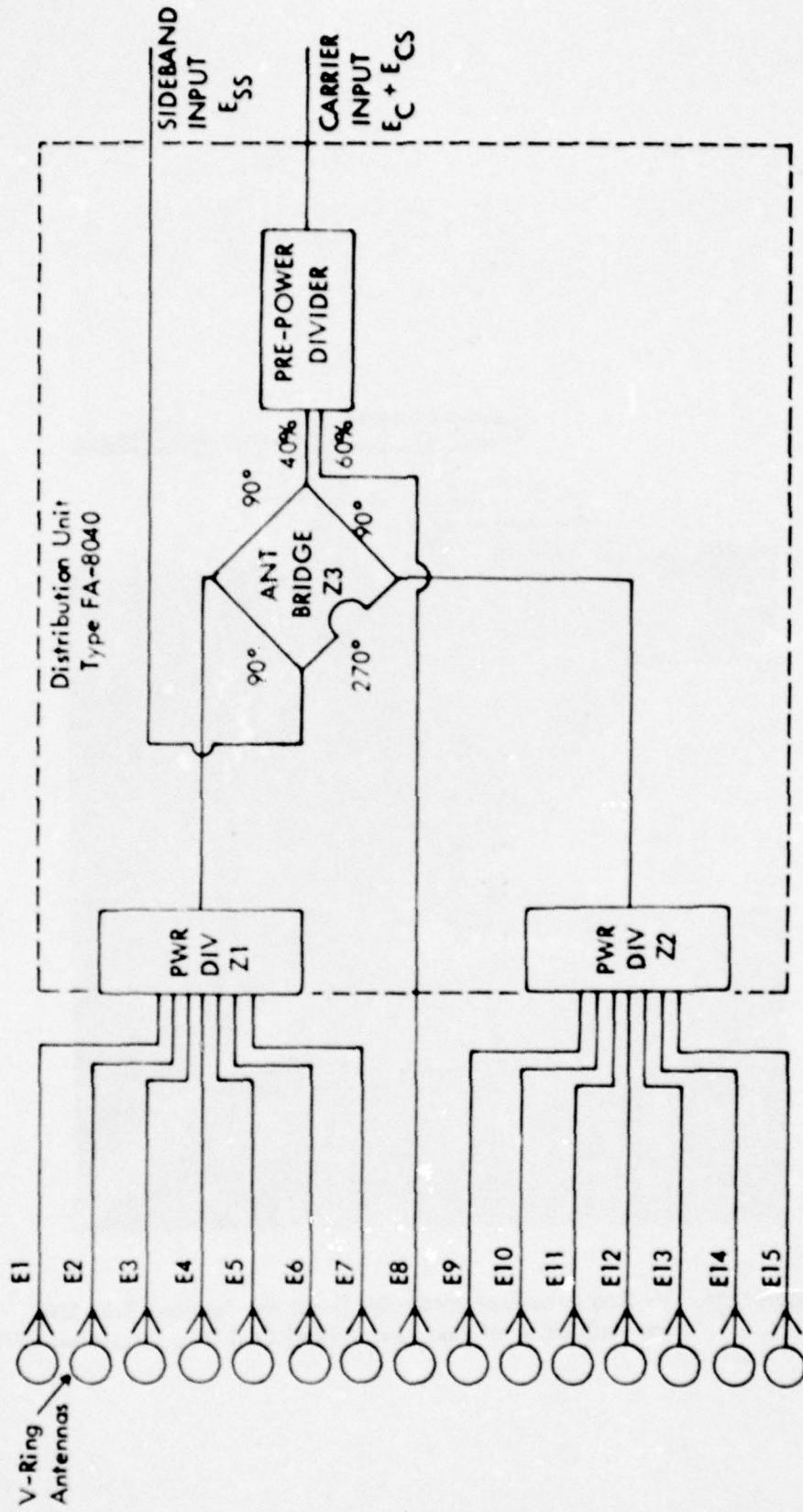
Figure 162. Type FA-8040 RF Distribution Unit Used with the V-Ring Localizer Array at the Tamiami Test Site in December 1978.

Fault Ant. No.	Measured Course Deviation (TMB) (°)	Measured Path Width(°)
Normal	0.05N	4.0
29°S/No. 9	0.2S	4.06
29°0/No. 9	0.5N	4.86
56°S/No. 9	0.15N	4.25
56°0/No. 9	1.0N	---
102°S/No. 9	0.5N	4.37
102°0/No. 9	0.4S	4.2
Sh/No. 10	0.0	4.3
29°S/No. 10	0.2S	4.25
29°0/No. 10	0.35N	4.26
56°0/No. 10	0.6N	4.64
Sh/No. 11	0.06N	4.2
Sh/No. 7	0.5N	4.26
Sh/No. 9	0.43S	4.16

Table 35. Experimental Results of Faulting the 15-Element V-Ring Localizer Array.
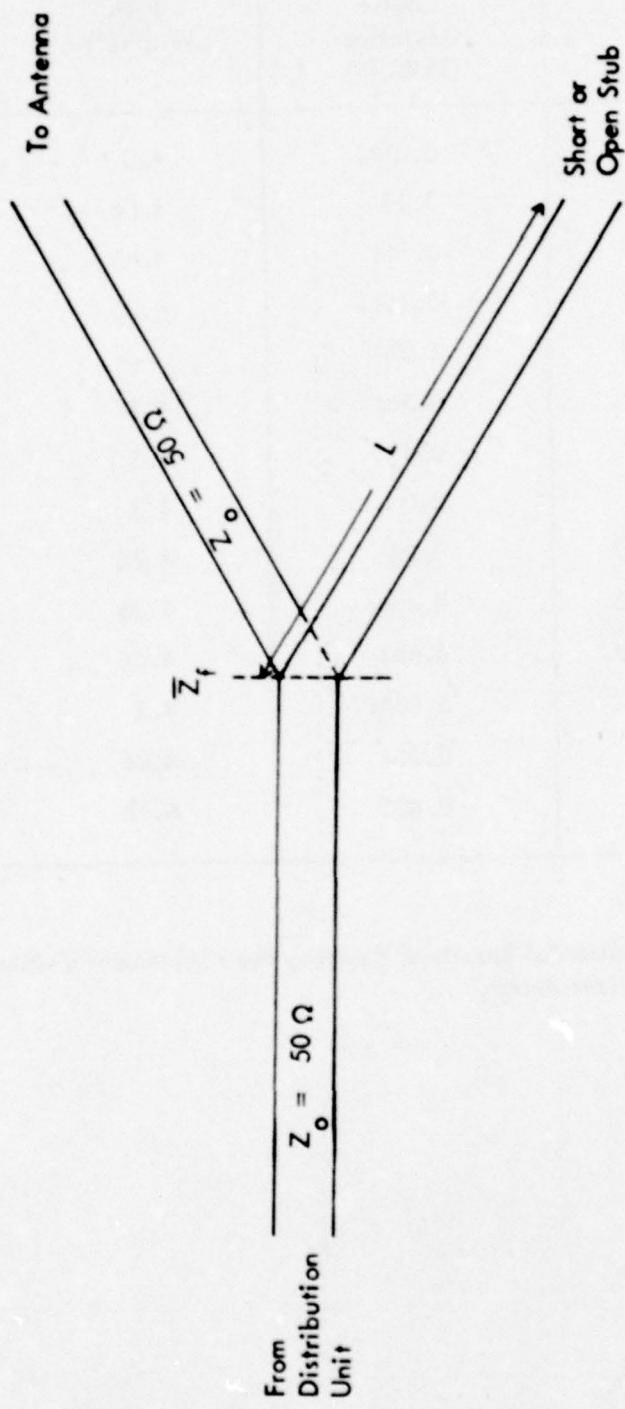
Figure 163. Diagram of the Stub Faulting Used to Effect a Complex Reflection Coefficient on Antenna Feedlines of the V-Ring Array.

The impedance Z_f at the fault is equal to the characteristic impedance of the transmission line, Z_o (or in this case $50\,\Omega$), in parallel with the impedance of the shorted or open stub some electrical distance L from the junction point. The impedance of the stub transformed back to the junction point is:

$$Z_{open} = -jZ_o \cot L \qquad \text{for the open and}$$

$$Z_{short} = jZ_o \tan L \qquad \text{for the shorted stub.}$$

The impedance Z_f is, in general, complex and associated with this complex impedance is a complex reflection coefficient at the junction point. It is this complex reflection coefficient that is used in the model. Similarly, it is this same complex reflection coefficient that determines the VSWR on the line. VSWR, however, is a scalar quantity and the unique identity of the complex reflection that results in any given VSWR is lost. This is because:

$$\bar{\rho} = \frac{\bar{Z}_f - \bar{Z}_o}{\bar{Z}_f + \bar{Z}_o}$$

and

$$VSWR = \frac{1 + |\bar{\rho}|}{1 - |\bar{\rho}|}$$

We see that the same VSWR on a transmission line can be achieved with an infinite number of complex reflection coefficients.

4. Discussion of Mathematical Model OULOC. OULOC is a Fortran program which computes the far field (or near field for that matter) radiation pattern from a defined set of antenna currents given in amplitude and phase. The problem of determining the maximum VSWR for an array of antennas must also include a preamble program that can accept CSB and SBO currents, for example, distribute these powers, calculate reflected powers and redistribute them to the array, and compute a final set of antenna currents in the presence of the VSWR or VSWR's that have been defined on the lines. The preamble program to accomplish this is called ANTENNA2. Both OULOC and ANTENNA2 appear in Appendix C.

The redistribution of reflected power back through the 7-way power dividers of the V-Ring array is the most significant aspect of having a non-trivial VSWR on any of the antenna feedlines. Referring to Figure 162, antenna bridge Z3 blocks any significant transfer of reflected power from one side of the array to the other. Additionally, redistribution of power back through the pre-power divider to or from the OC antenna E8 was measured at the Tamiami site and found to be at least 28 dB down from initial reflected power levels. Accordingly, the effects of reflected power on any antenna feedline are seen only on that same side of the array.

The scattering of reflected power entering the 7-way power dividers is defined by a data file available to the program ANTENNA2. These scattering parameters were

-413-

obtained from measured data taken on the Type FA-8040 distribution unit (S.N. 015) at the Tamiami site. Table 36 is a summary of these parameters in matrix form. Figure 164 is a diagram of the test setup used to obtain these data. This should be a symmetric matrix (i.e., FEED X, READ Y, should be the same as FEED Y, READ X). A spot check of a few of the values in the lower left half is made.

With other data files available to both OULOC and ANTENNA2, the model can be manipulated. This manipulation includes establishing the overall VSWR for the array as well as the increasing VSWR for each array element. In all cases it has been assumed that the overall average VSWR and one particular antenna is deteriorating (increasing VSWR). The results of a series of runs of the model are presented in the results section.

5. Results. As a matter of definition in the determination of the maximum allowable VSWR for the V-Ring array, "allowable" means that maximum value of VSWR existing at any antenna in the array which results in no more than 25% of the theoretically allowable tolerance being consumed. These identified far-field tolerances are three in number and are: (1) 15 µA CDI deflection on runway centerline, (2) 17% change in course width, and (3) a loss of clearance in localizer zones 1 and 2. Clearance required in zones 1 and 2 is 175 µA and 150 µA, respectively.

Ideally one would like to have a computer model such as OULOC/ANTENNA2 in every case where the operation of an array was in question due to a deteriorating VSWR on one element. Since this is not possible, the results of this study are given so that the technician or engineer concerned about such an occurrence can get some idea of the magnitude of his problem. This is done by presenting the results in Figure 165 as a graph. The single most important fact determining the maximum allowable VSWR that can be present on any antenna in the array is the condition of the remainder of the array. In the absence of detailed information about the complex impedance of all antennas in the array, the worst case is assumed in generating the data for Figure 165. This means that the entire array, except for the antenna in question, was given a VSWR that is a result of the worst possible complex reflection coefficient for that antenna. As could be expected, this results in what could be termed an ordered set of coefficients. The worst case for the V-Ring array is where the existing VSWR's on both sides of the array result from complex reflection coefficients at an angle of 0°. The best case is that resulting from reflection coefficient angle of 90° on both sides of the array. This information is not generally available to the field engineer. In most cases VSWR indications are obtained with a Bird wattmeter or equivalent.

In any case, Figure 165 is a result of this worst case situation. Given the average VSWR across the array, one can find the maximum value that can be tolerated on any element of the array. The horizontal sections of the plotted curves are a result of the requirement to maintain clearance in sectors 1 and 2. One interesting point on the graph of Figure 165 is that regardless of the angle on the complex reflections, all antennas in the array can deteriorate to at least 1.175:1 and no more than 25% of the theoretically allowable far-field tolerances will be consumed. The V-Ring array is quite tolerable of the best case reflections where this same point has a value of 1.43:1. This is an encouraging result which supports the operating standards and tolerances for the antenna feedline VSWR of 1.25:1 given in 6750.15A.

-414-

FEED → / READ ↓	1	2	3	4	5	6	7	INPUT
1	X	-28.0 dB -20°	-30.9 dB -13.5°	-34.7 dB -19.0°	-35.9 dB -20.9°	-37.7 dB -23.3°	-38.8 dB -24.6°	-20.9 dB -60.4°
2	-26.8 dB -18.9°	X	-34.9 dB -36.6°	-37.75 dB -40.0°	-39.85 dB -41.3°	-39.3 dB +14.7°	-40.8 dB +11.2°	-25.0 dB -65.0°
3	-29.7 dB -12.5°	-34.9 dB -36.6°	X	-38.5 dB +17.5°	-41.0 dB +12.9°	-44.5 dB -38.2°	-45.75 dB -38.9°	-27.9 dB -61.7°
4	-32.2 dB -18.0°	-37.45 dB -40.0°	-38.3 dB +17.6°	X	-40.2 dB +35.4°	-47.2 dB -39.0°	-48.4 dB -40.0°	-30.5 dB -60.0°
5	-34.2 dB -20.7°	-39.45 dB -41.2°	-40.6 dB +12.9°	-40.0 dB +35.4°	X	-49.1 dB -39.8°	-50.3 dB -40.5°	-32.45 dB -60.7°
6	-	-	-	-	-	X	-46.5 dB +33.0°	-34.0 dB -63.4°
7	-	-	-	-	-	-46.5 dB +33.0°	X	-35.25 dB -63.8°
INPUT	-	-	-	-32.7 dB -61.9°	-	-	-37.6 dB -65.8°	X

Table 36. Scattering Matrix for the 7-Way Power Divider Used in the FA-8040 Distribution Unit. Measured data are given as amplitude and phase.
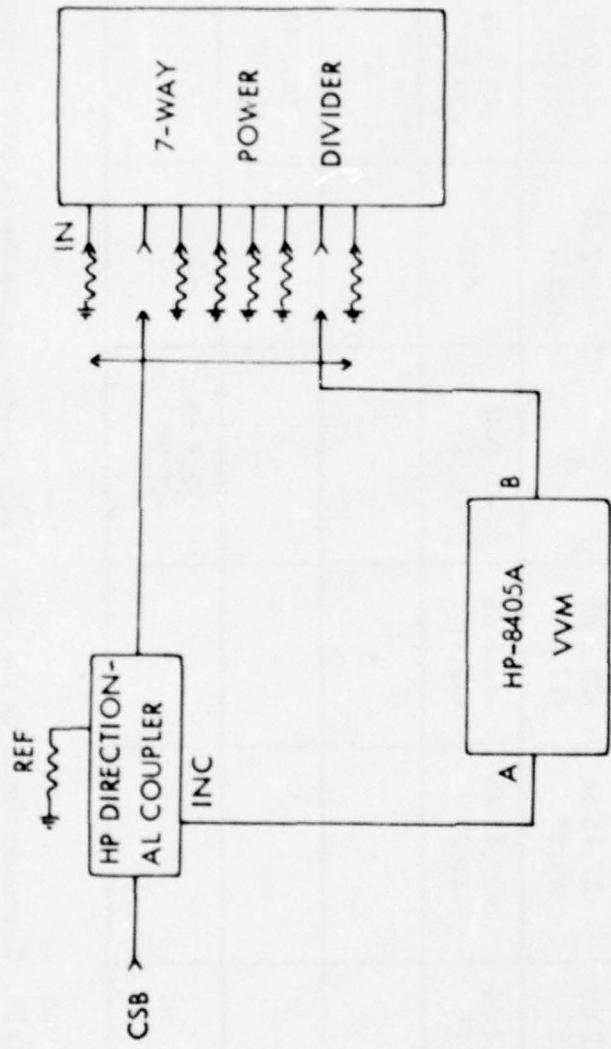
Figure 164.   Test Setup Used to Obtain the Matrix of Scattering Parameters for the 7-Way Power Divider in the Type FA-8040 Distribution Unit at the Tamiami Test Site, December 1978.
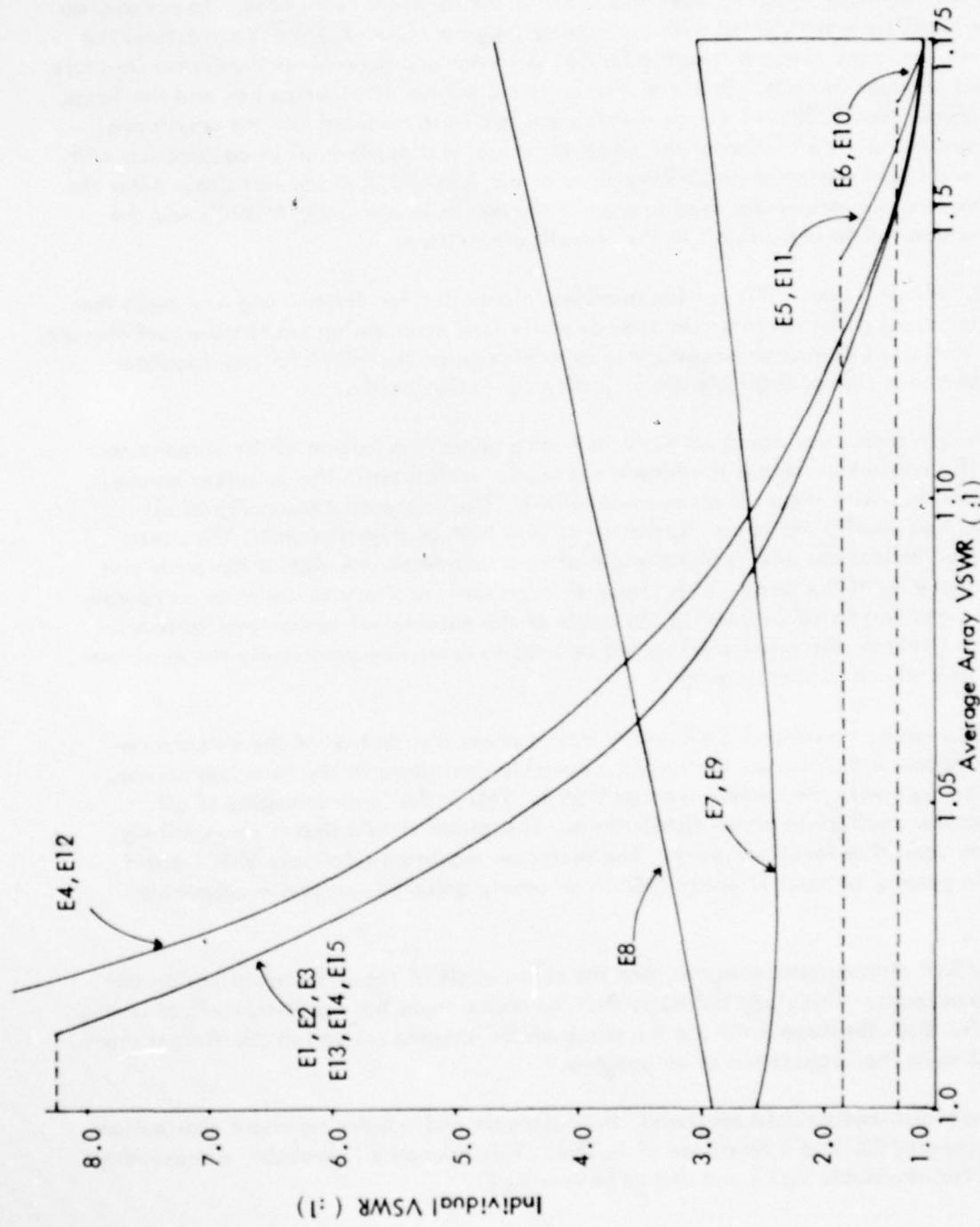
Figure 165. The Maximum Allowable VSWR for All Elements of the V-Ring Localizer Array Given the Average VSWR Across the Array. This is the identified worst case for the angle of the reflection coefficient.

D. Maximum VSWR Calculations for the 14-Element, O-Ring Localizer Array.

1. Summary and Conclusions. This report describes work performed to determine the maximum allowable VSWR on an O-Ring localizer array which will not degrade the performance of the localizer signal by more than 25% of the far-field tolerances. To accomplish this task the localizer was modeled with a computer program (OULOC) which calculates the redistribution of antenna currents from the faulted antennas and determines the course structure from the final antenna currents. Both the Wilcox self-clearing distribution box and the Texas Instruments Model No. 923801-1 course distribution box were modeled and the results are graphically presented. Validation of the computer model was carried out in conjunction with installation and flight testing of an O-Ring array at the Tamiami, Florida test site. After the validation process, the model was used to predict the maximum allowable VSWR's and the conclusions which follow are a result of the model's predictions.

2. Introduction. This section provides information for determining how much the VSWR on a localizer antenna array can degrade while still maintaining acceptable performance. This section contains information necessary to determine when the VSWR for any localizer antenna element has changed sufficiently to justify corrective action.

The worst-case, maximum VSWR results from a phase distribution of the antenna reflection coefficients which causes the largest allowable deviations in the localizer course, width and clearance with the smallest average VSWR. This is the most damaging of all possible reflection coefficient phase distributions. For both distribution units, the worst case represented reflections with a phase angle of zero degree on one side of the array and 90° on the other side of the array. This phase distribution is unlikely to occur on an operating localizer, and was found by varying the angle of the antenna reflection coefficients in the model. In general, the worst case cannot be used to determine practically the maximum allowable VSWR on a localizer antenna.

The best-case, maximum VSWR results from a phase distribution of the antenna reflection coefficients which causes the largest allowable deviations in the localizer course, width and clearance with the largest average VSWR. This is the least damaging of all possible reflection coefficient phase distributions. This phase distribution is also unlikely to occur on an operating localizer array. The best-case maximum allowable VSWR could not be used in general because it would lead to an overly optimistic maximum allowable VSWR.

The VSWR measurement does not take the phase angle of the antenna reflection coefficient into account. This study indicates that the phase angle has significant effect on the localizer path. Both the magnitude and the phase of the antenna reflection coefficient should be used to estimate the degradation of an antenna.

For both distribution units measured, the best-case and worst-case phase distributions bracket the current FAA VSWR tolerance of 1.25:1. This tolerance is probably a reasonably conservative yet attainable value and should be retained.

-418-

3. Significance of Maximum VSWR. The maximum VSWR calculations were based on the VSWR which would consume 25% of the far-field tolerance. The tolerances used were those for course, width, and clearance. The clearance parameter was not applied to the Texas Instruments distribution unit since it is normally used with a clearance array.

The worst-case maximum VSWR graphs (Figures 166 and 168) represent the phase distribution of the antenna reflection coefficients which consumed 25% of the far-field tolerance with the smallest value of VSWR. The phase distribution which produced this worst-case condition was a phase angle of zero degrees on one side of the array and 90° on the other side. This particular phase distribution caused far more disruption of the far-field path than any other phase distribution found. To use the worst-case maximum VSWR values would result in an overly pessimistic estimate of the maximum allowable VSWR and would not represent the effects which would be found on an array with the maximum value of VSWR and a more reasonable antenna reflection coefficient phase distribution.

The best-case, maximum VSWR graphs (Figures 167 and 169) represent the antenna reflection coefficient phase distribution which consumed 25% of the far-field tolerance with the largest value of VSWR. The best-case, maximum VSWR value could not be used as the maximum allowable VSWR because it would result in an overly optimistic value of VSWR.

An operating localizer array would fall between the values of the worst case and the best case. Thus for the Wilcox self-clearing distribution unit, the maximum allowable average VSWR would be between 1.037:1 (the worst-case value) and 1.5:1 (the best case value). Because of the wide variation between the best-case and worst-case VSWR values, the VSWR clearly is not the best parameter with which to measure antenna degradation.

The following items of information must be obtained before precise determination of the maximum allowable VSWR for a given antenna element can be made.

(a)   The complex impedances of the 13 undisturbed antennas.

(b)   Location of the element in question.

(c)   Line lengths to distribution box from each antenna.

(d)   A 14 by 14 matrix of redistribution parameters which are output voltages from each of thirteen ports when the remaining port is driven with a known voltage.

(e)   Margin above tolerance existing in clearance in localizer sectors one and two.

(f)   Certainty that course and course width are at nominal values.

4. Localizer Computer Model.

a. Development of the Mathematical Model. The basic modeling program, OULOC, which was developed at Ohio University in 1975-76, has been modified to improve the operation of the model in calculating the maximum allowable VSWR's of antenna arrays. The program is written in Fortran and calculates the theoretical values for DDM and CDI

-419-
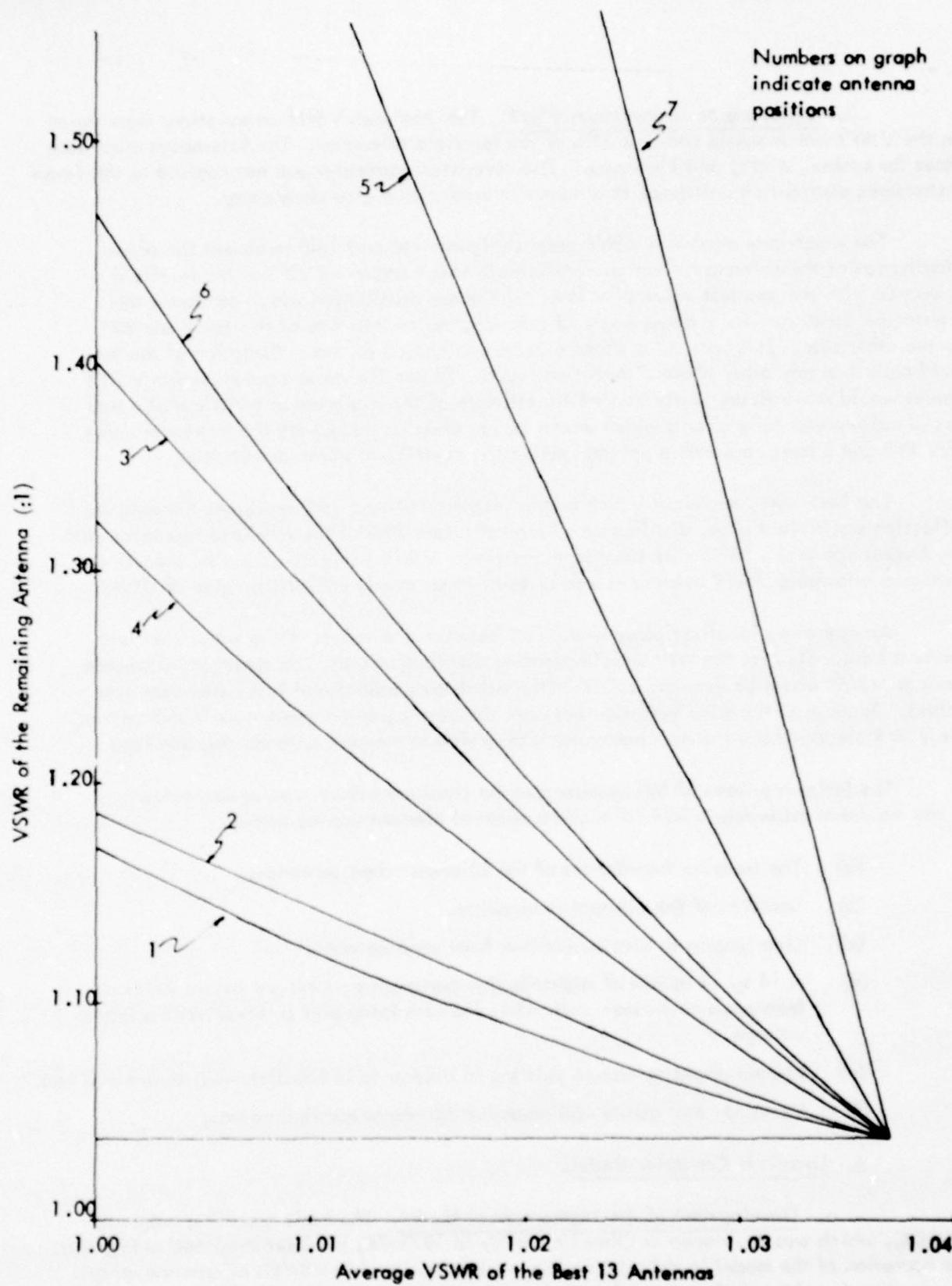
Figure 166. Worst-Case Maximum VSWR for the Wilcox Self-Clearing Distribution Unit with the 14-Element O-Ring Array.
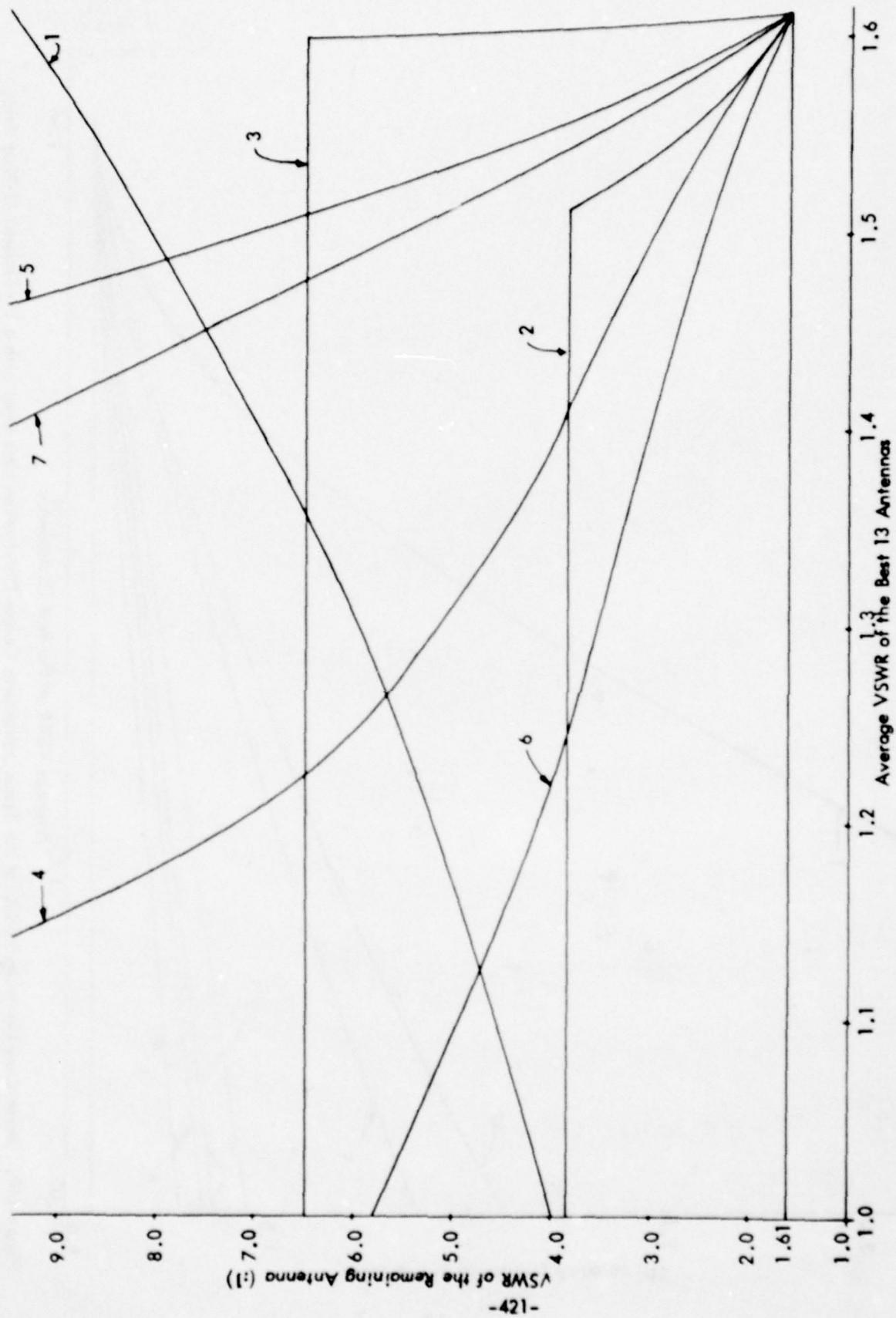
Figure 167. Best-Case Maximum VSWR for the Wilcox Self-Clearing Distribution Unit Used with a 14-Element O-Ring Array.

Figure 168. Worst-Case Maximum VSWR for the Texas Instruments Course Distribution Unit Used with a 14-Element O-Ring Array.
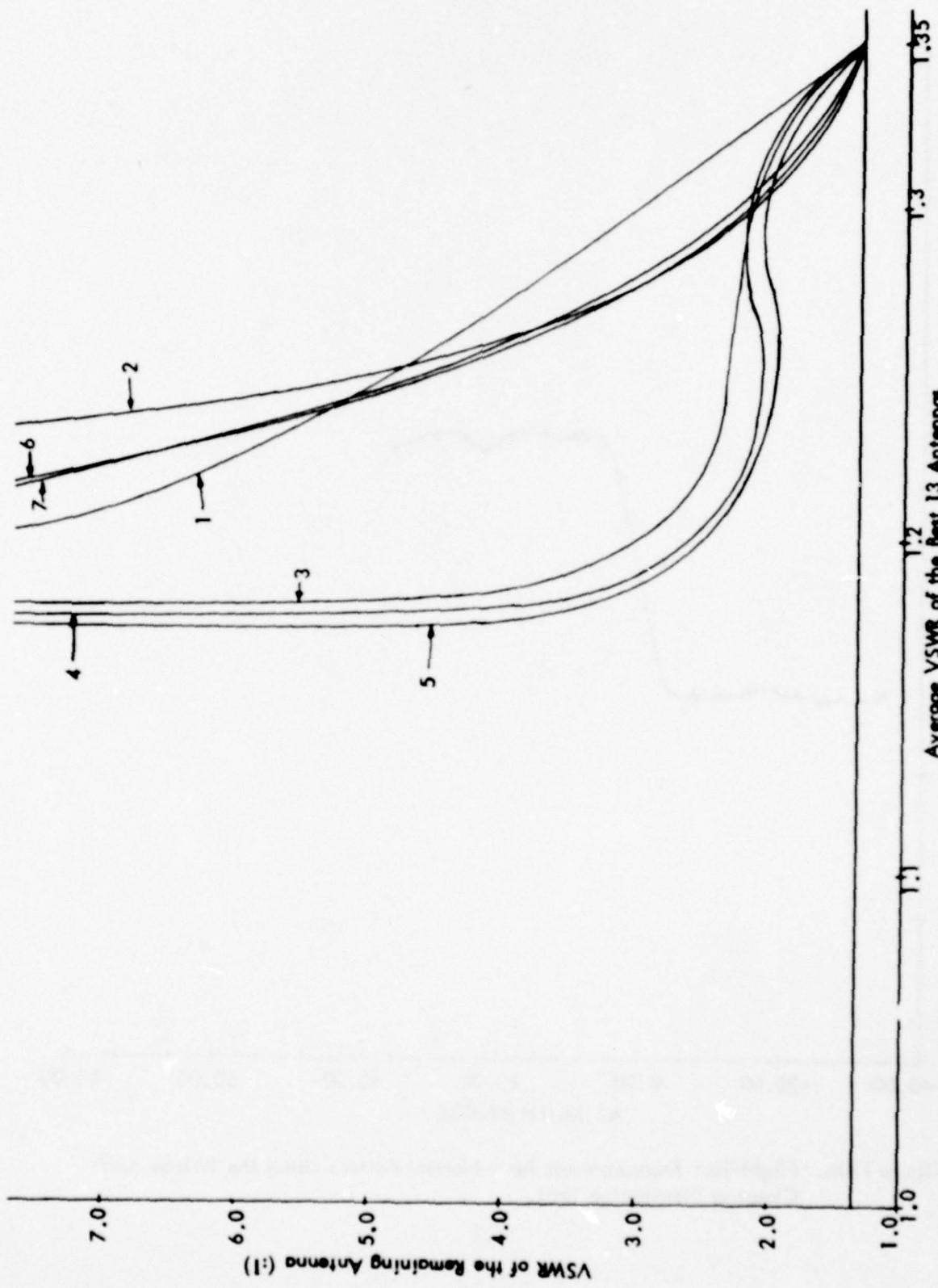
Figure 169. Best-Case VSWR for the Texas Instruments Coarse Distribution Unit Using a 14-Element O-Ring Array.
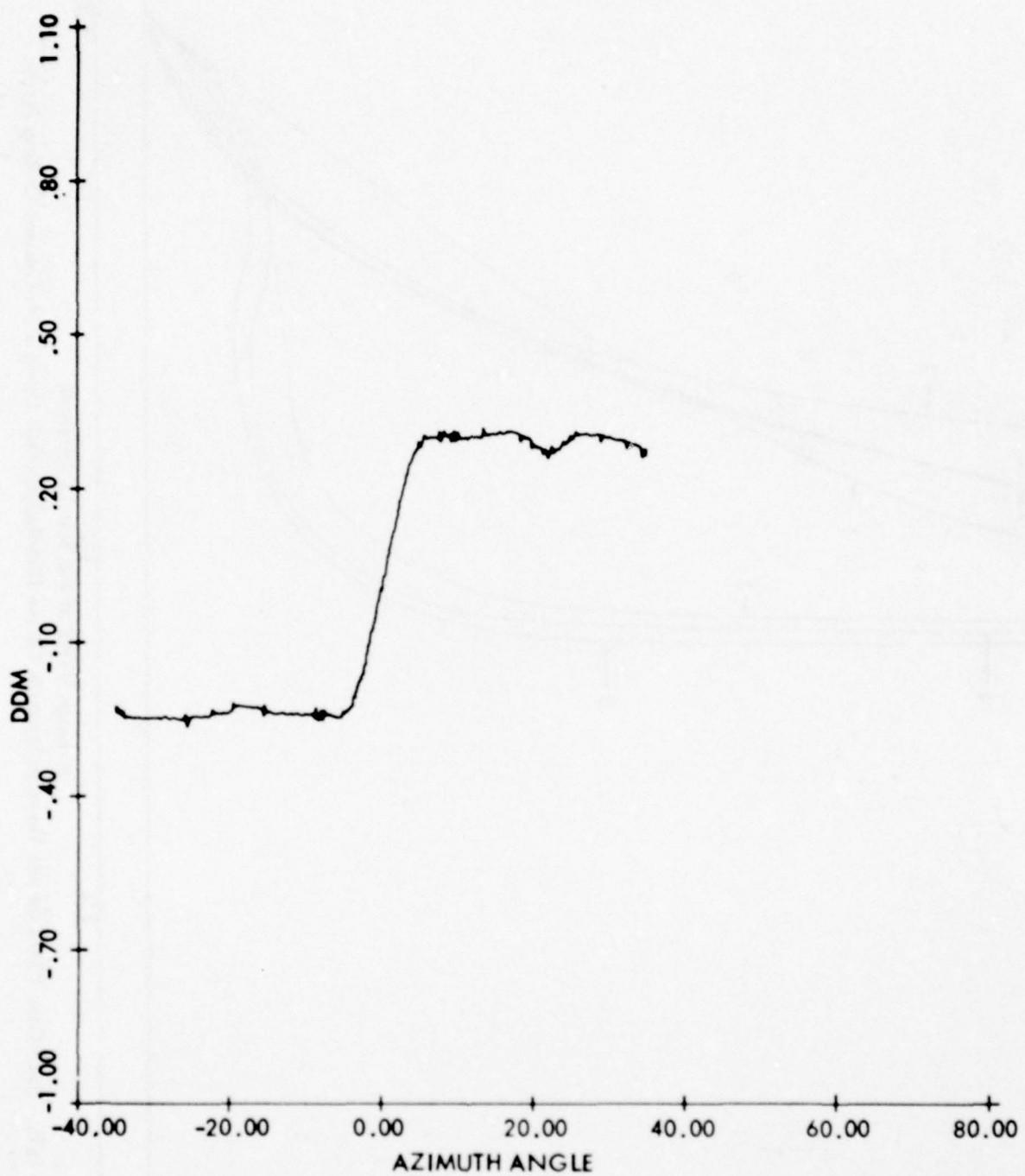
Figure 170a. Flight-Test Measurements for a Normal Pattern Using the Wilcox Self-Clearing Distribution Unit.

-424-
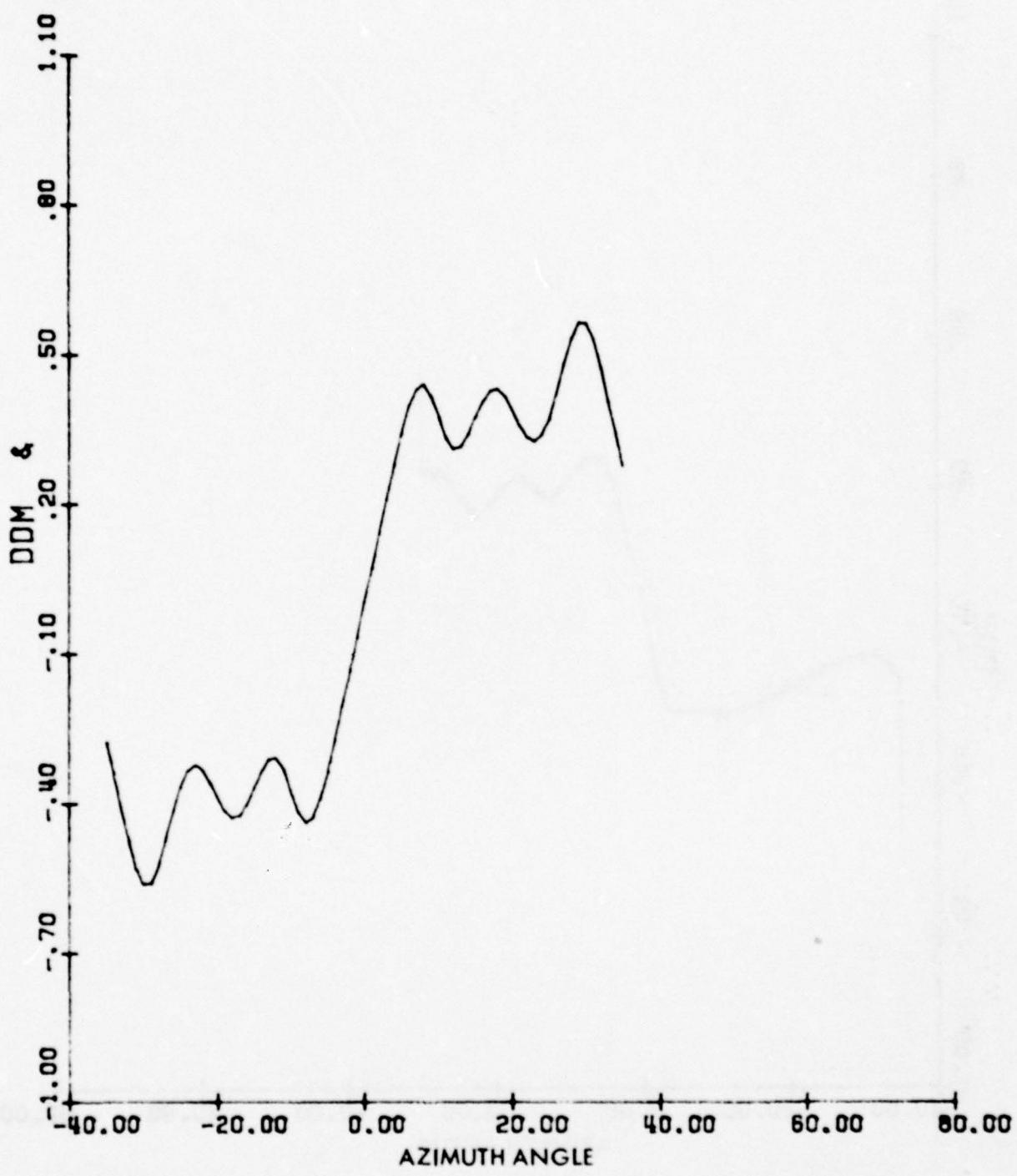
Figure 170b. Computer Model Calculations for a Normal Pattern
Using the Wilcox Self-Clearing Array.

-425-
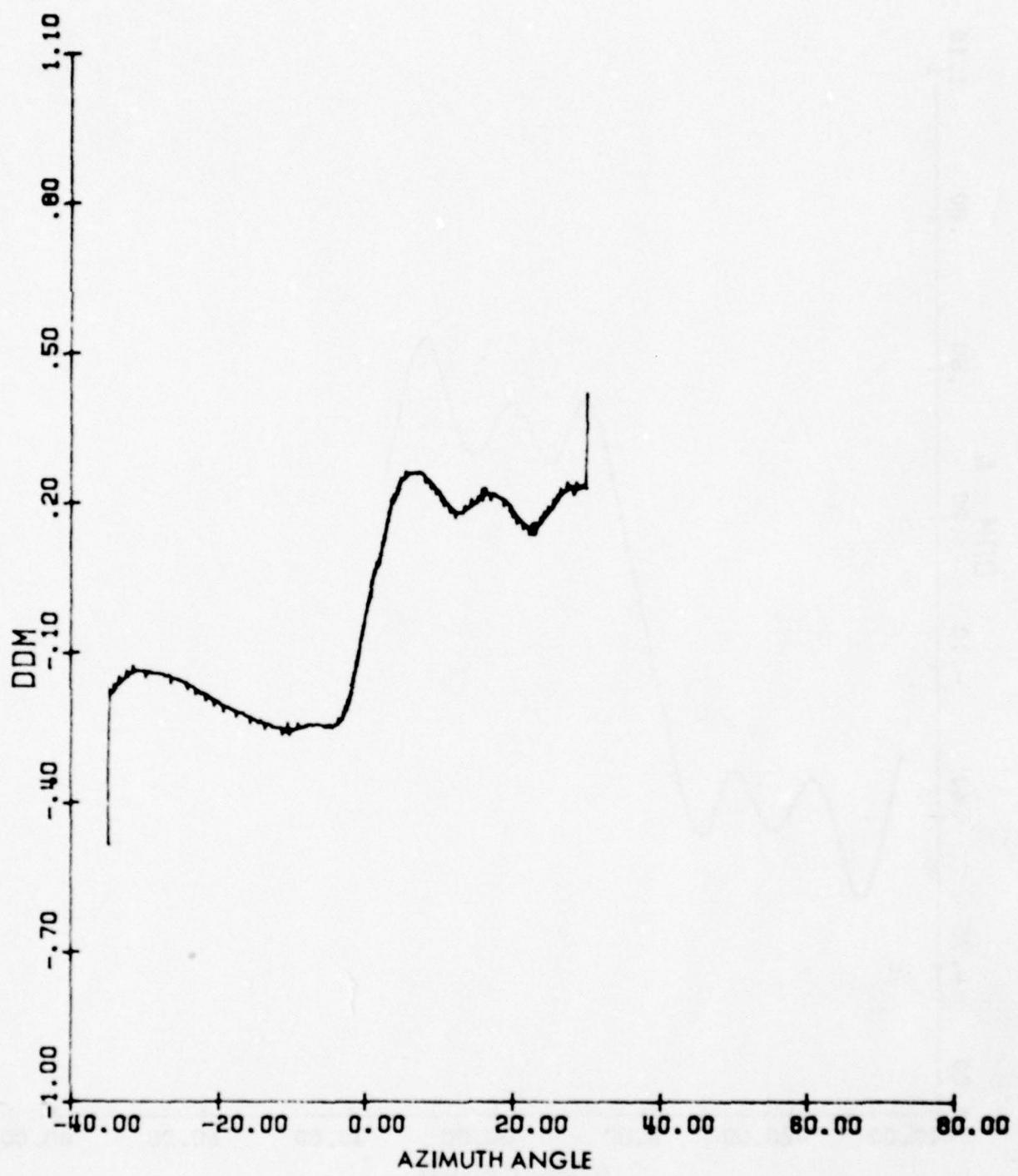
Figure 171a. Flight-Test Measurements with a 29° Open Stub
in Antenna 1 Left.

-426-
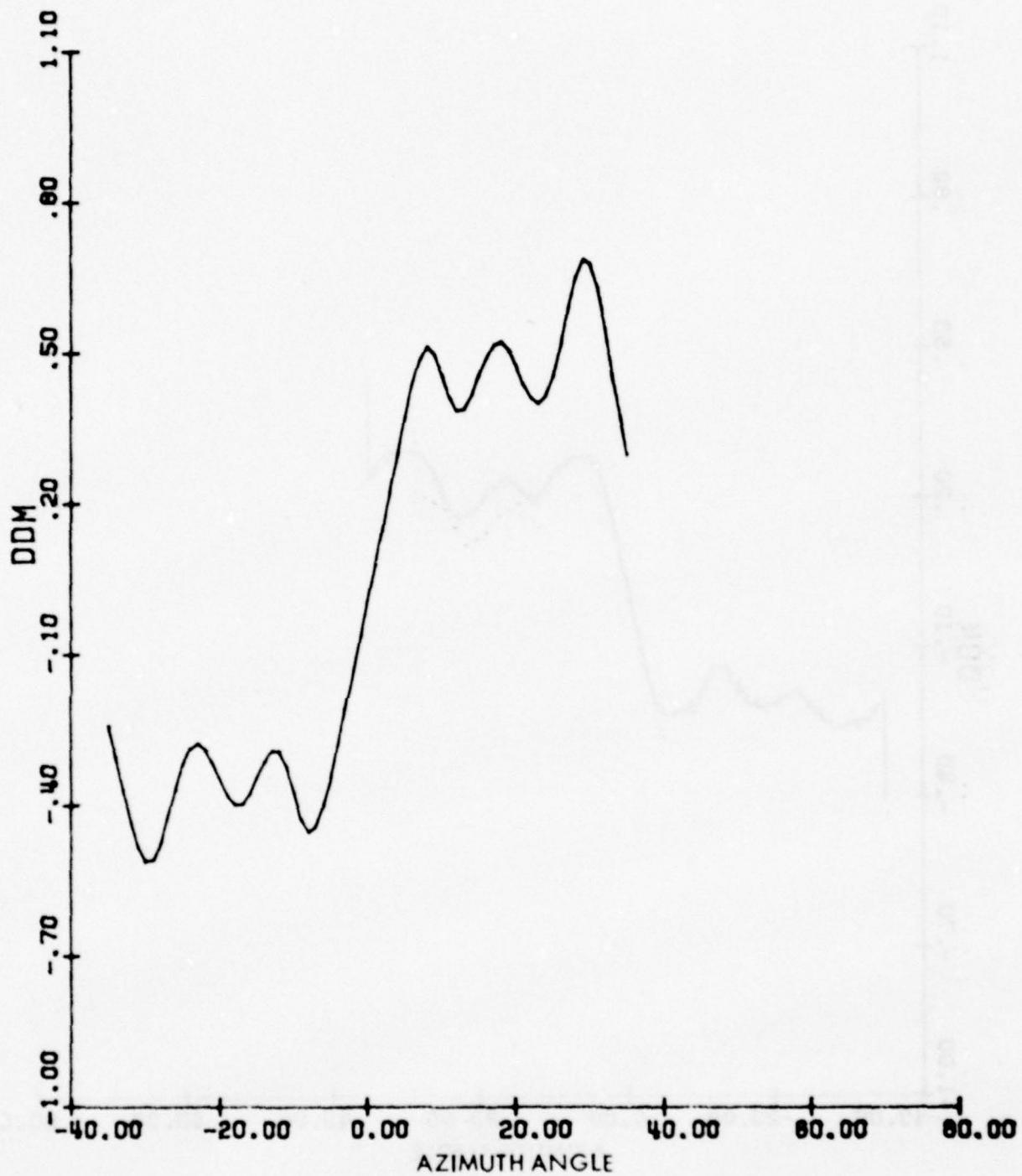
Figure 171b. Computer Model Calculations with a 29° Open Stub
in Antenna 1 Left.
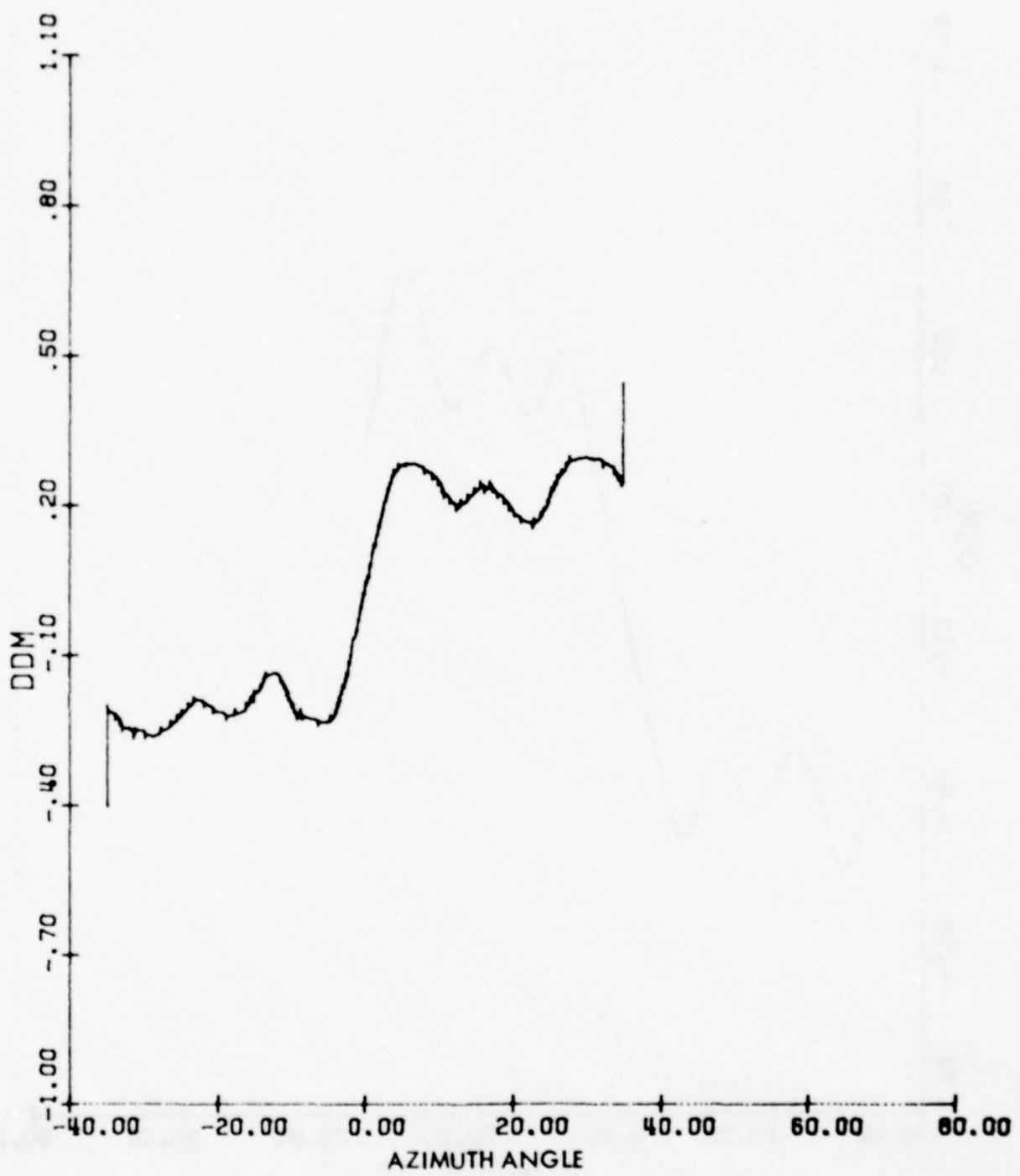
Figure 172a. Flight-Test Measurements with a 5° Shorted Stub in Antenna 1 Left.

-428-
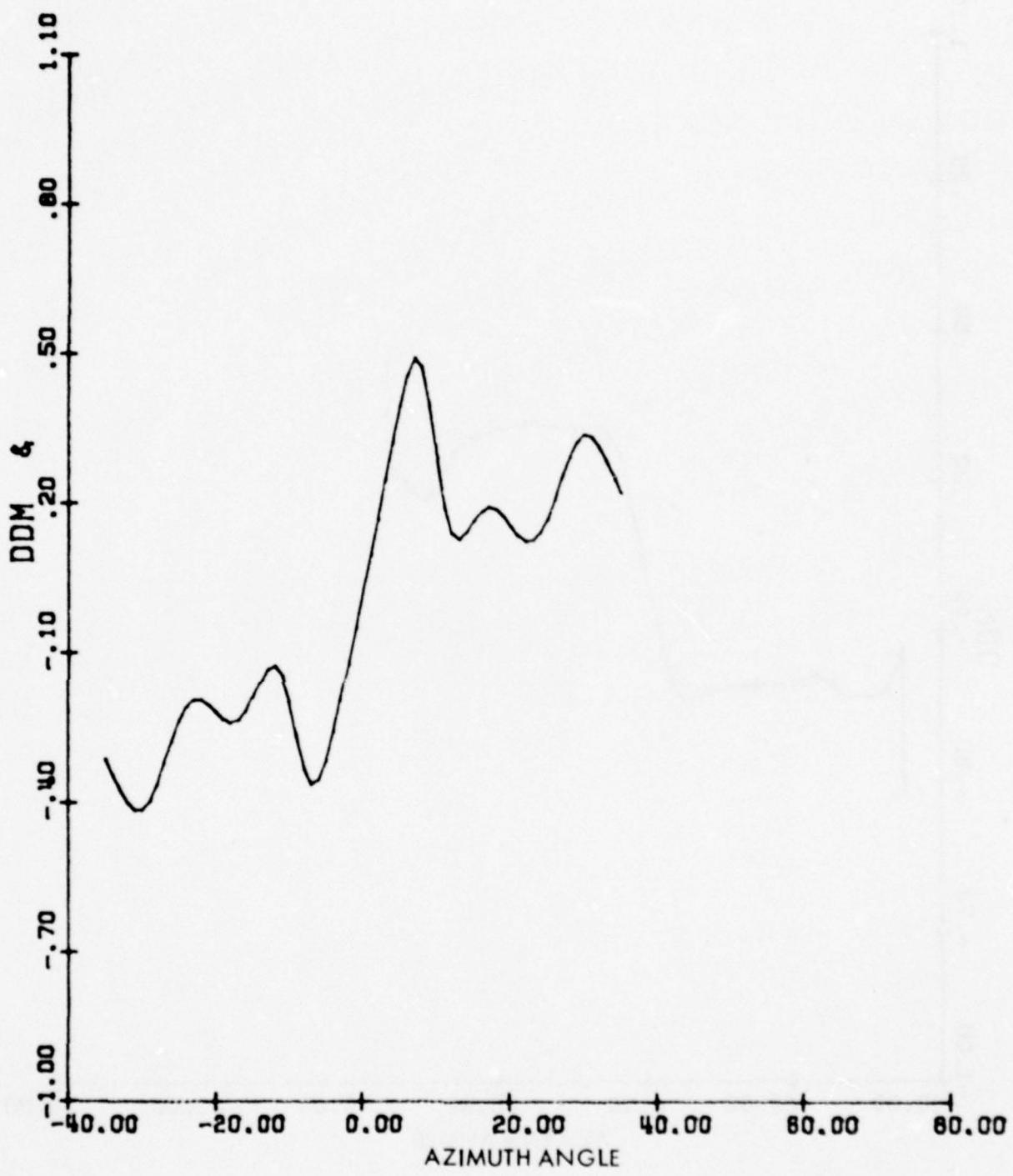
Figure 172b. Computer Model Calculations with a 5° Shorted Stub
in Antenna 1 Left.
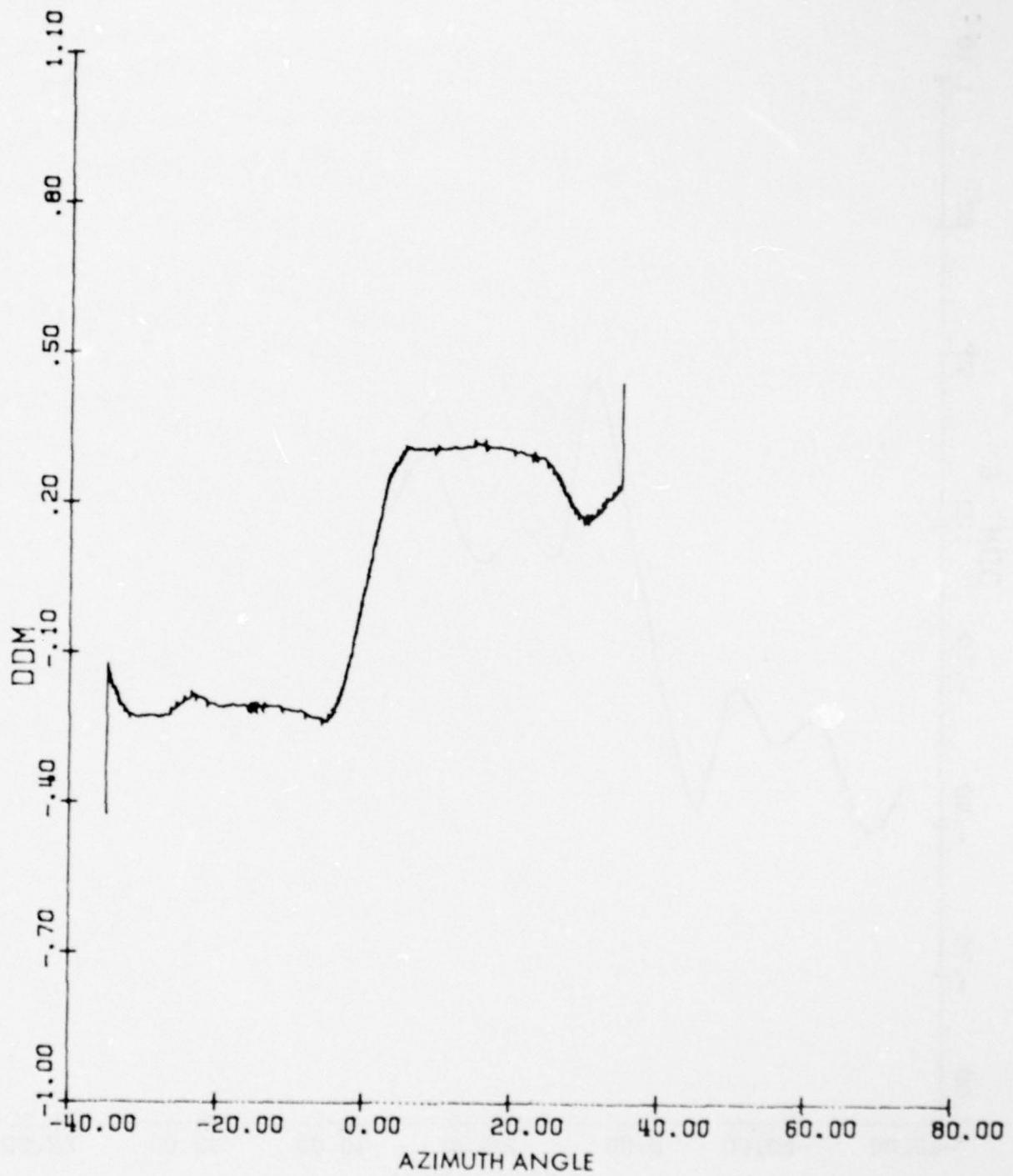
Figure 173a. Flight-Test Measurements with a 29° Shorted Stub in Antenna 1 Left.
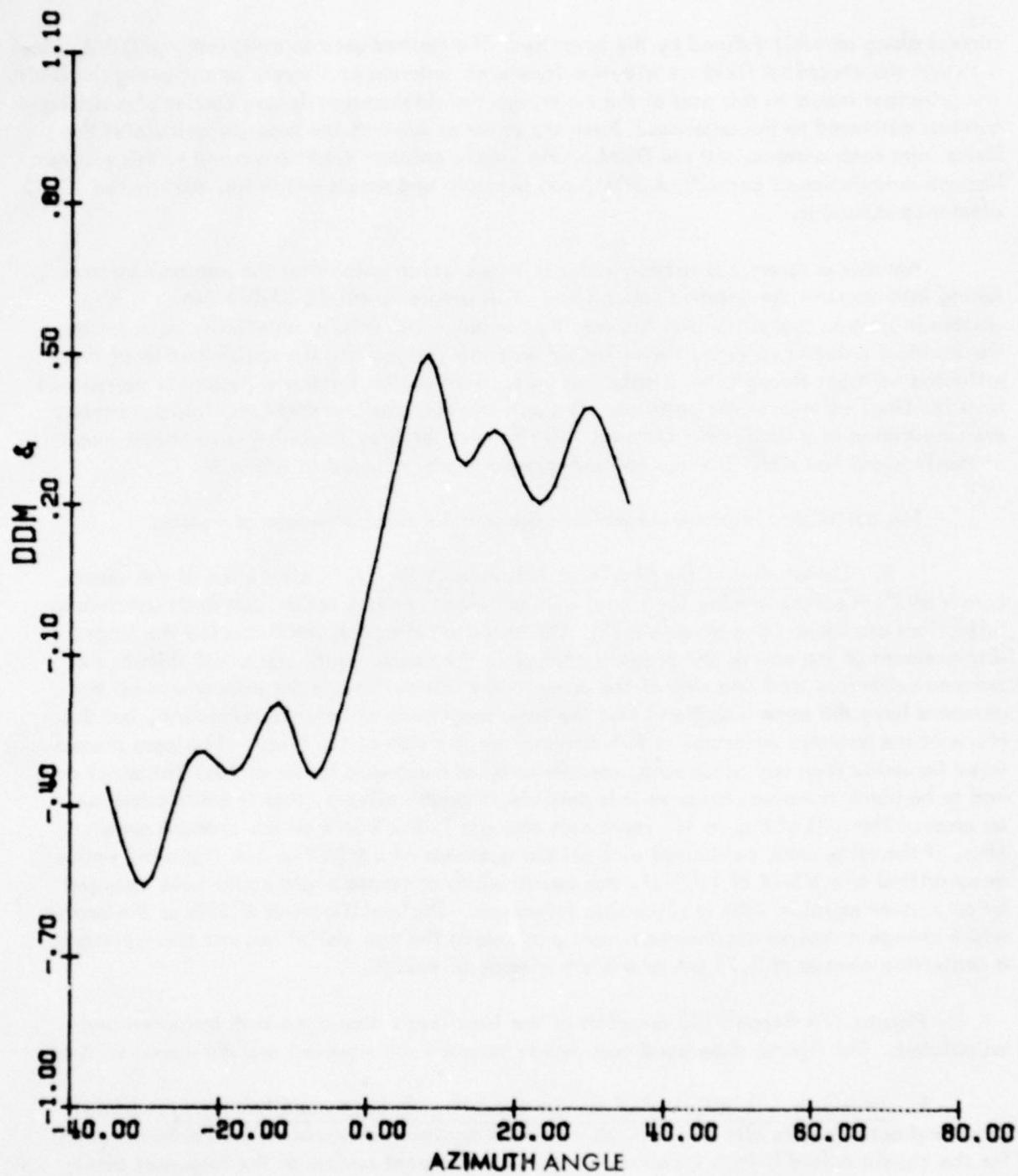
Figure 173b. Computer Model Calculations with a 29° Shorted Stub in Antenna 1 Left.

current along an orbit defined by the operator. The method used to calculate the DDM values is to sum the electrical field contribution from each antenna at discrete points along the orbit. The principal inputs to this part of the model are the sidebands-only and carrier plus sidebands currents delivered to the antennas. From the antenna currents the program calculates the fields from each antenna and the DDM at the sample points. Additions made to this program include calculation of centerline DDM, course width and points which fall outside the ICAO clearance standards.

Another program was written under this task which calculates the antenna currents taking into account the antenna reflections. This program, called ANTENNA3, is also written in Fortran and calculates the resultant antenna currents by repeatedly calculating the incident antenna voltage, the reflected antenna voltage and the redistribution of the reflected voltages through the distribution unit. The resultant antenna current is calculated from the final voltage at the antenna. The antenna currents and other required parameters are maintained in a data file. Data for this file was obtained through measurements made at the Tamiami test site. Listings for both programs are included in Appendix C.

The calculated results were within experimental error of measured values.

5. Calculation of the Maximum Allowable VSWR's. Calculation of the worst-case VSWR's involves running the model with different antenna reflections until worst-case reflections are found for a given VSWR. The antenna reflection which caused the largest displacement of the course and greatest change in the course width was a 90° shift in the antenna reflection from one side of the array to the other. This is the case where all the antennas have the same VSWR and thus the same magnitude of antenna reflection, but the phase of the antenna reflection is 90° different on one side of the array. This case proved to be far worse than any other case, sometimes by as much as a factor of 10. The worst case had to be used, however, because it is possible, though unlikely, that it could occur on an array. The axis of Figure 166 represents changes in the VSWR on the antenna array. Thus, if the array were calibrated with all the antennas at a VSWR of 1.0:1 and the entire array drifted to a VSWR of 1.037:1, the course width or course angle could have changed by an amount equal to 25% of allowable tolerance. The specification of 25% of the course width change or course displacement was specified in the task definition and corresponds to a centerline change of 3.75 μA or a width change of 4.25%.

Figures 170 through 173 are plots of the localizer's clearance both measured and calculated. The figures show good correlation between the modeled and the measured data.

E. Maximum VSWR Calculations for the Alford 8-Loop Localizer Array. Initial plans and actions were directed towards making a maximum allowable VSWR determination for the classic Alford 8-loop localizer array. A subsequent review of the resources available for execution of the V-Ring and O-Ring type array studies indicated that the 8-loop array should be disregarded, principally because the number of installations is steadily decreasing and application of the results would be very limited.

-432-

IV.   EDUCATION -- SEMINARS AND SHORT COURSES

A total of three ILS-related seminars and short courses have been conducted by Ohio University under Contract DOT-FA78WA-4062. The following is a summary of these educational support functions.

A. Capture Effect Glide Slope Seminar. A four day seminar on "The ILS Capture Effect Glide Slope" was presented at the FAA Academy in Oklahoma City from April 10 to April 14, 1978. Approximately 40 attendees took part in all or part of the seminar. Lecturers were Drs. Richard H. McFarland and Raymond Luebbers and Messrs. Raymond Croxford and Kent Chamberlin. The following is an outline for the material that was presented:

Antenna Fundamentals Review (1/2 Day)
   Maxwell's Equations
   Radiation Integral
   Dipole Antenna
   Array Theory
   Antenna Images
   Proximity Effects
   Reflector Antennas

CEGS Theory of Operation (1/2 Day)
   Antenna Patterns
   DDM
   Near Zone Behavior
   Receiver Processing

Terrain Effects (1/2 Day)
   Finite Conductivity
   Surface Roughness
   Uneven Terrain
   Other Environmental Effects
   Fresnel Zones
   Reflecting Plane Configurations (FAA Classification)
   Important and Unimportant Terrain Characteristics
   Siting Considerations

Computer Modeling (1/2 Day)
   Present Capabilities
   Modeling Process
   Calculating Perturbation Effects
   Examples of Troubleshooting with Models
   Validation with Measurements
   Accuracy of Input Data

Troubleshooting with Time Domain Reflectometer (1/2 Day)
Time Domain vs. Frequency Domain
Transmission Lines
Pulsed Transmission Lines--Bounce Diagrams
The Time Domain Reflectometer (Tektronix 1502 TDR)

Troubleshooting with Vector Voltmeter and Probes (1/2 Day)
The Vector Voltmeter
Directional Couplers
Effects of Uneven Cable Heating/Cooling
Probing Antenna Currents

ILS Monitoring (1/2 Day)
Chronological History of ILS Monitoring
Types and Purposes of Monitors
Integral Monitors
Near-Field Monitors
Relative Advantages and Disadvantages of Each

Engineering Flight Measurements Using Small Aircraft (1/2 Day)
Discussion of Parameters to be Measured
Calibration of Equipment
References for Aircraft Position
Data Acquisition and Analysis

B. Sideband Reference Seminar. A four day seminar on "The ILS Sideband Reference Glide Slope" was presented at the FAA Academy in Oklahoma City from November 13 to November 16, 1978. About 35 attendees were present for the lectures given by Drs. Richard H. McFarland and Raymond Luebbers and Mr. Raymond Croxford. The following outline summarizes the material that was presented:

Introduction
Introduction of Personnel
Statement of Objective of Seminar
Overview of Seminar Activities

The Sideband Reference, Image, Glide Slope System
Description
History
Motive for Implementation
Penalties for its Use

-434-

Theory of Operation
    Antenna Patterns
        Explanation of RF Patterns
        Applications
        SBR Patterns
    Distribution System
    Normal Conditions
    Antenna Offsets
    Operation under Abnormal Conditions
    Snow Effects (Discussed in Monitoring)

Siting
    A. General
        Theory behind Criteria
        Criteria for Roughness
        Reflection Zones
        Types of Siting Problems
        Acceptable and Unacceptable Obstructions
        Terrain Considerations
        Manual References
        Location of Transmitting Antennas
    B. Mathematical
        Use of Mathematical Predictions
        The Album, Its Preparation
        The Album, Its Use

Mathematical/Computer Aids Workshop
    Philosophy and Purpose
    Methods
    Demonstrations
    Type of Results

Monitoring
    Philosophy
        Analog vs. Fault Detection
        Reliability
        Outage Unacceptability
    Description of Existing Monitors (Near Field)
        360° – Amplitude
        270° (300°) Phase
    Sensitivity
    Counterpoise Requirement
        Function
        Fabrication
    Snow Effects
    Correlation with Far Field during System Perturbations
    Alarm Limits

<u>Monitoring</u> (continued)
    Integral Monitoring
        Virtues
        Implementation
        Verifying by Example

<u>Set-Up Techniques</u>
    General Approach
    Specific Measurements
    Phasing
        At Antennas
        Ground (Near Field) Phasing
        Far Field - Mid Mkr
        Airborne
    Confirmation of Performance Preparatory to Flight Check
    Perturbational Analysis

<u>Flight Check</u>
    Objective
    Limitations
    Tolerances
        Cat I
        Cat II
    Practicality of System Changes During Flight Check

<u>Troubleshooting</u>
    Examples of Need
    Methods of Approach
    Probe Measurements (with Vector Voltmeter)
    Time Domain Reflectometry
    Future Remote, Automatic Data Logging and Diagnostics

<u>Legal Considerations</u>
    Significance of Manuals and Written Instructions
    Documentation
    Examples from Current Cases

C. Sideband Reference Short Course. A one day short course on "The ILS Sideband Reference Glide Slope" was presented to 18 regional engineers and technicians on December 6 1978 at the Southern Region Headquarters in Atlanta, Georgia. The following is an outline for the material that was presented:

<u>Monitoring</u>
    A. Philosophy - Analog vs. Fault Detection
    B. The Integral Monitor
        1. Mechanization
            a. Width - (Amplitude)
            b. Path and Width, Mark ID, Cat II

Monitoring (continued)
    2. Sampling Probes
        a. Probe Measurements for FA9373 APC
                              8651 AIL
                              8730 Scanwell
        b. Handheld
        c. Rotatable - TI
  C. Near-Field Monitors
    1. Amplitude Detector
        a. Location of 360° Monitor Point
        b. Location of 360° Monitor Detector
    2. Phase Detector
        a. Location of Phase Detector
        b. Near-Field Profile
        c. Sensitivity
    3. Counterpoise
        a. Definition
        b. Equipotential Considerations
        c. Elevation Above Earth
        d. Orientation and Size
        e. Conductor Requirements
        f. Bonding
        g. Weather Effects - Pooling, Temperature

Snow Effects
  A. Monitors
  B. Far Field
  C. Procedures

Effects of System Perturbation
  A. Far-Field Response
  B. Near-Field Monitor Response

System Confirmation by Ground Checks
  A. Location of Ground Check Points
  B. CDI Profiles

    D. Notes and Critiques. For all presentations the attendees were provided with a complete set of lecture notes. Overhead projections, slides, and demonstrations complemented the traditional classroom presentations. Additionally, the Oklahoma City seminars were highlighted with real-time demonstrations of the operation of Ohio University's Computer Modeling Center. This was done via a telephone data link to the IBM 370/158 at Ohio University and proved to be a most favorably received aspect of the seminars.

    Critique questionnaires distributed at the end of the seminars provided Ohio University engineers with valuable information concerning subject matter for future seminars. Comments by attendees to the capture effect seminar determined in large part the choice of subject matter for the second four day presentation there--the sideband reference glide slope.

V. INVESTIGATORS AND ACKNOWLEDGEMENTS

This final report is the culmination of more than eighteen months of work by the engineering and support staffs at the Avionics Engineering Center, Department of Electrical Engineering, College of Engineering and Technology, Ohio University, Athens, Ohio. Contributions are from all levels from undergraduate student interns to postdoctoral and faculty, staff personnel. Similarly, a number of FAA personnel in the field, at headquarters, at the Aeronautical Center, and at Regional Offices have contributed in a variety of ways.

The following is a list of principal contributors and others who served to bring this work to a successful completion:

DR. RICHARD H. MCFARLAND has served as project director. He has also served as pilot for data collection and principal data analyst for the perturbational studies including an examination of anomalous path behavior at the Clarksburg, West Virginia sideband reference site. He authored the material on the SBR counterpoise. Dr. McFarland was a major contributor to both the Capture Effect and Sideband Reference Glide Slope Seminars conducted at the FAA Aeronautical Center, and the Sideband Reference Short Course given at the Southern Region Headquarters in Atlanta, Georgia.

MR. RAYMOND A. CROXFORD has served as project engineer and as technical editor for this final report. He has also served as principal field engineer for the experimental work. He is the author of the documentation of the response of the sideband reference system to specific faults, the response and character of the near field, a review of existing maintenance procedures, the series of perturbational studies at Eastern Region SBR sites, and the set-up and operation of the Alford 8-loop, V-Ring, and O-Ring localizers. Mr. Croxford provided the recommendations for improvements to the SBR system including path angle change by modulation unbalance and a scheme of fixed sideband power division. He has also served as a lecturer at both the Capture Effect and Sideband Reference Glide Slope Seminars conducted at the FAA Aeronautical Center, and the Sideband Reference Short Course given at Southern Region Headquarters.

DR. RAYMOND J. LUEBBERS has led the mathematical-based site prediction efforts which involved Messrs. T. Irvine, T. Mullins, J. Longworth, V. Ungvichian and Ms. L. Piecuch as team members. Included in his work has been the modeling of localizers and glide slopes, one example being the study of the glide-slope operation at Boston Logan Runway 22L. Additionally, Dr. Luebbers served as a lecturer at both the Capture Effect and Sideband Reference Glide Slope Seminars conducted at the FAA Aeronautical Center.

MR. KENT CHAMBERLIN was task engineer for the investigation of a deficiency in the FA-5723 clearance transmitter monitor. His work under this investigation included the design and fabrication of a recommended, auxiliary module for the monitor. Mr. Chamberlin also served as a lecturer at the Capture Effect Glide Slope Seminar conducted at the FAA Aeronautical Center.

-438-

VI. REFERENCES

[1]   vonHippel, Arthur R., Editor, "Dielectric Materials and Applications," MIT Press, 1954

[2]   "In-Service Improvements and Modernization of All Components of the Instrument Landing Systems," Vol. I,II, Final Report, Report No. FAA-RD-78-112,I, EER 35-1, Contract DOT-FA75WA-3549, Avionics Engineering Center, Ohio University, Athens, Ohio, July 1978, p. 4-10.

[3]   "Siting Criteria for Instrument Landing Systems," FAA Order 6750.16A, Federal Aviation Administration, August 18, 1973.

[4]   "In-Service Improvements and Modernization of All Components of the Instrument Landing Systems," op. cit., p. 6-1.

[5]   Ibid., p. 6-71.

[6]   Mitchell, Lawrence H., Raymond J. Luebbers, Vichate Ungvichian, and Richard H. McFarland, "Mathematical Modeling of Terrain Effects on ILS Glide-Slope Performance at Carswell AFB," Final Task Report (Carswell), EER 30-1, Avionics Engineering Center, Ohio University, Athens, Ohio, July 1977.

[7]   Luebbers, Raymond J., Richard H. McFarland, and Lawrence H. Mitchell, "Investigation of Glide Slope Performance at Malmstrom AFB," Final Task Report (Malmstrom), EER 30-2, Avionics Engineering Center, Ohio University, Athens, Ohio, September 1977.

[8]   "In-Service Improvements and Modernization of All Components of the Instrument Landing Systems," op. cit., p. 11-321.

[9]   United States Standard Flight Inspection Manual, FAA Handbook OA P 8200.1, May 30, 1973, p. 217-14.

[10]   "In-Service Improvements and Modernization of All Components of the Instrument Landing Systems," op. cit., p. 11-695.

[11]   Magnusson, P.G., Transmission Lines and Wave Propagation, Allyn and Bacon, Inc., Boston, Massachusetts, 1965, p. 307.

[12]   Kraus, J.D., Antennas, McGraw Hill Book Company, New York, 1950, pp. 303-304.

[13]   Antennas and Radiation Patterns Manual, FV-108, FAA Aeronautical Center, Oklahoma City, Oklahoma, 1966, p. 4-1ff.

[14] Instrument Landing System Concepts Catalog 40233, FAA Aeronautical Center, Oklahoma City, Oklahoma, 1976, p. 4-14.

[15] "Siting Criteria for Instrument Landing Systems," FAA Order 6750.16A, Federal Aviation Administration, 1973, p. 52, Appendix 3, p. 1-4.

[16] Chamberlin, Kent, "Capture Effect and Sideband Reference Glide Slope Performance in the Presence of Deep Snow," Report No. FAA-R-6750.1, prepared for the Federal Aviation Administration by Ohio University, Athens, Ohio, July 1978.

[17] File memorandum by Mr. Paul Maguire, Program Engineer, FAA New England Region, Reply reference ANE-431A, February 27, 1979.

[18] Site Survey Engineering Report, "Logan International Airport, Category I Instrument Landing System RWY 22L," prepared by Westinghouse Electric Corporation FIS Communications Programs under Contract No. DOT-FA73WA-3269, Task Order No. 1, Category A, Area I.

[19] United States Standard Flight Inspection Manual, Section 217.5, Tolerances, Paragraph (11).

[20] "In-Service Improvements and Modernization of All Components of the Instrument Landing Systems," op. cit., p. 4-363.

VII.   APPENDICES

APPENDIX A. MISCELLANEOUS SBR SET-UP TOPICS

One of the assigned tasks under Contract DOT-FA78WA-4062 was to study set-up procedures for the SBR glide slope and to suggest programs which would accomplish set-up and commissioning with minimum airborne checking. Theoretical study, computer modeling and actual real world testing at TMB have resulted in the following suggested routine:

(1) <u>Antenna Heights:</u>

a. Using the best available topographic information calculate (using OUGS if necessary) the required antenna heights for the desired glide-slope path angle, and the SBO/C power ratio for desired path width.

b. In the absence of specific calculated antenna heights, the proper theoretical heights above the surrounding terrain as well as offset can be obtained from Handbook 6750.6B.

(2) <u>Sideband Power Division</u>

Experimental and theoretical evidence reveals that a fixed sideband power division with antenna height adjustments to set the path angle is a desirable mode of operation for the sideband reference glide-slope system. Stability of the path angle is the critical concern. An alternate distribution scheme is presented here which replaces the variable divider with a fixer power division. The distribution scheme shown in Figure A-1 accomplishes a power division with the addition of only a single hybrid.
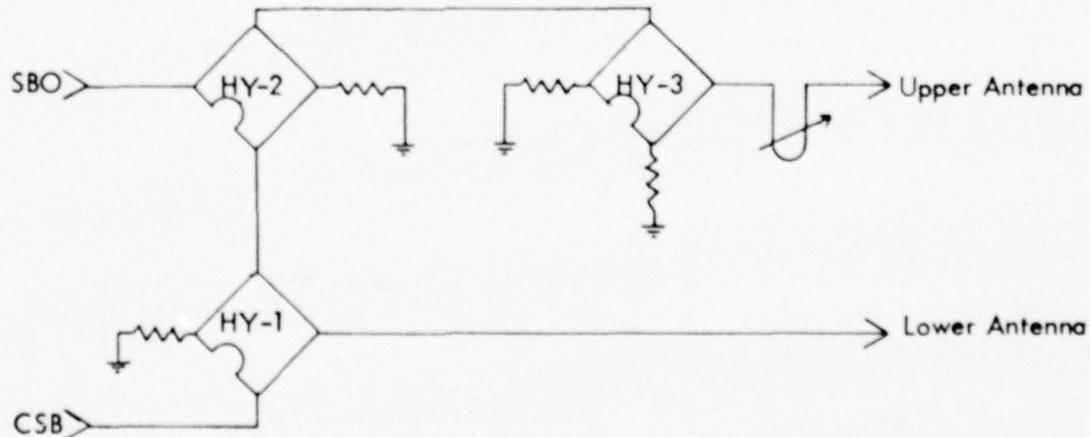
Figure A-1. Schematic of a Fixed Sideband Power Division Distribution Unit Implemented at Ohio University's Tamiami Test Site in March 1979. Hybrid HY-3 is the only component added to already existing hardware.

-442-

This distribution unit was implemented and tested at the Tamiami test site in March 1979. Hybrid HY-3 has been added to the standard network; Hybrid HY-2 is a hybrid which was already in use as a part of the variable power divider.

(3) Sideband Power Level

The total radiated sideband power should be equal to about 2% of the total carrier power. One indication of a sideband power level near the correct value is the DDM indication in the lower antenna line when the quadrature section is removed from the sideband line during carrier-to-sideband phasing. The value should be between .250 and .300 DDM in the 90 Hz. A setting of the sideband level for a DDM value in the lower antenna of about .265 at the same time that the sidebands are being phased will minimize resetting of the sideband power level and iterations to insure proper sideband phasing.

(4) CSB/SBO Phasing

Carrier-to-sideband phasing is essential for proper operation. This is accomplished by placing the sideband input line to the APCU in quadrature and observing the DDM reading in the lower antenna directional coupler DC-1. The sideband phaser on the transmitting equipment should be adjusted to indicate a zero DDM condition in the lower antenna line. This can also be accomplished by dummying the upper antenna output of the APCU and the upper antenna line and observing the DDM indication on the phase (path) detector. In either case, a zero DDM indication should be obtained when the sidebands are in quadrature. When the quadrature piece is removed from the sideband line, the DDM should go to between .250 and .300 into the 90 Hz. If the DDM shows 90 Hz, this indicates that the sidebands are now properly out-of-phase with the carrier. A 150 Hz indication, on the other hand, means that the sidebands and carrier are now in phase and an approximate 180° section should be either added to or taken out of either the sideband or the carrier line. It does not matter which line is shortened or lengthened. Following this change the sidebands must then be rechecked. The DDM level read is an indication of the sideband-to-carrier power-level ratio.

(5) Upper Antenna Phasing

The phasing of the upper antenna in the sideband reference system is one of the most difficult of the ground set-up procedures. It must be kept in mind that the only true indication of the proper antenna phasing of the system is that in the far field, on centerline. This is most closely approximated by airborne phasing done at very low elevation angles and several miles out on centerline. A number of approximations to this are available to the personnel on the ground.

Antenna phasing with the use of hand-held or jig-held probes to sample antenna currents is very repeatable and accurate. The vector voltmeter is used with an H-field probe held in place near each dipole. Amplitude and phase measurements result in an

-443-

effective amplitude and phase value for the antenna current which can be used to place the antenna current 180° out-of-phase.

Another method of phasing the upper antenna is possible if the phasing detector is already in place at the correct location. Ideally, the DDM value at the phasing detector when the antennas are phased properly is zero DDM. In practice there is some DDM value near zero that is present when the system is operating normally. A history of this value must be available from previous readings. The phasing detector is normally fed to the path monitor so that this DDM value appears there. The upper antenna phaser can be adjusted to return the path monitor channel to the reference DDM value.

In general, a ground phasing point should be as far as possible from the glide-slope mast. However, this "objective" often causes errors, because the greater the distance from the mast, the greater the number of sources of error in the phasing indications, such as reflections and terrain imperfections. The middle marker is an excellent location for phasing, IF a number of other requirements are met, because it is sufficiently far away from the facility, and usually has several conveniences, such as an antenna mounting point (for routine checks), power, and lights, plus ready access. However, these conveniences often cause the middle marker location to be used as a phasing point, even though it may be a poor location. A minimum distance for ground phasing is approximately 1500' (450m) from the facility, or about 500' (150m) beyond the threshold.

In addition to sufficient distance from the facility, a valid phasing point should meet the following conditions:*

1. All GS antennas must be line-of-sight from the phasing point.

2. No significant horizontal reflectors, such as overhead power lines, or fences, should be between the receiver and facility.

3. No significant terrain perturbations should exist between receiver and facility, such as ditches, banks, hills, mounds of dirt, etc.

4. Location should be on extended runway centerline or, if necessary, on the glide slope side of the runway as close to extended runway centerline as possible.

Once a phasing point has been selected on the basis of physical characteristics, two tests are needed to verify that the indications will be valid. These ensure that the signals reaching the receiver are due primarily to direct-radiated and ground-reflected signals, rather than unwanted multipath signals. The procedure is:

1. Make sure system modulation unbalance is zero, and the quadrature line section is 90 ± 2°. Using a directional antenna (not the localizer dipole supplied with

* Courtesy ANW-463, 1978.

-444-

the FA-8766 receivers), and holding the antenna at head height, obtain a quadrature indication in the null reference configuration, and slowly pan the antenna from side-to-side, approximately ± 30° away from being pointed directly at the antennas. Changes in DDM should not exceed .02. (If significant multipath reflections are present at the proposed phasing point, pointing the directive antenna at the reflection will increase its contribution to the total received signal, which will change the phase between carrier and sideband, and cause a change in the indicated quadrature DDM.)

2. With a quadrature indication at the proposed phasing point, remeasure the DDM at point 100-200' (30.5 - 61.0m) in front, behind, and to each side of the proposed point. Again, changes in the quadrature DDM should be very small, indicating that reflections are not significant and that proximity error is acceptably small.

If a proposed point meets the above requirements, it may be reasonably expected to provide good results; generally, systems aligned from such phasing points will pass airborne phasing tests without any additional phasing efforts.

(5) Threshold Measurements

The availability of a portable mast capable of elevating a probe to a height of 70' (21.3m) makes possible the examination of threshold or threshold-plane DDM measurements. A plot of the DDM structure in the vertical plane containing the threshold and extending from at least the runway centerline to the area directly in front of the antenna mast can provide both commissioning documentary data and periodic maintenance information. Time limitations prevent a comprehensive study of the suitability of such measurements; i.e., sensitivity to parametric changes in the transmitting system, effects of obstructions in the near field, measurement tolerances, etc.

One such series of measurements has been taken at the Ohio University test site at Tamiami, Florida while that site was in a sideband reference configuration. Figure A-2 is the result of these measurements. Threshold crossing height is seen to be 49.25' (15.01m). The ± 1 localizer dot for the Tamiami site is marked on the Figure. The DDM structure at the threshold and across the localizer indicates that the glide-path width in the area of the threshold is not uniform.

At the Tamiami site ± 1 localizer dot subtends a sector as viewed from boresight of 20-26°. An examination of typical amplitude and phase versus azimuth for the APC FA-8976 glide-slope antennas shows that the rate of change of these parameters in the vicinity of 20-30° from boresight is sufficient to cause an effective differential amplitude and/or phase between upper and lower antennas. The effect of relative amplitude and phase changes to the antenna drive currents is well documented in Appendix B of this report.

Additional study should be undertaken to determine the vulnerability of vertical guidance information as a function of azimuth-dependent antenna characteristics.

-445-
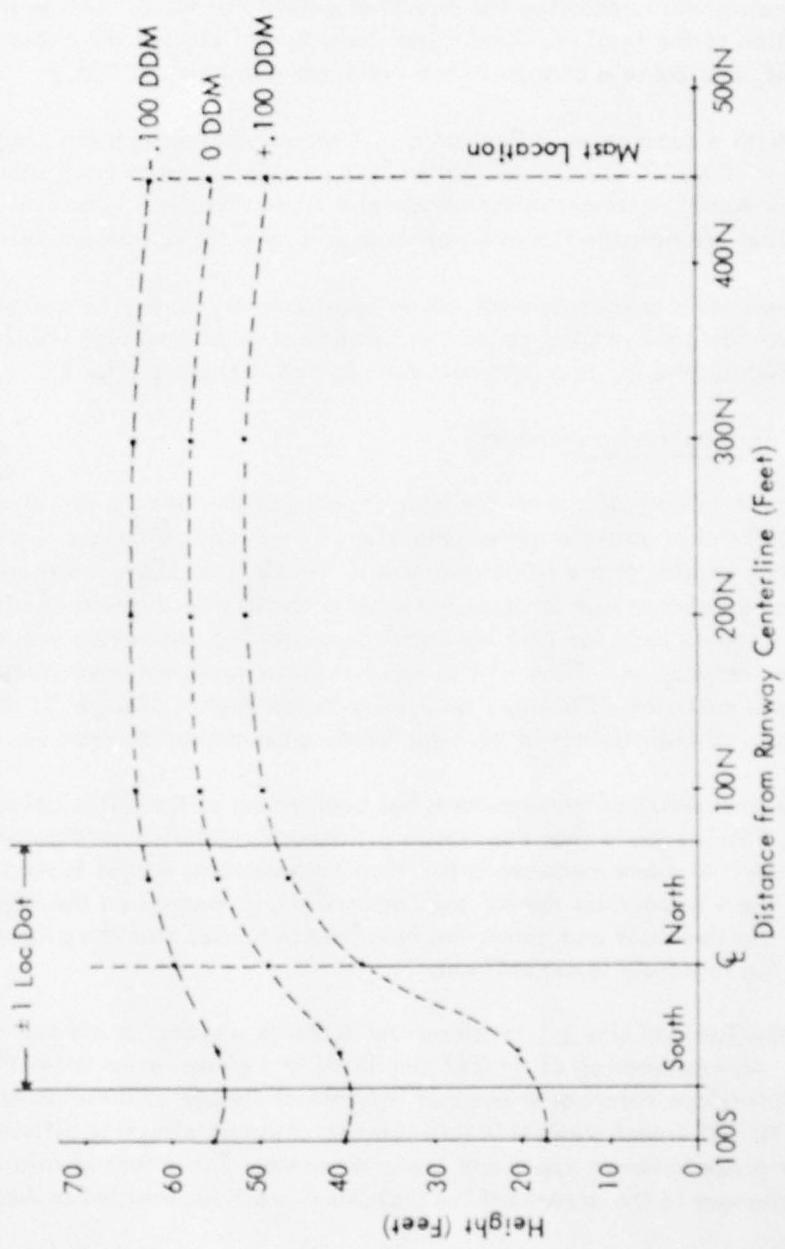
Figure A-2. Threshold Plane Probe Measurements Taken at the Tamiami Test Site, February 1979. Indicated on the graph is ± 1 localizer dot.

APPENDIX B. NEAR-FIELD MONITOR AND FAR-FIELD RESPONSE TO SYSTEM PERTURBATIONS

Figures B-1 through B-6 which follow give a graphic picture of the far-field response of the sideband reference system to various system perturbations including:

1. Carrier-to-sideband phasing
2. Upper antenna phasing
3. Lower and upper antenna attenuation
4. Carrier attenuation
5. Sideband attenuation

Each graph has two dependent variable scales, one on each side. The path angle is on the left, the path width is on the right. Out-of-tolerance conditions are identified as the cross-hatched area at the top and the bottom of the graph. The path angle is the solid line and the width is the dashed line. The parameter value beyond which the far field is out-of-tolerance is noted below each graph.

Figures B-7 through B-16 which follow show the Course Deviation Indicator (CDI) value in microamperes at both the amplitude and phase near-field monitors for system perturbations. These perturbations are the same as those for which the far-field values are computed in Figures B-1 through B-6.

-447-

Limits: Path – NA
Width –38.5°   +38.5°
(0.901)   (0.898)
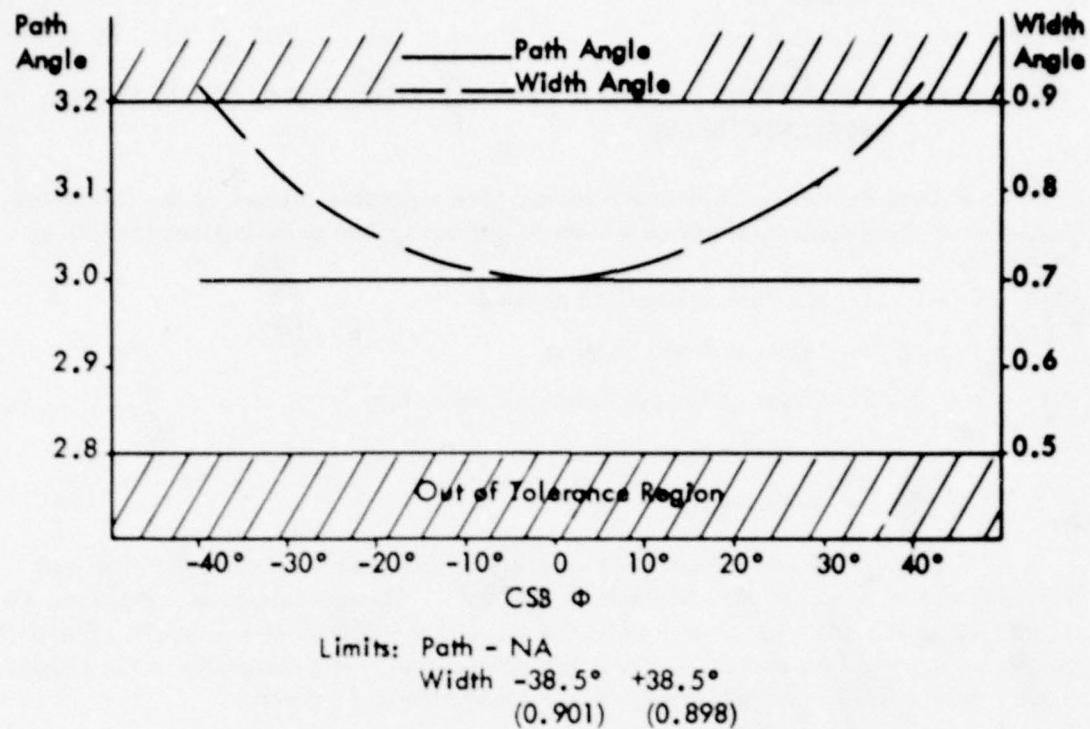
Figure B–1.   SBR Carrier to Sideband Phasing Far–Field Response.

Limits: Path –34°, +34°
Width –37.5°, +38°
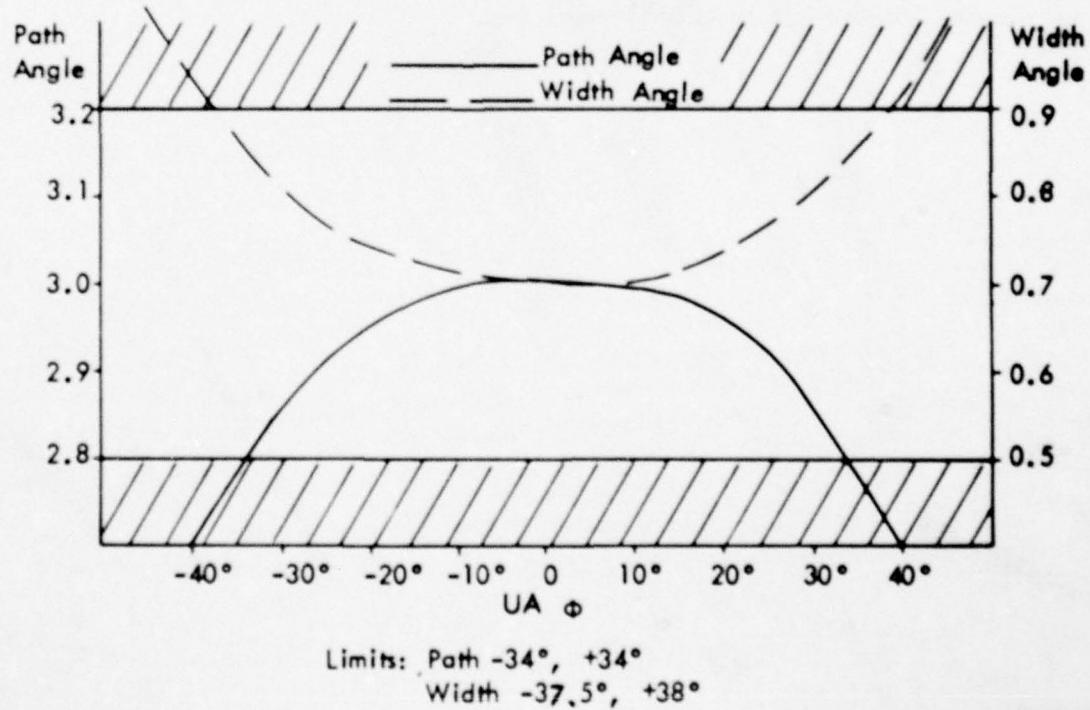
Figure B–2.   SBR Upper Antenna Phasing Far–Field Response.

-448-
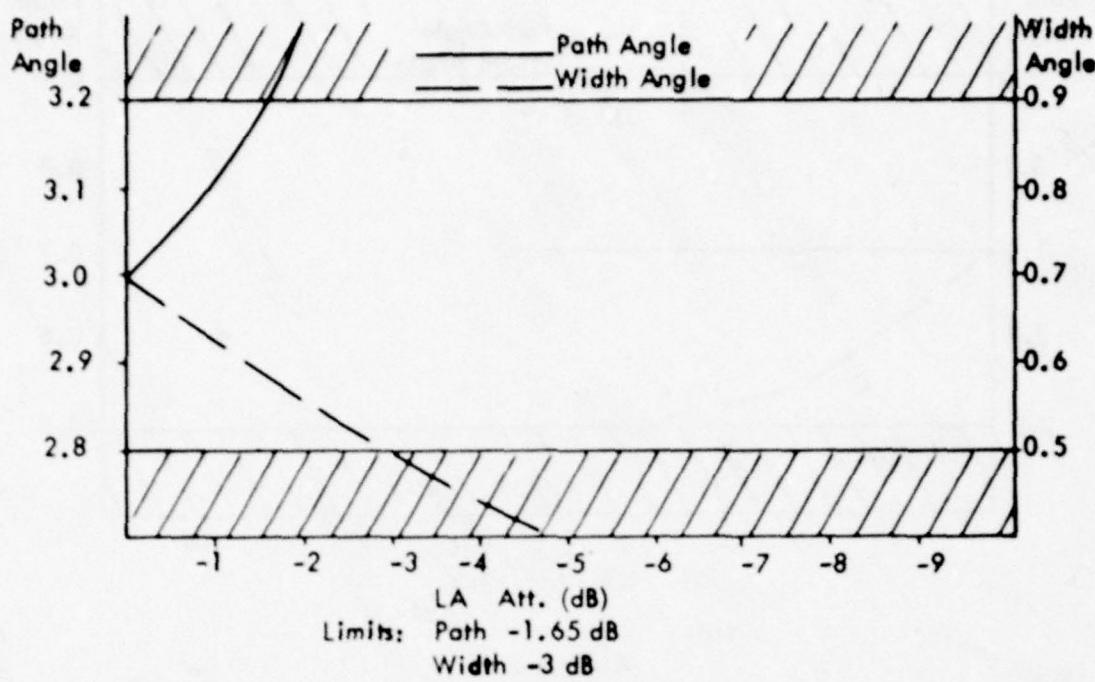
Figure B-3. SBR Lower Antenna Attenuation Far-Field Response.
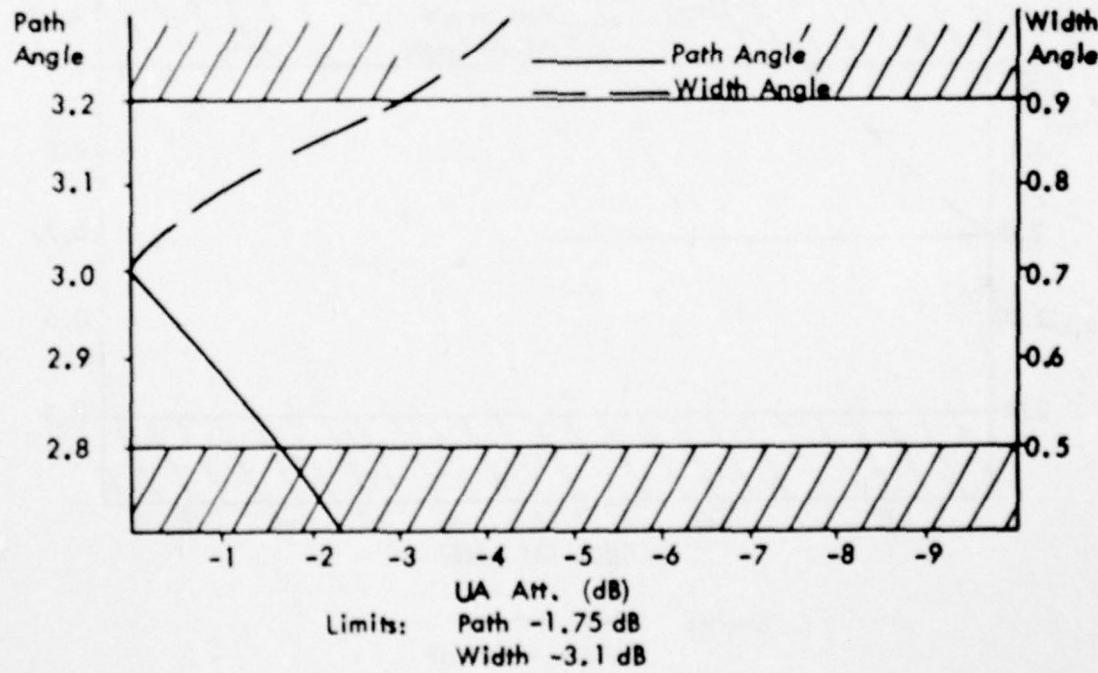
Figure B-4. SBR Upper Antenna Attenuation Far-Field Response.

-449-
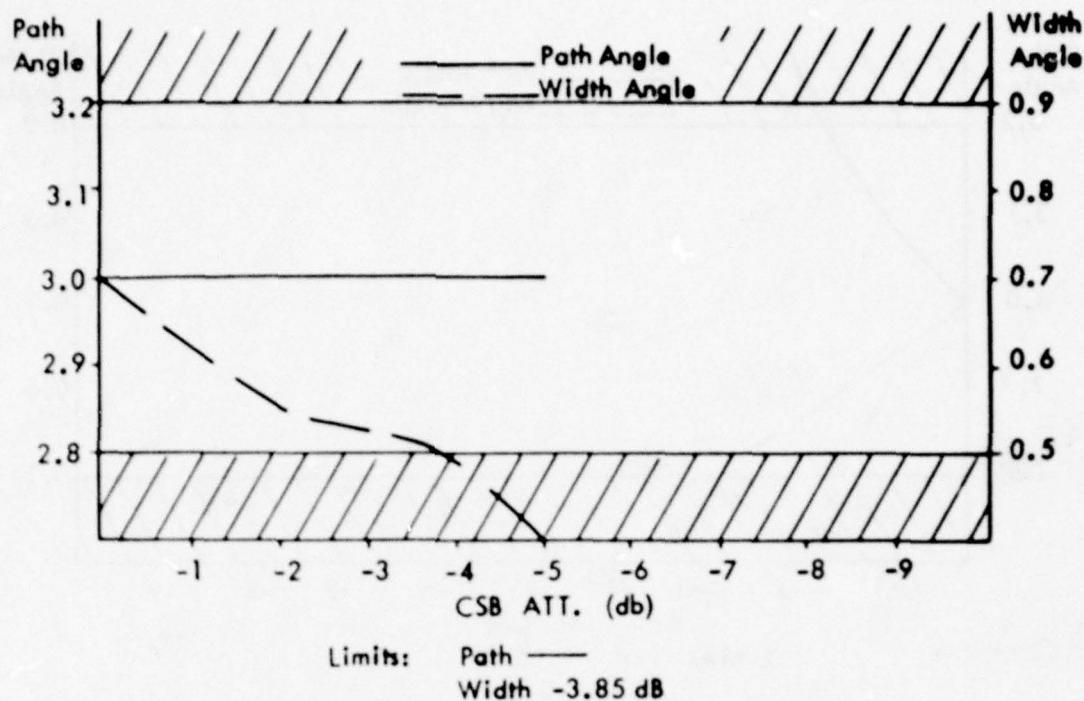
Figure B-5. SBR Carrier Attenuation Far-Field Response.
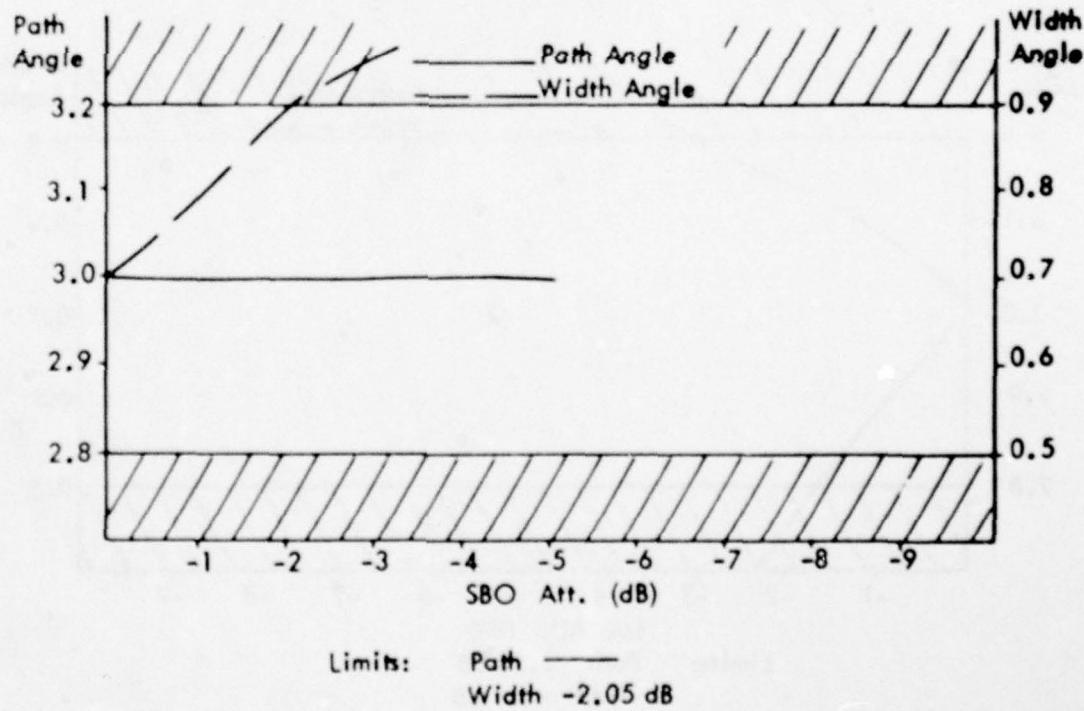
Figure B-6. SBR Sideband Only Attenuation Far-Field Response.

-450-
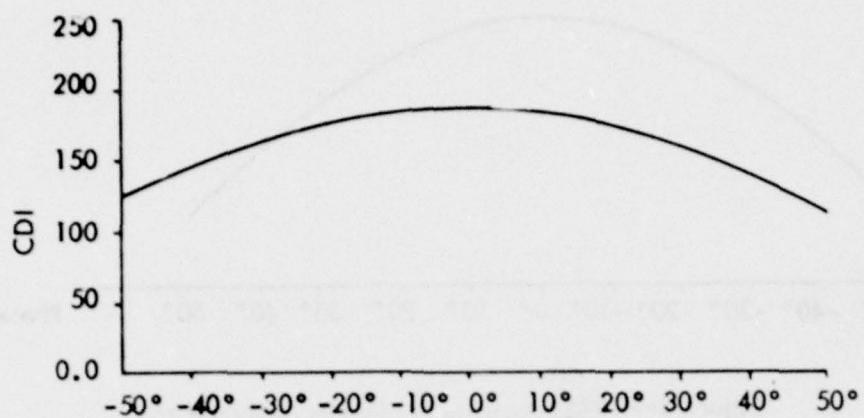
Figure B-7.   SBR Amplitude Monitor Response to
Carrier to Sideband Phasing.
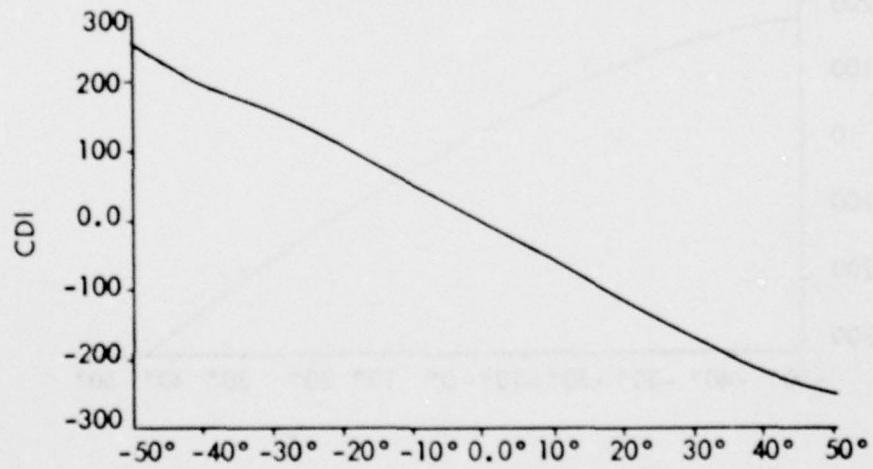
Figure B-8.   SBR Phase Monitor Response to
Carrier to Sideband Phasing.
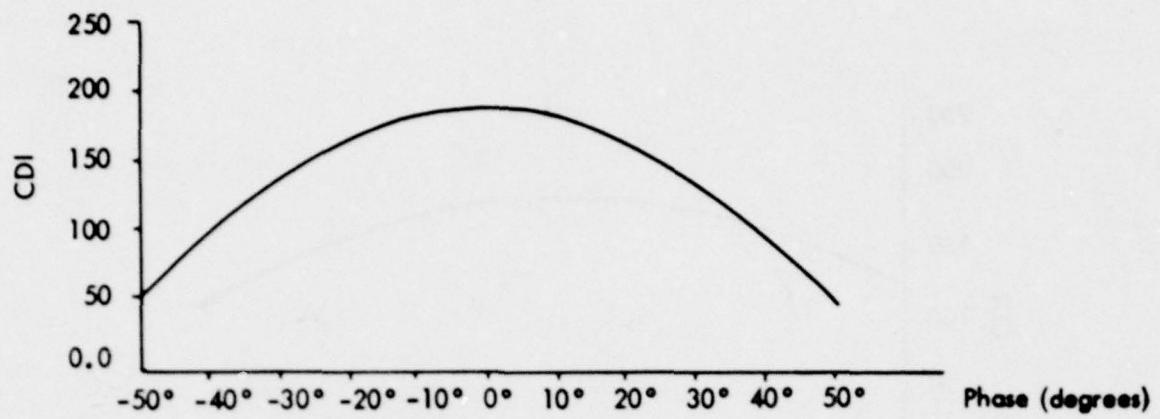
Figure B-9. SBR Amplitude Monitor Response to Upper Antenna Phasing.
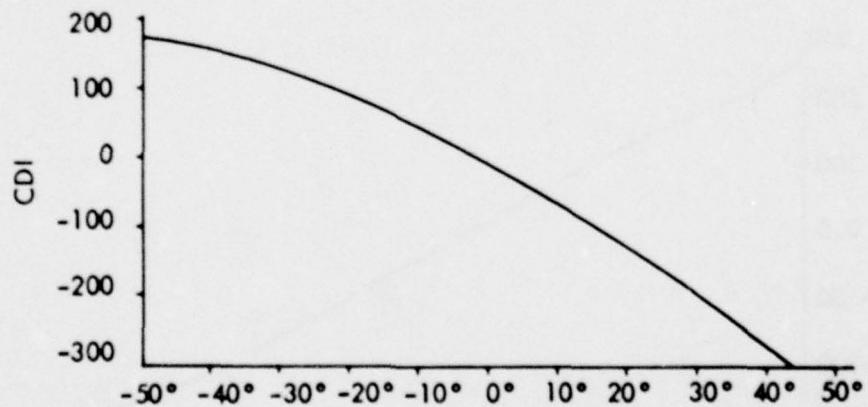
Figure B-10. SBR Phase Monitor Response to Upper Antenna Phasing.
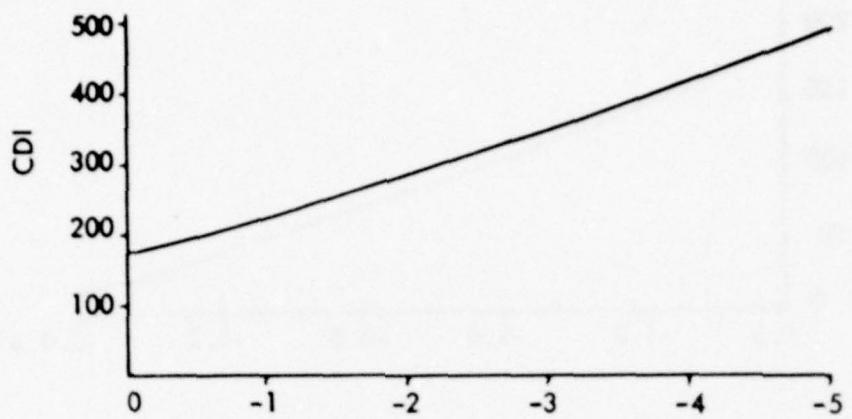
Figure B-11.   SBR Amplitude Monitor Response to
Lower Antenna Attenuation.
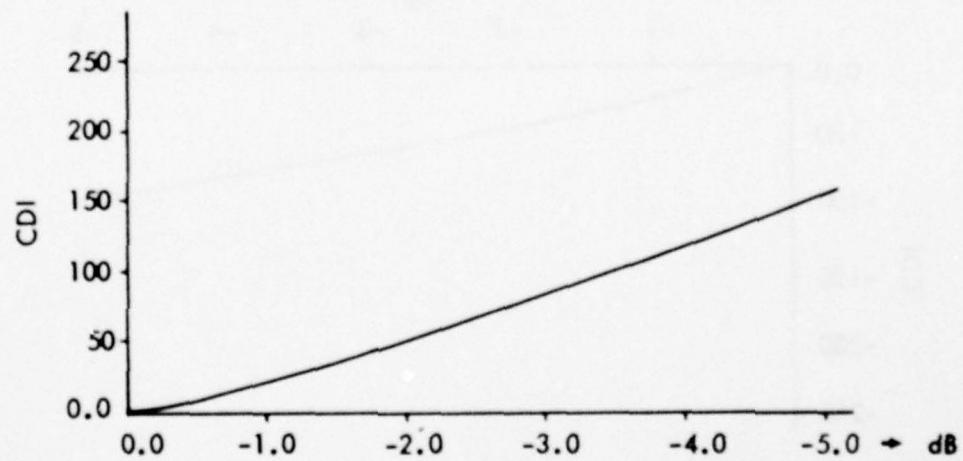
Figure B-12.   SBR Phase Monitor Response to
Lower Antenna Attenuation.

-453-
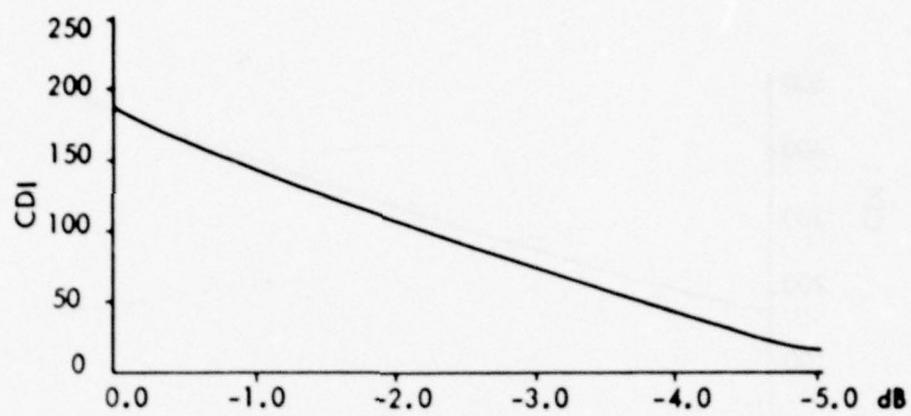
Figure B-13.   SBR Amplitude Monitor Response to
Upper Antenna Attenuation.
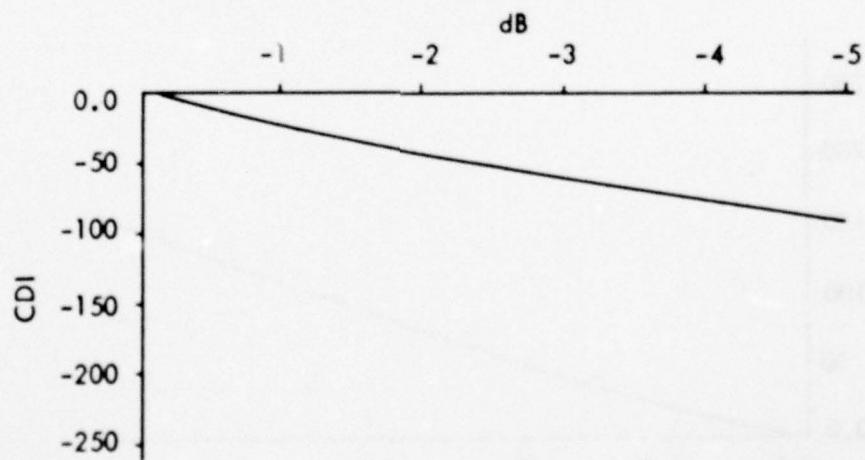
Figure B-14.   SBR Phase Monitor Response to
Upper Antenna Attenuation.

-454-
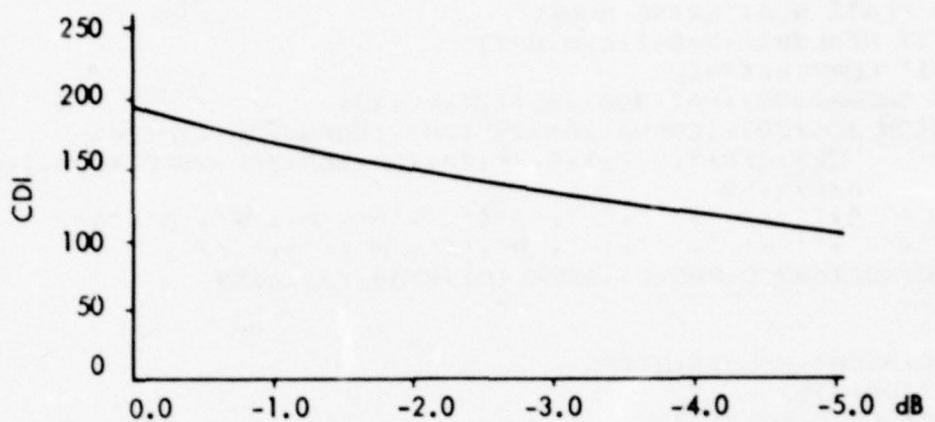
Figure B-15.   SBR Amplitude Monitor Response to
Sideband Attenuation.
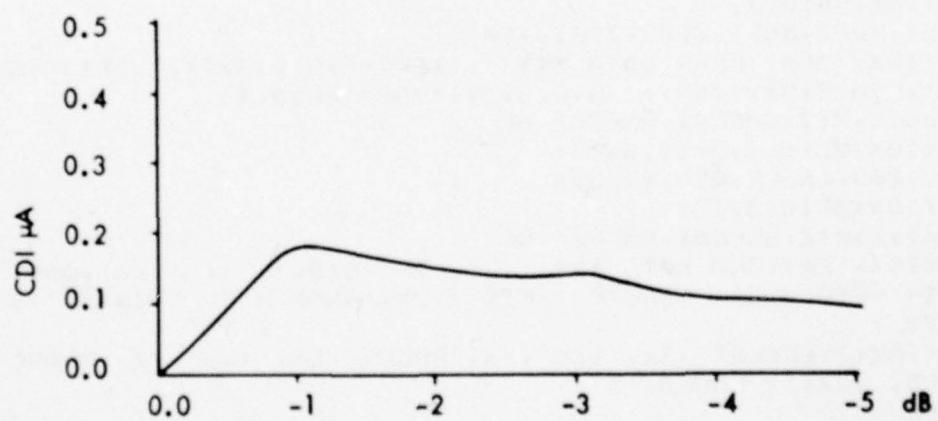
Figure B-16.   SBR Phase Monitor Response to
Sideband Attenuation.

APPENDIX C. PROGRAM LISTINGS

1. Listing of OULOC (Fortran)

```
TOF:
C   LOCALIZER PLATE SCATTERING MODEL
      IMPLICIT REAL*8(A,B,D-I,K,M,O-Z)
      IMPLICIT COMPLEX*16(C)
      REAL*4 OMEGA(300),PAT(300),XL(12),YL(12)
      DIMENSION ICS(20),ICSPHA(20),ISS(20),ISSPHA(20),ZP(20)
      COMMON        CES,CED,X,Y,Z,T,F,XP,ZA,XDP,YDP,ZDP,XDP2,XDP1,ZDP2,ZDP1
     C,TP,        K,F,R,RO
      DATA XL/' ',' ',' ',' ',' ',' ',' ','O','M','E','G','A'/
     C,YL/' ',' ',' ',' ',' ',' ','D','D','M',' ',' '/
      PHASE(C)=DATAN2(DIMAG(C),DREAL(C))*180./3.14159
C   READ DATA
      NI=0
      READ 30,NSCAT,NPLOTS,NTYPE
30    FORMAT(10X,3I5)
      IF(NSCAT.EQ.0)PRINT 31
31    FORMAT(10X,'THERE IS NO SCATTERER PRESENT')
      IF(NSCAT.NE.0)PRINT 32
32    FORMAT(10X,'THERE IS A SCATTERER PRESENT')
      PRINT 33,NPLOTS
33    FORMAT(10X,I1,'  PLOTS WILL BE MADE')
C   NN NOT PRESENTLY USED
      READ 40,NN,NE,M,XP,F,A
40    FORMAT(10X,2I5,4D10.3)
      PRINT 41,NE,M,XP,F,A
41    FORMAT(10X,'LOCALIZER DATA ***',2X,I5,1X,'ELEMENTS',5X,'M=',
     &F10.3,'XP=',G10.3,2X,'FREQ',F10.1,2X,'A RATIO=',F10.3)
      READ 50,XDP2,XDP1,ZDP2,ZDP1,YDP
50    FORMAT(10X,5D10.3)
      PRINT 51,XDP2,XDP1,ZDP2,ZDP1,YDP
51    FORMAT(10X,'SCATTERER DATA *** ','XDP2=',G10.3,2X,'XDP1=',G10.3,
     &'ZDP2=',G10.3,2X,'ZDP1=',G10.3,2X,'YDP=',G10.3)
      READ  60,X,RYZ,OMEGAI,OMEGAF,NP
60    FORMAT(10X,2D10.3,2F10.3,I5)
      READ 89,DB9,ANGLE,WID,NTENNA
89 FORMAT(10X,3F10.3,I5)
      PRINT 61,X,RYZ,OMEGAI,OMEGAF,NP
61    FORMAT(10X,'PATTERN DATA *** ',5X,'X=',G10.3,2X,'RYZ=',G10.3,2X,
     &'OMEGAI=',F10.3,2X,'OMEGAF=',F10.3,2X,'NUMBER OF POINTS=',I5)
      PRINT 71
71    FORMAT(10X,'ELEMENT',3X,'ICS',7X,'PHASE',5X,'ISS',7X,'PHASE',5X,
     &'X COORD.',2X,'Z COORD.')
      F=F*1.D6
      DO 3 JD=1,NE
      READ  70,ICS(JD),ICSPHA(JD),ISS(JD),ISSPHA(JD),XP,ZP(JD)
70    FORMAT(10X,4F10.3,2D10.3)
      PRINT 72,JD,ICS(JD),ICSPHA(JD),ISS(JD),ISSPHA(JD),XP,ZP(JD)
72    FORMAT(10X,I5,4(1X,F9.3),2(2X,G10.3))
3     CONTINUE
C   CONSTANTS
      PI=3.14159265
      $C=9.83569D8
      CJ=DCMPLX(0.D0,1.D0)
```

```
C   CALCULATE CONSTANTS
      K=2.*PI*F/$C
      R=DSQRT(X**2+RYZ**2)
      XDP=(XDP2+XDP1)/2.
      ZDP=(ZDP2+ZDP1)/2.
C   INCREMENT ORBITAL ANGLE OMEGA
      DO 1 J=1,NP
      T11=0.0
      T12=0.0
      OMEGA(J)=OMEGAI+(J-1.)*(OMEGAF-OMEGAI)/(NP-1.)
      O=OMEGA(J)*PI/180.
      Y=RYZ*DCOS(O)
      Z=RYZ*DSIN(O)
C   T IS POLAR ANGLE THETA IN RADIANS
      T=DARCOS(Z/R)
      P=DATAN2(Y,X)
      CESS=DCMPLX(0.D0,0.D0)
      CECS=DCMPLX(0.D0,0.D0)
      CESS2=DCMPLX(0.D0,0.D0)
      CECS2=DCMPLX(0.D0,0.D0)
C   CALCULATE FIELDS FOR EACH ANTENNA
      DO 2 JE=1,NE
      IPCS=ICSPHA(JE)*PI/180.
      IPSS=ISSPHA(JE)*PI/180.
      CISS=ISS(JE)*DCMPLX(DCOS(IPSS),DSIN(IPSS))
      CICS=ICS(JE)*DCMPLX(DCOS(IPCS),DSIN(IPCS))
      ZA=ZP(JE)
      RO=DSQRT(XP**2+ZA**2+YDP**2)
C   TP IS THE POLAR ANGLE IN RADIANS FROM THE ANTENNA TO THE CENTER OF TH
      TP=DARCOS((ZDP-ZA)/DSQRT((XDP -XP)**2+YDP**2+(ZDP-ZA)**2))
      CALL        DIRECT
      IF(NSCAT.EQ.0)GO TO 8
      CALL        SCAT
C   TOTAL FIELD IS SUM OF DIRECT AND SCATTERED
      CET=CED+CES
      CESS=CESS+CISS*CET*CJ
      CECS=CECS+CICS*CET
      ESS=CDABS(CESS)
      ECS=CDABS(CECS)
      ED=CDABS(CED)
      ES=CDABS(CES)
      ET=CDABS(CET)
      EDPHA=PHASE(CED)
8     CONTINUE
      CESS2=CESS2+CISS*CED*CJ
      CECS2=CECS2+CICS*CED
      ESS2=CDABS(CESS2)
      ECS2=CDABS(CECS2)
2     CONTINUE
      IF(NSCAT.EQ.0)GO TO 17
      DDM=ESS2
      DDM=-2.*M*A*DREAL(CESS/CECS)
      UA=DDM*150./.155
17    DDM2=ECS2
      DDM2=-2.*A*M*DREAL(CESS2/CECS2)
      UA2=DDM2*150./.155
      J2=J+NP
```

```
      PAT(J)=DDM
      IF(NSCAT.EQ.0)PAT(J)=DDM2
      IF(NPLOTS.EQ.2)PAT(J2)=DDM2
      IF(NPLOTS.EQ.2)OMEGA(J2)=OMEGA(J)
      PRINT 10,OMEGA(J),DDM,UA,DDM2,UA2
10    FORMAT(10X,5F15.4)
      X=0.155
      Y=0.0000
      Z1=0.2500
      IF (DDM2.GT.Y.AND.DDM2.LE.X.AND.OMEGA(J).GT.-6.0)DDM3=DDM2
      IF(DDM2.GE.X.AND.DDM2.LE.Z1.AND.OMEGA(J).GT.-6.0)DDM4=DDM2
      IF(DDM2.GT.Y.AND.DDM2.LE.X.AND.OMEGA(J).GT.-6.0)TH1=OMEGA(J)
      IF(DDM2.GE.X.AND.DDM2.LE.Z1.AND.OMEGA(J).GT.-6.0)TH2=OMEGA(J)
      X=-0.155
      Y=-0.000
      Z1=-0.250
      IF (DDM2.LT.Y.AND.DDM2.GE.X.AND.OMEGA(J).LT.6.0)DDM5=DDM2
      IF(DDM2.LE.X.AND.DDM2.GE.Z1.AND.OMEGA(J).LT.6.0)DDM6=DDM2
      IF(DDM2.LT.Y.AND.DDM2.GE.X.AND.OMEGA(J).LT.6.0)TH3=OMEGA(J)
      IF(DDM2.EQ.DDM6)TH4=OMEGA(J)
      W=-.080
      V=.08
      IF(DDM2.GT.W.AND.DDM2.LT.0.0)DDM8=DDM2
      IF(DDM2.GT.0.0.AND.DDM2.LT.V)DDM9=DDM2
      IF(DDM2.GT.W.AND.DDM2.LT.0.0)ALPHA2=OMEGA(J)
      IF(DDM2.GT.0.0.AND.DDM2.LT.V)ALPHA3=OMEGA(J)
      IF(OMEGA(J).EQ.0.0)DDMC=DDM2
      IF(OMEGA(J).EQ.0.0)UAC=UA2
      IF(DDM2.GE.-0.155.AND.OMEGA(J).LE.-10.0.AND.OMEGA(J).GE.-35.0)T11=
     11
      IF(DDM2.LE.0.155.AND.OMEGA(J).LE.-10.0.AND.OMEGA(J)
     1.GE.-35.0)WRITE (8,67)OMEGA(J)
      IF(DDM2.GE.-0.155.AND.OMEGA(J).GT.10.0.AND.OMEGA(J)
     1.LE.35.0)WRITE (8,67)OMEGA(J)
      IF(DDM2.LE.0.175.AND.OMEGA(J).LT.-3.0.AND.OMEGA(J).GE.-10.0)WRITE
     1(8,67)OMEGA(J)
      IF(DDM2.GE.-0.175.AND.OMEGA(J).GT.3.0.AND.OMEGA(J).LE.10.0)WRITE
     1 (8,67)OMEGA(J)
67    FORMAT(10X,F10.5)
      IF(DDM2.LE.0.155.AND.OMEGA(J).GE.10.0.AND.OMEGA(J).LE.35.0)T11=1.
      IF(DDM2.GE.-0.175.AND.OMEGA(J).LT.-3.0.AND.OMEGA(J).GE.-10.0)T12=1
      IF(DDM2.LE.0.175.AND.OMEGA(J).GT.3.0.AND.OMEGA(J).LE.10.0)T12=1.
      IF(T11.EQ.1.0.OR.T12.EQ.1.0)GO TO 37
      GO TO 39
37    NI=NI+1
39    T13=0.0
1     CONTINUE
      PER=DDM9/(DDM9-DDM8)
      ALPHA=ALPHA3-((ALPHA3-ALPHA2)*PER)
      PER1=(DDM4-0.155)/(DDM4-DDM3)
      THETA1=(TH2-((TH2-TH1)*PER1))
      PER2=(DDM6-X)/(DDM6-DDM5)
      THETA2=(TH4-((TH4-TH3)*PER2))
      THETA=THETA1-THETA2
      PER7=((THETA-WID)/(WID))*100.
      PRINT 99,DB9,ANGLE,NTENNA,ALPHA,WID,THETA,PER7,DDMC,UAC
```

1·0

2·8   2·5

3·15   2·2

3·5

1·1   2·0

1·8

1·25   1·4   1·6

NATIONAL BUREAU OF STANDARDS
MICROCOPY RESOLUTION TEST CHART
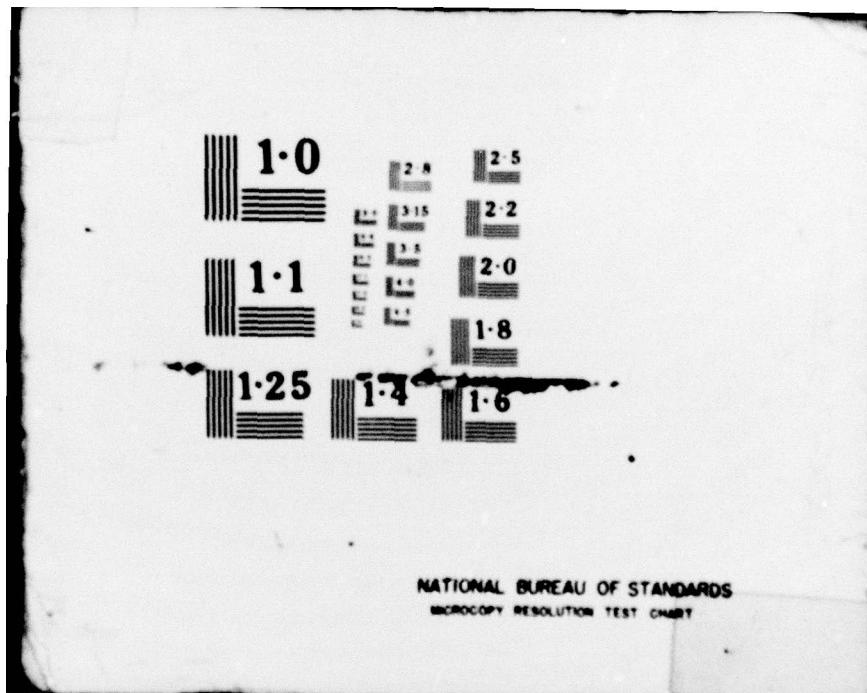
```
   99 FORMAT(10X,'****************'/10X,'RESULTS OF A',2F10.5,
      13X,'COMPLEX REFLECTION IN ANTENNA NUMBER',I5//35X,'NORMAL',3X,
      1'WITH FAULT'/10X,'ZERO DDM COURSE',10X,'0.00',5X,F10.5
      1/10X,'COURSE WIDTH',13X,F5.3,5X,F10.5/10X,'% CHANGE IN WIDTH'
      1,8X,'0.00',5X,F10.5/10X,'CENTERLINE DDM',11X,'0.00',5X,F10.5
      1/10X,'CENTERLINE UA',12X,'0.00',5X,F10.5)
   97 FORMAT(10X,'LOW CLEARANCE IN SECTORS 1 & 2',5X,'NONE')
      IF(NI.EQ.0)PRINT 97
      X=PER7
      Y=UAC
      PER8=DABS(X)
      UAC1=DABS(Y)
      IF(PER8.LT.17.0.AND.UAC1.LT.15.0.AND.NI.EQ.0)PRINT 79
   79 FORMAT(10X,'THE SYSTEM IS IN TOLERANCE'/10X,'***************')
      IF(NI.GT.0)PRINT 77
   77 FORMAT(10X,'LOW CLEARANCE IN SECTORS 1 & 2')
      IF(NI.GT.0)GO TO 47
      IF(NI.EQ.0)GO TO 48
      N=1
   47 DO 7 N=1,NI
      READ(9,69)PHI
   69 FORMAT(10X,F10.3)
      PRINT 98,PHI
   98 FORMAT(35X,F10.3)
7     CONTINUE
   48 IF(PER8.GT.17.0.OR.UAC1.GT.15.0.OR.NI.GT.0
      1)PRINT 88
   88 FORMAT(10X,'THE SYSTEM IS OUT OF TOLERANCE'/10X,'*************')
      IF(NPLOTS.EQ.0)GO TO 9
      IF(NTYPE.EQ.1)GO TO 19
      CALL MPLOT(OMEGA,PAT,NP,NPLOTS,XL,YL)
      GO TO 9
   19 CALL PLOTT(OMEGA,PAT,NP,NPLOTS,XL,YL)
9     CONTINUE
      STOP
      END
      SUBROUTINE DIRECT
      IMPLICIT REAL*8(A,B,D-I,K,M,O-Z)
      IMPLICIT COMPLEX*16(C)
      COMMON        CES,CED,X,Y,Z,T,P,XP,ZA,XDP,YDP,ZDP,XDP2,XDP1,ZDP2,ZDP1
     C,TP,         K,F,R,RO
      PHASE(C)=DATAN2(DIMAG(C),DREAL(C))*180./3.14159
      PI=3.14159265
      ETA=3.77D2
      CJ=DCMPLX(0.D0,1.D0)
      ZP=ZA
C  SINGLE ANTENNA PATTERN
      DIPAT=1.0D00
C  FOR TRAVELING WAVE DIPAT=DCOS(DCOS(T)*PI/2.)/DSIN(T)
C  RADIAL DISTANCE FROM RECEIVER TO ANTENNA
      RP=DSQRT((X-XP)**2+Y**2+(Z-ZP)**2)
      CEX=CDEXP(-CJ*K*RP)
      EX=CDABS(CEX)
      EXPHA=PHASE(CEX)
      CED=CJ    *ETA*CEX*DIPAT/(2.*PI*RP)
      RETURN
      END
```

-459-

```
      SUBROUTINE SCAT
      IMPLICIT REAL*8(A,B,D-I,K,M,O-Z)
      IMPLICIT COMPLEX*16(C)
      COMMON        CES,CED,X,Y,Z,T,P,XP,ZA,XDP,YDP,ZDP,XDP2,XDP1,ZDP2,ZDP1
     C,TP,         K,F,R,RO
      PHASE(C)=DATAN2(DIMAG(C),DREAL(C))*180./3.14159
C  CONSTANTS
      PI=3.14159265
      MUO=.383022977
      MUO=MUO*1.D-6
      CJ=DCMPLX(0.D0,1.D0)
      ZP=ZA
C  SINGLE ANTENNA PATTERN
C FOR TRAVELING WAVE  DIPAT=DCOS(DCOS(TP)*PI/2.)/DSIN(TP)
      DIPAT=1.0D00
C  COMPUTE SIN(U)/U
      IF((X.EQ.0.D0).AND.(XP.EQ.0.D0))GO TO 1
      VX=      K*(XDP2- XDP1)*(XP/RO+X/R)/2.
      UX=DSIN(VX)/VX
5     IF((Z.EQ.0.D0).AND.(ZP.EQ.0.D0))GO TO 2
      VZ=      K*(ZDP2- ZDP1)*(ZP/RO+Z/R)/2.
      UZ=DSIN(VZ)/VZ
6     CONTINUE
C  CALCULATE PHASE TERM
      CEX=CDEXP(CJ*K*( ( ZDP2+ZDP1)*(ZP/RO+Z/R)/2.
     &+(XDP2+XDP1)*(XP/RO+X/R)/2.-(RO+R                -Y*YDP/R)))
      CINT=    CEX*UX*UZ*(ZDP2-ZDP1)*(XDP2-XDP1)
      AX=YDP/DSQRT( XP**2+YDP**2)
      RI=RO-((XDP*XP)-(ZDP*ZP))/RO
      R2= R+YDP**2/(2*R)-(X*XDP+Y*YDP+Z*ZDP)/R
      CES=     F*MUO*DIPAT*AX*CINT       / (2.*PI*RI*R2)
      CES=CES*DSIN(T)
      GO TO 7
1     UX=1.D0
      GO TO 5
2     UZ=1.D0
      GO TO 6
7     RETURN
      END
```

2. <u>Listing of ANTENNA2 (Fortran)</u>

FILE: ANTENNA2 FORTRAN A

```
      COMPLEX A(15,15),B(15),C(15),DC(15),G(15),H(15),P,S(15),Q(15)
     1,DS(15),B1(15)
      DIMENSION Z(15)
      N=15
C SCATTER MATRIX PARAMETER DEFINITION
      DO 10 I=1,N
      READ 273,(A(I,J),J=1,N)
      DO 10 J=1,N
      A(I,J)=CMPLX((10**(REAL(A(I,J))/20))*COS(0.017453*AIMAG(A(I,J))),
     1(10**(REAL(A(I,J))/20))*SIN(0.017453*AIMAG(A(I,J))))
  273 FORMAT(3X,2F10.5)
   10 CONTINUE
C ANTENNA REFLECTION COEFFICIENTS
      READ 273,(B(J),J=1,N)
      DO 135 I=1,N
      B(I)=CMPLX((10**(REAL(B(I))/20))*COS(0.017453*AIMAG(B(I))),
     1(10**(REAL(B(I))/20))*SIN(0.017453*AIMAG(B(I))))
  135 B1(I)=B(I)
C INPUT POWER TRANSMISSION DATA
      READ 273,(DS(J),J=1,N)
      CALL CNVRT(DS,N)
      READ 273,(DC(J),J=1,N)
      CALL CNVRT(DC,N)
      DO 50 I=1,N
      DC(I)=CMPLX(50.,0.0)*DC(I)
      DS(I)=CMPLX(50.,0.0)*DS(I)
      H(I)=CMPLX(0.0,0.0)
      READ 273, Z(I)
   50 CONTINUE
      CALL RFLCT(A,B,C,DC,G,H,S,Q,N)
      DO 27 I=1,N
      DC(I)=CMPLX(SQRT(REAL(C(I))**2+AIMAG(C(I))**2),
     157.296*ATAN2(AIMAG(C(I)),REAL(C(I))))
   27 H(I)=CMPLX(0.0,0.0)
      CALL RFLCT(A,B1,C,DS,G,H,S,Q,N)
      DO 37 I=1,N
      DS(I)=CMPLX(SQRT(REAL(C(I))**2+AIMAG(C(I))**2),ATAN2(AIMAG(C(I)),
     1REAL(C(I)))*57.296)
   37 CONTINUE
      WRITE(7,100)
  100 FORMAT(10X,'     0     1     1')
      WRITE(7,110)
  110 FORMAT(10X,'    91    15',' .    0.3  ','0.0          ',
     1 '111.9       ','0.368     ')
      WRITE(7,120)
  120 FORMAT(10X,'    -.5       -8.5        4.0       -4.       150.
     1')
      READ 62,OMEGI,OMEGAF,NPT
   62 FORMAT(10X,2F10.3,I5)
      READ 67,DB9,ANGLE,WID,NTENNA
   67 FORMAT(10X,3F10.3,I5)
      WRITE(7,130)OMEGI,OMEGAF,NPT
  130 FORMAT(10X,'1000.       3168C.    ',2F10.3,I5)
      WRITE(7,89)DB9,ANGLE,WID,NTENNA
   89 FORMAT(10X,3F10.3,I5)
```

-461-

FILE: ANTENNA2 FORTRAN   A   OHIO UNIVERSITY AVIONICS ENGINEER

```
      DO 47 I=1,N
   47 WRITE(7,140) DC(I),DS(I),Z(I)
  140 FORMAT(10X,4F10.3,'      0.0  ',F10.7)
      STOP
      END
      SUBROUTINE RFLCT(A,B,C,D,G,H,S,Q,N)
      COMPLEX A(N,N),B(N),C(N),D(N),G(N),H(N),P,S(N),Q(N)
      PRINT 5
      DO 4 I=1,N
    4 PRINT 500,(A(I,J),J=1,N)
      PRINT 20,(B(I),I=1,N)
    5 FORMAT('STHE A MATRIX IS:')
   20 FORMAT(' ','THE B MATRIX IS:',/,1X,5(1PE10.3,1X,1PE10.3,3X),
     C/,6X,5(1PE10.3,1X,1PE10.3,3X),/,6X,5(1PE10.3,1X,1PE10.3,3X))
      PRINT 30,(D(J),J=1,N)
   30 FORMAT(' ','THE INPUT TRANSMISSION MATRIX IS:',/,
     C1X,5(1PE10.3,1X,1PE10.3,3X),2(/,6X,5(1PE10.3,1X,1PE10.3,3X)))
      P=CMPLX(1.0,0.0)
      PRINT 6
    6 FORMAT(' ','THE VOLTAGE AVAILABLE TO THE ANTENNA IS:')
      DO 300 K=1,10
      DO 50 J=1,N
      C(J)=H(J)
      G(J)=D(J)*P
   50 Q(J)=B(J)*C(J)
      CALL MULTIO(A,Q,S,N,N,1)
      DO 250 J=1,N
  250 H(J)=G(J)+S(J)
  300 PRINT 500,(H(J),J=1,N)
      DO 350 J=1,N
  350 C(J)=H(J)*(CMPLX(1.0,0.0)+B(J))
      PRINT 7
    7 FORMAT(' ','THE FINAL VOLTAGE AT THE ANTENNA IS')
      PRINT 500,(C(J),J=1,N)
  500 FORMAT(' ',5(2(1PE10.3,1X),2X),2(/,6X,5(1PE10.3,1X,1PE10.3,3X)))
      DO 17 J=1,N
      B(J)=50.*(1.+B(J))/(1.-B(J))
      CCOS=COS(ATAN2(AIMAG(C(J)),REAL(C(J))))
      CSIN=SIN(ATAN2(AIMAG(C(J)),REAL(C(J))))
      CMAG=SQRT((1./50.)*REAL(C(J)*C(J)/B(J)))
   17 C(J)=CMPLX(CCOS*CMAG,CSIN*CMAG)
      PRINT 8
    8 FORMAT(' THE ANTENNA CURRENTS ARE:')
      PRINT 500,(C(J),J=1,N)
      RETURN
      END
      SUBROUTINE MULTIO(A,B,C,N1,N2,N3)
      COMPLEX A(N1,N2),B(N2,N3),C(N1,N2)
      DO 1 I=1,N1
      DO 1 K=1,N3
      C(I,K)=CMPLX(0.0,0.0)
      DO 1 J=1,N2
    1 C(I,K)=C(I,K)+A(I,J)*B(J,K)
      RETURN
      END
```

-462-

```
      COMPLEX A(15,15),B(15),C(15),DC(15),G(15),H(15),P,S(15),Q(15)
     1,DS(15),B1(15)
      DIMENSION Z(15)
      N=15
C SCATTER MATRIX PARAMETER DEFINITION
      DO 10 I=1,N
      READ 273,(A(I,J),J=1,N)
      DO 10 J=1,N
      A(I,J)=CMPLX((10**(REAL(A(I,J))/20))*COS(0.017453*AIMAG(A(I,J))),
     1(10**(REAL(A(I,J))/20))*SIN(0.017453*AIMAG(A(I,J))))
  273 FORMAT(3X,2F10.5)
   10 CONTINUE
C ANTENNA REFLECTION COEFFICIENTS
      READ 273,(B(J),J=1,N)
      DO 135 I=1,N
      B(I)=CMPLX((10**(REAL(B(I))/20))*COS(0.017453*AIMAG(B(I))),
     1(10**(REAL(B(I))/20))*SIN(0.017453*AIMAG(B(I))))
  135 B1(I)=B(I)
C INPUT POWER TRANSMISSION DATA
      READ 273,(DS(J),J=1,N)
      CALL CNVRT(DS,N)
      READ 273,(DC(J),J=1,N)
      CALL CNVRT(DC,N)
      DO 50 I=1,N
      DC(I)=CMPLX(50.,0.0)*DC(I)
      DS(I)=CMPLX(50.,0.0)*DS(I)
      H(I)=CMPLX(0.0,0.0)
      READ 273, Z(I)
   50 CONTINUE
      CALL RFLCT(A,B,C,DC,G,H,S,Q,N)
      DO 27 I=1,N
      DC(I)=CMPLX(SQRT(REAL(C(I))**2+AIMAG(C(I))**2),
     157.296*ATAN2(AIMAG(C(I)),REAL(C(I))))
   27 H(I)=CMPLX(0.0,0.0)
      CALL RFLCT(A,B1,C,DS,G,H,S,Q,N)
      DO 37 I=1,N
      DS(I)=CMPLX(SQRT(REAL(C(I))**2+AIMAG(C(I))**2),ATAN2(AIMAG(C(I)),
     1REAL(C(I)))*57.296)
   37 CONTINUE
      WRITE(7,100)
  100 FORMAT(10X,'     0     1     1')
      WRITE(7,110)
  110 FORMAT(10X,'    91    15','     0.3  ','0.0    '
     1,'111.0     ','0.368     ')
      WRITE(7,120)
  120 FORMAT(10X,'     -.5      -8.5      4.0      -4.      150.
     ')
      READ 62,OMEGI,OMEGAF,NPT
   62 FORMAT(10X,2F10.3,I5)
      READ 67,DB9,ANGLE,WID,NTENNA
   67 FORMAT(10X,3F10.3,I5)
      WRITE(7,130)OMEGI,OMEGAF,NPT
  130 FORMAT(10X,'1000.      31680.    ',2F10.3,I5,
      WRITE(7,89)DB9,ANGLE,WID,NTENNA
```

```
   89 FORMAT(10X,3F10.3,I5)
      DO 47 I=1,N
   47 WRITE(7,140) DC(I),DS(I),Z(I)
  140 FORMAT(10X,4F10.3,'     0.0   ',F10.3)
      STOP
      END
      SUBROUTINE RFLCT(A,B,C,D,G,H,S,Q,N)
      COMPLEX A(N,N),B(N),C(N),D(N),G(N),H(N),P,S(N),Q(N)
      PRINT 5
      DO 4 I=1,N
    4 PRINT 500,(A(I,J),J=1,N)
      PRINT 20,(B(I),I=1,N)
    5 FORMAT('0THE A MATRIX IS:')
   20 FORMAT(' ','THE B MATRIX IS:',/,1X,5(1PE10.3,1X,1PE10.3,3X),
     C/,6X,5(1PE10.3,1X,1PE10.3,3X),/,6X,5(1PE10.3,1X,1PE10.3,3X))
      PRINT 30,(D(J),J=1,N)
   30 FORMAT(' ','THE INPUT TRANSMISSION MATRIX IS:',/,
     C1X,5(1PE10.3,1X,1PE10.3,3X),2(/,6X,5(1PE10.3,1X,1PE10.3,3X)))
      P=CMPLX(1.0,0.0)
      PRINT 6
    6 FORMAT(' ','THE VOLTAGE AVAILABLE TO THE ANTENNA IS:')
      DO 300 K=1,10
      DO 50 J=1,N
      C(J)=H(J)
      G(J)=D(J)*P
   50 Q(J)=B(J)*C(J)
      CALL MULTIO(A,Q,S,N,N,1)
      DO 250 J=1,N
  250 H(J)=G(J)+S(J)
  300 PRINT 500,(H(J),J=1,N)
      DO 350 J=1,N
  350 C(J)=H(J)*(CMPLX(1.0,0.0)+B(J))
      PRINT 7
    7 FORMAT(' ','THE FINAL VOLTAGE AT THE ANTENNA IS')
      PRINT 500,(C(J),J=1,N)
  500 FORMAT(' ',5(2(1PE10.3,1X),2X),2(/,6X,5(1PE10.3,1X,1PE10.3,3X)))
      DO 17 J=1,N
      B(J)=50.*(1.+B(J))/(1.-B(J))
      CCOS=COS(ATAN2(AIMAG(C(J)),REAL(C(J))))
      CSIN=SIN(ATAN2(AIMAG(C(J)),REAL(C(J))))
      CMAG=SQRT((1./50.)*REAL(C(J)*C(J)/B(J)))
   17 C(J)=CMPLX(CCOS*CMAG,CSIN*CMAG)
      PRINT 8
    8 FORMAT(' THE ANTENNA CURRENTS ARE:')
      PRINT 500,(C(J),J=1,N)
      RETURN
      END
      SUBROUTINE MULTIO(A,B,C,N1,N2,N3)
      COMPLEX A(N1,N2),B(N2,N3),C(N1,N2)
      DO 1 I=1,N1
      DO 1 K=1,N3
      C(I,K)=CMPLX(0.0,0.0)
      DO 1 J=1,N2
    1 C(I,K)=C(I,K)+A(I,J)*B(J,K)
      RETURN
```

```
      END
      SUBROUTINE CNVRT(D,N)
      COMPLEX D(N)
      DO 50 I=1,N
      D(I)=CMPLX(REAL(D(I))*COS(0.017453*AIMAG(D(I))),
     1REAL(D(I))*SIN(0.017453*AIMAG(D(I))))
50    CONTINUE
      RETURN
      END
```